# Anion-Templated Synthesis of Functional Interlocked Architectures

**Laura M. Hancock**

**Wadham College, University of Oxford**




A thesis submitted for the degree of Doctor of Philosophy

Inorganic Chemistry Laboratory
University of Oxford

Hilary Term, 2011

# Anion-Templated Synthesis of Functional Interlocked Architectures

Laura M. Hancock, Wadham College, University of Oxford

Abstract of thesis submitted for the degree of D. Phil.
Hilary Term 2011

This thesis explores the use of anions in the design and construction of interlocked architectures for applications in anion recognition and sensing, and to function as molecular machines upon a given stimulus.

***Chapter One*** introduces the field of anionic supramolecular chemistry focusing on host-guest chemistry and directed self-assembly. A review of the recognition and sensing of anionic guest species is given before strategies for the construction of interlocked architectures are discussed, and the potential functions of these structures considered.

***Chapter Two*** details the development of a novel anion-templation route for the synthesis of macrocycles and rotaxanes. The versatility of this route in constructing new [2]rotaxanes is explored by varying several features of the macrocyclic component, with emphasis on creating the most powerful anion complexant. Proton NMR spectroscopy is used to probe the anion binding properties of the rotaxanes, and X-ray crystallography and MD simulations are used to rationalize anion binding trends. The possibility of synthesizing catenanes for anion recognition *via* this new synthetic route is also investigated.

***Chapter Three*** investigates the appendage of transition metal complexes to rotaxanes to create interlocked host architectures capable of sensing anions *via* luminescence spectroscopy. The incorporation of rhenium(I) and ruthenium(II) polypyridyl complexes into the macrocyclic and axle component of [2]rotaxanes are described, before the anion binding studies of these structures using $^{1}$H NMR and luminescence spectroscopy are reported.

***Chapter Four*** describes the strategic synthesis of [2]rotaxanes designed to undergo molecular motion upon a given stimulus. Initially, the possibility of exploiting anions to stimulate the macrocyclic component of the [2]rotaxanes to translocate to a second station on the axle is investigated. The use of pyridine *N*-oxide as an integrated template for rotaxane formation is reported before the ability of these rotaxanes to undergo anion and pH driven molecular motion is explored. This chapter concludes with the construction of a calix[4]diquinone *N*-oxide containing [2]rotaxane capable of undergoing sodium- and barium-induced molecular pirouetting.

***Chapter Five*** provides synthetic procedures and characterisation details for compounds listed in this thesis.

***Chapter Six*** reports supplementary experimental information including titration protocols, X-ray crystal structures and MD simulations.

# Acknowledgements

Firstly, I must thank Prof. Paul Beer for giving me the opportunity to work in his research group, both as a Part II and DPhil student. I feel incredibly lucky to have worked with such a supportive and friendly supervisor.

I have thoroughly enjoyed supervising two excellent Part II students, Lydia and Sîan, who, as well as being talented students, have both provided fantastic company in the lab and contributed to making my DPhil really enjoyable. The Beer group has provided a really friendly atmosphere to work in, and special mention must go to Anna, Asha and (classic) Nick, who have been amazing colleagues and friends. I have learnt an incredible amount from them, and feel privileged to have worked alongside such talented chemists.
For crystallography, I am grateful to Chris and Nathan, who have given up their time to collect data and solve structures for me, both at Oxford and the Diamond Light Source.
For proof reading of this thesis, I would like to extend my whole-hearted appreciation to Lydia, Simon, (new) Nick, and Graeme.

Away from the Beer group, Dr. Nick Rees deserves special mention for endless help with NMR. The mass spectrometry department, Dr. Amber Thompson (crystallography) and the Faulkner group (loan of fluorimeter and UV-vis machine) have provided invaluable help over the course of my DPhil. I would also like to thank Prof. Vitor Félix, Dr. Sergio Santos and Dr. Sílvia Carvalho, who were responsible for carrying out the MD Simulations described in Chapter 2.

During the course of my DPhil I have benefited from Edward's constant encouragement, especially during the preparation of this thesis. I cannot express how appreciative I am for his generosity and understanding, as well as his reliable ability to make me smile.

Finally, I am indebted to my parents, whose unconditional love and support has enabled me to achieve all that I have. I dedicate this thesis to them.

# Table of Contents

**Preface** I
**Abstract of Thesis** I
**Acknowledgements** II
**Table of Contents** III
**Glossary** VII
**1 Introduction** 1
**1.1 Overview** 1
**1.2 Importance of Anions** 2
**1.3 Fundamental Principles of Anion Supramolecular Chemistry** 3
1.3.1 Challenges of Anion Complexation 3
1.3.2 Host-Guest Chemistry 4
1.3.3 Self-Assembly 6
1.3.4 Non-Covalent Interactions 7
1.3.5 Preorganisation 10
**1.4 Anion Receptor Chemistry** 11
1.4.1 Positively Charged Anion Receptors 12
1.4.2 Neutral Anion Receptors 15
1.4.3 Metal Containing Anion Receptors 21
**1.5 Anion Sensing** 22
1.5.1 Electrochemical Sensors 23
1.5.2 Luminescent Sensors 24
1.5.3 Colorimetric Sensors 27
**1.6 Displacement Assays** 28
**1.7 Templation** 30
1.7.1 Anion Templation 31
1.7.2 Interweaving Anion Templation 34
**1.8 Functional Applications of Interlocked Structures** 40
1.8.1 Modification of Properties 40
1.8.2 Molecular Machines 42
1.8.3 Anion Recognition and Sensing 45
**1.9 Project Objectives** 47
**1.10 References** 49
**2 Synthesis of Interlocked Structures for Chloride Recognition in Aqueous Solvent Media** 56
**2.1 Introduction** 56
2.1.1 Anion Recognition in Water 56
2.1.2 Mechanically Interlocked Structures 57
2.1.3 Chapter Objectives 59
**2.2 Macrocyclic Components** 60

2.2.1 Synthesis of Macrocycles **64**
2.2.2 Pseudorotaxane Formation **66**
**2.3 Synthesis, Characterisation and Anion Recognition of Novel [2]Rotaxanes** **69**
2.3.1 Synthesis of Axle Component **69**
2.3.2 Trial Rotaxane Synthesis **70**
2.3.3 Synthesis and Characterisation of Novel Monocationic Rotaxanes **72**
2.3.4 Investigations into the Role of the Templating Anion **81**
2.3.5 Anion Recognition Studies **84**
2.3.6 X-ray Crystal Structures **90**
2.3.7 Molecular Dynamics Simulations **92**
**2.4 Synthesis and Anion Recognition Properties of a Dicationic [2]Rotaxane** **98**
2.4.1 Synthesis and Characterisation **98**
2.4.2 Anion Recognition Studies **99**
**2.5 Synthesis and Anion Recognition Properties of [2]Catenanes** **102**
2.5.1 Macrocycle Synthesis **102**
2.5.2 Synthesis and Characterisation of [2]Catenanes **104**
2.5.3 Anion Recognition Studies **107**
2.5.4 X-ray Crystal Structures **109**
**2.6 Summary, Conclusions and Future Perspectives** **111**
**2.7 References** **113**
**3 Transition Metal Appended [2]Rotaxanes for Luminescent Anion Sensing** **115**
**3.1 Introduction** **115**
3.1.1 Photophysical Properties of Rhenium and Ruthenium Complexes **116**
3.1.2 Transition Metal Appended Anion Sensors **117**
3.1.3 Chapter Objectives **118**
**3.2 Incorporation of Transition Metal Reporter Motif into Macrocyclic Component** **119**
3.2.1 Macrocycle Synthesis and Characterisation **121**
3.2.2 Rotaxane Synthesis **124**
3.2.3 Anion Binding Studies **126**
*3.2.3.1 $^{1}$H NMR Spectroscopic Titrations* **126**
*3.2.3.2 Luminescence Titrations* **129**
3.2.4 Summary **132**
**3.3 Incorporation of Transition Metal Reporter Motif into Macrocyclic Component** **133**
3.3.1 Synthesis of Photo-active Thread Components **134**
3.3.2 Anion Binding Studies of Photo-active Thread Components **138**
*3.3.2.1 $^{1}$H NMR Spectroscopic Titrations* **138**
*3.3.2.2 Luminescence Titrations* **141**
3.3.3 Pseudorotaxane Studies **146**
*3.3.3.1 Macrocycle Synthesis* **146**
*3.3.3.2 $^{1}$H NMR Spectroscopic Titrations* **148**
*3.3.3.3 Luminescence Titrations* **151**
3.3.4 Synthesis of a Photo-active Rotaxane **152**

*3.3.4.1 Synthesis of Axle Components* **152**
*3.3.4.2 Synthesis and Characterisation of Rotaxane* **155**
3.3.5 Summary and Future Perspectives **157**
**3.4 Conclusion** **158**
**3.5 References** **159**
**4 Synthesis of [2]Rotaxanes for Molecular Motion** **161**
**4.1 Introduction** **161**
4.1.1 Molecular Motion in Rotaxanes **161**
4.1.2 Chapter Objectives **164**
**4.2 Novel Two Station Rotaxanes: Synthesis and Studies** **166**
4.2.1 Precursor Syntheses **168**
4.2.2 Rotaxane Synthesis and Characterisation **170**
**4.3 Re-design, Synthesis and Studies of a Novel Two Station Rotaxane Containing a Rigid Axle Component** **175**
4.3.1 Axle Precursor Synthesis **175**
4.3.2 Rotaxane Synthesis and Characterisation **177**
**4.4 Synthesis and Studies of Novel Pyridine *N*-oxide Rotaxanes** **180**
4.4.1 Pseudorotaxane Studies **181**
4.4.2 Rotaxane Synthesis and Characterisation **184**
4.4.3 pH-Switchable Molecular Motion Investigations **189**
**4.5 Construction of Calix[4]diquinone Containing [2]Rotaxanes for Cation-Induced Pirouetting Behaviour** **193**
4.5.1 Rotaxane Synthesis and Characterisation **195**
4.5.2 Investigations into Cation-Induced Pirouetting Behaviour **199**
4.5.3 Cation-Templated Synthesis of [2]Rotaxanes **203**
**4.6 Summary, Conclusions and Future Perspectives** **205**
**4.7 References** **209**
**5 Experimental** **211**
**5.1 General Information** **211**
5.1.1 Instrumental Methods **211**
5.1.2 Solvents and Reagents **211**
**5.2 Synthetic Procedures** **212**
5.2.1 Experimental Details for Chapter 2 **212**
5.2.2 Experimental Details for Chapter 3 **239**
5.2.3 Experimental Details for Chapter 4 **259**
**5.4 References** **271**
**Appendices** **AI**
**A.1. Titration Protocol** **AI**
A.1.1 $^{1}$H NMR Titrations **AI**
A.1.2 Luminescence Titrations **AII**
A.1.3 UV-vis Titrations **AIII**
**A.2 Job Plot Analysis** **AIII**

**A.3 Crystal Structure Data** **AIII**
A.3.1 Rotaxane **14**·Cl **AIII**
A.3.2 Rotaxane **22**·Cl **AV**
A.3.3 Catenane **32**·Cl **AVI**
A.3.4 Rotaxane **33**·$PF_6$ **AVIII**
A.3.5 Macrocycle **36**·$(PF_6)_2$ **AIX**
A.3.6 Ruthenium Nicotinamide Stopper **43**·$(PF_6)(NO_3)$ **AX**
**A.4 MD Simulations – Experimental Details** **AXI**
**A.5 References** **AXIII**

# Glossary

| | |
|---|---|
| **°** | degree |
| **Å** | Ångstrom |
| **$A^-$** | anion |
| **a.u.** | arbitrary units |
| **ADP** | adenosine diphosphate |
| ***anti*** | anticlinal |
| **aq** | aqueous |
| **Ar** | aromatic |
| **ATP** | adenosine triphosphate |
| **bipy** | 2,2′-bipyridine, 2,2′-bipyridyl |
| **br** | broad |
| **Bu** | butyl |
| **C** | centigrade |
| **Calc.** | calculated |
| **calix** | calix[4]diquinone |
| **Cat.** | catalytic |
| **CFTR** | cystic fibrosis transmembrane conductance regulator |
| **Cp** | cyclopentadienyl |
| **D** | dimensional |
| **d** | deuterated, diffuse (orbital), doublet |
| **DBU** | 1,8-diazobicyclo[5.4.0]undec-7-ene |
| **DCC** | *N*,*N*$^1$-dicyclohexylcarbodiimide |
| **dd** | double doublet |
| **DFT** | density functional theory |
| **DIPEA** | diisopropylethylamine |
| **DMAP** | 4-Dimethylaminopyridine |
| **DMF** | dimethylformamide |
| **DMSO** | dimethyl sulfoxide |
| **DNA** | deoxyribose nucleic acid |
| **EDCI** | 1-ethyl-3-(3-dimethylaminopropyl)carbodiimide) |

| | |
|---|---|
| **EI** | electron impact |
| **ESI** | electrospray ionisation |
| **Et** | ethyl |
| **f** | fundamental (orbital) |
| **Fc** | ferrocene |
| **FI** | field ionisation |
| **g** | gas, gram |
| **G** | Gibbs free energy |
| **GABA** | *gamma*-Aminobutyric acid |
| **GAFF** | general amber force field |
| **h** | hour |
| **HOMO** | highest occupied molecular orbital |
| **hq** | hydroquinone |
| **HRMS** | high resolution mass spectrometry |
| **Hz** | hertz |
| **IDD 594** | inhibitor (of aldose reductase) |
| **IR** | infra red |
| **ITC** | isothermal calorimetry |
| **J** | coupling constant |
| **K** | kelvin, association constant |
| $\mathbf{K_{app}}$ | apparent association constant |
| **kJ** | kilojoule |
| **L** | levorotary |
| **LC** | ligand centred |
| **LLE** | liquid-liquid extraction |
| **LMCT** | ligand metal charge transfer |
| **LUMO** | lowest unoccupied molecular orbital |
| **M** | molar, molecular ion (mass spectrometry), metal, mega |
| **m** | mulitplet |
| ***m/z*** | mass/charge (mass spectrometry) |
| **MALDI-TOF** | matrix assisted laser desorption/ionisation time of flight (mass spectrometry) |
| **Max** | maximum |

| | |
|---|---|
| **MC** | metal centred |
| **MD** | molecular dynamics |
| **Me** | methyl |
| **min** | minute |
| **mL** | millilitre |
| **MLCT** | metal ligand charge transfer |
| **mmol** | millimole |
| **MO** | molecular orbital |
| **mol** | mole |
| **MS** | mass spectrometry |
| **mV** | millivolt |
| **n** | stoichiometric variable |
| **NB** | no binding |
| ***n*-hex** | *n*-hexyl |
| **NHS** | *N*-hydroxysuccinamide |
| $\mathbf{N_{mass}}$ | average distances between anion and the centre of the binding cavity |
| **NMR** | nuclear magnetic resonance |
| **NOE** | nuclear overhauser effect |
| **NR** | no response |
| **ns** | nanosecond |
| ***o*** | *ortho* |
| **OAc** | acetate |
| **PET** | photoelectron transfer |
| **pH** | $-\log_{10}[H^+]$ |
| **phen** | phenanthroline |
| **Phth** | phthalimide |
| $\mathbf{pK_a}$ | $-\log_{10}[K_a]$ |
| **PMB** | *p*-methoxybenzyl |
| **ppm** | parts per million |
| **py** | pyridinium |
| **q** | quartet |
| **r** | radius |

| | |
|---|---|
| **R** | alkyl or aryl group |
| **RCM** | ring closing metathesis |
| **$R_f$** | retention factor |
| **RNA** | ribonucleic acid |
| **ROESY** | rotating frame nuclear overhause effect spectroscopy |
| **RT** | room temperature |
| **s** | singlet |
| **sept** | septet |
| ***syn*** | synclinal |
| **t** | triplet, tertiary |
| **TBA** | tetra(*n*-butyl)ammonium |
| **TBTA** | tris[(1-benzyl-1H-1,2,3-triazol-4-yl)methyl] amine |
| **td** | triple doublets |
| ***tert*** | tertiary |
| **THF** | tetrahydrofuran |
| **TLC** | thin layer chromatography |
| **Ts** | tosyl |
| **TTF** | tetrathiofulvane |
| **UHE** | ultra high efficiency |
| **UV** | ultra-violet |
| **vis** | visible |
| **X** | anion |
| **Y** | variable substituent |
| **δ** | chemical shift |
| **Δ** | heat, change |
| **ε** | extinction coefficient |
| **μW** | microwave irradiation |
| **λ** | wavelength |
| **χ** | mole fraction |

# Chapter 1: Introduction

## 1.1 Overview

The importance of supramolecular chemistry was first highlighted by the award of the Nobel Prize to Lehn,[1] Cram[2] and Pedersen[3] in 1987, by which point the field of cationic supramolecular chemistry was rapidly becoming an established field. In contrast, it can be argued that the supramolecular chemistry of anions has only developed significantly in the last two decades where anion receptor design and construction combined with the role of anions in membrane transport[4] and crystal engineering[5] has elevated anionic supramolecular chemistry such that its importance can now be considered almost equal to that of cations.

The research chronicled in this thesis explores the use of anions in the design and construction of supramolecular systems for functional applications, exploiting supramolecular chemistry's two principal disciplines: host-guest chemistry; and self-assembly. More specifically, of particular interest is harnessing the power of directed self-assembly (specifically anion templation) to create intricate interlocked architectures, designed to act as highly selective hosts for anionic guest species, or to undergo molecular motion upon a given stimulus.

With this ambitious target in mind, this chapter introduces the principles governing both host-guest chemistry and self-assembly, which are important considerations when designing the aforementioned systems. Specifically, the recognition and sensing of anionic guest species is comprehensively discussed before the ability of anions to act as templates is introduced. Attention will also be paid to the construction of interlocked structures, and some impressive examples of these molecules to exhibit sensory and molecular machine-like behaviour are provided.

## 1.2 Importance of Anions

The rapid growth of the field of anion supramolecular chemistry in the last two decades is not difficult to conceive given the crucial role that anions play in the natural world. In mammalian physiology anions, especially chloride, the recognition of which is central to this thesis, have important roles to play in many biological processes. Respiration relies on chloride to increase the blood's capacity for carbon dioxide in the form of bicarbonate,[6] whilst in the central nervous system the action of the chief inhibitory neurotransmitter (GABA) relies on the entry of chloride into specific neurons.[7] Chloride is also required to maintain the shape of the active site and aid activation (i.e. it is the cofactor) of the enzyme amylase.[8] Cross-membrane channels are responsible for the transport of anions and regulate the movement of essential metabolites across cell membranes. Genetic defects in the CFTR chloride channel are responsible for cystic fibrosis, a disease with devastating implications for the sufferer, and an example of the paramount importance of maintaining the flux of anions into and out of cells.[9]

Aside from chloride, many other anions are implicated in some way in the human body. DNA,[10] responsible for carrying and conserving the body's genetic code is a polyanion, as is ATP, the body's energy chemical.[11] Whilst these anions are crucial to maintain life, others are acutely toxic; cyanide inhibits the action of cytochrome c oxidase,[12] an important respiratory enzyme, and oxalate ingestion can cause permanent kidney and liver damage.[13]

Environmentally, phosphates and nitrates from agricultural fertilisers, cause eutrophication if they leech into rivers,[14] and nitrate and sulfate are present in acid rain.[15] Furthermore, the release of pertechnetate, a radioactive by-product of nuclear fuel processing, constitutes an example of the serious pollution impact that specific anions can have.[16]

Taking into consideration the importance of anions in biological systems, along with their impact in the environment, and numerous chemical roles, the importance of designing hosts for anionic guest species cannot be overstated. The following section summarises the key

factors synthetic chemists must consider when designing such systems, drawing on principles demonstrated in Nature.

## 1.3 Fundamental Principles of Anion Supramolecular Chemistry

### 1.3.1 Challenges of Anion Complexation

The reason the field of anion supramolecular chemistry was slow to develop compared to that of cations was primarily the result of the inherent characteristics of anions which make it more challenging to design appropriate receptor (host) systems.[17]

Firstly, anions are significantly larger than their isoelectronic cations (e.g. $r(Cl^-)$ = 1.69Å, $r(K^+)$ = 1.52 Å) and accordingly their charge to size ratio is smaller. This diffuse nature results in diminished electrostatic interactions between an anion and its receptor.

As well as size, shape is also a concern, with anions possessing a wide range of geometries (Figure 1.1), requiring a receptor with a complementary binding cleft to be designed for selective complexation. It should also be highlighted that many biologically relevant anions such as DNA and ATP have even more complex geometries further complicating receptor design. This is in contrast to cations, most of which are spherical in shape, making it facile to design an appropriate receptor.

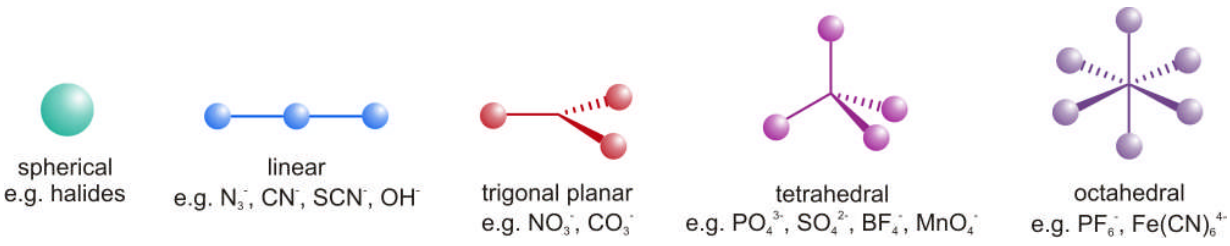



***Figure 1.1***. *Anion geometries.*

pH must also be a consideration since some anions, such as carboxylate, become protonated at low pH, and thus lose their negative charge. In addition, certain receptors may also be pH

sensitive; polyammonium receptors, for example, can themselves become deprotonated at high pH values where the anion exists, rendering them ineffective as anion receptors.

Finally, the role that solvent has to play in anion complexation cannot be underestimated. Anions exhibit large free energies of solvation relative to cations,[18, 19] and consequently hosts for anions must compete more effectively with the surrounding solvent media. The nature of the solvent media can also dramatically affect the ability of a host molecule to complex an anion. Polar protic solvent molecules form strong hydrogen bonds to the anion and thus receptors employing electrostatic interactions must be utilised in this media to effectively compete with solvent molecules for anion complexation. In contrast neutral receptors are most frequently observed to function in aprotic organic media. These solvent effects are discussed further in Section 1.4.

The selectivity of a receptor may also be influenced by the hydrophobicity of the anion, which is described by the Hofmeister series (Scheme 1.1). Hydrophobicity can be used by supramolecular chemists to design a receptor disposed towards larger anions with a lower charge, a feature which can be exploited in the extraction of anions from aqueous to organic solvent media.

organic anions > $ClO_4^-$ > $SCN^-$ > $I^-$ > salicylate > $NO_3^-$ > $Br^-$ > $Cl^-$ > $HCO_3^-$ > $H_2PO_4^-$ > $F^-$ > $SO_4^{2-}$ > $HPO_4^{2-}$

***Scheme 1.1.*** *Hofmeister series.*

### 1.3.2 Host-Guest Chemistry

Supramolecular chemistry is fundamentally based on the binding of a substrate by a host molecule, a principle first identified by Emil Fischer almost a century before supramolecular chemistry became a well-established field. This ‘lock and key’ hypothesis was used to illustrate the binding of a specific substrate, the key, in the active site of an enzyme, the lock, where components have complementary sizes and shapes to maximise binding interactions

(Figure 1.2a).[20] Despite this theory being an excellent basis to begin understanding enzyme-substrate complexation, in the 1950s Daniel Koshland proposed revisions to the 'lock and key' analogy proposing that the substrate could induce the enzyme to undergo moderate conformational change upon its binding (Figure 1.2b).[21] This extra flexibility actually serves to enhance recognition and selectivity.




***Figure 1.2.*** *Schematic representation of (a) Lock and Key hypothesis, and (b) induced fit theory.*

The concept of complementarity in nature serves as an important guide when designing abiotic receptors to ensure strong and selective binding of a specific anion. Explicit inspiration can be obtained from anion binding proteins in biological systems, where a combination of electrostatics and highly directional hydrogen bonds are deployed to ensure remarkable anion selectivity. The phosphate binding protein, responsible for the transport of *ortho*-phosphate in bacteria, is capable of forming twelve hydrogen bonds to the guest species.[22] Whilst eleven of these are protein hydrogen bond donor interactions, it is the single hydrogen bond acceptor residue in the protein that guarantees substrate selectivity for *ortho*-phosphate, which itself possesses one hydrogen bond donor. The single negative aspartate residue (shown in Figure 1.3a in blue) ensures that fully deprotonated anions (e.g. sulfate) cannot be included within the binding pocket due to steric repulsion with the carboxylate group. Interestingly mutagenesis of the arginine side chain to remove the electrostatic contribution results in no significant change in anion binding ability implying that the specific arrangement of hydrogen bond residues are more important in the protein's prolific anion recognition.

The aforementioned chloride transmembrane proteins employ a similar array of hydrogen bonds, (Figure 1.3b) with their selectivity attributed to the narrowest part of the channel where the tetrahedral coordination sphere of chloride is satisfied by four hydrogen bond donors.[23]

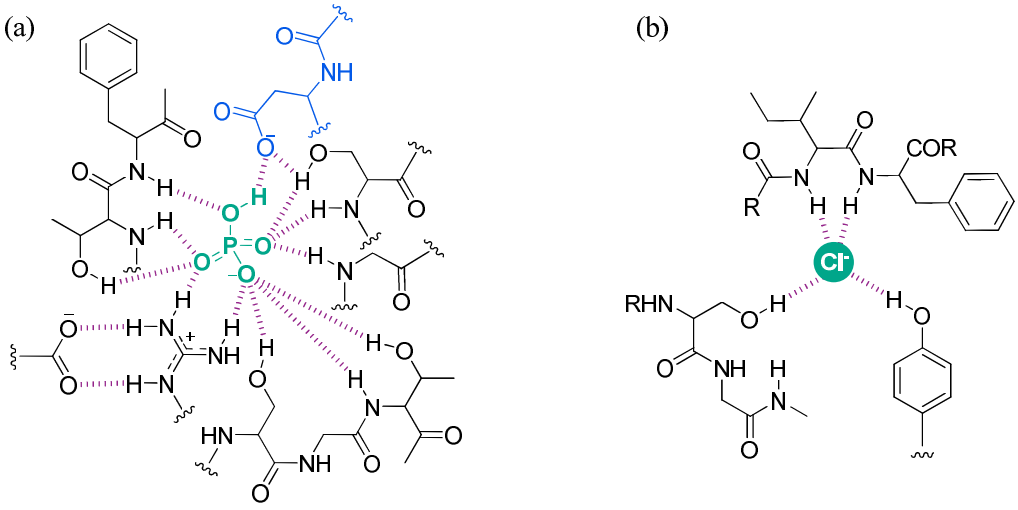



***Figure 1.3.*** *Anion binding sites of (a) Phosphate binding protein,[22] and (b) CFTR chloride transport channel.[23] Bound anions are shown in green.*

### 1.3.3 Self-Assembly

Self-assembly has been described as '*the spontaneous association of several molecular components into a discrete, non-covalently bound aggregate with a well defined structure*' (Figure 1.4) .[24]



***Figure 1.4****. Schematic representation of self-assembly.*

Self-assembly has been well documented in nature, and is especially crucial to the function of cells. It is demonstrated in the formation of double helical DNA through complementary hydrogen bonding of individual strands,[25] and in the construction of lipids to form the cell

membrane.[26] Self-assembly of incorrectly folded proteins into insoluble amyloid fibres are responsible for infectious prion-related neurodegenerative diseases.[27]

The self-assembly definition given above governs the phenomenon described as 'strict self-assembly' and requires the final product not only to spontaneously form when its components are present in the correct ratio, under the appropriate conditions, but also for the formation of the structure to be entirely reversible. The self-assembly described within this thesis has the alternative classification of 'directed self-assembly with post modification', where a template is used to direct the formation of the supramolecular assembly before a chemical reaction is used to 'lock' the structure. This factor results in the process no longer being reversible, and the resultant assembly can only be deconstructed by breaking a covalent bond.[28]

This type of self-assembly allows for the formation of mechanically interlocked molecules which have enormous potential for use as novel devices, sensors and machines.[29] From the perspective of a supramolecular chemist, the most important interlocked species are catenanes and rotaxanes. A catenane, deriving from the latin *catena* meaning chain, consists of *n* interlocked rings, whilst rotaxanes consists of an axle (*axis*) threaded through a macrocyclic wheel (*rota*). Technically interlocked structures can consist of any number of components,[30] and indeed polymeric rotaxanes[31] and catenanes[32] have been reported.[33] However, in terms of this project two component interlocked structures have most importance and thus this chapter will focus on these classes of rotaxane and catenane.

### 1.3.4 Non-Covalent Interactions

Both host-guest chemistry and self-assembly rely on the formation of non-covalent bonds which act to either complex a guest species or assist in the assembly of an intricate architecture. A covalent bond has a typical strength of 350 $kJmol^{-1}$ whereas an individual non-covalent interaction is significantly weaker, in the region of 1–250 $kJmol^{-1}$.[34] For this

reason several non-covalent interactions are often used in combination to create strong interactions between two or more species.

Electrostatic interactions are highly significant in supramolecular chemistry as their strength can be comparable to that of a covalent bond. They are based on the coulombic interaction between two species of opposite charge and fall into three categories: ion-ion (Figure 1.5a); ion-dipole (Figure 1.5b); and dipole-dipole. Although electrostatic interactions are non-directional in nature, dipoles must be suitably aligned for binding to be maximised.

Hydrogen bonds (Figure 1.5c) are a highly directional example of an ion-dipole electrostatic interaction and are ubiquitous in biological systems. Complementary base pairing of the DNA double helix occurs through hydrogen bonding and is responsible for its famous helical structure.[10] Cellulose, the polysaccharide constituent of plant cell walls, is a straight chain polymer whose chains are held together by multiple hydrogen bond interactions (Figure 1.6a).[35] The resultant microfibrils have great tensile strength, an important property for the rigidity of plant cell walls. Hydrogen bonds have also been extensively used by chemists in the formation of receptors for both neutral and ionic species, and to direct the assembly of more elegant architectures (e.g. ribbons and rosettes).[36]

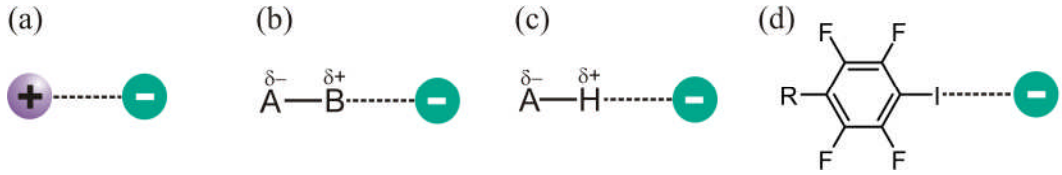



***Figure 1.5.*** *Non-covalent interactions: (a) ion-ion; (b) ion-dipole; (c) hydrogen bond; and (d) halogen bond.*

Analogous, and of comparable strength to the hydrogen bond is the halogen bond (Figure 1.5d), an interaction arising between an electron rich ion or dipole and an electrophilic halogen atom, usually appended to an electron withdrawing group.[37] Like hydrogen bonds, halogen bonds have a strong preference for linearity, but in contrast to hydrogen bonds are substantially larger and more polarisable. Halogen bonding has been strategically used in the

self-assembly of supramolecular architectures in the solid state, most extensively in crystal engineering,[38] however it is only recently that the potential of halogen bonding to direct the formation of structures in the solution phase has been realised.[39-43] The significance of halogen bonding in biological systems has also been highlighted in substrate specificity, binding and molecular folding.[44] In drug design, the action of human aldose reductase can be inhibited by the inhibitor compound IDD 594, whose inhibition strength is attributed to the O-Br halogen bond it forms with the enzyme (Figure 1.6b).[45] Within the specificity pocket of the protein-inhibitor complex, a short O-Br halogen bond contributes to inhibitor potency.

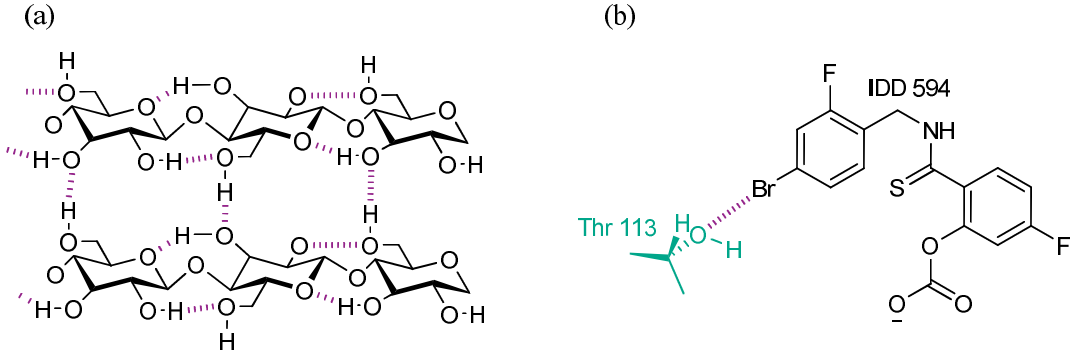



***Figure 1.6.*** *(a) Hydrogen bonds within and between cellulose molecules,[35] and (b) human aldose reductase-inhibitor complex showing a short Br-O halogen bond.[45]*

Both supramolecular and biological systems frequently contain aromatic rings giving rise to attractive π-π donor acceptor interactions which can occur in either an 'edge to face' or 'face to face' manner, (Figure 1.7a and b respectively) and are most powerful when charge-assisted. These interactions are also commonly employed in nature, for example in the tertiary structure of proteins,[46] and medically, in the intercalation of drugs into DNA.[47]

Aromatic rings can also form strong interactions with cationic species,[48] but due to the electron rich nature of π-systems fewer examples of anion-π interactions (Figure 1.7c) are reported. Recently the importance of this non-covalent force has been highlighted with reported examples of anion transport across lipid bilayer membranes assisted by the anion's interaction with a π-acidic aromatic surface.[49, 50]

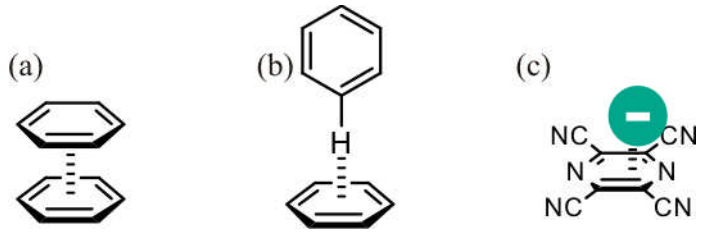



***Figure 1.7**. (a) Face to face, and (b) edge to face π-π stacking, and (c) anion-π interaction*[51]

### 1.3.5 Preorganisation

Another important concept in influencing the strength of interactions in supramolecular systems is preorganisation. Donald Cram suggested that this concept is fundamental to host-guest chemistry and demonstrated that receptors adopting a favourable binding conformation prior to substrate association possess a lower activation energy to guest binding, increasing the stability of the resultant complex.[2]

Preorganisation has been demonstrated in various simple anion receptors, Flood and co-workers providing a recent example (Figure 1.8).[52] Their aryl-triazole receptors displayed an enhanced affinity for chloride in $CD_2Cl_2$ when appended with hydroxyl groups capable of forming hydrogen bonds with the triazole nitrogen atoms, and thus preorganising the molecule prior to binding.

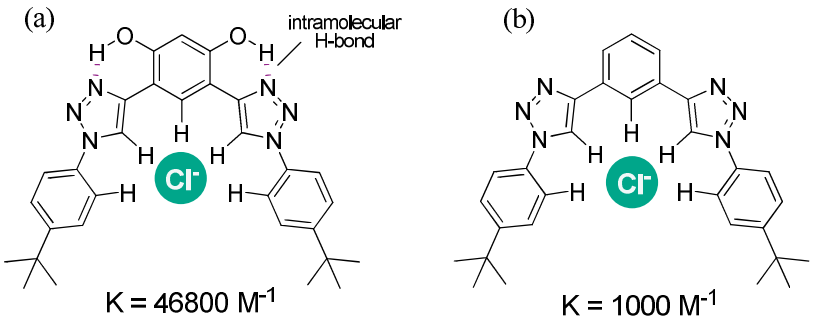



***Figure 1.8.** Association constants in $CD_2Cl_2$ of (a) preorganised and (b) non-preorganised aryl triazoles.*[52]

Related to the concept of preorganisation is the macrocyclic effect which refers to the greater stability of a macrocyclic complex compared to the complex of the open chain analogue. As well as preorganisation this amplified stability is attributed to a number of enthalpic and

entropic effects, including reduced solvation and greater rigidity of the macrocyclic component. Jurczak and Chmielewski's tetra-amide receptors exemplify this principle, with chloride recognition increasing forty-fold in the macrocyclic system compared to its open chain analogue in $d_6$-DMSO (Figure 1.9).[53] These systems benefit from additional preorganisation in the form of intramolecular hydrogen bonds between the pyridine nitrogen atom and amide protons.

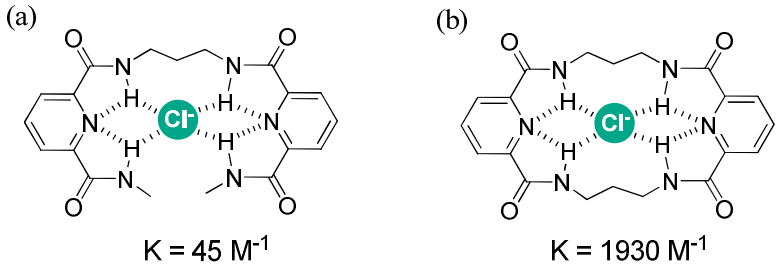



***Figure 1.9.*** *Example of the macrocyclic effect. Given association constants obtained in $d_6$-DMSO.*[53]

## 1.4 Anion Receptor Chemistry

The major theme of this thesis is the complexation of anions. Taking into account the design principles discussed above, this section aims to provide a brief overview of the vast area of anion receptor chemistry, highlighting strategies for anion recognition in various solvent media, including both archetypal examples and more recent advances. The field can be broadly resolved into two classifications of receptor: those possessing positive charge; and those that are neutral.

Receptors which utilise electrostatic interactions can compete with protic polar solvents, such as water and methanol, for the anion in question, whereas neutral host molecules are unlikely to exhibit sufficient anion binding affinities to energetically overcome anion desolvation. These molecules are more likely to function as anion receptors in aprotic solvents. Neutral receptors however may be able to function in more competitive polar solvents if the binding

domain is effectively shielded from solvent molecules, whereupon binding becomes entropically favourable.

### 1.4.1 Positively Charged Anion Receptors

The most discernable feature of anions is their negative charge, and hence an effective way to complex an anion strongly is for a potential receptor to be a positively charged, to exploit strong electrostatic interactions between the oppositely charged species.

Indeed, Park and Simmons utilised the strength of electrostatic interactions in combination with hydrogen bonds to create the first anion receptor in 1968 (Figure 1.10a).[54] The acidic ammonium protons were shown by $^{1}$H NMR spectroscopy (and later by X-ray crystallography[55]) to cooperatively bind the halide guest. This receptor signalled the beginning of the emergence of pH dependent polyammonium receptors for anion complexation.

Lehn and co-workers built on the seminal work of Park and Simmons by constructing a series of macrocyclic and macrotricyclic polyammonium based receptors whose cavity size could be designed to be of complementary size and shape for a specific anion.[56-59] For example, a cryptand bearing six protonated amine groups was shown to selectively recognise the linear azide anion, by virtue of its complementary cavity.[60]

A little later, it was discovered that polyammonium macrocyclic receptors could not only bind biologically relevant nucleotide phosphates (e.g. ATP, ADP) but also catalyse ATP hydrolysis (Figure 1.10b).[61, 62] This macrocycle displayed not only the highest binding affinity for ATP but also proved to be the most efficient catalyst when compared to similar macrocycles with different numbers of ammonium groups.

In more recent work, the tripodal tren-based polyammonium receptor reported by Bowman-James (Figure 1.10c), was shown to strongly complex dihydrogen phosphate

through three N-H···O hydrogen bonds, both in the solid state, and by $^{1}$H NMR titration experiments in $CDCl_3$.[63]

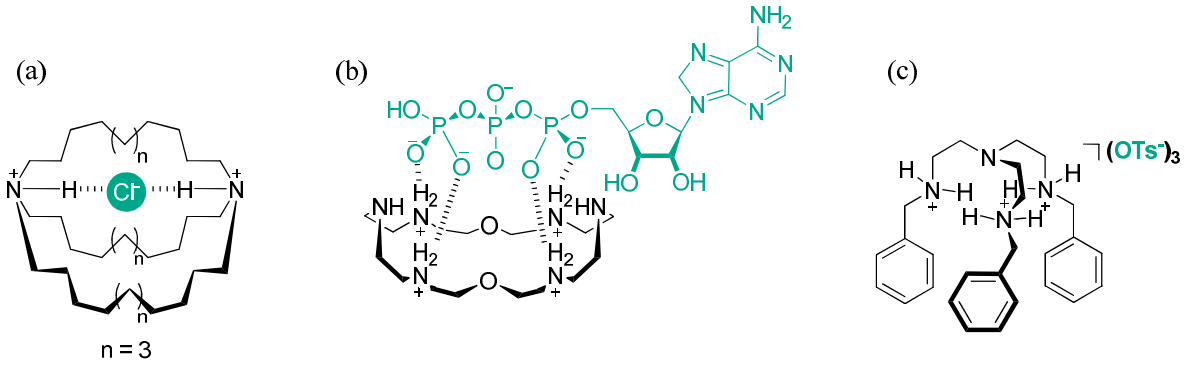



***Figure 1.10.*** *Polyammonium receptors: (a) Park and Simmons' kapitand;[54] (b) macrocycle capable of catalysing ATP hydrolysis;[61, 62] and (c) Bowman-James' tren receptor.[63]*

Whilst huge success has been achieved in using polyammonium receptors to complex anions in competitive solvent media, they are pH dependent and do not function at high pH values. Ways in which this issue can be overcome include using pH independent quaternary ammonium receptors such as Schmitchen's cage-like receptor (Figure 1.11a), capable of complexing halides in aqueous solvent media.[64-67]

Guanidinium and amidinium containing receptors are also attractive alternatives for anion complexation due to their high $pK_a$ values (13.6 and 12.4 respectively) arising from a high degree of delocalisation, and thus the receptors remain protonated over a large pH range. It should be noted however that guanidinium receptors have their own drawbacks such as their high energy of solvation in aqueous solvent media. Therefore receptors must often employ two or more guanidinium recognition groups to overcome this high solvation energy upon anion complexation. Anslyn and co-workers have demonstrated the power of incorporating three guanidinium groups into a tris-benzyl scaffold (Figure 1.11b) to bind the citrate anion in pure water.[68] They also discovered that replacing the guanidinium functionalities with ammonium groups caused diminished strength of association with citrate illustrating the potency of guanidinium in complexing oxoanions.

Further to the problem of high solvation is the fact that an anion may bind on either side of the guanidinium motif. This can be overcome by conformationally restraining the molecule to ensure binding only occurs on one side of the guanidinium. This can be achieved by preparing bicyclic guanidinium residues, exemplified by Schmitchen's preorganised foldable bis-guanidinium receptor (Figure 1.11c), shown to be an effective complexant of dicarboxylate anions (e.g. malonate, isophthalate) in $CD_3OD$.[69]

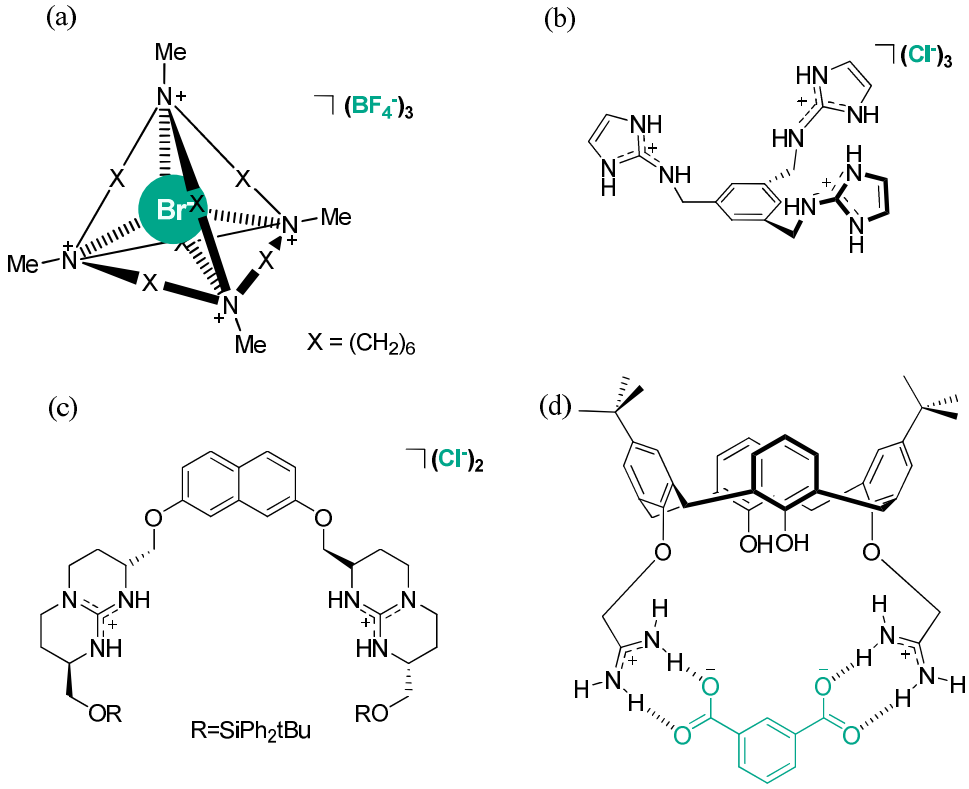



***Figure 1.11.*** *(a) Schmitchen's quaternary ammonium cage receptor[64] and examples of guanidinium receptors: (b) Anslyn's citrate selective receptor;[68] and (c) Schmitchen bicyclic receptor,[69] and (d) Gale's bis-carboxylate selective amidinium receptor.[70]*

Like guanidinium receptors, amidinium groups have a strong preference for oxoanions. Gale *et al.* harnessed the anion binding ability of two amidinium groups into a calix[4]arene scaffold (Figure 1.11d), which displayed affinity for bis-carboxylate anions in DMSO solution.[70, 71]

In recent years positively charged imidazolium,[72] and to a lesser extent triazolium motifs have emerged as important anion complexing groups due to their acidic C-H protons, capable of

undergoing charge-assisted hydrogen bonding with an anionic species. Similarly to the ammonium and guanidinium containing examples discussed previously, receptors containing two or more such groups can cooperatively complex the anion. To this end, Kang *et al.* designed a receptor with a glycouril backbone bearing two imidazolium groups capable of orienting themselves for the strong binding of acetate (Figure 1.12a) in 9:1 $CD_3CN/d_6$-DMSO.[73] Further preorganisation can be obtained by incorporating imidazolium moieties into a macrocycle such as that synthesised by Alcalde and co-workers (Figure 1.12b).[74, 75] This dicationic imidazololiophane exhibits a 1,2-alternative chair-like conformation in the solid state, where chloride is bound *via* a highly directional C-H···Cl interaction.

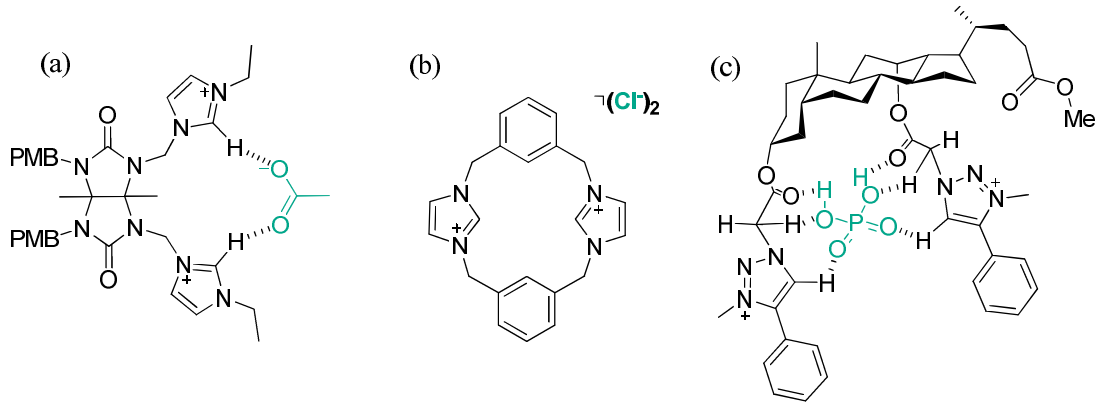



***Figure 1.12.*** *Receptors utilising acidic C-H groups: (a) Kang's acetate selective bis-imidazolium receptor;[73] (b) Alcalde's imidazoliophane macrocycle;[74] and (c) steroid-based 1,2,3-triazolium receptor.[76]*

More recently Pandey and Kumar have revealed the potential of the triazolium motif to be as prolific in anion complexation as imidazolium, with the synthesis of a steroid-based 1,2,3-triazolium receptor capable of selectively binding phosphate in preference to halides and acetate in $CDCl_3$ (Figure 1.12c).[76]

### 1.4.2 Neutral Anion Receptors

Whilst the previous section discussed the importance of electrostatic interactions in complexing anionic species, often in competitive protic polar solvent media, this section

focuses on neutral anion receptors. These generally rely on weaker non-covalent forces to bind the anion, and consequently operate in less competitive aprotic organic media. However, it may be possible for these receptors to achieve greater selectivity than their positively charged counterparts if they utilise multiple directional hydrogen bonding interactions for anion complexation.

Firstly, receptors containing N-H hydrogen bonds will be discussed. Such host systems account for a great majority of neutral anion receptors and utilise a range of functional groups. Much focus has been paid to amide based receptors, probably due to the extensive use of amide hydrogen bonding interactions in the anion binding domain of proteins. The work of Crabtree *et al.*, in 1997,[77] describing the isophthalamide functionality (Figure 1.13a) as an efficient anion complexant instigated the construction of a wide range of acyclic, macrocyclic,[78, 79] cage-like[80] and even mechanically interlocked receptors[81-83] based on the isophthalamide and related motifs. Simple isophthalamide itself was shown to strongly complex halide anions in $CD_2Cl_2$, whilst Jurczak demonstrated that the size of bis-isophthalamide macrocycles could be tuned to achieve greater selectivity of chloride binding in $d_6$-DMSO.[53] Bowman-James has synthesised an array of similar tetra-amide macrocycles, and has also incorporated the isophthalamide group into bicyclic and tricyclic cage structures. The bicyclic receptors showed enhanced fluoride binding affinity compared to two-dimensional analogues.[84-86] The elongated rigid tricyclic hosts (Figure 1.13b) displayed selectivity for linear anions such as $FHF^-$ in $d_6$-DMSO.[87]

Closely related to the amide group are ureas and thioureas. These motifs have been incorporated into many anion receptors and benefit from two parallel N-H hydrogen bond donor groups spaced a suitable distance apart to allow for interaction with a number of anionic species, especially Y-shaped anions such as carboxylate and nitrate. This is exemplified by Fabbrizzi whose urea receptor was shown to strongly complex acetate in

MeCN.[88] The binding mode of this Y-shaped anion was inferred from X-ray crystallography (Figure 1.13c). By contrast, Ghosh and co-workers have reported a tripodal urea receptor (Figure 1.13d), which exhibits preference for fluoride and dihydrogen phosphate over other halides and oxoanions in $d_6$-DMSO[89]. The X-ray crystal structure shows a fluoride anion encapsulated within the cavity created by the six convergent urea N-H hydrogen bonds.

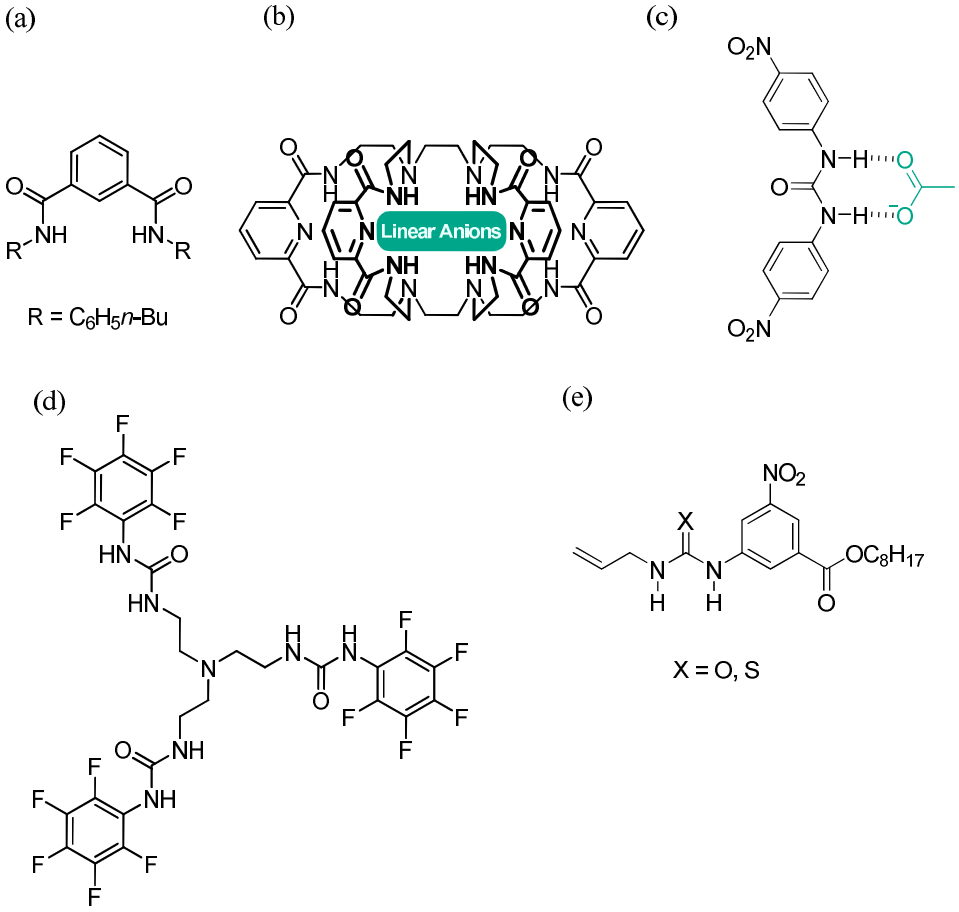



***Figure 1.13.*** *Receptors utilising N-H hydrogen bonds: (a) Crabtree's isophthalamide;[77] (b) Bowman-James' tricyclic receptor;[87] (c)Fabbrizzi's urea receptor capable of strongly binding Y-shaped anions;[88] (d) Ghosh's fluoride selective tripodal urea receptor;[89] and (e) Wilcox's thio(urea) recptor.[90]*

Generally thiourea N-H protons have enhanced acidity compared to their urea analogues rendering them more potent anion complexants, a feature recognised by Wilcox in his early receptors (Figure 1.13e).[90] However, it is important to note that the increased acidity of the thiourea protons may also have ramifications in terms of deprotonation of the receptor by highly basic anions.

Pyrroles also provide an acidic hydrogen bond donor to non-covalently bind an anion, and are intrinsic to many anion binding groups such as indoles, indolocarbazoles and calixpyrroles. Beer *et al*. have shown simple indolocarbazoles to be effective anion complexants,[91] whilst Jeong has incorporated them into macrocycles[92] and foldamers[93] for anion recognition. Wang and co-workers have reported an indolocarbazole with an extended π-system, capable of strongly sensing acetate and fluoride in DMSO *via* changes in the UV-vis spectrum (Figure 1.14a).[94] The selectivity for fluoride can be attributed to its size and basicity, whilst acetate's Y-shape is complementary to the two pyrrole hydrogen bonds held parallel by the structure's rigidity. Recently, a new heterocyclic motif has been reported by Curiel, named carbazolocarbazole, (Figure 1.14b) which bears a striking similarity to indolocarbazole and shows an enhanced binding affinity for acetate in $d_7$-DMF.[95] The authors attribute this improved strength of complexation to the more acute bite angle of the carbazolocarbazole as well as an additional binding stabilisation from the benzene C-H hydrogen bonds.

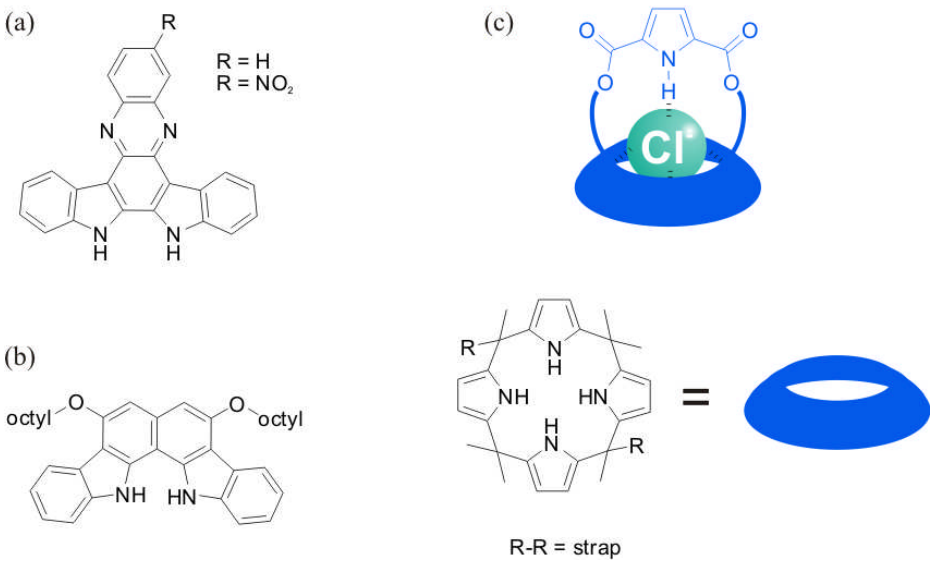



***Figure 1.14.*** *Pyrrole-based receptors: (a) Wang's indolocarbazole;[94] (b) Curiel's carbazolocarbazole;[95] and (c) Sesslers strapped calix[4]pyrrole receptor.[96]*

Since its emergence as an efficient host molecule for the small halide anions in the mid-1990s calix[4]pyrrole has been functionalised for a multitude of anion recognition purposes,[97]

including anion membrane transport.[98, 99] Sessler, the pioneer behind this class of receptor, has recently reported a strapped calixpyrrole receptor (shown schematically in Figure 1.14c), capable of binding fluoride and chloride in highly competitive aqueous solvent mixtures (4:1 $d_6$-DMSO/$D_2O$), whilst neither dihydrogen phosphate nor benzoate showed any evidence of complexation.[96] This selectivity reflects the three-dimensional nature of the structure, whereby the larger oxoanions cannot penetrate the binding cavity.

Comparatively less extensively used hydrogen bond donor groups in anion receptors are the hydroxyl and the C-H interactions. Hydroxyl groups have shown to form strong hydrogen bonds with anions, and recently Kondo *et al*. have demonstrated the ability of 1,3-disiloxane-1,1,3,3-tetraols to bind anions in $CD_3CN$.[100] These compounds showed higher affinity for halides than counterparts with only two hydroxyl groups indicating cooperative binding by all four O-H hydrogen bonds. At greater concentrations of chloride a switch in binding stoichiometry was observed with the receptor complexing two anions, each experiencing two hydroxyl hydrogen bonds (Figure 1.5a).

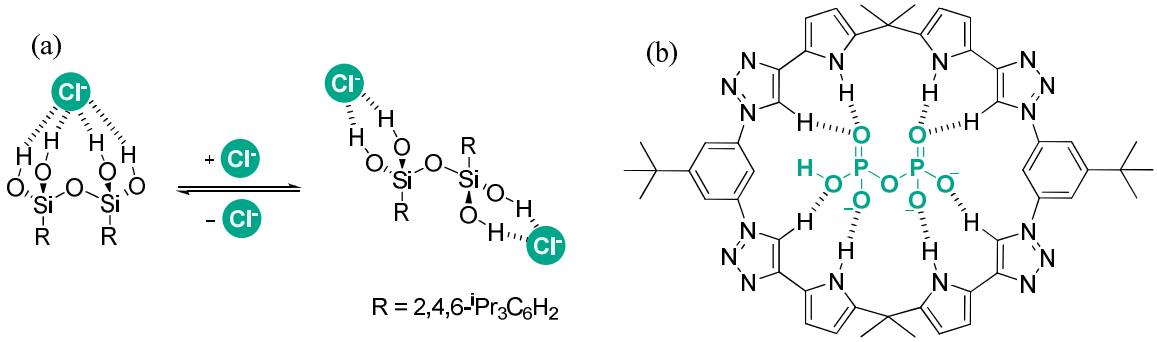



***Figure 1.15.*** *(a) Equilibrium showing two binding conformations of Kondo's silyl receptor with chloride[100] and (b) Sesslers pyrophosphate selective triazolophane macrocycle.[101]*

The value of the 1,2,3-triazolium group in anion receptor chemistry has already been discussed, however the important development of the neutral 1,2,3-triazole motif in providing an acidic C-H bond for anion binding should not be overlooked. Pioneering work in this field was carried out by Flood, who has synthesised macrocycles,[102] and more recently foldamers[103] bearing multiple triazole C-H hydrogen bonds oriented for selective chloride

binding. Sessler has recently used a similar principle to construct a macrocycle (Figure 1.15b) utilising both triazole C-H interactions and pyrrole N-H hydrogens bonds to create a cavity of complementary size to the biologically relevant anion pyrophosphate, as shown by solid state evidence.[101]

The first example of solution phase anion complexation *via* halogen bonding interactions was reported by Taylor *et al.* whereby a tripodal receptor bearing electropositive iodine atoms binds chloride in $d_6$-acetone (Figure 1.16a).[39] It should be noted that bromine and iodine are often the halides of choice in halogen bonding receptors due their more polarisable nature giving rise to greater electrophilicity and thus stronger halogen-anion interactions.

A number of receptors have been reported that contain Lewis acidic heteroatoms, such as boron,[104] silicon,[105] tin,[106] germanium[107] and mercury[108], capable of binding to an anion *via* the donation of electron density from the negatively charged species into a vacant orbital.

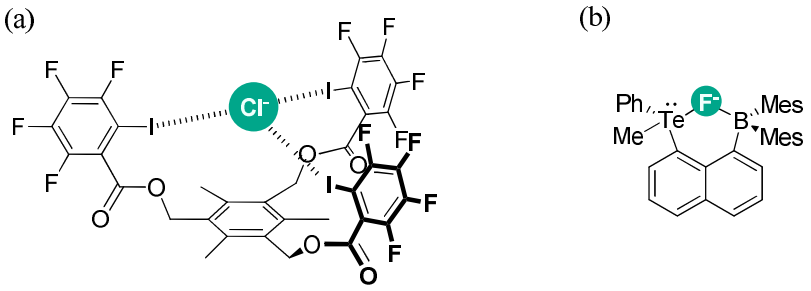



***Figure 1.16.*** *(a) Taylor's tripodal receptor utilising halogen bonding to complex chloride[39] and (b) Gabbaï's fluoride selective bidentate tellurium-boron receptor.[109]*

More recently, Gabbaï, has highlighted the ability of the heavier chalcogen atoms to complex an anionic guest species when in combination with a Lewis acidic boron centre.[109] A bidentate boron-tellurium receptor (Figure 1.16b) was shown to bind fluoride more strongly in methanol than the equivalent boron-sulphur containing molecule. This is attributed to the larger size of tellurium which results in the chalcogen atom being in closer proximity to the anion, leading to a stronger interaction compared with the sulphur analogue. These donor-

acceptor interactions between anion and polarisable electropositive tellurium atom are likened to the halogen bonding interactions discussed above.

### 1.4.3 Metal Containing Anion Receptors

A final class of anion receptors encompasses those possessing a metal centre, which may act to enhance binding affinity through an attractive columbic interaction with the anion, or to preorganise the receptor so that binding groups are in the correct orientation for effective association.[110, 111] Specific transition and lanthanide metals may also act as a reporter groups, signalling the occurrence of such an anion recognition event; this is discussed in more detail in the next section.

Lu and co-workers have utilised the strong electrostatic interaction between transition metals and anions in their dicobalt(II) cryptate (Figure 1.17a) which exhibits selective binding of chloride and bromide, whereas no evidence of fluoride and iodide complexation is observed.[112] This interesting selectivity trend is attributed to the rigidity of the receptor giving rise to a specifically sized binding cavity. An elegant example of a transition metal directed cage (Figure 1.17b) capable of anion recognition is provided by Fabbrizzi, which uses the octahedral coordination preference of iron(II) to assemble a tripodal imidazolium bipyridyl structure.[113] In the cage structure the three imidazolium C-H hydrogen bond donor fragments converge into the cavity which is of the correct size for complexing halide anions and azide in 4:1 $MeCN/H_2O$.

Recently, Steed *et al*. have demonstrated that building bis-thiourea ligands into organometallic complexes of $2^{nd}$ and $3^{rd}$ row transition metals can dramatically enhance anion binding.[114] The ruthenium complex shown in Figure 1.17ci is capable of strongly complexing chloride (of the order of $10^3$ $M^{-1}$) in competitive DMSO solution whilst little evidence of anion binding was provided for the free ligand. In addition to the role of the transition metal providing a positive charge to the receptor and increasing the acidity of the thiourea protons,

when coordinated to the ruthenium centre, the ligand is unable to undergo intramolecular hydrogen bonding interactions (Figure 1.17cii) which act to reduce the anion binding efficiency of the metal-free ligand.

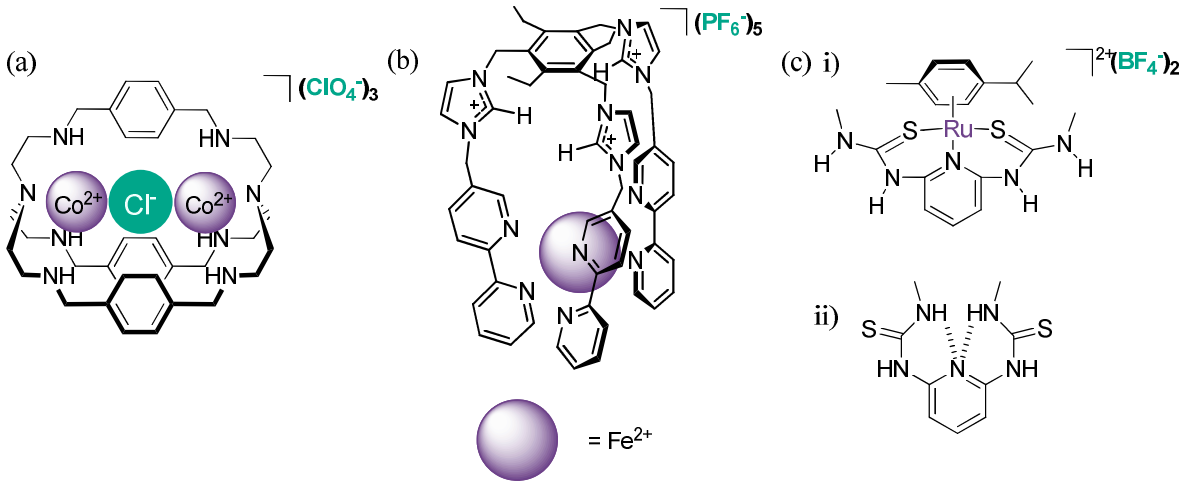



***Figure 1.17.*** *Metal containing anion receptors: (a) rigid dicobalt(II) cryptate with chloride selective cavity;[112] (b) Fabbrizzi's tripodal imidazolium cage;[113] and (c) Steed's thiourea ligand (i) appended to ruthenium and (ii) free, highlighting intramolecular hydrogen bonding between N-H protons and pyridine.[114]*

## 1.5 Anion Sensing

Each of the interactions described thus far can be exploited in the construction of anion sensors, provided an appropriate reporter group is incorporated into the receptor to allow for signalling of an anion recognition event (Figure 1.18).

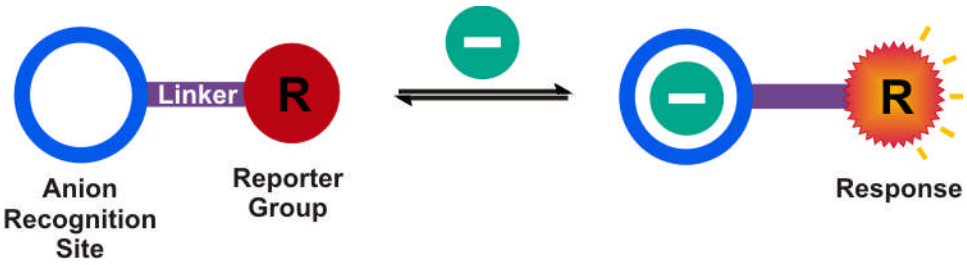



***Figure 1.18.*** *Schematic representation of anion sensing. Addition of an anion to the receptor induces a change in the physical properties of the reporter group: the response.*

Anion sensors usually take the form of an anion recognition unit, similar to those described in the previous section, linked to the reporter group, situated in close enough proximity such that

binding of the anion induces a macroscopic physical change in an optical (colorimetric or luminescent) or electrochemical property.

During the recent emergence of anion receptor chemistry numerous anion sensors have been reported; the following sections give examples of strategies that have been used for the macroscopic detection of anions.

### 1.5.1 Electrochemical Sensors

Electrochemical sensors combine a redox-active moiety and an anion recognition site in close proximity so that binding of an anion perturbs the redox potential of the redox metal centre. Both cobaltocenium and ferrocene have been extensively exploited in the construction of redox-active anion sensors by Beer and co-workers.[115] Binding of an anion by these receptors induces a cathodic shift of the metallocene redox couple since the anion stabilises the respective positively charged metallocenium species. The receptor depicted in Figure 1.19a exemplifies the behaviour displayed by such simple acyclic ferrocene receptors, with large cathodic shifts (up to 240 mV) observed upon addition of dihydrogen phosphate in the presence of a ten-fold excess of both hydrogen sulfate and chloride anions in MeCN solution.[116] Shinkai *et al.* have demonstrated the ability of a simple ferrocene boronic acid to selectively sense fluoride in 9:1 methanol/$H_2O$,[117, 118] and Aldridge has also utilised boron ferrocenyl derivatives in anion recognition units.[119] The sterically hindered ferrocene functionalised borane depicted in Figure 1.19b is able to detect the presence of fluoride and cyanide anions in MeCN *via* a cathodic shift of the receptor's ferrocene/ferrocenium redox couple, whilst possessing the additional advantage of being stable to air and moisture.

Aside from redox-active transition metal groups, a number of organic electrochemical sensors have been reported. Tetrathiafulvalene, which is capable of undergoing a one electron oxidation process, has been incorporated into a collection of calix[4]pyrrole receptors. The receptor shown in Figure 1.19c is capable of strongly complexing chloride and bromide in

dichloroethane solution, as determined by $^{1}$H NMR titration and ITC.[120] This halide anion complexation could also be monitored *via* cathodic shifts in the TTF redox couple as a function of chloride and bromide concentration in the same solvent, highlighting its potential in anion sensing.

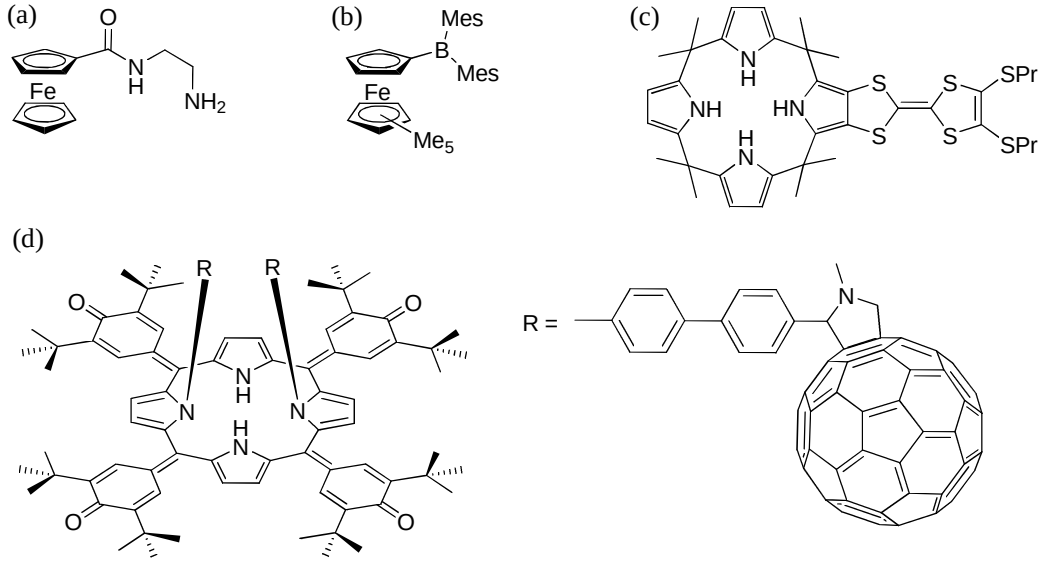



***Figure 1.19.*** *Electrochemical anion sensors: (a) Beer's dihydrogen phosphate selective amide appended ferrocene sensor;[116] (b) Aldridge's sterically hindered boron ferrocenyl receptor;[119] (c) Tetrathiofulvalene appended calix[4]pyrrole sensor;[120] and (d) bis-fullerene substituted oxoporphyrinogen sensor.[121]*

Recently Hill and co-workers have constructed a bis-fullerene substituted oxoporphyrinogen (Figure 1.19d) whose ability to complex fluoride at its hydrogen bonding core is signalled by a large cathodic shift of ~500 mV (upon 1.1 equivalents of $F^-$ in *o*-dichlorobenzene) of the oxoporphyrinogen redox couple.[121]

### 1.5.2 Luminescent Sensors

Receptors integrated with a luminescent reporter group are attractive for anion sensing since detection can often occur at very low concentrations, thus requiring only small quantities of the host species, coupled with the high sensitivity of luminescence detection techniques. The luminescence of a reporter group can be modulated upon anion binding by one of four mechanisms: photoelectron transfer (PET); electronic energy transfer; switching between

monomers and excimers; and the so-called rigidity effect. These phenomena can act to either enhance or quench luminescent emission intensity and may also alter the wavelength at which an excited state emits.

Certain transition metal complexes exhibit luminescence, the emission intensity of which can potentially be perturbed if appended in the vicinity of an anion recognition site. The photochemistry of $Ru(bipy)_3$ and related complexes is particularly well-known,[122] and consequently a number of anion receptors containing this luminescent moiety have been reported. A recent example couples two alkyl guanidinium groups and $Ru(bipy)_3$ to create a sensor (Figure 1.20a) capable of recognising the biologically relevant L-glutamate in MeCN, as signified by a four fold increase in photoluminescence intensity of the MLCT band with a concominant hypsochromic shift.[123] This increase in emission intensity is attributed to rigidification of the receptor upon anion binding resulting in less energy being lost through non-radiative pathways whilst the hypsochromic shift suggests that the anion raises the energy of the MLCT band.

As well as transition metals, lanthanides can also be incorporated into receptors for luminescent anion sensing. Since f-f transitions are Laporte forbidden, the direct excitation of lanthanide ions is inefficient and another mechanism is required. An organic chromophore in proximity to the lanthanide centre enables indirect excitation of the lanthanide *via* energy transfer from this sensitizing 'antenna' and subsequent emission from the long-lived lanthanide is observed. This concept is exemplified by Faulkner and co-workers in their lanthanide complex where, interestingly, the carboxylate functionalised TTF chromophore occupies a vacant coordination site rather than being covalently appended.[124] Figure 1.20b illustrates the intramolecular energy transfer occurring in this complex, a process which is disrupted by the addition of phosphate in methanolic solution, since this anion effectively

competes with the carboxylate groups to complex the lanthanide, and thus luminescence quenching is observed.

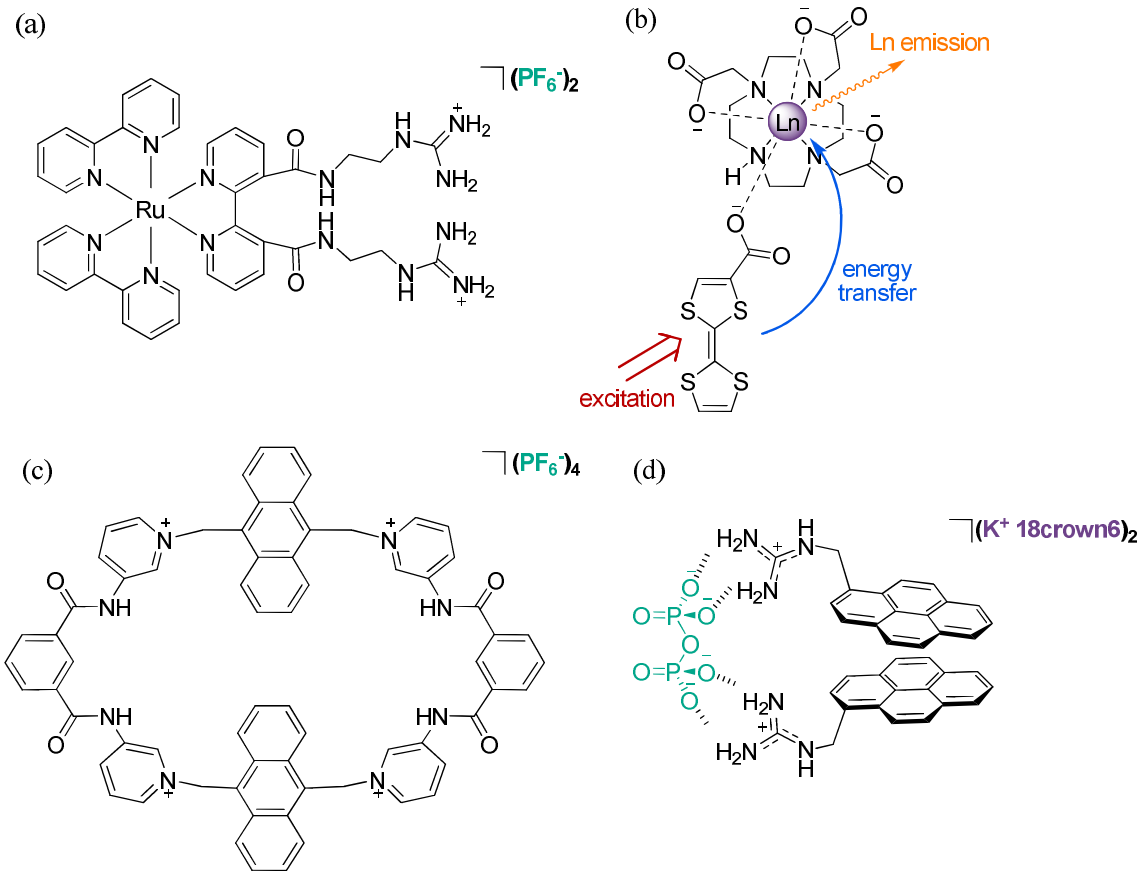



***Figure 1.20.*** *Luminescent anion sensors: (a) Sojic's bis-guanidinium ruthenium sensor;*[123] *(b) Faulkner's lanthanide complex showing energy transfer from the TTF chromophore to the lanthanide metal centre giving rise to luminescence;*[124] *(c) Ghosh's pyridinium-anthracene macrocycle capable of sensing carboxylate anions;*[125] *and (d) Teramae's pyrene receptor undergoing excimer formation in the presence of pyrophosphate.*[126]

Many organic fluorophores have also been employed in anion receptors for luminescent anion sensing. Anthracene can act as an effective sensor through ON-OFF or OFF-ON PET processes upon anion addition.[127] Indeed Ghosh *et al*. have designed a macrocyclic anthracene receptor (Figure 1.20c), whose fluorescence is quenched *via* a PET process from the adjacent pyridinium moiety, but in the presence of carboxylate anions this process is interrupted and fluorescence is restored.[125]

Another highly π-delocalised planar organic fluorophore is pyrene, whose most compelling feature is its ability to form excimers, a principle which has been used successfully in the

sensing of anions. A pyrene appended guanidinium receptor shows a band corresponding to monomer emission in the absence of anions, whilst, in methanol, the addition of pyrophosphate gives rise to a second structureless band at higher wavelength corresponding to the excimer.[126] The anion brings two receptors together through hydrogen bonding interactions with the guanidinium group, holding the pyrenes in close enough proximity to induce excimer formation (Figure 1.20d). Interestingly, a much weaker response was obtained with other anions such as acetate, dihydrogen phosphate and the halides, which is attributed to these smaller anions being less effective in simultaneously binding to two receptor molecules.

### 1.5.3 Colorimetric Sensors

Using a colour change to signal the presence of anions has arguably more appeal than using a fluorophore since no equipment is required and detection can be achieved by the naked eye. Steed and co-workers have developed a viologen based sensor (Figure 1.21a) that undergoes a colour change from colourless to deep purple upon addition of succinate, malonate and acetate, but remains unchanged by other anions including chloride and nitrate.[128] This colour change is suggestive of the formation of a charge-transfer complex between the carboxylate anions and the viologen, a phenomenon which was confirmed by DFT calculations. Gabbaï has developed a bidentate borane sensor (Figure 1.21b) that loses its intense yellow colour upon addition of fluoride as its LUMO becomes populated.[129]

A number of chromophore appended (thio)urea receptors have been reported to colorimetrically sense anions such as fluoride and acetate. Often the addition of these basic anions induces deprotonation of the acidic urea protons leading to increased conjugation in the system and thus a colour change is observed. An example is provided by Fabbrizzi and co-workers, who symmetrically furnished a urea receptor with the 1,8-naphthalimide chromophore (Figure 1.21c).[130] Upon addition of fluoride in DMSO the receptor undergoes stepwise deprotonation to give two distinct colour changes: orange to red; and red to blue,

whereas addition of less basic acetate and dihydrogen phosphate only cause a single deprotonation event.

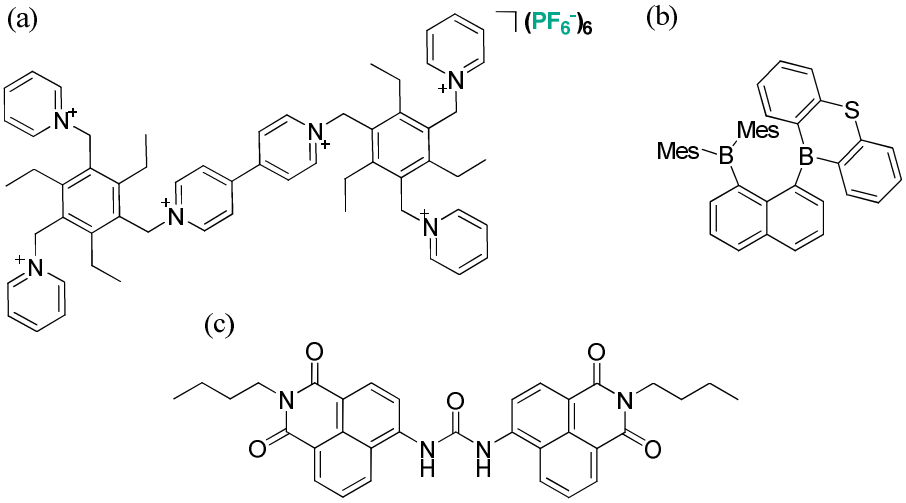



***Figure 1.21.*** *Colorimetric anion sensors: (a) Steed's viologen sensor for oxoanions;[128] (b) Gabbaï's fluoride selective borane sensor;[129] and (c) Fabbrizzi's 1,8-naphthalimide appended thiourea receptor capable of stepwise deprotonation upon addition of fluoride.[130]*

An alternative approach to the optical sensing of anions employs the use of displacement assays, the application of which is discussed in the following section.

## 1.6 Displacement Assays

Optical displacement assays comprise a receptor with a bound fluorophore or chromophore, such as a dye. They operate under the premise that a particular anion is able to complex to the receptor more strongly than this molecule and thus the dye becomes 'displaced' upon anion binding. Given that the particular microenvironment of a dye molecule influences its optical properties, release from the receptor will trigger a luminescent or colour change (Figure 1.22).

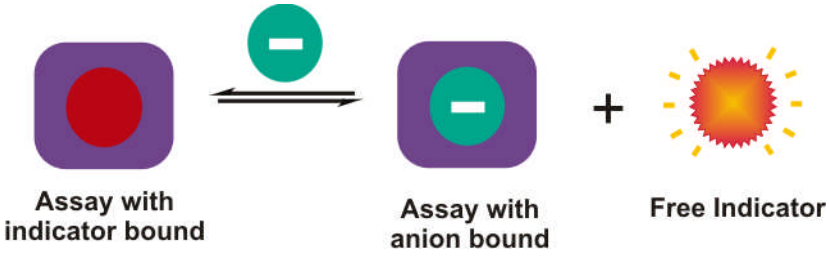



***Figure 1.22.*** *Schematic representation of displacement assay. An anion displaces the bound indicator, leading to a change in its optical properties upon release.*

Displacement assays for anions were pioneered by Anslyn and co-workers who used 5-carboxyfluorescein bound tris-guanidinium receptors to signal the presence of citrate anions.[131] More recently Vilar has adopted a similar approach to create an assay capable of detecting the presence of dihydrogen phosphate and acetate, but not a wide range of other anions tested.[132] The assay uses a thiolato-urea diplatinum complex bound to methyl red, which is coloured orange when bound but yellow when free in solution (i.e. when the anion displaces it from the receptor).

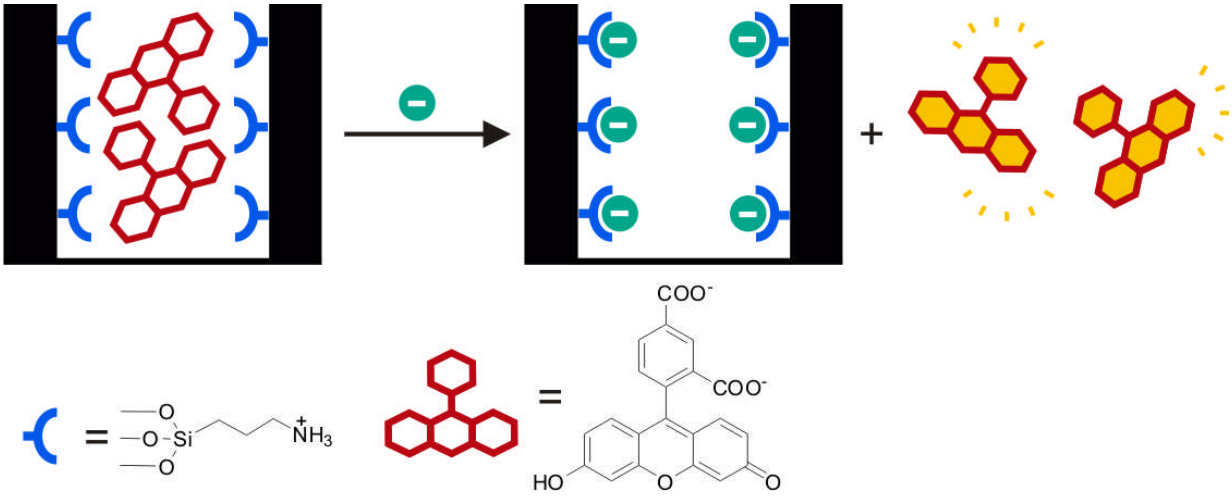



***Figure 1.23.*** *Schematic representation of Martínez-Máñez's displacement assay consisting of alkyl ammonium binding groups appended to silica linkers mounted on a mesoporous hybrid material. Initially the binding pockets complex 5-carboxyfluorescein which undergoes self quenching. Upon addition of anions the dye is released, and undergoes a colour change to signal the binding event.* [133]

Martínez-Máñez *et al.* have developed a range of assays employing binding groups appended to silica linkers which are covalently attached to a mesoporous hybrid material.[133, 134] In the absence of anions the pockets created are able to bind to 5-carboxyfluorescein; addition of an appropriate guest anion leads to the release of the dye and thus a colorimetric response. A number of anion binding moieties discussed in Section 1.4 are used with the most prolific being an alkyl ammonium group that shows remarkable selectivity for citrate in pure water (Figure 1.23).

## 1.7 Templation

The second key feature of this thesis is directed self-assembly and the potential of a specific anionic template to direct the formation of impressive molecular architectures.

Templation is abundant in Nature, with the replication of DNA proceeding *via* a templated synthesis[25] and the synthesis of proteins being templated by RNA.[135] In simplest terms, a template directs the formation of a specific product in a reaction that has the potential to yield a multitude of compounds, and remains distinct from a reagent since it plays no part in the intrinsic chemistry of a reaction. Pioneering work in the field of templation was carried out by Busch who classified templates as either thermodynamic or kinetic; the former acting to shift an equilibrium towards the formation of a particular component and the latter operating on irreversible reactions, orienting reactive groups in a particular way in order for the reaction to proceed towards a single product.[136] A templation reaction under thermodynamic control only requires that the template should bind more strongly to the target product than all other species present in the reaction. By contrast the requirements for a kinetic template are more complicated; in order to advocate the formation of the desired product the template must bind to the highest energy transition state thus lowering $\Delta G$, whilst lowering the energies of all intermediates and transition states through which the reaction proceeds.

Later, Sanders classified templation in terms of the topology of the template and final assembly, which can be defined as cyclisation, interweaving or linear (shown in Figure 1.24).[137]

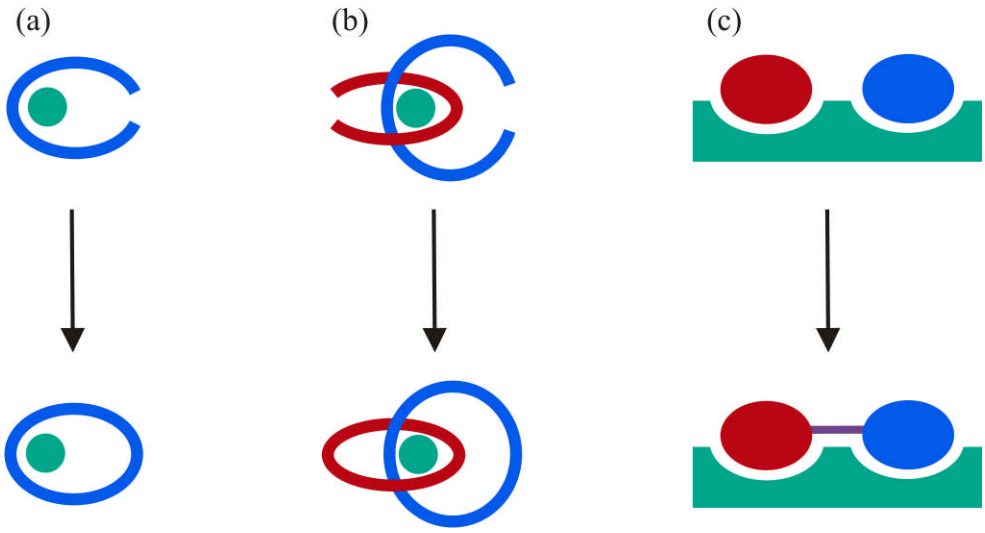



***Figure 1.24.*** *Classification of templation: (a) cyclisation; (b) interweaving; and (c) linear. The template is depicted in green.*[137]

The remainder of this section explores the first two classes, cyclisation and interweaving, using an anionic template. Similarly to anion receptor chemistry, the field of anion templation is much less well developed than its cationic counterpart, again due to the challenges that complexing anions pose. However in recent years some impressive examples of both serendipitous and strategic anion templation have been reported such that it can no longer be described as a fledgling field.

### 1.7.1 Anion Templation

Early examples of anion templation involved a certain degree of serendipity, usually where anions of different size and geometries were shown to control the assembly of polymetallic cage and cluster complexes.[138-142] An elegant example of this is provided by Dunbar and co-workers who showed the geometry of their metallocyclophanes could be directed by the addition of a particular anion (Figure 1.25).[143] Using the large $SbF_6^-$ anion gave a pentanuclear structure whereas $ClO_4^-$, $BF_4^-$ and $I^-$ directed the formation of molecular squares, and nitrate was responsible for a molecular triangle. It was also confirmed that the

pentagonal structure formed in the presence of $SBF_6^-$ could be converted to either the molecular square or triangle in the presence of the appropriate anions.

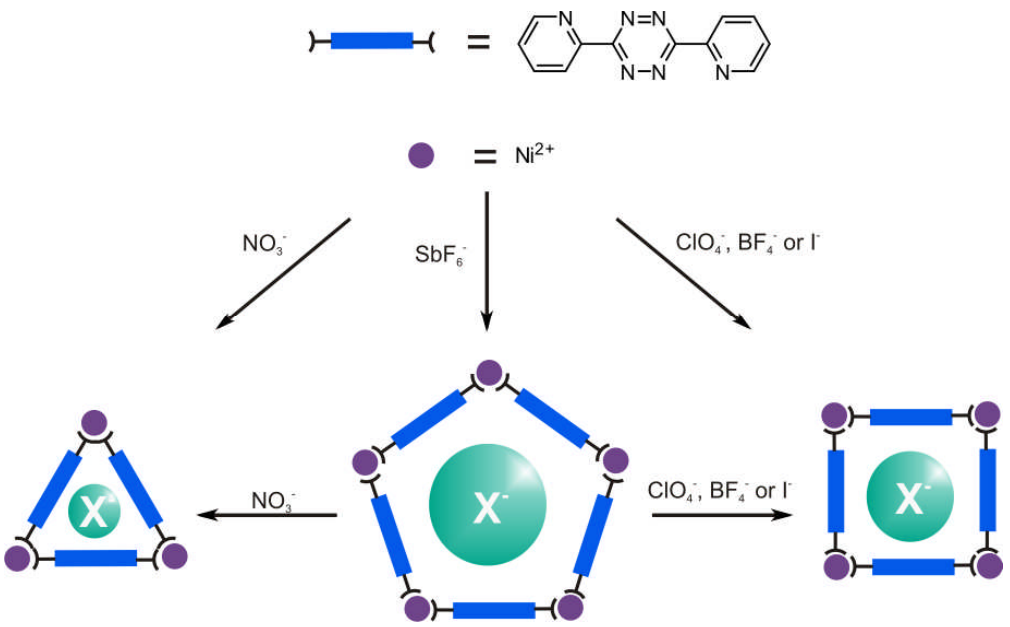



***Figure 1.25.*** *Schematic representation of Dunbar's anion-templated metallocyclophane. The geometry of the polygon is determined by the size of the templating anion.*[143]

In recent years, the strategic use of anions as templating agents has proved to be highly effective in directing the formation of molecules that would otherwise be inaccessible or low yielding. Sessler *et al.* have reported the anion-induced synthesis of pyrrole based macrocycles where the choice of acid used in the Schiff base reaction between a bis-amine and bis-aldehyde plays a pivotal role in defining product distribution.[144, 145] In the presence of sulphuric acid, the [2 + 2] macrocycle (Figure 1.26a) is the sole product whereas use of hydrochloric or hydrobromic acid results in mainly oligomeric products. This indicates the importance of the tetrahedral sulfate anion in directing the formation of this specific macrocycle.

Luis and co-workers have used a bis-carboxylate terephthalate template to direct the formation of pseudopeptidic macrocycles.[146, 147] In a recent example, they have utilised this anion templation approach to affect the outcome of a dynamic covalent mixture of pseudopeptidic oligoimines (Figure 1.26b).[148] The system is structurally disfavoured for

cyclization yet interactions with the bis-carboxylate anion constrain the precursors in such a position to form the macrocycle with the best fit for the template.

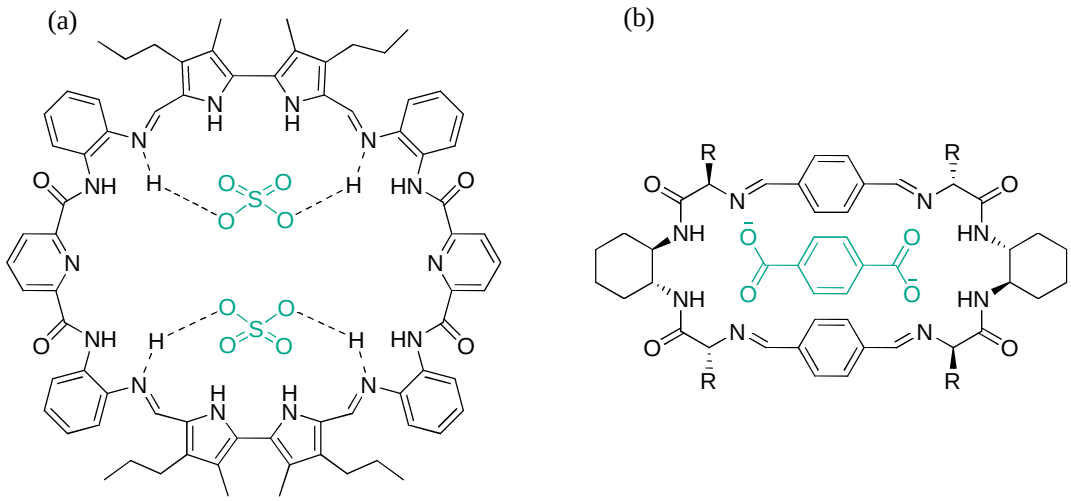



***Figure 1.26.*** *Anion-templated macrocycles: (a) Sessler's sulfate directed [2 + 2] diamidopyridine bipyrrole macrocycle;[144] and (b) example of Luis' dicarboxylate-templated structurally disfavoured macrocycle.[148]*

It has also been possible to use anions to mediate the formation of helices and foldamers from both linear and cyclic oligomers.[149] Gale and co-workers demonstrated the ability of fluoride to direct a simple isophthalamide to assemble into a double helix (Figure 1.27a), with X-ray crystal structure analysis confirming the placement of the anions held in position by N-H hydrogen bonds, with the helices wrapped around.[150]

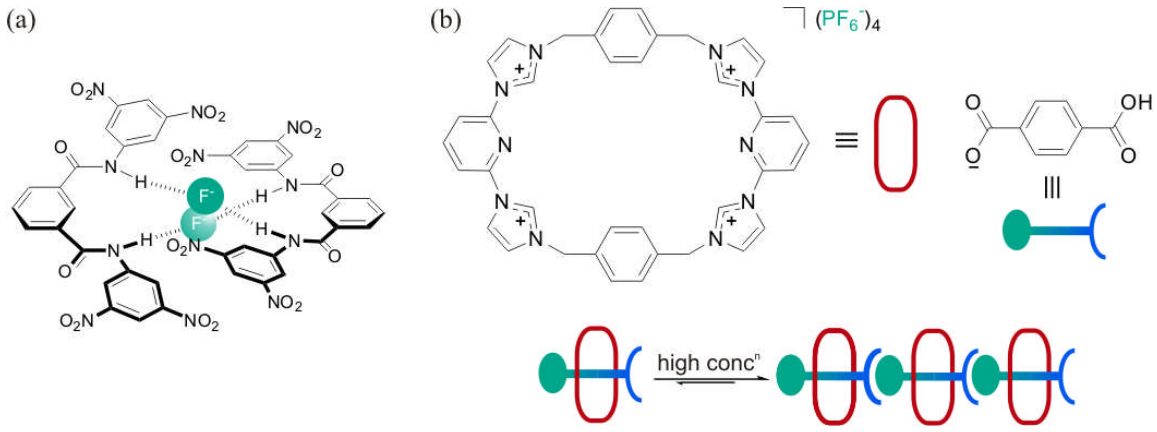



***Figure 1.27.*** *(a) Gale's fluoride directed double helix,[150] and (b) schematic representation of oligopseudorotaxane between a tetrakis-imidazolium macrocycle and monoteraphthalate anion.[151]*

Recently Sessler *et al.* have reported the formation of an oligopseudorotaxane, arising between a tetrakis-imidazolium macrocycle and a monoterephthalate anion.[151] At low concentrations the single pseudorotaxane species dominates, whereas at high concentrations hydrogen bond interactions between carboxylic acid and carboxylate groups cause the structure to self-assemble into a well defined 'molecular necklace' (Figure 1.27b).

### 1.7.2 Interweaving Anion Templation

In order for a template to be classified as interweaving it must possess the ability to direct two components to assemble in an orthogonal manner. This concept can then be expanded for the formation of templated interpenetrated structures (pseudorotaxanes) and ultimately for the construction of mechanically interlocked molecules. These three stages of interweaving anion templation are represented schematically in Figure 1.28, and examples of each are now discussed in turn.

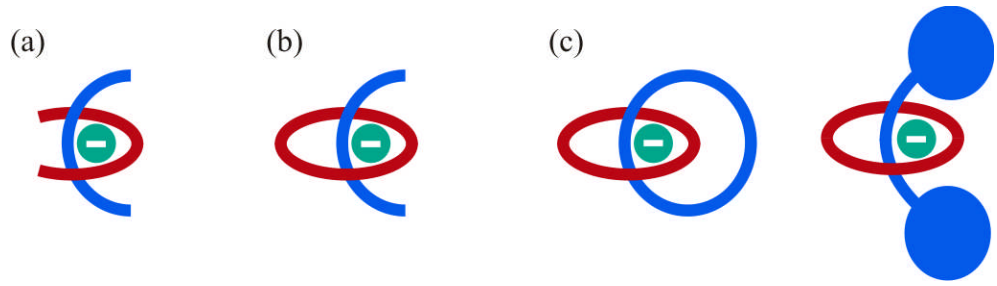



***Figure 1.28.*** *Interweaving anion templation: (a) Orthogonal array; (b) pseudorotaxane; and (c) catenane and rotaxane. Anions are shown in green.*

A simple example of an anion controlling the formation of an orthogonal array is provided by Schubert and co-workers who illustrated the ability of dianionic sulfate to direct the association of two receptors containing a phenyl-linked triazole-triazolium moiety (Figure 1.29a).[152] The formation of the octahedral bis-tridentate complex is attributed to the charge neutral nature of the complex whereby the doubly charged sulfate electrostatically satisfies two singly charged ligands, binding to the organic fragments *via* charge-assisted C-H

hydrogen bonds. Indeed, the bis-triazolium receptor is observed to only form a 1:1 complex with sulfate under the same conditions.

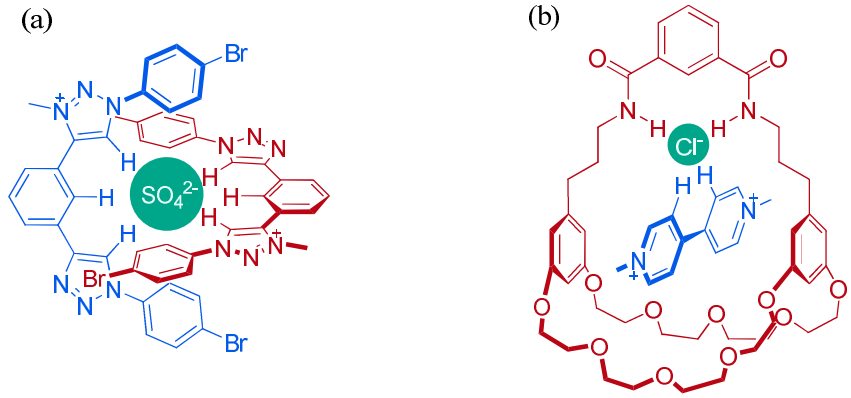



***Figure 1.29.*** *(a) Sulfate-templated orthogonal array between phenyl-linked triazolium-triazole ligands,*[152] *and (b) pseudorotaxane between isophthalamide-bridged cryptand and 4,4-bipyridinium thread.*[153]

Huang *et al.* have presented the ability of chloride to enhance the formation of pseudorotaxane formation between an isophthalamide bridged crown ether containing cryptand and a 4,4-bipyridinium thread component (Figure 1.29b).[153] In the absence of halide anion a weak interaction between the two components was observed *via* the pale yellow colour attributed to charge-transfer interactions between the electron rich phenyl and electron deficient bipyridinium units. Upon addition of chloride the intensity of this charge-transfer band increased indicating a greater stability of interpenetrated structure formation in the presence of this anion. The stability of this structure also requires the cryptand to be of complementary size cryptand to the bipyridinium-chloride complex, to maximise the strength of pseudorotaxane association.

Whilst both of the structures above are impressive on their own account, they can also be viewed as precursors to mechanically interlocked molecules. Various routes to these interlocked structures are highlighted in Figure 1.30.

Pseudorotaxanes often act as precursors to both catenanes and rotaxanes, with a clipping or stoppering reaction used to create the mechanically interlocked product.[154] Rotaxanes can also be formed at high temperatures or pressures where upon the stoppered axle is able to ‘slip’

through the macrocyclic wheel component.[155] Two halves of an axle can undergo chemical reaction within the macrocycle where the active template can either be preserved with the rotaxane's axle component or removed following the 'snapping' reaction.[156] It has also been possible for a small stopper to undergo a 'swelling' reaction to create an axle with stopper groups too large to allow for dethreading.[157, 158]

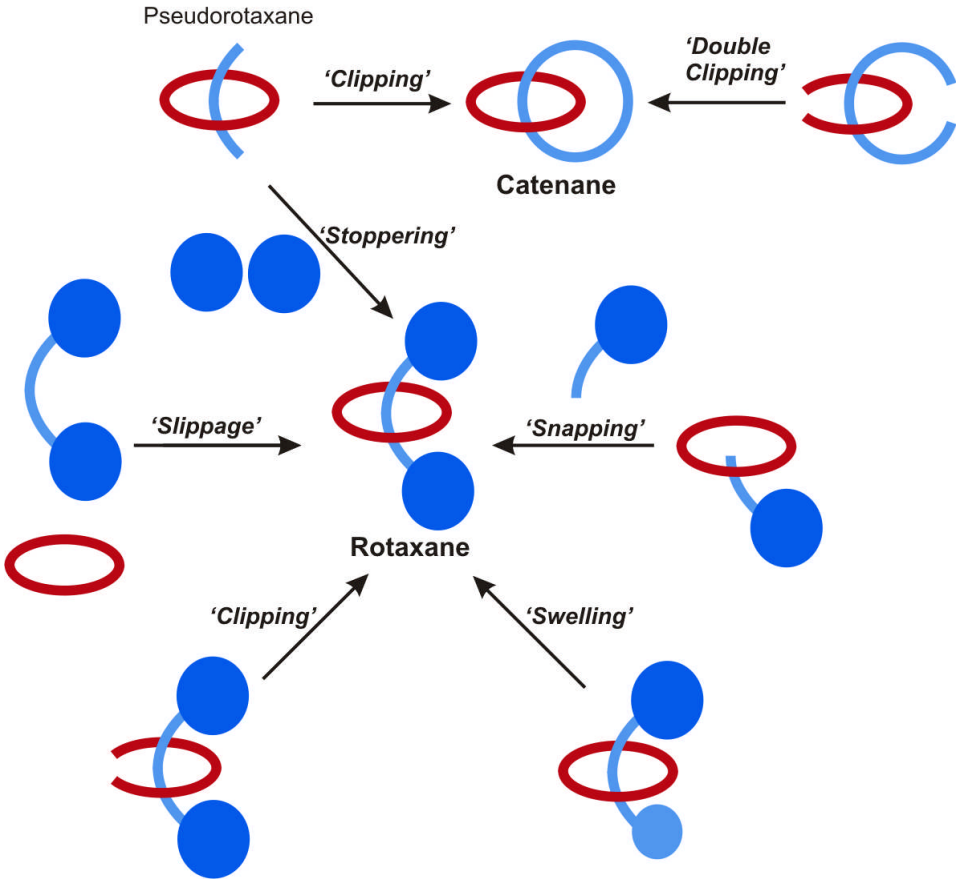
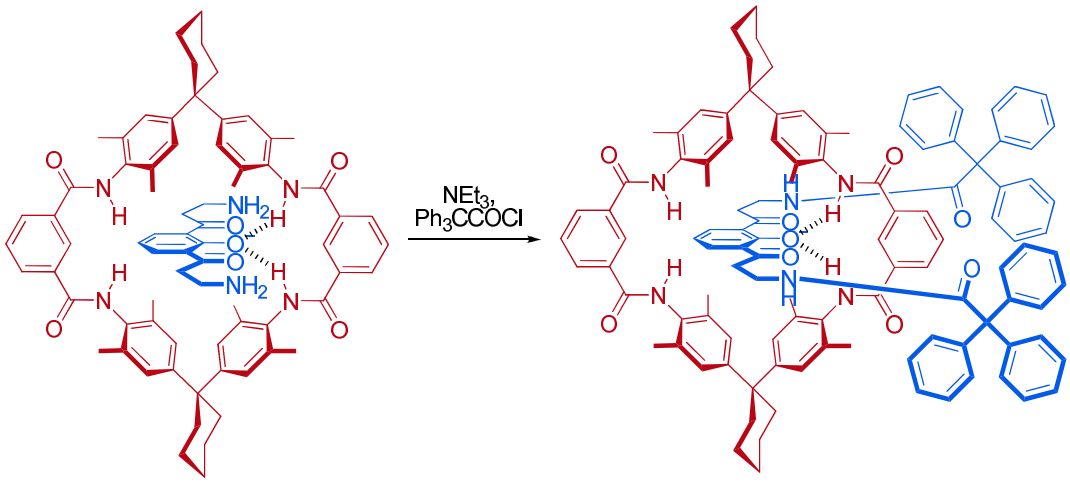



***Figure 1.30.*** *Strategies for interlocked structure formation.*

Early syntheses of interlocked species relied on statistical approaches which generally resulted in the target structure forming in low yields.[159, 160] Directed self-assembly methods allow for the more efficient construction of mechanically interlocked structures, most of which have employed cationic[161, 162] or neutral[163-166] templates, and it is only recently that anions have been employed in a similar role.

The first approaches to synthesise rotaxanes *via* anion templation involved complexing a phenoxide appended component within a tetralactam macrocycle, followed by reaction to yield the mechanically interlocked architecture.

Vögtle used this strategy whereby the templating phenolate underwent reaction with an acyl chloride derivative so that the template was not present in the final rotaxane structure.[167] In related work Schalley and co-workers used the hydrogen bond donating ability of a tetra-lactam macrocycle to complex a phenoxide unit appended with amine groups, before an acid chloride stoppering reaction yields the interlocked architecture (Scheme 1.2).[168]

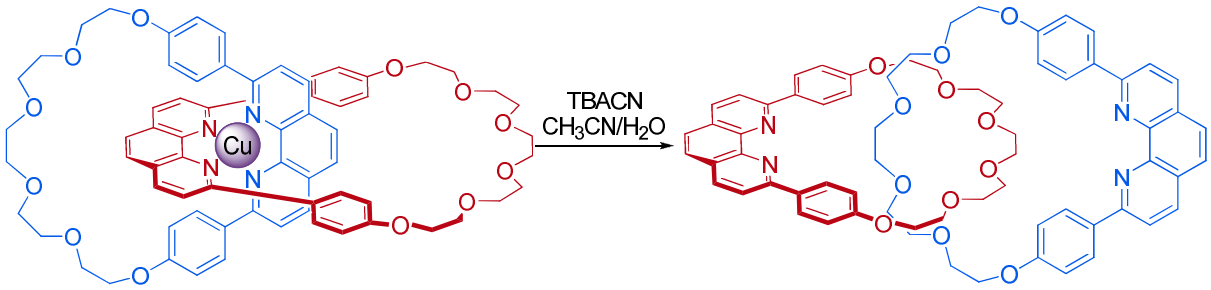



***Scheme 1.2.*** *Formation of Schalley's phenoxide-templated rotaxane by an acid chloride condensation reaction.*[168]

Crucially, in both of the aforementioned structures the template is either consumed in the rotaxanation reaction or an integral part of the rotaxane and thus cannot be removed to yield a three-dimensional cavity with the potential to complex a guest species.

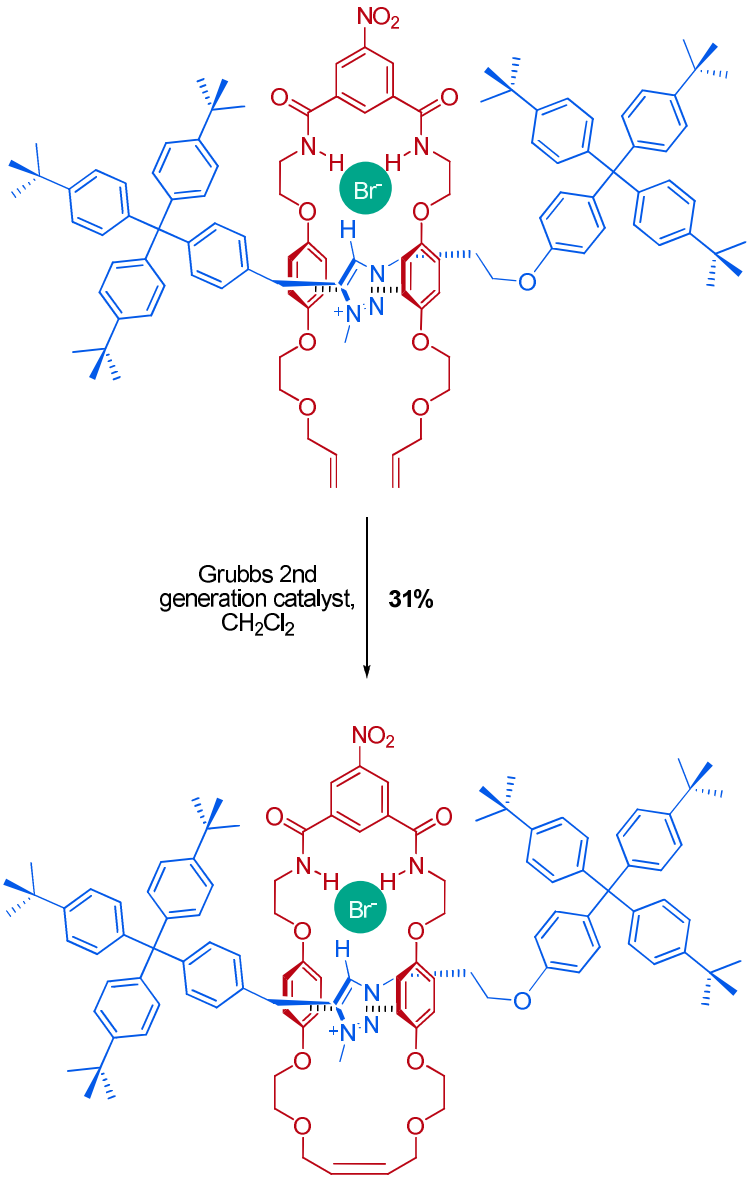
In order to construct such systems inspiration must be taken from the seminal work of Sauvage and co-workers who harnessed the tetrahedral coordination preference of Cu(I) cations to direct the formation of an assortment of mechanically interlocked molecules, for example the catenane shown in Scheme 1.3.[169] It was found that the 'free' catenane could be obtained by removal of the Cu(I) template using TBACN. Isolating the structure liberated

from the template has critical implications for the work carried out in this thesis, and is discussed further in later chapters.




***Scheme 1.3.*** *Removal of the templating cation from Sauvage's Cu(I) directed catenane.*[169]

Stimulated by this work, Beer *et al.* have developed a similar anion templation strategy for the formation of rotaxanes and catenanes.[81] A recent example of this strategy is provided by a bromide-templated rotaxane, consisting of a isophthalamide containing macrocycle and 1,2,3-triazolium axle component (Scheme 1.4).[170] The anion directs the orthogonal association of the bis-vinyl appended macrocycle precursor and the triazolium axle before Grubbs' catalysed ring closing metathesis yields the mechanically interlocked structure, in 31% yield, which is stabilised by charge-assisted π-π stacking interactions. Interestingly, in the presence of a chloride anion template, the yield of rotaxanation is reduced to 21% highlighting the importance of the complementary size of the bromide template in directing the formation of this structure. Following the removal of the anionic template a topologically unique three-dimensional interlocked cavity is exposed which can be exploited for anion complexation.




***Scheme 1.4.*** *Use of a distinct bromide template to direct the formation of a [2]rotaxane formed via Grubbs' RCM reaction.*[170]

Beer and co-workers have provided another impressive example of an anion directed interlocked structure formation with their sulfate-templated triply interlocked capsule (Figure 1.31).[171] A sulfate anion directs the association of two tripodal tris-urea precursors before a Huisgen 1,3-dipolar cycloaddition reaction is used to create the triply interlocked architecture. Interestingly $^{1}$H NMR analysis of the precursor with chloride and bromide indicated the formation of only 1:1 ligand-anion complexes indicating the formation of the

triply interlocked structure is reliant on the sulfate anion which demonstrates high coordination numbers allowing it to hydrogen bond to the twelve urea N-H protons.

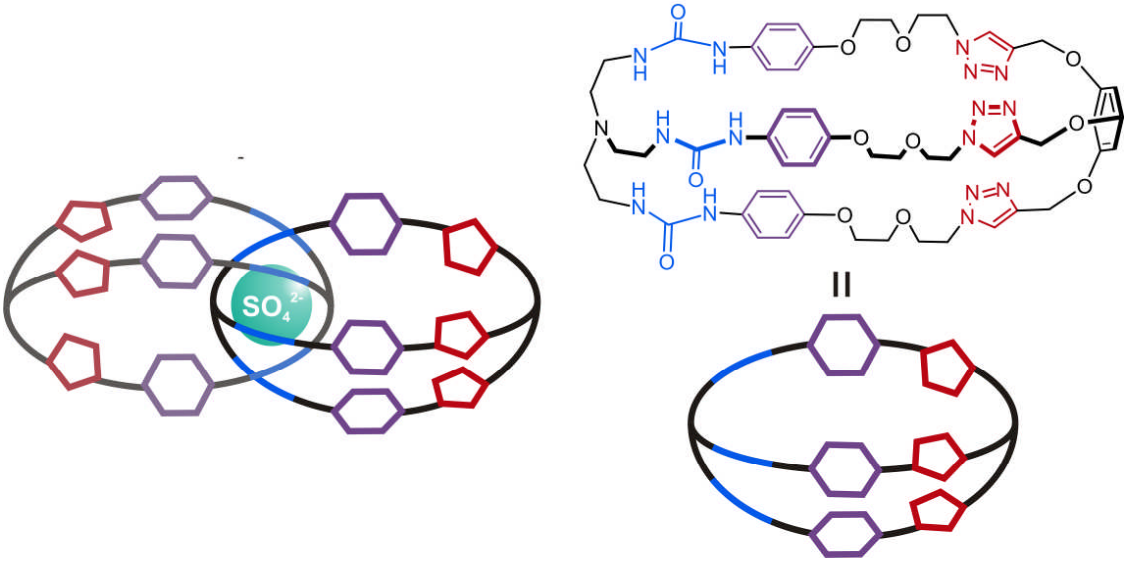



***Figure 1.31***. *Schematic representation of sulfate-templated triply interlocked capsule.*[171]

## 1.8 Functional Applications of Interlocked Structures

In the past supramolecular chemists have been satisfied by finding novel and efficient methods for the formation of elaborate interlocked molecular architectures, and indeed many impressive examples have been reported.[161, 172, 173] However, more recently, emphasis has shifted to creating mechanically interlocked structures capable of performing some useful function, with a view to using these structures in molecular devices. A brief overview of the main categories of functional interlocked structures is now discussed with emphasis placed on those examples that have relevance to this thesis.

### 1.8.1 Modification of Properties

Building particular functional groups into interlocked structures can act to modify their properties. This phenomenon is usually observed where this functional group constitutes part

of the axle component whereby encapsulation within the macrocyclic wheel acts to adjust a characteristic of this moiety, often protecting it from chemical degradation.

Recently Leigh and co-workers have used this approach to synthesise a pentapeptide containing [2]rotaxane (Figure 1.32a) where encapsulation of the peptide within a simple tetra-lactam macrocycle protects it from a wide range of peptidases.[174] With a view to providing a real function for this rotaxane, it was shown that when a self-immolative stopper group was incorporated the rotaxane could act as a propeptide delivery agent upon a given enzymatic stimuli.

Another group of chemicals that it may be beneficial to protect *via* encapsulation within a macrocycle are near IR dyes such as squaraines. When isolated many of these dyes are susceptible to nucleophilic attack since their HOMO-LUMO band gap is small, and are also hindered by their propensity to aggregate leading to broadening of their absorption bands. Smith *et al.* showed that it was possible to overcome these issues by enclosing the squaraine within the same macrocycle used by Leigh to protect his oligopeptide, to form a rotaxane (Figure 1.32b).[175]

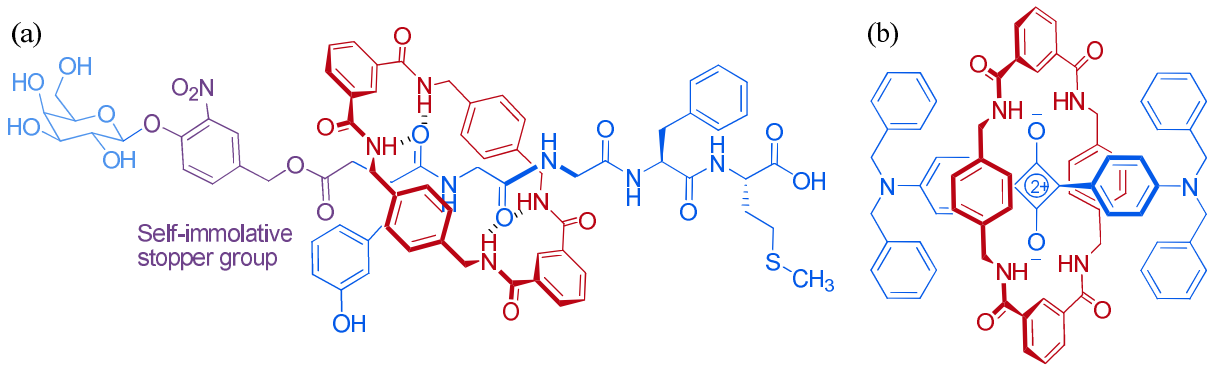



***Figure 1.32.*** *Protecting functional groups from chemical degradation with tetralactam macrocycles: (a) Leigh's pentapeptide rotaxane;[174] and (b) Smith's squaraine rotaxane.[175]*

They also showed properties of the squaraine could be further modified by encapsulation within structurally different tetra-lactam macrocycles,[176] and the implications of this for a functional use is detailed in Section 1.8.3.

### 1.8.2 Molecular Machines

Arguably the most exploited function of interlocked architectures is their use for molecular machine-like behaviour whereby some macroscopic stimuli initiates motion on the molecular scale. This function in particular has potential in terms of nanotechnological applications, which to some extent is already being realised.[177-181] The design of interlocked structures can be manipulated such that one component is capable of translocation relative to another component. In rotaxanes, the macrocycle can translate to an alternative site on the axle component, or remain at the same site and rotate upon its axis (Figure 1.33a). In catenanes, rotation of either macrocycle about the other is a possibility (Figure 1.33b).

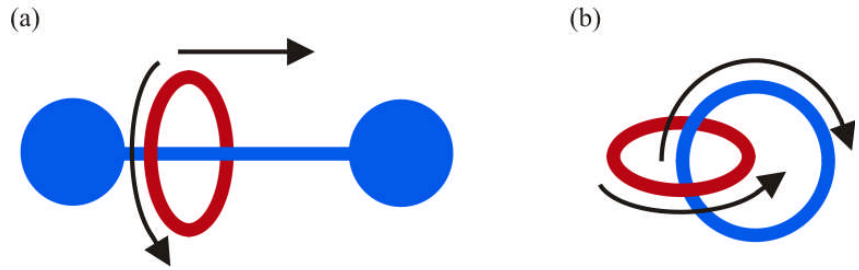
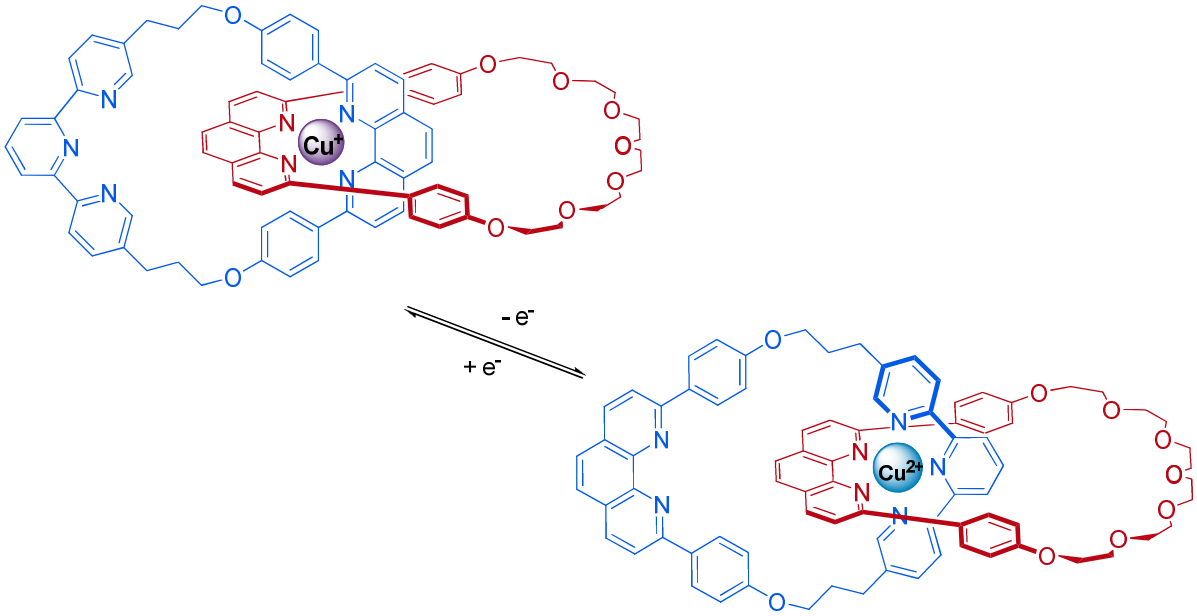



***Figure 1.33.*** *Schematic representation of types of molecular motion within mechanically interlocked structures: (a) [2]Rotaxane undergoing translational and pirouetting-type motion, and (b) rotation of one macrocycle within another in a [2]catenane.*

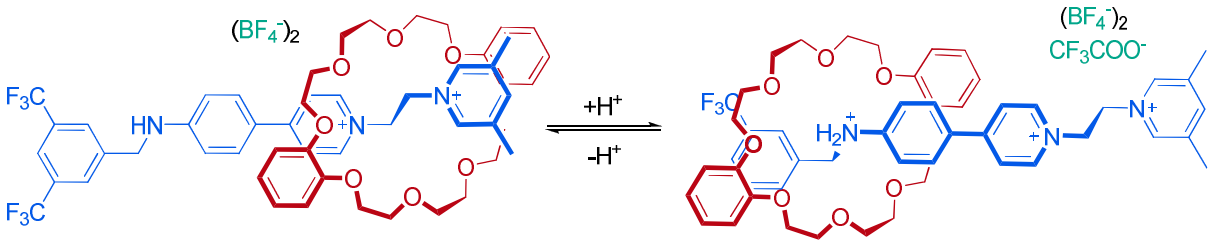
Examples of highly tuned molecular machines can be found in abundance in Nature, where they are broadly classified into two categories: rotary; and linear. RNA polymerase, responsible for synthesising RNA from DNA, carries out its function by moving processively along a molecule of the DNA template,[182] and has been categorised with other motor proteins such as myosin[183] and kinesin[184]. The stimulus for movement in these examples is provided by chemical energy obtained from the hydrolysis of ATP. Supramolecular systems benefit from being susceptible to a large range of stimuli for molecular motion including electrochemical, optical and chemical methods, and examples of some interlocked structures designed to undergo motion upon the application of a variety of stimuli are now described.

An early example of a molecular machine was provided by Sauvage and co-workers who synthesised a bistable catenane whose two forms can be interconverted electrochemically by utilising the different coordination preferences of the two redox states of the Cu(I)/Cu(II) couple (Scheme 1.5).[185] In the Cu(I) state the cation prefers to satisfy its tetrahedral coordination preference complexing to both phenanthroline units whereas upon oxidation to Cu(II) it is more favourable to adopt the phenanthroline-terpyridine five-coordinate complex and thus induce a rotation of one ring within the other. This process was shown to be fully reversible by applying a reduction potential to the divalent state.



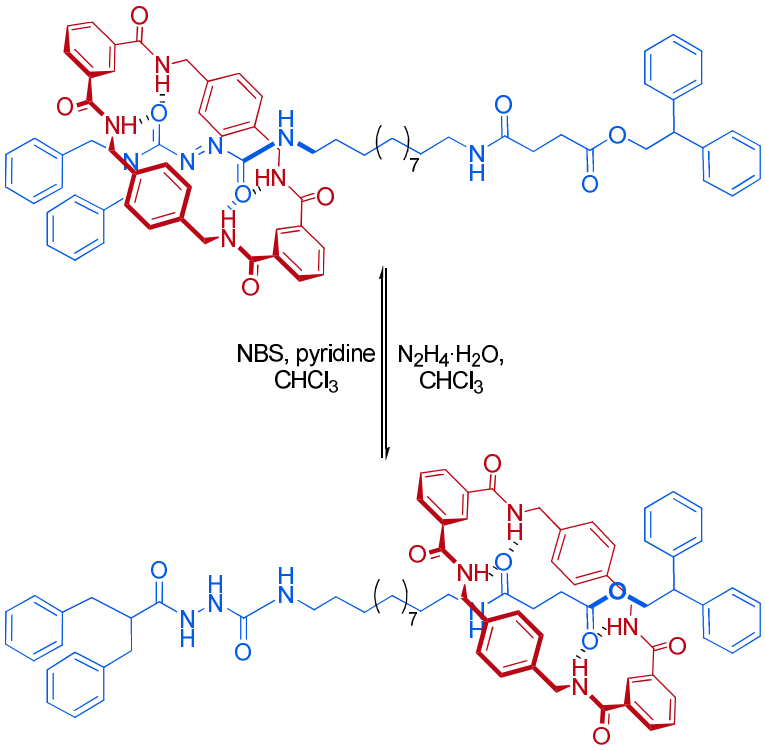

***Scheme 1.5***. *Electrochemically-induced rotational motion within a [2]catenane, utilising the different coordination preferences of the Cu(I)/Cu(II) redox couple.*[185]

A great number of rotaxanes containing macrocycles capable of shuttling between two sites controlled by pH have been reported, many of which exploit the strong interaction of dialkyl- and dibenzyl-ammonium groups with crown ethers, and the ease at which the former can be deprotonated.[29] Indeed Loeb *et al.* showed that their crown ether macrocycle component prefers to reside upon the charged bis-pyridinium ethane unit at neutral pH, but undergoes translocation to the ammonium group upon addition of acid (Scheme 1.6).[186]




***Scheme 1.6.*** *Loeb's acid-base controlled molecular shuttle.*[186]

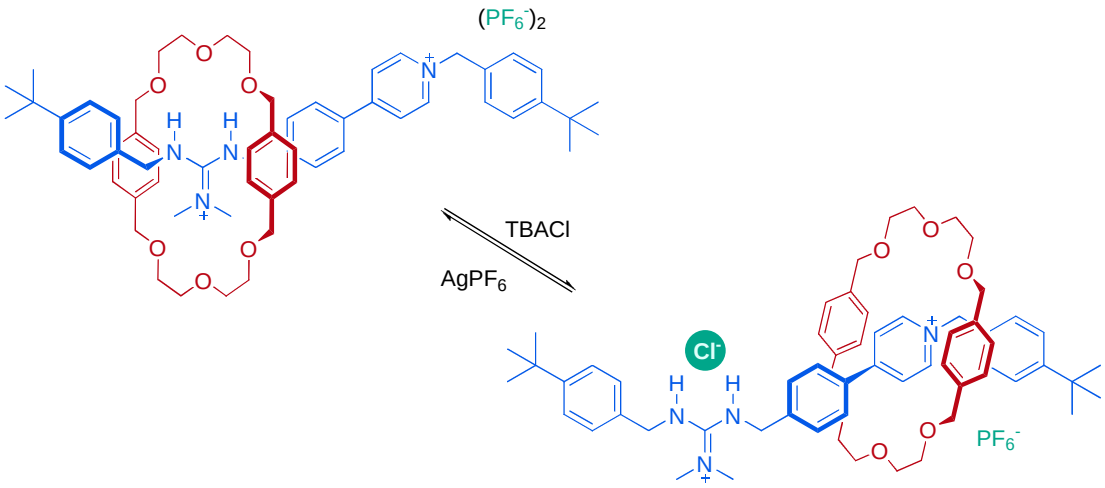
It has also been possible to induce molecular motion *via* other chemical stimuli and recently Berná *et al.* have shown they can induce shuttling within a two station rotaxane by hydrogenation/dehydrogenation of the azo functionality (Scheme 1.7).[187] Interestingly, translation of the macrocycle could also be attained in a continuous cycle through a catalysed ester bond formation whereby the rotaxane behaves as an organocatalyst.




***Scheme 1.7.*** *Berná's rotaxane capable of undergoing molecular motion via hydrogenation/dehydrogenation.*[187]

Unsurprisingly, like the field of anion receptor chemistry and templation, the use of anions to trigger molecular motion is a notably underdeveloped area. Early examples of these type of machines operated under pH control, involving deprotonation of a phenol moiety to create the

corresponding anion.[188, 189] More recently anions distinct from the interlocked structure have been used to induce motion, an example of which is Chiu's chloride controlled molecular switch (Scheme 1.8).[190] In the absence of anions, the macrocycle resides over the guanidinium moiety, whereas the addition of chloride translocates the macrocycle to the pyridinium station. The strong complexation of the chloride to the guanidinium group results in it being sterically unfavourable for the macrocycle to reside in its original position hence the movement observed.




***Scheme 1.8.*** *Chloride-induced molecular motion within a two station rotaxane.*[190]

This example suggests that there may be great potential in using anions to translocate a macrocyclic component to an alternative site along the axle component. Moreover, their negative charge may be exploited in order to create a molecular machine driven by electrostatic effects and the recently acquired accessibility of anionic supramolecular chemistry may lead to this area becoming an established field.

### 1.8.3 Anion Recognition and Sensing

A final use for mechanically interlocked structures and perhaps the most important in terms of the work described in this thesis is their ability to act as anion receptors and sensors. A wide range of acyclic and macrocyclic receptors for anion recognition and sensing purposes have

already been examined in this introduction, however interlocked host species may provide the additional benefit of possessing a three-dimensional binding domain for the strong and selective binding of an anionic guest.

To this end, Jeong and co-workers have synthesised a catenane where the acidic N-H protons of two indolocarbazole fragments converge into a three-dimensional cavity to bind anions (Figure 1.34).[191] This catenane was observed, by an enhancement of the fluorescence emission band, to complex chloride over an order of magnitude more strongly than other anions tested in 99:1 acetone/$H_2O$, including acetate which is considerably more basic. This selectivity is attributed to the complementary size and shape of the cavity to chloride, which is encapsulated in the cavity, bound by four N-H hydrogen bonds.

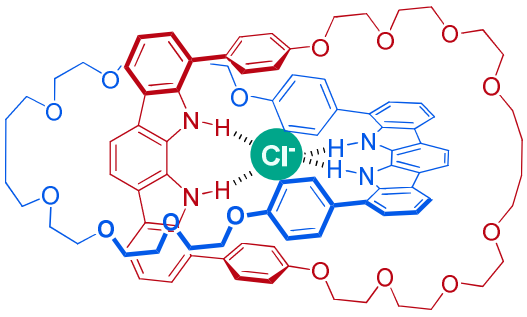



***Figure 1.34.*** *Jeong's [2]catenane capable of selectively complexing chloride.*[191]

Impressively, Smith *et al.* have constructed a squaraine rotaxane that acts to modify the properties of the squaraine, undergo anion-induced molecular motion and ultimately act as an effective anion sensor.[192] When encapsulated within the particular tetra-lactam macrocycle as part of the rotaxane shown in Figure 1.35a, the squaraine fragment experiences a significant reduction in its fluorescence intensity compared to the free dye. Addition of chloride anions to this structure in $CHCl_3$ acts to displace the macrocycle from the squaraine due to strong binding of the anion within the macrocycle's isophthalamide cleft, and the macrocycle translocates to an alternative site on the rotaxane's axle component (Figure 1.35b). Upon this movement the squaraine's luminescence intensity is restored and thus the rotaxane acts as a

chloride sensor. It proved possible to fabricate this sensory rotaxane into dipsticks capable of sensing chloride in aqueous solution *via* a 'turn-on' fluorescence response.

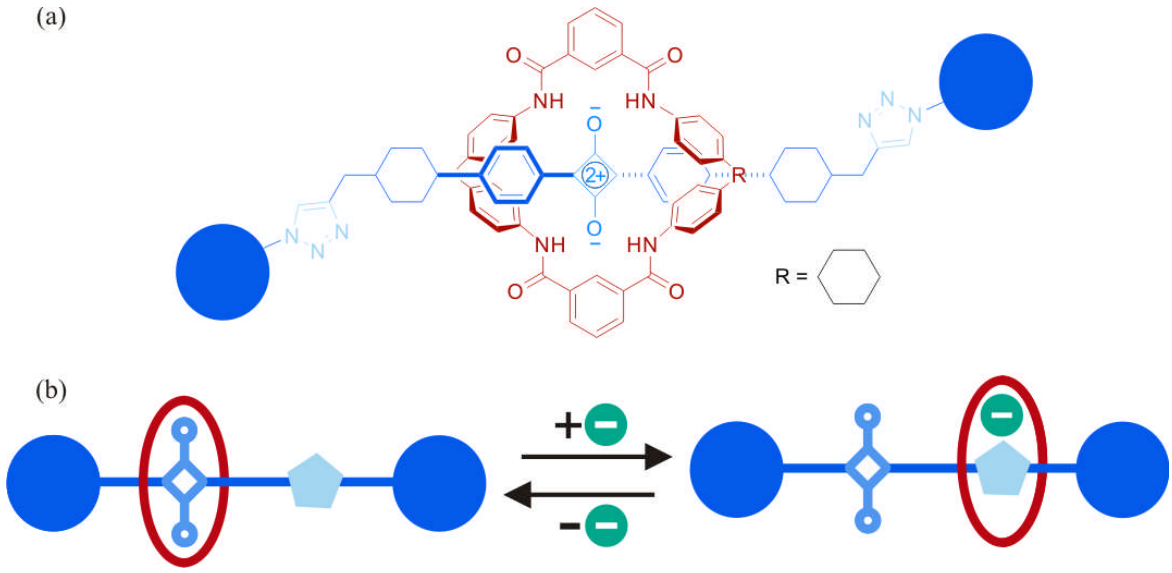



***Figure 1.35.*** *(a) Smith's squaraine [2]rotaxane, and (b) schematic representation of chloride-induced molecular motion restoring the luminescence intensity of the squaraine moiety.*[192]

## 1.9 Project Objectives

The overriding ambition of this project is to exploit strategic anion templation for the assembly of interlocked molecular architectures capable of executing some useful function. The first application focuses on the recognition and sensing of anionic guest species, and the second involves the use of charged species to induce molecular motion within a mechanically interlocked species.

Discovering efficient methods for the synthesis of rotaxanes and catenanes (Figure 1.36a) is crucial for this work, and initial efforts will be directed towards novel anion templation procedures for their formation, as detailed in ***Chapter Two***. The ability of the mechanically interlocked species to bind anions is then investigated with particular focus on complexation in aqueous solvent media.

A natural extension of this project is to incorporate a reporter group into the interlocked structure in order to sense the presence of an anion (Figure 1.36b). Investigations into appending a transition metal lumophore to either the macrocycle or axle component of a rotaxane, and the subsequent rotaxane's ability to sense anions *via* luminescence comprises the contents of ***Chapter Three***.

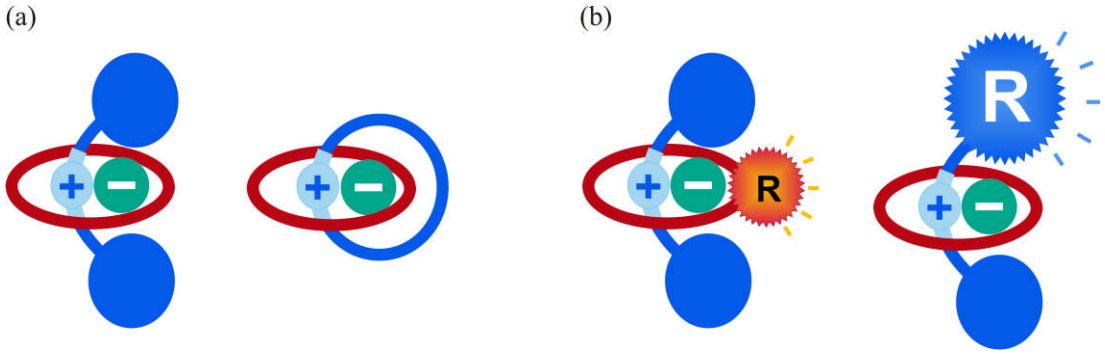



***Figure 1.36.*** *Schematic representations of: (a) [2]Rotaxane and [2]catenane capable of complexing anions; and (b) [2]rotaxanes incorporating reporter groups to sense the present of anions via changes in their luminescence intensity.*

***Chapter Four*** describes efforts towards constructing rotaxanes capable of machine-like behaviour, with initial work concentrating on the synthesis of a structure designed to undergo anion-induced molecular motion (Figure 1.37).

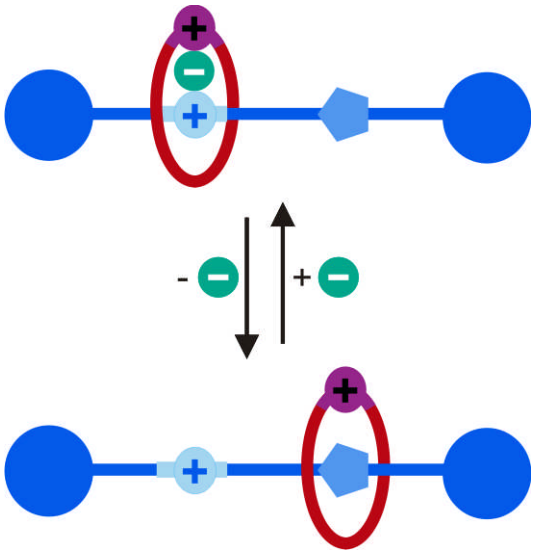



***Figure 1.37.*** *Schematic representation of a two-station [2]rotaxane capable of undergoing anion-induced molecular motion.*

The remainder of Chapter 4 focuses on the use of the pyridine *N*-oxide motif as an integrated template for rotaxane formation, and the potential of these rotaxanes to undergo pH-, anion- and cation-induced molecular motion.

## 1.10 References


1. J.-M. Lehn, *Angew. Chem., Int. Ed. Engl.*, 1988, **27**, 89-112.
2. D. J. Cram, *Angew. Chem., Int. Ed. Engl.*, 1988, **27**, 1009-1020.
3. C. J. Pedersen, *Angew. Chem., Int. Ed. Engl.*, 1988, **27**, 1021-1027.
4. J. T. Davis, O. Okunola and R. Quesada, *Chem. Soc. Rev.*, 2010, **39**, 3843-3862.
5. R. Custelcean, *Chem. Soc. Rev.*, 2010, **39**, 3675-3685.
6. W. D. McCardle, F. I. Katch and V. L. Katch, *Essentials of Exercise Physiology* Lea & Febiger, University of Michigan, 1994.
7. S. Ebihara, K. Shirato, N. Harata and N. Akaike, *J. Physiol. Lond.*, 1995, **484**, 77-86.
8. G. D. Brayer, Y. Luo and S. G. Withers, *Protein Sci.*, 1995, **4**, 1730-1742.
9. A. L. Berger, C. O. Randak, L. S. Ostedgaard, P. H. Karp, D. W. Vermeer and M. J. Welsh, *Journal of Biological Chemistry*, 2005, **280**, 5221-5226.
10. J. D. Watson and F. H. C. Crick, *Nature*, 1953, **171**, 737-738.
11. J. M. Berg, J. L. Tymoczko and L. Stryer, *Biochemistry 6th Ed.*, W.H. Freeman & Co., New York, 2006.
12. G. E. Isom and J. L. Way, *Toxicology and Applied Pharmacology*, 1984, **74**, 57-62.
13. A. M. Davison, S. J. Cameron, J.-P. Grünfield, C. Ponticelli, E. Ritz, C. Winearls and C. van Epersele, *Oxford Textbook of Clinical Nephrology, 3rd Ed.*, OUP, New York, 2005.
14. A. J. P. Smolders, L. P. M. Lamers, E. Lucassen, G. Van der Velde and J. G. M. Roelofs, *Chemistry and Ecology*, 2006, **22**, 93-111.
15. S. A. Watmough, J. Aherne, C. Alewell, P. Arp, S. Bailey, T. Clair, P. Dillon, L. Duchesne, C. Eimers, I. Fernandez, N. Foster, T. Larssen, E. Miller, M. Mitchell and S. Page, *Environmental Monitoring and Assessment*, 2005, **109**, 1-36.
16. J. L. H. Eersels, M. J. Travis and J. D. M. Herscheid, *Journal of Labelled Compounds & Radiopharmaceuticals*, 2005, **48**, 241-257.
17. J. L. Sessler, P. A. Gale and W.-S. Cho, *Anion Receptor Chemistry*, RSC, Cambridge, 2006.
18. W. M. Latimer, K. S. Pitzer and C. M. Slansky, *J. Chem. Phys.*, 1939, **7**, 108-111.
19. G. Hummer, L. R. Pratt and A. E. Garcia, *J. Phys. Chem.*, 1996, **100**, 1206-1215.
20. E. Fischer, *Ber. Dtsch. Chem. Ges.*, 1894, **27**, 2985-2993.
21. D. E. Koshland Jr., *Proc. Natl. Acad. Sci. U.S.A.*, 1958, **44**, 98-104.
22. H. Luecke and F. A. Quiocho, *Nature*, 1990, **347**, 402-406.
23. R. Dutzler, E. B. Campbell, M. Cadene, B. T. Chait and R. MacKinnon, *Nature*, 2002, **415**, 287-294.
24. J.-M. Lehn and P. Ball, in *The New Chemistry*, ed. N. Hall, CUP, Cambridge, 2000, p. 9.
25. L. Stryer, *Biochemistry 4th Ed.*, W.H. Freeman & Co., New York, 1995.
26. H. G. L. Coster, *Aust. J. Phys.*, 1999, **52**, 117-140.
27. J. Collinge, *Annu. Rev. Neurosci.*, 2001, **24**, 519-550.
28. J. S. Lindsey, *New J. Chem.*, 1991, 153-180.

29. V. Balzani, A. Credi and M. Venturi, *Molecular Devices and Machines - A Journey into the Nanoworld*, Wiley-VCH, Weinheim, 2003.
30. O. Safarowsky, B. Windisch, A. Mohry and F. Vögtle, *J. Prakt. Chem.*, 2000, **342**, 437-444.
31. A. Harada, A. Hashidzume, H. Yamaguchi and Y. Takashima, *Chemical Reviews*, 2009, **109**, 5974-6023.
32. D. A. Leigh and R. A. Smith, in *Cyclic Polymers, 2nd Ed.*, ed. J. A. Semlyen, Kluwer, Dordecht, 2000, pp. 561-600.
33. F. M. Raymo and J. F. Stoddart, *Chemical Reviews*, 1999, **99**, 1643-1664.
34. P. A. Atkins and J. de Paula, *Atkins' Physical Chemistry, 7th Ed.*, OUP, New York, 2002.
35. Y. Nishiyama, P. Langan and H. Chanzy, *J. Am. Chem. Soc.*, 2002, **124**, 9074-9082.
36. J. W. Steed and J. L. Atwood, *Supramolecular Chemistry, 2nd Ed.*, Wiley-VCH, Chichester, 2009.
37. P. Metrangolo and G. Resnati, *Chem. Eur. J.*, 2001, **7**, 2511-2519.
38. P. Metrangolo, F. Meyer, T. Pilati, G. Resnati and G. Terraneo, *Angew. Chem., Int. Ed.*, 2008, **47**, 6114-6127.
39. M. G. Sarwar, B. Dragisic, S. Sagoo and M. S. Taylor, *Angew. Chem., Int. Ed.*, 2010, **49**, 1674-1677.
40. C. J. Serpell, N. L. Kilah, P. J. Costa, V. Félix and P. D. Beer, *Angew. Chem., Int. Ed.*, 2010, **49**, 5322-5326.
41. M. G. Sarwar, B. Dragisic, L. J. Salsberg, C. Gouliaras and M. S. Taylor, *J. Am. Chem. Soc.*, 2010, **132**, 1646-1653.
42. N. L. Kilah, M. D. Wise, C. J. Serpell, A. L. Thompson, N. G. White, K. E. Christensen and P. D. Beer, *J. Am. Chem. Soc.*, 2010, **132**, 11893-11895.
43. A. Caballero, N. G. White and P. D. Beer, *Angew. Chem., Int. Ed*, 2011, **50**, 1845-1848.
44. P. Auffinger, F. A. Hays, E. Westhof and P. S. Ho, *Proceedings of the National Academy of Sciences of the United States of America*, 2004, **101**, 16789-16794.
45. E. I. Howard, R. Sanishvili, R. E. Cachau, A. Mitschler, B. Chevrier, P. Barth, V. Lamour, M. Van Zandt, E. Sibley, C. Bon, D. Moras, T. R. Schneider, A. Joachimiak and A. Podjarny, *Proteins: Struct., Funct., and Bioinf.*, 2004, **55**, 792-804.
46. E.-I. Kim, S. Paliwal and C. S. Wilcox, *J. Am. Chem. Soc.*, 1998, **120**, 11192-11193.
47. W. Saenger, *Principles of Nucleic Acid Structure*, Springer-Verlag, New York, 1984.
48. J. C. Ma and D. A. Dougherty, *Chem. Rev.*, 1997, **97**, 1303-1324.
49. V. Gorteau, M. D. Julliard and S. Matile, *J. Membrane Sci.*, 2008, **321**, 37-42.
50. J. Mareda and S. Matile, *Chem. Eur. J.*, 2009, **15**, 28-37.
51. Y. S. Rosokha, S. V. Lindeman, S. V. Rosokha and J. K. Kochi, *Angew. Chem., Int. Ed.*, 2005, **44**, 2178-2178.
52. S. Lee, Y. Hua, H. Park and A. H. Flood, *Org. Lett.*, 2010, **12**, 2100-2102.
53. M. J. Chmielewski and J. Jurczak, *Chem. Eur. J.*, 2005, **11**, 6080-6094.
54. C. H. Park and H. E. Simmons, *J. Am. Chem. Soc.*, 1968, **90**, 2431-2432.
55. R. A. Bell, G. G. Christoph, F. R. Fronczek and R. E. Marsh, *Science*, 1975, **190**, 151-152.
56. E. Graf and J. M. Lehn, *J. Am. Chem. Soc.*, 1975, **97**, 5022-5024.
57. E. Graf and J. M. Lehn, *J. Am. Chem. Soc.*, 1976, **98**, 6403-6405.
58. J. P. Kintzinger, J. M. Lehn, E. Kauffmann, J. L. Dye and A. I. Popov, *J. Am. Chem. Soc.*, 1983, **105**, 7549-7553.
59. B. Dietrich, J. Guilhem, J. M. Lehn, C. Pascard and E. Sonveaux, *Helv. Chim. Acta*, 1984, **67**, 91-104.

60. J. M. Lehn, E. Sonveaux and A. K. Willard, *J. Am. Chem. Soc.*, 1978, **100**, 4914-4916.
61. S. Suzuki, H. T. and A. Nakahara, *Bioorg. Chem.*, 1973, **2**, 145-154.
62. S. Suzuki and A. Nakahara, *Bioorg. Chem.*, 1975, **4**, 250-258.
63. M. A. Hossain, J. A. Liljegren, D. Powell and K. Bowman-James, *Inorg. Chem.*, 2004, **43**, 3751-3755.
64. F. P. Schmidtchen, *Angew. Chem., Int. Ed. Engl.*, 1977, **16**, 720-721.
65. F. P. Schmidtchen, *Chem. Ber.*, 1980, **113**, 864-874.
66. F. P. Schmidtchen, *Chem. Ber.*, 1981, **114**, 597-607.
67. F. P. Schmidtchen and G. Muller, *J. Chem. Soc., Chem. Commun.*, 1984, 1115-1116.
68. A. Metzger, V. M. Lynch and E. V. Anslyn, *Angew. Chem., Int. Ed. Engl.*, 1997, **36**, 862-865.
69. P. Schiessl and F. P. Schmidtchen, *J. Org. Chem.*, 1994, **59**, 509-511.
70. S. Camiolo, P. A. Gale, M. I. Ogden, B. W. Skelton and A. H. White, *J. Chem. Soc., Perkin Trans. 2*, 2001, 1294-1298.
71. S. Camiolo, P. A. Gale, M. E. Light and M. B. Hursthouse, *Supramol. Chem.*, 2001, **13**, 613-618.
72. Z. Xu, S. K. Kim and J. Yoon, *Chem. Soc. Rev.*, 2010, **39**, 1457-1466.
73. H. Kim, S. In and J. Kang, *Supramol. Chem.*, 2006, **18**, 141-145.
74. E. Alcalde, N. Mesquida and L. Perez-Garcia, *Eur. J. Org. Chem*, 2006, 3988-3996.
75. E. Alcalde, N. Mesquida, M. Vilaseca, C. Alvarez-Rua and S. Garcia-Granda, *Supramol. Chem.*, 2007, **19**, 501-509.
76. A. Kumar and P. S. Pandey, *Org. Lett.*, 2008, **10**, 165-168.
77. K. Kavallieratos, S. R. deGala, D. J. Austin and R. H. Crabtree, *J. Am. Chem. Soc.*, 1997, **119**, 2325-2325.
78. A. Szumna and J. Jurczak, *Eur. J. Org. Chem.*, 2001, **2001**, 4031-4039.
79. M. A. Hossain, J. M. Llinares, D. Powell and K. Bowman-James, *Inorg. Chem.*, 2001, **40**, 2936-2937.
80. A. P. Bisson, V. M. Lynch, M.-K. C. Monahan and E. V. Anslyn, *Angew. Chem., Int. Ed. Engl.*, 1997, **36**, 2340-2342.
81. M. D. Lankshear and P. D. Beer, *Acc. Chem. Res.*, 2007, **40**, 657-668.
82. M. S. Vickers and P. D. Beer, *Chem. Soc. Rev.*, 2007, **36**, 211-225.
83. J. J. Gassensmith, J. M. Baumes and B. D. Smith, *Chem. Commun.*, 2009, 6329-6338.
84. S. O. Kang, J. M. Llinares, D. Powell, D. VanderVelde and K. Bowman-James, *J. Am. Chem. Soc.*, 2003, **125**, 10152-10153.
85. S. O. Kang, D. VanderVelde, D. Powell and K. Bowman-James, *J. Am. Chem. Soc.*, 2004, **126**, 12272-12273.
86. S. O. Kang, D. Powell and K. Bowman-James, *J. Am. Chem. Soc.*, 2005, **127**, 13478-13479.
87. S. O. Kang, V. W. Day and K. Bowman-James, *Inorg. Chem.*, 2010, **49**, 8629-8636.
88. M. Boiocchi, L. Del Boca, D. E. Gómez, L. Fabbrizzi, M. Licchelli and E. Monzani, *J. Am. Chem. Soc.*, 2004, **126**, 16507-16514.
89. I. Ravikumar, P. S. Lakshminarayanan, M. Arunachalam, E. Suresh and P. Ghosh, *Dalton Trans.*, 2009, 4160-4168.
90. P. J. Smith, M. V. Reddington and C. S. Wilcox, *Tetrahedron Lett.*, 1992, **33**, 6085-6088.
91. D. Curiel, A. Cowley and P. D. Beer, *Chem. Commun.*, 2005, 236-238.
92. N.-K. Kim, K.-J. Chang, D. Moon, M. S. Lah and K.-S. Jeong, *Chem. Commun.*, 2007, 3401-3403.
93. J.-M. Suk and K.-S. Jeong, *J. Am. Chem. Soc.*, 2008, **130**, 11868-11869.
94. T. Wang, Y. Bai, L. Ma and X.-P. Yan, *Org. Biomol. Chem.*, 2008, **6**, 1751-1755.

95. D. Curiel, M. Mas-Montoya, G. Sanchez, R. A. Orenes, P. Molina and A. Tarraga, *Org. Biomol. Chem.*, 2010, **8**, 4811-4814.
96. D.-W. Yoon, D. E. Gross, V. M. Lynch, C.-H. Lee, P. C. Bennett and J. L. Sessler, *Chem. Commun.*, 2009, 1109-1111.
97. P. A. Gale, J. L. Sessler, V. Král and V. Lynch, *J. Am. Chem. Soc.*, 1996, **118**, 5140-5141.
98. M. G. Fisher, P. A. Gale, J. R. Hiscock, M. B. Hursthouse, M. E. Light, F. P. Schmidtchen and C. C. Tong, *Chem. Commun.*, 2009, 3017-3019.
99. J. L. Sessler, V. Král, T. V. Shishkanova and P. A. Gale, *Proc. Natl. Acad. Sci. U.S.A.*, 2002, **99**, 4848-4853.
100. S. Kondo, N. Okada, R. Tanaka, M. Yamamura and M. Unno, *Tetrahedron Lett.*, 2009, **50**, 2754-2757.
101. J. L. Sessler, J. J. Cai, H. Y. Gong, X. P. Yang, J. F. Arambula and B. P. Hay, *J. Am. Chem. Soc.*, 2010, **132**, 14058-14060.
102. Y. Li and A. H. Flood, *Angew. Chem., Int. Ed.*, 2008, **47**, 2649-2652.
103. Y. Hua and A. H. Flood, *J. Am. Chem. Soc.*, 2010, **132**, 12838-12840.
104. H. E. Katz, *Organometallics*, 1987, **6**, 1134-1136.
105. K. Tamao, T. Hayashi and Y. Ito, *J. Organomet.Chem.*, 1996, **506**, 85-91.
106. M. Newcomb, Y. Azuma and A. R. Courtney, *Organometallics*, 1983, **2**, 175-177.
107. S. Aoyagi, K. Tanaka and Y. Takeuchi, *J. Chem Soc., Perkin Trans. 2*, 1994, 1549-1553.
108. V. B. Shur, I. A. Tikhonova, A. I. Yanovsky, Y. T. Struchkov, P. V. Petrovskii, S. Y. Panov, G. G. Furin and M. E. Volpin, *J. Organomet. Chem.*, 1991, **418**, 29-32.
109. H. Zhao and F. P. Gabbai, *Nat. Chem.*, 2010, **2**, 984-990.
110. V. Amendola and L. Fabbrizzi, *Chem. Commun.*, 2009, 513-531.
111. D. J. Mercer and S. J. Loeb, *Chem. Soc. Rev.*, 2010, **39**, 3612-3620.
112. J. M. Chen, X. M. Zhuang, L. Z. Yang, L. Jiang, X. L. Feng and T. B. Lu, *Inorg. Chem.*, 2008, **47**, 3158-3165.
113. V. Amendola, M. Boiocchi, B. Colasson, L. Fabbrizzi, M. J. R. Douton and F. Ugozzoli, *Angew. Chem., Int. Ed.*, 2006, **45**, 6920-6924.
114. M. L. Soriano, J. T. Lenthall, K. M. Anderson, S. J. Smith and J. W. Steed, *Chem. Eur. J.*, 2010, **16**, 10818-10831.
115. P. D. Beer, P. A. Gale and G. Z. Chen, *J. Chem. Soc., Dalton Trans.*, 1999, 1897-1910.
116. P. D. Beer, A. R. Graydon, A. O. M. Johnson and D. K. Smith, *Inorg. Chem.*, 1997, **36**, 2112-2118.
117. C. Dusemund, K. Sandanayake and S. Shinkai, *J. Chem Soc., Chem. Commun.*, 1995, 333-334.
118. H. Yamamoto, A. Ori, K. Ueda, C. Dusemund and S. Shinkai, *Chem. Commun.*, 1996, 407-408.
119. A. E. J. Broomsgrove, D. A. Addy, C. Bresner, I. A. Fallis, A. L. Thompson and S. Aldridge, *Chem. Eur. J.*, 2008, **14**, 7525-7529.
120. K. A. Nielsen, W. S. Cho, J. Lyskawa, E. Levillain, V. M. Lynch, J. L. Sessler and J. O. Jeppesen, *J. Am. Chem. Soc.*, 2006, **128**, 2444-2451.
121. J. P. Hill, M. E. El-Khouly, R. Charvet, N. K. Subbaiyan, K. Ariga, S. Fukuzumi and F. D'Souza, *Chem. Commun.*, 2010, **46**, 7933-7935.
122. J. P. Sauvage, J. P. Collin, J. C. Chambron, S. Guillerez, C. Coudret, V. Balzani, F. Barigelletti, L. Decola and L. Flamigni, *Chem. Rev.*, 1994, **94**, 993-1019.
123. E. Berni, I. Gosse, D. Badocco, P. Pastore, N. Sojic and S. Pinet, *Chem. Eur. J.*, 2009, **15**, 5145-5152.

124. S. J. A. Pope, B. P. Burton-Pye, R. Berridge, T. Khan, P. J. Skabara and S. Faulkner, *Dalton Trans.*, 2006, 2907-2912.
125. K. Ghosh and A. R. Sarkar, *Tetrahedron Lett.*, 2009, **50**, 85-88.
126. S. Nishizawa, Y. Kato and N. Teramae, *J. Am. Chem. Soc.*, 1999, **121**, 9463-9464.
127. T. Gunnlaugsson, H. D. P. Ali, M. Glynn, P. E. Kruger, G. M. Hussey, F. M. Pfeffer, C. M. G. dos Santos and J. Tierney, *Journal of Fluorescence*, 2005, **15**, 287-299.
128. S. J. Dickson, E. V. B. Wallace, A. N. Swinburne, M. J. Paterson, G. O. Lloyd, A. Beeby, W. J. Belcher and J. W. Steed, *New J. Chem.*, 2008, **32**, 786-789.
129. S. Sole and F. P. Gabbai, *Chem. Commun.*, 2004, 1284-1285.
130. D. Esteban-Gomez, L. Fabbrizzi and M. Liechelli, *J. Org. Chem.*, 2005, **70**, 5717-5720.
131. S. C. McCleskey, A. Metzger, C. S. Simmons and E. V. Anslyn, *Tetrahedron*, 2002, **58**, 621-628.
132. C. Mendoza, J. Benet-Buchholz, M. A. Pericas and R. Vilar, *Dalton Trans.*, 2009, 2974-2985.
133. M. Comes, M. D. Marcos, R. Martinez-Manez, F. Sancenon, J. Soto, L. A. Villaescusa and P. Amoros, *Chem. Commun.*, 2008, 3639-3641.
134. M. Comes, E. Aznar , M. Moragues, M. D. Marcos, R. Martínez-Máñez, F. Sancenón, J. Soto, L. A. Villaescusa, L. Gil and P. Amorós, *Chem. Eur. J.*, 2009, **15**, 9024-9033.
135. J. D. Watson, *Science*, 1963, **140**, 17-26.
136. M. C. Thompson and D. H. Busch, *J. Am. Chem. Soc.*, 1964, **86**, 213-217.
137. S. Anderson, H. L. Anderson and J. K. M. Sanders, *Acc. Chem. Res.*, 1993, **26**, 469-475.
138. B. Hasenknopf, J. M. Lehn, B. O. Kneisel, G. Baum and D. Fenske, *Angew. Chem., Int. Ed. Eng.*, 1996, **35**, 1838-1840.
139. X. Yang, C. B. Knobler and M. F. Hawthorne, *Angew. Chem., Int. Ed. Engl.*, 1991, **30**, 1507-1508.
140. Z. Zheng, C. B. Knobler and M. F. Hawthorne, *J. Am. Chem. Soc.*, 1995, **117**, 5105-5113.
141. R. L. Paul, Z. R. Bell, J. C. Jeffery, J. A. McCleverty and M. D. Ward, *Proc. Natl. Acad. Sci. U.S.A.*, 2002, **99**, 4883-4888.
142. S. P. Argent, T. Riis-Johannessen, J. C. Jeffery, L. P. Harding and M. D. Ward, *Chem. Commun.*, 2005, 4647-4649.
143. C. S. Campos-Fernández, B. L. Schottel, H. T. Chifotides, J. K. Bera, J. Bacsa, J. M. Koomen, D. H. Russell and K. R. Dunbar, *J. Am. Chem. Soc.*, 2005, **127**, 12909-12923.
144. E. A. Katayev, G. Dan Pantos, M. D. Reshetova, V. N. Khrustalev, V. Lynch, Y. A. Ustynyuk and J. L. Sessler, *Angew. Chem., Int. Ed.*, 2005, **44**, 7386-7390.
145. E. A. Katayev, N. V. Boev, V. N. Khrustalev, Y. A. Ustynyuk, I. G. Tananaev and J. L. Sessler, *J. Org. Chem.*, 2007, **72**, 2886-2896.
146. M. Bru, I. Alfonso, M. I. Burguete and S. V. Luis, *Angew. Chem., Int. Ed.*, 2006, **45**, 6155-6159.
147. I. Alfonso, M. Bolte, M. Bru, M. I. Burguete, S. V. Luis and J. Rubio, *J. Am. Chem. Soc.*, 2008, **130**, 6137-6144.
148. M. Bru, I. Alfonso, M. Bolte, M. I. Burguete and S. V. Luis, *Chem. Commun.*, 2010, **47**, 283-285.
149. H. Juwarker and K. S. Jeong, *Chem. Soc. Rev.*, 2010, **39**, 3664-3674.
150. S. J. Coles, J. G. Frey, P. A. Gale, M. B. Hursthouse, M. E. Light, K. Navakhun and G. L. Thomas, *Chem. Commun.*, 2003, 1462-1462.

151. H. Y. Gong, B. M. Rambo, E. Karnas, V. M. Lynch and J. L. Sessler, *Nat. Chem.*, 2010, **2**, 406-409.
152. B. Schulze, C. Friebe, M. D. Hager, W. Gunther, U. Kohn, B. O. Jahn, H. Gorls and U. S. Schubert, *Org. Lett.*, 2010, **12**, 2710-2713.
153. K. Zhu, L. Wu, X. Yan, B. Zheng, M. Zhang and F. Huang, *Chem. Eur. J.*, 2010, **16**, 6088-6098.
154. C. Dietrich-Buchecker and J.-P. Sauvage, eds., *Molecular Catenanes, Rotaxanes and Knots. A Journey Through the World of Molecular Topology*, Wiley-VCH, Weinheim, 1999.
155. M. Asakawa, P. R. Ashton, R. Ballardini, V. Balzani, M. Bělohradský, M. T. Gandolfi, O. Kocian, L. Prodi, F. M. Raymo, J. F. Stoddart and M. Venturi, *J. Am. Chem. Soc.*, 1997, **119**, 302-310.
156. K. D. Hänni and D. A. Leigh, *Chem. Soc. Rev.*, 2010, **39**, 1240-1251.
157. P. R. Ashton, S. R. L. Everitt, M. Gomez-Lopez, N. Jayaraman and J. F. Stoddart, *Tetrahedron Lett.*, 1997, **38**, 5691-5694.
158. J.-L. Ko, S.-H. Ueng, C.-W. Chiu, C.-C. Lai, Y.-H. Liu, S.-M. Peng and S.-H. Chiu, *Chem. Eur. J.*, 2010, **16**, 6950-6960.
159. E. Wasserman, *J. Am. Chem. Soc.*, 1960, **82**, 4433-4434.
160. I. T. Harrison and S. Harrison, *J. Am. Chem. Soc.*, 1967, **89**, 5723-5724.
161. J. P. Sauvage, *Acc. Chem. Res.*, 1990, **23**, 319-327.
162. J. D. Crowley, S. M. Goldup, A.-L. Lee, D. A. Leigh and R. T. McBurney, *Chem. Soc. Rev.*, 2009, **38**, 1530-1541.
163. C. A. Hunter, *J. Am. Chem. Soc.*, 1992, **114**, 5303-5311.
164. D. G. Hamilton, N. Feeder, L. Prodi, S. J. Teat, W. Clegg and J. K. M. Sanders, *J. Am. Chem. Soc.*, 1998, **120**, 1096-1097.
165. G. Brancato, F. Coutrot, D. A. Leigh, A. Murphy, W. J. K. Y. and F. Zerbetto, *Proc. Natl. Acad. Sci. U.S.A.*, 2002, **99**, 4967-4971.
166. G. Wenz, B.-H. Han and A. MÃ¼ller, *Chemical Reviews*, 2006, **106**, 782-817.
167. G. M. Hubner, J. Glaser, C. Seel and F. Vogtle, *Angew. Chem., Int. Ed.*, 1999, **38**, 383-386.
168. P. Ghosh, O. Mermagen and C. A. Schalley, *Chem. Commun.*, 2002, 2628-2629.
169. C. O. Dietrich-Buchecker, J. P. Sauvage and J. M. Kern, *J. Am. Chem. Soc.*, 1984, **106**, 3043-3045.
170. K. M. Mullen, J. Mercurio, C. J. Serpell and P. D. Beer, *Angew. Chem., Int. Ed.*, 2009, **48**, 4781-4784.
171. Y. Li, K. M. Mullen, T. D. W. Claridge, P. J. Costa, V. Felix and P. D. Beer, *Chem. Commun.*, 2009, 7134-7136.
172. D. B. Amabilino and J. F. Stoddart, *Chemical Reviews*, 1995, **95**, 2725-2828.
173. R. Jäger and F. Vögtle, *Angew. Chem., Int. Ed. Engl.*, 1997, **36**, 930-944.
174. A. Fernandes, A. Viterisi, F. Coutrot, S. Potok, D. A. Leigh, V. Aucagne and S. Papot, *Angew. Chem., Int. Ed.*, 2009, **48**, 6443-6447.
175. E. Arunkumar, C. C. Forbes, B. C. Noll and B. D. Smith, *J. Am. Chem. Soc.*, 2005, **127**, 3288-3289.
176. J. J. Gassensmith, L. Barr, J. M. Baumes, A. Paek, A. Nguyen and B. D. Smith, *Org. Lett.*, 2008, **10**, 3343-3346.
177. J. E. Green, J. W. Choi, A. Boukai, Y. Bunimovich, E. Johnston-Halperin, E. DeIonno, Y. Luo, B. A. Sheriff, K. Xu, Y. S. Shin, H. R. Tseng, J. F. Stoddart and J. R. Heath, *Nature*, 2007, **445**, 414-417.
178. K. Patel, S. Angelos, W. R. Dichtel, A. Coskun, Y. W. Yang, J. I. Zink and J. F. Stoddart, *J. Am. Chem. Soc.*, 2008, **130**, 2382-2383.

179. B. K. Juluri, A. S. Kumar, Y. Liu, T. Ye, Y. W. Yang, A. H. Flood, L. Fang, J. F. Stoddart, P. S. Weiss and T. J. Huang, *ACS Nano*, 2009, **3**, 291-300.
180. C. R. Thomas, D. P. Ferris, J. H. Lee, E. Choi, M. H. Cho, E. S. Kim, J. F. Stoddart, J. S. Shin, J. Cheon and J. I. Zink, *J. Am. Chem. Soc.*, 2010, **132**, 10623-10625.
181. H. A. Meng, M. Xue, T. A. Xia, Y. L. Zhao, F. Tamanoi, J. F. Stoddart, J. I. Zink and A. E. Nel, *J. Am. Chem. Soc.*, 2010, **132**, 12690-12697.
182. M. D. Wang, M. J. Schnitzer, H. Yin, R. Landick, J. Gelles and S. M. Block, *Science*, 1998, **282**, 902-907.
183. A. Landesberg, Y. Landesberg, S. Sideman and H. E. D. J. Ter Keurs, 972, 119., *Ann. N. Y. Acad. Sci.*, 2002, **972**, 119-126.
184. W. H. Mather and R. F. Fox, *Biophys. J.*, 2006, **91**, 2416-2426.
185. A. Livoreil, C. O. Dietrich-Buchecker and J. P. Sauvage, *J. Am. Chem. Soc.*, 1994, **116**, 9399-9400.
186. S. J. Vella, J. Tiburcio and S. J. Loeb, *Chem. Commun.*, 2007, 4752-4754.
187. J. Berná, M. Alajarin and R. A. Orenes, *J. Am. Chem. Soc.*, 2010, **132**, 10741-10747.
188. C. M. Keaveney and D. A. Leigh, *Angew. Chem., Int. Ed.*, 2004, **43**, 1222-1224.
189. K.-Y. Ng, V. Felix, S. M. Santos, N. H. Rees and P. D. Beer, *Chem. Commun.*, 2008, 1281-1283.
190. T. C. Lin, C. C. Lai and S. H. Chiu, *Org. Lett.*, 2009, **11**, 613-616.
191. M. K. Chae, J. M. Suk and K. S. Jeong, *Tetrahedron Lett.*, 2010, **51**, 4240-4242.
192. J. J. Gassensmith, S. Matthys, J. J. Lee, A. Wojcik, P. V. Kamat and B. D. Smith, *Chem. Eur. J.*, 2010, **16**, 2916-2921.

# Chapter 2: Synthesis of Interlocked Structures for Chloride Recognition in Aqueous Solvent Media

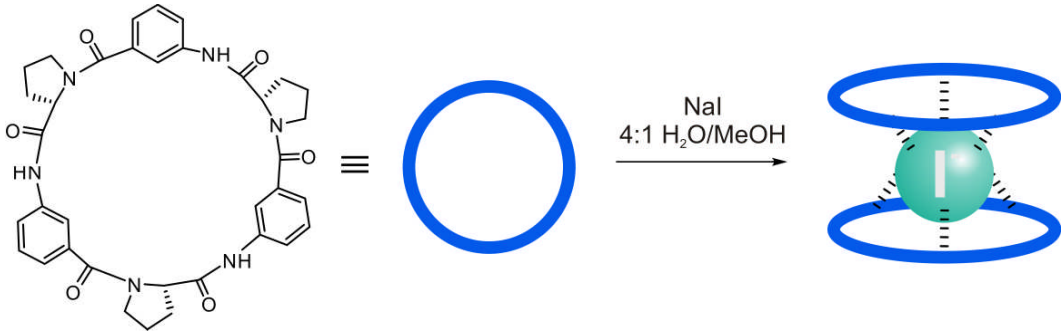
## 2.1 Introduction

### 2.1.1 Anion Recognition in Water

In recent years a multitude of receptors have been reported that demonstrate impressive affinities for anions in organic solvent media.[1] Despite this, great interest has evolved in designing host molecules for recognition of anions in aqueous solvent media for potential use in detection of biologically relevant molecules and environmental pollutants.[2] In order to achieve this, the anion's high energy of hydration must be overcome to ensure binding to the host molecule is energetically favourable. Naturally occurring proteins demonstrate that this is achievable by 'burying' the binding pocket deep within the protein structure, utilising convergent hydrogen bonds for strong and selective anion binding.[3, 4] Surrounded by lipophilic organic fragments, this pocket is shielded from the bulk solvent, increasing the efficacy and strength of anion complexation. To achieve comparable strengths of anion binding in synthetic receptors, it is necessary for chemists to take inspiration from these natural systems, and design three-dimensional structures with solvent-protected cavities.

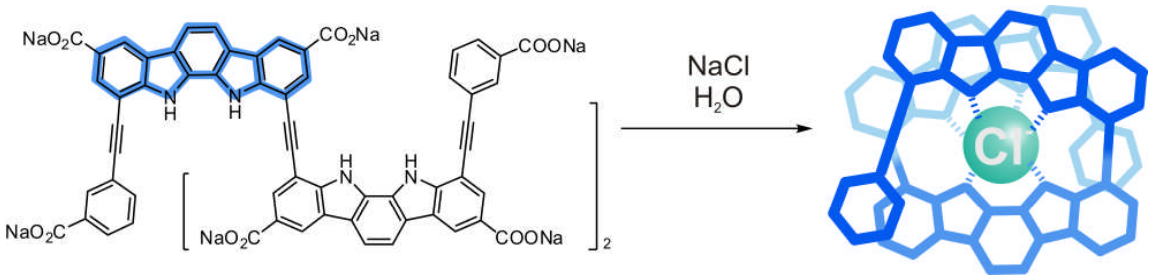
To this end, Kubik *et al*. have synthesised a cyclic hexapeptide macrocycle that complexes sulfate and halide anions with 2:1 binding stoichiometry in 80% aqueous solvent media (Scheme 2.1).[5] Crystallographic evidence of the iodide salt shows the anion residing between two macrocyclic components, resembling a molecular capsule, where binding occurs *via* hydrogen bonding interactions with the six amide groups. Microcalorimetric investigations indicate that entropy governs the binding of the anion within the cavity created by the two

macrocycles, where the anion is released from solvent during complex formation, and is then shielded from the surrounding solvent when complexed.




***Scheme 2.1.*** *Association of peptide macrocycles around an iodide ion to form a 'molecular capsule'.*[5]

More recently Jeong and co-workers have linked three indolocarbazole units to create a foldamer structure, possessing an internal cavity capable of chloride complexation in pure water.[6] The helical conformation of the structure provides a tubular cavity, where again the anion is shielded from competing solvent molecules (Scheme 2.2).



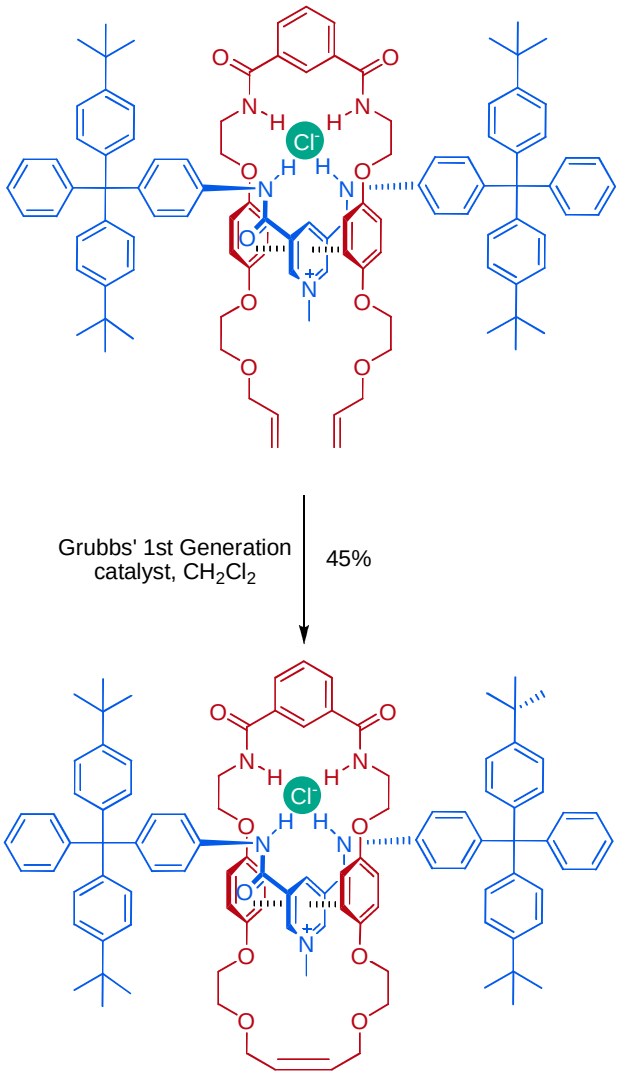

***Scheme 2.2.*** *Jeong's indolocarbazole foldamer.*[6]

A strategy for creating a protected binding environment for the selective complexation of anions, employed by the Beer group, utilises mechanically interlocked structures containing a three-dimensional binding cavity. The synthesis of these structures and their potential as receptors for anions is discussed in the next section.

### 2.1.2 Mechanically Interlocked Structures

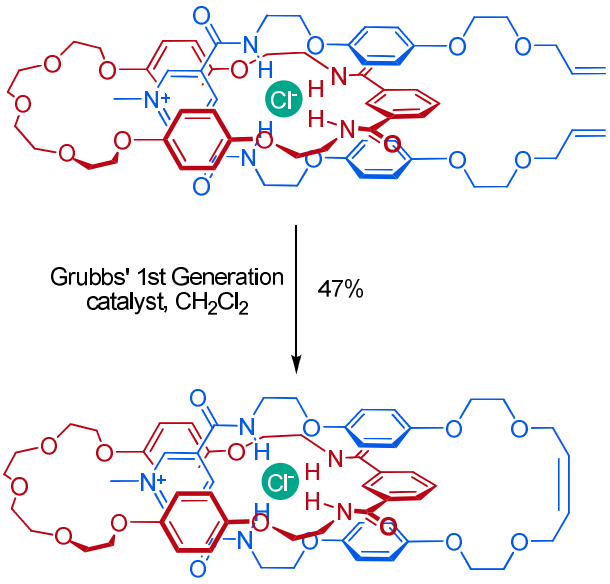
The construction of interlocked molecules, such as catenanes and rotaxanes, is invariably less trivial than classical organic synthesis, and relies on templation for the assembly of

components (Chapter 1). For a number of years the Beer group has employed a successful anion templation strategy for the synthesis of rotaxanes (Scheme 2.3) and catenanes (Scheme 2.4) incorporating Crabtree's halide binding isophthalamide unit, and a new 3,5-bis-amide substituted pyridinium analogue.[7-9]




***Scheme 2.3.*** *Synthesis of a [2]rotaxane via Grubbs' RCM reaction.*[7]

The positively charged pyridinium unit complexes a chloride anion whose unsaturated coordination sphere allows for the orthogonal binding of a second species containing the isophthalamide unit. Ring closing metathesis (RCM) using Grubbs' catalyst is used to form the interlocked species, with π-π stacking interactions stabilising the structures.




***Scheme 2.4.*** *Synthesis of a [2]catenane via Grubbs' RCM reaction.*[8]

Upon removal of the templating halide anion, these structures were observed to have a strong binding affinity for chloride in a competitive 1:1 $CDCl_3/CD_3OD$ solvent mixture, whilst the more basic oxoanions ($H_2PO_4^-$ and $OAc^-$) were bound weakly. This selectivity is attributed to the complementary size and shape of the interlocked cavity for the chloride anion, and opposes the trend predicted on basicity grounds.

While the use of Grubbs' catalyst for the synthesis of interlocked structures has been successful for a variety of systems, its expense makes it desirable to explore alternative synthetic routes. In addition Grubbs' catalyst is unsuitable for use in reactions where a component contains a ligating functional group such as pyridyl. It appears that such groups are capable of complexing to the ruthenium centre of the catalyst thus disrupting the catalytic cycle.

### 2.1.3 Chapter Objectives

With the disadvantages of Grubbs' catalyst in mind, this chapter details the development of a new synthetic strategy, combining anion templation and π-π stacking, for the formation of rotaxanes. The versatility of this new route will be explored by systematically altering the

size, geometry and electronic nature of the macrocyclic wheel component, with particular focus on the impact these alterations have on yield of rotaxane formation.

The target rotaxane host systems are shown in Figure 2.1, displaying the three-dimensional binding cavity. Importantly, the ability of these new rotaxanes to act as hosts for anionic guest species in competitive aqueous solvent mixtures will be studied. By implementing the aforementioned variations in the macrocyclic component of the rotaxane it may be possible to tune the three-dimensional binding cavity for stronger anion recognition and greater selectivity.

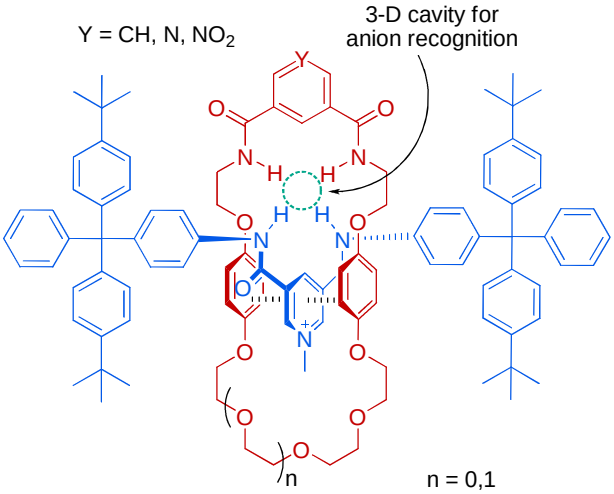



***Figure 2.1.*** *Example of target rotaxane, containing an anion binding cavity.*

Finally, the new synthetic pathway is exploited further in the construction of [2]catenanes, and the anion recognition properties of the new structures are also explored.

## 2.2 Macrocyclic Components

Macrocycles are a key component of both rotaxanes and catenanes, and their design for incorporation into these interlocked systems requires careful consideration. The formation of rotaxanes and catenanes is driven by a number of intermolecular forces that act to stabilise the interlocked assembly, and the target macrocycle contains a number of moieties to enable

favourable interactions with an appropriate π-electron deficient ion pair component (Figure 2.2).

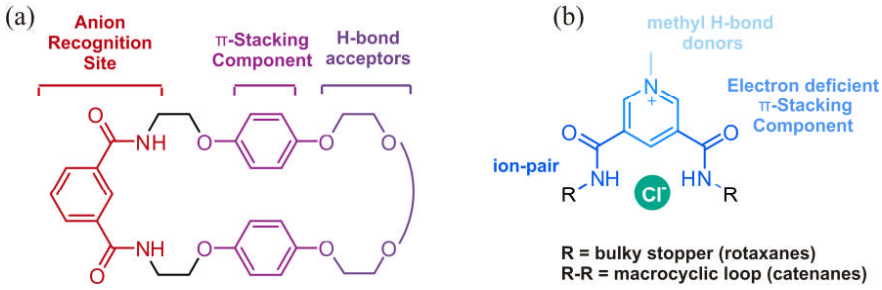



***Figure 2.2.*** *(a) Target macrocyclic component, and (b) ion-pair species.*

The isophthalamide group provides a recognition site for chloride,[10] whilst the electron rich hydroquinone aromatic groups can undergo π-π stacking with an appropriate electron deficient aromatic surface to stabilise the interlocked structure. Additional stabilisation may arise from hydrogen bonding interactions between the polyether chain of the neutral macrocyclic component and the pyridinium *N*-methyl group of the ion-pair species.

Despite the importance of these macrocyclic components, their synthesis within the Beer group has always presented a challenge, invariably involving lengthy multiple-step syntheses giving poor yields of the final product. The target macrocycles for inclusion in anion-templated interlocked and interpenetrated structures have been synthesised by two main routes in recent years, highlighted in Figure 2.3.[11, 12]

Both procedures involve traditional high dilution techniques where the two macrocycle precursor reactants are slowly added to a large volume of solvent. In a dilute solution an intramolecular reaction to form a cyclic product is more likely than various separate reactants colliding to form oligomeric side products.[13]

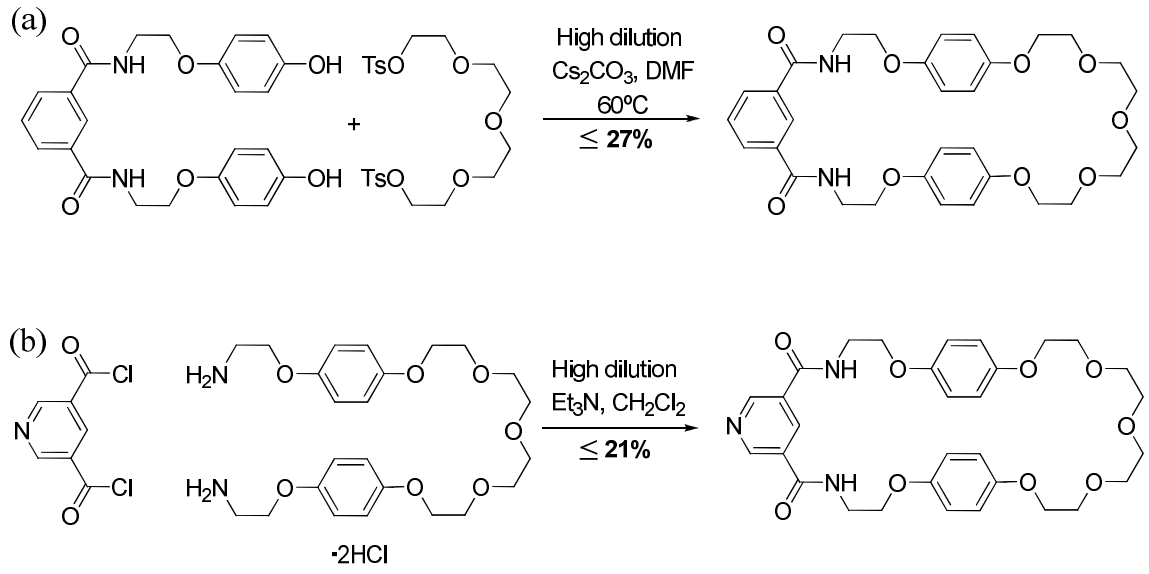
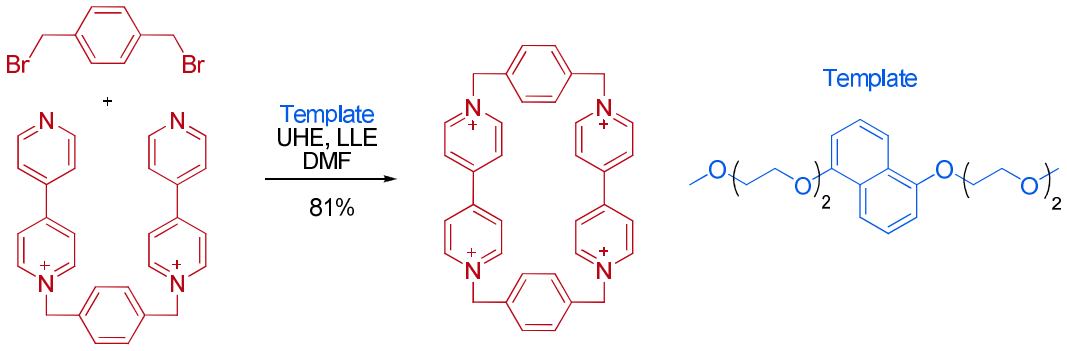



***Figure 2.3.*** *Synthetic pathways for the formation of macrocycles using high dilution conditions.*

It is necessary for route (a) to be carried out at elevated temperatures due to the limited solubility of the bis-phenol appended isophthalamide precursor, which can favour the aforementioned oligomeric side-products by increasing the entropy of the system. This factor may be responsible for the relatively low yield of the reaction, deemed to be notoriously unreliable with yields ranging from 0 – 27%. Route (b), developed slightly later, did not prove much more rewarding, with a maximum yield of 21% for macrocycle formation. Since the successful formation of macrocycles is a crucial factor in this project, it was important to employ a different strategy for their synthesis. It should also be noted that using the large volumes of organic solvent necessary for high dilution conditions is neither cost-effective nor environmentally friendly.

Supramolecular chemists have been employing metal cation templates for the synthesis of macrocycles since the revolutionary work of Busch in the 1960s,[14-16] whilst Stoddart has used a variety of electron rich organic templates to enhance the yield of formation of the tetracationic 'box'. The template providing the greatest enhancement in yield is a napthoquinone derivative, and its prolific templating effect is attributed to a combination of

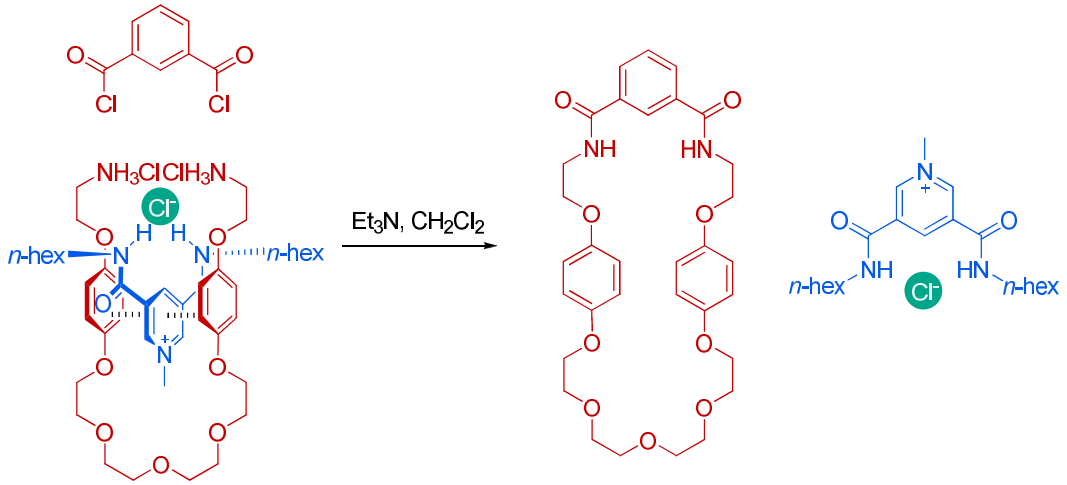
electrostatics and π-π stacking, as well as its complementary size match for the macrocycle (Scheme 2.5).[17]




***Scheme 2.5.*** *Synthesis of Stoddart's tetracationic 'box' via templation with naphthoquinone derivative.*[17]

To a lesser degree anions have also been used in the templation of macrocycles.[18-20]

The target macrocycles have been observed to form stable pseudorotaxane assemblies with an electron deficient pyridinium thread component, when in the presence of a chloride anion.[11]

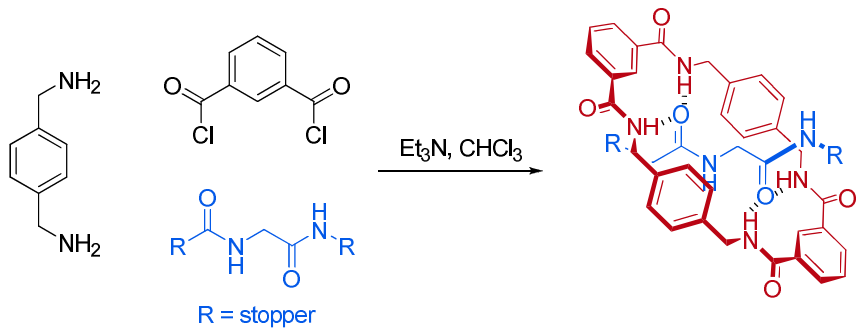



***Scheme 2.6.*** *Proposed macrocycle synthesis using pyridinium ion-pair template.*

It was thought that the strength of this association could be exploited to template the formation of the target macrocycles, from suitable precursors. It was decided that acid chloride-amine condensation route (b) would be more appropriate for this synthetic method since route (a) necessitated the use of elevated temperatures which is entropically unfavourable for the association of a template with macrocycle precursors. Also this pyridinium cation-chloride anion templating strategy would be aided by charge-assisted π-π

stacking interactions between the electron rich hydroquinone rings and the electron deficient pyridinium surface (Scheme 2.6).

Interestingly, an analogous templating strategy was employed by Leigh *et al.*, who showed that by taking a simple bis-amine and isophthaloyl dichloride in the presence of a stoppered dipeptide template it was possible to form [2]rotaxanes in good yields *via* a hydrogen bond directed 'clipping' strategy (Scheme 2.7).[21] In related work, it was shown that the free macrocyclic component could be isolated when the stopper contained an ester linkage, which could be subjected to transesterification conditions to disassemble the interlocked structure.[22]




***Scheme 2.7.*** *Synthesis of dipeptide rotaxane via a hydrogen bond directed clipping strategy. Cleavage of the bulky stopper groups yields the free macrocycle.*[22]

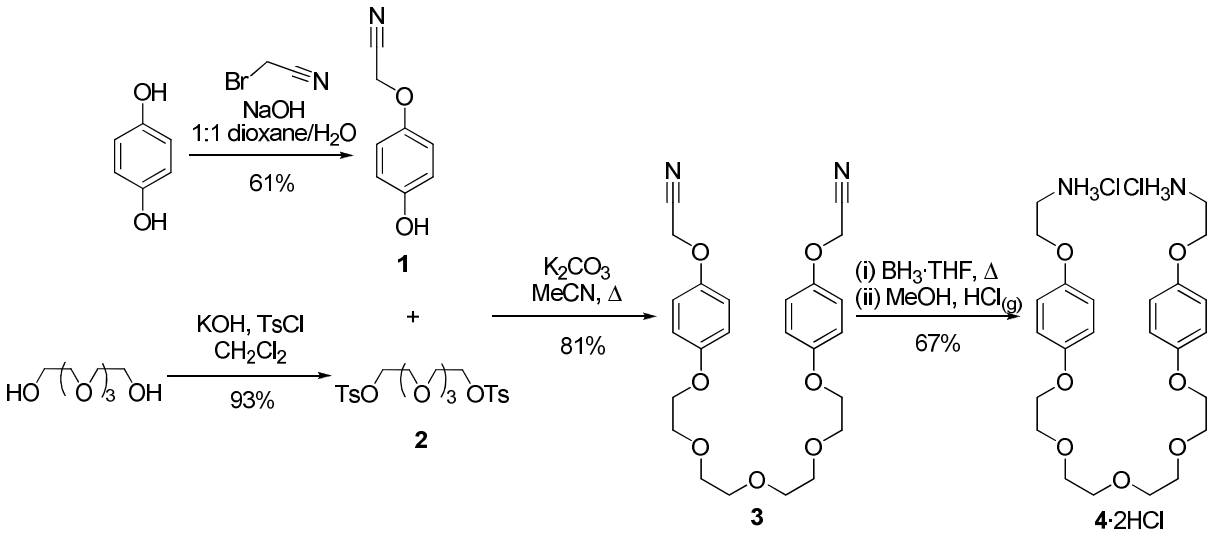
In the proposed pyridinium chloride ion-pair templating strategy the anion is envisaged to be a substitute for the electron rich carbonyl oxygen in Leigh's system, which should partake in similar hydrogen bonding interactions with the isophthalamide binding unit during the reaction to form a macrocycle.

### 2.2.1 Synthesis of Macrocycles

All compounds in this section are characterised by $^{1}$H NMR, and $^{13}$C NMR and HRMS (ESI) where novel.

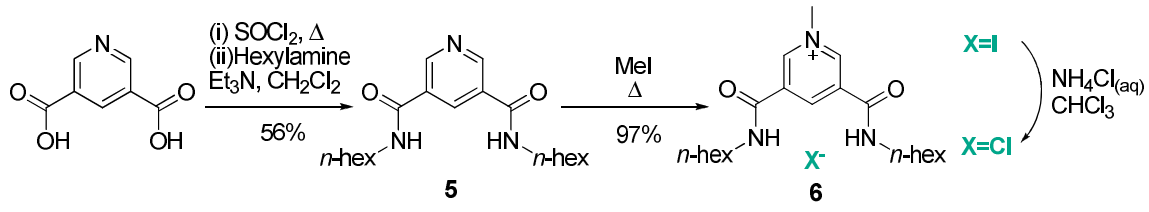
The synthesis of the bis-amine macrocycle precursor **4**·2HCl[12] is depicted in Scheme 2.8, and began with the monofunctionalisation of hydroquinone with bromoacetonitrile in the presence of NaOH in a water/dioxane mixture to give compound **1** in 61% yield. Tosylation of

tetraethylene glycol using KOH and tosyl chloride in $CH_2Cl_2$ gave **2** in 93% yield which was then coupled with two equivalents of **1** by heating at reflux in MeCN with $K_2CO_3$. Compound **3** was reduced using borane in THF, and **4** was purified by precipitating as the hydrogen chloride salt to give compound **4**·2HCl in 67% yield.




***Scheme 2.8.*** *Synthesis of bis-amine macrocycle precursor.*

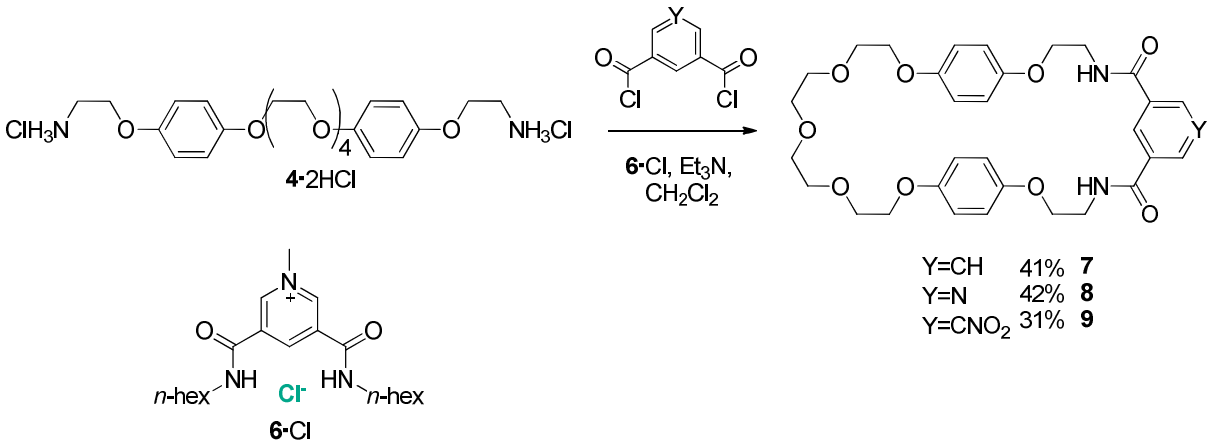
The 3,5-pyridinium bis-amide template[11] was synthesised according to Scheme 2.9. 3,5-Pyridine dicarboxylic acid was converted to the corresponding acid chloride by heating at reflux in $SOCl_2$. This was then used immediately in the condensation reaction with hexylamine in the presence of $Et_3N$ in $CH_2Cl_2$ to give **5** in 56% yield. Alkylation using iodomethane gave **6**·I in 97% which was then converted to the target template **6**·Cl by washing with aqueous $NH_4Cl$.




***Scheme 2.9.*** *Synthesis of pyridinium template.*

With both the bis-amine macrocycle precursor **4**·2HCl and the template **6**·Cl in hand, it was possible to attempt macrocyclisation reactions (Scheme 2.10). The bis-amine **4**·2HCl, was

stirred with a large excess of $Et_3N$ in $CH_2Cl_2$ with **6**·Cl until all material had dissolved, followed by the addition of the appropriate acid chloride. Following acidic aqueous workup, the material was subjected to column chromatography where removal of the pyridinium template component proved facile and the target macrocycles **7**, **8** and **9** were isolated in 41%, 42% and 31% yield respectively.




***Scheme 2.10.*** *Synthesis of macrocycles via a templation methodology.*

This was extremely pleasing since using the same starting materials, only omitting the pyridinium chloride template resulted in macrocycle **8** forming in only 21% yield. By introducing the template it has been possible to double the yield of the final step of this macrocyclisation. The slightly lower yield of macrocycle **9** is attributed to purification problems due to contamination with a side product from the reaction which may be the [2 + 2] macrocycle.

### 2.2.2 Pseudorotaxane Formation

Following the isolation of macrocycle **8**, a $^1$H NMR pseudorotaxane study was carried out in order to determine the strength of association with the pyridinium thread component **6**·Cl in the deuterated equivalent of the reaction solvent $CH_2Cl_2$. Macrocycle **8** is of particular interest since it has not previously been possible to synthesise interlocked structures with pyridine containing components due to the limitations of Grubbs' catalyst. The formation of this

proposed pseudorotaxane was probed by $^{1}$H NMR titration, whereby a solution of **6**·Cl is added in aliquots to a solution of **8** whilst the chemical shift perturbations are monitored for evidence of interpenetrated structure formation (Figure 2.4).

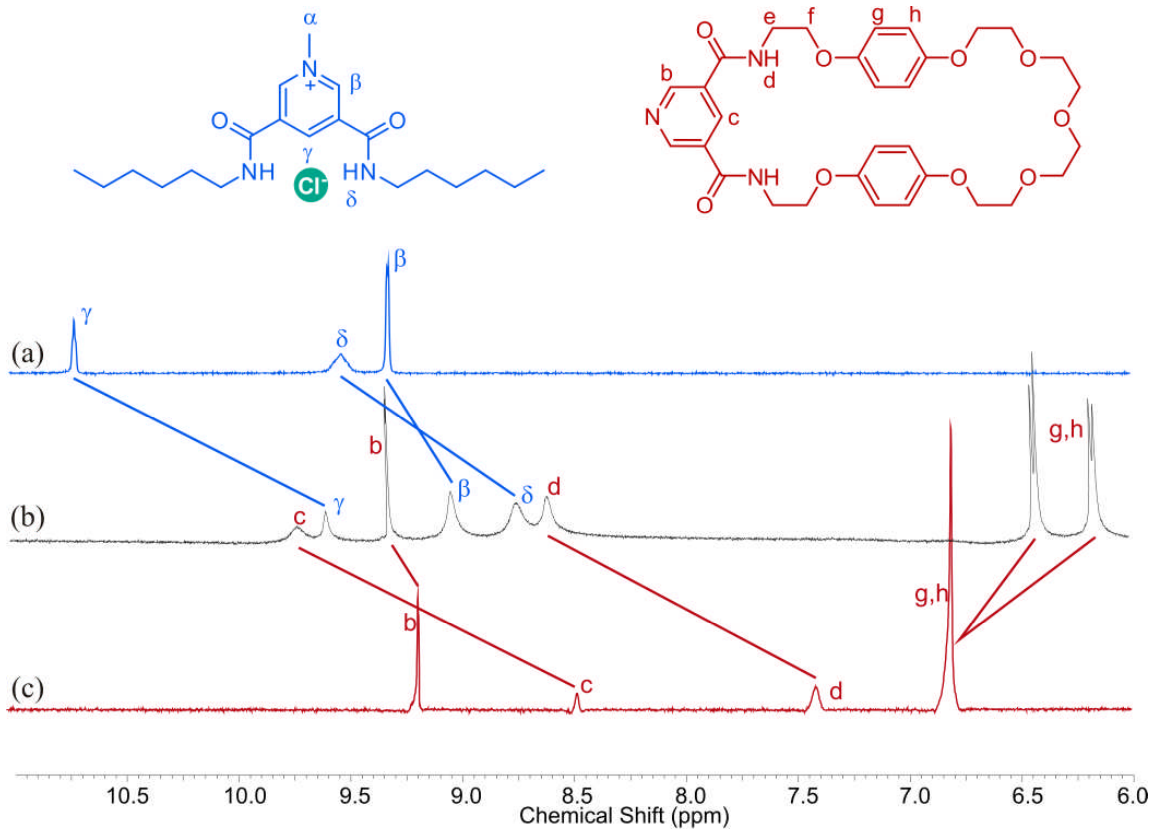



***Figure 2.4*** *$^{1}$H NMR in $CD_2Cl_2$ at 293K of (a) pyridinium thread* ***6***·*Cl, (b) 'pseudorotaxane', 1:1 macrocycle* ***8****/pyridinium thread* ***6***·*Cl, and (c) macrocycle* ***8****.*

Since there is strong ion-pairing between the pyridinium threading component and its chloride counteranion, they are assumed to remain associated throughout the titration. Addition of **6**·Cl to macrocycle **8** resulted in perturbations of a number of signals corresponding to protons directly involved in pseudorotaxane formation which is observed to be fast on the NMR timescale. Downfield shifts of signals corresponding to macrocycle cavity protons *d* and *c* signify binding of chloride within the cleft, and this process is further demonstrated in the upfield shifts of the thread cavity protons $\gamma$ and $\delta$ as the chloride becomes polarized away from this unit. Whilst examination of these aforementioned cavity protons of both macrocycle and thread are useful indicators for pseudorotaxane formation, abstraction of the chloride

anion by the macrocycle can also be responsible for these chemical shift perturbations. It is therefore more reliable to use the chemical shift perturbations of the macrocycle hydroquinone protons to probe interpenetrated structure assembly since any changes can only be the result of pseudorotaxane formation. In this case, both signals corresponding to these protons are observed to move significantly upfield ($\Delta\delta$ = –0.38 ppm and $\Delta\delta$ = –0.64 ppm for protons *g* and *h* respectively at 1:1 **8**/**6**·Cl) which is indicative of π-π stacking interactions with the electron deficient pyridinium surface.

The chemical shift perturbations of hydroquinone protons *g* and *h* were monitored as a function of the amount of **6**·Cl added, to give the titration curves displayed in Figure 2.5. Using the computer programme winEQNMR2[23] it should be possible to obtain an association constant for pseudorotaxane formation from this titration data. However this association proved to be greater than the limits for winEQNMR2 (i.e. $K > 10^4$ $M^{-1}$) indicating that this pseudorotaxane assembly is extremely stable in non-competitive solvents such as $CH_2Cl_2$.

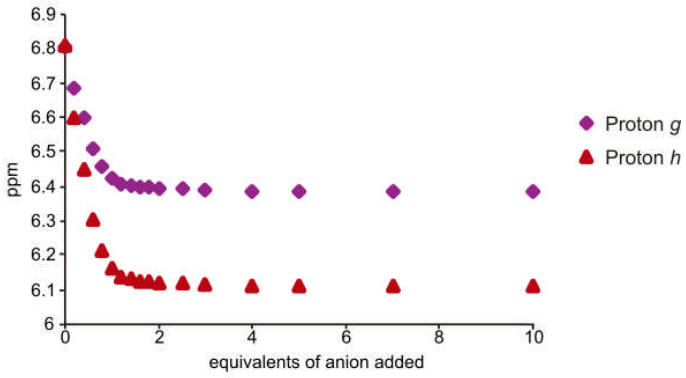



***Figure 2.5.*** *Change in chemical shift of protons g and h on addition of pyridinium thread* ***6***·*Cl to a solution of macrocycle* ***8*** *in* $CD_2Cl_2$ *at* $3.08\times 10^{-3}$ *M and 293 K.*

Given this result, and the success using the pyridinium component **6**·Cl as a template for the formation of macrocycles, it was anticipated that a similar synthetic procedure could be utilised for the synthesis of rotaxanes by replacing the thread component with an appropriate stoppered axle.

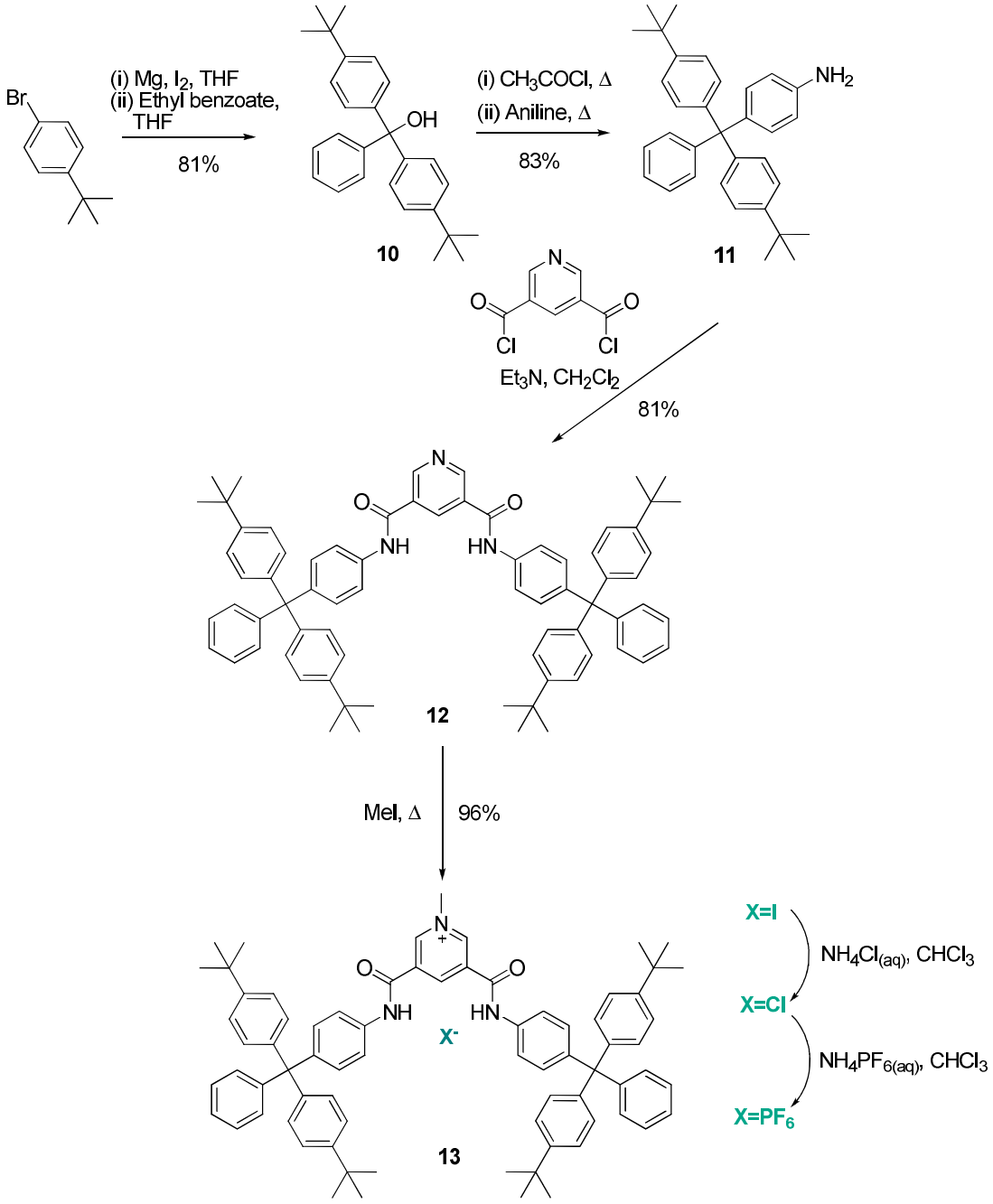
# 2.3 Synthesis, Characterisation and Anion Recognition Properties of Novel [2]Rotaxanes

All novel compounds described in the remainder of this chapter are characterised by $^{1}H$ and $^{13}C$ NMR and HRMS (ESI).

## 2.3.1 Synthesis of Axle Component

Before embarking on rotaxane synthesis, it was necessary to synthesise an appropriate pyridinium containing axle component. An axle previously utilised in successful rotaxane formation was chosen, the synthesis of which is depicted in Scheme 2.11.[7]

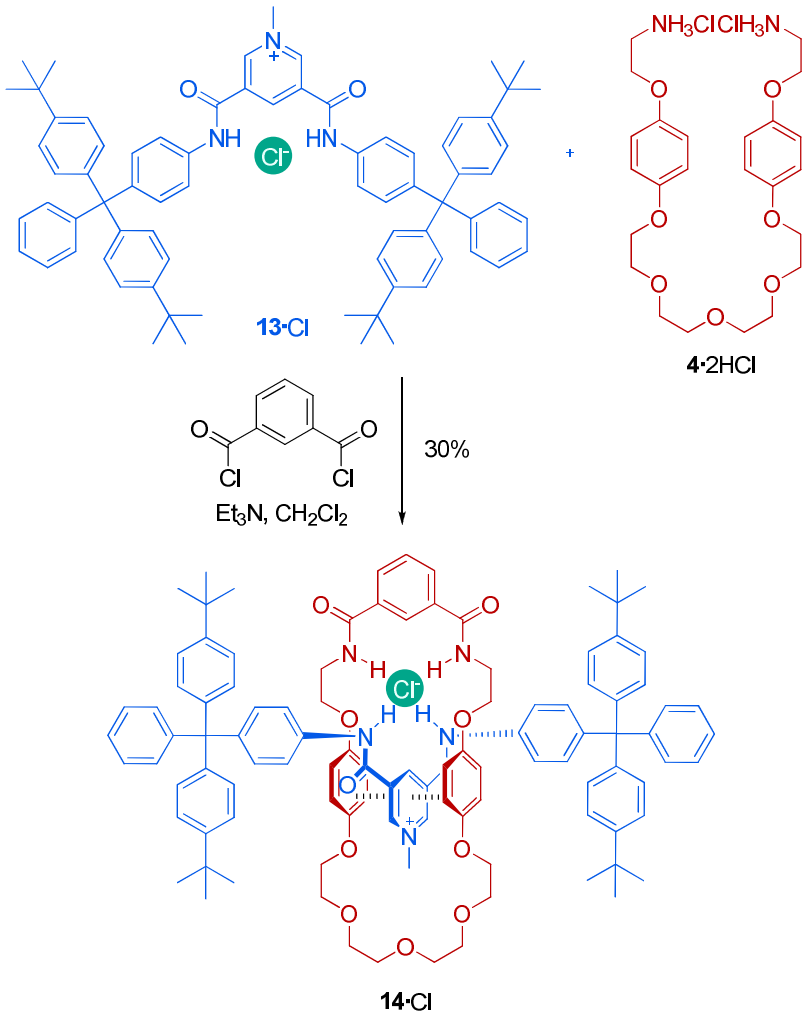
1-Bromo-4-*tert*-butylbenzene was converted to the Grignard intermediate by reacting with magnesium in the presence of iodine in THF, before ethyl benzoate was added, and the reaction heated under reflux to give **10** in 81%. This was then heated in acetyl chloride, followed by reaction with aniline at 105 ºC to give the stopper group **11**[24] in 83% yield. Condensation of 3,5-bis(chlorocarbonyl) pyridine in $CH_2Cl_2$ with two equivalents of **11** produced the pyridine bis-amide **10**, in 81%, which was alkylated in 96% yield using iodomethane. It was possible to convert the axle **13**·I to the chloride and hexafluorophosphate salts by washing a solution of **13**·I with an aqueous solution of the corresponding ammonium salts.




***Scheme 2.11.*** *Synthesis of axle component* ***13****.*

## 2.3.2 Trial Rotaxane Synthesis

With the necessary precursor components in hand, attempts to prepare a [2]rotaxane *via* the novel synthetic route, shown in Scheme 2.12, were undertaken.




***Scheme 2.12.*** *Synthesis of [2]rotaxane* ***14****·Cl.*

Conditions similar to those employed in the templated synthesis of macrocycle **7** – **9** were used, where the precursors **13**·Cl and **4**·2HCl were stirred for thirty minutes with a large excess of $Et_3N$ in order to deprotonate and thus solubilise **4**·2HCl. Commercially available isophthaloyl dichloride was added to the solution, which was then stirred for one hour. Following acidic work-up and preparative TLC it was possible to isolate the target rotaxane was isolated in a reasonable yield of 30%.

During purification of the rotaxane by preparative TLC it was noted that there were numerous fluorescent yellow by-products, none of which corresponded to axle or macrocyclic components. It proved impossible to elucidate the structures of any of these by-products by $^1$H NMR or mass spectrometry (ESI), and given the colour it was proposed that they arise

from decomposition of the axle component **13**·Cl during the reaction. In order to assess this theory, the axle was added to separate $CH_2Cl_2$ portions of the other reaction components, bis-amine **4**·2HCl, isophthaloyl dichloride and $Et_3N$. TLC analysis revealed no effect with either **4**·2HCl or isophthaloyl dichloride, however almost instantaneously several new highly fluorescent spots were observed in the TLC of the mixture of **13**·Cl and $Et_3N$. Given pyridinium's known susceptibility to nucleophiles[25, 26] it is postulated that the decomposition occurs *via* nucleophilic attack at the *para* position. It was thought a more hindered base such as DIPEA may not cause such decomposition, but unfortunately the same highly fluorescent species were also observed when this base was used instead. To solve this problem, and potentially increase the yield of the rotaxanation reaction, it was necessary to minimise the amount of time that the axle component remained in solution with $Et_3N$. This could be achieved if the free amine **4** was isolated before the reaction, and $Et_3N$ was added immediately before the acid chloride. The results of this new synthetic rotaxanation protocol are discussed in the next section.

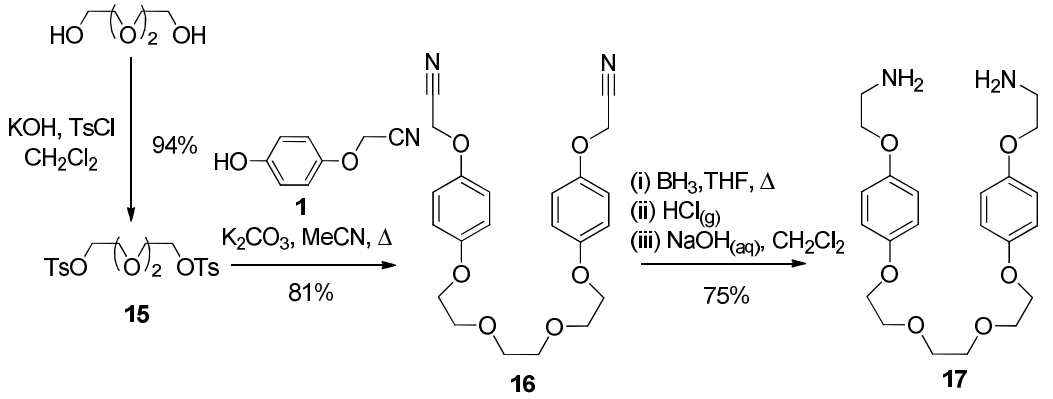
### 2.3.3 Synthesis and Characterisation of Novel Monocationic Rotaxanes

Following the successful synthesis of rotaxane **14**·Cl *via* a new methodology, and with the ultimate objective of tuning the three-dimensional binding cavity for strong and selective anion recognition, the versatility of this route was investigated.

The anion binding unit could be varied both electronically, by altering the substituents of the isophthalamide unit, whilst the size of the macrocycle can be reduced by altering the length of the polyether chain. More ambitiously, it may be possible to influence π- π stacking events by incorporating a more electron rich polyaromatic π system.

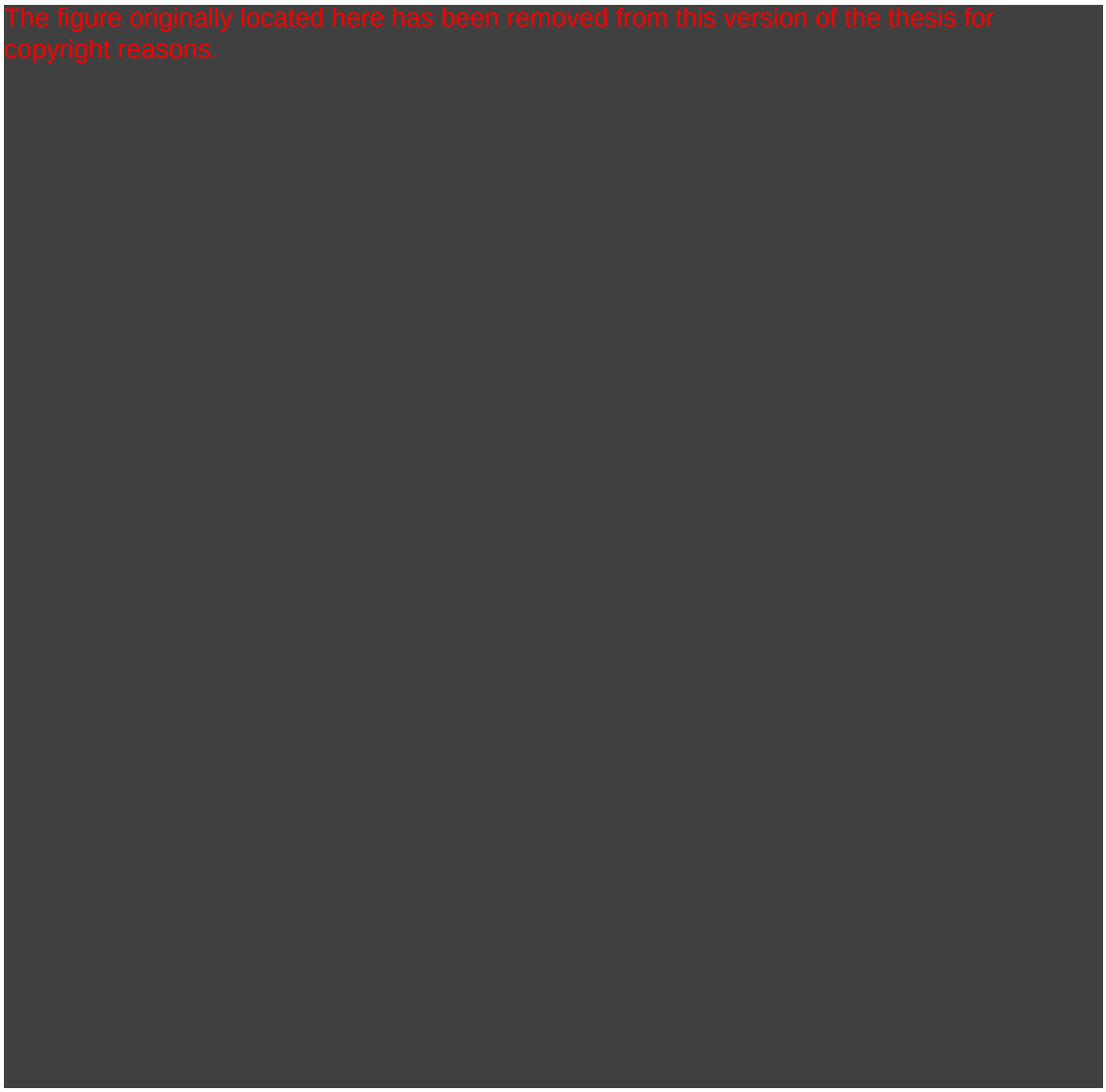
In order to synthesise rotaxanes with a smaller macrocyclic component a bis-amine precursor with a four-oxygen containing polyether chain was prepared (Scheme 2.13).

Triethylene glycol was converted to the corresponding bis-tosylate by reaction with tosyl chloride in the presence of potassium hydroxide in $CH_2Cl_2$ to give **15**[27] in 94% yield which was then reacted with compound **1** by heating with $K_2CO_3$ in MeCN to give **16** in 81% yield. Reduction to the bis-amine **17** was achieved by heating with borane in THF and was purified by precipitating as the hydrogen chloride salt. The free bis-amine **17** along with its five-oxygen polyether analogue **4** was obtained by washing with aqueous NaOH.




***Scheme 2.13.*** *Synthesis of smaller bis-amine precursor **17**.*

Following isolation of these target bis-amine precursors, a range of rotaxanes containing isophthalamide, 3,5-bis-amide pyridine and nitro-substituted isophthalamide macrocyclic anion recognition groups were prepared. The synthesis of six novel rotaxanes is outlined in Scheme 2.14. The free bis-amine component (either **4** or **17**) was stirred with the axle **13**·Cl for ten minutes in dry $CH_2Cl_2$, followed sequentially by addition of 2.5 equivalents of $Et_3N$ and the appropriate bis-acid chloride. After acidic workup and preparative TLC the six novel rotaxanes were isolated in yields of between 36 and 60%. Importantly, modification of the synthetic procedure by significantly reducing the amount of $Et_3N$ used in the reaction has resulted in an increase in the yield of rotaxane **14**·Cl to 60%.




***Scheme 2.14.*** *Synthesis of [2]rotaxane.*

It is noteworthy that the yield for the formation of the five-oxygen polyether containing rotaxanes is notably higher than those of the four-oxygen polyether rotaxane analogues. This may be attributed to unfavourable steric interaction between the pyridinium *N*-methyl group and the four-oxygen polyether chain. Further insight into this theory is obtained from MD simulations which are discussed later.

Evidence for [2]rotaxane formation was initially obtained by $^{1}$H NMR. The $^{1}$H NMR spectrum of rotaxane **14**·Cl, along with spectra of the component axle **13**·Cl and macrocycle **7** are given in Figure 2.6.




***Figure 2.6.*** *$^{1}H$ NMR in $CDCl_3$ at 293K of (a) axle **13**·Cl (b) [2]rotaxane **14**·Cl and (c) macrocycle **7**.*

The [2]rotaxane **14**·Cl displays considerable upfield shifts of the amide $\delta$ and para pyridinium proton $\gamma$ corresponding to polarisation of the chloride anion away from the binding cleft as a result of halide anion recognition by the macrocycle's isophthalamide cavity. This is further signified by downfield shifts of the amide *d* and cavity isophthalamide proton *c* as they become deshielded by the halide's negative charge. The proton signal associated with the hydroquinone environments, *g* and *h*, of the macrocycle has moved upfield and split appreciably which is characteristic of π-π donor-acceptor interactions between the electron rich hydroquinones and the positively charged electron deficient pyridinium motif. Finally, the signal corresponding to the methyl protons $\alpha$, of the pyridinium axle has moved

significantly upfield, indicative of hydrogen bonding between these protons and the oxygens of the macrocycle's polyether chain.

Further confirmation of the interlocked nature of [2]rotaxane **14**·Cl was obtained by 2D ROESY NMR (shown in Figure 2.7).

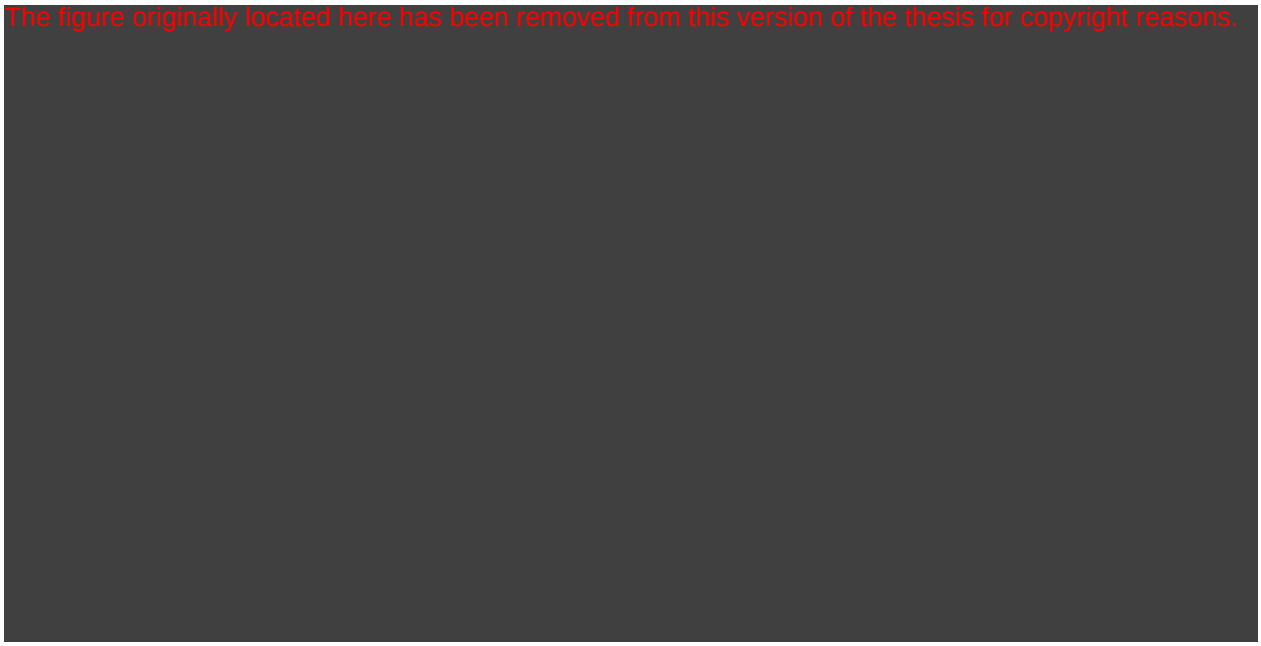



***Figure 2.7.*** *$^{1}H$ -$^{1}H$ ROESY spectrum of [2]rotaxane **14**·Cl in $CD_2Cl_2$ at 293K. Cross couplings are shown on the schematic diagram on the right.*

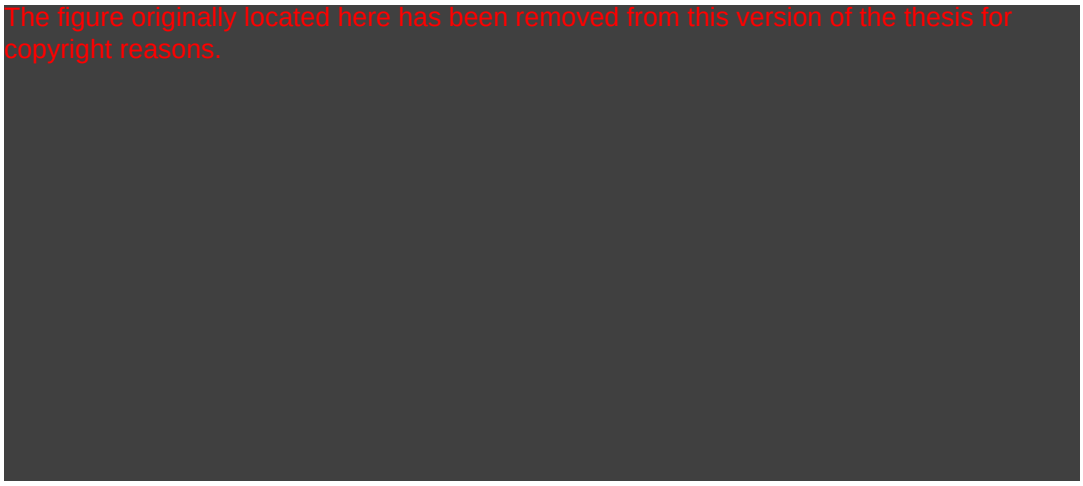
The $^{1}$H NMR ROESY spectrum displays a number of through-space correlations between the two separate components of the [2]rotaxane. Important interactions include **4** ($\beta \rightarrow g,h$) and **3** ($\delta \rightarrow g,h$), characteristic of π-π stacking between the protons of the electron rich hydroquinone unit and electron deficient pyridinium unit suggesting the axle component is threaded through the annulus of the macrocycle. Interaction **6** ($\delta \rightarrow d$) confirms the cavity amide protons are in close proximity as they converge into the binding domain to complex chloride. NOEs **5** ($\varepsilon \rightarrow g,h$), **7** ($\varepsilon \rightarrow c$), and **8** ($\varepsilon \rightarrow d$), indicate the axle stoppers are close in space to both the macrocycle cavity and hydroquinone protons, confirming the axle resides in the macrocycle in the orientation depicted. Finally, interactions **1** ($\alpha \rightarrow f,i\text{-}l$) and **2** ($\alpha \rightarrow g,h$) reveal the pyridinium methyl protons are in close proximity to both the polyether chain of the

macrocycle (through hydrogen bonding interactions previously described), and also the hydroquinone protons.

Further variation of the anion binding unit of the macrocyclic component was achieved by incorporating a sulfonamide motif into the [2]rotaxane. Since sulfonamides (p$K_a \approx 9 - 10$) are about 5 p$K_a$ units more acidic than amides (p$K_a \approx 14 - 15$), their hydrogen bond donating ability is amplified and consequently a rotaxane containing such a group may display a increased affinity for anions.

The synthesis of this rotaxane was carried out under analogous conditions described in Scheme 2.14, using benzene-1,3-disulfonyl dichloride as the 'clipping' component, and is shown in Scheme 2.15.

A noticeably lower yield was obtained for the formation of rotaxane **23**·Cl, indicating that the chloride template is playing a less efficient role in this synthesis which may also be a consequence of benzene-1,3-disulfonyl dichloride having slightly different geometric requirements than its isophthalamide analogues. Interestingly, Crabtree *et al.* observed weaker anion binding of their sulfonamide receptors compared to the isophthalamide systems,[28] a factor that also supports the lower rotaxane yield observed here, and may result in this rotaxane being a weaker complexant of anions compared to related isophthalamide systems, despite their enhanced hydrogen bond donor ability.




***Scheme 2.15.*** *Synthesis of sulfonamide containing rotaxane* ***23****·Cl.*

In addition to varying the electronic properties of the macrocycle's anion binding unit, geometric requirements for the new synthetic route were tested by attempting the preparation of *ortho* and *para* aryl amide containing [2]rotaxanes. The acid chlorides used in the 'clipping' step of the rotaxanation reaction, along with the original isophthaloyl dichloride are shown in Figure 2.8.

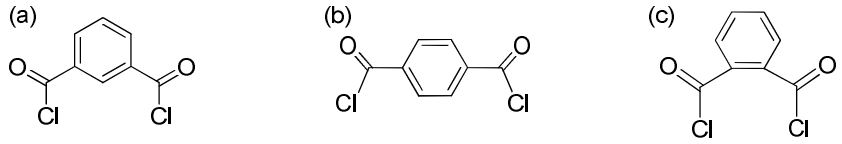


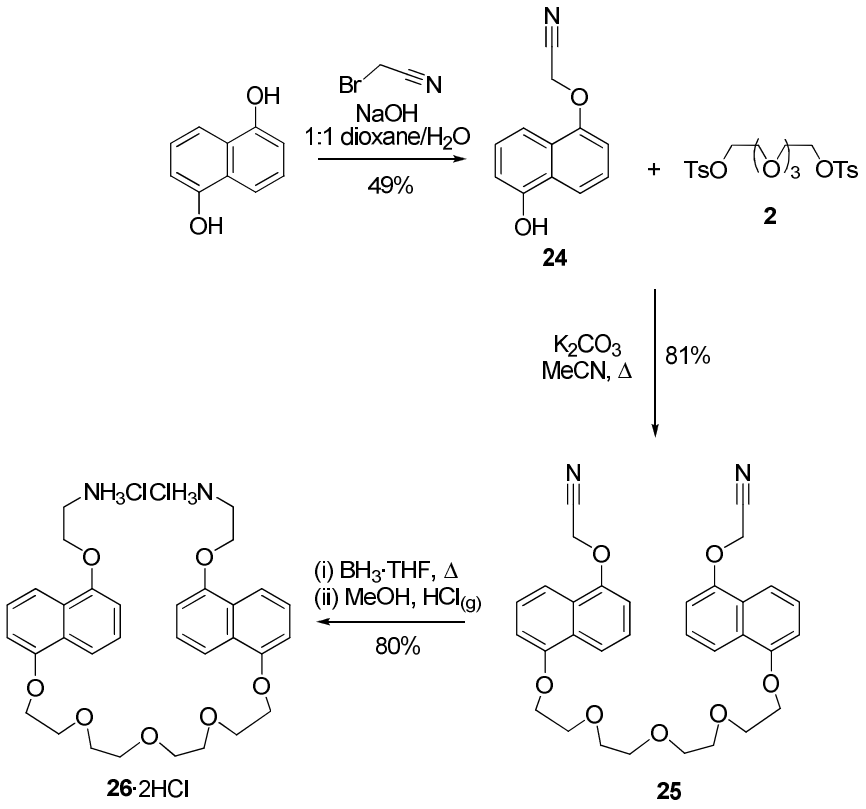

***Figure 2.8.*** *(a) isophthaloyl dichloride, (b) terephthaloyl dichloride, and (c) phthaloyl dichloride.*

Analogous synthetic procedures using phthaloyl chloride and terephthaloyl chloride proved unsuccessful with no evidence of rotaxane formation in either $^{1}$H NMR or mass spectrometry (ESI).

In both cases it appears rotaxanation is unfavourable, probably on account of weak association with the chloride anion template, where with phthalamide the amide protons are possibly too close together and the terephthalamide protons are too far apart to cooperatively complex chloride. These factors may also inhibit favourable π-π stacking interactions between the hydroquinone and axle pyridinium units. These observations highlight the importance of the geometry of the isophthalamide chloride anion recognition motif in mechanical bond formation.

One final variation to the macrocyclic wheel component involved replacing the hydroquinone motif with naphthoquinone, with the idea that including this more electron rich aromatic component would enhance π-π stacking interactions with the pyridinium unit of the axle and further stabilise rotaxane formation.

A naphthoquinone containing bis-amine component was synthesised according to Scheme 2.16.

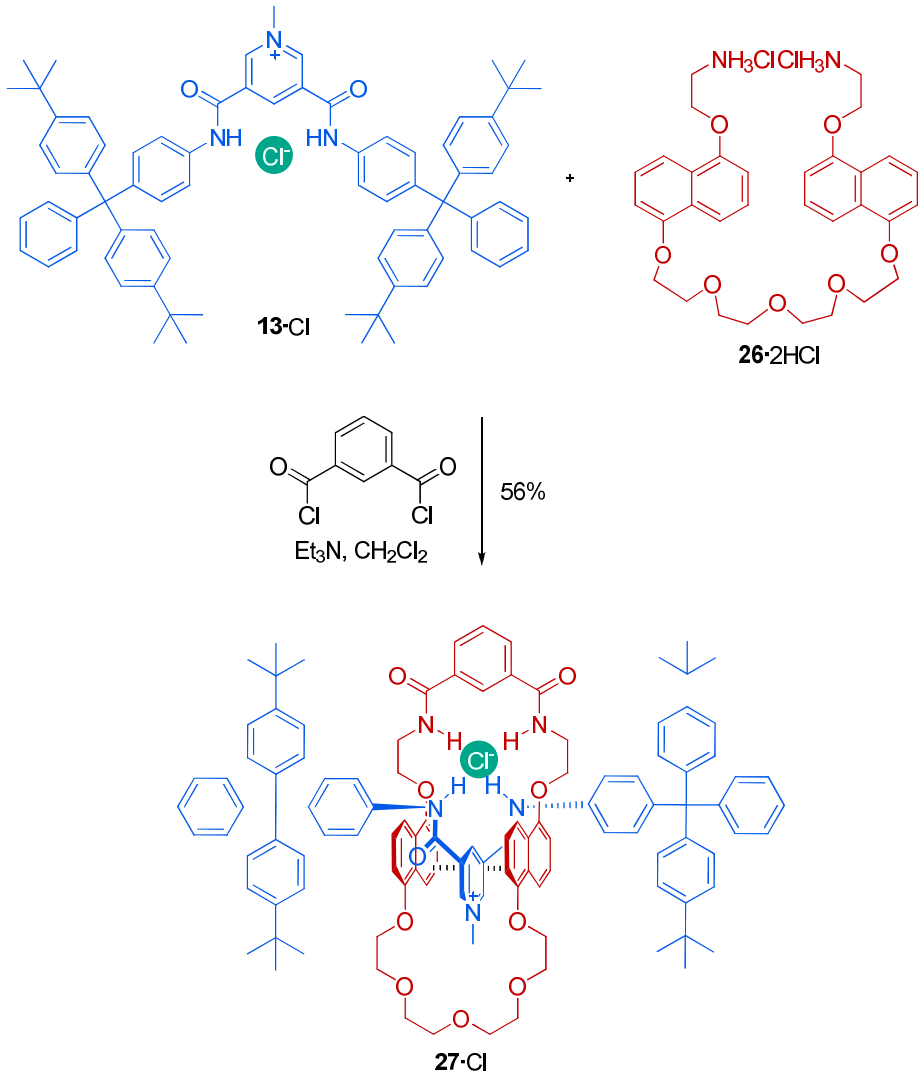



***Scheme 2.16.*** *Synthesis of naphthoquinone containing bis-amine.*

Naphthalen-1,5-diol was monofunctionalised with bromoacetonitrile in the presence of NaOH in 1:1 dioxane/water in 49% yield giving compound **24**. This was heated with **2** and $K_2CO_3$ in MeCN to give **25** in 81% yield which was then reduced using borane in THF. The hydrogen chloride salt of **26** was precipitated using gaseous HCl. Unfortunately, upon addition of base to **26**·2HCl substantial decomposition was observed and thus it was decided to attempt the rotaxanation using **26**·2HCl.

The synthesis of naphthoquinone rotaxane **27**·Cl is outlined in Scheme 2.17. Isophthaloyl dichloride was added to a mixture of axle **13**·Cl, bis-amine **26**·2HCl and $Et_3N$ in $CH_2Cl_2$, before acidic workup and preparative TLC gave **27**·Cl in 56% yield. Given the original synthetic route (i.e. having an excess of $Et_3N$ present in the reaction mixture for thirty minutes before the acid chloride was added) was employed in this rotaxane synthesis this yield is very impressive, in fact almost double that obtained for the hydroquinone containing analogue under the same conditions. This highlights the strength of interaction between the

naphthoquinone and pyridinium units, and also the significant role π-π stacking interactions play in the formation of the rotaxane architectures.




***Scheme 2.17.*** *Synthesis of napthoquinone containing [2]rotaxane.*

The $^{1}$H NMR spectrum of rotaxane **27**·Cl, along with those of its component parts for comparison are given in Figure 2.9. Similar to the hydroquinone analogue **14**·Cl, the peaks corresponding to the axle's cavity and amide protons *γ* and *δ* are shifted upfield compared to the component axle, whereas the macrocycle protons *c* and *d* are shifted downfield as a result of the chloride residing between the two components in the cleft of the rotaxane. In addition, naphthoquinone protons *h*, *i*, *k* and *l* have moved significantly upfield compared to the free macrocycle, a consequence of π-π stacking with the axle pyridinium unit.

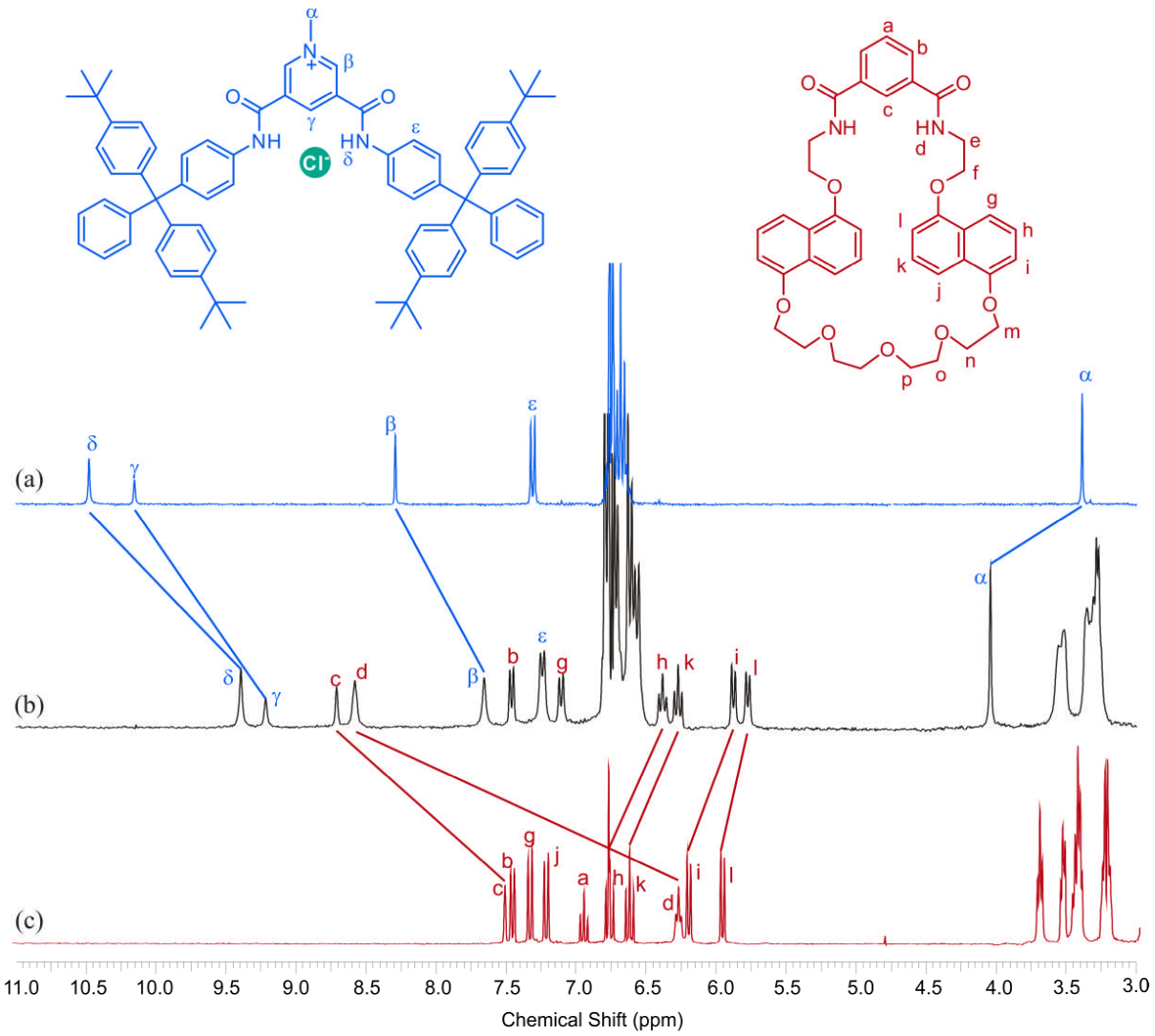



***Figure 2.9.*** *$^1$H NMR in $CDCl_3$ at 293K of (a) axle **13**·Cl, (b) [2]rotaxane **27**·Cl, and (c) component macrocycle.*

## 2.3.4 Investigations into the Role of the Templating Anion

This new synthetic route has proved highly successful and versatile in the formation of a variety of rotaxane structures in good yields. However, the exact mechanism of the reaction is unclear. Figure 2.10 highlights a proposed mechanistic pathway whereby the bis-amine precursor associates around the axle component, driven by charge-assisted π-π stacking interactions between the electron rich hydroquinone and the electron deficient aromatic surfaces, possibly in combination with anion templation.

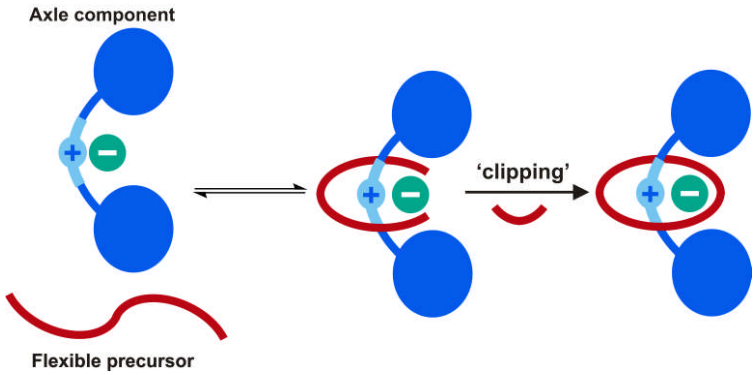



***Figure 2.10.*** *Proposed mechanistic pathway.*

To determine whether this association between the bis-amine precursor and the pyridinium axle is occurring, a $^{1}$H NMR spectrum of a 1:1 mixture of the two components in $CD_2Cl_2$ was examined (Figure 2.11).

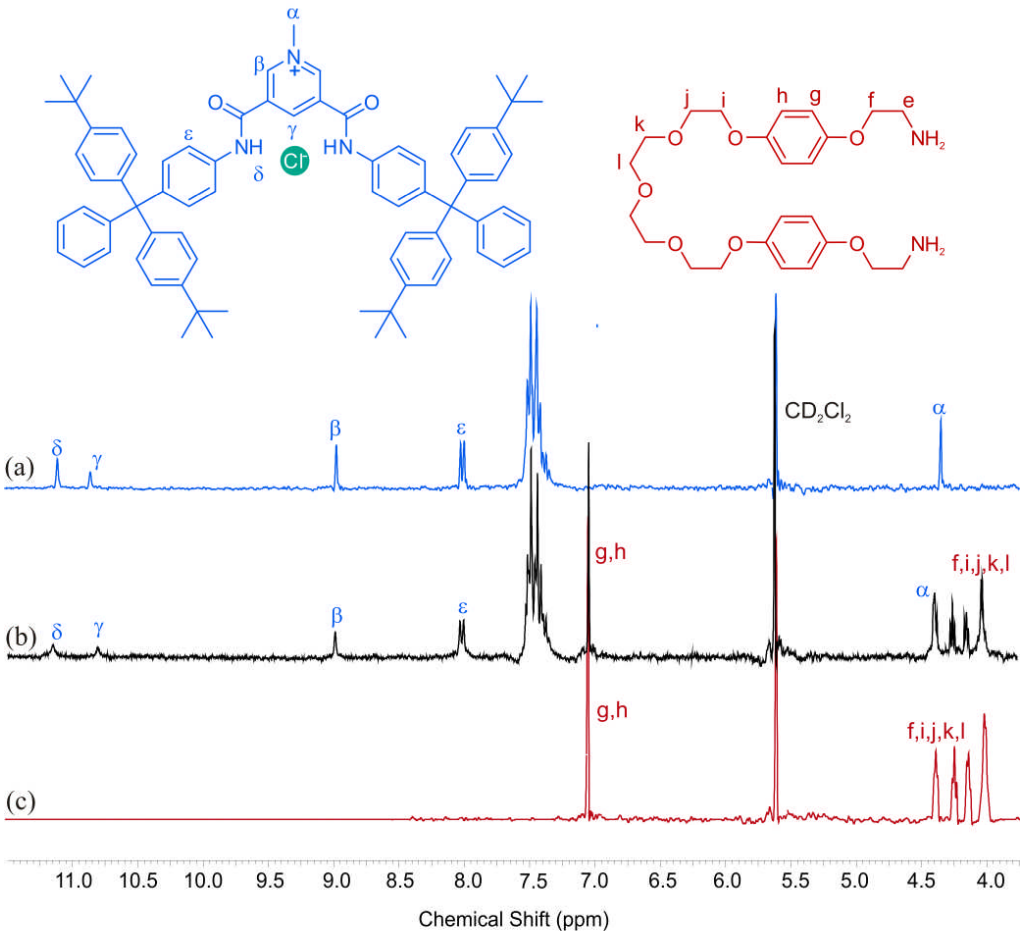



***Figure 2.11.*** *$^{1}$H NMR in $CD_2Cl_2$ at 293K of (a) pyridinium axle **13**·Cl, (b) 1:1 mixture of **13**·Cl/**4**, and (c) bis-amine **4**.*

No evidence of the aforementioned π-π stacking interactions was noted in this $^{1}$H NMR spectrum which suggests rotaxanation must proceed *via* an intermediate assembly of components (Figure 2.12), whereby an amine has reacted with one acid chloride group. The chloride anion, through hydrogen bonding, templates the intramolecular amide ring closing condensation reaction around the pyridinium axle component orienting the second amine in the correct position to react with the other acid chloride group to afford the interlocked product. If this postulate is correct, the halide anion must play a crucial role in the synthesis of these rotaxanes, and in order to confirm this, the reaction needs to be carried out in the absence of the anion.

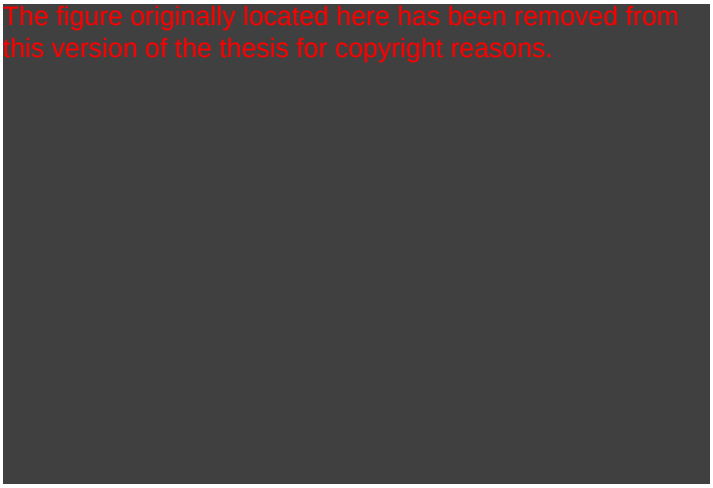



***Figure 2.12.*** *Proposed rotaxane intermediate.*

Since the 'clipping' step of the rotaxanation involves the release of chloride, the condensation reaction was undertaken out using an activated ester which was synthesised by reacting isophthalic acid with *N*-hydroxysuccinamide in the presence of the coupling reagent DCC (Scheme 2.18). The reaction was carried out with both chloride and the hexafluorophosphate salts of the pyridinium axle component **13**. In the presence of the chloride anion template the yield of the rotaxanation reaction was 42% whilst the rotaxane was obtained in only 16% yield when **13**·$PF_6$ was used. Thus the presence of chloride as a templating reagent is significant for enhancing the yield of rotaxane production.




***Scheme 2.18.*** *Synthesis of rotaxane* ***14*** *via DCC coupling reaction.*

To replicate the original reaction conditions (since using the activated ester requires longer reaction times compared to the acid chloride reaction which can be assumed to be almost instantaneous) the acid chloride condensation was carried out in the presence of two equivalents of $AgPF_6$ to precipitate the chloride generated during the condensation reaction. The yield of this reaction was observed to be approximately 15%, only a quarter of that when chloride anion was present. This is another positive indication that the yield of the reaction is highly dependant on the presence of the chloride anion, and it is very likely that the reaction goes *via* the intermediate proposed in Figure 2.12.

### 2.3.5 Anion Recognition Studies

In order to study the anion binding properties of the novel rotaxanes it was necessary to exchange the chloride templating anion for the non-coordinating hexafluorophosphate anion. This was achieved in quantitative yield by washing a solution of the rotaxane in $CHCl_3$ with aqueous $NH_4PF_6$. The $^1H$ NMR spectra of rotaxane **14** before and after anion exchange to the hexafluorophosphate salt are shown in Figure 2.13.

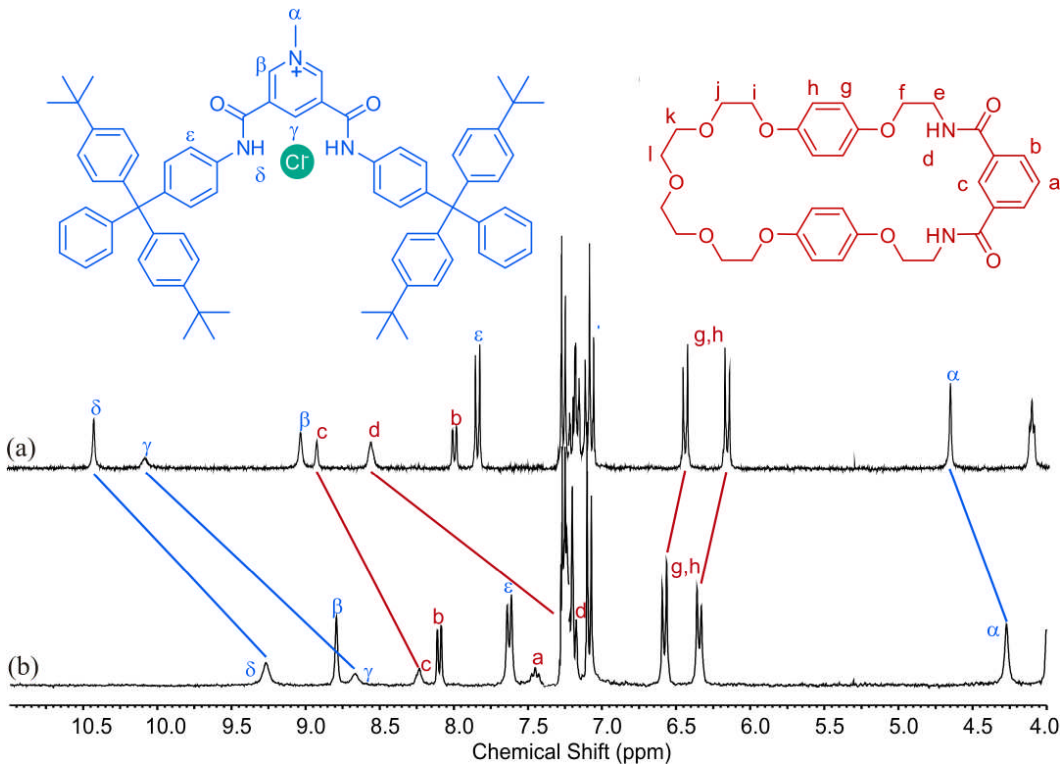



***Figure 2.13.*** *$^1$H NMR in $CDCl_3$ at 293K of (a) rotaxane **14**·Cl and (b) rotaxane **14**·$PF_6$.*

The most notable difference in the spectrum of **14**·$PF_6$ compared to **14**·Cl is that the protons residing within the interlocked cavity of the rotaxane (*δ*, *γ*, *c* and *d*) are observed to have moved upfield, which is consistent with the chloride anion being removed from this cleft. Interestingly, the peak corresponding to the pyridinium *N*-methyl protons *α* also moves upfield upon anion exchange whilst the hydroquinone peaks are observed to move slightly downfield. This is likely to result from a small conformational change of the cationic pyridinium axle within the macrocyclic wheel since chloride is no longer present to lock the two components in place. Crucially, despite the small peak shift for the hydroquinone protons, they still remain upfield and spilt compared to the free macrocycle (Figure 2.6c) indicating that the interlocked nature of the rotaxane has been preserved upon anion exchange. Indeed 2D ROESY evidence (Figure 2.14) confirms that the structure remains interlocked with cross coupling interactions observed between the pyridinium and hydroquinone protons. Through space correlations between cavity and stopper protons are also present.




***Figure 2.14.*** *$^{1}H$ -$^{1}H$ ROESY spectrum of [2]rotaxane **14**·$PF_6$ in $CDCl_3$ at 293K. Cross couplings are shown on the schematic diagram on the right.*

All the rotaxanes, where the macrocyclic component contained hydroquinone functionalities, exhibited similar $^{1}H$ NMR spectral differences to rotaxane **14**, upon chloride to hexafluorophosphate anion exchange. However the naphthoquinone containing rotaxane **27**·$PF_6$ was observed to undergo substantial decomposition upon anion exchange, as observed by both $^{1}H$ NMR and TLC. This disappointing result indicates that the presence of the chloride anion is essential in maintaining the integrity of the rotaxane structure. Unfortunately this meant that no further studies could be carried out on rotaxane **27**·$PF_6$.

The anion binding properties of the rotaxanes (**14, 18 – 23**)·$PF_6$ were investigated initially by $^{1}H$ NMR titration experiments with tetra butyl ammonium (TBA) salts of $Cl^-$, $H_2PO_4^-$ and $OAc^-$ in 1:1 $CDCl_3$/$CD_3OD$. TBA was chosen as the countercation since it is considered to be essentially non-competitive for the anions in question in the solvent system used. The binding of anions in the rotaxanes' binding cleft was demonstrated to be fast on the NMR timescale and it was possible to monitor the chemical shift perturbations of cavity protons *c* and *γ*, and *ortho* pyridinium proton *β* as a function of concentration of anion. It was not possible to use the amide protons *d* and *δ* since they had exchanged for deuterium in this protic solvent

media. WinEQNMR2 was unable to determine association constant values for chloride binding in this solvent system as the halide is bound extremely strongly ($K > 10^4$ $M^{-1}$). In stark contrast the axle **13**·$PF_6$ only weakly binds chloride in this solvent mixture ($K = 125$ $M^{-1}$), and exhibits a pronounced selectivity preference for the basic dihydrogen phosphate and acetate anions.[7] Interestingly the novel sulfonamide containing [2]rotaxane **23**·$PF_6$ proved to be a relatively weaker complexant of chloride, exhibiting an association constant of 1500 $M^{-1}$ in 1:1 $CDCl_3/CD_3OD$, which correlates with the rotaxane's relatively lower yield and confirms that the halide anion is a less efficient templating reagent.

Analogous anion binding titrations were undertaken in the presence of 10% water, and the same proton signals followed to aid understanding of the anion binding mode, and obtain quantitative association constant data. Addition of chloride to the rotaxanes resulted in the expected downfield perturbation of cavity protons *c* and *γ*, as a consequence of deshielding in the presence of the electronegative anion (Figure 2.15a).

Conversely, addition of the oxoanions acetate and dihydrogen phosphate resulted in an upfield shift perturbation of pyridinium cavity proton *γ*, presumably as a consequence of a conformational change in the [2]rotaxane since these anions are too large to penetrate the interlocked binding cavity, and consequently associate externally. Moreover only negligible changes in chemical shift was observed for the proton signal representing macrocycle cavity proton *c* indicating that the binding of the oxoanions is more reliant on electrostatics, associating with the positively charged axle component rather than in the cleft created by convergent hydrogen bond donors (Figure 2.15c).




***Figure 2.15.*** *$^1$H NMR in 45:45:10 $CDCl_3/CD_3OD/D_2O$ at 293K of (a) rotaxane **14**·$PF_6$ + 1 eq. TBACl, (b) rotaxane **14**·$PF_6$, and (c) rotaxane **14**·$PF_6$ + 1 eq. TBAOAc.*

Titration curves for the binding of the anions were obtained by plotting chemical shift perturbation as a function of equivalents of anion added to the respective rotaxane and those obtained for protons $\beta$ and $\gamma$ are given in Figure 2.16.




***Figure 2.16.*** *Chemical shift perturbations of protons (a) β and (b) γ on addition of $Cl^-$, $OAc^-$ and $H_2PO_4^-$ (as TBA salts) to a solution of [2]rotaxane* ***14***$\cdot PF_6$ *in 45:45:10 $CDCl_3/CD_3OD/D_2O$ at 1.91 × $10^{-3}$M and 293 K. Symbols represent experimental data points; continuous lines represent calculated curves.*

Association constants were calculated from the titration data using winEQNMR2, and are reported in Table 2.1.

| | **14**·$PF_6$ | **18**·$PF_6$ | **19**·$PF_6$ | **20**·$PF_6$ | **21**·$PF_6$ | **22**·$PF_6$ |
|---|---|---|---|---|---|---|
| $Cl^-$ | 1190 | 1500 | 1800 | 860 | 1450* | 1175 |
| $OAc^-$ | 120 | 60 | 170 | 110 | 120 | 150 |
| $H_2PO_4^-$ | 180 | 110 | 180 | 120 | 250 | 200 |

**Table 2.1:** *Association constants, K ($M^{-1}$), of [2]rotaxanes with $Cl^-$, $OAc^-$ and $H_2PO_4^-$ in 45:45:10 $CDCl_3/CD_3OD/D_2O$ at 1.91 × $10^{-3}$M and 293 K. Obtained by monitoring proton β. Error < 10%, * error < 15%.*

All rotaxanes are observed to bind chloride strongly even in this competitive aqueous solvent mixture, whereas the oxoanions are complexed only weakly, despite the greater basicity of these anions. These results indicate that the respective interlocked binding pocket is of complementary size to chloride. Whilst the pseudotetrahedral binding environment created by the convergent amide groups is able to satisfy the coordination sphere of the spherical chloride anion, the cavity is not large enough to encapsulate the oxoanions which is reflected in the lower association constant values and the upfield chemical shift perturbations of the cavity proton γ discussed earlier.

Of the monocationic rotaxanes, those with the larger polyether macrocyclic component were observed to complex chloride significantly more strongly which contrasts to what might be predicted on grounds of preorganisation. This may be attributed to the binding of chloride causing unfavourable steric interactions between the pyridinium *N*-methyl group of the axle and the polyether chain of the smaller macrocycle which is suggested in the solid state structure of **22**·Cl (Figure 2.19) and further rationalised in MD simulations (see Section 2.3.7).

As expected, the rotaxanes containing the electron withdrawing pyridine **18**·$PF_6$, and nitro-isophthalamide **19**·$PF_6$, functionalities display an enhanced binding affinity for chloride. This is a consequence of the increased acidity of the amide protons, and thus their hydrogen bond donor ability.

### 2.3.6 X-ray Crystal Structures

Confirmation of the ability of the rotaxanes to encapsulate chloride within their respective three-dimensional interlocked cavities was obtained by single crystal X-ray structures of the chloride salts of two rotaxanes.

Yellow crystals suitable for single crystal X-ray diffraction structural analysis of rotaxanes **14**·Cl (Figure 2.17) and **22**·Cl (Figure 2.18) were grown by gaseous diffusion of diisopropyl ether into dichloromethane and benzene solutions respectively.

Data collection was undertaken at beamline I19 of Diamond Light Source, and the structures solved by Dr. Christopher Serpell and Dr. Nathan Kilah. The structures confirm the interlocked nature of the respective systems, and the location of the chloride anion in the interlocked binding site, fully encapsulated by the orthogonal amide hydrogen bonding array.




***Figure 2.17.*** *X-ray crystal structure of* 14·*Cl. Disorder and non-protic hydrogens omitted for clarity.*

The distance between the chloride anion and the centre of the binding pocket ($N_{mass}$) defined by the four nitrogen atoms of the N-H binding sites (two amide nitrogens of the pyridinium axle and two amide nitrogens of the macrocycle) were calculated at 0.567 ± 0.001 Å for **14**·Cl and 0.649 ± 0.003 Å for **22**·Cl, suggesting that the binding pocket of **14** is more favourably disposed to chloride inclusion, which is consistent with the results obtained by solution $^{1}$H NMR binding experiments.

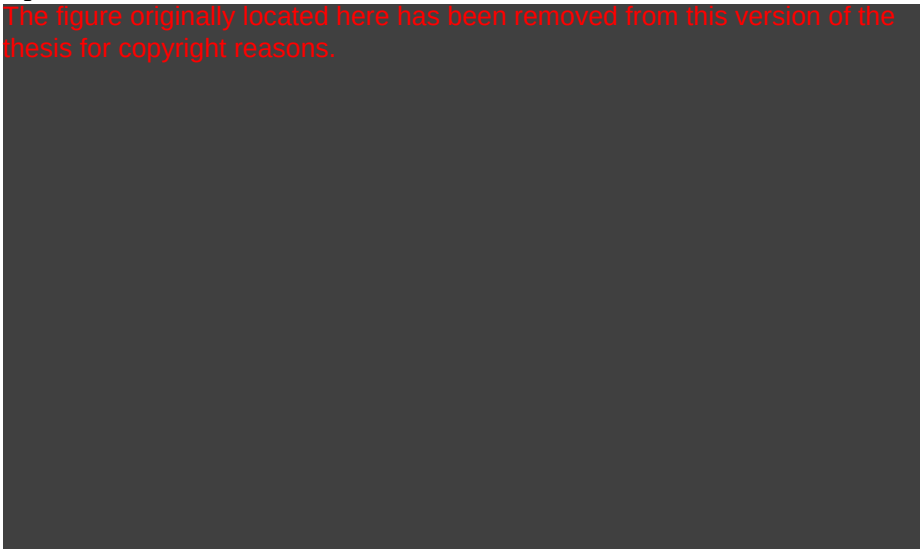



***Figure 2.18.*** *X-ray crystal structure of* ***22***·*Cl. Disorder and non-protic hydrogens omitted for clarity.*

The hydroquinone and pyridinium rings have adopted coplanar positions in these structures, which may be indicative of the face to face π-π stacking interactions, presumed to stabilise the interlocked structures.

Earlier postulates suggested that the different lengths of the macrocyclic polyether chain and the interactions that may occur with the pyridinium *N*-methyl group of the axle may play an important role in both the yield of formation and anion complexing ability of the [2]rotaxanes. This is apparent in these crystal structures where the longer polyether chain of **14**·Cl appears to have the capacity to swing back and forth over the pyridinium *N*-methyl group with ease, whereas it is less clear that **22**·Cl possesses the necessary degrees of freedom for this process to occur readily. The greater conformational flexibility in **14**·Cl may allow an induced-fit mechanism to operate more successfully thus increasing its ability to bind chloride. The features observed in the solid state can be further explored by examining the solution state molecular dynamics simulations described in the next sub-section.

### 2.3.7 Molecular Dynamics Simulations

Molecular dynamics (MD) simulations using Amber 10 software[29] and general Amber force field (GAFF) parameters,[30] carried out by the group of Prof. Vitor Felix at the University of Aveiro, can provide further insight into the results discussed in the previous sections. The aims of this collaborative work were to further rationalise both the differences in yields of formation and anion binding trends between the four- and five-oxygen polyether containing rotaxanes, and to obtain solution state structures for these rotaxanes with various bound anions to confirm theories regarding preferential chloride recognition. In addition, it was of interest to gain an understanding as to why the sulfonamide containing rotaxane binds chloride less strongly than its isophthalamide analogue.

To begin with, suitable *syn-syn* low energy co-conformations for the rotaxane associations **14**·Cl, **20**·Cl and **23**·Cl were generated in the gas phase through the quenched MD approach

(see Appendix A.4), then immersed in an equilibrated cubic box solvent mixture of $CHCl_3$/MeOH/$H_2O$ (45:45:10) and subjected to classical MD simulations for 10 ns. The MD snapshots of the representative binding arrangements for rotaxanes **14**·Cl (a), **20**·Cl (b) and **23**·Cl (c) are shown in Figure 2.19.




***Figure 2.19.*** *Snapshots of (a)* ***14****·Cl, (b)* ***20****·Cl , and (c)* ***23****·Cl taken at 5 ns of MD simulation. Carbon atoms of the macrocycle and pyridinium axle are shown in gray and yellow, respectively. Hydrogen bonds are represented as orange dashed lines. For clarity reasons, only the N-methyl and N-H hydrogen atoms are shown.*

For all three rotaxanes the main structural features observed in the gas phase were retained in the solution phase over the entire MD simulation, and are consistent with those observed in the crystal structure of **14**·Cl where the chloride anion is bound by four amide N-H hydrogen bonds, two from each of the macrocyclic isophthalamide and pyridinium amide axle components.

The average distances between the chloride anion and the centre of the binding cavity ($N_{mass}$), along with the distances between the hydroquinone and pyridinium rings for the

aforementioned rotaxanes are recorded in Table 2.2. This data gives important insight into the stability of the rotaxane structures and thus the yield of rotaxanation.

| Rotaxane | Distances (Å) | | |
|---|---|---|---|
| | $N_{mass}\cdots Cl^-$ | hq···py rings | |
| **14**·Cl | 1.360±0.23 | 4.061±0.37 | 3.834±0.34 |
| **20**·Cl | 1.424±0.33 | 4.763±0.45 | 3.918±0.32 |
| **23**·Cl | 3.391±2.08 | 4.652±0.51 | 4.652±0.51 |

***Table 2.2.*** *Average distances (with standard deviations) between $Cl^-$ and the centre of the binding cavity, and between the macrocycle hydroquinone rings (hq) and axle pyridinium (py) ring of rotaxanes **14**·Cl, **20**·Cl and **23**·Cl . The standard deviations were calculated for N = 50000.*

Both rotaxanes **14**·Cl and **20**·Cl possess short $N_{mass}\cdots Cl^-$ distances with small standard deviations indicating that the halide anion fits well within the three-dimensional cavity, tightly hydrogen bonded to the four N-H protons. Rotaxane **14**·Cl has a noticeably shorter $N_{mass}\cdots Cl^-$ distance than **20**·Cl reflecting the greater yield and anion binding strength observed experimentally. The average distance between the hydroquinone and pyridinium rings is also smaller for **14**·Cl indicating that π-π stacking interactions are more effective, thus acting to further stabilise the structure compared to **20**·Cl, where it is unlikely that two simultaneous hydroquinone-pyridinium π- π stacking interactions exist.

In contrast to **14**·Cl and **20**·Cl, the sulphonamide containing rotaxane **23**·Cl displays an increased average $N_{mass}\cdots Cl^-$ distance of 3.391 Å with a very large standard deviation of 2.08 Å. This suggests that the orthogonal assembly between the axle and the macrocycle containing the sulfonamide motif is not particularly stable, which may account for the rotaxane's reduced yield of formation compared to the isophthalamide containing analogues. This less efficient chloride anion templation, may be the result of different conformational restrictions imposed by the macrocycle's R-$SO_2$-R tetrahedral fragment on the N-H directionality compared to the isophthalamide group. This can be seen in Figure 2.21c where

the two macrocyclic N-H binding groups from the macrocycle are observed to be out of the plane of the ring whilst in the isophthalamide counterparts (Figure 2.21a and b), they lie almost in the plane.

Additional evidence for the differences in yields between the four- and five-oxygen containing rotaxanes can be obtained by examining the grid contours representing the histogram built using the spatial positions occupied by the carbon of the axle's pyridinium *N*-methyl group over the entire simulation time for both rotaxanes **14**·Cl and **20**·Cl (Figure 2.20).

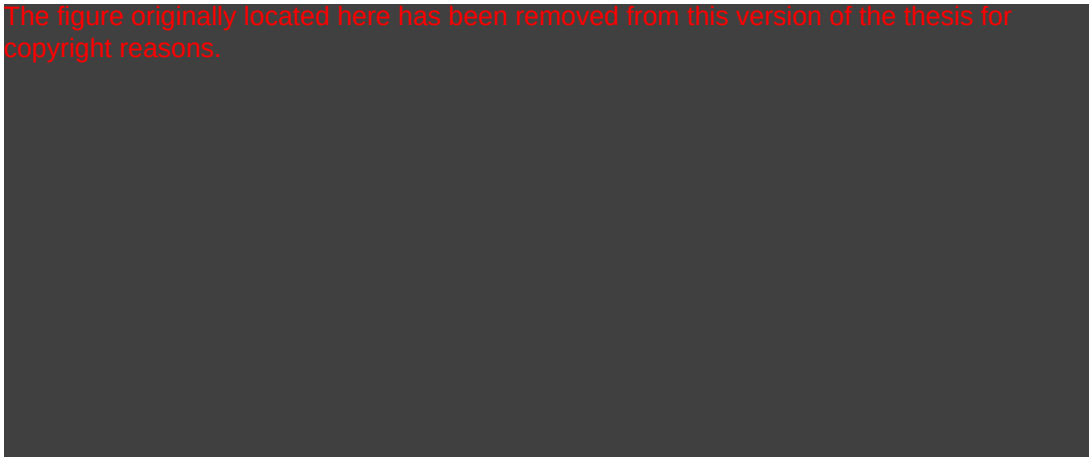



**Figure 2.20.** *Grid representation (red) of the histograms for the location of the methyl carbon atom in the pyridinium axle (yellow) over the 10 ns simulation in (a)* ***14****·Cl and (b)* ***20****·Cl. A density contour value of 10 was used.*

For **14**·Cl the density of the methyl carbon atom is located within the macrocycle's polyether chain and evenly distributed on both sides of the macrocyclic cavity. This indicates that the methyl group of the axle can occupy the same plane as the macrocycle's polyether chain and is able to swing back and forth. As a consequence of this spatial disposition, the average C···O distance between the pyridinium *N*-methyl group and the aliphatic oxygen atoms of polyether chain (1.599±0.41 Å), suggests that the interlocked structure of **14**·Cl is stabilized by $H_2C$-H···O ($\delta^+$-$\delta^-$) interactions. Evidence for these hydrogen bonding interactions are also observed by comparing the relevant protons in the $^1$H NMR spectra of the rotaxane and free axle. In contrast, for **20**·Cl, the carbon atom density is out of the plane of the macrocycle at

all times due to the shorter length of the polyether chain, demonstrating that the size of the macrocycle determines the conformation of the interlocked structure due to steric interactions, and ultimately has an impact on the yield of rotaxane formation and subsequently its anion binding abilities.

Evidence for the anion binding trends determined by $^1$H NMR titrations can be obtained by again looking at MD snapshots of the rotaxanes when complexed to the three anions, and comparing average $N_{mass}\cdots X^-$ and hydroquinone-pyridinium distances (Table 2.3).

| **Rotaxane** | **Distances (Å)** | | |
|---|---|---|---|
| | **$N_{mass}\cdots X^-$** | **hq···py rings** | |
| **14**·Cl | 1.360±0.23 | 4.061±0.37 | 3.834±0.34 |
| **14**·OAc | 1.800±0.18 | 4.104±0.54 | 4.322±0.58 |
| **14**·$H_2PO_4$ | 3.391±2.08 | 4.815±0.74 | 4.815±0.74 |

***Table 2.3.*** *Average distances (with standard deviations) between the anions (X = $Cl^-$, $OAc^-$ or $H_2PO_4^-$) and the centre of the binding cavity, and between the macrocycle hydroquinone rings (hq) and axle pyridinium (py) ring of rotaxane **14**. The standard deviations were calculated for N = 50000.*

The average $N_{mass}\cdots X^-$ distances are significantly longer for **14**·OAc (1.800 Å) and **14**·$H_2PO_4$, (2.015 Å) compared to **14**·Cl (1.360 Å) indicating that the oxoanions are more weakly bound, which corroborates the trend observed in the experimental association constants (Table 2.3). Furthermore, this structural parameter also shows that, contrary to chloride, the polyatomic anions are located outside the interlocked binding pocket as can be observed in the MD snapshots of rotaxane **14**, with $Cl^-$ (a), $OAc^-$ (b), and $H_2PO_4^-$ (c) represented in Figure 2.21.

Whilst chloride is fully encapsulated within the interlocked binding cleft, with the pyridinium *N*-methyl group located within the polyether chain, significant distortion of the axle component within the macrocycle occurs upon binding of the oxoanions, which are complexed outside the cavity. These distortions provide increased exposure of this cavity to the solvent media and thus justify the significantly weakened binding, and may also account

for the notable upfield perturbations of the pyridinium proton $\gamma$ observed in the acetate and dihydrogen phosphate NMR titration experiments discussed in Section 2.3.4.

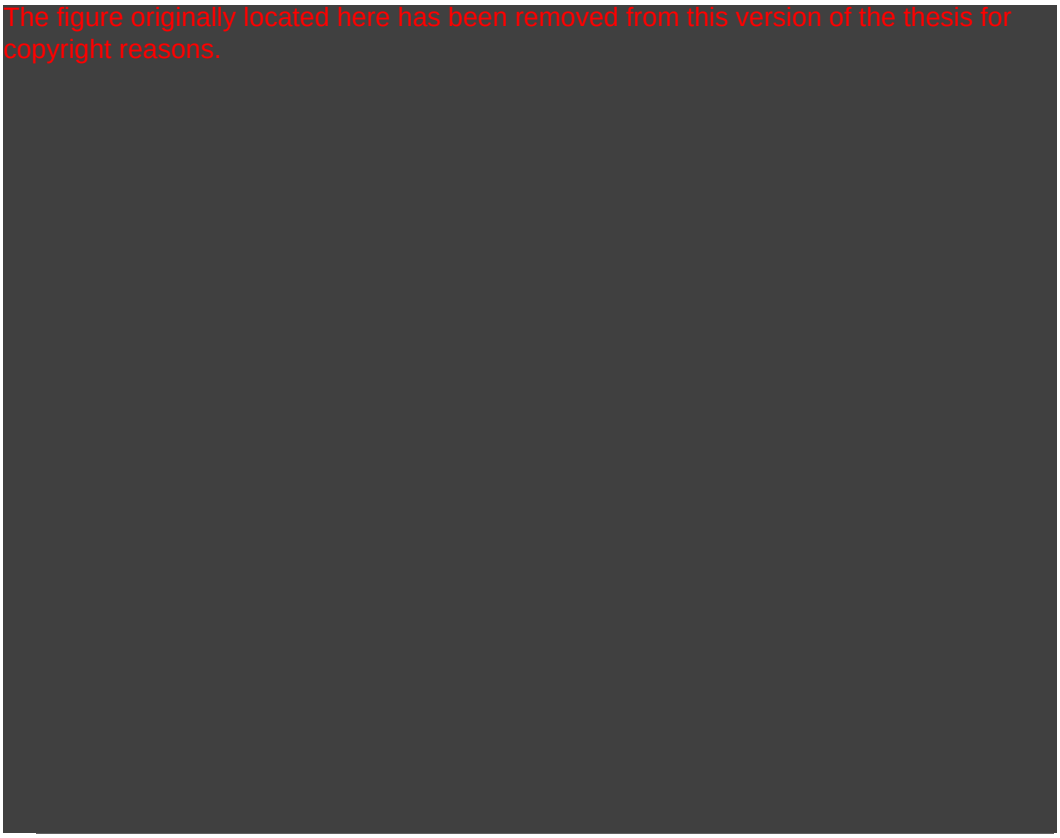



***Figure 2.21.*** *Snapshots of (a)* ***14***·*Cl taken at 5 ns, and (b)* ***14***·*OAc and (c)* ***14***·$H_2PO_4$ *taken at 6 ns of MD simulation. Carbon atoms of the macrocycle and pyridinium axle are shown in gray and yellow, respectively. Hydrogen bonds are represented as orange dashed lines. For clarity reasons, only the N-methyl and N-H hydrogen atoms are shown. The polyatomic anions are drawn in ball and stick style.*

Figure 2.22 displays the different orientations observed for the pyridinium axle in representative snapshots of **14**·Cl, **14**·OAc, and **14**·$H_2PO_4$. From $Cl^-$ to $OAc^-$ to $H_2PO_4^-$, the orthogonal coordination environment becomes increasingly distorted and reflects the strength of binding $Cl^- > OAc^- > H_2PO_4^-$ calculated experimentally.

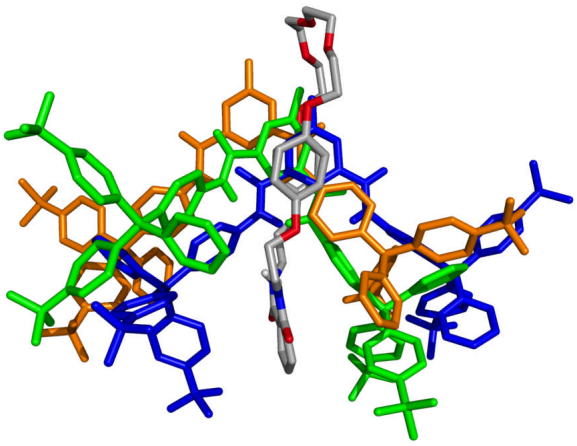


***Figure 2.22.*** *Superposition of the rotaxane structures* ***14***·*Cl (blue),* ***14***·*OAc (green) and* ***14***·$H_2PO_4$ *(orange) showing the different axle orientations.*

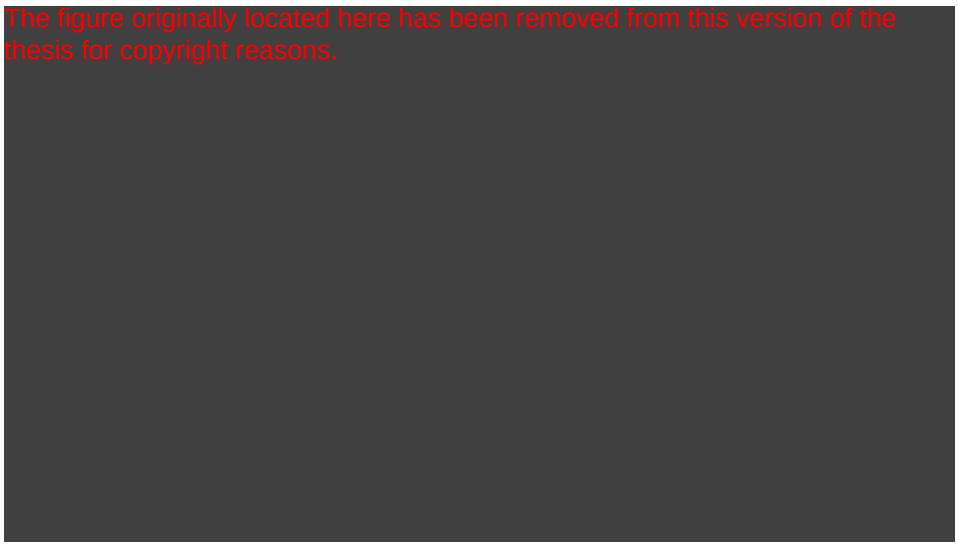
## 2.4 Synthesis and Anion Recognition Properties of a Novel Dicationic [2]Rotaxane

The strength of chloride complexation in aqueous solvent media of the monocationic rotaxane described in Section 2.3 is a very positive indication that the three-dimensional cavities of interlocked structures can be exploited for strong anion binding by shielding the binding domain from competing solvent molecules.

It may be possible to construct host molecules capable of exhibiting a higher affinity for chloride if the positive charge of the rotaxane is increased. In order to investigate the effect of increasing charge of the rotaxane, a novel dicationic rotaxane was prepared; the synthesis and binding studies of which are discussed in the following section.

### 2.4.1 Synthesis and Characterisation

The novel dicationic rotaxane was prepared with relative synthetic ease by simple alkylation of pyridine containing rotaxane **18**·$PF_6$ by heating at reflux in iodomethane. Once the alkylating agent was removed, the new rotaxane **28**·(I)($PF_6$) could be fully converted to the hexafluorophosphate salt by washing with aqueous $NH_4PF_6$ (Scheme 2.19).




***Scheme 2.19.*** *Synthesis of dicationic rotaxane* ***28***$\cdot(PF_6)_2$.

The $^1$H NMR spectrum of **28**$\cdot(PF_6)_2$ is given in Figure 2.23 and shows the presence of a new signal corresponding to the methyl pyridinium protons *a* of the macrocycle. It is also important to note the continued presence of the split hydroquinone proton peaks *g* and *h*, indicating that the structure remains interlocked following the alkylation.

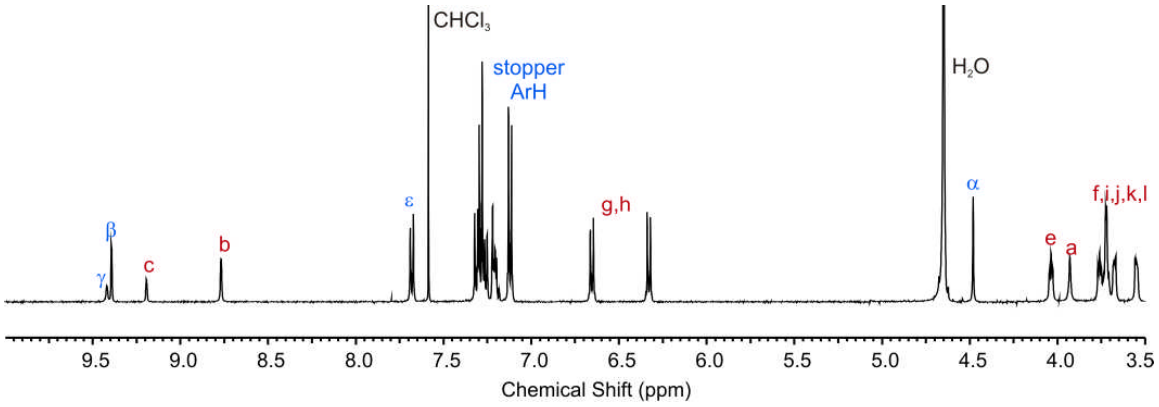



***Figure 2.23.*** *$^1$H NMR of* ***28***$\cdot(PF_6)_2$ *in 1:1* $CDCl_3/CD_3OD$ *at 293K.*

## 2.4.2 Anion Recognition Studies

The anion recognition properties of the dicationic rotaxane were initially investigated qualitatively by comparison of the $^1$H NMR spectra of the hexafluorophosphate and chloride salts of the rotaxane in $CDCl_3$ (Figure 2.24i)

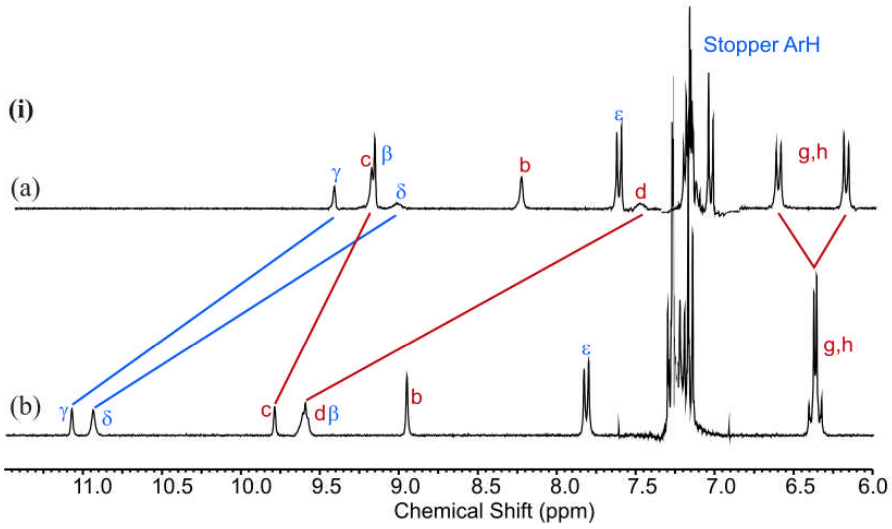



**Figure 2.24.** *(i) $^1$H NMR in $CDCl_3$ at 293K of (a) **28**·$(PF_6)_2$, and (b) **28**·$Cl_2$, and (ii) difference in chemical shifts of protons c, d, γ and δ between **28**·$(PF_6)_2$ and **28**·$Cl_2$.*

Considerable downfield shifts are seen in the cavity protons upon conversion to the chloride salt consistent with strong binding of the halide anion within the rotaxane's three-dimensional binding cleft (Figure 2.24ii). More interestingly, and in contrast to its monocationic counterparts, the dicationic rotaxane **28**·$Cl_2$ displays convergence of the hydroquinone proton signals, whilst in **28**·$(PF_6)_2$ they remain split. It is suggested that the strong complexation of chloride causes a slight contraction in the binding cavity leading to the pyridinium axle component assuming a position closer to the macrocyclic wheel than in the monocationic rotaxanes. This may cause the hydroquinone protons to experience a different environment within the ring currents of the pyridinium aromatic surface.

Quantitative anion titration experiments were carried out in 45:45:10 $CDCl_3/CD_3OD/D_2O$ in an identical manner to those described in Section 2.3.5, and the dicationic rotaxane **28**·$(PF_6)_2$ complexes chloride with an association constant of 3000 $M^{-1}$, double the value (1500 $M^{-1}$) noted with the monocationic rotaxane **18**·$PF_6$. This high association constant is attributed to the increased favourable electrostatic interactions provided by the cationic pyridinium motif of the macrocyclic component.

Anion binding studies were repeated in a solvent system containing a higher percentage of water. The limiting factor of these studies was the solubility of the rotaxane which contains large lipophilic stopper groups. Therefore the anion binding properties of rotaxane **28**·$(PF_6)_2$ were investigated in 65:35 $d_6$-acetone/$D_2O$. As observed for the monocationic systems cavity pyridinium proton $\gamma$ shifted downfield upon addition of chloride. However, in this solvent system, negligible chemical shift perturbations of the signal corresponding to proton $\gamma$ were observed upon addition of the oxoanions, acetate and dihydrogen phosphate. The association curves for the binding of these anions in this highly competitive aqueous solvent mixture are shown in Figure 2.25, and the association constants calculated from winEQNMR2 analysis of the titration data are given in Table 2.4.

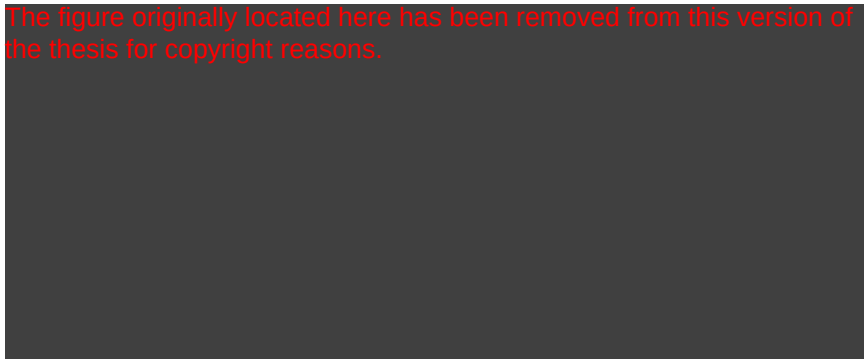



***Figure 2.25.*** *Chemical shift perturbations of protons γ and on addition of $Cl^-$, $OAc^-$ and $H_2PO_4^-$ (as TBA salts) to a solution of [2]rotaxane **32**·$PF_6$ in 65:35 $d_6$-acetone/$D_2O$ at 1.91 × $10^{-3}$M and 293 K. Symbols represent experimental data points; continuous lines represent calculated curves.*

| | $Cl^-$ | $OAc^-$ | $H_2PO_4^-$ |
|---|---|---|---|
| **28**·$(PF_6)_2$ | 500 | NB | NB |

***Table 2.4.*** *Association constants, K ($M^{-1}$), of [2]rotaxane **28**·$(PF)_2$ with $Cl^-$, $OAc^-$ and $H_2PO_4^-$ and in 65:35 $d_6$-acetone/$D_2O$ at 1.91 × $10^{-3}$M and 293K. Obtained by monitoring proton γ. Error < 10%. NB denotes no binding.*

Remarkably, chloride is still bound with considerable strength in 35% water, whereas no binding of oxoanions is observed. This rotaxane displays total selectivity for chloride over the more basic dihydrogen phosphate and acetate anions in this solvent mixture, which is

again attributed to the complementary size and shape of chloride for the rotaxane's binding cavity.

## 2.5 Synthesis and Anion Recognition Properties of [2]Catenanes

Following the success of synthesising [2]rotaxanes *via* the new synthetic route utilising anion templation and π-π stacking, it was of interest to determine whether catenanes could be formed using a similar route only replacing the pyridinium axle component with an appropriate positively charged macrocycle (Figure 2.26).

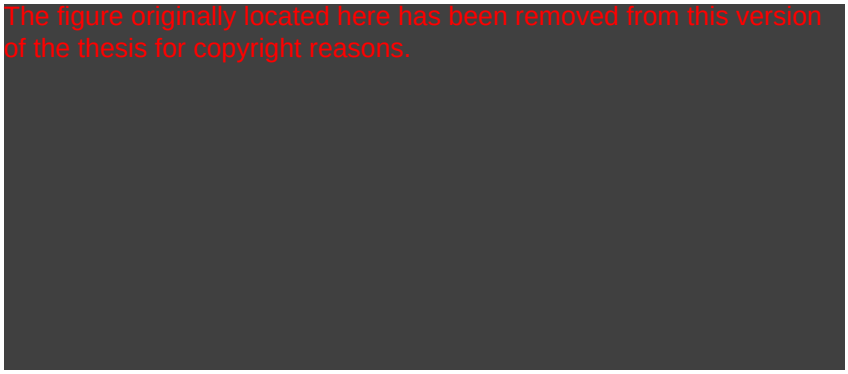
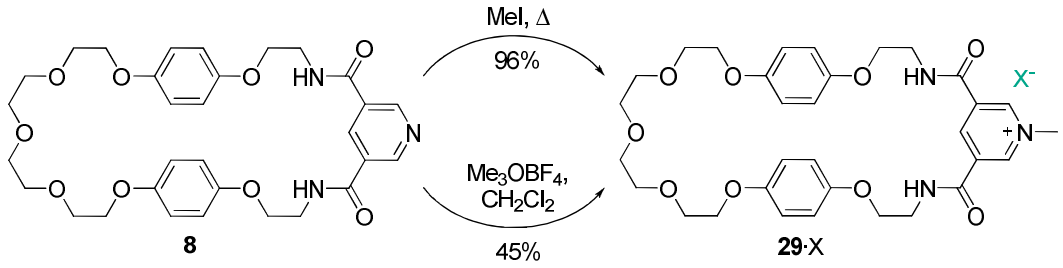



***Figure 2.26.*** *Schematic representation of catenane synthesis.*

### 2.5.1 Macrocycle Synthesis

A pyridinium macrocycle component was synthesised by simply alkylating macrocycle **8** by heating at reflux in iodomethane (Scheme 2.20) to give **29**·Cl in 96% yield.

Macrocycle **29**·I proved fairly insoluble in common organic solvents suitable for catenation reactions. However it was hoped that anion exchange to the non-coordinating hexafluorophosphate salt might improve solubility. Unfortunately, due to its inherent solubility, anion exchange proved challenging and preparing the macrocycle as the tetrafluroborate salt was undertaken (Scheme 2.20).

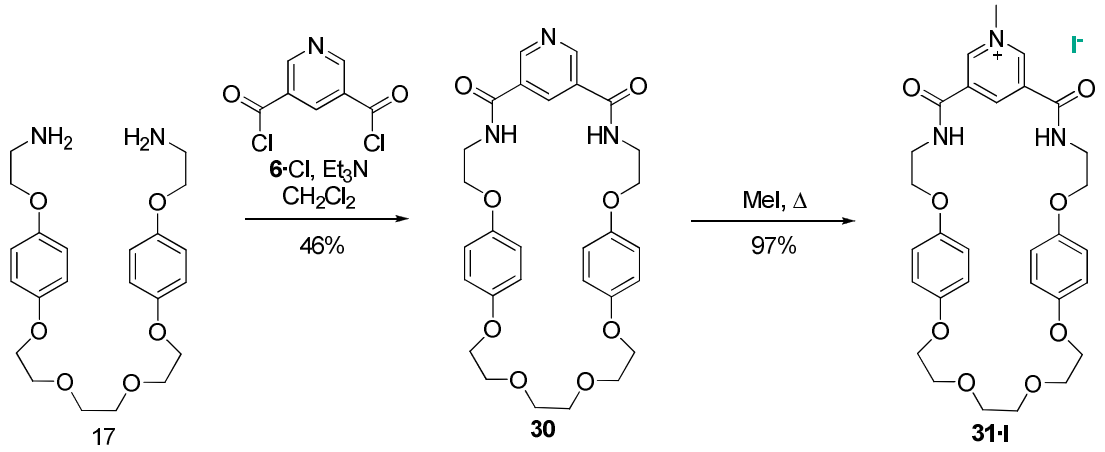



***Scheme 2.20.*** *Synthesis of pyridinium macrocycle* ***29****·X.*

Trimethyloxonium tetrafluoroborate was used to form macrocycle **29**·$BF_4$, but in much lower yields than those obtained with iodomethane (45% compared with 96%). A significant amount of macrocycle **8** was recovered from the reaction mixture despite efforts to force the reaction to completion using large excesses of $Me_3OBF_4$ and longer reaction times. It is postulated that since the alkylating agent liberates $HBF_4$ on contact with any trace amount of water, this strong acid could protonate the macrocycle's pyridine group, inhibiting the alkylation reaction.

Even as the lipophilic tetrafluoroborate salt the macrocycle had only partial solubility in solvents suitable for catenanation reactions ($CH_2Cl_2$ or MeCN) and would only dissolve in solvents too competitive for interlocked structure assembly or incompatible with acid chloride condensation reactions. Therefore it was deemed a macrocycle with greater solubility would be required if catenane formation was to be successful.

This was achieved with the preparation of the smaller four-oxygen polyether containing pyridinium macrocycle **31**·I. The synthesis of the new pyridinium macrocycle is outlined in Scheme 2.21. The condensation of 3,5-pyridine dicarbonyl dichloride with bis-amine **17** in the presence of templating reagent **6**·Cl and $Et_3N$ in dry $CH_2Cl_2$ afforded macrocycle **30** in 46% yield following acidic work-up and column chromatography. Alkylation with iodomethane gave pyridinium macrocycle **31**·I in 97% yield.




***Scheme 2.21.*** *Synthesis of pyridinium macrocycle* ***31****·I.*

Fortuitously, the new pyridinium macrocycle **31**·I, proved to have much greater solubility than **29**·I in all solvents, and thus anion exchange to the chloride salt was attempted by repeatedly washing a $CHCl_3$ solution of **31**·I with aqueous $NH_4Cl$. Unfortunately it was discovered that macrocycle **31** had partial water solubility and following anion exchange the majority of the macrocycle was to be found in the aqueous layers. Instead an anion exchange resin was used to convert macrocycle **31** to the chloride salt, but this too proved unsuccessful with the macrocycle sticking to the resin and most material was lost.

Given that iodide has been proved to be an ineffective template for interlocked structure, it was hoped that it might be possible to synthesise [2]catenanes using macrocycle **31**·I combined with a source of chloride anions to act as the templating anions. This is discussed in the next section.

## 2.5.2 Synthesis and Characterisation of Novel [2]Catenanes

The syntheses of two novel catenanes were carried out according to Scheme 2.22. Isophthaloyl dichloride was added to a solution of the appropriate bis-amine, **31**·I and $Et_3N$ in dry $CH_2Cl_2$ and stirred for one hour. Following acidic work-up and preparative TLC catenanes **32**·Cl and **33**·Cl were isolated in 35% and 29% yields respectively. These yields are significantly lower than those obtained for rotaxane formation, and may be a consequence of

purification problems (contamination with the isophthalamide neutral macrocycle resulted in preparative TLC being carried out twice) and the more topologically constrained nature of the [2]catenane. In addition, in this particular synthesis, it is necessary for the acid chloride 'clipping' to take place within the confines of the pyridinium macrocycle, which may, for steric reasons, make the formation of catenanes less favourable.




***Scheme 2.22.*** *Synthesis of [2]catenanes.*

The new [2]catenanes were characterised by $^{1}$H NMR, $^{13}$C NMR and HRMS (ESI). The $^{1}$H NMR spectrum of catenane **33**·Cl along with those of the component pyridinium and neutral macrocycles for comparison are given in Figure 2.27.

The catenane spectrum displays upfield shifts of cavity proton *γ* and amide proton *δ*, and a reduction in splitting of the hydroquinone proton signal *η, θ,* both of which are consistent with the chloride anion becoming polarised away from the pyridinium macrocycle towards the amide binding cleft of the isophthalamide macrocycle. This is further signified by the large downfield perturbation of the cavity proton, *c* and amide proton *d* signals, as they become deshielded by the anion's negative charge. Finally, the large upfield shift and splitting of the hydroquinone proton signal *g, h,* of the isophthalamide macrocycle is characteristic of π-π donor-acceptor stacking interactions between these hydroquinone protons and the electron deficient pyridinium group.

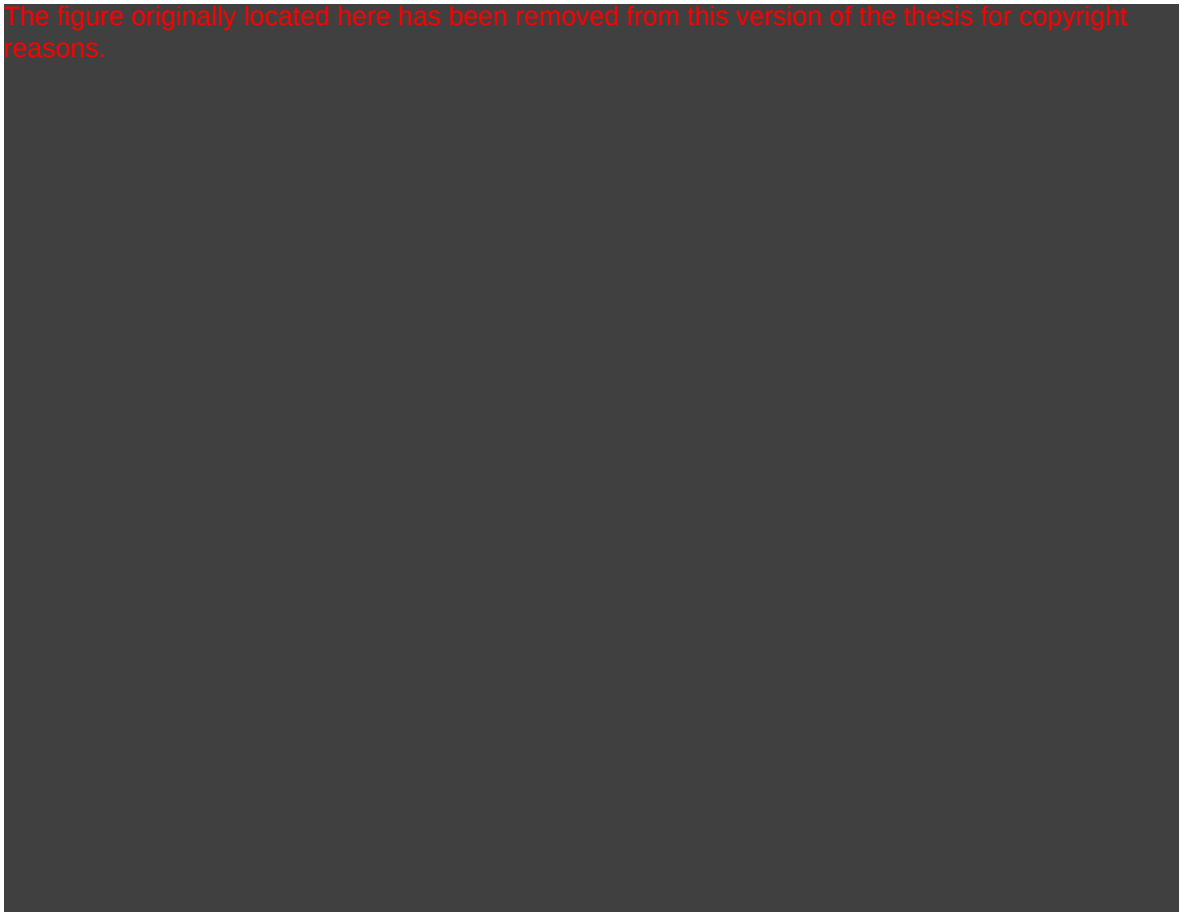



***Figure 2.27.*** *$^1$H NMR in $CDCl_3$ at 293K of (a) pyridinium **31**·I + 1 eq. TBACl, (b) [2]catenane **33**·Cl and (c) component macrocycle.*

Further evidence for the interlocked nature of the catenane structures was obtained from 2D $^1$H ROESY NMR, the spectrum of catenane **33**·Cl is given in Figure 2.28.

Cross coupling interactions exist between hydroquinone protons of the neutral macrocyclic component and the pyridinium protons exemplified by correlations **1** ($\gamma \rightarrow g,h$), **2** ($\beta \rightarrow g,h$) and **3** ($\delta \rightarrow g,h$). A through space correlation **6** ($\delta \rightarrow c$) also exists between amide proton of the pyridinium macrocycle and cavity proton of the neutral macrocycle, as they converge into the cleft to bind chloride. Interactions **4** ($b \rightarrow \eta,\theta$) and **5** ($c \rightarrow \eta,\theta$) reveal the isophthaloyl and hydroquinone protons are also in close proximity.

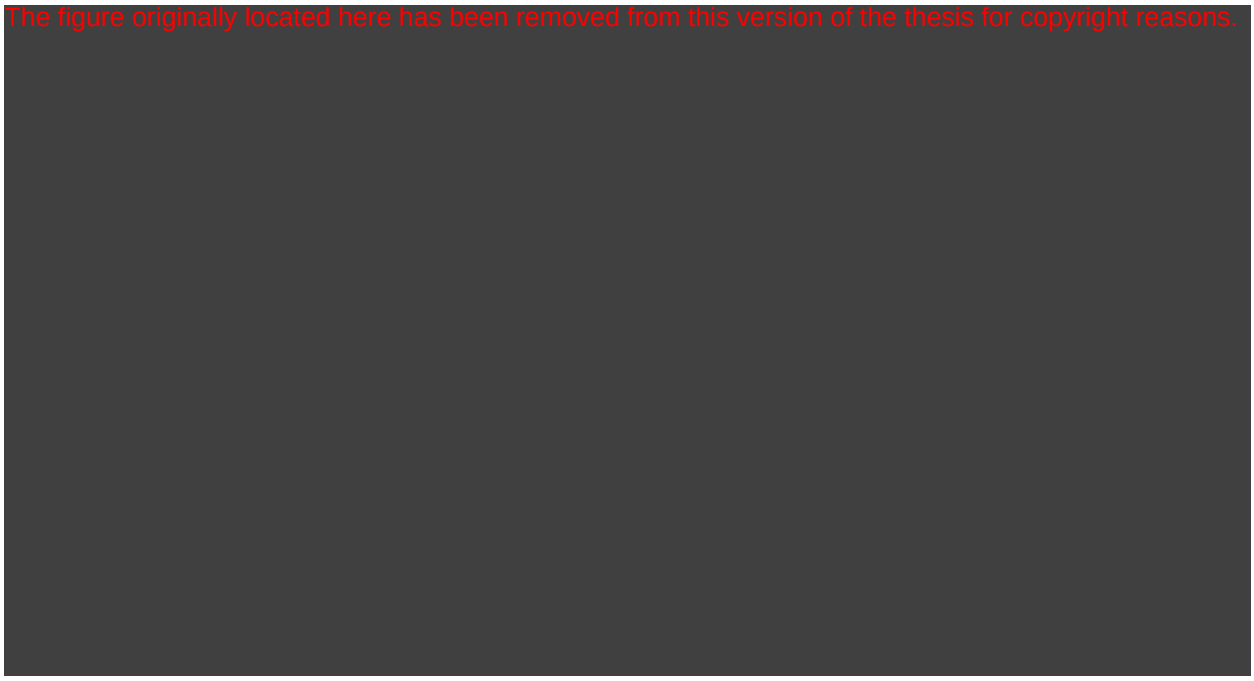



***Figure 2.28.*** *$^{1}H$ -$^{1}H$ ROESY spectrum of [2]rotaxane **33**·Cl in $CDCl_3$ at 293K. Cross couplings are shown on the schematic diagram on the right.*

### 2.5.3 Anion Recognition Studies

In order to determine the ability of the novel [2]catenanes to complex anions, the chloride templating anion was exchanged for the non-coordinating hexafluorophosphate salt by washing chloroform solutions of **32**·Cl and **33**·Cl with aqueous $NH_4PF_6$.

Anion binding studies were carried out using $^{1}H$ NMR titration experiments, as discussed in Section 2.3.5, in a 1:1 $CDCl_3/CD_3OD$ solvent mixture. Addition of anions to a solution of the catenane receptor resulted in a number of chemical shift perturbations of protons in the vicinity of the interlocked cavity. The titration curves for the addition of anions to catenane **32**·$PF_6$ are shown in Figure 2.31.

The addition of chloride, acetate and dihydrogen phosphate to **32**·$PF_6$ and **33**·$PF_6$ produced downfield shifts of *ortho* pyridinium proton $\beta$ whilst cavity pyridinium proton $\gamma$ was shown to move downfield upon addition of chloride but upfield in the presence of the oxoanions. Interestingly, in contrast to the [2]rotaxanes, cavity proton *c* of the neutral macrocyclic component was observed to move downfield for all three anions, whereas negligible shifts

were observed in this proton when the oxoanions were added to the rotaxanes. The upfield movement of proton $\gamma$ upon the addition of dihydrogen phosphate and acetate implies that there is still some conformational change upon the binding of these oxoanions.

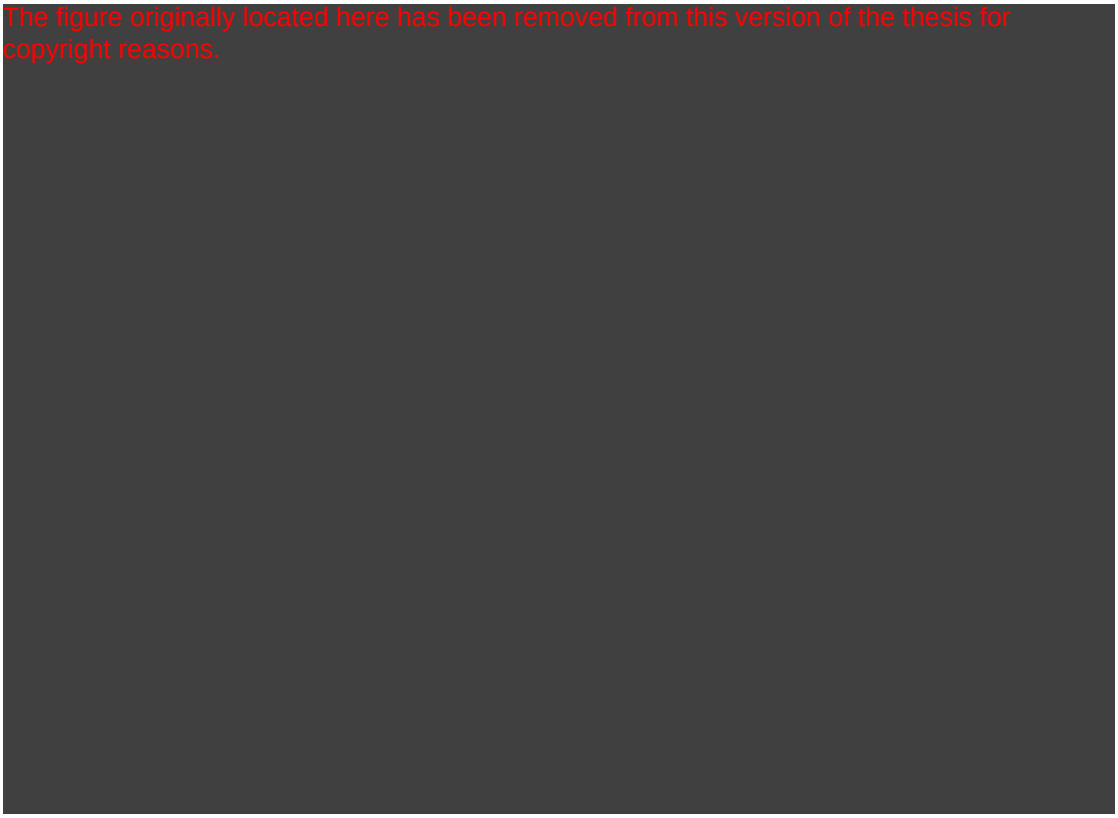



***Figure 2.29.*** *Chemical shift perturbations of protons (a)* β *, (b)* γ *and (c)* c *on addition of* $Cl^-$*,* $OAc^-$ *and* $H_2PO_4^-$ *(as TBA salts) to a solution of [2]catenane* ***32***$\cdot PF_6$ *in 1:1* $CDCl_3/CD_3OD$ *at 1.91 ×* $10^{-3}$*M and 293 K. Symbols represent experimental data points; continuous lines represent calculated curves.*

WinEQNMR2 analysis of the titration data determined 1:1 stoichiometric association constants, given in Table 2.5.

| | $Cl^-$ | $OAc^-$ | $H_2PO_4^-$ |
|---|---|---|---|
| **32**·$PF_6$ | 1650 | 210 | 630 |
| **33**·$PF_6$ | 880 | 160 | 540 |

**Table 2.5:** *Association constants, K (*$M^{-1}$*), of [2]catenane* ***32***$\cdot PF_6$ *and* ***33***$\cdot PF_6$ *with* $Cl^-$*,* $OAc^-$ *and* $H_2PO_4^-$ *in 1:1* $CDCl_3/CD_3OD$ *at 1.91 ×* $10^{-3}$*M and 293K. Obtained by monitoring proton* β *. Error < 10%.*

Both catenanes strongly complex chloride in this competitive solvent mixture and the basic oxoanions are bound considerably more weakly. This may be a consequence of chloride being of complementary size and geometry to be encapsulated within the catenane binding cavity whilst the considerably larger oxoanions associate peripherally. Interestingly acetate is bound more weakly than dihydrogen phosphate despite its greater basicity.

Interestingly, catenane **32**·$PF_6$ is observed to complex chloride significantly more strongly than catenane **33**·$PF_6$, which may be the result of the latter catenane possessing a more topologically constrained conformation, where unfavourable steric interactions between the pyridinium *N*-methyl group and the four-oxygen polyether chain of the neutral macrocycle results in anion complexation being less favourable.

Importantly the [2]catenanes exhibit relatively lower binding affinities for chloride than their analogous rotaxane systems in 1:1 $CDCl_3$/$CD_3OD$. In the rotaxane the amides appended to the axle's pyridinium motif are aromatic in nature, compared to the catenanes where the analogous amide protons are aliphatic. Aromatic amide protons are more acidic than their aliphatic counterparts due to delocalisation of electron density into the benzene rings and thus are capable of more strongly complexing anions.

### 2.5.4 X-ray Crystal Structures

Single crystals of **32**·Cl suitable for single crystal X-ray diffraction structural analysis were grown by slow evaporation of a $CHCl_3$/acetone solution of the catenane. The structure (Figure 2.30), solved by Dr. Nathan Kilah, confirms the interlocked nature of the [2]catenane, and the location of chloride, encapsulated within the binding cavity's orthogonal hydrogen bonding array.

As well as the hydrogen bonding interactions between the halide anion and interlocked receptor, other important non-covalent forces acting to stabilise the catenane are highlighted. Both π-π donor-acceptor stacking interactions between the pyridinium surface and at least one

hydroquinone ring are observed, as well as hydrogen bonds between the pyridinium *N*-methyl protons and the polyether oxygens of the neutral macrocyclic component.




***Figure 2.30.*** *X-ray crystal structure of* ***32****·Cl. Disorder and non-protic hydrogens omitted for clarity.*

In addition, it was possible to grow single crystals of **33**·$PF_6$, by slow evaporation of a $CHCl_3$/MeOH solution of the catenane which was solved by Dr. Christopher Serpell. Interestingly, the structure (Figure 2.31) shows the amides of both macrocyclic components adopting a *syn-anti* confomation in the absence of the templating chloride anion.

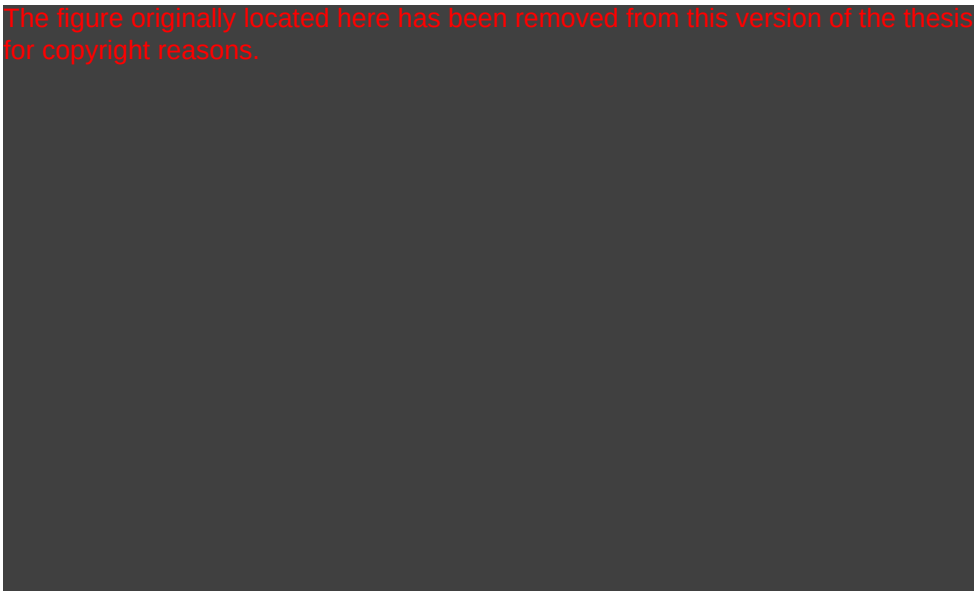



***Figure 2.31.*** *X-ray crystal structure of* ***32****·$PF_6$. Non-protic hydrogens omitted for clarity.*

Intramolecular hydrogen bonding between carbonyl oxygen and amide protons of opposing macrocycles (dotted lines) exists to stabilise the structure in the absence of chloride, whilst the

hexafluorophosphate anion is shown to be wholly non-coordinating. Only a minor change in conformation is required in order to re-establish the tetrahedral hydrogen bonding array for anion coordination, implying that complexation of anionic guests can occur *via* an induced-fit mechanism with low energetic barriers.[31]

## 2.6 Summary, Conclusions and Future Perspectives

A new versatile synthetic methodology that combines chloride anion templation with π-π stacking interactions has been developed for the synthesis of macrocycles, rotaxanes and catenanes, which eliminates the need for the expensive Grubbs' RCM catalyst.

Using this method it has been possible to double the yield of formation of important macrocyclic components by utilising a 3,5-pyridinium bis-amide thread as a template, the removal of which, following the macrocycle synthesis, is facile using column chromatography.

As an extension of this macrocycle synthesis, a variety of [2]rotaxanes have been synthesised by replacing the template with a stoppered pyridinium axle component. It has been possible to exploit the versatility of the new synthetic route by varying the size of the macrocycle, the electronic nature of the macrocycle's anion binding component and also the electron rich aromatic units of the macrocycle. Interestingly, rotaxanes containing the larger five-oxygen polyether macrocyclic component are produced in higher yield, a factor attributed to unfavourable steric interactions between the axle pyridinium *N*-methyl group and the polyether chain in the smaller four-oxygen polyether analogue which is further supported by molecular dynamics simulations.

Following removal of the chloride template $^{1}$H NMR anion titration binding investigations demonstrated the ability of the rotaxanes' three-dimensional binding domains to exhibit high degrees of chloride anion selectivity in competitive aqueous solvent media (45:45:10

$CDCl_3/CD_3OD/D_2O$) in preference to the more basic oxoanions. This binding trend was rationalised by assuming that the oxoanions are too large to fit within the three-dimensional binding cavity and thus associate peripherally. Molecular dynamics simulations corroborate this theory, where the oxoanions are demonstrated to bind externally to the binding cavity causing appreciable distortion in the rotaxane structure, whilst near total encapsulation of chloride is observed. X-ray structural analysis confirms the position of the chloride within the three-dimensional binding cleft.

The rotaxane host's chloride anion binding affinity can be further enhanced and tuned *via* attachment of electron withdrawing substituents to the macrocycle's isophthalamide motif and by increased positive charge with macrocycle pyridinium group modification. In particular, the orthogonal cavity disposition of two 3,5-bis-amide substituted pyridinium motifs of the dicationic rotaxane **28**·$(PF_6)_2$ impressively enables this interlocked host to recognize chloride in 35% water, wherein no evidence of binding oxoanions, acetate and dihydrogen phosphate, is detected.

It has also been possible to synthesise [2]catenanes *via* adaptation of novel synthetic pathway by replacing the axle component with a pyridinium containing macrocycle. The anion binding properties were again probed by $^1$H NMR titration experiments and like their rotaxane analogues the novel [2]catenanes were found to bind chloride in preference to the more basic oxoanions in 1:1 $CDCl_3/CD_3OD$. However these catenane host molecules were found to bind chloride significantly less strongly than the equivalent rotaxanes, a feature that can be attributed to the absence of the relatively more acidic aromatic amide protons.

To conclude, the versatility of a new synthetic method has been demonstrated by extensively varying the macrocycle component of [2]rotaxanes, and synthesising [2]catenanes. It may be possible to further exploit this route by replacing the pyridinium *N*-methyl group with alternative positively charged anion binding motifs.

Future efforts to construct chloride selective interlocked host molecules should be focused on rotaxanes since they are shown to be superior complexants of anions. The design and manipulation of mechanically bonded rotaxane molecules for luminescent anion sensing applications is investigated in the following chapter.

## 2.7 References


1. J. L. Sessler, P. A. Gale and W.-S. Cho, *Anion Receptor Chemistry*, RSC, Cambridge, 2006.
2. S. Kubik, *Chem. Soc. Rev.*, 2010, **39**, 3648-3663.
3. H. Luecke and F. A. Quiocho, *Nature*, 1990, **347**, 402-406.
4. J. W. Pflugrath and F. A. Quiocho, *Nature*, 1985, **314**, 257-260.
5. S. Kubik, R. Goddard, R. Kirchner, D. Nolting and J. Seidel, *Angew. Chem., Int. Ed.*, 2001, **40**, 2648-2651.
6. J.-M. Suk and K.-S. Jeong, *J. Am. Chem. Soc.*, 2008, **130**, 11868-11869.
7. J. A. Wisner, P. D. Beer, M. G. B. Drew and M. R. Sambrook, *J. Am. Chem. Soc.*, 2002, **124**, 12469-12476.
8. M. R. Sambrook, P. D. Beer, J. A. Wisner, R. L. Paul and A. R. Cowley, *J. Am. Chem. Soc.*, 2004, **126**, 15364-15365.
9. M. R. Sambrook, P. D. Beer, M. D. Lankshear, R. F. Ludlow and J. A. Wisner, *Org. Biomol. Chem.*, 2006, **4**, 1529-1538.
10. K. Kavallieratos, S. R. deGala, D. J. Austin and R. H. Crabtree, *J. Am. Chem. Soc.*, 1997, **119**, 2325-2325.
11. J. A. Wisner, P. D. Beer and M. G. B. Drew, *Angew. Chem., Int. Ed.*, 2001, **40**, 3606-3609.
12. K.-Y. Ng, V. Felix, S. M. Santos, N. H. Rees and P. D. Beer, *Chem. Commun.*, 2008, 1281-1283.
13. J. W. Steed and J. L. Atwood, *Supramolecular Chemistry*, Wiley, Chichester, 2009.
14. M. C. Thompson and D. H. Busch, *J. Am. Chem. Soc.*, 1962, **84**, 1762-1763.
15. M. C. Thompson and D. H. Busch, *J. Am. Chem. Soc.*, 1964, **86**, 213-217.
16. M. C. Thompson and D. H. Busch, *J. Am. Chem. Soc.*, 1964, **86**, 3642-3650.
17. C.-H. Sue, S. Basu, A. C. Fahrenbach, A. K. Shveyd, S. K. Dey, Y. Y. Botros and J. F. Stoddart, *Chem. Sci.*, 2010, **1**, 119-125.
18. D. Meshcheryakov, V. Böhmer, M. Bolte, V. Hubscher-Bruder, F. Arnaud-Neu, H. Herschbach, A. Van Dorsselaer, I. Thondorf and W. Mögelin, *Angew. Chem., Int. Ed.*, 2006, **45**, 1648-1652.
19. E. A. Katayev, G. Dan Pantos, M. D. Reshetova, V. N. Khrustalev, V. Lynch, Y. A. Ustynyuk and J. L. Sessler, *Angew. Chem., Int. Ed*, 2005, **44**, 7386-7390.
20. M. Bru, I. Alfonso, M. I. Burguete and S. V. Luis, *Angew. Chem., Int. Ed.*, 2006, **45**, 6155-6159.
21. D. A. Leigh, A. Murphy, J. P. Smart and A. M. Z. Slawin, *Angew. Chem., Int. Ed*, 1997, **36**, 728-732.
22. A. G. Johnston, D. A. Leigh, A. Murphy, J. P. Smart and M. D. Deegan, *J. Am. Chem. Soc.*, 1996, **118**, 10662-10663.
23. M. J. Hynes, *J. Chem. Soc., Dalton Trans.*, 1993, 311-312.

24. H. W. Gibson, S.-H. Lee, P. T. Engen, P. Lecavalier, J. Sze, Y. X. Shen and M. Bheda, *J. Org. Chem*, 1993, **58**, 3748-3756.
25. U. Eisner and J. Kuthan, *Chem. Rev.*, 1972, **72**, 1-42.
26. D. M. Stout and A. I. Meyers, *Chem. Rev.*, 1982, **82**, 223-243.
27. K. M. Bonger, R. van den Berg, L. H. Heitman, A. P. Izjerman, J. Oosterom, K. M. Timmers, H. S. Overkleeft and G. A. van der Marel, *Biorg. Med. Chem*, 2007, **15**, 4841-4856.
28. K. Kavallieratos, C. M. Bertao and R. H. Crabtree, *J. Org. Chem.*, 1999, **64**, 1675-1683.
29. D. A. Case, *AMBER 10*, University of California, San Francisco, 2008.
30. J. Wang, R. M. Wolf, J. W. Caldwell, P. A. Kollman and D. A. Case, *J. Comput. Chem.*, 2004, **25**, 1157-1174.
31. A. N. Swinburne, M. J. Paterson, A. Beeby and J. W. Steed, *Chem. Eur. J.*, 2010, **16**, 2714-2718.

# Chapter 3: Transition Metal Appended [2]Rotaxanes for Luminescent Anion Sensing

## 3.1 Introduction

Following the success in utilising a new synthetic procedure to construct interlocked host architectures for selective chloride recognition, as detailed in Chapter 2, focus shifted to incorporating a reporter group into such an interlocked receptor to allow for the macroscopic detection of anions.

Due to the inherent sensitivity of detection techniques, coupled with the low concentrations of the host molecule required for detection, luminescence was chosen as the sensing mechanism. A variety of inorganic and organic fluorophores are known (see Chapter 1),[1] however rhenium(I) and ruthenium(II) bipyridyl complexes are attractive for incorporation into luminescent anion sensors since they exhibit chemical stability and their optical properties are well established.[2] In addition, polypyridyl ligands can be appropriately functionalised for integration into a range of receptors. In this case, rotaxanes were chosen as the interlocked host structure since the more topologically constrained nature of [2]catenanes make functionalisation with the bulky polypyridyl transition metal complex more challenging. Conversely, it may be possible to decorate either the macrocyclic or axle component of a [2]rotaxane in such a way that the transition metal polypyridyl group is in proximity to the interlocked binding site facilitating the luminescent sensing of the anionic guest species.

### 3.1.1 Photophysical Properties of Rhenium and Ruthenium Complexes

Octahedral polypyridyl complexes of both rhenium(I) and ruthenium(II) exhibit low-spin $d_6$ configurations giving rise to the molecular orbital diagram shown in Figure 3.1a. A number of electronic transitions between energy levels are possible, including metal d-d and ligand π-π* transitions, and ligand to metal and metal to ligand charge transfer bands. The latter is most important in terms of the photophysical properties of these complexes, where absorption of a photon of appropriate wavelength excites an electron from the fully occupied $t_{2g}$ metal-centred orbital to the ligand π* orbital. Intersystem crossing from the singlet MLCT to the triplet MLCT is efficient since both metals are considered to be 'heavy atoms' and it is generally assumed that luminescence occurs from the triplet state (Figure 3.1b).

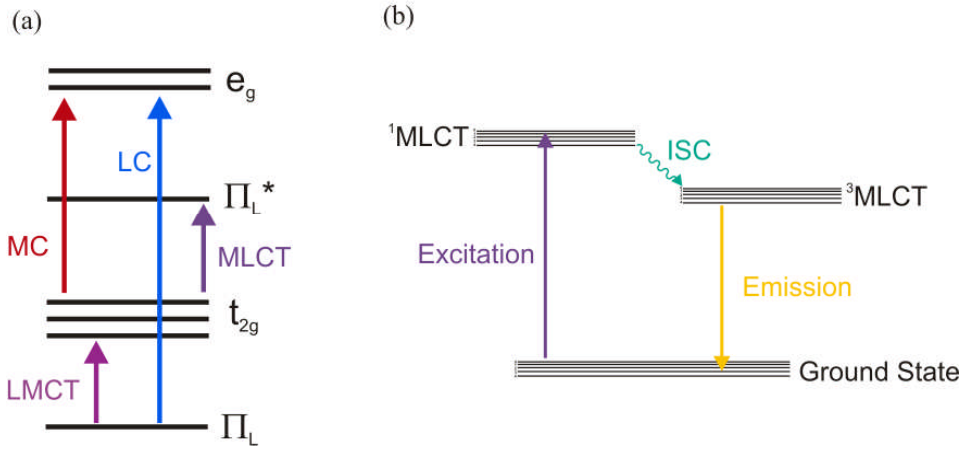



***Figure 3.1.*** *(a) Example of a partial MO diagram and (b) Jablonski diagram, for Re(I)/Ru(II) complexes.*

The objective when designing an appropriate anion sensor containing these transition metals is for the presence of a bound anion to perturb the intensity and wavelength of this emission. The following section discusses examples of anion sensing rhenium(I) and ruthenium(II) bipyridyl receptors.

### 3.1.2 Transition Metal Appended Anion Sensors

Many acyclic anion sensors have exploited the photophysical properties of rhenium(I) and ruthenium(II) bipyridyl motifs for luminescent anion recognition. Lees and coworkers appended rhenium(I) bipyridyl complexes in close proximity to an isophthalamide anion binding fragment (Figure 3.2a), whereby quenching of the $^3$MLCT band was observed upon addition of anions in $CH_2Cl_2$, with cyanide, acetate and the halides shown to bind most strongly.[3] This reduction in emission intensity was tentatively accredited to hydrogen bonding interactions between the amide protons and anions causing the lowest excited state to switch from a bipy-based $^3$MLCT state to an amide-pyridine $^3$MLCT state, thereby enhancing non-radiative decay.

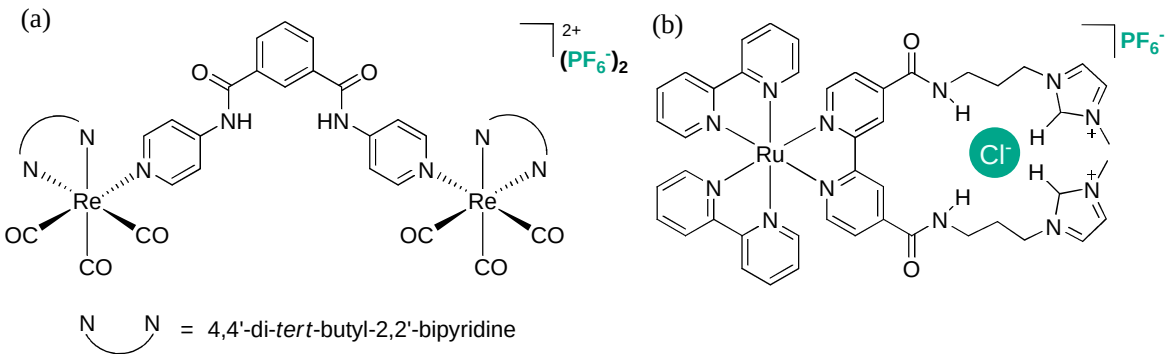



***Figure 3.2.*** *Anion sensors incorporating transition metal complexes: (a) Lees' rhenium(I) receptor;[3] and (b) Beer's ruthenium(II) imidazolium receptor.[4]*

A major incentive for the integration of a transition metal into an anion receptor is that the metal often provides an additional positive charge to the molecule, and may enhance anion binding through electrostatic interactions.[5, 6] Ruthenium(II) complexes containing neutral ligands are dicationic and are therefore well placed to satisfy this requirement. Vickers and Beer have developed a potent anion sensor by functionalising an amide appended ruthenium(II) bipyridyl complex with imidazolium units (Figure 3.2b).[4] The receptor was shown to be selective for chloride in 9:1 MeCN/$H_2O$, which can be attributed to the size of the cavity, created by four convergent charge-assisted hydrogen bonds, and showed both a

luminescence emission enhancement and hypsochromic shift of the $^{3}$MLCT band upon anion binding. The enhancement of the emission intensity was attributed to a rigidification of the receptor upon anion binding, therefore reducing energy lost through non-radiative pathways. Meanwhile the $^{3}$MLCT band hypsochromic shift can be explained by assuming that the electron in the MLCT dπ* formally resides on the bis-amide bipyridine ligand, which is energetically unfavourable in the presence of an anion.

The examples above illustrate ways in which anions may perturb the luminescence emission intensity of the MLCT of rhenium(I) and ruthenium(II) bipyridyl based anion receptors, and demonstrate factors to be considered when designing photo-active mechanically interlocked structures.

### 3.1.3 Chapter Objectives

This chapter aims to exploit the synthetic versatility of polypyridyl ligands (namely 2,2′-bipyridine and 1,10-phenanthroline) for incorporation into either the macrocyclic or axle component of [2]rotaxanes, with a view to complexing a photo-active transition metal.

Firstly, functionalisation of the macrocyclic component to incorporate metal lumophores is explored, with initial focus on the synthesis of photo-active macrocycles *via* the novel synthetic strategy detailed in Chapter 2. It is hoped that this route can also be exploited for the ambitious synthesis of 2,2′-bipyridine functionalised rotaxanes, which can subsequently be appended with the appropriate rhenium(I) or ruthenium(II) complex. Ultimately, the anion recognition and sensing properties of the photo-active rotaxanes are investigated through a combination of $^{1}$H NMR and luminescence spectroscopy (Figure 3.3a).

The second section of this chapter explores the possibility of incorporating a transition metal complex into the axle component of a [2]rotaxane, whereby this motif constitutes one of the bulky stopper groups. The anion recognition and sensing properties of an amide appended phenanthroline bis-bipyridyl ruthenium(II) motif are investigated *via* incorporation into

simple acyclic receptors to determine the suitability of the motif for integration into rotaxane host systems. As precursors to these structures the ability of these receptors to form pseudorotaxanes with appropriate macrocyclic components is explored by both $^{1}$H NMR and luminescence spectroscopy. Finally, the synthesis of a rotaxane containing a photo-active axle component is attempted with the ultimate objective of investigating its anion sensing properties (Figure 3.3b).

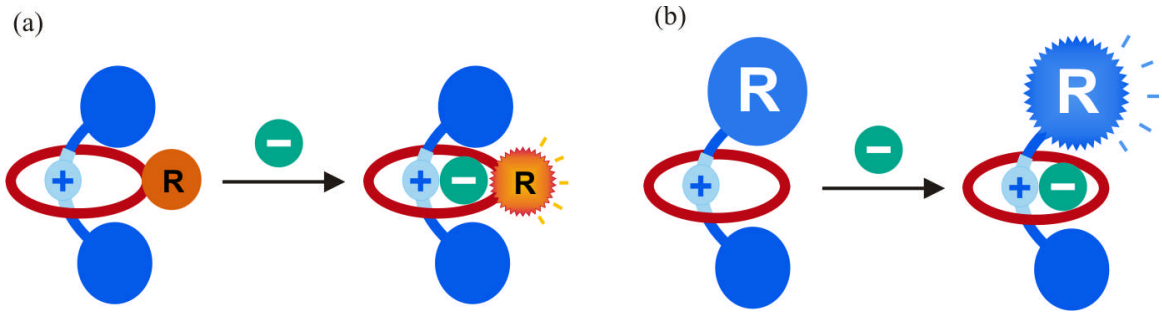



***Figure 3.3.*** *Schematic representation of anion sensing where reporter group is appended to (a) macrocyclic and (b) axle components.*

## 3.2 Incorporation of Transition Metal Reporter Motif into Macrocyclic Component

Incorporating the 4,4′-bis-amide-2,2′-bipyridyl motif into macrocycles facilitates the subsequent complexation of transition metals. Indeed a range of transition metals with both octahedral and square planar coordination preference have been incorporated into these cyclic structures.[2] An illustrative example is provided by Beer and co-workers who appended a calix[4]arene framework with an amide functionalised ruthenium(II) bipyridine anion binding unit (Figure 3.4).[7]

This macrocycle exhibited a dramatic increase in MLCT luminescence intensity upon addition of dihydrogen phosphate in DMSO, which was attributed to increased rigidification of the

host-anion complex compared to the free receptor, disfavouring energy loss through non-radiative decay pathways.

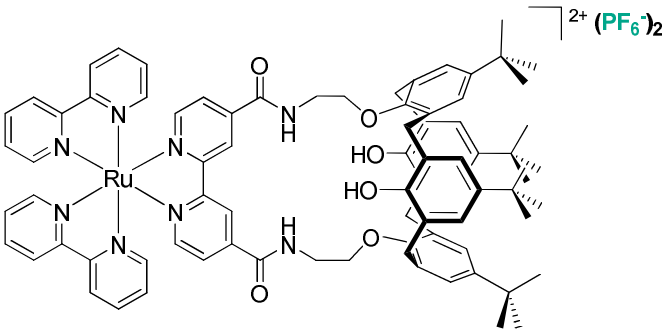



***Figure 3.4.*** *Beer's Ru(II) calix[4]arene macrobicycle.*[7]

The macrocycles described in Chapter 2 were shown to undergo strong association with a pyridinium ion-pair thread, and by appropriately modifying the macrocyclic component it has been shown that a series of luminescent pseudorotaxanes can be assembled (Figure 3.5).[8]

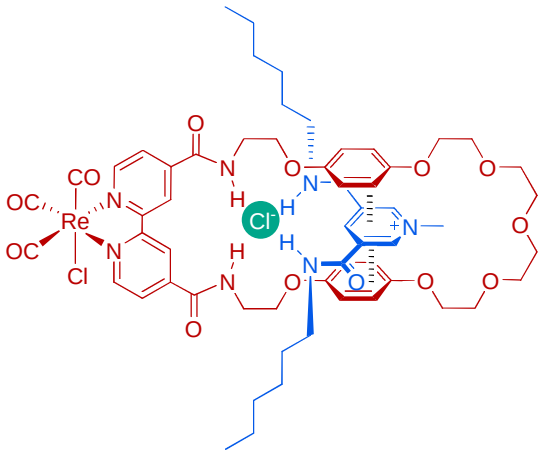


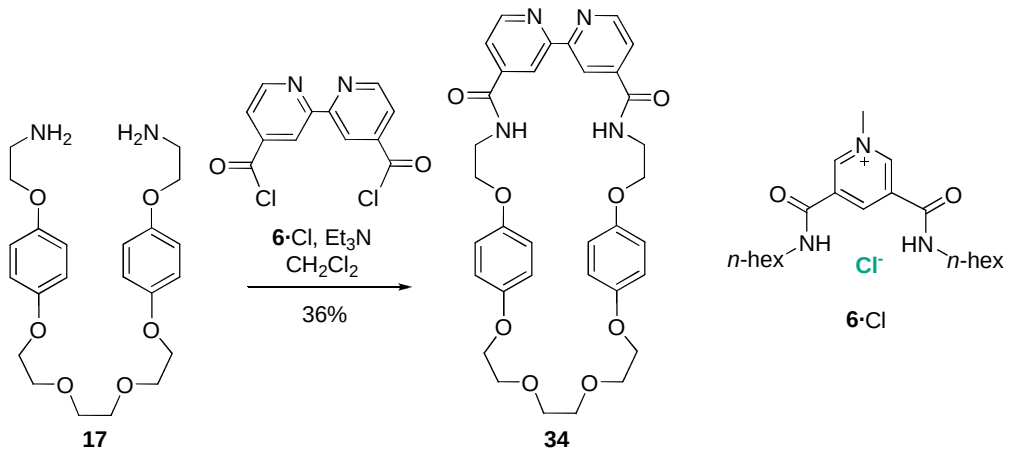

***Figure 3.5.*** *Chloride-templated photo-active pseudorotaxane.*[8]

Importantly, the presence of the pyridinium ion-pair thread causes an enhancement of the rhenium(I) complex's MLCT emission intensity, despite evidence that the pyridinium motif can quench luminescence through formation of charge transfer complexes.[9] These results are positive indications that the analogous rotaxane would also display luminescent properties, and may be capable of sensing anions through perturbation of the MLCT emission band.

### 3.2.1 Macrocycle Synthesis and Characterisation

A structurally similar bipyridyl bis-amide macrocycle to that shown in Figure 3.5 was chosen as the macrocycle component in the new photo-active rotaxane design. Due to the relatively larger bis-amide 'bite-size' of the 4,4′-bis-amide-2,2′-bipyridyl group as compared to the isophthalamide motif, it was thought the *tert*-phenyl stopper groups used thus far may not be sufficiently bulky to prevent dethreading of the axle component. It is possible to prepare an axle containing larger stopper groups, but synthetically it is easier to use the smaller four-oxygen polyether macrocycle component.

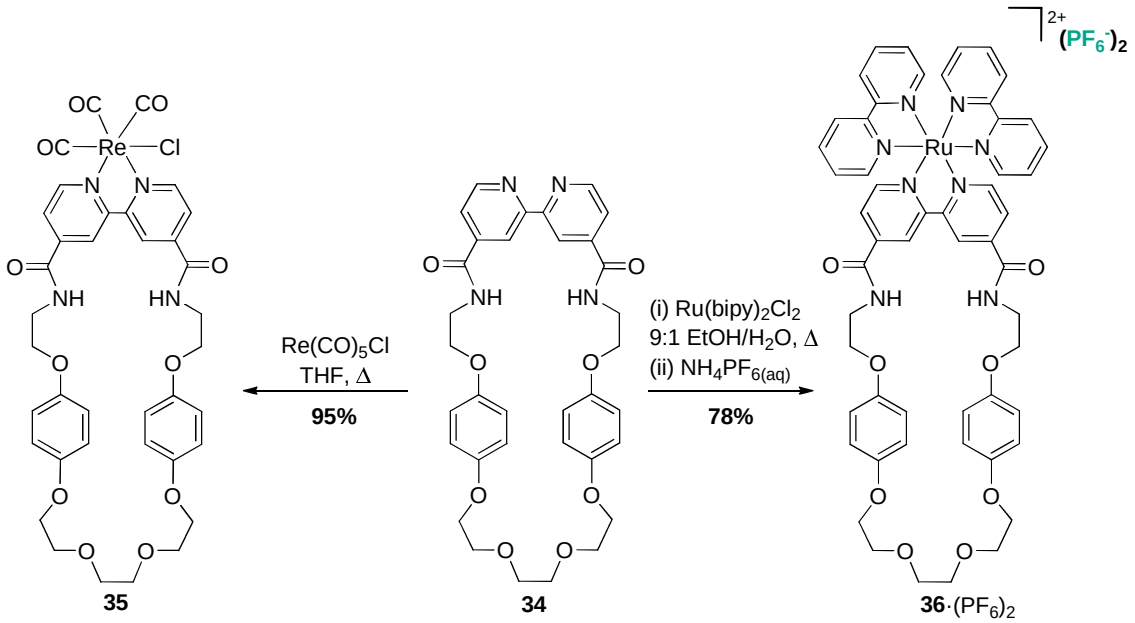
The synthesis of the bis-amine precursor **17** is described in Chapter 2. The target bipyridine macrocycle was prepared *via* an acid chloride condensation of bis-amine **17** with 4,4′-bis(chlorocarbonyl)-2,2′-bipyridine in the presence of the pyridinium template **6**·Cl (Scheme 3.1).




***Scheme 3.1.*** *Synthesis of macrocycle* ***34****.*

Following column chromatography the macrocycle was isolated in 36% yield, suggesting that the templation method used in Chapter 2 can be successful when the geometry of the bis-acid chloride used in the 'clipping' step of the reaction deviates from that of the standard isophthalamide. This also has positive implications for the possibility of synthesising similarly functionalised rotaxanes by this method.

Heating macrocycle with either $Re(CO)_5Cl$ or $Ru(bipy)_2Cl_2$ (Scheme 3.2) afforded the corresponding metal complexes in good yields. For the ruthenium(II) appended macrocycle, anion exchange to the non-coordinating hexafluorophosphate salt was achieved by precipitation with aqueous $NH_4PF_6$.




***Scheme 3.2.*** *Synthesis of transition metal appended macrocycles.*

A combination of $^1H$ and $^{13}C$ NMR and HRMS (ESI) were used in order to determine whether the procedure to complex the transition metal had been successful.

Since the new rhenium macrocycle **35** contains no new proton environments, $^{13}C$ NMR was used to verify that the complexation of rhenium had occurred *via* the presence of new carbon signals at 197.5ppm and 189.5ppm corresponding to the carbonyl ligands of the metal complex (Figure 3.6).

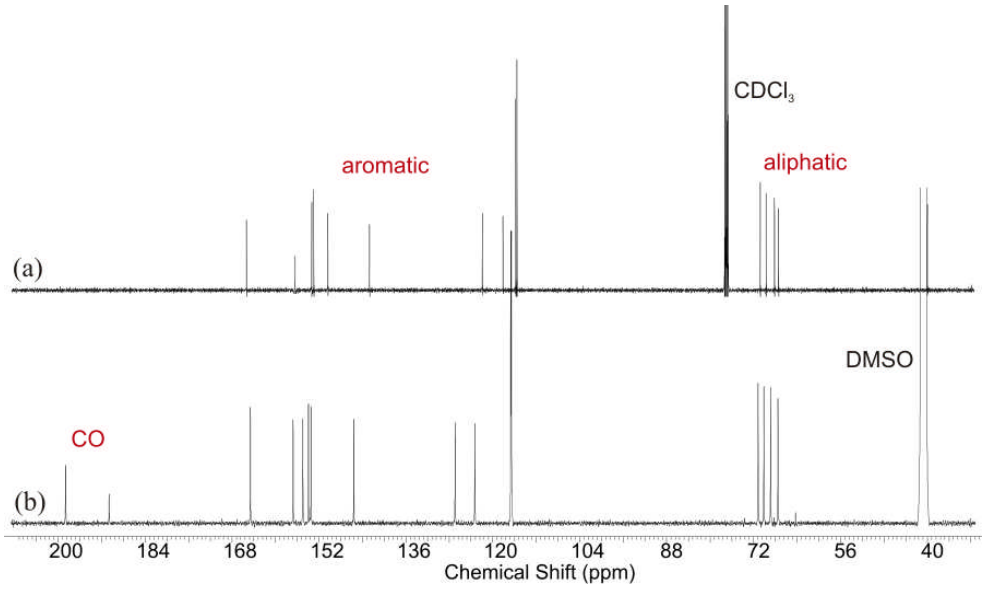



***Figure 3.6.*** *$^{13}C$ NMR spectra at 293 K of (a) macrocycle **34** in $CDCl_3$, and (b) macrocycle **35** in $d_6$-DMSO.*

The $^{1}H$ NMR spectra of bipyridine macrocycle **34** and the new ruthenium(II) appended macrocycle **36**·$(PF_6)_2$ are shown in Figure 3.7.

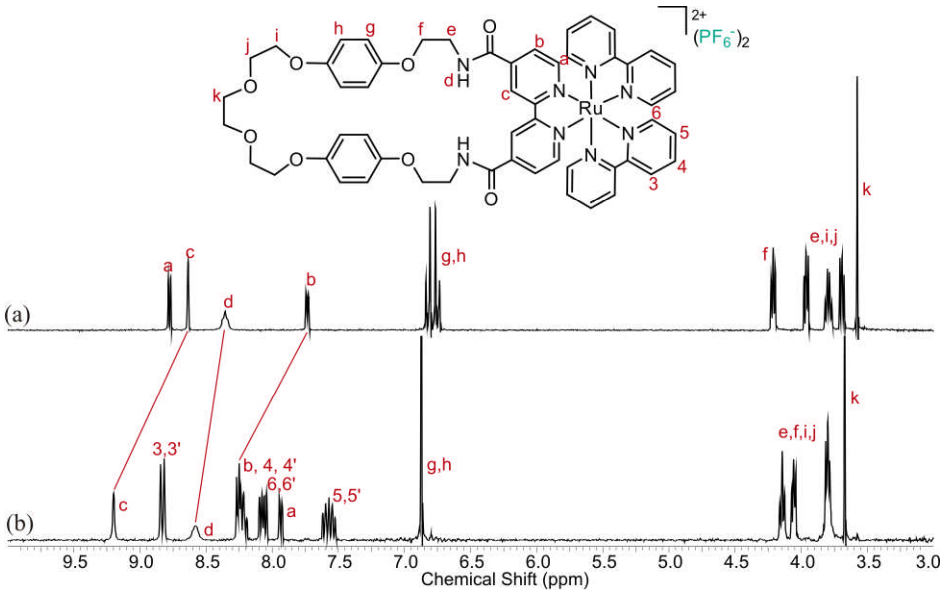



***Figure 3.7.*** *$^{1}H$ NMR spectra in $d_6$-acetone at 293 K of (a) macrocycle **34** and (b) macrocycle **36**·$(PF_6)_2$.*

A number of new peaks are observed in the aromatic region of the spectrum of **36**·$(PF_6)_2$ corresponding to sixteen new bipyridyl protons. In addition bipyridyl protons *b* and *c*, as well as amide *d* signals of the macrocycle have moved downfield due to the presence of the positively charged ruthenium centre causing deshielding.

It was also possible to grow single crystals of macrocycle **36**·$(PF_6)_2$ suitable for X-ray diffraction structural analysis by slow evaporation of a solution of the macrocycle from $d_6$-acetone. The preliminary structure was solved by Dr. Nathan Kilah, and is shown in Figure 3.8. Macrocycle amide groups are shown to adopt a *syn-syn* conformation.

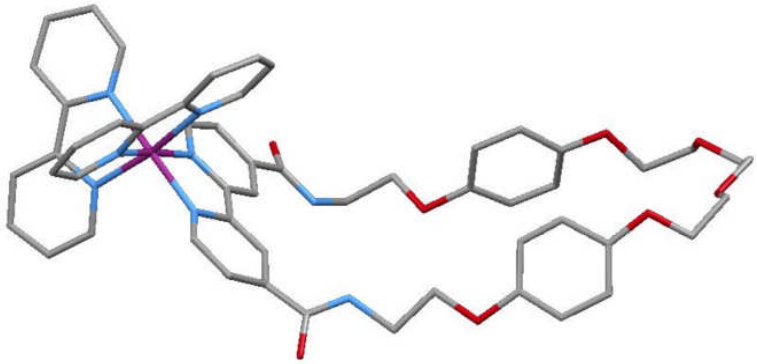
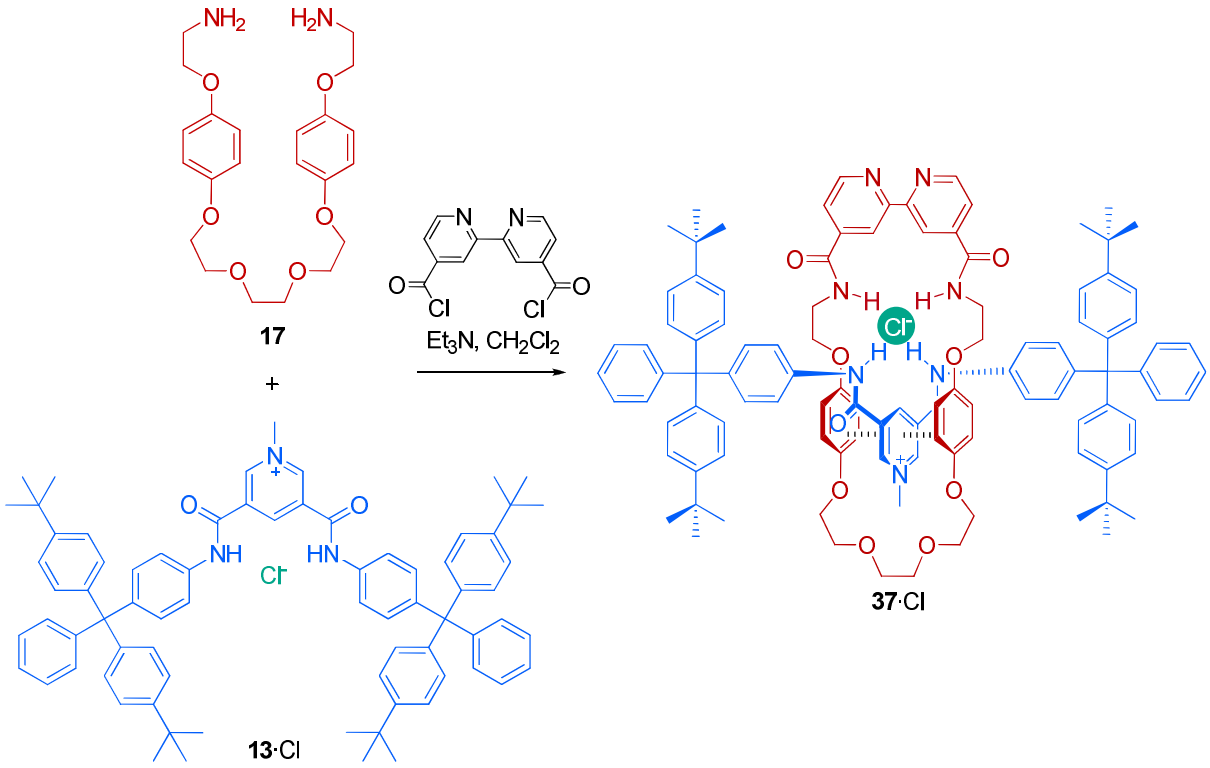


***Figure 3.8****. Crystal structure of macrocycle* ***36****·(*$PF_6$*)*$_2$*. Hydrogen atoms and counteranions are omitted for clarity.*

### 3.2.2 Rotaxane Synthesis

Having successfully prepared the bipyridine containing macrocycles, an analogous procedure (Scheme 3.3) was used to synthesise a bipyridine containing [2]rotaxane. In accordance with the rotaxane syntheses in Chapter 2, 4,4'-bis(chlorocarbonyl)-2,2′-bipyridine was added to a solution of bis-amine **17,** axle **13**·$Cl^{10}$ and $Et_3N$ in dry $CH_2Cl_2$ to form rotaxane **37**·Cl.

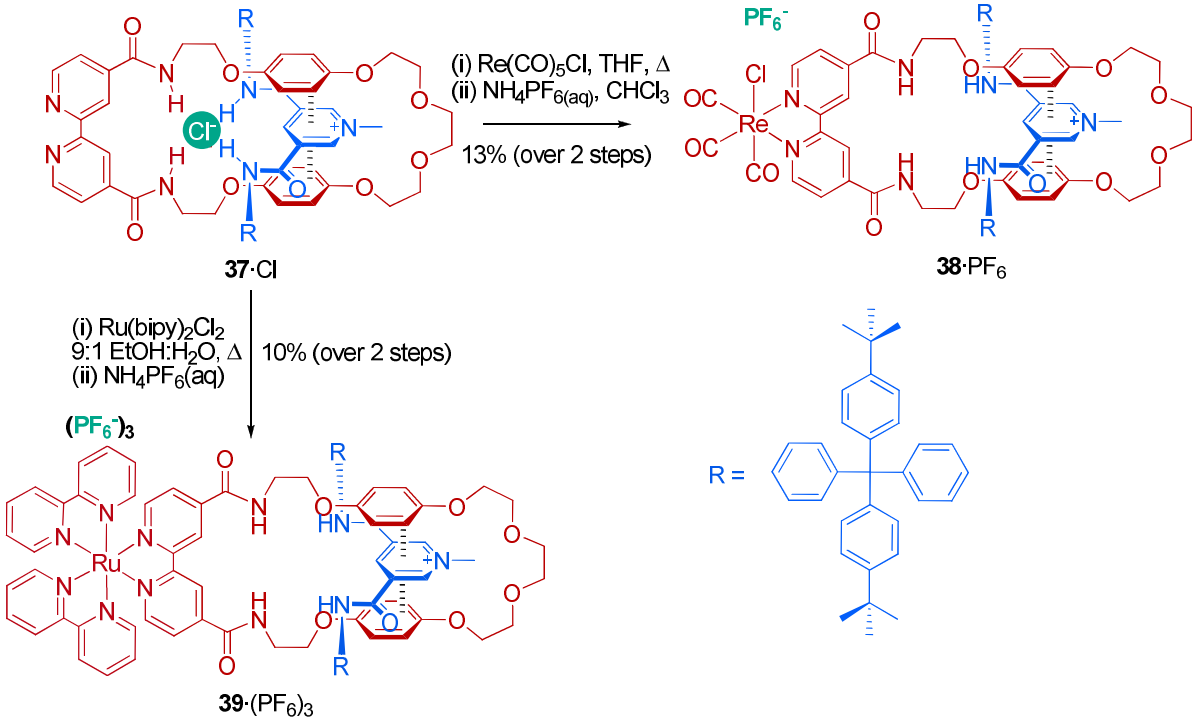



***Scheme 3.3.*** *Synthesis of rotaxane* ***37****·Cl.*

Chromatographic purification proved a significant challenge, with the axle **13**·Cl, rotaxane **37**·Cl and bipyridine macrocycle **34**, a side product of the rotaxanation reaction, having very similar $R_f$ values. This is presumably a result of the pyridine groups increasing the polarity of both the macrocycle and rotaxane. It was possible to separate the axle **13**·Cl from the crude reaction mixture by exploiting its insolubility in MeCN. However efforts to separate the rotaxane and macrocycle components proved futile and it was concluded that purification *via* metal complexation might prove possible.

Scheme 3.4 shows the synthesis of the rhenium(I) and ruthenium(II) rotaxanes **38**·$PF_6$ and **39**·$(PF_6)_3$, achieved by heating the contaminated rotaxane mixture with the appropriate metal complex. Fortunately, following transition metal complexation, it was possible to separate the macrocycle and rotaxane components using chromatographic techniques, and the rhenium(I) and ruthenium(II) appended [2]rotaxanes were isolated in 13% and 10% yield respectively (calculated from bis amine **17** and axle **13**·Cl).

These novel rotaxanes were characterised by $^{1}H$ and $^{13}C$ NMR, and HRMS (ESI).




***Scheme 3.4.*** *Synthesis of transition metal appended rotaxanes.*

## 3.2.3 Anion Binding Studies

### *3.2.3.1 $^{1}H$ NMR Spectroscopic Titrations*

Following the isolation of the two transition metal appended [2]rotaxanes **38**·$PF_6$ and **39**·$(PF_6)_3$, $^{1}H$ NMR anion binding titrations were carried out following the protocol used in Chapter 2. The chemical shift perturbations of axle cavity proton $\gamma$ and macrocycle cavity proton *c* were monitored upon addition of anion in aqueous solvent mixtures. The titrations of **38**·$PF_6$ with $Cl^-$, $H_2PO_4^-$ and $OAc^-$ anions were carried out in 9:1 $d_6$-acetone/$D_2O$. Figure 3.9 shows the $^{1}H$ NMR spectra of **38**·$PF_6$ before and after the addition of one equivalent of TBACl in this solvent mixture.

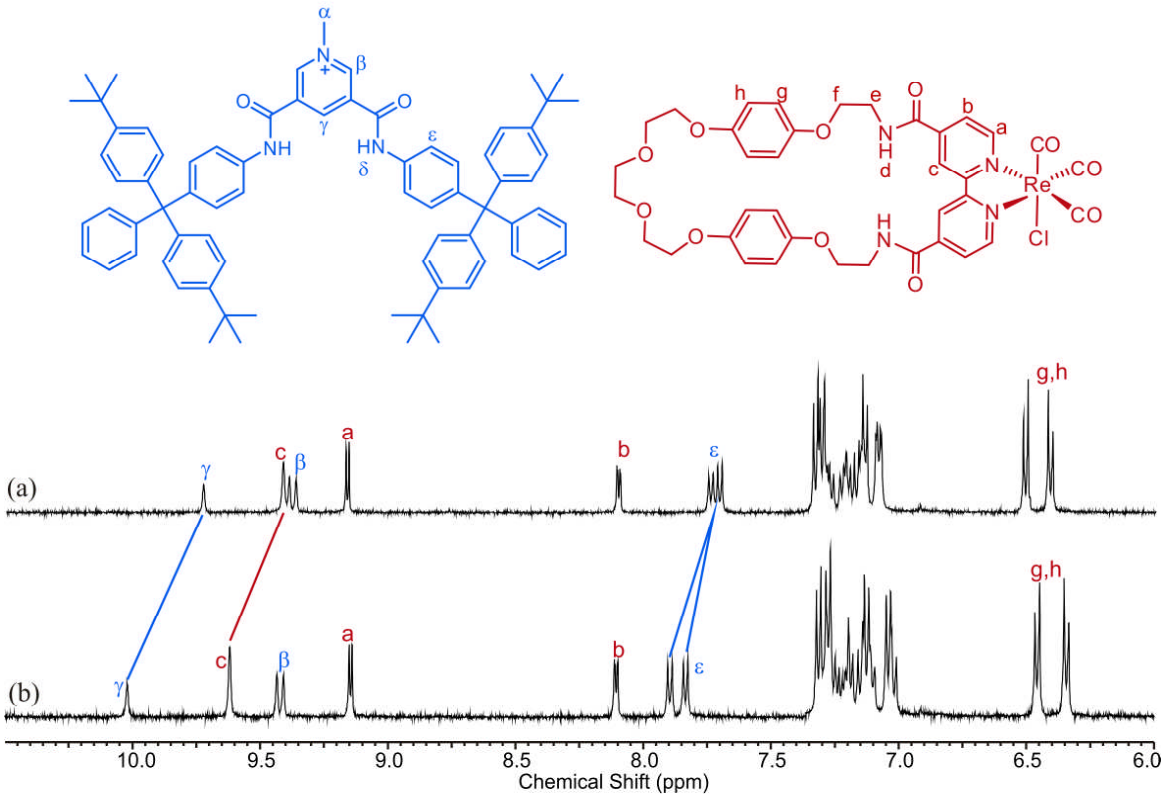



***Figure 3.9.*** *$^1$H NMR spectra in 9:1 $d_6$-acetone/$D_2O$ at 293 K of rotaxane **38**·$PF_6$ in the (a) absence and (b) presence, of 1 eq. TBACl.*

Significant downfield shifts of protons *c* and *γ* were observed upon addition of chloride indicating that the halide anion is bound in the interlocked cavity. Interestingly, splitting of the signal corresponding to stopper proton *ε* occurs upon addition of chloride implying that the anion induces a conformational change in the [2]rotaxane whereby the complex exhibits a degree of asymmetry.

Conversely, akin to the rotaxanes described in Chapter 2, an upfield shift of pyridinium axle proton *γ* were observed upon addition of $H_2PO_4^-$ and $OAc^-$, indicating that the interlocked cavity is also not of sufficient size and complementary shape for the inclusion of these anions. The binding isotherms, obtained by plotting the chemical shift perturbation of pyridinium proton *γ* versus equivalents of anion (Figure 3.10), were used by winEQNMR2[11] to determine anion association constants which are reported in Table 3.1.

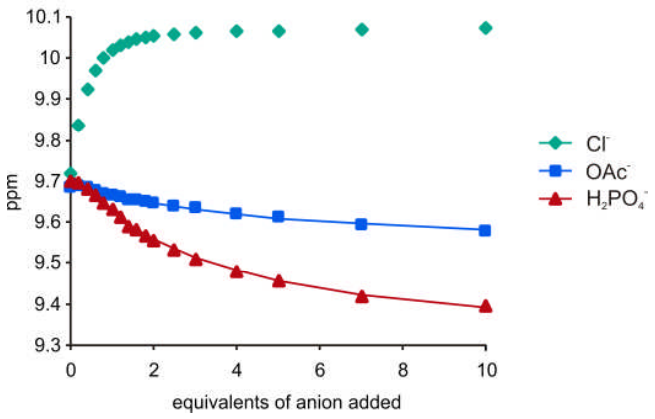



***Figure 3.10.*** *Chemical shift perturbations of proton γ on addition of $Cl^-$, $OAc^-$ and $H_2PO_4^-$ (as TBA salts) to a solution of [2]rotaxane* ***14***$\cdot PF_6$ *in 9:1 $d_6$-acetone/$D_2O$ at 1.43 × $10^{-3}$ M and 293 K. Symbols represent experimental data points; continuous lines represent calculated curves.*

Rotaxane **38**$\cdot PF_6$ strongly complexes chloride in a 10% aqueous solvent system, and winEQNMR2 is unable to determine an association constant value. The oxoanions are bound considerably less strongly, reflecting their peripheral association.

| | $Cl^-$ | $OAc^-$ | $H_2PO_4^-$ |
|---|---|---|---|
| **K ($M^{-1}$)** | > $10^4$ | 160 | 240 |

***Table 3.1****. Association constants of [2]rotaxane* ***38***$\cdot PF_6$ *with $Cl^-$, $H_2PO_4^-$ and $OAc^-$ in 9:1 $d_6$-acetone/$D_2O$ at 1.43 × $10^{-3}$ M and 293 K Obtained by monitoring proton γ. Error < 15%.*

Analogous $^1$H NMR binding titration experiments were carried out with rotaxane **39**$\cdot(PF_6)_3$, in 7:3 $d_6$-acetone/$D_2O$ since it was anticipated that the strength of chloride association would be enhanced compared to the rhenium analogue given the increased electrostatic contribution from the dicationic ruthenium(II) metal centre. Unfortunately, due to a limited supply of rotaxane, it was only possible to carry out anion binding titrations with $Cl^-$ and $H_2PO_4^-$ anions. Upon addition of these anions to **39**$\cdot(PF_6)_3$, similar chemical shift perturbations were observed as for rotaxane **38**$\cdot PF_6$. The winEQNMR2 determined association constants for **39**$\cdot(PF_6)_3$ are given in Table 3.2.

| | $Cl^-$ | $H_2PO_4^-$ |
|---|---|---|
| **K ($M^{-1}$)** | 1500 | 130 |

***Table 3.2.*** *Association constants of [2]rotaxane* ***39***$\cdot(PF_6)_3$ *with* $Cl^-$ *and* $H_2PO_4^-$ *(as TBA salts) in 7:3* $d_6$*-acetone /*$D_2O$ *at 293 K. Obtained by monitoring proton γ. Error < 10%.*

Even in 30 % water chloride is still complexed strongly, whereas $H_2PO_4^-$ is bound over an order of magnitude more weakly, again illustrating the potency of these three-dimensional interlocked cavities for both strong and selective anion complexation and effective shielding from surrounding solvent molecules when the anion is encapsulated within the binding domain.

It was hoped that the strength of chloride association exhibited by these transition metal appended rotaxanes in aqueous solvent mixtures would be reflected in their ability to sense this anion *via* luminescence spectroscopy in aqueous media. This is explored in the next section.

### *3.2.3.2 Luminescence Titrations*

In order to confirm whether complexation of an anion by the rotaxanes would result in significant ground state perturbations, simple UV-vis titrations were carried out initially by addition of anions to a solution of receptors **38**$\cdot PF_6$ and **39**$\cdot(PF_6)_3$ in acetone/$H_2O$ mixtures (9:1 and 7:3 respectively). Only negligible changes were observed in the UV-vis spectra of both rotaxanes upon addition of anions and attention turned to investigate whether anions perturbed luminescence MLCT spectra of the rotaxanes.

The MLCT absorption and emission wavelength, along with the emission intensity for both rotaxanes in the aqueous solvent systems are given in Table 3.3. The relative emission intensity of the rhenium rotaxane **38**$\cdot PF_6$ was observed to be over an order of magnitude smaller than for the equivalent ruthenium rotaxane **39**$\cdot(PF_6)_3$ at the same concentration. This can be attributed to the lower energy of the rhenium $e_g$ orbital, placing it nearer in energy to

the MLCT and thus thermal population of the $e_g$ from the MLCT can occur.[12] This will in turn lead to an increase in non-radiative decay from this orbital and hence luminescence emission intensity is diminished.

| Rotaxane | $\lambda_{absorption}$ (nm) | $\lambda_{max\ emission}$ (nm) | Intensity (a.u.) |
|---|---|---|---|
| **38**·$PF_6$ | 395 | 660 | 11 |
| **39**·$(PF_6)_3$ | 475 | 672 | 550 |

*Table 3.3. MLCT wavelengths of absorption and emission, and emission intensity of metal appended rotaxanes **38**·$PF_6$ (in 9:1 acetone/$H_2O$) and **39**·$(PF_6)_3$ (in 7:3 acetone/$H_2O$) at 1 × $10^{-4}$ M.*

Luminescence titrations were carried out by separately adding portions of $Cl^-$, $Br^-$, $OAc^-$ and $H_2PO_4^-$ to a solution of rhenium rotaxane **38**·$PF_6$ in 9:1 acetone/$H_2O$. The addition of all anions, with the exception of acetate, produced an increase in luminescence emission intensity, concomitant with appreciable hypsochromic shifts in $\lambda_{max}$ (Table 3.4). The former may result from an increased rigidification of the rotaxane structure upon addition of anion leading to less energy being lost through non-radiative pathways. It is also conceivable that the rhenium complex experiences quenching by the pyridinium motif and this quenching pathway is partially blocked in the presence of a bound anion, again leading to an enhancement in the emission intensity. The hypsochromic shift of the MLCT band may be rationalised by considering that the excited electron formally resides on the bis-amide bipyridyl ligand. This results in the excited electron being in proximity to the anion, and the resultant electrostatic repulsion between the negative species raises the energy of the MLCT. The emission spectrum for the addition of chloride to the rotaxane is given in Figure 3.11.

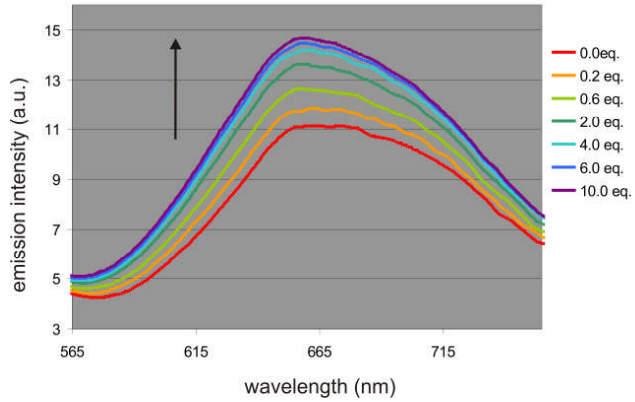



***Figure 3.11.*** *Luminescence emission enhancement upon addition of TBACl to rotaxane* ***38***·$PF_6$ *in 9:1 acetone/$H_2O$ at 1 × $10^{-4}$ M and 293 K.*

Table 3.4 reports the percentage increase and change in $\lambda_{max}$ upon anion addition. SPECFIT[13] was used to calculate association constants from the emission spectra, and these are also given in Table 3.4. Rotaxane **38**·$PF_6$ was observed to bind chloride more strongly than bromide and $H_2PO_4^-$, which correlates with the association constant data obtained by $^1$H NMR spectroscopy. It is unclear as to why the rotaxane does not sense the presence of acetate since this anion is complexed with an association constant of similar magnitude to dihydrogen phosphate. Interestingly, despite the weaker association of $H_2PO_4^-$, this oxoanion causes a much larger increase in emission intensity than either chloride or bromide concomitant with a large hypsochromic shift of the MLCT emission band.

| | $Cl^-$ | $Br^-$ | $OAc^-$ | $H_2PO_4^-$ |
|---|---|---|---|---|
| **$\Delta_{intensity}$ (%)†** | 30 | 20 | 0 | 160 |
| **$\Delta\lambda_{max}$‡ (nm)†** | 3.5 | 2 | - | 7 |
| **log K** | 3.30 | 3.05* | NR | 2.69 |

***Table 3.4.*** *Percentage increase and change in wavelength of emission maxima intensity, and association constants of [2]rotaxane* ***38***·$PF_6$ *with $Cl^-$, $Br^-$, $OAc^-$ and $H_2PO_4^-$ in 9:1 acetone /$H_2O$ at 1 × $10^{-4}$ M and 293 K. Error < 10%, * error < 15%. † upon addition of 50 eq. of anion. ‡ hypsochromic (blue shift). NR denotes no response.*

Analogous luminescence titrations were undertaken with ruthenium rotaxane **39**·$(PF_6)_3$ in 7:3 acetone/$H_2O$. The percentage increase and change in $\lambda_{max}$ are reported in Table 3.5.

| | $Cl^-$ | $Br^-$ | $H_2PO_4^-$ |
|---|---|---|---|
| $\Delta_{intensity}$ (%)† | 8 | 10 | 4 |
| $\Delta\lambda_{max}$‡ (nm) † | 2 | 0.5 | 1 |

***Table 3.5.*** *Percentage increase and change in wavelength of emission maxima intensity,of [2]rotaxane* ***39***$\cdot(PF_6)_3$ *with* $Cl^-$, $Br^-$,*and* $H_2PO_4^-$ *in 7:3 acetone /*$H_2O$ *at 1 ×* $10^{-4}$ *M and 293 K. † upon addition of 100 eq. of anion. ‡ bathchromic (red shift).*

Whilst all anions tested were observed to cause an increase in emission intensity, this enhancement was relatively small, (Figure 3.12) (especially when compared to the enhancement for the rhenium analogue) and only minor shifts are observed in $\lambda_{max}$. Importantly, the bathochromic nature of this shift is in direct contrast with that seen for the rhenium rotaxane, and is difficult to explain.

SPECFIT was unable to determine anion association constant values, possibly as a result of the relatively small emission intensity enhancements observed.

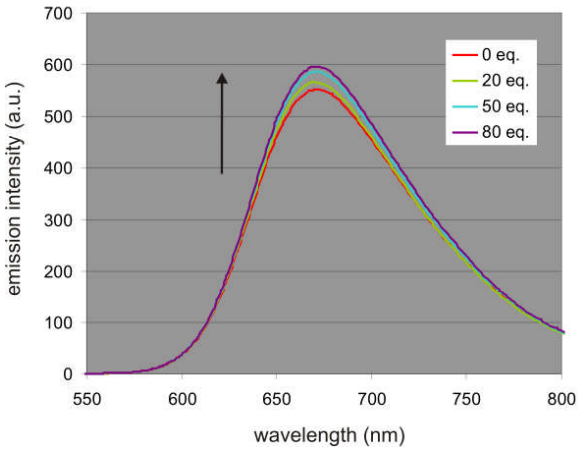



***Figure 3.12.*** *Luminescence emission enhancement upon addition of TBACl to rotaxane* ***39***$\cdot(PF_6)_3$ *in 7:3 acetone/*$H_2O$ *at 1 ×* $10^{-4}$ *M and 293 K.*

### 3.2.4 Summary

It has been possible to further exploit the new method for rotaxane formation discussed in Chapter 2 with the successful synthesis of two novel rotaxanes, where a transition metal lumophore is appended to the macrocyclic component. Both rotaxanes are capable of strongly

and selectively binding chloride in preference to more basic oxoanions, a consequence of their topologically unique binding cavities. In particular the ruthenium(II) appended rotaxane **39**·$(PF_6)_3$ exhibits an impressive high binding affinity for chloride in 30 % water.

The rhenium(I) appended rotaxane **38**·$PF_6$ is capable of sensing anions *via* luminescence spectroscopy with an observed enhancement of the MLCT emission intensity upon addition of anions. Quantitative luminescence titrations reveal chloride to be bound most strongly, correlating with the association constant data obtained from $^1$H NMR spectroscopic titrations. Whilst being the stronger complexant of anions, ruthenium rotaxane **39**·$(PF_6)_3$ displayed only relatively small MLCT emission band enhancements upon addition of anions, which is difficult to rationalise.

## 3.3 Incorporation of Transition Metal Reporter Motif into Axle Component

A relatively simple way of incorporating a transition metal reporter group into the axle component of a [2]rotaxane is to replace one of the bulky stopper groups with the metal complex. The complex must be of sufficient size to prevent dethreading of the macrocyclic component. The following section focuses on ruthenium(II) polypyridyl complexes since the rhenium(I) bipyridyl motif was considered not to be large enough to serve as a stoppering group. Balzani and Stoddart have demonstrated the ability of a tris-bipyridyl ruthenium(II) complex to act as stopper group in their rotaxane capable of undergoing photochemically driven molecular shuttling (Figure 3.13).[14]

Liu and co-workers have also used ruthenium complexes as stoppers in their cyclodextrin rotaxane.[15]

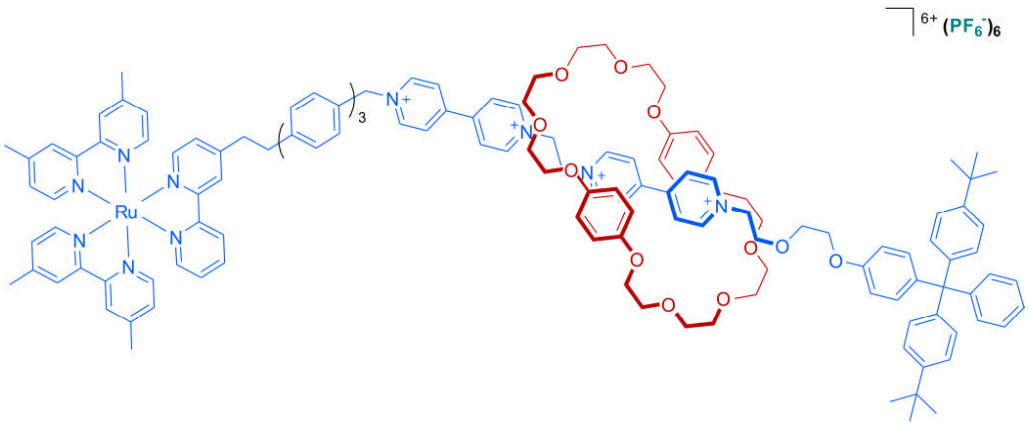



***Figure 3.13.*** *Stoddart and Balzani's molecular 'abacus' incorporating a Ru(II)complex as a stopper group.*[14]

It was hoped that functionalising 1,10-phenanthroline with an amine substituent would enable target thread and axle components, containing a pyridinium anion binding cleft to be prepared (Figure 3.14). Initial efforts focused on the synthesis and study of two potential threading components, containing an amide-functionalised phenanthroline bis-bipyridyl ruthenium(II) motif designed to sense anions *via* luminescence spectroscopy.

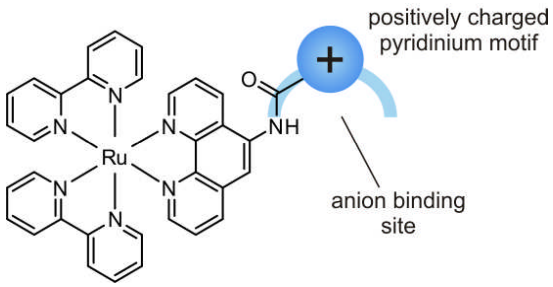


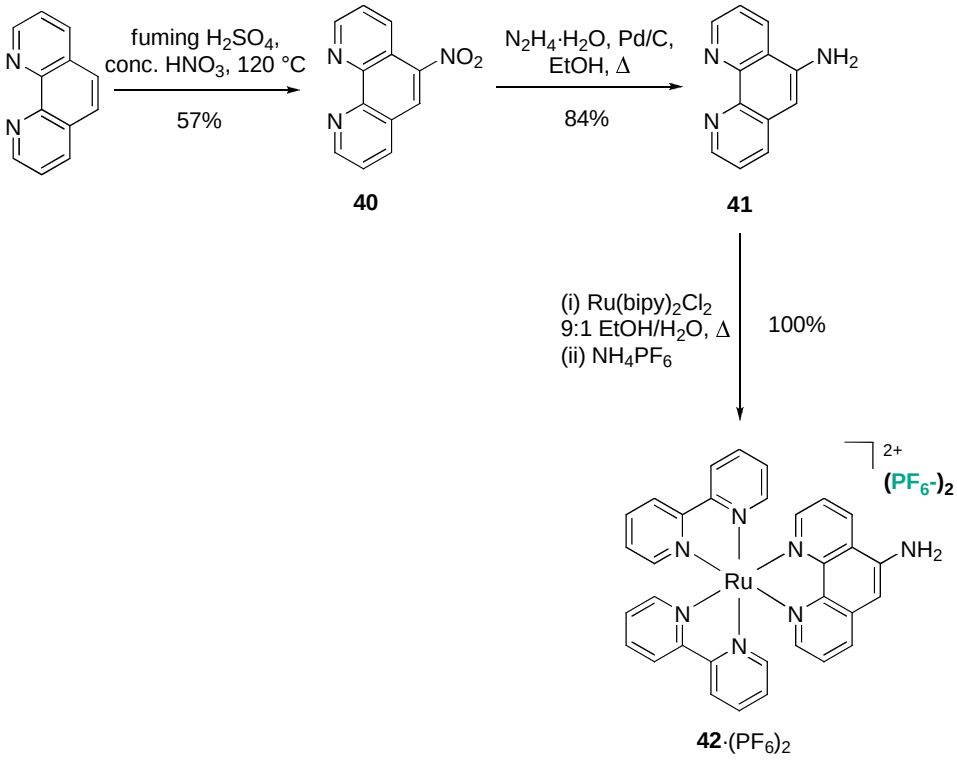

***Figure 3.14.*** *Design of Ru(II) containing photo-active thread component.*

### 3.3.1 Synthesis of Photo-Active Thread Components

All novel compounds synthesised in this section were characterised by $^{1}$H NMR and $^{13}$C NMR, and HRMS (ESI).

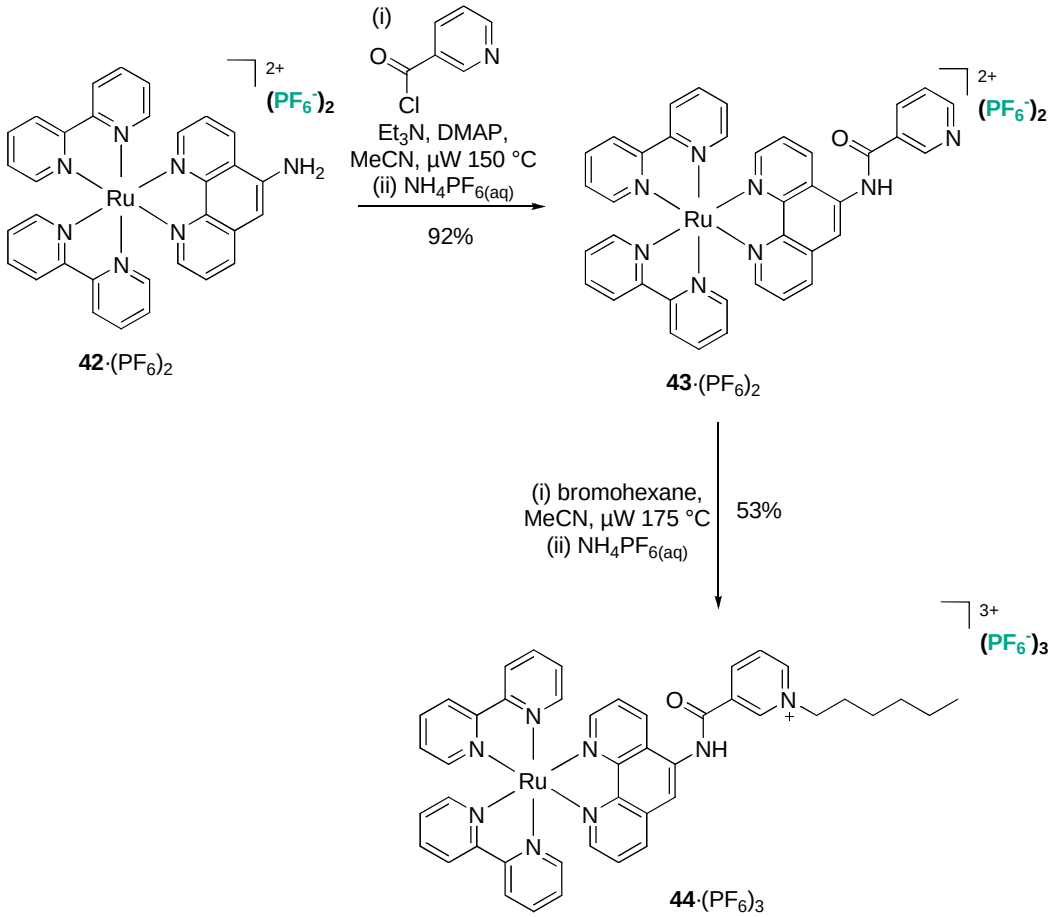
The ruthenium(II) stopper group for covalent attachment to potential pyridinium based threading components was synthesised according to Scheme 3.5. Nitration of 1,10-phenthroline to give compound **40** was achieved using a mixture of fuming $H_2SO_4$ and concentrated $HNO_3$.[16] Compound **40** was reduced using a mixture of hydrazine and Pd/C[17]

and the resulting amine **41** was chelated to the ruthenium(II) centre to produce **42**·$(PF_6)_2$ by heating at reflux with $Ru(bipy)_2Cl_2$, followed by anion exchange using excess $NH_4PF_6$.




***Scheme 3.5.*** *Synthesis of amine appended Ru(II) stopper group* ***42***·$(PF_6)_2$.

The synthesis of a ruthenium appended pyridinium nicotinamide thread component is outlined in Scheme 3.6. The acid chloride condensation reaction of amine **42**·$(PF_6)_2$ with nicotinoyl chloride in $CH_2Cl_2$ was initially attempted at room temperature, however even after 24 hours no reaction was observed to have taken place. The reaction was attempted again using microwave irradiation at 150 °C, replacing $CH_2Cl_2$ with MeCN. After one hour the reaction was observed to have gone to completion, and **43**·$(PF_6)_2$ was isolated in 92% yield following column chromatography and anion exchange using aqueous $NH_4PF_{6(aq)}$. This reaction highlights the power of microwave synthesis in giving high reaction yields even when the starting materials have low reactivity. The synthesis of target thread **44**·$(PF_6)_3$ was achieved by subjecting a solution of **43**·$(PF_6)_2$ and 1-bromohexane in MeCN to microwave irradiation at 175 °C.




***Scheme 3.6.*** *Synthesis of pyridinium nicotinamide thread component* ***45***·$(PF_6)_3$.

During the synthesis of **44**·$(PF_6)_3$ it was possible to grow crystals suitable for X-ray crystal structural analysis of **43**·$(PF_6)(NO_3)$ from slow evaporation of an acetone solution. The structure (Figure 3.15), solved by Christopher Serpell, shows the nitrate anion bound in a cleft created by the amide proton and the pyridine proton in the 4' position. In contrast, the non-coordinating hexafluorophosphate anion is associating peripherally, in proximity of the positively charged ruthenium centre.

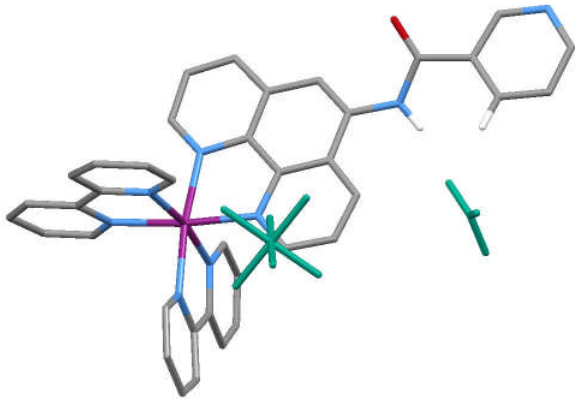
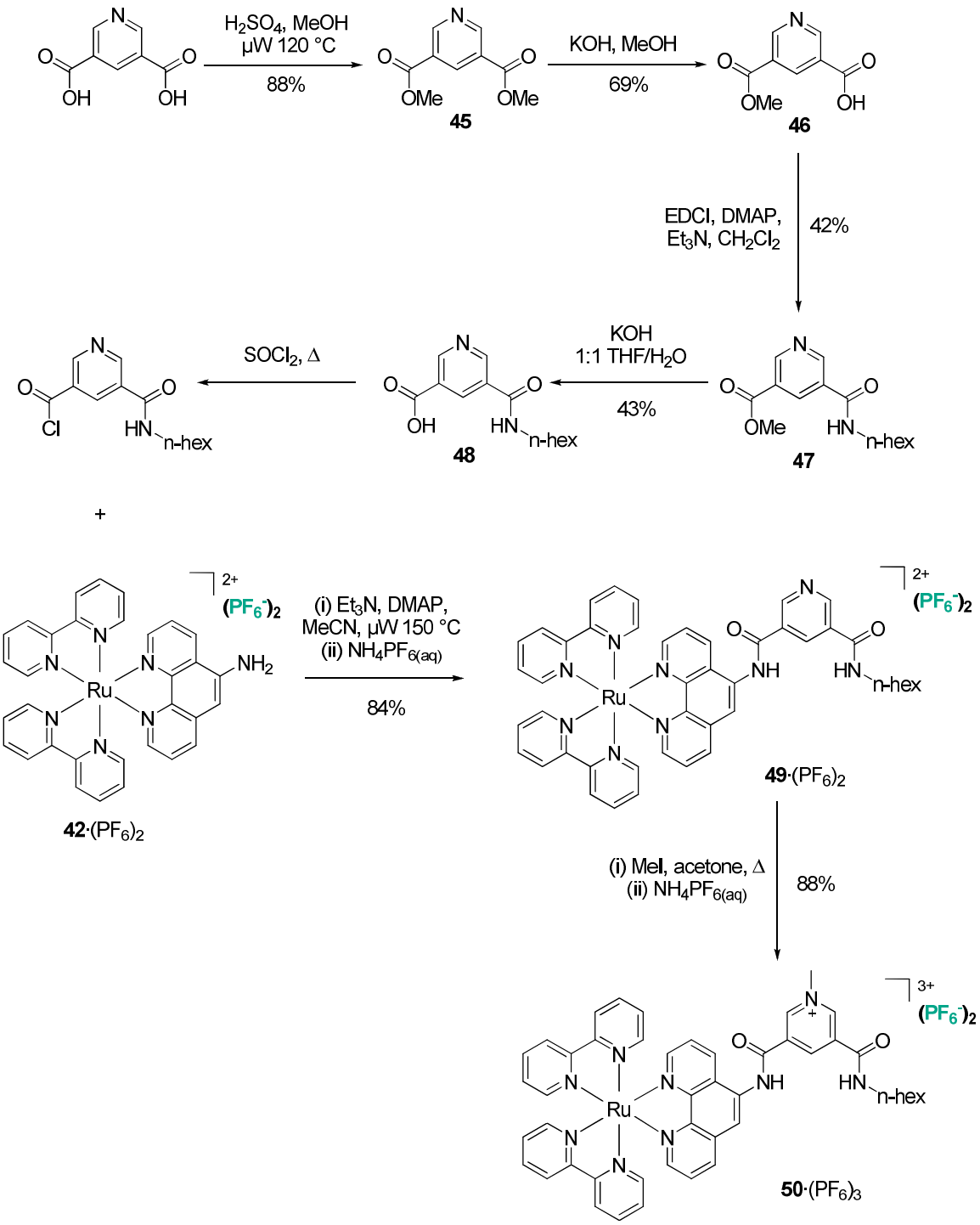


***Figure 3.15.*** *Crystal structure of* ***43***$\cdot(PF_6)(NO_3)$*. Non-protic hydrogens are omitted for clarity.*

Along with the pyridinium nicotinamide thread, it was of interest to synthesise a 3,5-bis-amide pyridinium *N*-methyl thread, analogous to the system that proved so successful in forming interlocked structures in Chapter 2. In order to append one ruthenium stopper complex to this thread monofunctionalisation of 3,5-bis-carboxy pyridine needs to be established. This was achieved by adaptation of literature procedures, and the synthesis of thread **50**$\cdot(PF_6)_3$ is shown in Scheme 3.7. Pyridine 3,5-dicarboxylic acid was converted to the corresponding methyl ester **45** by microwave irradiation in a mixture of methanol and concentrated $H_2SO_4$. Monohydrolysis using 1.1 equivalents of KOH in MeOH, afforded **46**[18] which was subsequently coupled to *n*-hexylamine using EDCI in the presence of $Et_3N$ and DMAP in dry $CH_2Cl_2$ giving **47** in 42% yield. The second ester group was hydrolysed using KOH in 1:1 THF/$H_2O$ to give **48**, which was converted to the corresponding acid chloride *via* reflux with $SOCl_2$ and reacted with amine **42**$\cdot(PF_6)_2$ under microwave irradiation. Anion exchange was achieved with aqueous $NH_4PF_6$, followed by methylation of **49**$\cdot(PF_6)_2$ with iodomethane and anion exchange gave the target thread component **50**$\cdot(PF_6)_2$ in 88% yield.




***Scheme 3.7.*** *Synthesis of 3,5-pyridinium bis-amide thread* ***50***·*$(PF_6)_3$.*

## 3.3.2 Anion Binding Studies of Photo-active Thread Components

### *3.3.2.1 $^1$H NMR Spectroscopic Titrations*

Before quantitative $^1$H NMR titration experiments to determine the strength of association of certain anions with the photo-active thread components were undertaken, it was important to

establish whether coordinating anions would bind in the pyridinium nicotinamide cleft, or merely associate electrostatically with the positively charged ruthenium. Two possible conformations of thread **44**·$(PF_6)_2Cl$ are given in Figure 3.16. The second conformation (b) supports the solid state evidence obtained for **43**·$(NO_3)(PF_6)$ (Figure 3.16).

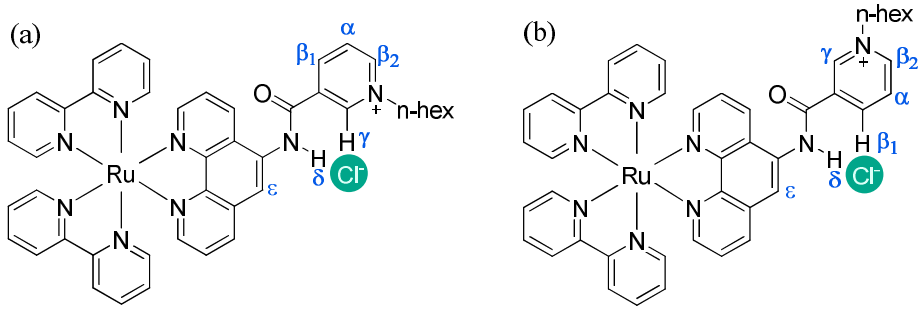



***Figure 3.16.*** *Possible conformations of thread* ***44***·$(PF_6)$ *upon addition of* $Cl^-$.

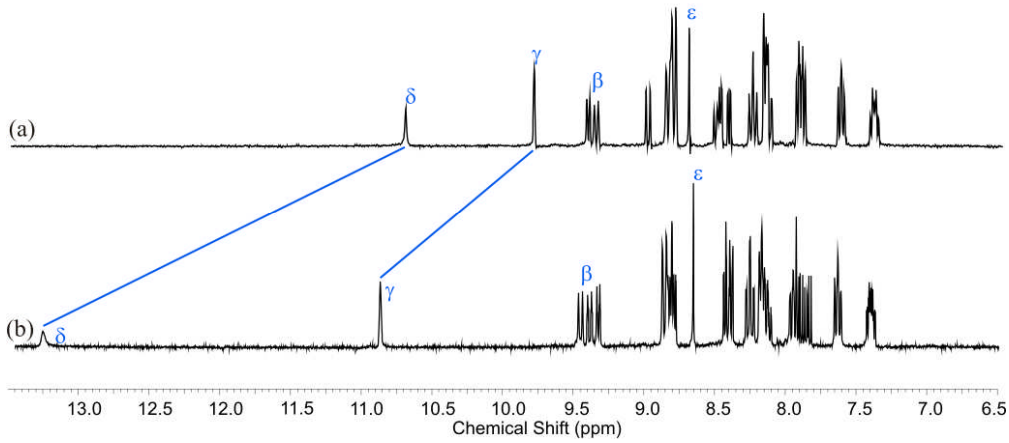



***Figure 3.17.*** *$^1H$ NMR spectra of* ***44***·$(PF_6)_3$ *at 293 K in* $d_6$*-acetone in the (a) absence and (b) presence, of 1 eq. TBACl.*

Addition of one equivalent of TBACl to **44**·$(PF_6)_3$ in $d_6$-acetone produced a considerable downfield shift of amide proton $\delta$ (+ 2.54 ppm) indicating a strong hydrogen bonding interaction with the halide anion (Figure 3.17). Pyridinium proton $\gamma$ is also observed to shift downfield (+ 1.06 ppm), whilst proton $\beta_1$ is perturbed very little, indicating that the binding conformation illustrated in Figure 3.16a is favoured upon addition of chloride. This is an encouraging observation in terms of potential pseudorotaxane formation since if conformation (b) was adopted this may impede threading through an appropriate macrocyclic component.

Quantitative $^1$H NMR titration experiments with both receptors **44**·$(PF_6)_3$ and **50**·$(PF_6)_3$ were carried out with the TBA salts of $Cl^-$, $Br^-$, $OAc^-$ and $H_2PO_4^-$ in 9:1 $d_6$-acetone/$D_2O$, as described in Chapter 2. Addition of anions to the receptors induced a number of chemical shift perturbations in the $^1$H NMR spectra, notably the cavity pyridinium proton $\gamma$. It was not possible to monitor amide protons $\delta$ due the protic nature of the solvent mixture leading to exchange of these protons for deuterium. The titration curves for the binding of anions, with thread **44**·$(PF_6)_3$ are shown in Figure 3.18a. The addition of bromide and chloride were observed to cause downfield perturbations of the cavity pyridinium proton γ, with Job plot analysis (Figure 3.18b) indicating a 1:1 receptor/anion binding stoichiometry.

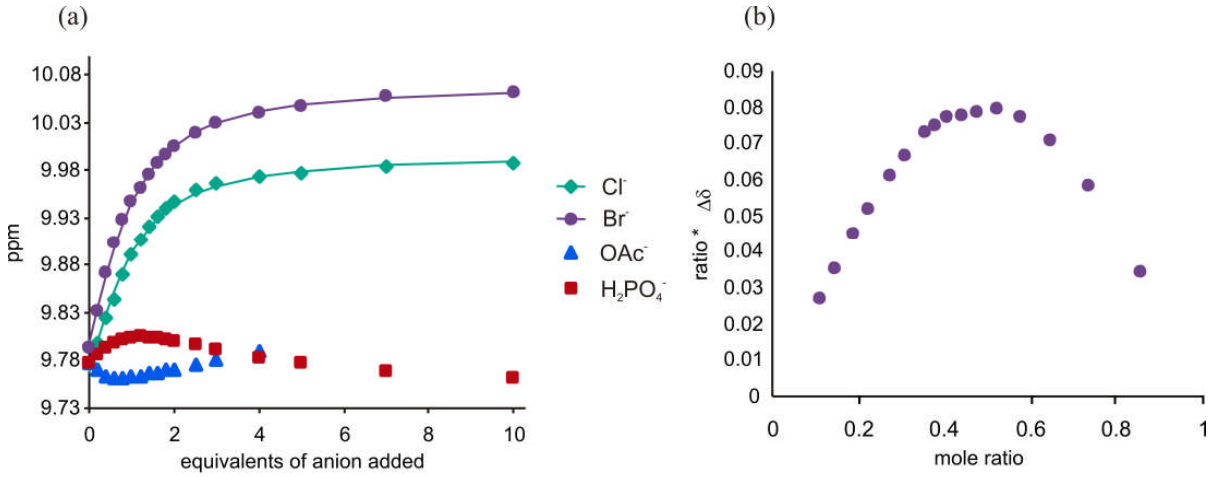



***Figure 3.18.*** *In 9:1 $d_6$-acetone/$D_2O$ at 1.91 × $10^{-3}$M and 293 K: (a) Chemical shift perturbations of protons γ on addition of $Cl^-$, $Br^-$, $OAc^-$ and $H_2PO_4^-$ (as TBA salts) to a solution of receptor **44**·$(PF_6)_3$. Symbols represent experimental data points; continuous lines represent calculated curves; (b) Pseudo-Job Plot of addition of TBABr to receptor **44**·$(PF_6)_3$.*

Conversely, unusual binding isotherms were obtained for the addition of both acetate and dihydrogen phosphate, with the titration curve changing direction at one equivalent for both anions. This may be explained by a change in binding stoichiometry from 1:1 to 1:2, however it is difficult to account for the upfield chemical shift perturbations since only downfield perturbations are usually observed for the binding of anions in acyclic systems.

Similar phenomena were observed in the addition of halide and oxoanions to **50**·$(PF_6)_3$. The 1:1 stoichiometric association constants for the binding of chloride and bromide were determined using winEQNMR2 (Table 3.6).

| | $Cl^-$ | $Br^-$ |
|---|---|---|
| **44**·$(PF_6)_3$ | 1300 | 1400 |
| **50**·$(PF_6)_3$ | 800 | 400 |

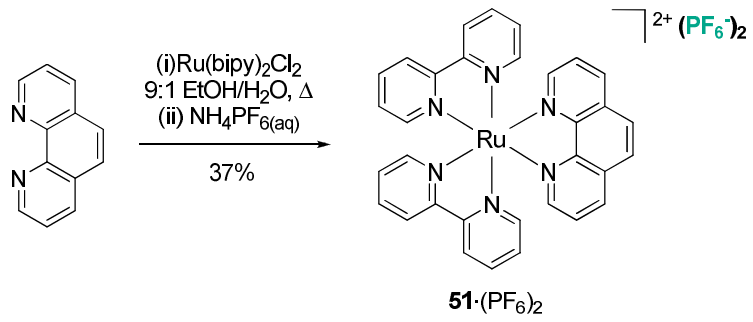
***Table 3.6.*** *Association constants, K ($M^{-1}$), of receptors **44**·$(PF_6)_3$ and **50**·$(PF_6)_3$ with $Cl^-$ and $Br^-$ in 9:1 $d_6$-acetone/$D_2O$ at 293 K Obtained by monitoring proton γ. Error < 10%.*

The pyridinium nicotinamide receptor **44**·$(PF_6)_3$ binds chloride and bromide with similar strength which is attributed to the interplay between chloride's higher charge density and basicity, and bromide being less heavily solvated in this aqueous solvent medium. The pyridinium receptor **50**·$(PF_6)_3$, on the other hand, exhibits selectivity for chloride over bromide, presumably due to a better size match between the smaller halide anion and the cavity of this receptor.

### *3.3.2.2 Luminescence Titrations*

Before embarking upon luminescence titration experiments of the target thread compounds it was important to determine whether the simple ruthenium bis-bipyridyl phenanthroline[19] complex undergoes any interaction with anions.

The synthesis of this model compound was achieved by heating 1,10-phenanthroline with $Ru(bipy)_2Cl_2$, followed by anion exchange with aqueous $NH_4PF_6$ (Scheme 3.8).




**51**·$(PF_6)_2$

***Scheme 3.8.*** *Synthesis of model Ru(II) complex.*

As expected $^1$H NMR titration of TBACl with a solution of **51**·$(PF_6)_2$ in 9:1 $d_6$-acetone/$D_2O$ resulted in negligible shifts of any signals indicating that simple anion exchange does not appreciably perturb the proton environments of this complex.

UV-visible and luminescence titrations were also carried out to determine whether the presence of anions resulted in perturbations of either the absorption or emission spectrum of the MLCT band of the complex. The wavelengths of the absorption and emission bands, along with the emission intensity are reported in Table 3.7.

| Receptor | $\lambda_{absorption}$ (nm) | ε ($M^{-1}cm^{-1}$) | $\lambda_{max\ emission}$ (nm) | Intensity (a.u.) |
|---|---|---|---|---|
| **51**·$(PF_6)_2$ | 448 | 17200 | 615 | 360 |

***Table 3.7.*** *Wavelengths of MLCT absorption and emission, extinction coefficient and emission intensity of complex* ***51***·$(PF_6)_2$ *in 9:1 acetone/*$H_2O$ *at 293 K.*

The UV-vis spectrum of complex **51**·$(PF_6)_2$ in acetone was not observed to change upon addition of either chloride or acetate (chosen to test since it is a basic oxoanion with a different geometry to chloride). However, significant quenching (~ 30%) of the MLCT emission band was induced upon addition of both anions indicating that the model compound is capable of luminescently sensing anions. This may be the result of collisional quenching, where the energy lost through non-radiative pathways is increased. The latter is a well-known phenomenon in the presence of chloride,[9] but it is unclear whether acetate anions could cause the same effect. In addition, the presence of anions causes a bathochromic shift (8 nm after 50 equivalents of both TBACl and TBAOAc) of the emission band, indicating the presence of anion stabilises the MLCT in some way.

Figure 3.19a demonstrates the emission spectrum of **51**·$(PF_6)_2$ upon addition of chloride, whilst the graph in Figure 3.19b shows the association curve of both anions at 615 nm.

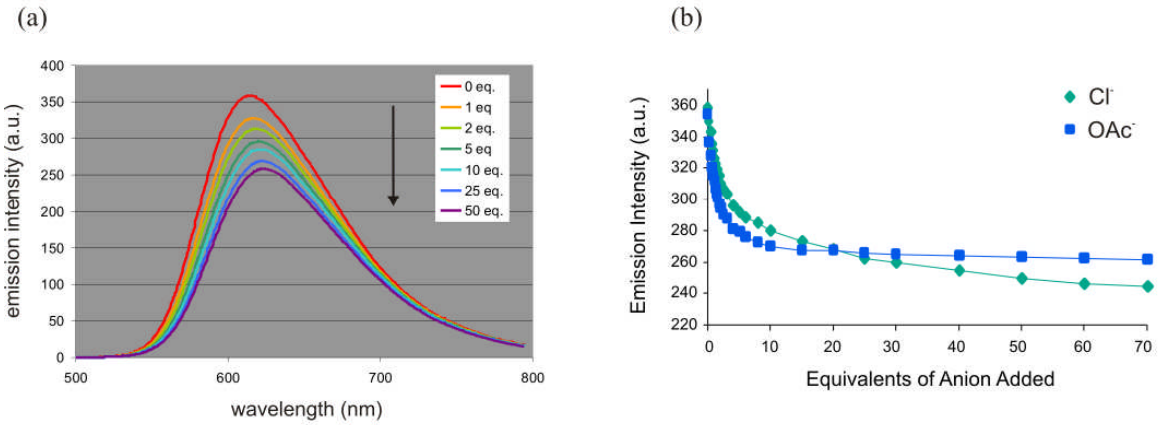



***Figure 3.19.*** *(a) Luminscence emission reduction of* ***51***$\cdot(PF_6)_2$ *upon addition of* $Cl^-$ *and (b) Luminescence emission intensity of* ***51***$\cdot(PF_6)_2$ *as function of equivalents of anion added at 615 nm, at* $1 \times 10^{-4}$*M and 293 K in 9:1 acetone/*$H_2O$*.*

The SPECFIT computer programme was used to calculate the association constants of **51**$\cdot(PF_6)_2$ with chloride and acetate (from the emission spectra) which are given in Table 3.8.

| | $Cl^-$ | $OAc^-$ |
|---|---|---|
| **log K** | 3.5 | 3.9 |

**Table 3.8.** *Association constant of* ***51***$\cdot(PF_6)_3$ *with* $Cl^-$ *and* $OAc^-$ *in 9:1* $d_6$*-acetone/*$D_2O$ *at 293 K. Error < 10%.*

The complex is observed to sense both anions with a relatively large association constant in acetone. These results are an important consideration when measuring the anion sensing capability of the target threads, such that any similar perturbations observed should be attributed to the interaction of anions with the ruthenium complex itself rather than through its anion recognition site. Conversely, if an increase in emission intensity is observed it can be solely accredited to the complexation of the anions in its specific binding domain.

Luminescence titrations with threads **44**$\cdot(PF_6)_3$ and **50**$\cdot(PF_6)_3$ were carried out in 9:1 acetone/$H_2O$, for solubility purposes and also to allow comparisons to made with the results obtained using $^1$H NMR spectroscopy. The wavelengths of the absorption and emission bands, along with the emission intensity of both threads **44**$\cdot(PF_6)_3$ and **50**$\cdot(PF_6)_3$, and also the model system **51**$\cdot(PF_6)_2$ for comparison are reported in Table 3.9.

| Receptor | $\lambda_{absorption}$ (nm) | ε ($M^{-1}cm^{-1}$) | $\lambda_{max\ emission}$ (nm) | Intensity (a.u.) |
|---|---|---|---|---|
| **44**·$(PF_6)_3$ | 452 | 18600 | 619 | 290 |
| **50**·$(PF_6)_3$ | 452 | 17400 | 616 | 200 |
| **51**·$(PF_6)_2$ | 448 | 17200 | 615 | 335 |

***Table 3.9.*** *Wavelengths of MLCT absorption and emission, extinction cooefficient, and emission intensity of complex* ***44***·$(PF_6)_2$, ***50***·$(PF_6)_3$ *and* ***51***·$(PF_6)_3$ *in 9:1 acetone/$H_2O$ at 1× $10^{-4}$M and 293 K.*

Compared to model compound **51**·$(PF_6)_2$, the MLCT absorption and emission bands of threads **44**·$(PF_6)_3$ and **50**·$(PF_6)_3$ are observed at slightly longer wavelengths, which can be attributed to the electron withdrawing nature of the appended amide group(s) leading to the excited state being lower in energy. In addition, the emission intensity was observed to be considerably lower for both thread systems, which is unsurprising given that pyridinium is known to quench luminescence through electron transfer.[9]

Anion luminescence titrations were carried out by adding aliquots of TBA salts to solutions of receptor **44**·$(PF_6)_3$, and monitoring the emission spectra following each addition. It was not possible to complete the titration with $H_2PO_4^-$ due to precipitation problems

It should be noted that no appreciable change in the UV-vis spectrum of the receptors was observed upon addition of anions.

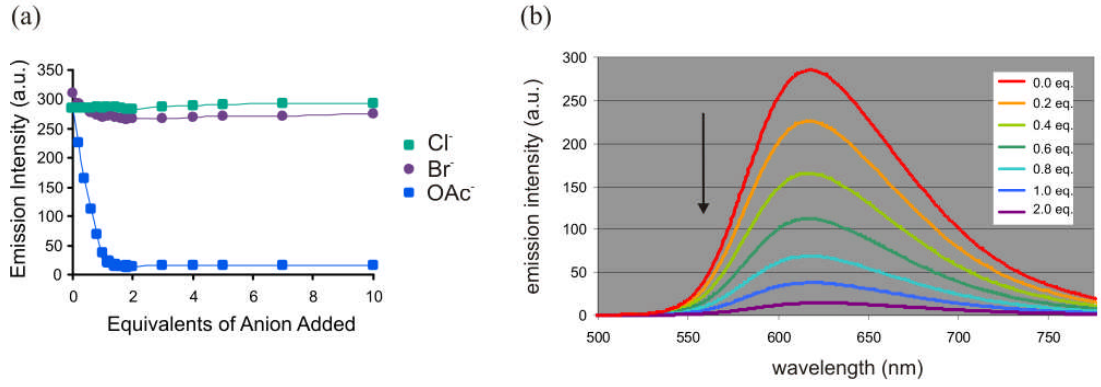



***Figure 3.20.*** *(a) Luminescence emission intensity of* **44**·$(PF_6)_3$ *as function of equivalents of anion added at 619 nm, and (b) Luminescence emission reduction of* **44**·$(PF_6)_2$ *upon addition of TBAOAc, at 1 x $10^{-4}$ M and 293 K in 9:1 acetone/$H_2O$.*

Disappointingly Figure 3.20 shows chloride and bromide induce only negligible changes in the emission intensity, with the thread seemingly unable to sense the presence of these halide anions. It is thought that a combination of factors may contribute to these observations, with possible enhancement of MLCT emission intensity *via* thread rigidification on anion binding opposing an anion quenching effect (as for model system **51**·$(PF_6)_2$). Overall this results in the emission intensity appearing unchanged. In contrast, a dramatic effect is seen upon addition of acetate with almost total quenching of the emission intensity after the addition of only two equivalents of anion.

Analogous luminescence titrations were carried out with thread **50**·$(PF_6)_3$, with chloride, bromide and acetate. Whilst bromide again induced no response, chloride caused a 20% enhancement in the MLCT (Figure 3.20a) and it was possible to use SPECFIT to calculate an association constant (log K = 4.42 (error < 15%)).

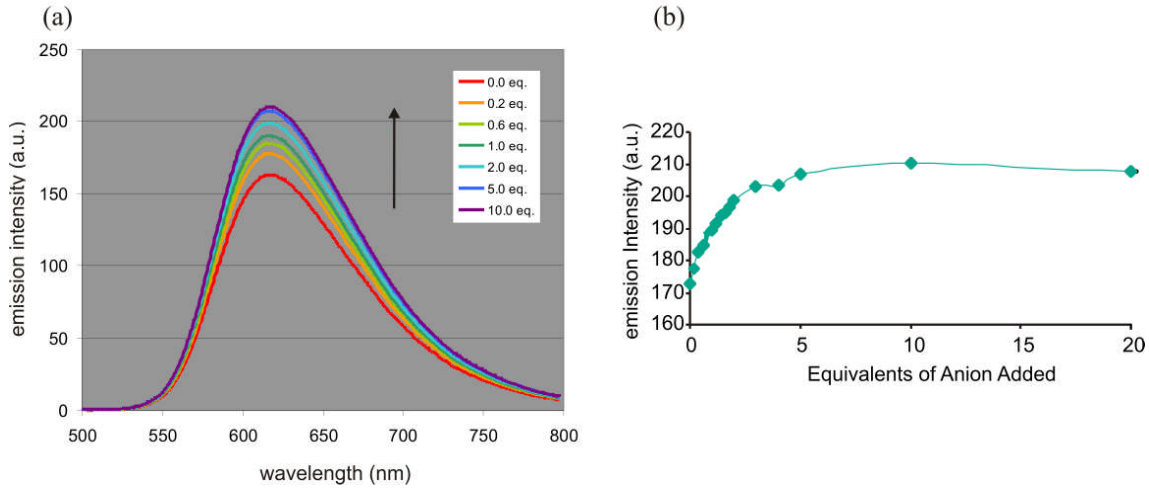



***Figure 3.21.*** *(a) Luminscence emission enhancement of* ***50***·$(PF_6)_3$ *upon addition of TBACl and (b) Luminescence emission intensity of* ***50***·$(PF_6)_3$ *as function of equivalents of* $Cl^-$ *added, at 616 nm, at 1 x* $10^{-4}$ *M and 293 K in 9:1 acetone/*$H_2O$.

It is conceivable that receptor **50**·$(PF_6)_3$ undergoes greater rigidification upon anion binding than **44**·$(PF_6)_3$, due to it possessing two anion binding amide protons. This leads to a greater enhancement of emission intensity due to less energy being lost through non-radiative

pathways, and the competing quenching effect of the anion, as seen for the model system **51**·$(PF_6)_2$, is overcome.

Addition of acetate to thread **50**·$(PF_6)_3$ again caused almost 100% quenching of the MLCT emission intensity band. It was proposed that this quenching may be due to a deprotonation event since acetate is considerably more basic than the halides, and therefore a number of tests were carried out to verify this postulate. The amide protons appended to the dicationic ruthenium complex are the most acidic in the system and are thus most susceptible to deprotonation. In which case, similar quenching should be observed upon addition of acetate to the thread precursors **43**·$(PF_6)_2$ and **49**·$(PF_6)_2$ as they also possess these acidic amide protons. Indeed, the same luminescence quenching is observed upon addition of acetate to these compounds.

Furthermore, addition of TBAOH to the systems produced total quenching of the luminescence emission intensity, whilst subsequent addition of TFA restored the luminescence intensity as the amide is reprotonated.

Deprotonation of amide protons results in a free nitrogen lone pair which is known to quench luminescence emission through PET.[20]

## 3.3.3 Pseudorotaxane Studies

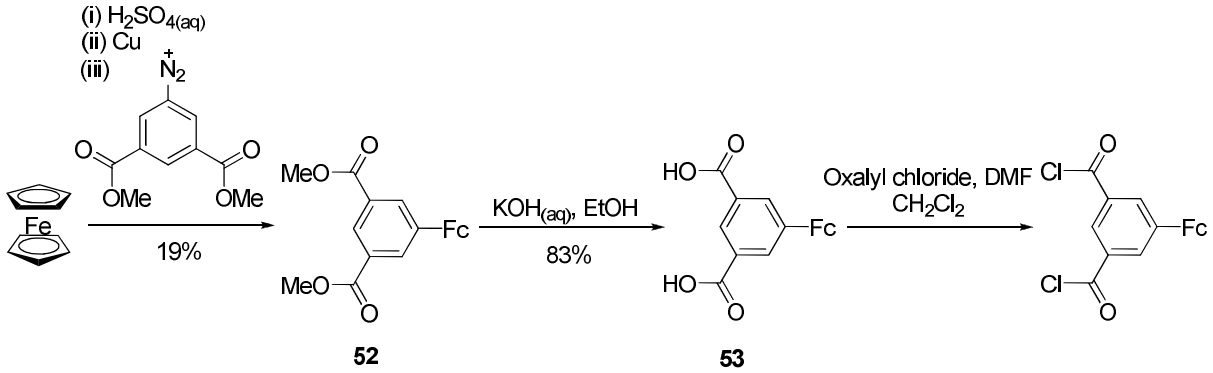
### *3.3.3.1 Macrocycle Synthesis*

The macrocycles chosen for attempted anion-templated pseudorotaxane formation with ruthenium threads **44**·$(PF_6)_3$ and **50**·$(PF_6)_3$ bear resemblance to those used in Chapter 2, only appended with different functional groups. A *tert*-butyl appended macrocycle **54** was chosen since it has greater solubility than its unsubstituted analogue. It has been reported by Beer *et al*. that ferrocene is capable of quenching MLCT luminescence when in proximity to a ruthenium(II) bis-bipyridyl metal centre *via* intramolecular electron and energy transfer

processes.[21, 22] Therefore a ferrocene appended macrocycle **55** may be used as a potential probe for signalling pseudorotaxane formation *via* a luminescent response.

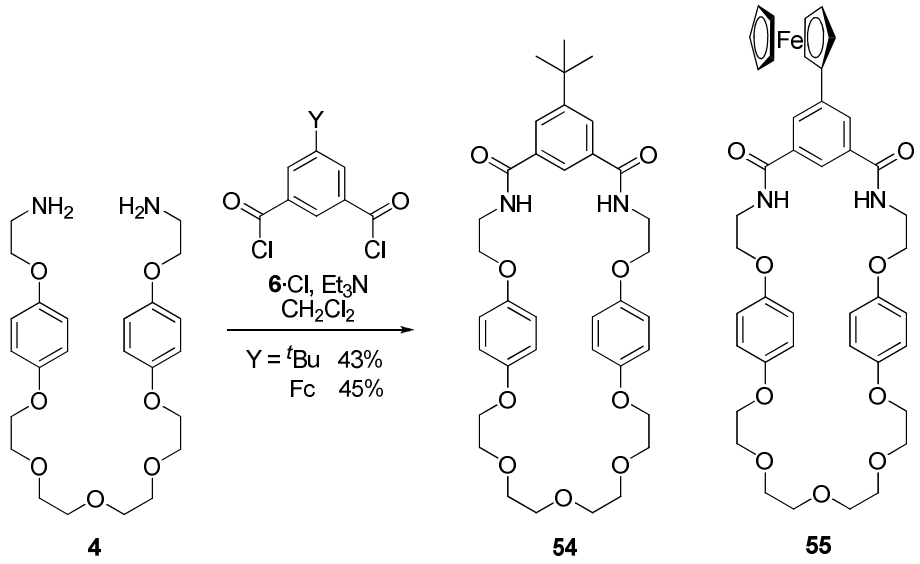
Both macrocycles were synthesised *via* an acid chloride condensation reaction, the macrocyclisation templated by the pyridinium thread **6**·Cl, as described in Chapter 2. The ferrocene subsitituted isophthaloyl dichloride was synthesised according to a procedure adapted by Nicholas Evans, shown in Scheme 3.9.

Ferrocene was oxidized to ferrocenium with $H_2SO_4$ whilst dimethyl 5-aminoisophthalate was converted to the corresponding diazonium salt using $NaNO_2$ in $H_2O$. Coupling of these precursors was undertaken in the presence of Cu powder, and the ferrocene appended ester **52** was isolated following addition of ascorbic acid and aqueous workup. Ester hydrolysis was achieved using KOH in EtOH to give **53**, before oxalyl chloride was used to convert the bis-acid to the corresponding bis-acid chloride.




***Scheme 3.9.*** *Synthesis of ferrocene appended isophthaloyl dichloride.*

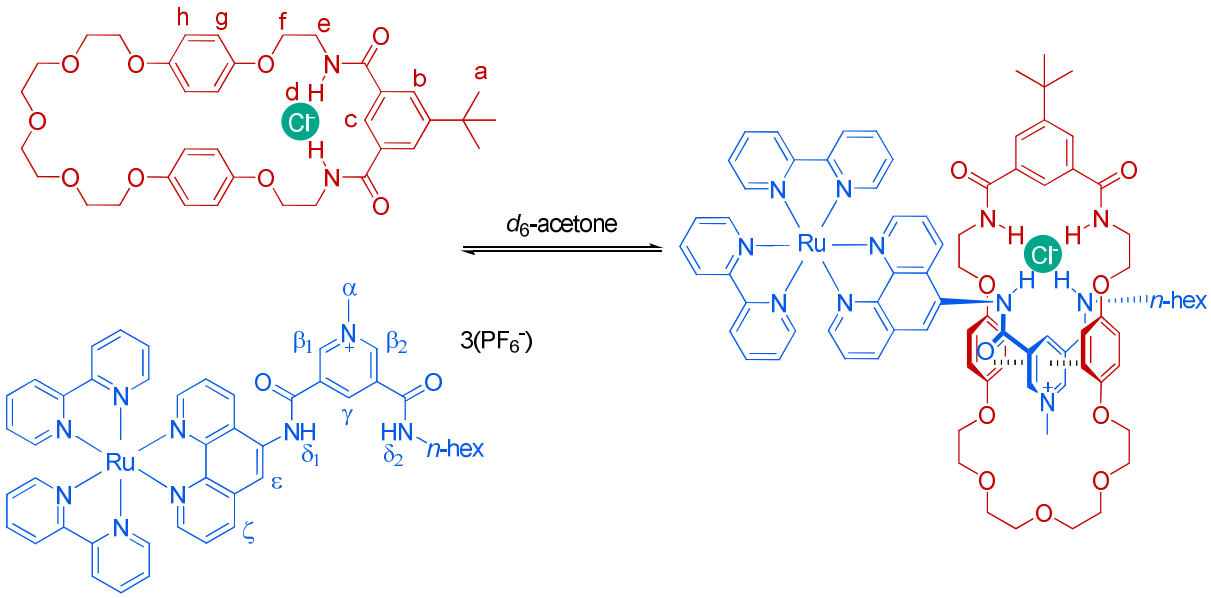
The synthesis of target macrocycles **54** and **55** was achieved by addition of the appropriate bis-acid chloride to a solution of bis-amine **4**, template **6**·Cl and $Et_3N$ in dry $CH_2Cl_2$ (Scheme 3.10). Following acidic workup and column chromatography macrocycles **54** and **55** were isolated in yields of 43% and 45% respectively, and characterised by $^1$H NMR, $^{13}$C NMR and HRMS (ESI).




***Scheme 3.10.*** *Synthesis of macrocycles **54** and **55**.*

### *3.3.3.2 $^1$H NMR Spectroscopic Titrations*

The ability of **44**·$(PF_6)_3$ and **50**·$(PF_6)_3$ to undergo pseudorotaxane formation with macrocycle **54** was initially investigated *via* $^1$H NMR titration experiments in $d_6$-acetone. Unlike pseudorotaxane titrations carried out previously in this thesis, it was not possible to add aliquots of the chloride ion-pair thread to a solution of the macrocycle, as **44**·$(PF_6)_2$(Cl) and **50**·$(PF_6)_2$(Cl) (formed by addition of one equivalent of TBACl to the hexafluorophosphate salt of the thread) were not soluble in $d_6$-acetone at the concentrations required. Therefore, one equivalent of TBACl was added to macrocycle **54** in $d_6$-acetone solution to form the chloride complex **54**·Cl which, upon addition of a potential threading derivative, could template the interpenetration process resulting in the orthogonal arrangement of the two components according to Scheme 2.11.




***Scheme 2.11.*** *Pseudorotaxane formation between thread* ***50***$\cdot(PF_6)_3$ *and macrocycle complex* ***54***$\cdot$*Cl.*

Upon addition of one equivalent of TBACl to macrocycle **54**, chemical shift perturbations of various proton signals were observed in the $^1$H NMR spectrum. The $^1$H NMR spectrum of the new pseudorotaxane species **54**$\cdot$**50**$\cdot(PF_6)_2(Cl)$ along with those of the free thread **50**$\cdot(PF_6)_3$ and **54**$\cdot Cl^-$ for comparison are shown in Figure 3.22.

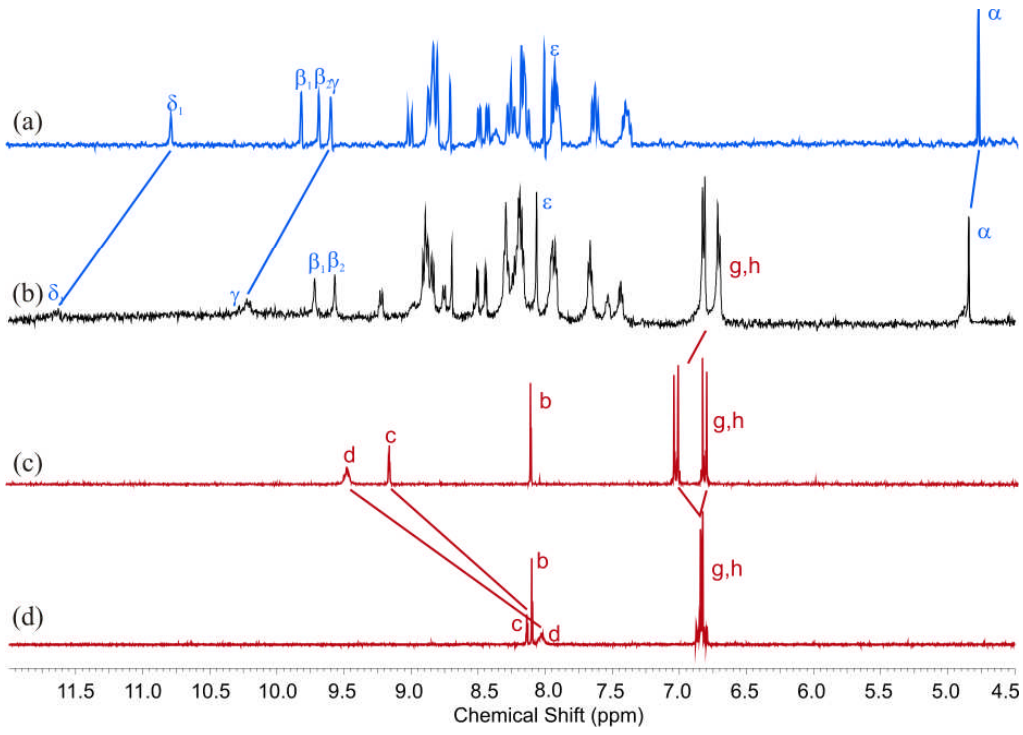



***Figure 3.22.*** *$^1$H NMR spectra in $d_6$-acetone at 293 K of (a) thread* ***50***$\cdot(PF_6)_3$*, (b) 1:1:1* ***50***$\cdot(PF_6)_3$*/****54****/TBACl, (c) macrocycle* ***54*** *+ 1 eq. TBACl, and (d) macrocycle* ***54****.*

Both cavity proton *c* and amide proton *d* shifted downfield upon chloride complexation in the isophthalamide cleft of macrocycle **54**, whilst the hydroquinone protons were observed to move downfield and split as a consequence of chloride complex-induced asymmetry.

Upon addition of thread **50**·$(PF_6)_3$ macrocycle hydroquinone protons were observed to remain split, and shifted upfield, which is a direct consequence of charge-assisted π-π stacking with the electron deficient pyridinium group. In addition, amide protons $\delta$ and cavity protons $\gamma$ of the thread were observed to move downfield suggesting chloride is bound in the pyridinium cleft. Thread **44**·$(PF_6)_3$ was shown to form a similar pseudorotaxane assembly in the presence of **54**·$Cl^-$.

Plotting the chemical shift perturbations of hydroquinone protons *g* and *h* against equivalents of thread species produced titration curves, and winEQNMR2 analysis determined apparent association constants for the interpenetration process of both threads with the chloride complex of macrocycle **54** to be greater than $10^4$ $M^{-1}$.

Further evidence for interpenetration was obtained using 2D ROESY NMR, and the spectrum of **54**·**50**·$(PF_6)_2(Cl)$ is shown in Figure 3.23.

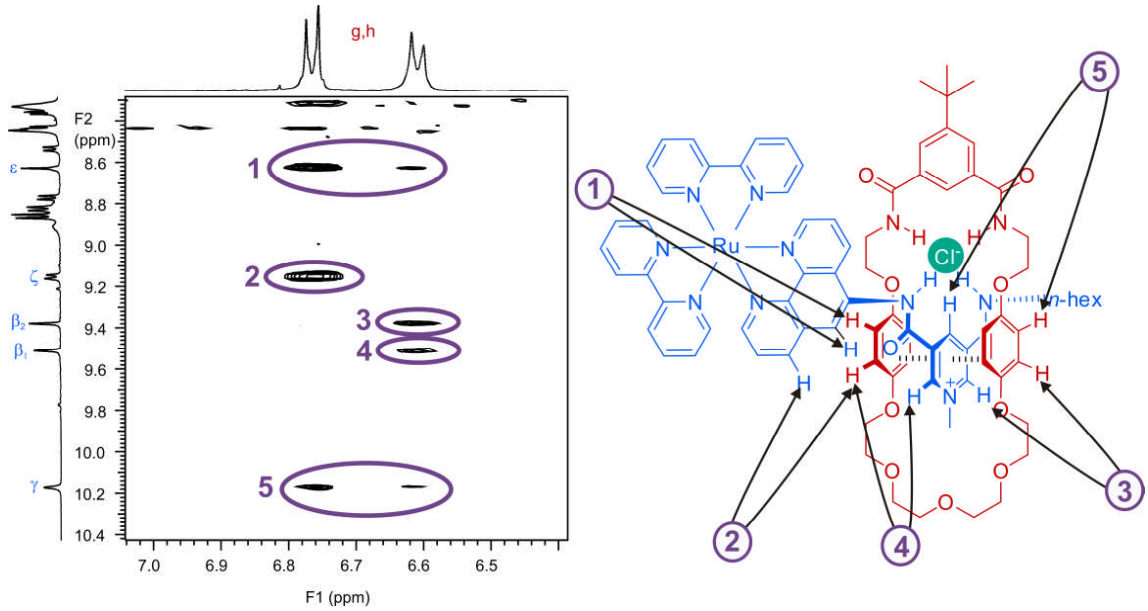



***Figure 3.23.*** *$^1H$ -$^1H$ ROESY spectrum of pseudorotaxane* ***54·50***·$(PF_6)_2Cl$ *in $d_6$-acetone at 293K. Cross couplings are shown on the schematic diagram on the right.*

Cross coupling interactions were observed between the macrocycle hydroquinone protons and thread protons in proximity to the anion binding site. Interactions **1** ($\varepsilon \rightarrow g,h$) and **2** ($\zeta \rightarrow g,h$) exist between phenanthroline protons and hydroquinone protons, whilst **3** ($\beta_1 \rightarrow g,h$), **4** ($\beta_1 \rightarrow g,h$) and **5** ($\gamma \rightarrow g,h$) denote through space correlations between hydroquinone and pyridinium protons.

### *3.3.3.3 Luminescence Titrations*

Following the success in forming chloride-templated pseudorotaxanes with the ruthenium appended threads, investigations to establish whether pseudorotaxane formation could be signalled *via* luminescence spectroscopy were undertaken. Luminescence titrations were performed whereby portions of the ferrocene macrocycle **55** were added to a 1:1 mixture of **44**·$(PF_6)_3$/TBACl in MeCN. Significant quenching (~ 50% after 5 equivalents) of the MLCT emission band was observed upon addition of the macrocycle to 1:1 **44**·$(PF_6)_3$/TBACl (Figure 3.24a). A plot of equivalents of macrocycle added versus the emission intensity is shown in Figure 3.24b. The MLCT emission quenching is indicative of interpenetrative assembly where the ferrocene moiety is in proximity to the ruthenium(II) stopper and induces quenching *via* intramolecular electron and energy transfer processes

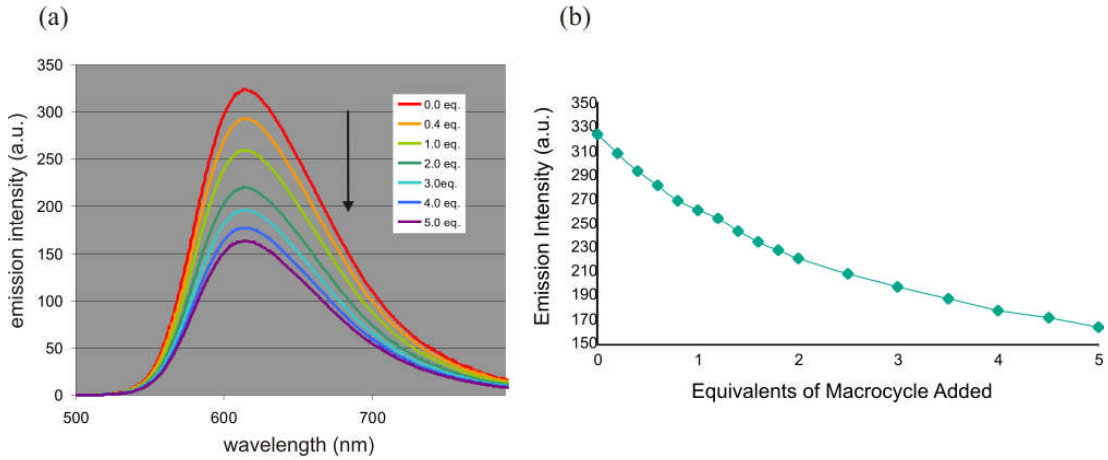



***Figure 3.24.*** *(a) Luminscence emission reduction of* ***44***·$(PF_6)_2Cl$ *upon addition of ferrocene macrocycle* ***55*** *and (b) Luminescence emission intensity of* ***44***·$(PF_6)_2Cl$ *as function of equivalents of macrocycle added, at 614 nm, at 1 x* $10^{-4}$ *M and 293 K in MeCN.*

SPECFIT was used to calculate an apparent association constant for this interpenetrative assembly process (log $K_{app}$ = 3.57 (error < 5%)).

### 3.3.4 Synthesis of Photo-active Rotaxane

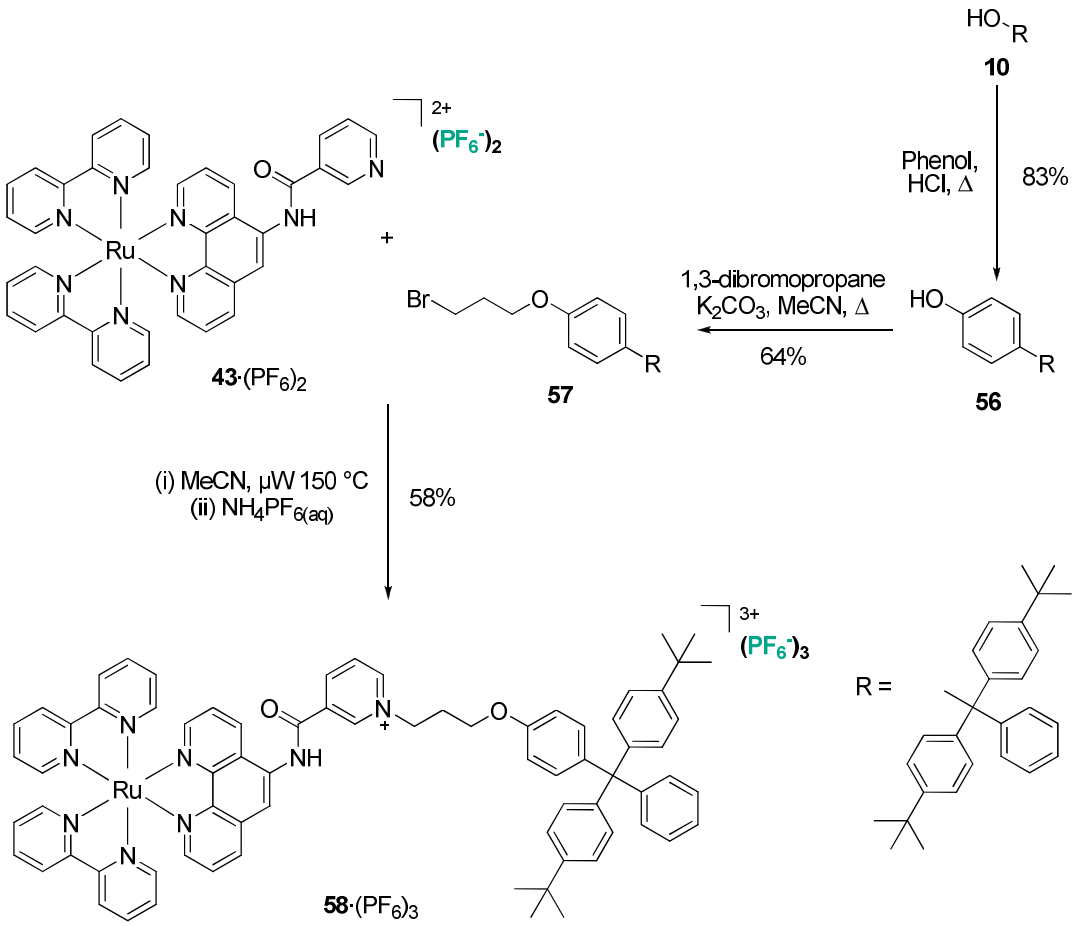
Given the success in forming pseudorotaxanes with the ruthenium appended threads **44**·$(PF_6)_3$ and **50**·$(PF_6)_3$, efforts were directed towards the synthesis of novel photo-active rotaxanes. Despite the disappointing halide responsive luminescence behaviour of pyridinium nicotinamide thread **50**·$(PF_6)_3$ itself, it was hoped that incorporation of the motif into an interlocked structure may result in an improved anion sensing ability through rigidification of the interlocked structure upon addition of anions.

In the first instance it was necessary to replace the hexyl chain of the thread components with a bulky stopper group to prevent dethreading from the macrocyclic component.

#### *3.3.4.1 Synthesis of Axle Components*

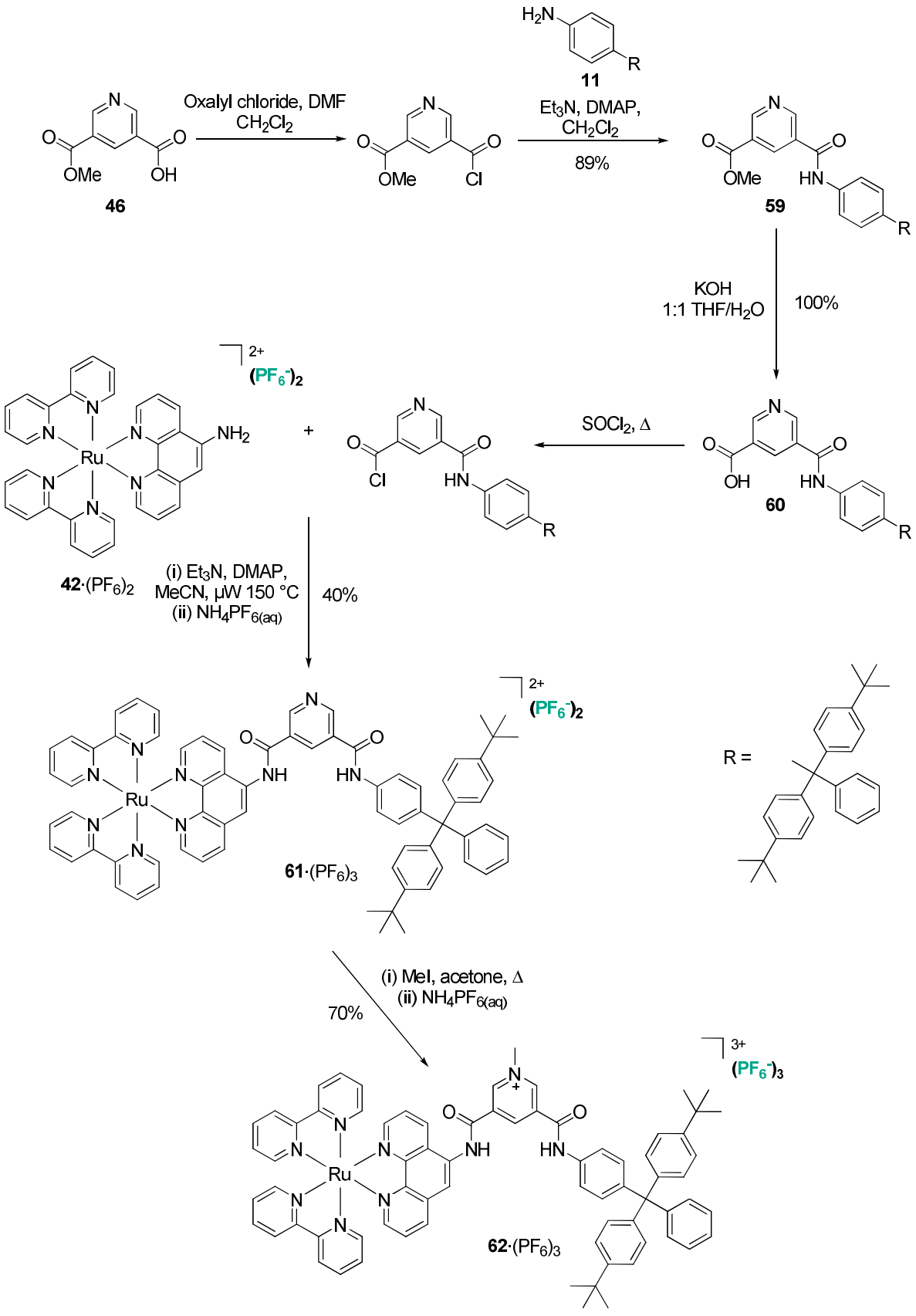
The synthesis of the pyridinium nicotinamide axle component is shown in Scheme 3.12, and began with the formation of the phenolic stopper component **56** *via* reaction of compound **10** with phenol in the presence of HCl. Stopper **56**[23] was reacted with one equivalent of 1,3-dibromopropane in MeCN in the presence of $K_2CO_3$ to give **57**[24] in 64%. Reaction of **43**·$(PF_6)_3$ and **57** was carried out in MeCN under microwave irradiation at 150 °C. Following column chromatography and anion exchange with aqueous $NH_4PF_6$, axle **58**·$(PF_6)_3$ was isolated in 58% yield.

After very small periods of time in solution ($CH_2Cl_2$, MeCN), significant decomposition of axle **58**·$(PF_6)_3$ was observed, which may be the result of an unstable pyridinium-alkyl bond. Unfortunately the inherent instability of this axle implied that it would not be suitable for reactions to form new photo-active rotaxanes, and therefore attention was turned to the synthesis of the pyridinium *N*-methyl axle component (Scheme 3.13).




***Scheme 3.12.*** *Synthesis of pyridinium nicotinamide axle* ***58***·*$(PF_6)_3$.*

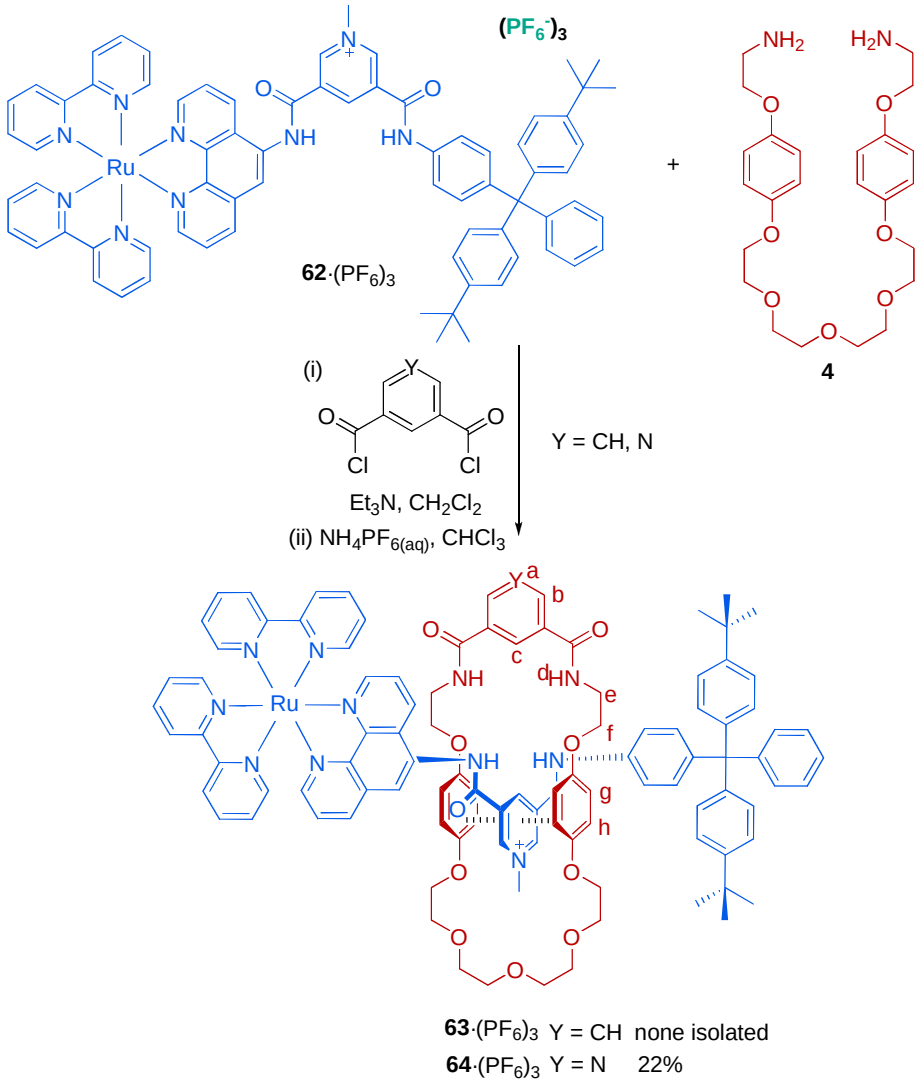
Compound **46** was converted to the corresponding acid chloride using oxalyl chloride in dry $CH_2Cl_2$ with a catalytic amount of DMF, which, upon condensation with amine stopper **11** in the presence of $Et_3N$ and DMAP in $CH_2Cl_2$ gave **59** in 89% yield. Ester hydrolysis was achieved using KOH in 1:1 THF/$H_2O$ to give **60** which was subsequently converted to the acid chloride. Reaction of this compound with amine **42**·$(PF_6)_3$ was carried out using microwave irradiation in MeCN with $Et_3N$ and DMAP to afford **61**·$(PF_6)_3$ in 40% yield after anion exchange. Methylation by heating with iodomethane in acetone, followed by anion exchange gave the target pyridinium axle compound **62**·$(PF_6)_3$ in 70%.




***Scheme 3.13.*** *Synthesis of axle component* ***62***·$(PF_6)_3$.

### *3.3.4.2 Synthesis and Characterisation of Rotaxane*

With axle component **62**·$(PF_6)_3$ in hand it was possible to carry out a rotaxanation reaction, shown in Scheme 3.14.




***Scheme 3.14.*** *Synthesis of rotaxanes.*

The bis-acid chloride clipping procedure employed in the successful synthesis of rotaxanes in Chapter 2 was used, initially with isophthaloyl dichloride. However, the rotaxane **63**·$(PF_6)_3$ produced had identical solubility properties and $R_f$ value to the axle **62**·$(PF_6)_3$ and despite numerous attempts the two components could not be separated. Since pyridine containing compounds are known for their high polarity it was decided to use 3,5-bis(chlorocarbonyl) pyridine in the clipping step of the rotaxanation reaction in the hope that this would aid better

chromographic separation of rotaxane and axle components. Following repeated column chromatography (with several eluents) and anion exchange, it was possible to isolate rotaxane **64**·$(PF_6)_3$ with minor contaminants in 22% yield. This yield is considerably lower than that obtained for the rotaxanes with symmetrical non-photo-active axles (Chapter 2), which may result from loss of material during the more lengthy purification procedure. It is also possible that the phenanthroline moiety may be sterically inhibiting the association of the macrocycle precursor and axle component during the condensation reaction. Evidence for the formation of rotaxane **64**·$(PF_6)_3$ was obtained by $^1$H NMR spectroscopy and mass spectrometry. The $^1$H NMR spectrum revealed characteristic upfield shifts and splitting of the macrocycle hydroquinone protons, indicative of π-π stacking interactions between hydroquinone and pyridinium surfaces.

The electrospray mass spectrum of **64**·$(PF_6)_3$ along with the isotope model for comparison is given in Figure 3.25. The observed mass of 1941.6499 is in good agreement with the isotope model (1941.6500) and provides strong evidence for successful formation of the rotaxane.

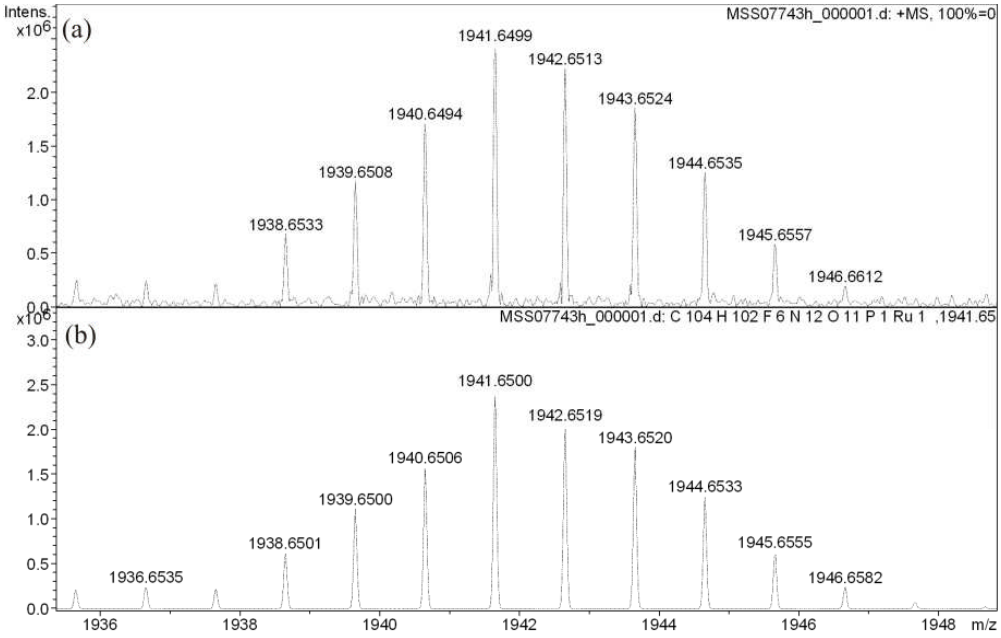



***Figure 3.25.*** *(a) Measured ESI mass spectrum and (b) theoretical isotope model, for* **64**·$(PF_6)_3$ *[M − $PF_6$ − H]$^+$.*

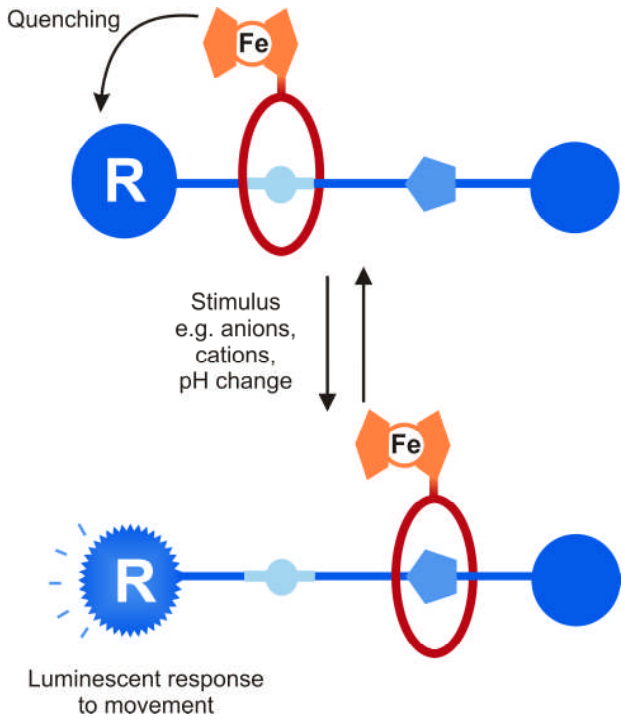
The challenging multi-step synthesis and purification of rotaxane **64**·$(PF_6)_3$, combined with the lengthy synthesis of its component axle, meant that it was not possible to obtain an adequate amount of the rotaxane of sufficient purity for subsequent anion binding and sensing titration experiments.

### 3.3.5 Summary and Future Perspectives

New ruthenium(II) phenanthroline bis-bipyridyl appended stopper groups have been prepared for incorporation into a number of photo-active thread and axle components. The ability of this moiety to bind and sense anions in aqueous solvent media, when incorporated into appropriately designed pyridinium receptors was investigated *via* $^1$H NMR and luminescence titration experiments. Proton NMR studies reveal these pyridinium receptors are capable of strongly complexing halide anions, whilst there seems to be several complex equilibria involved in the binding of oxoanions. The ability of these systems to sense anions is more ambiguous, with acetate causing a near total quenching of the MLCT emission band which is attributed to deprotonation of the highly acidic amide proton(s) causing PET quenching. Pyridinium nicotinamide receptor **44**·$(PF_6)_3$ is unable to sense halide anions, whereas receptor **50**·$(PF_6)_3$ undergoes a 20% increase in MLCT emission intensity upon addition of chloride, but does not detect the presence of bromide. These observations are tentatively attributed to the interplay between two competing factors, where the anion itself acts a luminescence quencher whilst the rigidification of the receptor upon anion binding acts to enhance emission intensity. Due its greater flexibility, receptor **50**·$(PF_6)_3$ undergoes substantial rigidification upon addition of anions, which may account for its ability to sense chloride.

Both threads are capable of undergoing pseudorotaxane formation with an appropriate macrocyclic component *via* chloride anion templation, and, upon construction of a suitable ruthenium(II) appended pyridinium axle component **63**·$(PF_6)_3$, it was possible to synthesise a [2]rotaxane.

Functionalisation of the macrocyclic component with ferrocene allowed for pseudorotaxane formation to be probed by luminescence spectroscopy. Upon addition of the ferrocene macrocycle to thread **44**·$(PF_6)_3$ in the presence of chloride, a significant quenching of MLCT emission intensity was observed indicative of pseudorotaxane assembly where the ferrocene is in proximity to the ruthenium stopper and can therefore quench its luminescence *via* intramolecular electron and energy transfer processes. In the future this phenomenon may be useful for probing molecular motion in a two-station [2]rotaxane (Scheme 3.15). The construction of appropriate bistable [2]rotaxanes for molecular motion is discussed in the next chapter.




***Scheme 3.15.*** *Schematic representation of luminescent response to molecular motion.*

## 3.4 Conclusions

The work in this chapter has shown that it is possible to functionalise [2]rotaxanes with photo-active transition metal complexes, on either the macrocycle or axle component. Using the subsequent rotaxanes for anion sensing has produced varied results. Preliminary

observations suggest that rotaxanes with appended rhenium(I) bipyridyl complexes are capable of sensing the presence of anions, with similar binding trends observed in both $^{1}$H NMR and luminescence studies. By contrast, whilst ruthenium(II) bipyridyl systems are stronger anion complexants due to increased electrostatic contributions, their anion sensing capabilities have proved complicated. This may be the result of various complex luminescence mechanisms upon anion addition. Greater success may be sought by incorporating ruthenium(II) complexes into bistable rotaxanes for detecting molecular motion *via* luminescence spectroscopy.

## 3.5 References


1. R. Martínez-Máñez and F. Sancenón, *Chem. Rev.*, 2003, **103**, 4419-4476.
2. P. D. Beer and S. R. Bayly, *Topics in Current Chemistry*, 2005, **255**, 125-162.
3. S.-S. Sun, A. J. Lees and P. Y. Zavalij, *Inorg. Chem.*, 2003, **42**, 3445-3453.
4. M. S. Vickers, K. M. Martindale and P. D. Beer, *J. Mater. Chem.*, 2005, **15**, 2784-2790.
5. V. Amendola and L. Fabbrizzi, *Chem. Commun.*, 2009, 513-531.
6. D. J. Mercer and S. J. Loeb, *Chem. Soc. Rev.*, 2010, **39**, 3612-3620.
7. F. Szemes, D. Hesek, Z. Chen, S. W. Dent, M. G. B. Drew, A. J. Goulden, A. R. Graydon, A. Grieve, R. J. Mortimer, T. Wear, J. S. Weightman and P. D. Beer, *Inorg. Chem.*, 1996, **35**, 5868-5879.
8. D. Curiel, P. D. Beer, R. L. Paul, A. Cowley, M. R. Sambrook and F. Szemes, *Chem. Commun.*, 2004, 1162-1163.
9. J. R. Lakowicz, *Principles of Fluorescence Spectroscopy*, Springer, New York and London, 1983.
10. J. A. Wisner, P. D. Beer, M. G. B. Drew and M. R. Sambrook, *J. Am. Chem. Soc.*, 2002, **124**, 12469-12476.
11. M. J. Hynes, *J. Chem. Soc., Dalton Trans.*, 1993, 311-312.
12. D. J. Stufkens and A. Vlcek, *Coord. Chem. Rev.*, 1998, **177**, 127-179.
13. *SPECFIT, 2.02*, Spectrum Software Associates, Chapel Hill, NC.
14. P. R. Ashton, R. Ballardini, V. Balzani, A. Credi, K. R. Dress, E. Ishow, C. J. Kleverlaan, O. Kocian, J. A. Preece, N. Spencer, J. F. Stoddart, M. Venturi and S. Wenger, *Chem. Eur. J.*, 2000, **6**, 3558-3574.
15. G. Chen, J. Xia, Z. Li, G.-A. Yu, S. Jin and S. H. Liu, *J. Organomet. Chem.*, **695**, 323-326.
16. G. F. Smith and F. W. Cagle, *J. Org. Chem.*, 1947, **12**, 781-784.
17. K. Binnemans, P. Lenaerts, K. Driesen and C. Gorller-Walrand, *J. Mater. Chem.*, 2004, **14**, 191-195.
18. J. P. Collman, R. A. Decreau and S. Costanzo, *Org. Lett.*, 2004, **6**, 1033-1036.
19. W. Huang and T. Ogawa, *Polyhedron*, 2006, **25**, 1379-1385.

20. M. K. P. Leung, C.-F. Chow and M. H. W. Lam, *J. Mater. Chem.*, 2001, **11**, 2985-2991.
21. P. D. Beer, A. R. Graydon and L. R. Sutton, *Polyhedron*, 1996, **15**, 2457-2461.
22. P. D. Beer, F. Szemes, V. Balzani, C. M. Sala, M. G. B. Drew, S. W. Dent and M. Maestri, *J. Am. Chem. Soc.*, 1997, **119**, 11864-11875.
23. H. W. Gibson, S.-H. Lee, P. T. Engen, P. Lecavalier, J. Sze, Y. X. Shen and M. Bheda, *J. Org. Chem*, 1993, **58**, 3748-3756.
24. H. Zheng, W. Zhou, J. Lv, X. Yin, Y. Li, H. Liu and Y. Li, *Chem. Eur. J.*, 2009, **15**, 13253-13262.

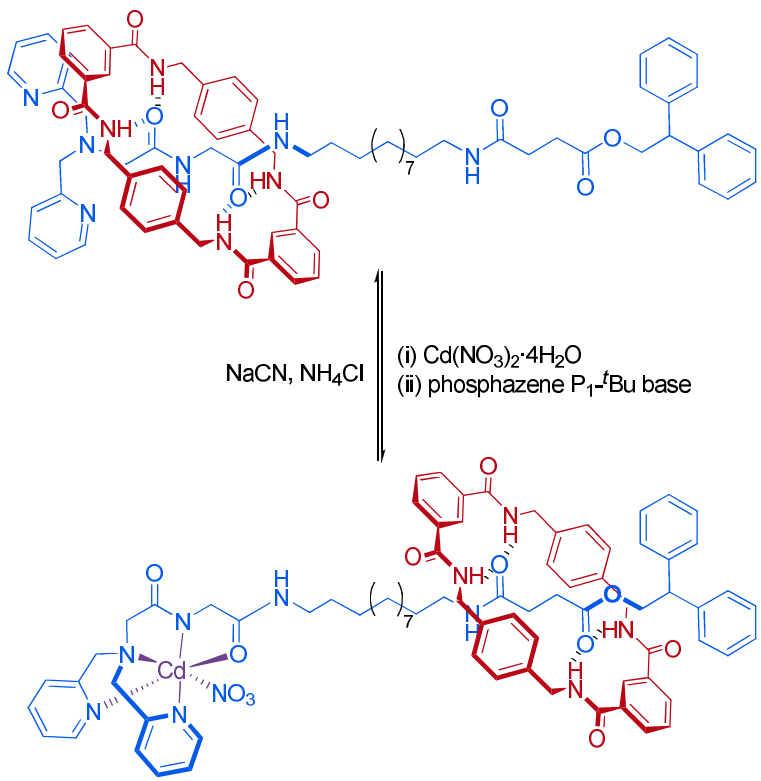
# Chapter 4: Synthesis of [2]Rotaxanes for Molecular Motion

## 4.1 Introduction

### 4.1.1 Molecular Motion in [2]Rotaxanes

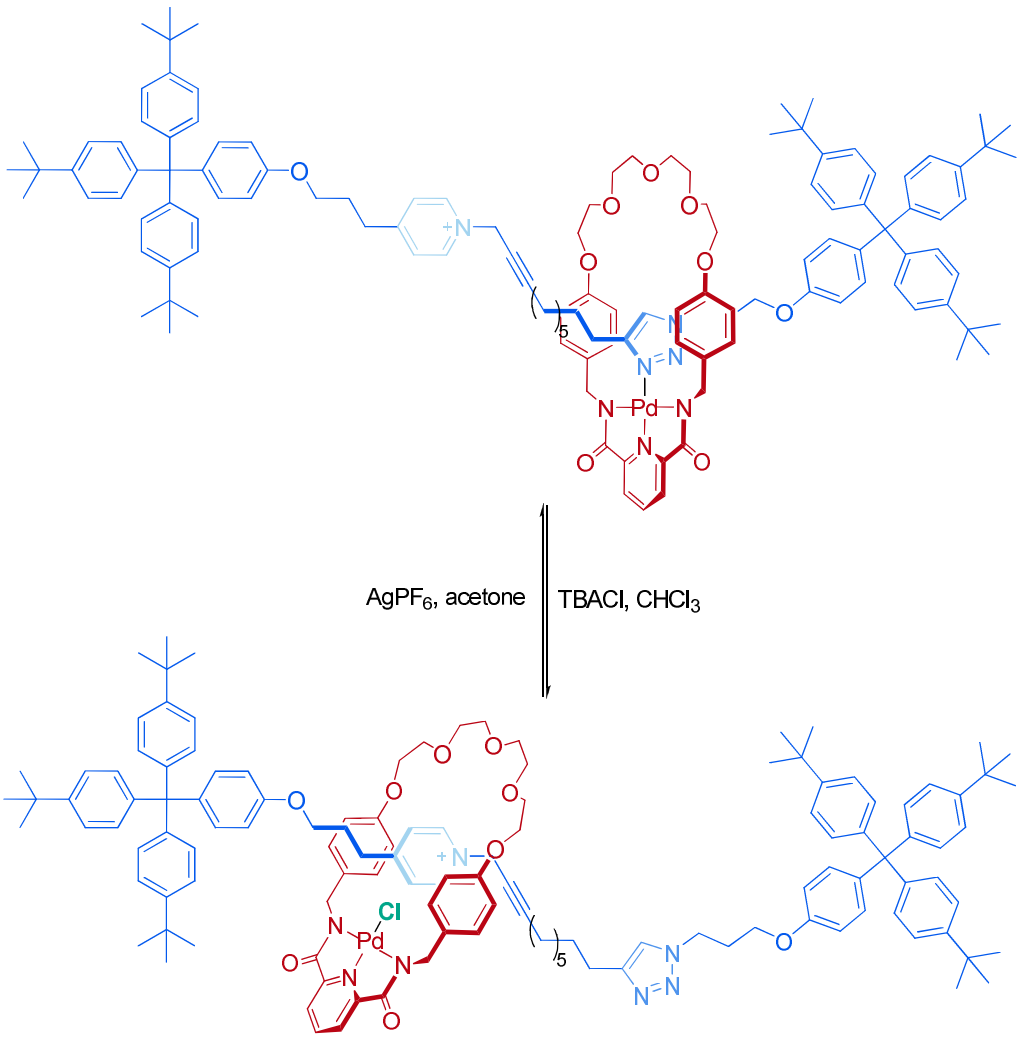
The concept of using various stimuli to induce molecular motion in artificial interlocked systems was introduced in Chapter 1. This chapter focuses specifically on the use of ions to stimulate motion within strategically designed [2]rotaxanes.

Examples of both cation- and anion-induced molecular motion have appeared in the recent literature, however there are considerably fewer anion-dependent machine-like systems due to the challenges of anion complexation (discussed in Section 1.3.1).




***Scheme 4.1.*** *Leigh's Cd(II)-induced molecular shuttle.*[1]

Many cation-induced molecular machines employ the preferred coordination geometries of transition metal d-orbital configurations.[2-5] Indeed Leigh and co-workers have designed various cation-induced molecular shuttles utilizing such a principle.[6, 7] This group have also been responsible for providing an example of a molecular shuttle where the addition of metal cations acts to translocate the macrocyclic component to an alternative site on the axle (Scheme 4.1).[1] Coordination of a Cd(II) ion at the bis-pyridyl tertiary amine axle terminus causes a conformational change such that it is no longer favourable for the tetra-amide macrocycle to reside here *via* hydrogen bonding, and the macrocycle moves to the second weaker hydrogen bonding site.




***Scheme 4.2.*** *Leigh's chloride-induced molecular shuttle.*[8]

The same researchers have demonstrated that the ability of chloride to displace weak nitrogen donors from the square planar coordination sphere of palladium(II) complexes can be exploited to construct an anion-switchable molecular shuttle (Scheme 4.2).[8]

Both of the molecular machines illustrated above are examples of rotaxanes undergoing translational motion of the macrocyclic wheel along the axle component. Rotational motion of the macrocycle around the axle is much rarer. Sauvage has produced an elegant example of this 'pirouetting' motion in a rotaxane where both the macrocycle and axle components are functionalised with porphyrin complexes (Figure 4.1a).[9] In the presence of Cu(I) ions the macrocycle adopts a conformation where the phenanthroline units of the macrocycle and axle form an orthogonal complex around the cation. However, when the Cu (I) ion is removed, the macrocycle undergoes a rotation of 180° to adopt a conformation where all porphyrin units are stacked, stabilised by the weak interactions between the Zn(II) and Au(III) ions (Figure 4.1b). Upon addition of Cu(I) the macrocycle reverts to its original position.

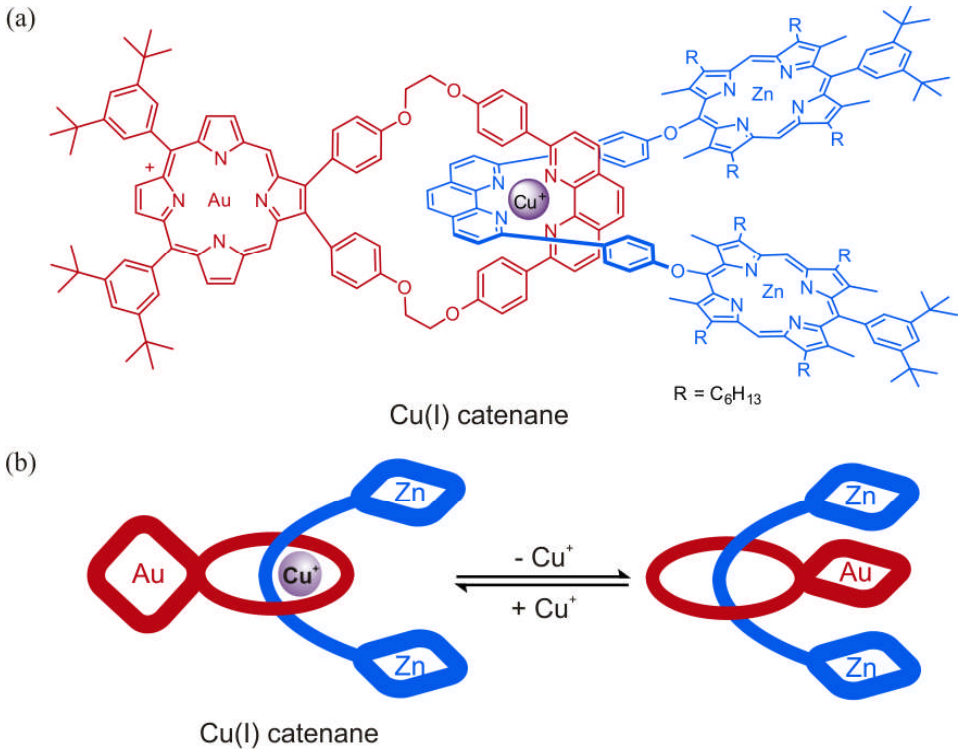
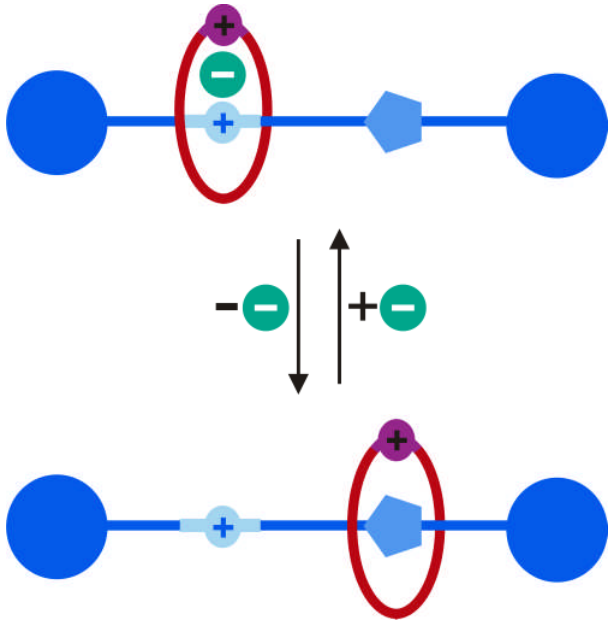



***Figure 4.1.*** *(a) Sauvage's Cu(I)-templated [2]rotaxane functionalised with porphyrin units, (b) schematic representation of rotational molecular motion upon demetallation.*[9]

### 4.1.2 Chapter Objectives

The main objective of this chapter is to synthesise functional rotaxanes for use as molecular machines, capable of undergoing either translational or rotational motion.

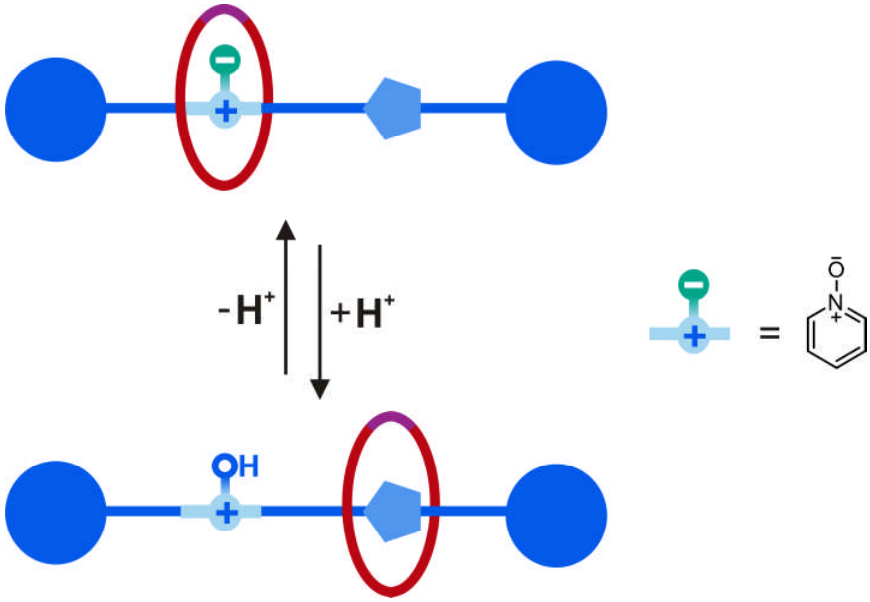
Since all rotaxanes in this thesis to this point have been designed for anion recognition, initial efforts will focus on the construction of a two station [2]rotaxane capable of undergoing translational motion upon addition of anions. If such a system is designed whereby one station on the axle is positively charged and the other is neutral, then it is anticipated that a positively charged macrocycle will only reside at the positive station in the presence of anions. In the absence of anions, unfavourable repulsive electrostatic interactions between macrocyclic and axle pyridinium units will induce movement of the macrocycle to the second neutral station. This is depicted schematically in Scheme 4.3.



***Scheme 4.3.*** *Schematic representation of chloride-induced molecular shuttling*

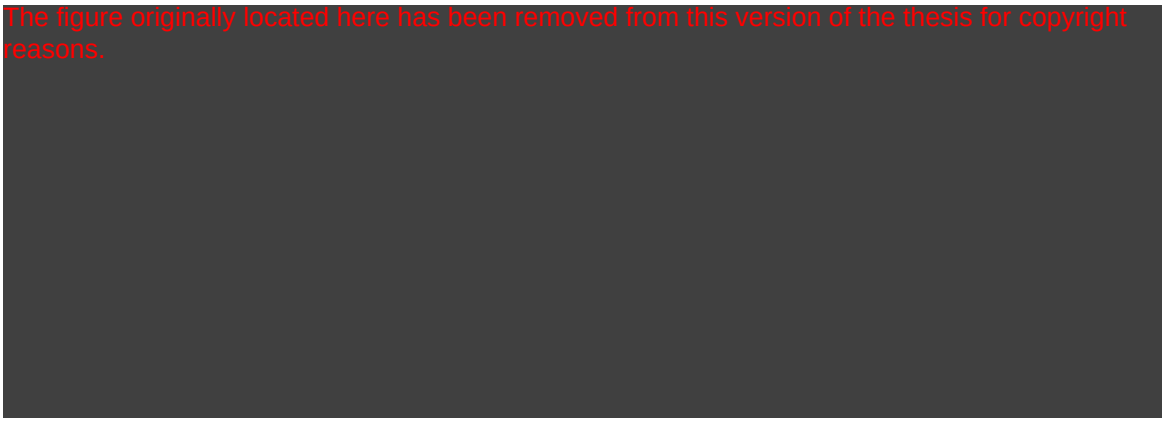
The construction of rotaxanes containing axles functionalised with pyridine *N*-oxide to act as an integrated template will also be investigated. The inherent properties of pyridine *N*-oxide may make it a suitable group for inclusion in molecular machines since protonation of the

appended oxygen may result in movement away from the anion binding domain where it resides (Scheme 4.4).




***Scheme 4.4.*** *Schematic representation of pyridine N-oxide rotaxane undergoing pH-induced molecular motion.*

More ambitiously, if an appropriately designed heteroditopic macrocycle is functionalised with an anion binding site at one end and cation binding receptor at the other, it may be possible to induce pirouetting of the macrocycle around the axle component by addition and removal of cations. This idea relies on the pyridine *N*-oxide component being able to occupy a vacant coordination site of the metal cation bound by the macrocycle. It is anticipated that, in the absence of cations, the pyridine *N*-oxide will be bound by the anion binding motif, whereas upon addition of cations, a half rotation will occur such that the pyridine *N*-oxide coordinates to the cation (Scheme 4.5). It has been shown that an appropriate calix[4]diquinone macrocycle functionalised with an isophthalamide unit can strongly bind both anions and cations,[10] and therefore might be suitable for inclusion in the target [2]rotaxane.

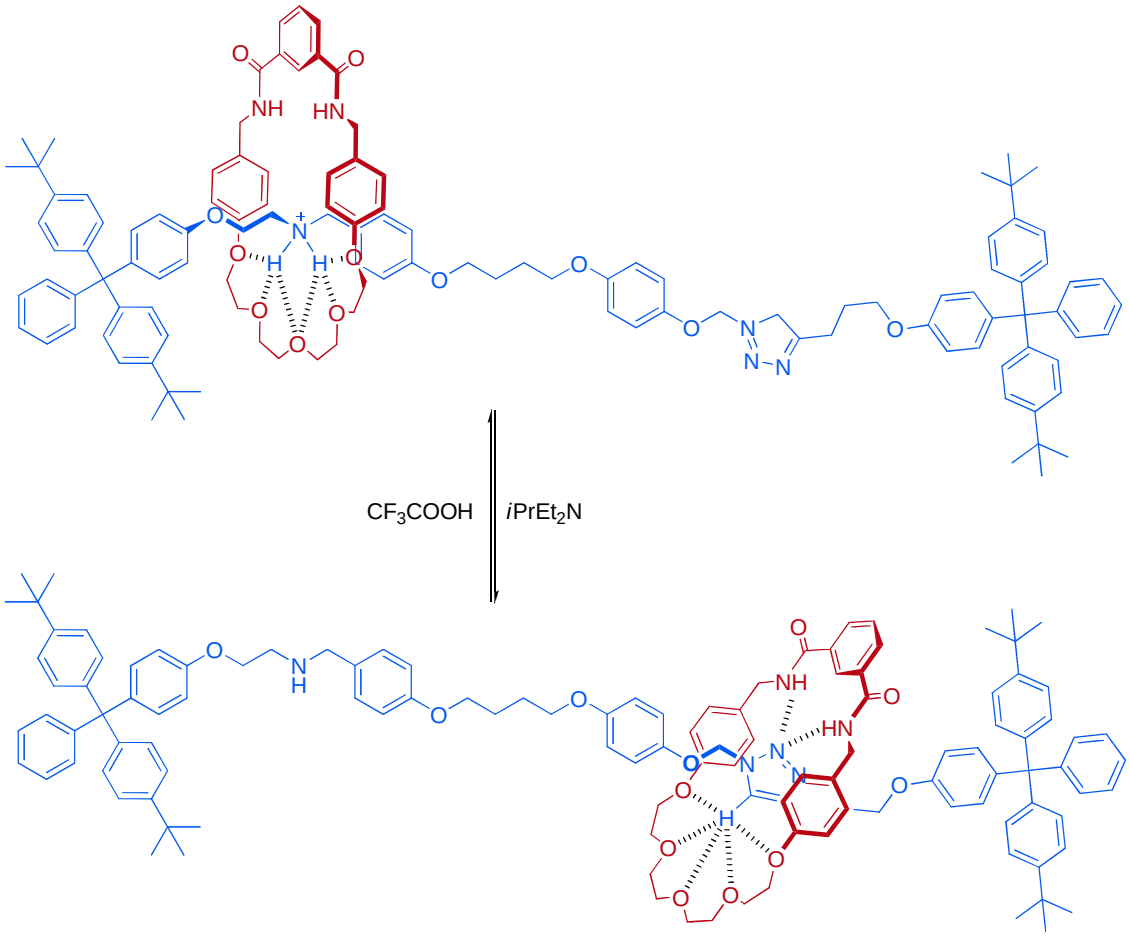



***Scheme 4.5.*** *Schematic representation of cation-induced pirouetting of a calix[4]diquinone containing [2]rotaxane.*

## 4.2 Novel Two Station Rotaxane: Synthesis and Studies

In order to design and construct a rotaxane capable of undergoing some form of molecular motion, it must firstly be possible to use a synthetically accessible route to construct the interlocked molecule. Secondly, it is necessary for there to be two bistable isomers of the molecule which can be interconverted upon a given stimulus. Both conditions can be satisfied by using a Huisgen 1,3-dipolar cycloaddition (referred to as 'click reaction' from now on for simplicity) between an alkyne and azide, creating a triazole moiety which can then act as a second station.

Li *et al.* have reported a rotaxane system where an isophthalamide-polyether macrocycle resides at a dialkylammonium site under acidic conditions, however upon addition of base the macrocycle moves to a triazole station.[11] This motion can be reversed by re-protonation of the axle dialkyl amine. The authors propose that the polarised nature of the triazole unit gives rise to favourable hydrogen bonding interactions with both the isophthalamide cleft and the polyether chain (see Scheme 4.6).




***Scheme 4.6.*** *Li's acid/base controlled molecular shuttle.*[11]

Inspired by this work, a two station axle was designed whereby one station is a positively charged anion binding motif and the other is a neutral triazole (Figure 4.2). Since the 3,5-pyridinium bis-amide motif has been shown to undergo chloride-templated pseudorotaxane formation with appropriate macrocyclic components this was chosen as the positively charged station. The macrocyclic component of the target [2]rotaxane was chosen as the pyridinium macrocycle used in Chapter 2 of this thesis for catenane formation. It is postulated that in the presence of chloride the macrocycle will reside over the axle pyridinium station, where the two components form a strong orthogonal complex around the chloride anion, stabilized by hydrogen bonding and electrostatics. Upon removal of anion, it is anticipated that the mutual electrostatic repulsion will induce movement of the pyridinium macrocycle away from the

positively charged pyridinium station towards the triazole motif, where hydrogen bonding interactions would stabilize the new co-conformation.

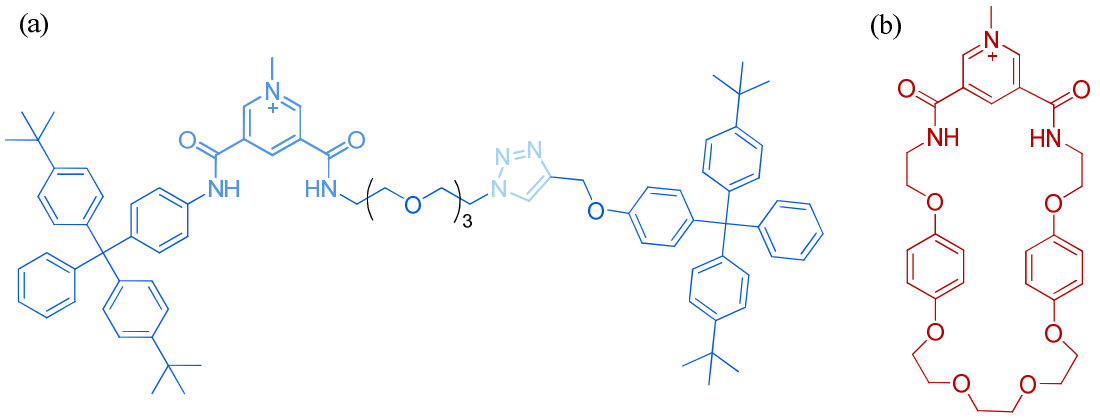


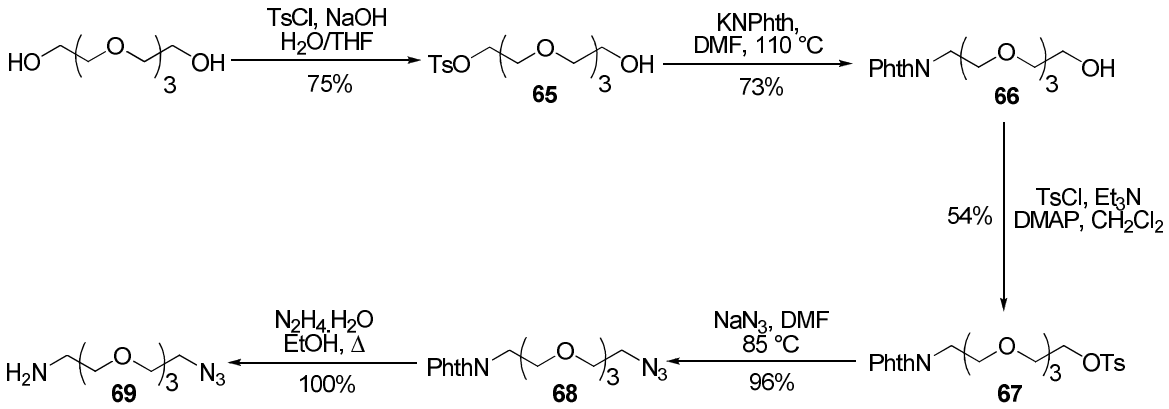

***Figure 4.2**. Design of components for two station rotaxane: (a) axle; and (b) macrocycle.*

To ensure that the stations remain distinct a polyether chain of appreciable length was chosen as the spacer group between pyridinium and triazole motifs.

### 4.2.1 Precursor Syntheses

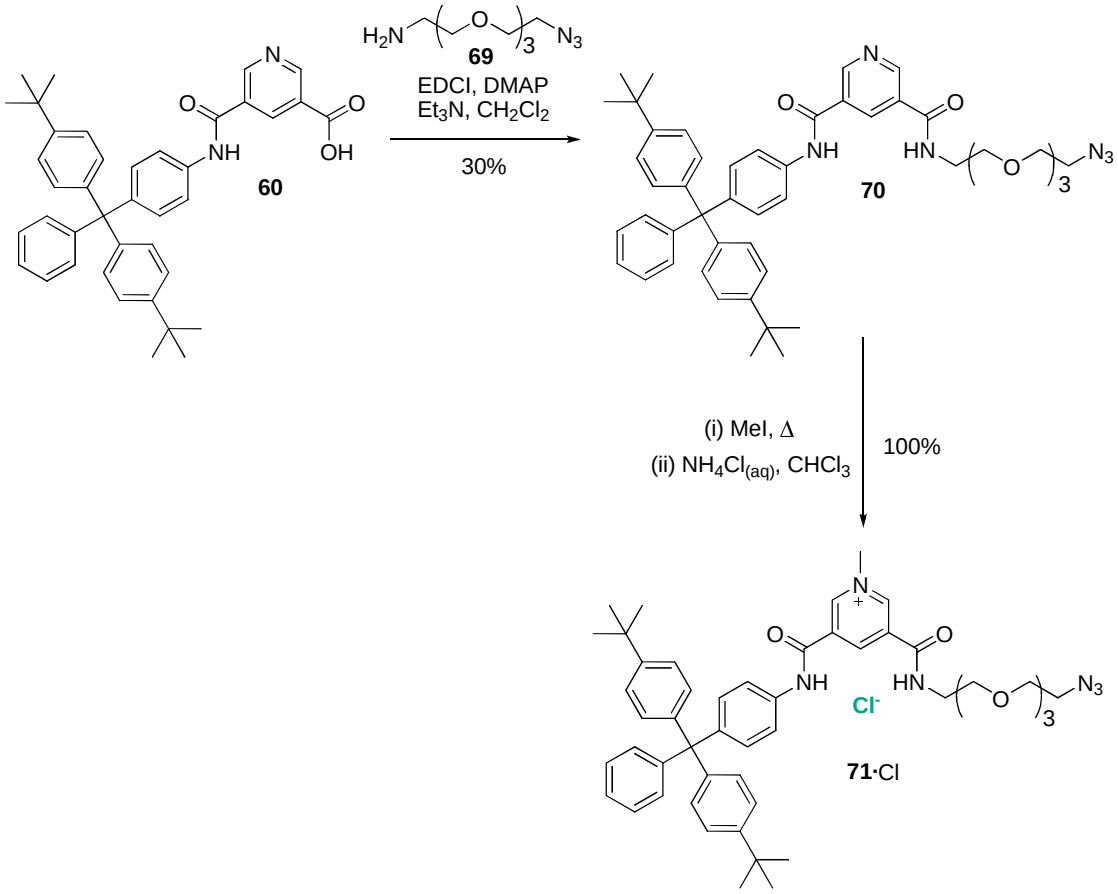
All novel compounds reported in this section were characterised by $^{1}$H NMR, $^{13}$C NMR and HRMS (ESI).

The synthesis of the axle precursor component began with the preparation of an asymmetric amine-azide component **69**, depicted in Scheme 4.7.




***Scheme 4.7.** Synthesis of azide-amine precursor **69**.*

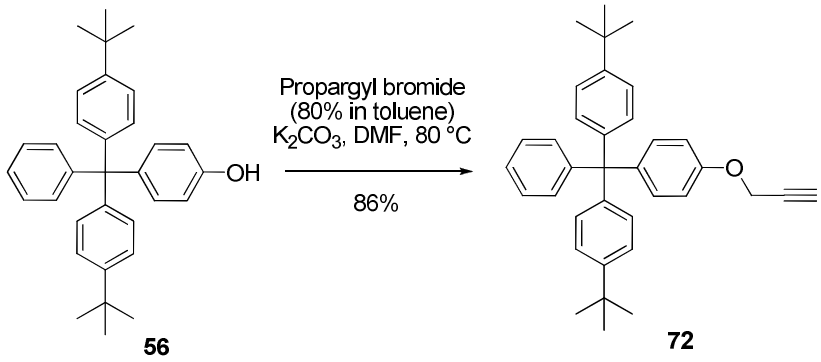
Mono-tosylation of tetraethylene glycol was achieved *via* reaction with a substoichiometric amount of tosyl chloride in the presence of NaOH in 1:1 $H_2O$/THF to give compound **65** in 75% yield. This was then reacted with potassium phthalamide by heating in DMF to give **66**[12] in 73%, whose alcohol functionality was converted to the corresponding tosylate **67**[12] by reaction with tosyl chloride in the presence of $Et_3N$ and DMAP in dry $CH_2Cl_2$. Compound **68**[13] was synthesised *via* conversion of the tosylate to the azide analogue by heating with sodium azide in DMF. Finally, the synthesis of asymmetric amine-azide derivative **69**[13] was achieved *via* removal of the phthalimide protecting group by heating with hydrazine in ethanol. The synthesis of the pyridinium axle precursor is outlined in Scheme 4.8, and began with the EDCI mediated coupling reaction between compounds **60** and **69** in the presence of DMAP and $Et_3N$ in $CH_2Cl_2$.




***Scheme 4.8.*** *Synthesis of pyridinium axle precursor* ***71****·Cl.*

It was necessary to leave the reaction for several days to react, by which time substantial decomposition of compound **60** had occurred, accounting for the low yield of this coupling step. Following purification of compound **70**, methylation was achieved by heating with MeI, and anion exchange carried out by washing a solution of **71**·I in $CHCl_3$ with aqueous $NH_4Cl$.

An appropriate alkyne functionalised stopper group, for use in the click reaction was synthesised according to Scheme 4.9. Phenol stopper **56** was heated with propargyl bromide and $K_2CO_3$ in DMF at 80 °C to yield alkyne stopper **72** in 86% yield following aqueous workup and a silica plug.

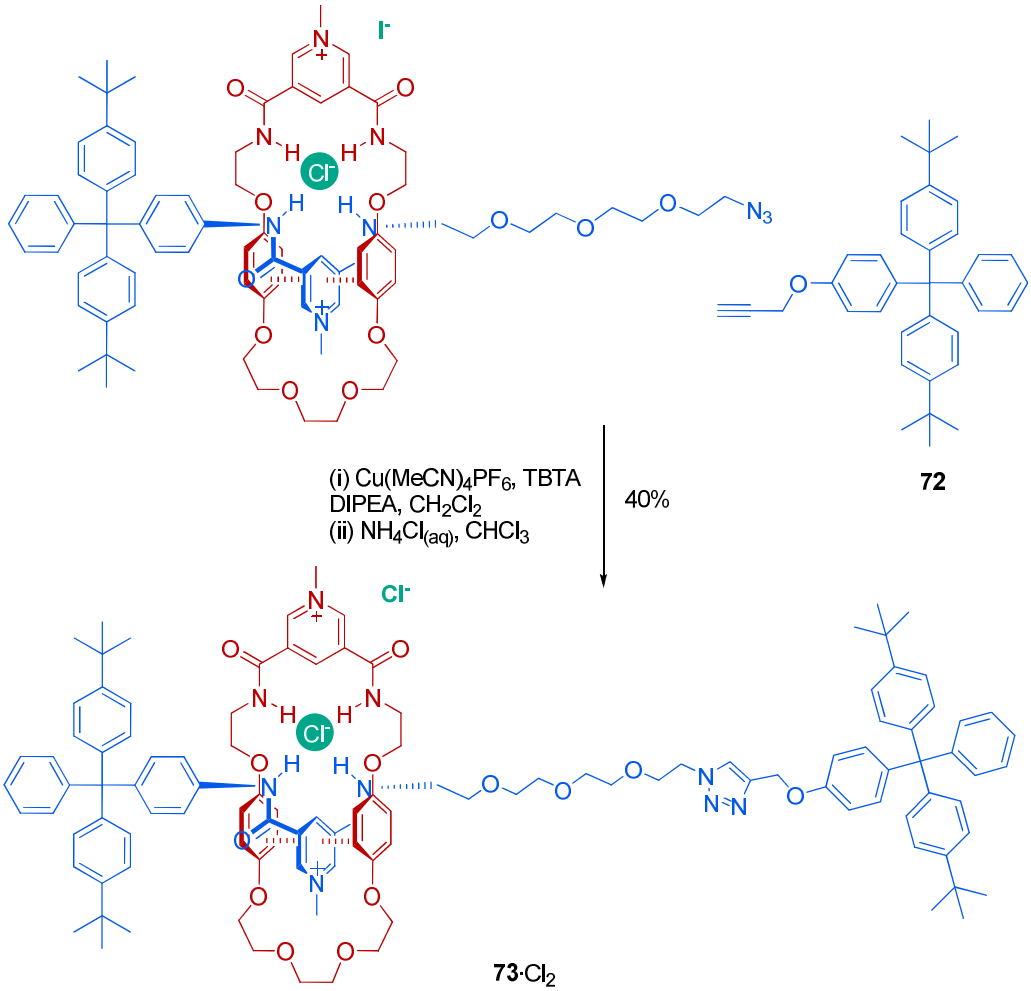



***Scheme 4.9.*** *Synthesis of alkyne functionalised stopper **72**.*

## 4.2.2 Rotaxane Synthesis and Characterisation

With all components in hand, the copper(I) catalysed click reaction was carried out to form a two station [2]rotaxane (Scheme 4.10).

Macrocycle **31**·I, azide appended axle precursor **71**·Cl and alkyne stopper **72** were stirred in degassed $CH_2Cl_2$ for fifteen minutes before $Cu(MeCN)_4PF_6$, TBTA and DIPEA were added. The reaction was left for sixteen hours, then subjected to acidic work-up, preparative TLC and conversion to the bis-chloride salt using $NH_4Cl_{(aq)}$ giving **73**·$Cl_2$ in 40% yield. It is thought that the reaction could proceed in a higher yield but was hindered by DIPEA-induced decomposition of the two pyridinium motifs, akin to that described in Section 2.3.2.




***Scheme 4.10.*** *Synthesis of rotaxane* ***73***·$Cl_2$.

The novel rotaxane was initially characterised by $^1$H NMR. The $^1$H NMR spectrum of rotaxane **73**·$Cl_2$, along with that of the component axle (as the hexafluorophosphate salt) and macrocycle **31**·Cl for comparison are given in Figure 4.3. These spectra suggest that the rotaxane is adopting a conformation where the macrocycle is residing over the axle's pyridinium station in the presence of chloride anions, as anticipated. This is exemplified by a large upfield shift of the macrocycle hydroquinone protons *g* and *h* upon rotaxane formation resulting from charge-assisted π-π stacking interactions with the electron deficient pyridinium surface. In addition, only minor changes in chemical shift values between free axle and rotaxane of protons *ζ*, *η* and *θ* in the vicinity of the triazole station are observed, again providing evidence for the aforementioned co-conformation

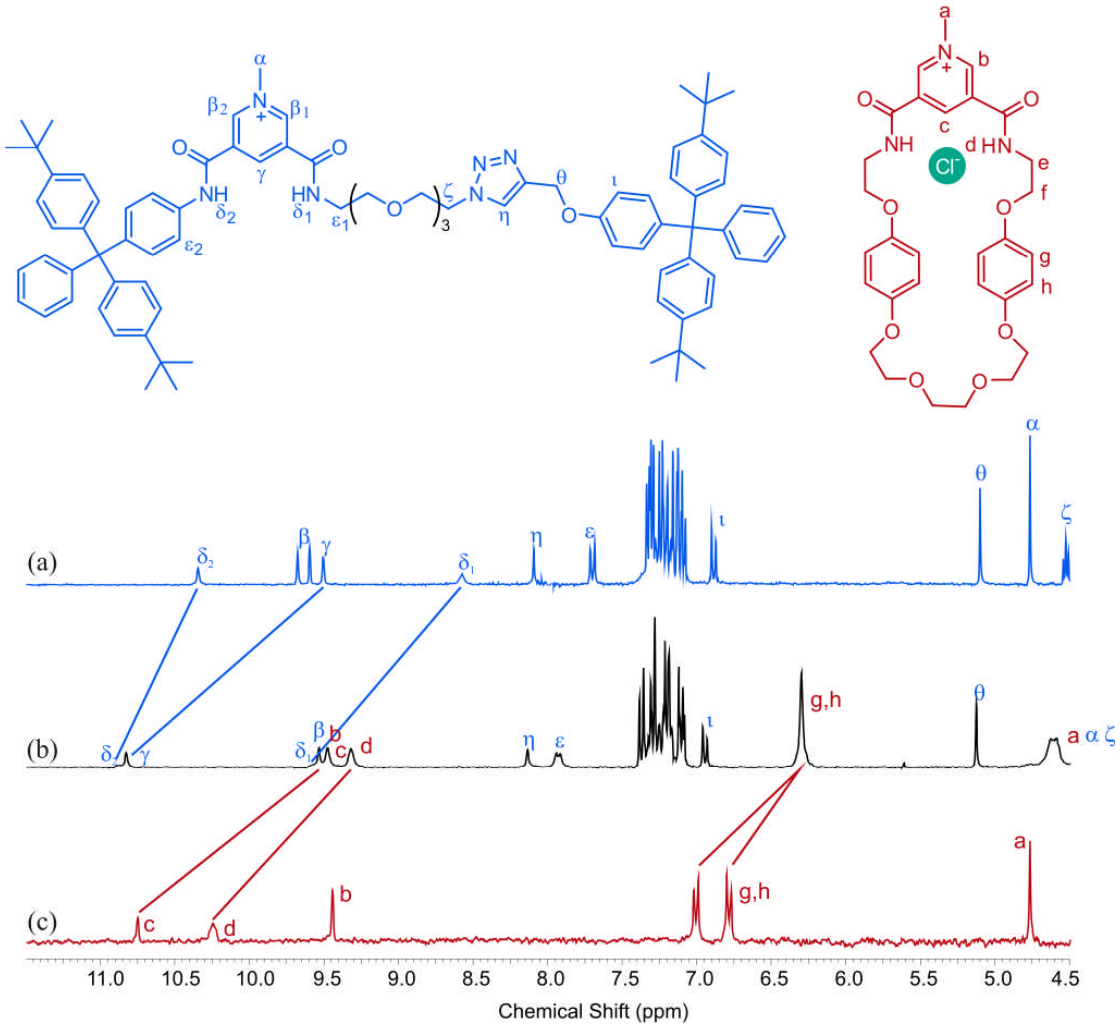



***Figure 4.3.*** *$^1$H NMR in $d_6$-acetone at 293K of (a) component axle, (b) [2]rotaxane* ***73***$\cdot Cl_2$ *and (c) pyridinium* ***31***$\cdot I$ *+ 1 eq. TBACl.*

Removal of the chloride anions was achieved by washing a solution of **73**$\cdot Cl_2$ in $CHCl_3$ with aqueous $NH_4PF_6$. The $^1$H NMR spectra of the chloride and hexafluorophosphate salts of rotaxane **73** are given in Figure 4.4. A number of chemical shift perturbations are observed upon converting to the hexafluorophosphate salt, namely the upfield shift of peaks corresponding to protons *b*, *c*, *d*, *β*, *γ*, $\delta_1$ and $\delta_2$. This is consistent with the chloride anion being removed from the cavity, rather than an indication of translational movement to the triazole station. In addition, the increased splitting of the hydroquinone protons *g* and *h* may also be a direct consequence of anion exchange, and is consistent with the simple dicationic rotaxane **28**$\cdot X_2$ described in Chapter 2. Disappointingly, there were no shifts apparent in

protons in the vicinity of the triazole unit ($\zeta$, $\eta$ and $\theta$) which strongly implies that these protons remain in a similar environment, suggesting that the macrocycle maintains its original position at the axle's pyridinium station.

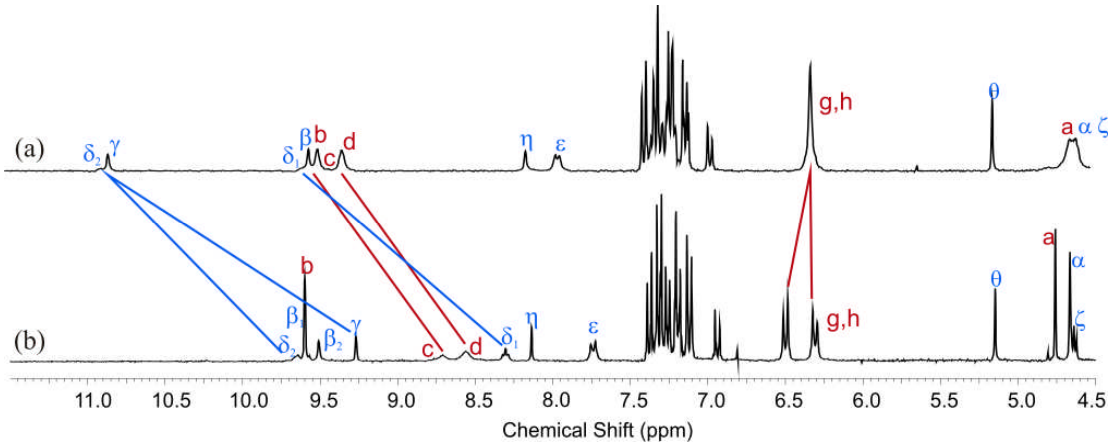



***Figure 4.4.*** *$^1$H NMR in $d_6$-acetone at 293K of (a) rotaxane **73**·$Cl_2$ and (b) rotaxane **73**·$(PF_6)_2$.*

Two-dimensional ROESY NMR was used to confirm this theory, and the spectrum of **73**·$(PF_6)_2$ is given in Figure 4.5. A number of through space correlations between macrocycle hydroquinone protons and protons in the vicinity of the pyridinium unit are observed. Interactions **1** ($\beta_1 \rightarrow g,h$), **5** ($\beta_1 \rightarrow g,h$) and **2** ($\gamma \rightarrow g,h$) occur between pyridinium and hydroquinone protons and **4** ($\delta_1 \rightarrow$ g,h) shows through space correlation between the axle aliphatic amide and hydroquinone protons. Stopper and methyl protons are also observed to be close in space to the macrocycle by interactions **3** ($\varepsilon_2 \rightarrow g,h$) and **7** ($\alpha \rightarrow g,h$). All evidence obtained from 2D ROESY NMR discussed thus far supports the theory that the macrocycle continues to reside at the axle's pyridinium station. However a further cross coupling interaction **6** ($\theta \rightarrow g,h$) between the macrocycle hydroquinone protons and the protons residing adjacent to the triazole group begins to complicate this conclusion. Interaction **6** indicates that, in solution, the macrocycle resides in close proximity to the triazole unit for an appreciable amount of time.

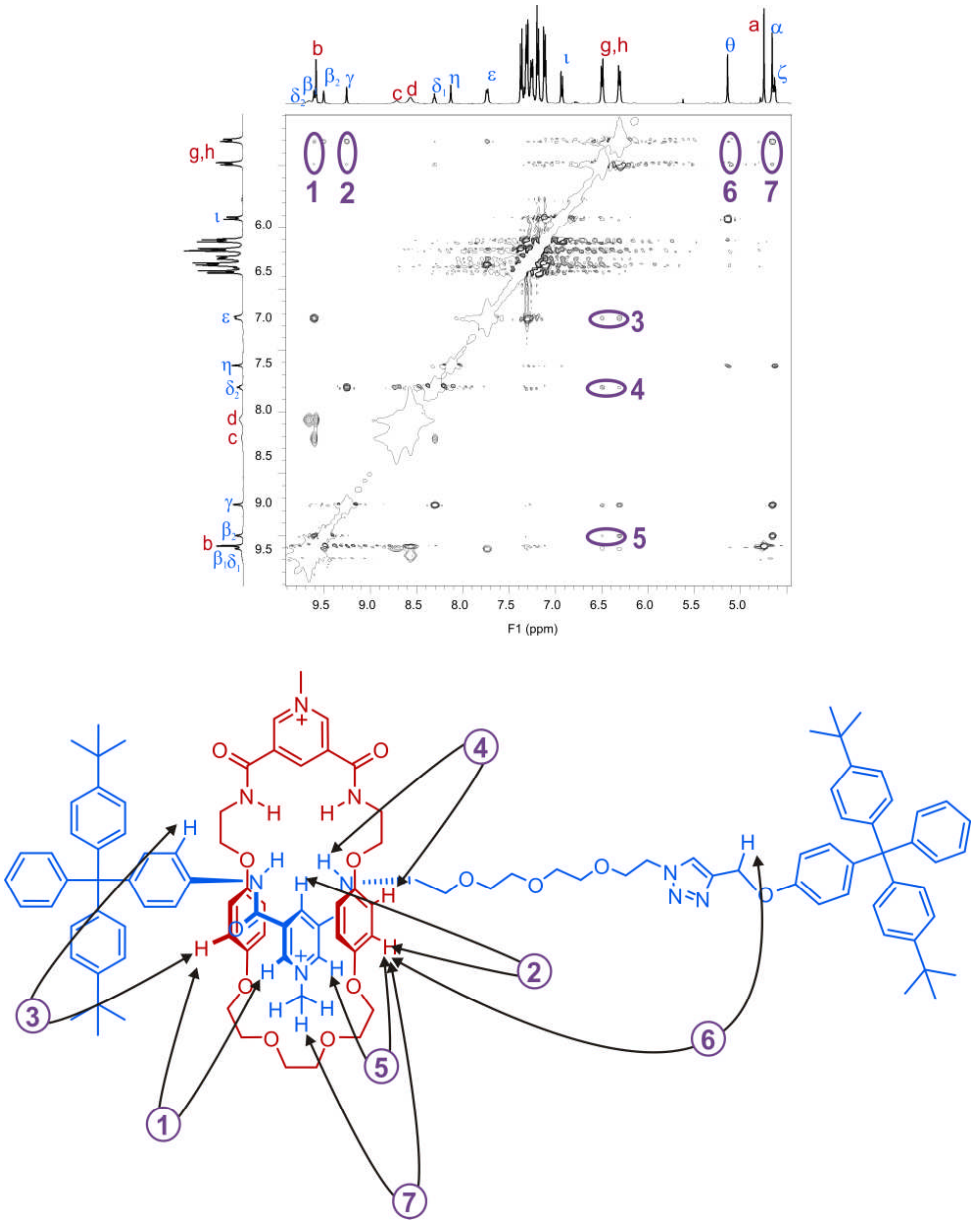



***Figure 4.5.*** *$^1$H -$^1$H ROESY spectrum of [2]rotaxane* ***73***$\cdot(PF_6)_2$ *in $d_6$-acetone at 293K. Cross couplings are shown on the schematic diagram below.*

It was initially thought that the macrocycle could be shuttling between the two sites, and if this motion was fast compared to the NMR timescale then only a single set of peaks corresponding to an average of the two positions would be observed. In order to verify this postulate, low temperature $^1$H NMR was used in an attempt to slow the shuttling motion and hopefully lead to the resolution of the two isomers in the $^1$H NMR spectrum. Proton NMR spectra of rotaxane **73**$\cdot(PF_6)_2$ in $d_6$-acetone were obtained at 0, –20, –40, –60 and –75 ºC (the limiting factor being the freezing point of acetone). Even at –75 ºC, the same $^1$H NMR

spectrum was observed with no splitting of the peaks that might suggest the macrocycle was shuttling between the pyridinium and triazole sites.

It is possible that the anomalous cross coupling interaction **6** could arise from a 'coiling' of the axle component. Polyether chains are highly flexible which could result in the axle folding in on itself (Figure 4.6). It can be argued that in this conformation the electron rich triazole nitrogen backbone could interact with the acidic amide protons of the macrocycle in the absence of the coordinating anion.

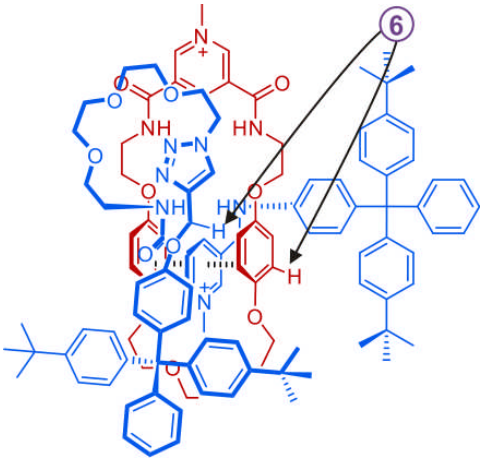



***Figure 4.6.*** *Postulated conformation of rotaxane* ***73***$\cdot(PF_6)_2$.

## 4.3 Re-design, Synthesis and Studies of a Novel Two Station Rotaxane Containing a Rigid Axle Component

The postulated 'coiled' conformation of rotaxane **73**$\cdot(PF_6)_2$ necessitates a re-design of the axle component where the flexible polyether linker is replaced by a more rigid spacer to avoid interaction of the macrocycle with both pyridinium and triazole sites. The synthesis of a new axle precursor incorporating such a rigid spacer group is discussed in the following section.

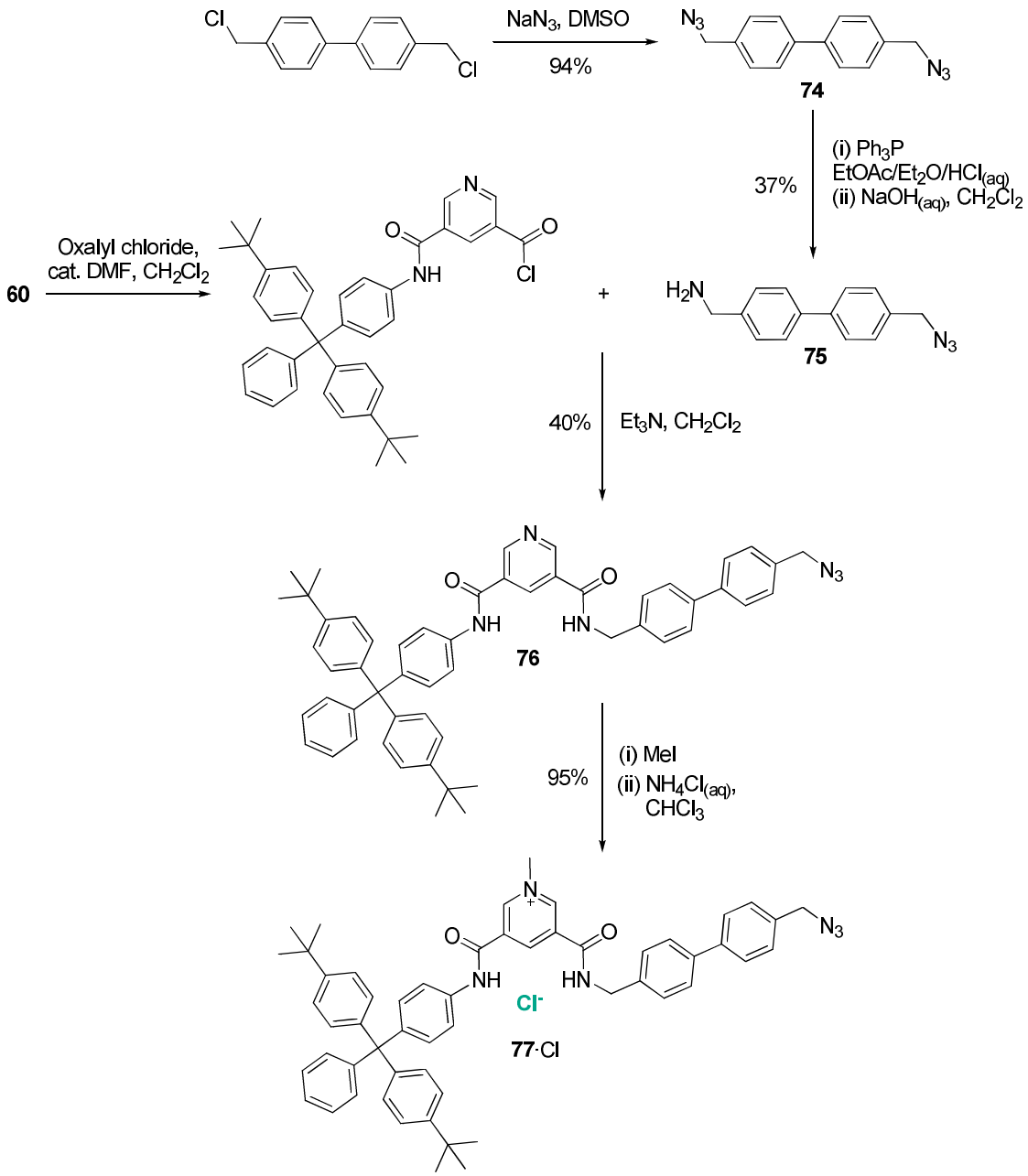
### 4.3.1 Axle Precursor Synthesis

All novel compounds in this section are characterised by $^{1}$H NMR, $^{13}$C NMR and HRMS (ESI).

A brief literature search revealed that the commercially available 4,4′-bis(chloromethane)-1,1′-biphenyl could be easily converted (in two steps) to the corresponding rigid biphenyl compound **74** functionalised with both azide and amine functionalities, necessary for click and acid chloride reactions respectively.

The synthesis of the new axle precursor component **77**·Cl is depicted in Scheme 4.11. 4,4′-Bis(chloromethyl)-1,1′-biphenyl was converted to the corresponding bis-azide **74** by reaction with sodium azide in DMSO, followed by precipitation with water. The reduction of a single azide component to its corresponding amine was achieved using triphenylphosphine in the biphasic solvent mixture 1:1:1 EtOAc/$Et_2O$/10% $HCl_{(aq)}$.[14] The formation of the bis-amine is inhibited by precipitation of the hydrogen chloride salt of **75**, achieved in the acidic reaction conditions. This precipitation also results in no further purification being required. The free amine **75** was obtained by suspending **75**·HCl in a biphasic 10% $NaOH_{(aq)}$/$CH_2Cl_2$ mixture and stirring until all solid had dissolved.

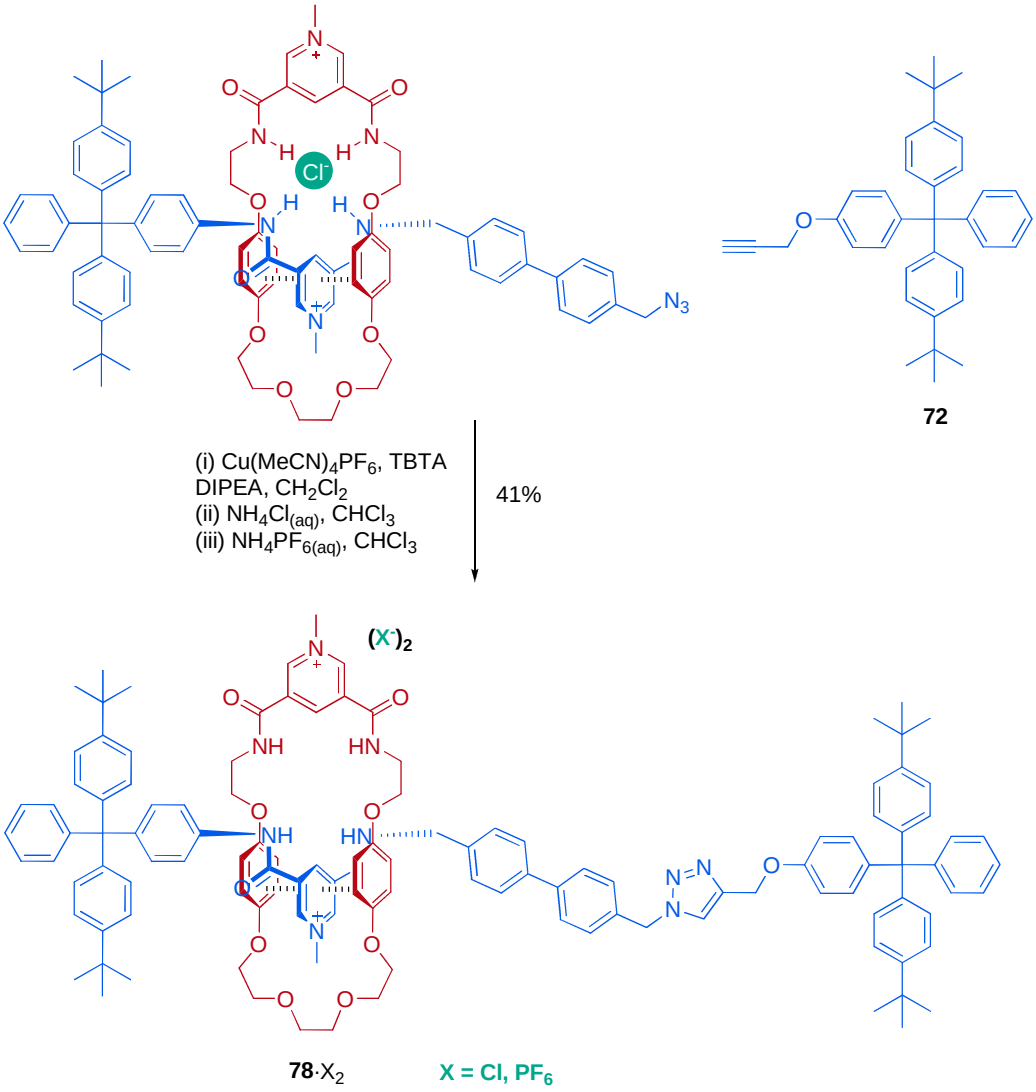
Since the EDCI coupling of compound **60** with amine **69** was fairly low yielding and time consuming, it was decided to convert **60** to its corresponding acid chloride for reaction with amine **75**. In Chapter 3, this conversion from acid to acid chloride was achieved using thionyl chloride, but a considerable amount of decomposition of **60** was observed, possibly as a result of amide cleavage. Instead, oxalyl chloride, requiring milder conditions, was used for this conversion and the subsequent acid chloride condensed with amine **75** in the presence of $Et_3N$ in dry $CH_2Cl_2$. Following acidic workup and column chromatography, compound **76** was isolated in 40% yield, which although low for an acid chloride condensation reaction, is appreciably higher than for the EDCI coupling of **60** and **69**, and was observed to take two hours instead of four days. Compound **76** was methylated using iodomethane, and converted to the chloride salt using aqueous $NH_4Cl$ to give **77**·Cl in 95% yield.




***Scheme 4.11.*** *Synthesis of rigid axle precursor* ***76***·*Cl.*

## 4.3.2 Rotaxane Synthesis and Characterisation

The target rotaxane **78**·$Cl_2$ was synthesised using the same procedure for the synthesis of rotaxane **73**·$Cl_2$.




***Scheme 4.12.*** *Synthesis of rotaxane* ***78***·$X_2$.

The synthesis, highlighted in Scheme 4.12, began by dissolving macrocycle **31**·I, azide appended axle precursor **77**·Cl and alkyne stopper **72** in degassed $CH_2Cl_2$ and stirring for fifteen minutes before the copper(I) catalyst, TBTA and DIPEA were added. The reaction was left for sixteen hours, then subjected to acidic workup, preparative TLC and conversion to the bis-chloride salt using aqueous $NH_4Cl$ before the rotaxane **78**·$Cl_2$ was isolated in 41% yield. In addition, it was easy to convert to the hexafluorophosphate salt, in quantitative yield, *via* washing a $CHCl_3$ solution with aqueous $NH_4PF_6$.

It was hoped that comparison of the $^1$H NMR spectra of the chloride and hexafluorophosphate salts of rotaxane **78** would reveal the ability of the rotaxane to undergo anion-induced molecular shuttling.

The $^1$H NMR spectra of **78**·$Cl_2$ and **78**·$(PF_6)_2$ are given in Figure 4.7.

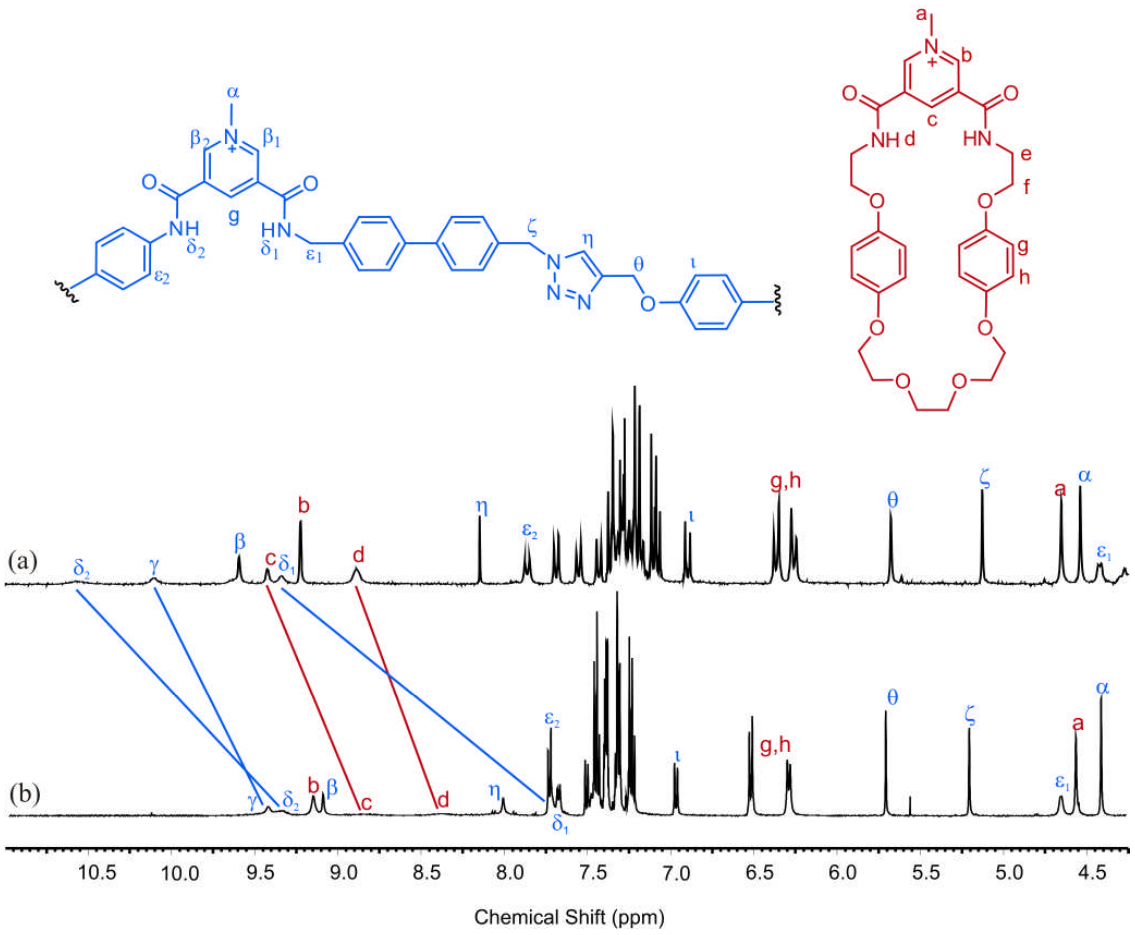



***Figure 4.7.*** *$^1$H NMR in $d_6$-acetone at 293 K of (a) rotaxane* ***78***·*$Cl_2$ and (b) rotaxane* ***78***·*$(PF_6)_2$.*

Disappointingly, again the chemical shift perturbations of the rotaxane upon exchange from the chloride to hexafluorophosphate salt only appear to correlate with removal of the halide anion from the interlocked amide cavity rather than as a result of molecular motion. Upfield chemical shift perturbations of the axle *para* pyridinium proton *γ* and amide protons *δ*, and macrocycle cavity *c* and amide protons *d* are consistent with removal of the halide anion, whilst the shift of hydroquinone protons *g* and *h* correspond to the axle pyridinium *N*-methyl unit rotating out of the plane of the macrocycle to avoid unfavourable steric interactions with

the polyether chain (see Chapter 2). Negligible shifts are observed in protons $\zeta$, $\eta$ and $\theta$ which are in the vicinity of the triazole 'station', indicating the macrocycle remains stationed at the pyridinium axle site.

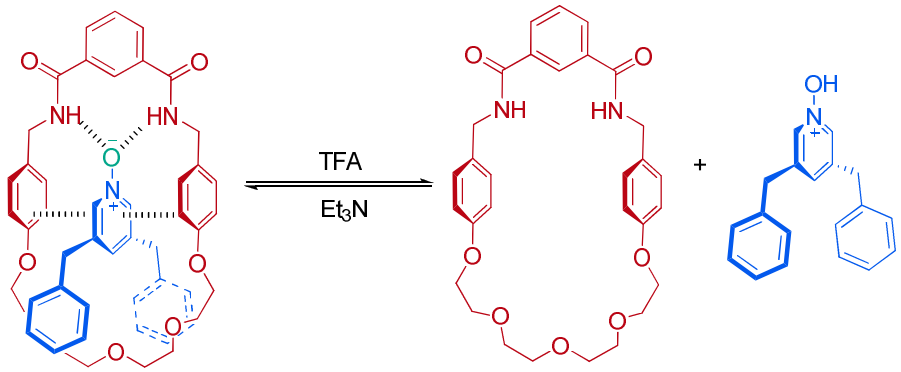
Two-dimensional ROESY spectroscopy confirmed the position of the macrocycle at the pyridinium axle station in both **78**·$Cl_2$ and **78**·$(PF_6)_2$, and thus confirmed that this rotaxane was incapable of undergoing anion-induced molecular motion.

In spite of the repulsive electrostatic interactions between the two positively charged axle and macrocycle pyridinium components, this conformation remains energetically favourable for the rotaxane. It is postulated that the charge-assisted π-π stacking interactions between macrocycle hydroquinone units and the axle pyridinium surface are strong enough to overcome the electrostatic repulsion between positively charged axle and macrocycle components. In order to construct an anion-switchable molecular shuttle, it is necessary to alter the design of the rotaxane. Efforts towards this are detailed in the next section.

## 4.4 Synthesis and Studies of Novel Pyridine *N*-oxide [2]Rotaxanes

Recently Jiang *et al.* have reported the ability of a pyridine *N*-oxide thread component to undergo pseudorotaxane formation with an isophthalamide functionalised macrocycle, with X-ray crystal structure analysis confirming the orientation of the thread within the macrocycle, as shown in Scheme 4.13.[15]

In addition it was demonstrated that addition of acid to the system could disrupt pseudorotaxane formation by protonation of the pyridine *N*-oxide oxygen.




***Scheme 4.13.*** *Jiang's pH-switchable pyridine N-oxide pseudorotaxane.*[15]

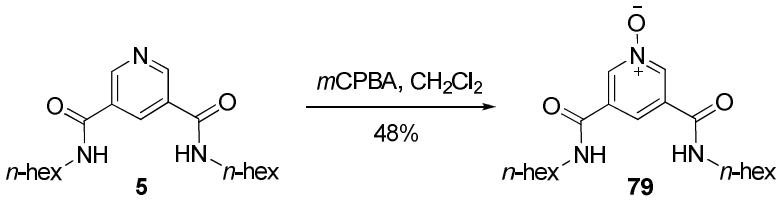
It was thought that it might also be possible to displace, or change the orientation of the pyridine *N*-oxide thread component on addition of anions, whereby the anion would preferentially associate in the isophthalamide cleft. It may also be possible to extend this system by incorporation into a [2]rotaxane to create an anion-switchable molecular shuttle, akin to the squaraine rotaxane of Smith and coworkers described in Chapter 1. Whilst Hoffart and Loeb have used pyridine *N*-oxide at the termini of rotaxanes for the construction of MOFs[16, 17] and Leigh *et al*. have used nitrone in rotaxane templation,[18] this rotaxane would constitute the first example of using the pyridine N-oxide motif in the template construction of an interlocked structure.

In addition, if such a rotaxane could be synthesised it should be capable of undergoing pH-induced molecular motion, similar to that described by Jiang and coworkers (Scheme 4.13).

### 4.4.1 Pseudorotaxane Studies

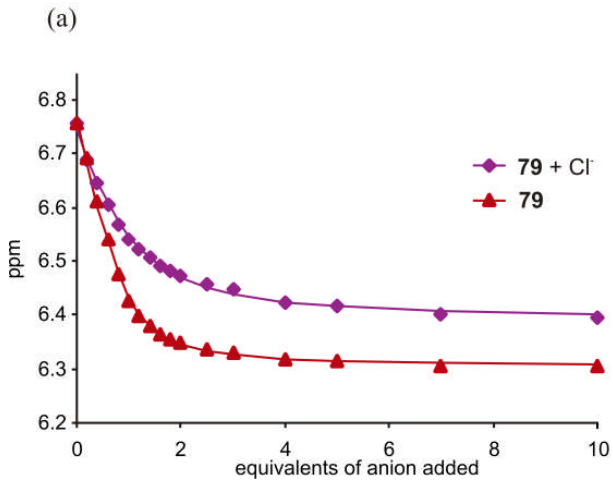
Although the macrocycles used thus far are structurally very similar to Jiang's system, it was important to determine the strength of association of these macrocycles with a pyridine *N*-oxide threading component before efforts were directed to the construction of a pyridine *N*-oxide interlocked structure. It was also of interest to determine if the presence of chloride would enhance the stability of the pseudorotaxane, and thus whether anion-induced molecular motion in this system could be achieved.

An appropriate pyridine *N*-oxide thread was synthesised according to Scheme 4.14. Pyridine thread **5** was oxidized using *m*CPBA in dry $CH_2Cl_2$. Following basic workup and column chromatography the target thread **79** was isolated in 48% yield.




***Scheme 4.14.*** *Synthesis of pyridine N-oxide thread **79**.*

Pseudorotaxane titrations were carried out as described in Section 2.2.2. In separate titrations aliquots of a solution of thread **79** with and without one equivalent of TBACl were added to a solution of macrocycle **54**.




(b)

| | **79** | **79 + Cl⁻** |
|---|---|---|
| **K ($M^{-1}$)** | 5950 | 1830 |

***Figure 4.8.*** *(a) Average chemical shift perturbations of protons g and h on addition of **79** and **79** + TBACl to a solution of macrocycle **54** in $CDCl_3$ at 1.43 x $10^{-3}$M and 293 K. Symbols represent experimental data points; continuous lines represent calculated curves. (b) Association constants, K ($M^{-1}$), of macrocycle **54** with **79** and **79** + TBACl in $CDCl_3$. Obtained by monitoring the average chemical shift of protons g and h . Error < 10%.*

A number of chemical shift perturbations were observed upon addition of both guest species, notably an upfield shift of the signals corresponding to the hydroquinone protons indicating the formation of a pseudorotaxane species. The titration curves (equivalents of anion added against average chemical shift of hydroquinone protons *g* and *h*) for the binding of both **79** and **79**·$Cl^-$ with macrocycle **54** are shown in Figure 4.8a. Job plot analysis indicated 1:1

stoichiometry, and winEQNMR[19] was used to calculate the association constants for pseudorotaxane assembly (tabulated in Figure 4.8b).

Interestingly, thread **79** forms a more stable pseudorotaxane assembly in the absence of chloride, which may be rationalised by examining the $^1$H NMR spectra of **54**·**79** and **54**·**79**·$Cl^-$ complexes compared to their free components (Figure 4.9).

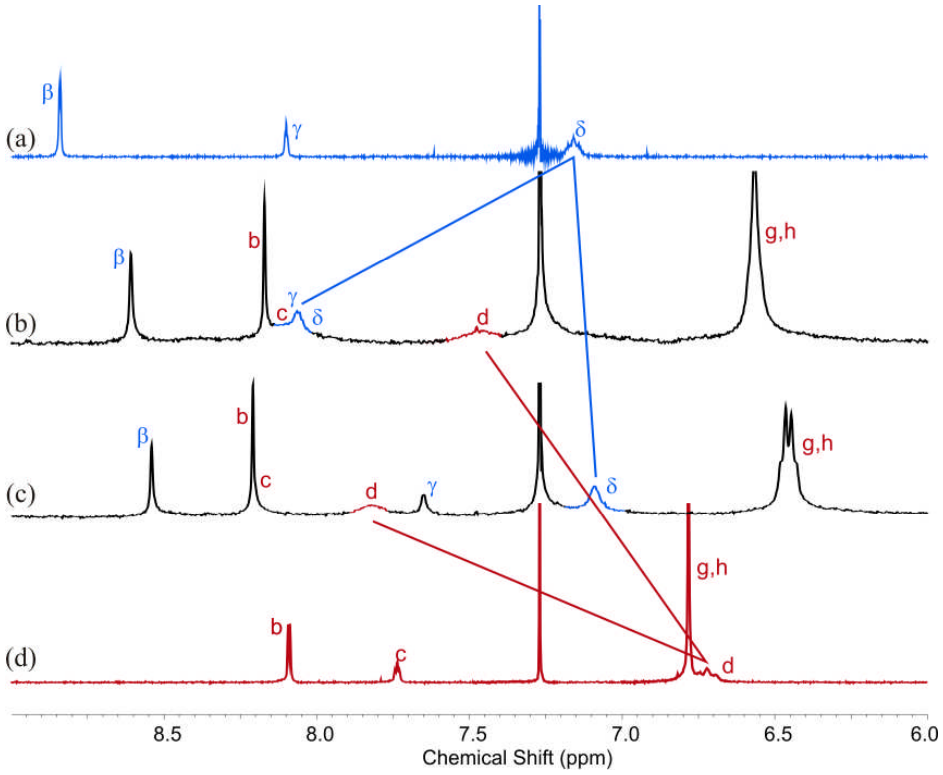



***Figure 4.9.*** *$^1$H NMR spectra in $CDCl_3$ at 293 K of (a) thread **79**, (b) macrocycle **54** + thread **79** + TBACl, (c) macrocycle **54** + thread **79**, (d) macrocycle **54**.*

The pseudorotaxane formed between macrocycle **54** and thread **79** in the absence of halide anion is shown in spectrum c, where the macrocycle amide protons *d* have shifted considerably downfield (> 1 ppm) compared to the free macrocycle, indicating the pyridine *N*-oxide oxygen atom resides in the isophthalamide binding domain (Figure 4.10a). In this conformation, the environment of thread amide protons *δ* remains unchanged, as confirmed by a negligible shift of this signal in the $^1$H NMR spectrum.

In contrast, spectrum (b), the chloride-templated pseudorotaxane, shows both macrocycle *d* and pyridine *N*-oxide *δ* amide protons are shifted downfield compared to their separate

components. In the presence of chloride the amides of both thread and macrocycle converge creating an orthogonal binding cavity to accommodate the halide anion (Figure 1.10b). The pyridine *N*-oxide oxygen is now situated in proximity to the electronegative oxygens of the macrocycle's polyether chain giving rise to electrostatic repulsion and thus a less stable pseudorotaxane assembly results.

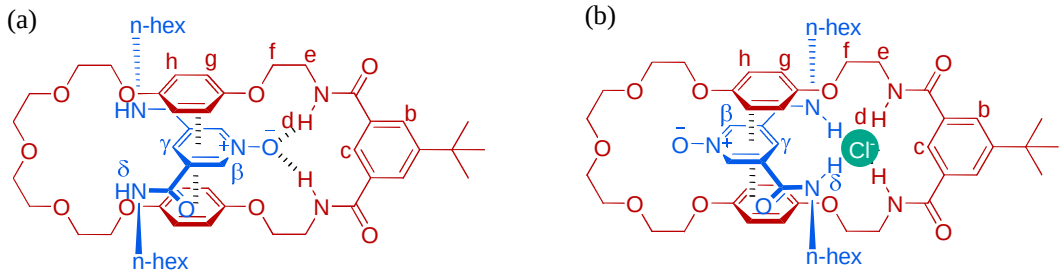


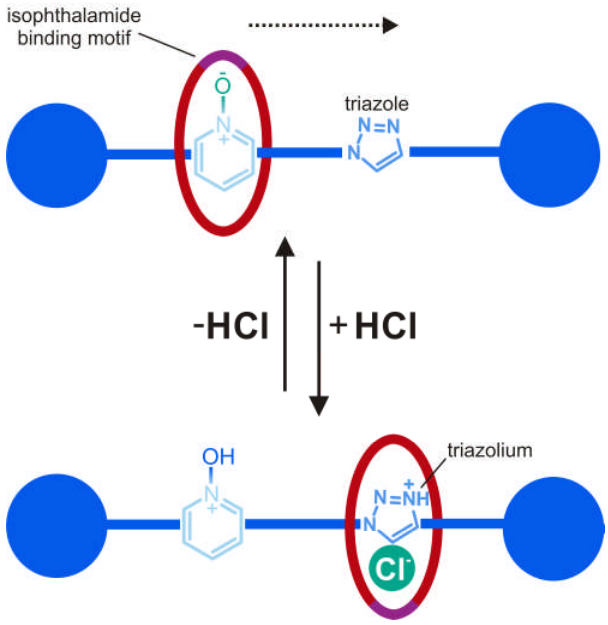

**Figure 4.10.** *Predicted conformation of pseudorotaxane **54·79** in (a) absence and (b) presence of chloride anions.*

Given the strength of these pseudorotaxane assemblies, it was anticipated that it should be possible to construct rotaxanes containing the same components. It was decided to carry out the rotaxanation reaction in the absence of a chloride anion template since the interpenetrated association of components was shown to be stronger in the absence of the halide anion.

It should also be noted that the diminished stability of **54·79**·$Cl^-$ compared to **54·79** suggests chloride is unlikely to displace the pyridine *N*-oxide component from the isophthalamide cleft. Therefore attention was focused on designing a system capable of undergoing molecular motion upon changes in pH, akin to the Jiang's switchable pseudorotaxane.

### 4.4.2 Rotaxane Synthesis and Characterisation

For synthetic ease axle precursor **76** was converted to the target pyridine *N*-oxide derivative **80**. Moreover the triazole motif may act as a second station in a pH-switchable molecular machine. This proposed motion can be visualised using the schematic given in Figure 4.15.

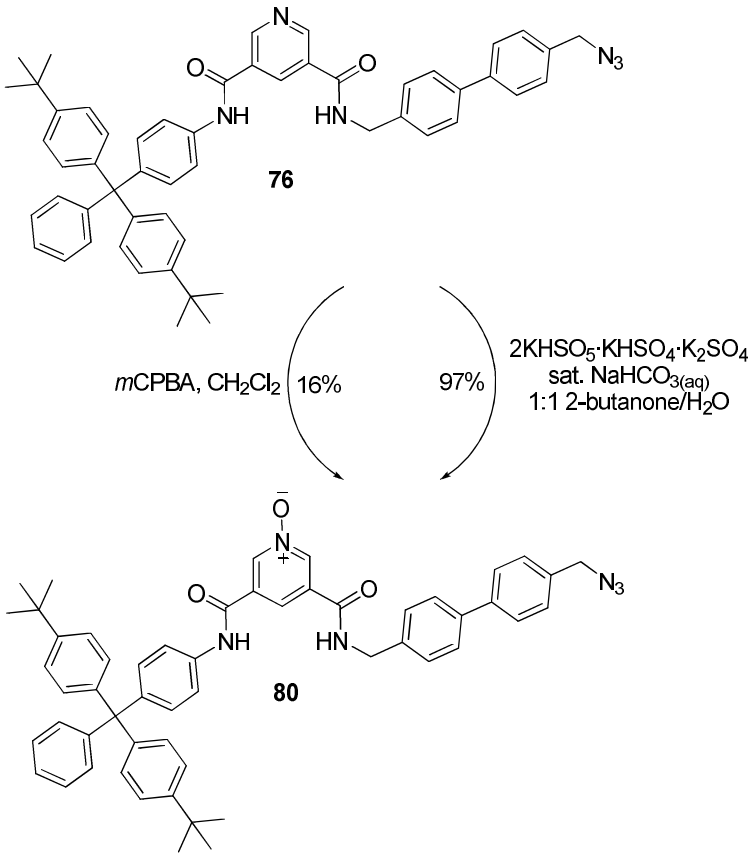



***Scheme 4.15.*** *Schematic representation of HCl-induced molecular shuttling in a two station pyridine N-oxide/triazole [2]rotaxane.*

Upon addition of acid, it is anticipated that the pyridine *N*-oxide moiety will become protonated and lose its binding affinity for the macrocycle's isophthalamide cleft. It is possible that the triazole moiety may also become protonated, thus taking on characteristics of the methyl triazolium system discussed in Section 1.7.2. Both of these factors may contribute to the macrocycle translocating from the pyridine *N*-oxide station to the triazolium station, with this form being further stabilised by the presence of chloride acting to cooperatively associate the macrocycle around the axle triazolium station.

The synthesis of the azide functionalised pyridine *N*-oxide precursor **80** is depicted in Scheme 4.16. Initially oxidation of **76** was attempted under analogous conditions to those used for the synthesis of the model pyridine thread **79** with *m*CPBA in $CH_2Cl_2$. However only low yields of approximately 16% could be obtained for the conversion of **76** to **80** and thus a new procedure was attempted. Potassium peroxymonosulfate (or Oxone®) is a powerful oxidising agent known for its non-toxic nature, stability and versatility, and was therefore chosen as an alternative for the oxidation of **76**.[20] Reaction of Oxone® and **76** was carried out in the

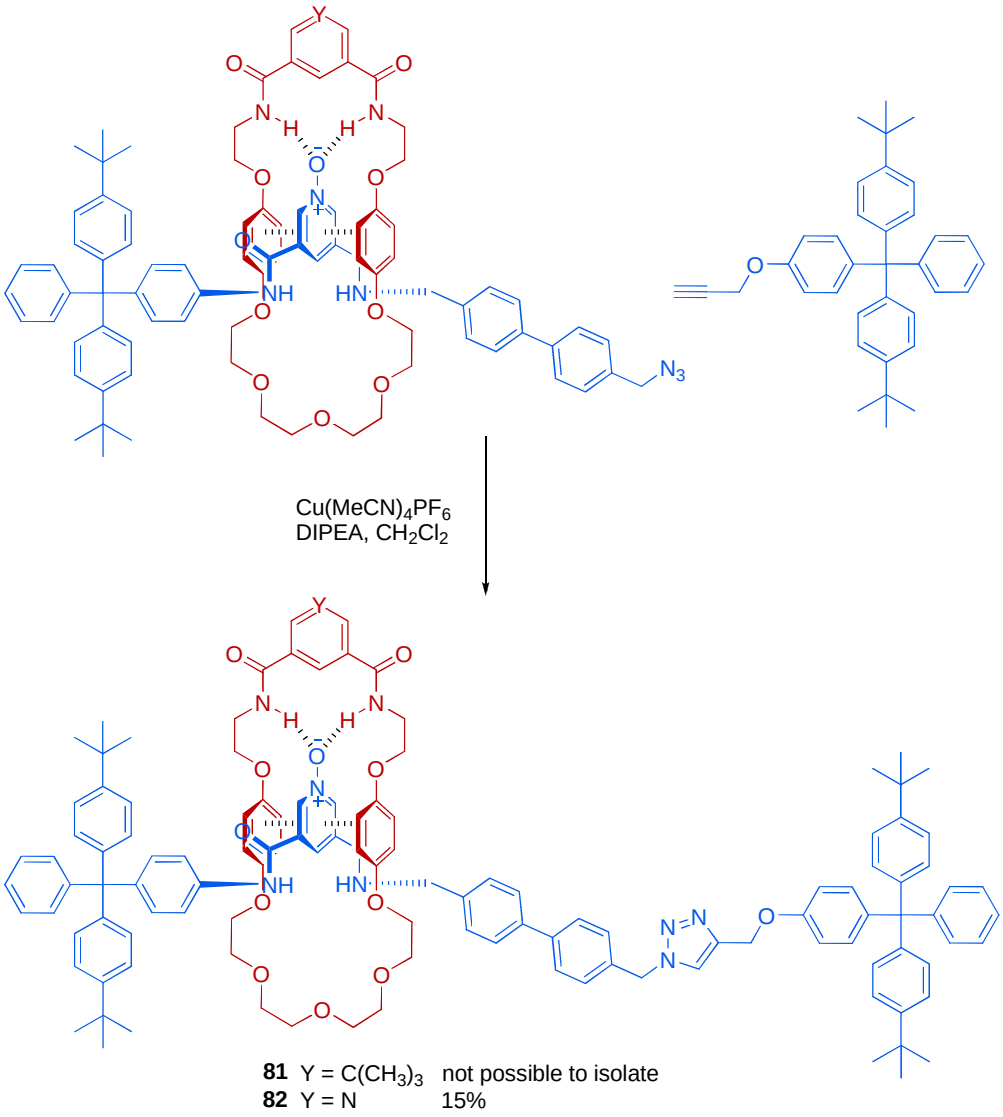
presence of $NaHCO_3$ in 1:1 butan-2-one/$H_2O$. Following addition of NaCl and aqueous work-up compound **80** was isolated in 97%, a considerable improvement on the yield obtained with *m*CPBA.




***Scheme 4.16.*** *Synthesis of pyridine N-oxide axle precursor* ***80****.*

The first attempt at synthesising a pyridine *N*-oxide containing rotaxane was undertaken using the *tert*-butyl appended isophthalamide macrocycle used for the pseudorotaxane studies discussed in Section 4.2.1 (Scheme 4.17). A mixture of precursor **80**, macrocycle **54** and stopper **72** was stirred for fifteen minutes in degassed $CH_2Cl_2$ before the addition of DIPEA and $Cu(MeCN)_4PF_6$. Purification of rotaxane **81** was initially attempted *via* preparative TLC, however despite $^1H$ NMR confirming the presence of the target rotaxane, the similarity in $R_f$ values of the three components (rotaxane, axle and macrocycle) made it impossible to isolate **81**. In order to overcome these purification issues it was decided to employ the strategy used in Section 3.3.5.2, whereby a pyridine functionalised macrocycle may change the polarity of

the rotaxane and hopefully result in easier purification. The same rotaxanation conditions were used as for the formation of rotaxane **81** with macrocycle **8**. Following preparative TLC the target rotaxane **82** was isolated in 15% yield.




***Scheme 4.17.*** *Synthesis of pyridine N-oxide containing [2]rotaxanes* ***81*** *and* ***82****.*

Rotaxane **82** was characterised by $^{1}$H NMR, $^{13}$C NMR and HRMS (ESI). The $^{1}$H NMR spectrum of rotaxane **82** along with the spectra of its component parts are given in Figure 4.11. Macrocycle cavity *c* and amide protons *d* are observed to shift downfield in the rotaxane indicating the presence of the pyridine *N*-oxide negative oxygen dipole in the macrocycle anion binding cleft. Hydroquinone protons *g* and *h* have moved upfield as a consequence of

π-π stacking interactions with the electron deficient polarised pyridine *N*-oxide surface of the axle. These interactions are further signified by upfield shifts of the signals corresponding axle protons *β*, *γ* and *δ*.

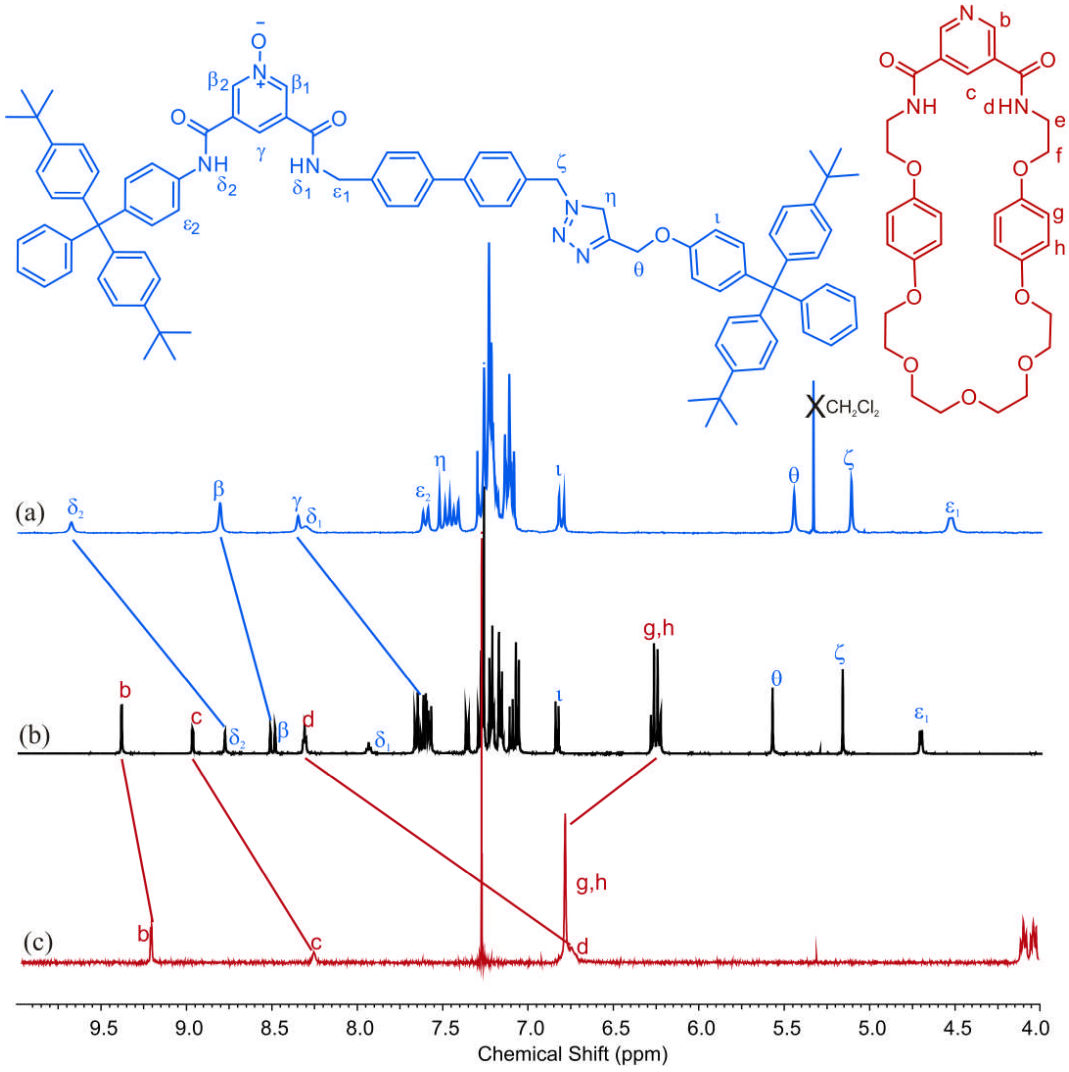



***Figure 4.11.*** *$^1$H NMR spectra in $CDCl_3$ at 293 K of (a) component axle, (b) [2]rotaxane* ***82*** *and (c) macrocycle* ***8****.*

Further evidence for the formation of the [2]rotaxane and the position of the macrocyclic component at the pyridine *N*-oxide station was obtained by 2D ROESY NMR (Figure 4.12). Interactions **1** (*δ* → *g*,*h*), **2** (*β* → *g*,*h*) and **3** (*δ* → *g*,*h*) confirm that the macrocycle is stationed at the pyridine *N*-oxide motif, whilst interactions **4** (*β* → *c*) and **5** (*β* → *d*) indicate that pyridine *ortho* protons are in close proximity to the isophthalamide cleft. Arguably the latter

can only occur if the axle adopts a position whereby the pyridine *N*-oxide oxygen points into the macrocycle's isophthalamide cleft.

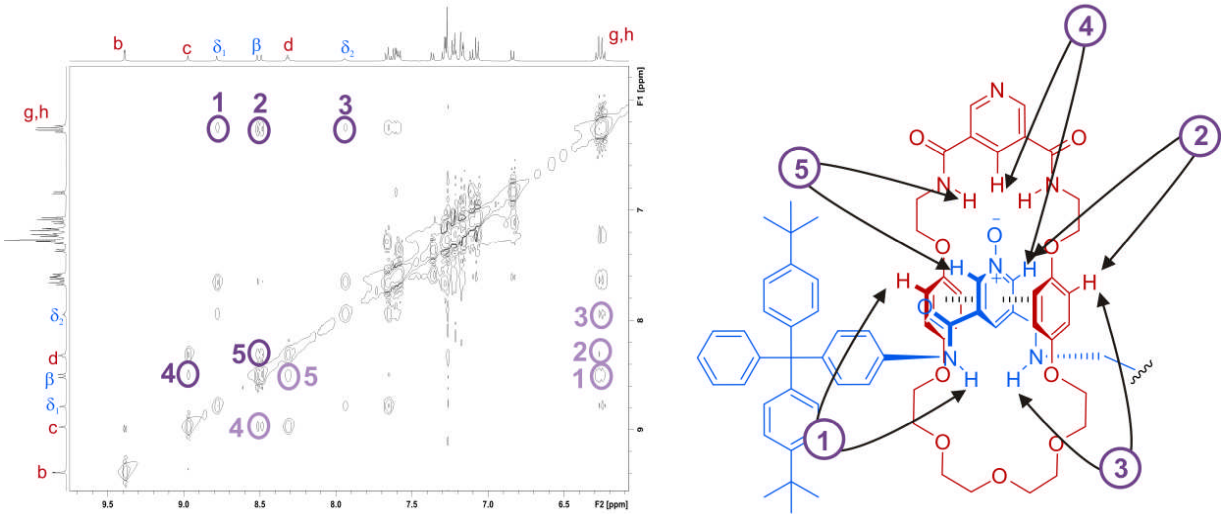



***Figure 4.12.*** *$^{1}H$ -$^{1}H$ ROESY spectrum of [2]rotaxane* ***82*** *in $CDCl_3$ at 293K. Cross couplings are shown on the schematic diagram on the right.*

## 4.4.3 pH-Switchable Molecular Motion Investigations

Following the successful synthesis and isolation of the novel pyridine *N*-oxide rotaxane **82**, attention was turned to the potential of using this interlocked structure as a pH-induced molecular shuttle. At the beginning of this section it was suggested that such translational motion may be induced *via* protonation of both the pyridine *N*-oxide unit, removing its ability to coordinate to the isophthalamide cleft, and the triazole moiety, creating a positively charged station capable of undergoing possible anion-templated association with the isophthalamide macrocycle, assisted by π-π stacking.

In order to ascertain the ability of the rotaxane to undergo such translational motion, a titration was carried out whereby TFA was added incrementally to a solution of rotaxane **82** in $CHCl_3$ ($^{1}H$ NMR spectra of selected additions of TFA are given in Figure 4.13). It should be noted that the presence of the pyridine macrocycle provides a third basic site available for protonation.

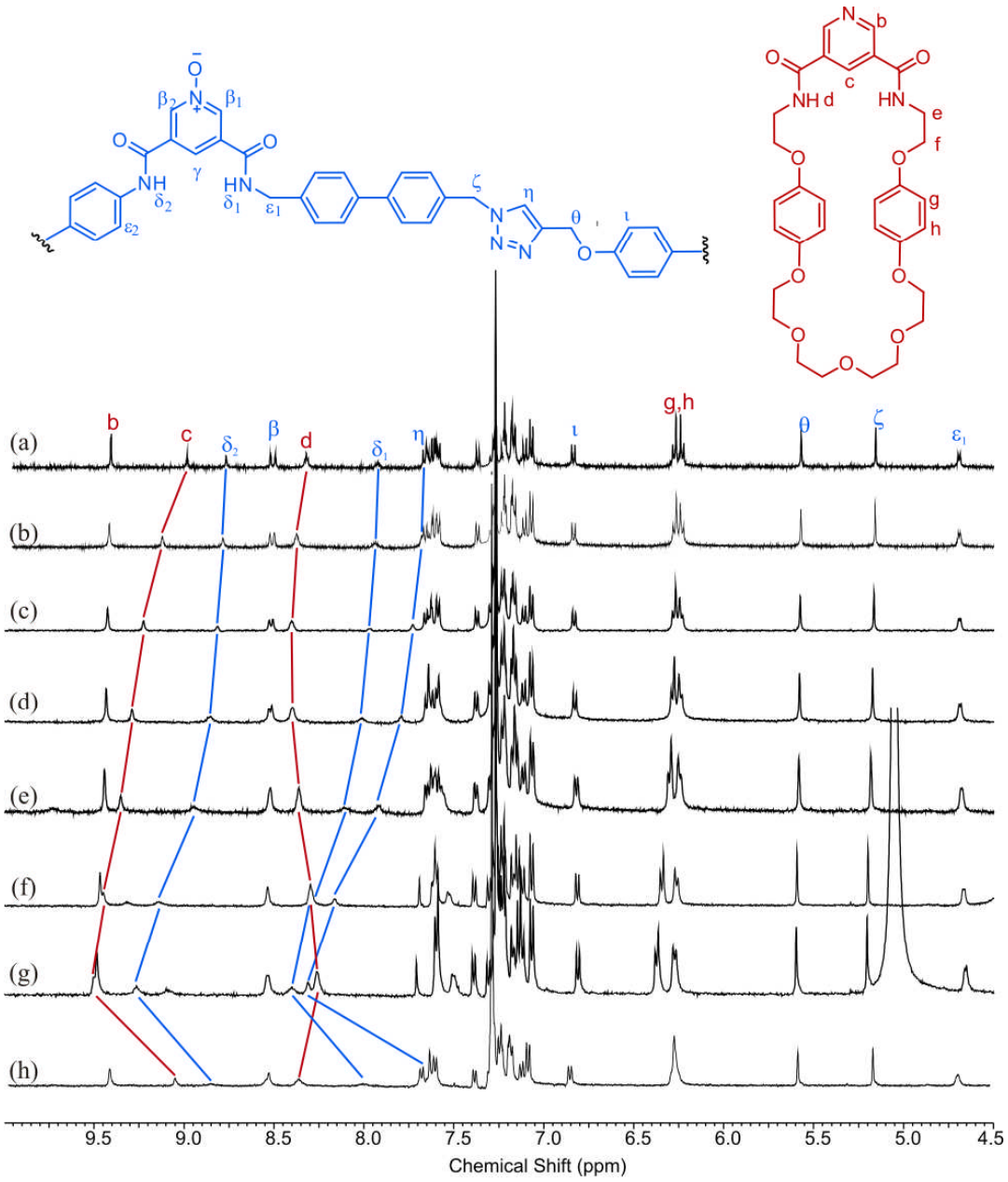



***Figure 4.13.*** *$^1$H NMR spectra in $CDCl_3$ at 293 K of rotaxane* ***82*** *with (a) 0, (b) 1, (c) 2, (d) 3, (e) 5, (f) 10 and (g) 15 equivalents of TFA, and (h) with 15 equivalents of TFA + 15 equivalents of DBU.*

Upon addition of TFA to the rotaxane, chemical shift perturbations of peaks corresponding to a number of protons are observed. Of those peaks that move, the majority are observed to shift downfield, which is to be expected considering the introduction of positive charge to the macrocycle anion binding motif and axle pyridine *N*-oxide unit. In addition protonation of the axle's triazole motif induces a downfield shift of triazole proton *η*. Interestingly, macrocycle amide proton *d* initially moves to higher chemical shift values followed by, at approximately

2.5 equivalents of TFA, a change of direction to shift appreciably upfield as further equivalents of acid are added. This can be rationalised considering the protonation processes involved upon addition of TFA. Firstly protonation of the macrocyclic pyridine results in a downfield shift of the amide proton *d*, before protonation of the axle pyridine *N*-oxide and triazole. Protonation of pyridine *N*-oxide results in disruption of the hydrogen-bonding interactions between this motif and the macrocycle's isophthalamide amide protons thus it is no longer favourable to be bound in the macrocycle cavity. However, conversely to previous predictions there is no evidence that following pyridine *N*-oxide protonation the macrocycle shifts to the protonated triazolium station as the chemical shift of protons $\theta$ and $\zeta$ remains unchanged.

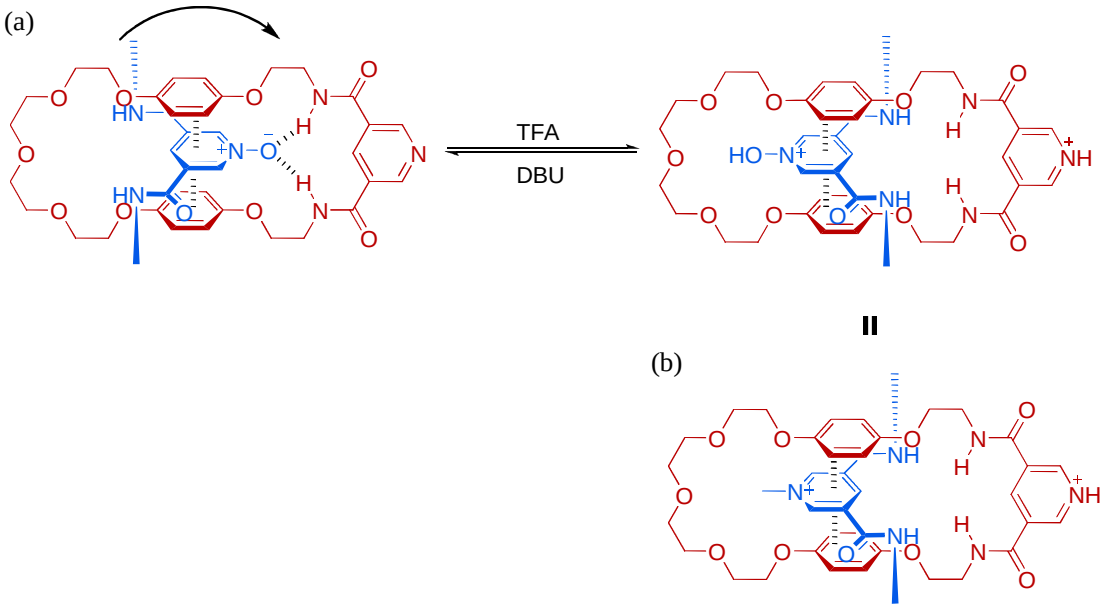



***Figure 4.14.*** *(a) pH-induced molecular rotation in N-oxide containing [2]rotaxane* ***82****, (b) equivalent pyridinium rotaxane.*

It is postulated that the rotaxane can undergo a rotation of the macrocycle (Figure 4.14a) around the axle rather than translocation to the triazolium station. It is noted that the new protonated pyridine *N*-oxide bears a striking resemblance to the pyridinium *N*-methyl motif used extensively in this thesis and observed to undergo very strong π-π stacking interactions

with macrocycle hydroquinone units (Figure 4.14b). There are few examples reported to date of such a pirouetting motion within rotaxane architectures.[11, 21-23]

It was possible to reverse this motion by addition of DBU, where all shifted peaks were observed to return to their original position. This confirms that any motion occurring is a result of protonation of various sites rather than a consequence of ionic strength of the solution.

Addition of excess TBACl to the triply protonated rotaxane caused negligible chemical shift perturbations of any protons other than those of macrocycle and pyridinium cavities indicating binding of halide anion in the amide binding domain. It appears that chloride is acting to further stabilise this new conformation rather than acting as a stimulus to move the macrocycle to the triazolium station.

Further investigations into the position of the macrocycle in relation to the axle after addition of acid were carried out using 2D ROESY spectroscopy. Figure 4.15 depicts a portion of the ROESY spectrum of rotaxane **82** following the addition of 10 equivalents of TFA.

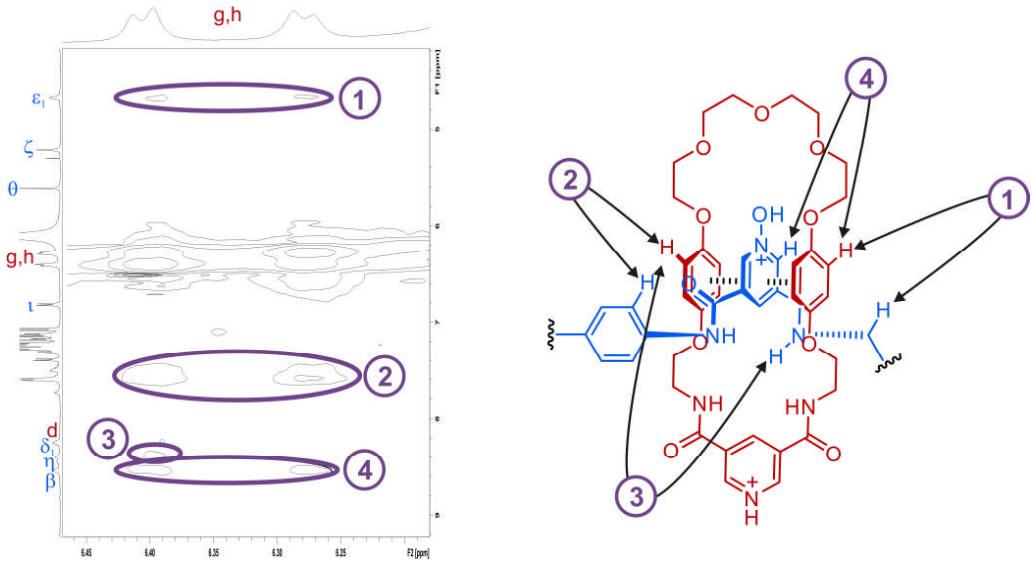


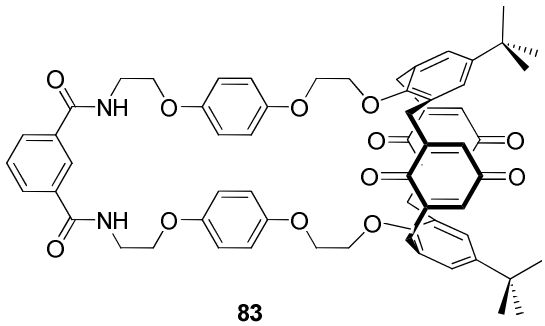

***Figure 4.15***. *$^{1}$H -$^{1}$H ROESY spectrum of [2]rotaxane **82** + 10 eq. TFA in $CDCl_3$ at 293K. Cross couplings are shown on the schematic diagram on the right.*

Confirmation of the position of the macrocycle over the axle's protonated pyridine *N*-oxide station was obtained by observation of through space cross coupling interactions between the macrocycle hydroquinone protons and various protons in the vicinity of the protonated pyridine *N*-oxide motif.

It should also be noted that addition of excess TBACl to the neutral rotaxane **82** in $CDCl_3$, produced no appreciable chemical shift perturbations, which is consistent with evidence obtained from pseudorotaxane formation, where the presence of chloride acts to destabilise the association of macrocycle and axle.

## 4.5 Construction of Calix[4]diquinone Containing [2]Rotaxanes for Cation-Induced Pirouetting Behaviour

The final section of this chapter explores the incorporation of a calix[4]diquinone macrocycle (Figure 4.16) into [2]rotaxanes, with a view to create cation-induced molecular machines. Macrocycle **83**, kindly supplied by Dr. Alex Leontiev, has previously been incorporated into rotaxanes, that have demonstrated the ability to undergo cation-induced molecular motion.[10]




**83**

***Figure 4.16.*** *Calix[4]diquinone macrocycle* ***83****.*[10]

The rotaxane was shown to adopt the conformation shown in Figure 4.17a in the absence of anions or cations, but upon addition of barium(II) cations the macrocycle was observed to move away from the axle pyridinium unit (4.17b). This movement is attributed to electrostatic

and steric repulsion between the cation and the cationic pyridinium *N*-methyl motif, induced by strong binding of barium at the calix[4]diquinone. Importantly, it was not possible to induce this translational motion in the presence of monocationic alkali metals such as sodium.

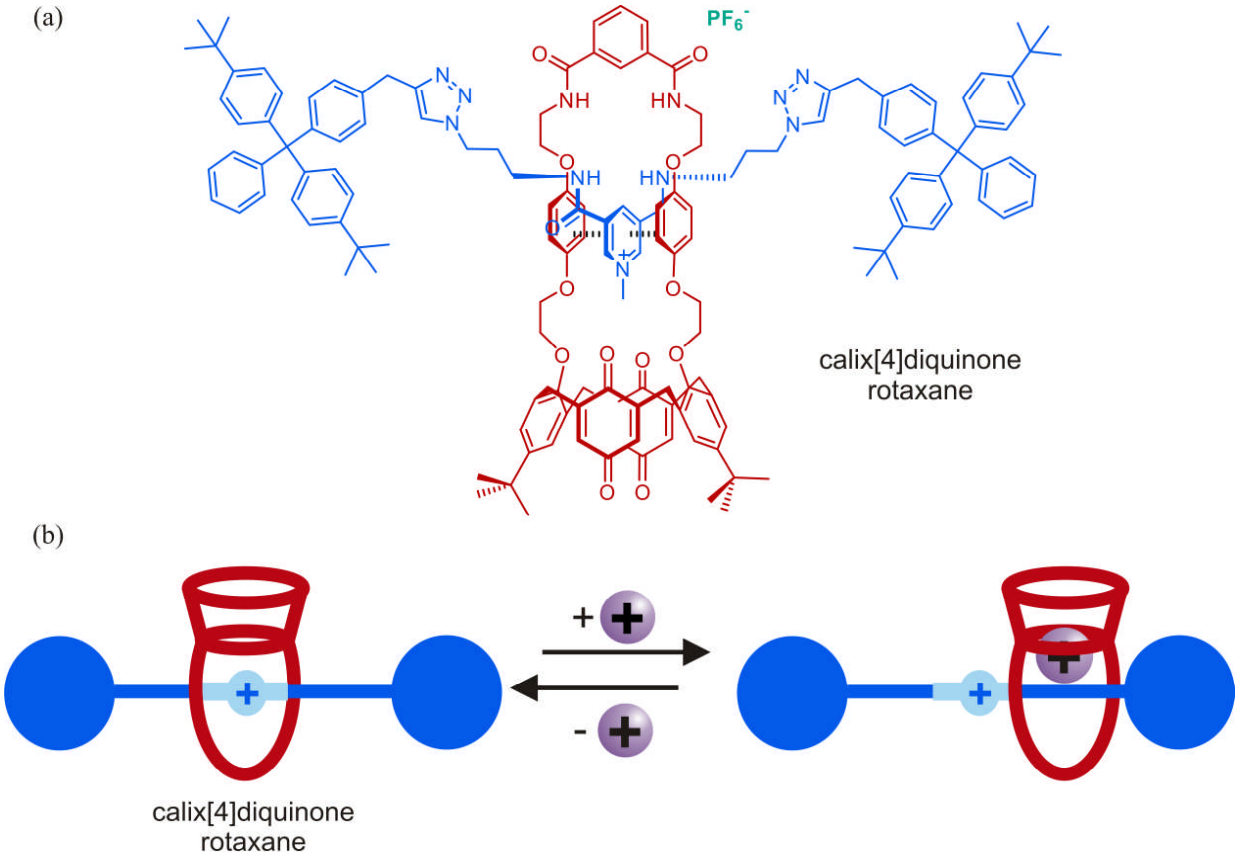



***Figure 4.17.*** *(a) Beer's calix[4]diquinone [2]rotaxane, and (b) schematic representation of cation-induced molecular motion.*[10]

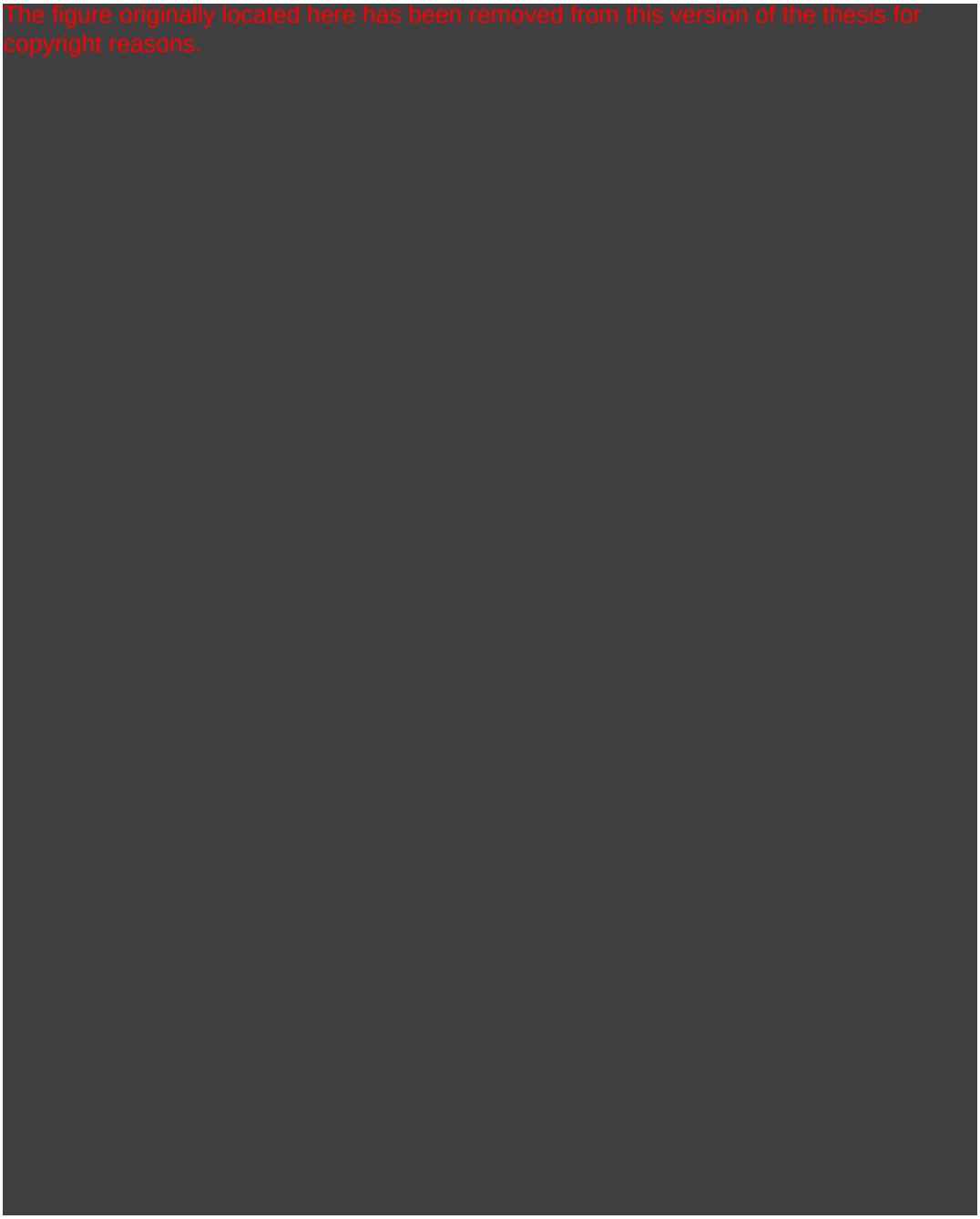
The strong binding of barium cations by the macrocyclic component could be harnessed for a different kind of molecular motion, when incorporated into a rotaxane containing the pyridine *N*-oxide axle described in the previous section. It is assumed that the rotaxane would adopt the same conformation as rotaxane **82** in the absence of cations, however complexation of barium at the calix[4]diquinone recognition site may induce a 180 degree macrocycle rotation as the axle pyridine *N*-oxide coordinates to the metal cation. This rotary motion critically relies on the complexation of barium and pyridine N-oxide being significantly more

favourable than that of pyridine N-oxide-amide hydrogen-bonding interactions in the isophthalamide cleft of the macrocycle.

### 4.5.1 Rotaxane Synthesis and Characterisation

The available pyridine *N*-oxide functionalised compound **80** was chosen as an axle precursor to the target rotaxane. This compound has the added advantage of having excellent solubility in $CH_2Cl_2$, whereas simpler pyridine *N*-oxide components have been found to be much less soluble in this solvent.

The target rotaxane **84** was synthesised according to Scheme 4.18. Macrocycle **83**, axle precursor **80** and stopper **72** were stirred for fifteen minutes in degassed $CH_2Cl_2$ before the addition of $Cu(MeCN)_4PF_6$ and DIPEA. The reaction was stirred for sixteen hours before preparative TLC was used to isolate rotaxane **84** in 10% yield.




***Scheme 4.18.*** *Synthesis of rotaxane* ***84****.*

The novel rotaxane was initially characterised by $^{1}$H NMR. The spectrum of rotaxane **84**, along with its component axle and macrocycle are given in Figure 4.18.




***Figure 4.18.*** *$^{1}$H NMR spectra in $CDCl_3$ at 293 K of (a) component axle, (b) [2]rotaxane **84** and (c) macrocycle **83**.*

It was anticipated that the spectrum of **84** would closely resemble that of the analogous pyridine *N*-oxide rotaxane, only with additional signals corresponding to the protons of the calix[4]diquinone motif. Indeed, signals corresponding to macrocycle cavity *c* and amide *d* protons were observed to move downfield upon rotaxane formation, implying the axle pyridine *N*-oxide oxygen is bound in the macrocycle isophthalamide cleft. In addition

hydroquinone protons *g,h* of the macrocycle and pyridine *N*-oxide protons $\beta$ and $\gamma$ are observed to move upfield as a result of π-π stacking interactions.

However, in addition to the aforementioned movement of peaks, a number of signals in the calix[4]diquinone unit exhibited unusual shifts in the $^1$H NMR spectrum. Protons *l* and *m* corresponding to the quinone and phenyl protons of the calix[4]diquinone units are observed to shift considerably upfield (> 0.5 ppm) and undergo splitting upon rotaxane formation. Also, calix[4]diquinone methylene protons $k_1$ and $k_2$, observed as two doublets in the macrocycle spectrum, have undergone further splitting to yield four doublets, each of which integrate to two protons. The splitting of these peaks indicates asymmetry within the system, possibly a manifestation of the asymmetrical axle component. No splitting is observed for macrocycle protons other than those in the vicinity of the calix[4]diquinone protons, although it is possible that the two environments give rise to coincidental signals for the other protons. However the asymmetry of the axle does not account for the large upfield movement of the quinone *l* and phenyl *m* protons and 2D ROESY spectroscopy (Figure 4.19) was used to provide further insight.

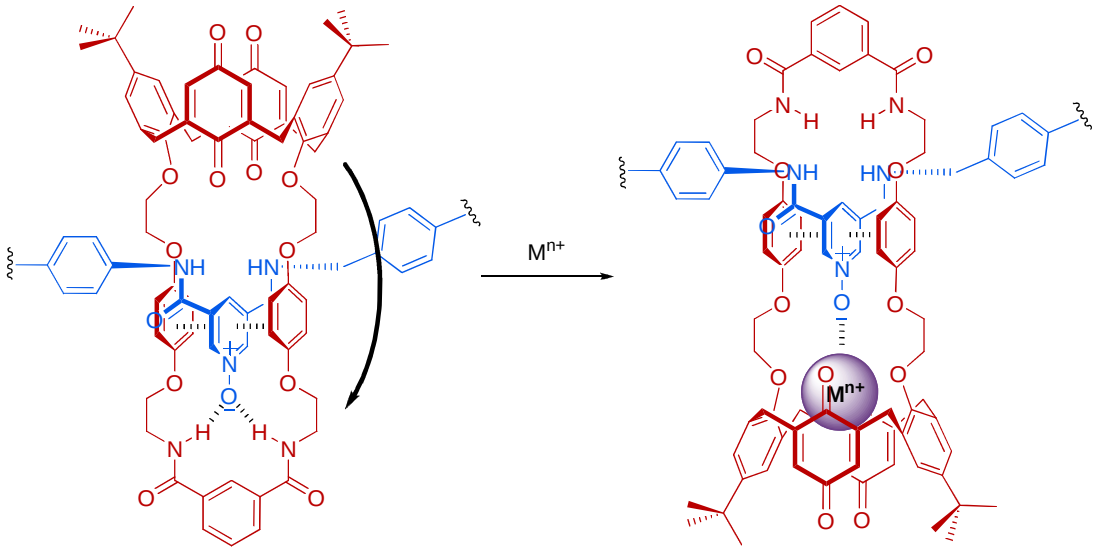
Expected correlations **1** ($\delta_2 \rightarrow g,h$), **2** ($\beta_1 \rightarrow g,h$), **3** ($\gamma \rightarrow g,h$) and **4** ($\varepsilon_2 \rightarrow g,h$) were observed between macrocycle hydroquinone protons and protons in the vicinity of the pyridine *N*-oxide motif whilst interaction **6** ($\beta_2 \rightarrow d$) indicates that the axle pyridine *N*-oxide oxygen is pointing into the isophthalamide cleft. More interestingly, a number of cross coupling interactions (**5**) exist between the calix[4]diquinone protons and the phenyl linker of the axle. It is possible that π-π stacking interactions are occurring between the two aromatic systems thus accounting for the unusual chemical shift values for the signals corresponding to the calix[4]diquinone protons. These non-covalent interactions may also be responsible for the asymmetry observed in the rotaxane's $^1$H NMR spectrum.




***Figure 4.19.*** *$^{1}H$ -$^{1}H$ ROESY spectrum of [2]rotaxane **84** in $CDCl_3$ at 293K. Cross couplings are shown on the schematic diagram on the right.*

## 4.5.2 Investigations into Cation-Induced Pirouetting Motion

Following the isolation of the target rotaxane **84**, $^{1}H$ NMR investigations into the potential of the interlocked structure to undergo a cation-induced pirouetting motion were carried out. The anticipated pirouetting motion of the rotaxane upon addition of cations is depicted in Scheme 4.19.




***Scheme 4.19.*** *Anticipated cation-induced pirouetting motion of rotaxane **84**.*

It was decided that investigations would be carried out with both barium(II) and sodium(I) cations in order to ascertain whether the anticipated pirouetting motion of the rotaxane was dependent upon the charge of the cation. The perchlorate salts of these cations were used as perchlorate can be considered a non-coordinating cation.

These $^{1}$H NMR experiments were carried out in 5:1 $CDCl_3/CD_3CN$ since the perchlorate salts of barium and sodium are insoluble in 100% $CDCl_3$. Figure 4.20 shows the spectra of rotaxane **84** before (a) and after (b) the addition of one equivalent of barium perchlorate.

The figure originally located here has been removed from this version of the thesis for copyright reasons.

***Figure 4.20.*** *$^{1}$H NMR spectra in 5:1 $CDCl_3/CD_3CN$ at 293 K of rotaxane **84** in the (a) absence and (b) presence of $Ba(ClO_4)_2$.*

A number of chemical shift perturbations are observed upon addition of the dication. Notably macrocycle amide proton *d* is observed to move upfield indicating that the axle pyridine *N*-oxide motif is no longer bound in the macrocycle's isophthalamide cleft. In addition, increased splitting of the hydroquinone protons *g* and *h* is observed indicating an alternative

position of the pyridine *N*-oxide unit between the hydroquinone surfaces. The majority of protons in the vicinity of the pyridine *N*-oxide motif were also observed to shift upfield implying that they may now reside in a different environment. Interestingly, the diquinone and phenyl protons of the calix[4]diquinone unit are observed to move upfield whilst the splitting seen in methylene proton signals $k_1$ and $k_2$ is removed. This may be a result of the axle phenyl linker being too far away from the calix[4]diquinone unit to undergo any π- π stacking interactions in the new conformation.

Although the multitude of shifts observed are indicative of a pirouetting motion occurring upon barium cation addition, 2D ROESY NMR was used in an attempt to obtain definitive proof. Unfortunately, due to a large number of overlapping proton signals in the new conformation it was impossible to confirm that the pirouetting motion had occurred. However, no cross coupling interactions between the macrocycle protons and any protons in the vicinity of the triazole unit were observed indicating that it was unlikely that translational motion had taken place.

In order to determine whether it was possible to reverse the molecular motion described above and thus create a switchable molecular machine it was important to be able to sequester the barium cations from the rotaxane. The easiest way to remove barium cations is to use a source of sulfate and thus precipitate $BaSO_4$. One equivalent of $(TBA)_2SO_4$ was added to a 1:1 mixture of rotaxane **84** and $Ba(ClO_4)_2$ in 5:1 $CDCl_3/CD_3CN$. The $^1H$ NMR spectrum of the resultant solution is given in Figure 4.21 along with that of rotaxane **84** in the presence and absence of $Ba(ClO_4)_2$ for comparison.




***Figure 4.21.*** *$^{1}$H NMR spectra in 5:1 $CDCl_3$/$CD_3CN$ at 293 K of (a)* ***84****, (b)* ***84*** *+ 1 eq. $Ba(ClO_4)_2$ and (c)* ***84*** *+ 1 eq. $Ba(ClO_4)_2$ + 1 eq. $(TBA)_2SO_4$.*

A virtually identical spectrum was obtained upon addition of $(TBA)_2SO_4$ to that observed for the rotaxane itself. This indicates not only that the barium cations have been successfully removed from the rotaxane but also that the observed molecular motion is reversible.

An analogous $^{1}$H NMR titration study using sodium perchlorate resulted in very similar $^{1}$H NMR shifts being observed (Figure 4.22b).




***Figure 4.22.*** *$^{1}$H NMR spectra in 5:1 $CDCl_3$/$CD_3CN$ at 293 K of rotaxane* ***84*** *in the presence of 1 eq. (a) $Ba(ClO_4)_2$ and (b) $NaClO_4$.*

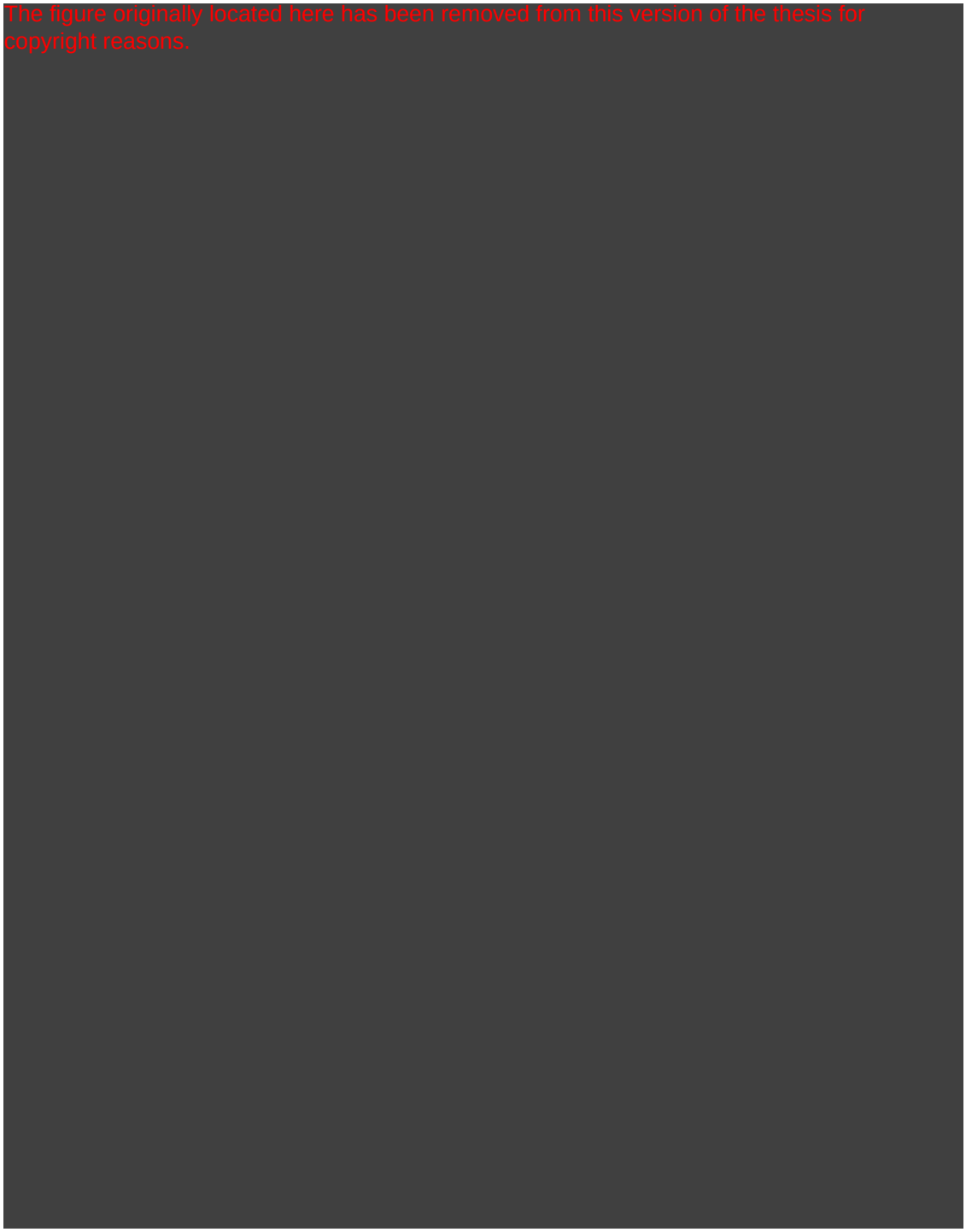
This implies that the type of motion occurring in the presence of sodium cations is the same as when barium cations are added, and thus changing the charge of the cation does not affect the molecular pirouetting process. The only discernable difference in $^{1}$H NMR spectra is the position of hydroquinone protons *g* and *h*, which is to be expected considering the smaller ionic radius of sodium causing the pyridine *N*-oxide to adopt a slightly different position amid the hydroquinone units.

### 4.5.3 Cation-Templated Synthesis of [2]Rotaxanes

The preliminary studies described above suggest that it is possible to stimulate rotaxane **84** to undergo rotational motion of the macrocyclic wheel component around the axle upon addition of cations.

Since this pirouetting molecular motion is dependent on the pyridine *N*-oxide oxygen atom coordinating to the cation, it may be possible to enhance the yield of formation of this rotaxane by using a templating barium or sodium cation.

Due to the solubility properties of the perchlorate salts, they were added to a $CH_2Cl_2$ solution of macrocycle **83**, axle precursor **80** and stopper **72** in MeCN, with the latter solvent making up 1.25% of the total solution volume. In this solvent mixture, $NaClO_4$ remained dissolved throughout the reaction, whilst the less soluble $Ba(ClO_4)_2$ was observed as a suspension. In spite of this the reaction was continued with DIPEA and a copper(I) catalyst added to mediate the click reaction.




***Scheme 4.20.*** *Cation-templated syntheses of rotaxane* ***84.***

Following preparative TLC rotaxane **84** was isolated in 28% and 50% yields after templation with barium and sodium cations respectively. In both cases the free rotaxane **84** was isolated (i.e. in the absence of its templating cation) which is presumed to be a consequence of the cations being lost during preparative TLC due to the high affinity of charged species with silica. The yield of rotaxane formation has increased three fold by templation with barium

cations despite $Ba(ClO_4)_2$ remaining suspended throughout the reaction, whilst templation with sodium has resulted in a five-fold increase. These significant increases in yields provide unequivocal evidence for the cation-mediated templation of this pyridine *N*-oxide axle containing rotaxane. This also constitutes one of few reported examples of the alkali and alkaline earth metal cation template synthesis of interlocked molecular assemblies.[24-26]

Arguably, the greater yield obtained by sodium templation is a direct consequence of $NaClO_4$ remaining soluble throughout the reaction rather than monocationic sodium being a more effective template for this reaction than dicationic barium. In order to confirm this theory, the reactions should be repeated in pure MeCN in which all components would be soluble. Unfortunately, a limited supply of starting materials meant that this was not possible.

It can be argued that the large enhancement of rotaxane yield in the presence of these metal cations provides further evidence for the cation-mediated pirouetting motion described in the previous section. These increased yields can only be explained by assuming that the axle's pyridine *N*-oxide oxygen donor atom coordinates to the calix[4]diquinone macrocycle bound cation, which facilitates interpenetration and pseudorotaxane assembly. If, on the other hand, the pyridine *N*-oxide motif remains bound by the macrocycle isophthalamide cleft, no advantage would be gained on addition of $Ba^{2+}$ or $Na^{+}$, as the respective metal cation would merely be complexed by the calix[4]diquinone unit and hence only act as a spectator.

## 4.6 Summary, Conclusions and Future Perspectives

It has been possible to use click chemistry to construct a [2]rotaxane **73**·$X_2$ (Figure 4.23) where the axle component contains two potential stations; a pyridinium and triazole motif, linked by a polyether spacer. Despite the rotaxane being designed as an anion switchable molecular shuttle, driven by unfavourable electrostatic interactions between the positively charged macrocycle and axle pyridinium groups, the macrocyclic component was shown to

reside at the pyridinium station in both the presence and absence of chloride. However **73**·$(PF_6)_2$ was also shown, by 2D ROESY spectroscopy, to be in close proximity to the triazole station, which was attributed to a folding of the polyether linked flexible axle such that the triazole was able to associate in the amide cavity, left vacant by removal of the halide anion.

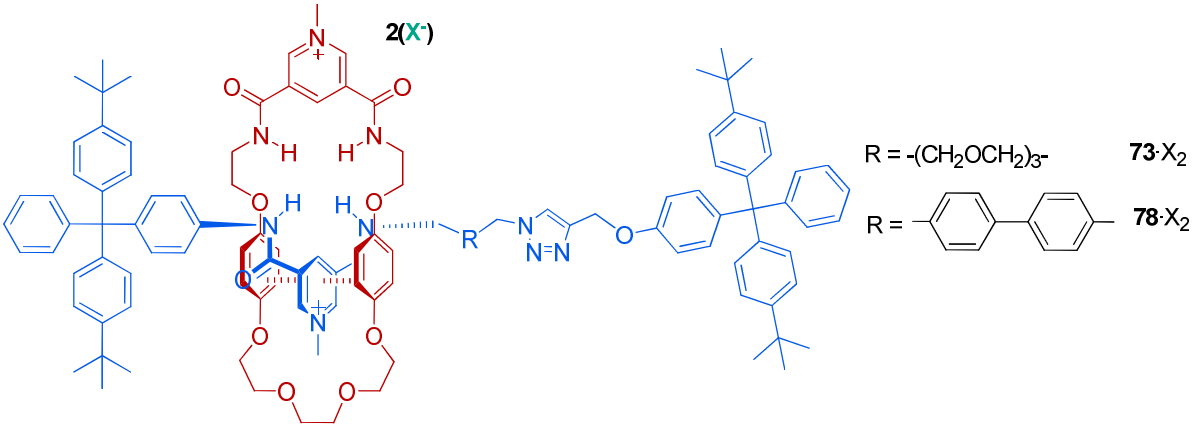


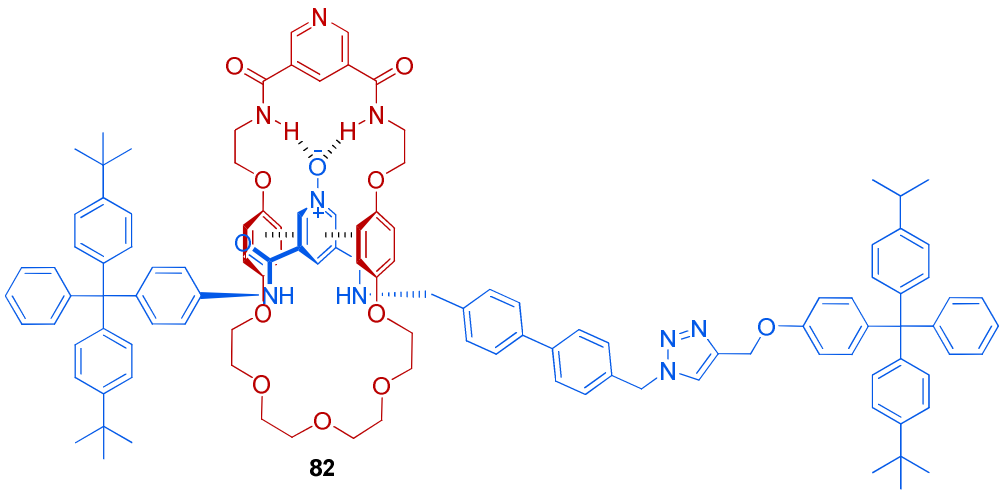

***Figure 4.23.*** *Novel two-station rotaxanes.*

Following this observation a new rotaxane **78**·$Cl_2$ was designed whereby the axle component contained a rigid biphenyl spacer group to circumvent the 'coiling' observed in the previous rotaxane. Formation of this rotaxane was successful, but again the macrocycle was shown to reside over the axle pyridinium station in both chloride and hexafluorophosphate salts. It was concluded that the strength of the charge-assisted π-π stacking interactions between macrocycle hydroquinone and axle pyridinium aromatic surfaces was capable of counteracting the unfavourable repulsive electrostatic interactions between pyridinium macrocycle and axle components.

It may be possible to construct an anion-switchable molecular shuttle of similar design if the axle pyridinium moiety were replaced with another functional group. Imidazolium or triazolium could be used as they capable both of undergoing pseudorotaxane formation with an appropriate macrocycle, however the resultant pseudorotaxane assemblies are less stable than the equivalent pyridinium *N*-methyl containing assembly.[27, 28] This may be a

consequence of the smaller planar surface of these heterocycles resulting in diminished π-π stacking interactions with the macrocycle hydroquinone unit.

Investigations were also carried out into the possibility of using pyridine *N*-oxide as a motif for interlocked structure formation. Templation using pyridine *N*-oxide was successful for the rotaxane formation, where the pyridine *N*-oxide oxygen of the axle was shown to reside, *via* hydrogen bonding, in the isophthalamide cleft of the macrocycle (Figure 4.24).




**82**

***Figure 4.24.*** *Novel pyridine N-oxide rotaxane* ***82****.*

Upon addition of acid to the rotaxane, the macrocycle undergoes rotational motion (Figure 4.25a) as the hydrogen bonding interactions of the pyridine *N*-oxide motif with the amide cleft are broken upon protonation of the *N*-oxide group. This molecular motion was shown to be reversible by addition of base. It may be possible to exploit this phenomenon further in the construction of a pyridine *N*-oxide containing catenane (Figure 4.21b).

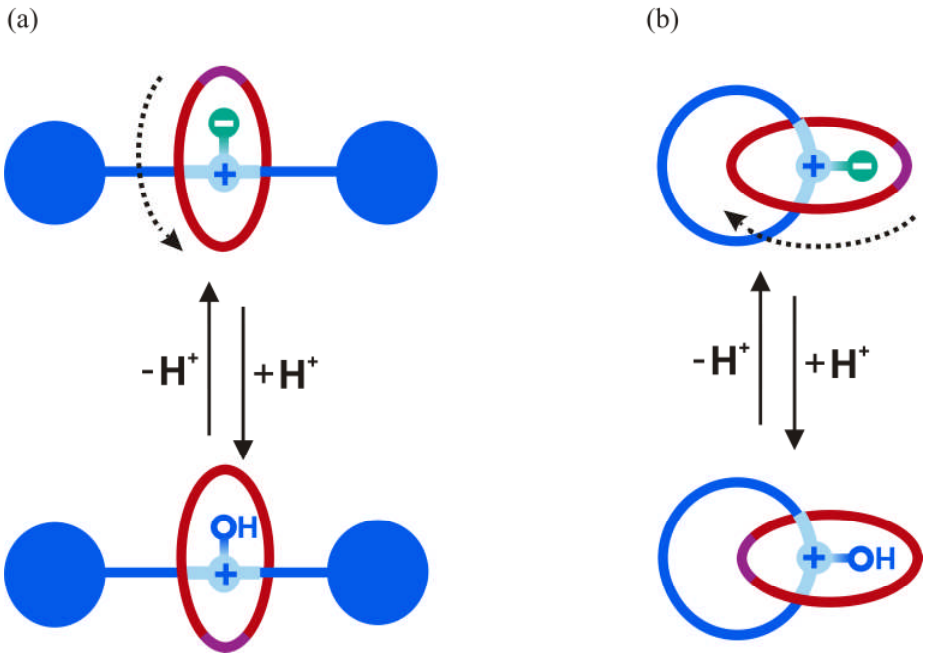



***Figure 4.25.*** *Schematic representation of pH controlled molecular rotation in pyridine N-oxide containing (a) rotaxane and (b) catenane.*

It was also possible to synthesise a novel rotaxane **84** whereby the polyether chain of the isophthalamide macrocycle was replaced with a calix[4]diquinone unit. In the absence of metal cations the rotaxane is shown, by 2D ROESY NMR to adopt a conformation where the axle pyridine *N*-oxide oxygen donation is bound by the isophthalamide cleft of the macrocycle. Preliminary results suggest that addition of barium and sodium cations induce a pirouetting molecular motion of the macrocycle around the axle whereby the pyridine *N*-oxide moved from being coordinated in the macrocycle's isophthalamide cleft to adopting a vacant coordination site of the calix[4]diquinone-bound metal cation (Scheme 4.21).

The figure originally located here has been removed from this version of the thesis for copyright reasons.

***Scheme 4.21.*** *Schematic representation of cation-induced pirouetting-type motion in a [2]rotaxane.*

In the case of barium this motion could be reversed by addition of sulfate anions.

Finally, repetition of the rotaxane synthesis in the presence of barium and sodium cations caused a substantial increase in yield, indicative of the aforementioned conformation where the pyridine *N*-oxide of the axle coordinates to the macrocycle-bound cation. This rotaxane

## 4.7 References


1. D. S. Marlin, D. G. Cabrera, D. A. Leigh and A. M. Z. Slawin, *Angew. Chem., Int. Ed.*, 2006, **45**, 77-83.
2. J. P. Sauvage, *Chem. Commun.*, 2005, 1507-1510.
3. J. P. Collin, V. Heitz, S. Bonnet and J. P. Sauvage, *Inorg. Chem. Commun.*, 2005, **8**, 1063-1074.
4. B. Champin, P. Mobian and J. P. Sauvage, *Chem. Soc. Rev.*, 2007, **36**, 358-366.
5. S. Sharma, G. J. E. Davidson and S. J. Loeb, *Chem. Commun.*, 2008, 582-584.
6. J. D. Crowley, S. M. Goldup, A.-L. Lee, D. A. Leigh and R. T. McBurney, *Chem. Soc. Rev.*, 2009, **38**, 1530-1541.
7. J. D. Crowley, K. D. Hänni, D. A. Leigh and A. M. Z. Slawin, *Journal of the American Chemical Society*, 2010, **132**, 5309-5314.
8. M. J. Barrell, D. A. Leigh, P. J. Lusby and A. M. Z. Slawin, *Angew. Chem., Int. Ed.*, 2008, **47**, 8036-8039.
9. M. Linke, J. C. Chambron, V. Heitz and J. P. Sauvage, *J. Am. Chem. Soc.*, 1997, **119**, 11329-11330.
10. A. V. Leontiev, C. A. Jemmett and P. D. Beer, *Chem. Eur. J.*, 2011, **17**, 816-825.
11. H. Zheng, W. Zhou, J. Lv, X. Yin, Y. Li, H. Liu and Y. Li, *Chem. Eur. J.*, 2009, **15**, 13253-13262.
12. M. D. Lankshear, I. Dudley, K.-M. Chan, S. M. Santos, V. Felix and P. D. Beer, *Chem. Eur. J.*, 2008, **14**, 2248-2263.
13. M. Gonçalves, K. Estieu-Gionnet, T. Berthelot, G. Laïn, M. Bayle, X. Canron, N. Betz, A. Bikfalvi and G. Déléris, *Pharm. Res.*, 2005, **22**, 1411-1421.
14. D. E. Phipps and P. D. Beer, *Tetrahedron Lett.*, 2009, **50**, 3454-3457.
15. M. Chen, S. Han, L. Jiang, S. Zhou, F. Jiang, Z. Xu, J. Liang and S. Zhang, *Chem. Commun.*, 2010, **46**, 3932-3934.
16. D. J. Hoffart and S. J. Loeb, *Angew. Chem. Int. Ed.*, 2005, **44**, 901-904.
17. D. J. Hoffart and S. J. Loeb, *Supramol. Chem.*, 2007, **19**, 89-93.
18. D. M. D'Souza, D. A. Leigh, L. Mottier, K. M. Mullen, F. Paolucci, S. J. Teat and S. Zhang, *J. Am. Chem. Soc.*, 2010, **132**, 9465-9470.
19. M. J. Hynes, *J. Chem. Soc., Dalton Trans.*, 1993, 311-312.
20. B. R. Travis, M. Sivakumar, G. O. Hollist and B. Borhan, *Org. Lett.*, 2003, **5**, 1031-1034.
21. L. Raehm, J.-M. Kern and J.-P. Sauvage, *Chem. Eur. J.*, 1999, **5**, 3310-3317.
22. J.-M. Kern, L. Raehm, J.-P. Sauvage, B. Divisia-Blohorn and P.-L. Vidal, *Inorg. Chem.*, 2000, **39**, 1555-1560.
23. I. Murgu, J. M. Baumes, J. Eberhard, J. J. Gassensmith, E. Arunkumar and B. D. Smith, *J. Org. Chem.*, 2011, **76**, 688-691.
24. S. L. Castro, O. Just and O. S. Rees Jr, *Angew. Chem., Int. Ed.*, 2000, **39**.

25. G. Kaiser, T. Jarrosson, S. Otto, Y.-F. Ng, A. D. Bond and J. K. M. Sanders, *Angew. Chem. Int. Ed.*, 2004, **43**, 1959-1962.
26. S.-Y. Hsueh, C.-C. Lai, Y.-H. Liu, S.-M. Peng and S.-H. Chiu, *Angew. Chem. Int. Ed.*, 2007, **46**, 2013-2017.
27. M. R. Sambrook, P. D. Beer, J. A. Wisner, R. L. Paul, A. R. Cowley, F. Szemes and M. G. B. Drew, *J. Am. Chem. Soc.*, 2005, **127**, 2292-2302.
28. K. M. Mullen, J. Mercurio, C. J. Serpell and P. D. Beer, *Angew. Chem., Int. Ed.*, 2009, **48**, 4781-4784.

# Chapter 5: Experimental

## 5.1 General Information

### 5.1.1 Instrumental Methods

All instrumentation used was located in the Chemistry Research Laboratory, University of Oxford. NMR spectra were obtained using DPX 200, Varian Mercury 300, AVII 500 (for $^{13}C$ cryoprobe) and Unity Plus 500 spectrometers at 293 K. The internal standards for $^{19}F$ and $^{31}P$ NMR were $CFCl_3$ and $H_3PO_4$ respectively. Low resolution electrospray mass spectrometry was performed using a Micromass LCT Premier XE spectrometer and high resolution electrospray mass spectrometry to four decimal places was achieved with Bruker microTOF and Bruker FT-ICR-MS spectrometers. Electron impact and field ionisation mass spectrometry was carried out using a Micromass GCT spectrometer, fitted with a temperature programmed solid probe inlet. MALDI mass spectra were obtained using a Waters MALDI micro spectrometer. Reactions carried out under microwave irradiation used a Biotage Initiator 2.0 microwave.

### 5.1.2 Solvents and Reagents

Commercially available solvents and chemicals were used without further purification unless stated. Where dry solvents were used, they were degassed with nitrogen, dried by passing through an MBraun MPSP-800 column and then used immediately. Water was deionised in all cases and microfiltered prior to use through a Milli-Q® Millipore machine.

$Cu(MeCN)_4PF_6$ and TBTA were prepared by Nicholas White and stored in a desiccator prior to use. $Ru(bipy)_2Cl_2$ was prepared by Thomas Lake and macrocycle **83**[1] was kindly provided by Dr. Alexandre Leontiev.

Where it is not stated, acid chlorides were prepared by suspending in thionyl chloride (10 mL) and heating at reflux for 16 h, followed by the removal of $SOCl_2$ by distillation, and immediate use in the appropriate reaction. This is with the exception of isophthaloyl dichloride which is available commercially. Gaseous HCl was prepared by adding concentrated $H_2SO_4$ *via* a dropping funnel to a NaCl. The HCl was delivered to the required solution by rubber tubing appended with a glass nozzle.

## 5.2 Synthetic Procedures

### 5.2.1 Experimental Details for Chapter 2

**General Procedure for Rotaxane Synthesis**

Axle **13**·Cl (100 mg, 0.093 mmol) and the appropriate bis-amine (0.093 mmol) were dissolved in dry $CH_2Cl_2$ (20 mL) and stirred under $N_{2(g)}$ for 15 min. Triethylamine (24 μL, 0.23 mmol) was added to the reaction mixture followed immediately by addition of the appropriate acid chloride (0.093 mmol) in dry $CH_2Cl_2$ (5 mL). The reaction was stirred under $N_{2(g)}$ for 1 h before washing with 10% $HCl_{(aq)}$ (2 × 25 mL) and $H_2O$ (2 × 25 mL). The organic layer was dried over anhydrous $MgSO_4$, the solvent removed *in vacuo*, and the resulting crude yellow solid purified by preparative TLC.

**General Procedure for Rotaxane Anion Exchange to Hexafluorophosphate Salt**

The rotaxane was dissolved in $CHCl_3$ (15 mL) and washed with 0.1 M $NH_4PF_{6(aq)}$ (10 × 10 mL) and $H_2O$ (2 × 10 mL). The organic layer was dried over $MgSO_4$, and the solvent removed *in vacuo* to give a yellow solid in quantitative yield.

**4-cyanatophenol (1):**

NaOH (8.43 g, 211 mmol) and hydroquinone (11.6 g, 105 mmol) were dissolved in degassed 1:1 dioxane/water (300 mL) and stirred under $N_{2(g)}$. A solution of bromoacetonitrile (7.34 mL, 105 mmol) in degassed dioxane (50 mL) was added to the above mixture. The reaction

mixture was stirred for 1 h, degassing throughout, its progress being monitored by TLC. Once the reaction had gone to completion, it was acidified with 1 M $HCl_{(aq)}$ and extracted with $CH_2Cl_2$ (3 × 200 mL). The solution was dried over anhydrous $MgSO_4$ and the solvent removed *in vacuo*. The resulting brown oil was purified using column chromatography (silica; 98:2 $CH_2Cl_2$/MeOH) giving the product as a yellow oil (9.55 g, 61%).

**$^1$H NMR** (300 MHz, $CDCl_3$) δ (ppm): 6.89 (2H, d, $^3J$ = 9.1 Hz, Ar*H*), 6.83 (2H, d, $^3J$ = 9.4 Hz, Ar*H*), 5.03 (1H, br s, ArO*H*), 4.72 (2H, s, C$H_2$CN). **$^{13}$C NMR** (75.5 MHz, $CDCl_3$) δ (ppm): 151.6, 150.4, 116.9, 116.3, 115.4, 54.9. **HRMS (ESI):** *m/z* calc. for $C_8H_7NO_2$ $[M + NH_4]^+$: 167.0814; found 167.0815.[2]

**Bis-tosylate tetraethylene glycol (2)[3]:**

Tetraethylene glycol (5 mL, 22.8 mmol) was dissolved in $CH_2Cl_2$ (50 mL), then TsCl (8.73 g, 45.8 mmol) was added and the solution cooled to 0 °C. Powdered KOH (16.8 g, 300 mmol) was added portionwise, keeping the mixture at 0 °C and the reaction was stirred for 3 h at this temperature. Dichloromethane (50 mL) was added, the mixture poured onto ice water (150 mL), and the organic layer separated. The aqueous layer was extracted with $CH_2Cl_2$ (3 × 100 mL), then the combined organic layers were washed with $H_2O$ (100 mL) and dried over anhydrous $MgSO_4$ before the solvent was removed *in vacuo*. Any remaining TsCl was removed by triturating with $Et_2O$ (4 × 25 mL) to give the product as a colourless oil (10.7 g, 93%).

**$^1$H NMR** (200 MHz, $CDCl_3$) δ (ppm): 8.80 (4H, d, $^3J$ = 8.3 Hz, Ar*H*), 7.34 (4H, d, $^3J$ = 8.3 Hz, Ar*H*), 4.16 (4H, t, $^3J$ = 4.5 Hz, C$H_2$), 3.68 (4H, t, $^3J$ = 4.8 Hz, C$H_2$), 3.57 (8H, s, $CH_2$), 2.45 (6H, s, C$H_3$). **MS (ESI):** *m/z* calc. for $C_{22}H_{30}O_9S_2$ $[M + NH_4]^+$: 525.1; found: 525.1.[3]

**5-oxygen polyether bis-nitrile (3)[2]:**

Compound **1** (1.50 g, 10.1 mmol) and bis-tosylate **2** (2.53 g, 5.03 mmol) were dissolved in dry MeCN (100 mL). Potassium carbonate (1.39 g, 10.1 mmol) was added and the mixture heated at reflux for 48 h. The reaction was cooled to RT, filtered to remove $K_2CO_3$, and the solvent removed *in vacuo*. The sticky pale brown solid was redissolved in $CHCl_3$ (75 mL), filtered and the solvent removed *in vacuo* to give a white oily solid (1.87 g, 81%).

**$^1$H NMR** (300 MHz, $CDCl_3$) δ (ppm): 6.87 – 6.95 (8H, m, Ar*H*), 4.71 (4H, s, C$H_2$CN) 4.09 (4H, t, $^3J$ = 4.8 Hz, C$H_2$), 3.85 (4H, t, $^3J$ = 4.8 Hz, C$H_2$), 3.68 – 3.76 (8H, m, C$H_2$). **MS (ESI):** *m/z* calc. for $C_{24}H_{28}N_2O_7$ $[M + Na]^+$: 479.2 found: 479.2.[2]

**5-oxygen polyether bis-amine (4):**

Bis-nitrile **3** (1.87 g, 4.10 mmol) was dissolved in dry THF (100 mL) and added dropwise to 1 M $BH_3$·THF (30 mL, 30.0 mmol) which had been preheated to 70 °C. Once the addition of compound **3** was complete the solution was heated at reflux for 4 h under $N_{2(g)}$. The solution was then cooled to RT and MeOH was added with care to quench the reducing agent until bubbling had ceased. The solvent was reduced by ¾ *in vacuo*, then $HCl_{(g)}$ bubbled through the solution for 30 min. The precipitate was collect by vacuum filtration, washed with cold MeOH (50 mL) and hexane (2 × 50 mL), and dried under vacuum. The white solid was suspended in $CH_2Cl_2$ (50 mL), 10% $NaOH_{(aq)}$ (50 mL) was added and the biphasic mixture stirred vigorously for 30 min. The organic phase was washed with $H_2O$ (100 mL), dried over anhydrous $MgSO_4$, and the solvent removed *in vacuo* to give an oily white solid (1.28 g, 75%).

**$^1$H NMR** (300 MHz, $CDCl_3$) δ (ppm): 6.84 (8H, s, Ar*H*), 4.08 (4H, t, $^3J$ = 4.8 Hz, C$H_2$), 3.94 (4H, t, $^3J$ = 5.1 Hz, C$H_2$), 3.84 (4H, t, $^3J$ = 4.8 Hz, C$H_2$), 3.68 – 3.76 (8H, m, C$H_2$), 3.06 (4H, t, $^3J$ = 5.1 Hz, C$H_2$). **$^{13}$C NMR** (75.5 MHz, $CDCl_3$) δ (ppm): 153.1, 115.5, 115.3, 70.7, 70.6, 69.8, 68.0, 41.6. **MS (ESI):** *m/z* calc. for $C_{22}H_{32}N_2O_6$ $[M + H]^+$: 465.26; found 465.26.

**Pyridine Thread (5)[4]:**

3,5-Pyridine dicarboxylic acid (1.31 g, 7.8 mmol) was dissolved in $SOCl_2$ (20 mL) and heated at reflux under $N_{2(g)}$ for 16 h until the solution became homogeneous. The $SOCl_2$ was removed by distillation and the residue was redissolved in dry $CH_2Cl_2$ (20 mL). This solution was then added dropwise to a solution of hexylamine (1.1 mL. 8.37 mmol) and $Et_3N$ (2.0 mL, 14.3 mmol) in dry $CH_2Cl_2$ (100 mL) at 0 ˚C. The reaction mixture was stirred for 2 h then washed with 10% citric $acid_{(aq)}$ (2 × 100 mL) and water (2 × 100 mL). The organic phase was dried over anhydrous $MgSO_4$ and the solvent removed *in vacuo* to yield the product as an off-white solid (1.45 g, 56%).

**$^1$H NMR** (300 MHz, $CDCl_3$) δ (ppm): 9.10 (2H, s, Ar*H*), 8.45 (1H, s, Ar*H*), 6.43 (2H, br t, $^3J$ = 5.7 Hz, N*H*), 3.49 (4H, q, $^3J$ = 7.0 Hz, C$H_2$NH), 1.65 (4H, m, C$H_2$), 1.35 (4H, m, C$H_2$), 0.91 (6H, t, $^3J$ = 6.7 Hz, C$H_3$). **MS (ESI):** *m/z* calc. for $C_{19}H_{31}N_3O_2$ $[M + H]^+$: 333.2; found 333.3.[4]

**Pyridinium Thread (6·Cl)[4]:**

Pyridine thread **5** (1.39 g, 4.18 mmol) and MeI (2 mL) were dissolved in $CHCl_3$ (50 mL) and the solution heated at reflux under $N_{2(g)}$ for 48 h. The reaction mixture was cooled to RT and the solvent and MeI were removed *in vacuo* to give **6**·I as an orange solid. This was redissolved in $CHCl_3$ (100 mL) and washed with 1 M $NH_4Cl_{(aq)}$ solution (8 × 100 mL) and $H_2O$ (2 × 100 mL). The organic phase was dried over anhydrous $MgSO_4$, and the solvent removed *in vacuo* to give a yellow solid (1.20 g, 75%).

**$^1$H NMR** (300 MHz, $CDCl_3$) δ (ppm): 10.72 (1H, s, Ar*H*), 9.59 (2H, br t, $^3J$ = 5.2 Hz, N*H*), 9.26 (2H, s, Ar*H*), 4.54 (3H, s, $N^+$C$H_3$), 3.49 (4H, m, C$H_2$NH), 1.76 (4H, m, C$H_2$), 1.34 (12H, m, C$H_2$), 0.89 (6H, t, $^3J$ = 7.0 Hz, C$H_3$). **MS (ESI)**: *m/z* calc for $C_{20}H_{34}N_3O_2$·Cl $[M - Cl]^+$: 348.3; found: 348.3.[4]

**Isophthalamide 5-oxygen polyether macrocycle (7)**[5]:

Bis-amine **4**·2HCl (500 mg, 0.93 mmol), pyridinium thread **6**·Cl (355 mg, 0.93 mmol) and $Et_3N$ (3 mL, 21.5 mmol) were dissolved in dry $CH_2Cl_2$ (40 mL) and stirred until all solid had dissolved. Isophthaloyl dichloride (189 mg, 0.93 mmol) in dry $CH_2Cl_2$ (20 mL) was added dropwise, and the reaction mixture stirred for 1 h. The solution was washed with 10% $HCl_{(aq)}$ (2 × 50 mL) and $H_2O$ (2 × 50 mL), then dried over anhydrous $MgSO_4$ and the solvent removed *in vacuo*. The resulting bright yellow solid was purified by column chromatography (silica; 95:5 $CHCl_3$/MeOH) to yield pale yellow material which was subsequently washed with cold MeOH (2 × 10 mL) to give the product as a white solid (553 mg, 41%).

**$^1$H NMR** (300 MHz, $d_6$-acetone) δ (ppm): 8.04 (2H, dd, $^3J$ = 7.7 Hz, $^4J$ = 1.7 Hz, isophthalamide $H^4$ & $H^6$), 7.98 (1H, t, $^4J$ = 1.7 Hz, isophthalamide $H^2$), 7.55 (1H, t, $^3J$ = 7.7 Hz, isophthalamide $H^5$), 6.78 (10H, s, hydroquinone Ar*H* & N*H*), 4.09 (4H, t, $^3J$ = 4.8 Hz, C$H_2$), 4.04 (4H, t, $^3J$ = 5.0 Hz, C$H_2$), 3.83 – 3.89 (8H, m, C$H_2$), 3.68 – 3.74 (8H, m, C$H_2$). **$^{13}$C NMR** (75.5 MHz, 3:1 $CDCl_3$/$CD_3OD$) δ (ppm): 167.8, 153.2, 152.7, 134.2, 131.0, 129.2, 125.6, 115.6, 115.4, 70.6, 70.6 (*sic*), 69.7, 68.1, 67.2, 39.7. **HRMS (ESI):** *m/z* calc. for $C_{32}H_{38}N_2O_9$ $[M + Na]^+$: 617.2470; found 617.2471.[4]

**Pyridine 5-oxygen polyether macrocycle (8)**[5]**:**

3,5-Pyridine dicarbonyl dichloride (190 mg, 0.93 mmol) was dissolved in dry $CH_2Cl_2$ (20 mL) and added dropwise to a solution of bis-amine **4**·2HCl (500 mg, 0.93 mmol), pyridinium thread **6**·Cl (357 mg, 0.93 mmol) and $Et_3N$ (3 mL, 21.5 mmol) in $CH_2Cl_2$ (50 mL) that had been stirred vigorously for 30 min. The reaction mixture was left to stir for 16 h, then washed with 10% $HCl_{(aq)}$ solution (2 × 50 mL) and $H_2O$ (50 mL). The organic layer was dried over anhydrous $MgSO_4$, and the solvent removed *in vacuo* to yield a crude yellow solid. This was purified using column chromatography (silica; 96:4 $CHCl_3$/MeOH) to give a white solid (0.232 g, 42%).

**$^{1}$H NMR** (300 MHz, $CDCl_3$) δ (ppm): 9.20 (2H, s, pyridine *H*$^{2}$ & *H*$^{6}$), 8.24 (1H, s, pyridine *H*$^{4}$), 6.77 (8H, s, hydroquinone Ar*H*), 6.73 (2H, br s, N*H*), 4.09 (4H, t, $^{3}J$ = 4.9 Hz, C$H_2$NH), 4.03 (4H, t, $^{3}J$ = 4.9 Hz, C$H_2$), 3.81-3.89 (4H, m, C$H_2$), 3.69 (8H, m, C$H_2$). **$^{13}$C NMR** (75.5 MHz, 3:1 $CDCl_3$/$CD_3OD$) δ (ppm): 165.4, 153.0, 152.5, 150.8, 133.0, 129.4, 115.4, 115.1, 70.4, 69.4, 67.8, 66.8, 39.6. **HRMS (ESI):** *m/z* calc for $C_{31}H_{37}N_3O_9$ $[M + H]^+$: 596.2603; found: 596.2605.[2]

**Nitro isophthalamide 5-oxygen polyether macrocycle (9)[5]:**

5-Nitro isophthaloyl dichloride (231 mg, 0.93 mmol) was dissolved in $CH_2Cl_2$ (20 mL) and added dropwise to a solution of bis-amine **4**·2HCl (500 mg, 0.93 mmol), pyridinium thread **6**·Cl (0.355 g, 0.93 mmol) and $Et_3N$ (2 mL, 14.3 mmol) in dry $CH_2Cl_2$ that had been stirring vigorously for 30 min. The solution was stirred for 1 h, washed with 10% $HCl_{(aq)}$ (2 × 50 mL) and $H_2O$ (2 × 50 mL), then dried over $MgSO_4$ and the solvent removed *in vacuo*. The resulting yellow solid was purified by column chromatography (silica; 94:6 $CH_2Cl_2$/MeOH) to give a yellow solid (185 mg, 31%).

**$^{1}$H NMR** (300 MHz, $d_6$-DMSO) δ (ppm): 9.09 (2H, t, $^{3}J$ = 5.3 Hz, N*H*), 8.71 (3H, s, isophthalamide *H*$^{2}$, *H*$^{4}$ & *H*$^{6}$), 6.80 – 6.88 (8H, m, hydroquinone Ar*H*), 4.09 (4H, t, $^{3}J$ = 5.0 Hz, C$H_2$), 3.95 – 3.98 (4H, m, C$H_2$), 3.64 – 3.70 (8H, m, C$H_2$), 3.51 – 3.56 (8H, m, C$H_2$) **$^{13}$C NMR** (75.5 MHz, $d_6$-DMSO) δ (ppm): 164.2, 152.5, 147.9, 136.1, 131.8, 124.4, 115.4, 115.2, 70.0, 69.9, 69.0, 67.5, 66.5. **HRMS (ESI):** *m/z* calc. for $C_{32}H_{37}N_3O_{11}$ $[M + Na]^+$: 662.2320; found 662.2321.

**Bis(4-tert-butylphenyl)(phenyl)methanol (10)[6]:**

Magnesium turnings (1.46 g, 60.1 mmol) were heated at 110 °C under $N_{2(g)}$ in a three-necked flask for 16 hours, then the flask was cooled to RT and dry THF (10 mL) added. Iodine (cat.) was added, followed by the dropwise addition of 1-bromo-4-*tert*-butyl benzene (9.76 mL, 56.3 mmol) in dry THF (30 mL). The mixture was heated at 40 ºC until the solution began to

effervesce and lose its red/brown colour then stirred for 2 h under $N_{2(g)}$. A solution of methyl benzoate (3.3 mL, 26.8 mmol) in dry THF (4 mL) was added dropwise over 20 min and the mixture heated at reflux for 16 h under $N_{2(g)}$. The solution was cooled to RT, neutralised with 10% $HCl_{(aq)}$ and extracted with hexane (2 × 100 mL). The combined organic layers were washed with $H_2O$ (2 × 100 mL), dried over anhydrous $MgSO_4$, and the solvent removed *in vacuo*. The pale brown oil was recrystallised from MeOH to give a white solid (8.09 g, 81%).

**$^1$H NMR** (300 MHz, $CDCl_3$) δ (ppm): 7.16 – 7.33 (13H, m, Ar*H*), 2.75 (1H, s, O*H*), 1.31 (18H, s, $^t$Bu). **MS (ESI)**: *m/z* calc. for $C_{27}H_{32}O$ $[M - OH]^+$: 355.2; found: 355.3.[6]

**4-(bis(4-tert-butylphenyl)(phenyl)methyl)aniline (11)[6]:**

Compound **10** (6.00 g, 16.1 mmol) was dissolved in acetyl chloride (30 mL) and heated at reflux for 16 h. The acetyl chloride was removed by distillation, giving a white solid which was immediately dissolved in aniline (30 mL). The mixture was heated at 105 °C for 48 h, during which a colour change from orange to purple was observed. The reaction mixture was cooled to RT, poured onto 10% $HCl_{(aq)}$ (300 mL) and stirred for 20 min before the purple precipitate was collected by vacuum filtration. The solid was washed with sat. $K_2CO_{3(aq)}$ (50 mL) and $H_2O$ (50 mL) before being dissolved in $CH_2Cl_2$ (150 mL) and dried with anhydrous $MgSO_4$. The solvent volume was reduced by ¾, filtered through a silica plug and the solvent removed *in vacuo* to give a pale brown solid which was recrystallised from toluene/hexane to give a white solid (2.61 g, 36%).

**$^1$H NMR** (300 MHz, $CDCl_3$) δ (ppm): 7.30 (9H, m, Ar*H*), 7.14 (4H, d, $^3J$ = 8.80 Hz, Ar*H*), 7.02 (2H, d, $^3J$ = 8.80 Hz, Ar*H*), 6.61 (2H, d, $^3J$ = 8.80 Hz, Ar*H*), 3.63 (2H, br s, N$H_2$), 1.35 (18H, s, $^t$Bu). **MS (ESI)**: *m/z* calc. for $C_{33}H_{37}N$ $[M + MeCN + H]^+$: 489.3; found: 489.3.[6]

**Pyridine Axle (12)[7]:**

3,5-Pyridine dicarbonyl dichloride (0.228 g, 1.12 mmol) was dissolved in dry $CH_2Cl_2$ (10 mL), added dropwise to a solution of stopper **11** (1.00 g, 2.23 mmol) and $Et_3N$ (1 mL,

7.17 mmol) in dry $CH_2Cl_2$ (50 mL), and the reaction stirred for 4 h under $N_{2(g)}$. The solvent was removed *in vacuo*, and EtOH (50 mL) added to the resulting yellow residue. The mixture was heated at reflux for 1 h, and then filtered to give a pale yellow solid (0.932 g, 81%).

**$^1$H NMR** (300 MHz, $CDCl_3$) δ (ppm): 10.62 (2H, br s, N*H*), 9.23 (1H, d, $^3J$ = 2.1 Hz, pyridine $H^4$), 8.74 (2H, t, $^4J$ = 2.1 Hz, pyridine $H^2$ & $H^6$), 7.68 (4H, d, $^3J$ = 9.0 Hz, Ar*H*NH), 7.09 – 7.34 (30H, m, Ar*H*), 1.26 (36H, s, $^t$Bu). **MS (ESI):** *m/z* calc. for $C_{73}H_{75}N_3O_2$ $[M + MeCN + NH_4]^+$: 1084.6; found: 1084.6.[7]

**Pyridinium Axle Iodide salt (13·I)[7]:**

Pyridine axle **12** (400 mg, 0.389 mmol) was suspended in MeI (10 mL), the mixture stirred at reflux under $N_{2(g)}$ for 72 h and the solvent was removed *in vacuo* to give a bright yellow solid in quantitative yield (454 mg, 100%).

**$^1$H NMR** (300 MHz, $d_6$-DMSO) δ (ppm): 10.94 (2H, s, N*H*), 9.64 (2H, s, pyridinium $H^2$ & $H^6$), 9.49 (1H, s, pyridinium $H^4$), 7.66 (4H, d, $^3J$ = 8.90 Hz, Ar*H*NH), 7.09 – 7.35 (30H, m, Ar*H*), 4.49 (3H, s, $N^+CH_3$), 1.26 (36H, s, $^t$Bu*H*). **MS (ESI)**: *m/z* calc. for $C_{74}H_{78}N_3O_2$·I $[M - I]^+$: 1040.6; found: 1040.5.[7]

**Pyridinium Axle Chloride salt (13·Cl)[7]:**

Axle **13**·I (350 mg, 0.30 mmol) was suspended in $CHCl_3$ (200 mL) and washed with 1 M $NH_4Cl_{(aq)}$ solution (8 × 200 mL) and $H_2O$ (2 × 100mL). The organic phase was dried over anhydrous $MgSO_4$ and the solvent removed *in vacuo* giving a bright yellow solid (291 mg, 90%).

**$^1$H NMR** (300 MHz, $CDCl_3$) δ (ppm): 10.98 (2H, br s, N*H*), 10.66 (1H, s, pyridinium $H^4$), 8.79 (2H, s, pyridinium $H^2$ & $H^6$), 7.80 (4H, d, $^3J$ = 8.77 Hz, Ar*H*NH), 7.16 – 7.27 (30H, m, Ar*H*), 5.30 (3H, s, $N^+CH_3$), 1.29 (36H, s, $^t$Bu). **MS (ESI)**: *m/z* calc. for $C_{74}H_{78}N_3O_2$·Cl $[M - Cl]^+$: 1040.6; found: 1040.6.[7]

**Pyridinium Axle Hexafluorophosphate salt (13·$PF_6$):**

Axle **13**·Cl (100 mg, 0.093 mmol) was dissolved in $CHCl_3$ (30 mL) and washed with 1 M $NH_4PF_{6\ (aq)}$ solution (10 × 20 mL) and $H_2O$ (2 × 20 mL). The organic phase was dried over anhydrous $MgSO_4$ and the solvent removed *in vacuo* giving a yellow solid (109 mg, 99%).

**$^1$H NMR** (300MHz, $CDCl_3$) δ (ppm): 9.15 (1H, s, pyridinium $H^4$), 9.02 (2H, br s, N*H*), 8.77 (2H, s, pyridinium $H^2$ & $H^6$), 7.53 (4H, d, $^3J$ = 8.8 Hz, Ar*H*NH), 7.11 – 7.26 (30H, m, Ar*H*), 4.05 (3H, s, $N^+CH_3$), 1.29 (36H, s, $^t$Bu). **$^{19}$F NMR** (282.4 MHz, $CDCl_3$) δ (ppm): −72.7 (d, $^1J$ = 712 Hz, P$F_6$); **$^{31}$P NMR** (121.6 MHz, $CDCl_3$) δ (ppm): −144.2 (sept, $^1J$ = 712 Hz, $PF_6$); **MS (ESI)**: *m/z* calc. for $C_{74}H_{78}N_3O_2$·$PF_6$ $[M - PF_6]^+$: 1040.6; found: 1040.5.[7]

**Isophthalamide Rotaxane 5-oxygen polyether chain Chloride salt (14·Cl):**

**METHOD 1:** Axle **13**·Cl (50 mg, 0.046 mmol), bis-amine **4**·2HCl (30 mg, 0.046 mmol) and $Et_3N$ (1 mL, 7.17 mmol) were dissolved in dry $CH_2Cl_2$ (20 mL) and stirred vigorously under $N_{2(g)}$ for 30 min. A solution of isophthaloyl dichloride (9.5 mg, 0.047 mmol) in $CH_2Cl_2$ (5 mL) was added and the reaction stirred under $N_{2(g)}$ for 1 h before washing with 10% $HCl_{(aq)}$ (2 × 25 mL) and $H_2O$ (2 × 25 mL). The organic layer was dried over anhydrous $MgSO_4$, the solvent removed *in vacuo*, and the resulting crude yellow solid purified by preparative TLC (silica; 95:5 $CHCl_3$/MeOH) to give a yellow solid (23 mg, 30%).

**METHOD 2:** Following general procedure for rotaxane synthesis using bis-amine **2** (60 mg, 0.093 mmol) and isophthaloyl dichloride (19 mg, 0.093 mmol). Preparative TLC (silica; 95:5 $CHCl_3$/MeOH) gave a yellow solid (91 mg, 60%).

**METHOD 3:** Isophthalic acid (8.3 mg, 0.05 mmol) was suspended in dry MeCN (5 mL) and *N*-hydroxysuccinamide (13.8 mg, 0.12 mmol), then *N*,*N*′-dicyclohexylcarbodiimide (22.7 mg, 0.11 mmol) were added. The reaction mixture was stirred at RT for 16 h, and then filtered. The filtrate was concentrated *in vacuo*, redissolved in dry $CH_2Cl_2$ (2 mL) and added to a solution of axle **13**·Cl (50 mg, 0.046 mmol), bis-amine **4** (21.5 mg, 0.046 mmol) and $Et_3N$ (16

μL, 0.115 mmol) in $CH_2Cl_2$ (10 mL). The solution was stirred under $N_{2(g)}$ for 16 h, then washed with 10% $HCl_{(aq)}$ (2 × 15 mL) and $H_2O$ (2 × 15 mL), dried over anhydrous $MgSO_4$, and the solvent removed *in vacuo*. The resulting crude material was purified by preparative TLC (silica; 95:5 $CHCl_3$/MeOH) to yield the product as a yellow solid (32 mg, 41%).

**$^1$H NMR** (300 MHz, $CDCl_3$) δ (ppm): 10.40 (2H, s, axle N*H*), 10.06 (1H, s, pyridinium $H^4$), 9.02 (2H, s, pyridinium $H^2$ & $H^6$), 8.91 (1H, s, isophthalamide $H^2$), 8.54 (2H, br s, macrocycle N*H*), 7.99 (2H, d, $^3J$ = 7.5 Hz isophthalamide $H^4$ & $H^6$), 7.83 (4H, d, $^3J$ = 8.4 Hz, Ar*H*NH), 7.05 – 7.27 (31H, m, stopper Ar*H* & isophthalamide $H^5$), 6.44 (4H, d, $^3J$ = 8.6 Hz, hydroquinone Ar*H*), 6.16 (4H, d, $^3J$ = 8.6 Hz, hydroquinone Ar*H*), 4.66 (3H, s, $N^+CH_3$), 4.11 (4H, t, $^3J$ = 4.5 Hz, C$H_2$), 3.71 – 3.74 (20H, m, C$H_2$), 1.33 (36H, s, $^t$Bu). **$^{13}$C NMR** (75.5 MHz, $CDCl_3$) δ (ppm): 167.0, 158.2, 153.7, 151.7, 148.3, 146.9, 145.3, 144.5, 143.5, 134.8, 133.6, 133.4, 131.7, 131.5, 131.0, 130.6, 128.5, 127.3, 125.7, 124.9, 124.2, 120.2, 114.7, 114.6, 70.7, 70.5, 70.0, 68.2, 65.6, 63.8, 49.6, 40.7, 34.3, 31.3. **HRMS (ESI):** *m/z* calc. for $C_{106}H_{116}N_5O_{11}$ $[M - Cl]^+$: 1635.8699; found: 1635.8654.

**Isophthalamide Rotaxane 5-oxygen polyether chain Hexafluorophosphate salt (14·$PF_6$):**

**METHOD 1:** Following the general procedure for rotaxane anion exchange using rotaxane **14**·Cl (75 mg, 0.045 mmol) to give **14**·$PF_6$ as a yellow solid (80 mg, 100%).

**METHOD 2:** Isophthalic acid (8.3 mg, 0.05 mmol) was suspended in dry MeCN (5 mL) and *N*-hydroxysuccinamide (13.8 mg, 0.12 mmol), then *N*,*N*′-dicyclohexylcarbodiimide (22.7 mg, 0.11 mmol) were added The reaction mixture was stirred at RT for 16 h and then filtered. The filtrate was concentrated *in vacuo*, redissolved in dry $CH_2Cl_2$ (2 mL) and added to a solution of axle **13**·$PF_6$ (55 mg, 0.046 mmol), bis-amine **4** (21.5 mg, 0.046 mmol) and $Et_3N$ (16 μL, 0.115 mmol) in $CH_2Cl_2$ (10 mL). The solution was stirred under nitrogen for 16 h, then washed with 10% $HCl_{(aq)}$ (2 × 15 mL) and $H_2O$ (2 × 15 mL), dried over anhydrous $MgSO_4$,

and the solvent removed *in vacuo*. The resulting crude material was purified by preparative TLC (silica; 95:5 $CHCl_3$/MeOH) to yield the product as a yellow solid (15 mg, 20%).

**$^1$H NMR** (300 MHz, $CDCl_3$) δ (ppm): 9.26 (2H, s, axle N*H*), 8.78 (2H, s, pyridinium $H^2$ & $H^6$), 8.66 (1H, s, pyridinium $H^4$), 8.22 (1H, s, isophthalamide $H^2$), 8.09 (2H, d, $^3J$ = 7.6 Hz isophthalamide $H^4$ & $H^6$), 7.62 (4H, d, $^3J$ = 8.4 Hz, Ar*H*NH), 7.44 (1H, t, $^3J$ = 7.3 Hz, isophthalamide $H^5$), 7.07 – 7.26 (32H, m, stopper Ar*H* & isophthalamide N*H*), 6.57 (4H, d, $^3J$ = 8.9 Hz, hydroquinone Ar*H*), 6.34 (4H, d, $^3J$ = 8.9 Hz, hydroquinone Ar*H*), 4.26 (3H, s, $N^+CH_3$), 4.11 (4H, m, $CH_2$), 3.95 – 4.00 (20H, m, $CH_2$), 1.32 (36H, s, $^t$Bu). **$^{13}$C NMR** (75.5 MHz, $CDCl_3$) δ (ppm): 166.9, 158.6, 152.9, 151.7, 148.6, 146.8, 145.0, 144.4, 143.3, 134.5, 133.9, 131.9, 131.6, 131.0, 130.6, 129.0, 127.4, 125.8, 124.3, 123.5, 119.8, 115.9, 114.7, 70.6, 70.4, 70.0, 67.5, 66.9, 63.8, 49.3, 39.7, 34.3, 31.3; **$^{19}$F NMR** (282.4 MHz, $CDCl_3$) δ (ppm): −70.0 (d, $^1J$ = 710 Hz, $PF_6$); **$^{31}$P NMR** (121.6 MHz, $CDCl_3$) δ (ppm): −144.0 (sept, $^1J$ = 710 Hz, $PF_6$); **HRMS (ESI):** *m/z* calc.for $C_{106}H_{116}N_5O_{11}$ $[M - PF_6]^+$: 1635.8699; found: 1635.8691.

**Triethylene glycol bis-tosylate (15)[3]:**

Triethylene glycol (5 mL, 37.4 mmol) was dissolved in $CH_2Cl_2$ (50 mL), tosyl chloride (14.3 g, 74.8 mmol) was added and the mixture cooled to 0 ˚C using an ice bath. Powdered KOH (16.8 g, 300 mmol) was carefully added portionwise and the temperature kept below 0 ˚C. The reaction was stirred for 3 h at 0 ˚C, and then $CH_2Cl_2$ (50 mL) and ice water (100 mL) were added. The organic layer was separated and the aqueous layer extracted with $CH_2Cl_2$ (2 × 50 mL). The combined organic layers were washed with $H_2O$ (50 mL) and dried over anhydrous $MgSO_4$. The solvent was removed *in vacuo* to yield compound **2** as a white solid (16.0 g, 94%).

**$^1$H NMR** (300 MHz, $CDCl_3$) δ (ppm): 7.81 (4H, d, $^3J$ = 8.4 Hz, Ar*H*), 7.35 (4H, d, $^3J$ = 8.4 Hz, Ar*H*), 4.15 (4H, t, $^3J$ = 4.8 Hz, $CH_2$), 3.66 (4H, t, $^3J$ = 4.8 Hz, $CH_2$), 3.54 (4H, s,

C*H*$_2$), 2.45 (6H, s, C*H*$_3$); **MS (ESI):** *m/z* calc. for $C_{20}H_{26}O_8S_2$ $[M + NH_4]^+$: 476.1; found: 476.1.[3]

**4-oxygen polyether bis-nitrile (16)[2]:**

Compound **1** (2.24 g, 15.3 mmol) and bis-tosylate **15** (3.50 g, 7.64 mmol) were dissolved in dry MeCN (150 mL) before $K_2CO_3$ (2.16 g, 15.6 mmol) was added and the mixture was refluxed under $N_2$ for 24 h. The mixture was cooled to RT, the $K_2CO_3$ removed by filtration and the solvent was removed *in vacuo*. The resulting residue was redissolved in $CHCl_3$ (75 mL), filtered and the solvent removed *in vacuo* to obtain compound **16** as a pale yellow oily solid in 81% yield (2.54 g, 5.15 mmol). N.B. If oxidation of the starting material **1** has begun to occur the final product will be a dark brown, and the pure product can be obtained by carrying out a silica gel plug (70:30 $CH_2Cl_2$/EtOAc).

**$^1$H NMR** (300 MHz, $CDCl_3$) δ (ppm): 6.92 (8H, s, Ar*H*), 4.71 (4H, s, C*H*$_2$CN), 4.11 (4H, t, $^3J$ = 4.8 Hz, C*H*$_2$), 3.86 (4H, t, $^3J$ = 4.8 Hz, C*H*$_2$), 3.76 (4H, s, C*H*$_2$); **$^{13}$C NMR** (75.5 MHz, $CDCl_3$) δ (ppm): 154.7, 150.7, 116.5, 115.7, 115.4, 70.8, 69.7, 67.9, 54.7; **HRMS (ESI):** *m/z* calc. for $C_{22}H_{24}N_2O_6$ $[M + NH_4]^+$: 430.1973; found: 430.1975.

**4-oxygen polyether bis-amine (17):**

A 1 M solution of $BH_3$·THF (16 mL, 16 mmol) was heated to 70°C and then a solution of bis-nitrile **16** (0.80 g, 1.94 mmol) in dry THF (40 mL) was added dropwise over a period of 15 min. The reaction mixture was then heated at reflux under $N_{2(g)}$ for 4 h. The reaction was cooled to RT and methanol (50 mL) added very slowly, releasing $H_{2(g)}$. The solvent was reduced by ¾, then $HCl_{(g)}$ was bubbled into the solution forming a white precipitate which was collected by vacuum filtration. The white solid was washed with methanol (50 mL) and hexane (50 mL), and left to dry under vacuum for 1 h. The solid was then suspended in $CH_2Cl_2$ (30 mL), 10% $NaOH_{(aq)}$ (30 mL) was added and the biphasic mixture stirred vigorously for 30 min. The organic phase was washed with $H_2O$ (50 mL), dried over

anhydrous $MgSO_4$, and the solvent removed *in vacuo* to give an oily white solid (0.61 g, 75%).

**$^1$H NMR** (300 MHz, $CDCl_3$) δ (ppm): 6.84 (8H, s, hydroquinone Ar*H*), 4.09 (4H, t, $^3J$ = 4.9 Hz, C$H_2$), 3.93 (4H, t, $^3J$ = 5.2 Hz, C$H_2$), 3.84 (4H, t, $^3J$ = 4.9 Hz, C$H_2$), 3.75 (4H, s, C$H_2$), 3.06 (4H, t, $^3J$ = 5.2 Hz, C$H_2$); **$^{13}$C NMR** (75.5 MHz, $CDCl_3$) δ (ppm): 153.0, 129.3, 115.6, 115.4, 70.8, 69.9, 68.1, 41.7; **HRMS (ESI)**: *m/z* calc. for $C_{22}H_{32}N_2O_6$ $[M + H]^+$: 421.2333; found: 421.2330.

**Pyridine Rotaxane 5-oxygen polyether chain Chloride salt (18·Cl):**

Following the general procedure for rotaxane synthesis using bis-amine **4** (60 mg, 0.093 mmol) and pyridine dicarbonyl dichloride (19 mg, 0.093 mmol). Preparative TLC (silica; 9:1 $CHCl_3$/MeOH) gave a yellow solid (91 mg, 60%).

**$^1$H NMR** (300 MHz, $CDCl_3$) δ (ppm): 10.31 (2H, br s, axle N*H*), 10.03 (1H, s, pyridinium $H^4$), 9.30 (1H, s, pyridine $H^4$), 9.21 (2H, s, pyridine $H^2$ & $H^6$), 8.99 (2H, s, pyridinium $H^2$ & $H^6$), 8.45 (2H, br s, macrocycle N*H*), 7.82 (4H, d, $^3J$ = 8.8 Hz, Ar*H*NH), 7.02 – 7.26 (30H, m, Ar*H*), 6.45 (4H, d, $^3J$ = 9.1 Hz, hydroquinone *H*), 6.17 (4H, d, $^3J$ = 9.1 Hz, hydroquinone *H*) 4.67 (3H, s, $N^+CH_3$), 4.07 (4H, t, $^3J$ = 4.6, C$H_2$), 3.68 – 3.75 (16H, m, C$H_2$), 3.49 (4H, m, C$H_2$) 1.31 (36H, s, $^t$Bu); **$^{13}$C NMR** (75.5 MHz, $CDCl_3$) δ (ppm): 165.3, 158.1, 153.6, 152.7, 151.8, 148.4, 146.8, 145.4, 144.9, 143.4, 134.6, 133.6, 131.8, 131.0, 130.5, 127.6, 127.3, 125.8, 124.3, 120.4, 114.8, 114.7, 77.2, 70.7, 70.5, 70.0, 68.3, 65.6, 63.7, 49.7, 40.7, 34.3, 31.3; **HRMS (ESI)** *m/z* calc. for $C_{105}H_{115}N_6O_{11}$·Cl $[M - Cl]^+$: 1636.8651; found: 1636.8229.

**Pyridine Rotaxane 5-oxygen polyether chain Hexafluorophosphate salt (18·$PF_6$):**

Following the general procedure for rotaxane anion exchange using rotaxane **18**·Cl (75 mg, 0.045 mmol) to give **18**·$PF_6$ as a yellow solid (80 mg, 100%).

**$^1$H NMR** (300 MHz, $CDCl_3$) δ (ppm): 9.31 (2H, br s, axle N*H*), 9.30 (2H, s, pyridine $H^2$ & $H^6$), 8.80 (1H, s, pyridinium $H^4$), 8.71 (2H, s, pyridinium $H^2$ & $H^6$), 8.49 (1H, s, pyridine $H^4$),

7.62 (4H, d, $^{3}J$ = 8.86 Hz, NHAr*H*), 7.07 – 7.27 (32H, m, macrocycle N*H* & stopper Ar*H*), 6.45 (4H, d, $^{3}J$ = 8.70 Hz, hydroquinone Ar*H*), 6.17 (4H, d, $^{3}J$ = 8.70 Hz, hydroquinone Ar*H*) 4.11 (3H, s, $N^{+}CH_3$), 4.00 (4H, t, $^{3}J$ = 4.70, $CH_2$NH), 3.72 (16H, m, $CH_2$), 3.58 (4H, m, $CH_2$) 1.31 (36H, s, $^{t}$Bu); **$^{13}$C NMR** (75.5 MHz, $CDCl_3$) δ (ppm): 165.3, 158.1, 153.6, 152.7, 151.8, 148.4, 146.8, 145.4, 144.9, 143.4, 134.6, 133.6, 131.8, 131.0, 130.5, 127.6, 127.3, 125.8, 124.3, 120.4, 114.8, 114.7, 109.9, 77.2, 70.7, 70.5, 70.0, 68.3, 65.6, 63.8, 49.7, 40.7, 34.3, 31.3; **$^{19}$F NMR** (282.4 MHz, $CDCl_3$) δ (ppm): −70.0 (d, $^{1}J$ = 713 Hz, P$F_6$); **$^{31}$P NMR** (121.6 MHz, $CDCl_3$) δ (ppm): −144.0 (sept, $^{1}J$ = 713 Hz, $PF_6$); **HRMS (ESI):** *m/z* calc. for $C_{105}H_{115}N_6O_{11}{\cdot}PF_6$ $[M - PF_6]^{+}$: 1636.8651; found: 1636.8436.

**Nitro Isophthalamide Rotaxane 5-oxygen polyether chain Chloride salt (19·Cl):**

Following the general procedure for rotaxane synthesis using bis-amine **4** (60 mg, 0.093 mmol), and 5-nitroisophthaloyl dichloride (23 mg, 0.093 mmol). Preparative TLC (silica; 93:7 $CHCl_3$/MeOH) gave a yellow solid (87 mg, 55%).

**$^{1}$H NMR** (300 MHz, $CDCl_3$) δ (ppm): 10.27 (2H, s, axle N*H*), 10.02 (1H, s, pyridinium $H^4$), 9.37 (1H, s, isophthalamide $H^4$), 8.99 (2H, s, isophthalamide $H^2$ & $H^6$), 8.91 (2H, d, $^{4}J$ = 1.2 Hz, pyridinium $H^2$ & $H^6$), 8.68 (2H, t, $^{3}J$ = 3.8 Hz, macrocycle N*H*), 7.86 (4H, d, $^{3}J$ = 8.8 Hz, Ar*H*NH), 6.99 – 7.26 (30H, m, Ar*H*), 6.47 (4H, d, $^{3}J$ = 9.1 Hz, hydroquinone Ar*H*), 6.17 (4H, d, $^{3}J$ = 9.1 Hz, hydroquinone Ar*H*), 4.71 (3H, s, $N^{+}CH_3$), 4.13 (4H, t, $^{3}J$ = 4.7 Hz, $CH_2$), 3.72 – 3.77 (20H, m, $CH_2$), 1.32 (36H, s, $^{t}$Bu); **$^{13}$C NMR** (75.5 MHz, $CDCl_3$) δ (ppm): 158.0, 153.3, 151.8, 148.5, 146.7, 145.3, 144.8, 143.3, 137.1, 135.2, 134.7, 133.6, 131.8, 130.9, 130.5, 130.0, 127.3, 126.4, 125.8, 124.2, 120.3, 114.7, 70.7, 70.5, 70.0, 68.4, 65.4, 63.7, 49.8, 41.0, 34.3, 31.3; **HRMS (ESI):** *m/z* calc. for $C_{106}H_{116}N_6O_{13}{\cdot}Cl$ $[M - Cl]^{+}$: 1680.8556; found: 1680.8631.

**Nitro Isophthalamide Rotaxane 5-oxygen polyether chain Hexafluorophosphate salt (19·$PF_6$):**

Following the general procedure for anion exchange using rotaxane **19**·Cl (75 mg, 0.044 mmol) to give **19**·$PF_6$ as a yellow solid (80 mg, 100%).

**$^1$H NMR** (300 MHz, $CDCl_3$) δ (ppm): 9.93 (2H, br s, axle N*H*), 8.97 (3H, s, pyridinium $H^2$, $H^4$ & $H^6$), 8.65 (2H, s, isophthalamide $H^2$ & $H^6$), 8.51 (1H, s, isophthalamide $H^4$), 7.65 (4H, d, $^2J$ = 8.5 Hz, Ar*H*NH), 7.07–7.28 (32H, m, Ar*H* & macrocycle N*H*), 6.64 (4H, d, $^2J$ = 8.1 Hz, hydroquinone Ar*H*), 6.35 (4H, d, $^2J$ = 8.1 Hz, hydroquinone Ar*H*), 4.03 – 4.06 (7H, m, $N^+CH_3$ & -$CH_2$-), 3.70–3.75 (16H, m, $CH_2$), 3.57 (4H, br s, $CH_2$), 1.32 (36H, s, $^t$Bu). **$^{13}$C NMR** (75.5 MHz, $CDCl_3$) δ (ppm): 164.5, 158.8, 153.0, 151.6, 148.7, 146.7, 145.2, 144.6, 143.3, 136.1, 134.5, 134.0, 132.0, 131.0, 130.5, 127.4, 126.3, 125.9, 124.3, 119.8, 115.9, 114.7, 70.6, 70.5, 70.1, 67.3, 66.7, 63.8, 49.4, 39.9, 34.3, 31.3; **$^{19}$F NMR** (282.4 MHz, $CDCl_3$) δ (ppm): −70.0 (d, $^1J$ = 713 Hz, P$F_6$); **$^{31}$P NMR** (121.6 MHz, $CDCl_3$) δ (ppm): −144.0 (sept, $^1J$ = 713 Hz, *P*$F_6$); **HRMS (ESI):** *m/z* calc.for $C_{106}H_{116}N_6O_{13}$·$PF_6$ $[M - PF_6]^+$: 1680.8556; found: 1680.8534.

**Isophthalamide Rotaxane 4-oxygen polyether chain Chloride salt (20·Cl):**

Following the general procedure for rotaxane synthesis using bis-amine **17** (46 mg, 0.093 mmol), isophthaloyl dichloride (19 mg, 0.093 mmol). Preparative TLC (silica; 9:1 $CHCl_3$/MeOH) gave a yellow solid (62 mg, 42%).

**$^1$H NMR** (300 MHz, 1:1 $CDCl_3$/$CD_3OD$) δ (ppm): 9.58 (1H, s, pyridinium $H^4$), 9.46 (2H, s, pyridinium $H^2$ & $H^6$), 8.80 (1H, t, $^4J$ = 1.5 Hz, isophthalamide $H^2$), 7.95 (2H, dd, $^3J$ = 7.9 Hz, $^4J$ = 1.5 Hz, isophthalamide $H^4$ & $H^6$) 7.68 (4H, d, $^3J$ = 8.7 Hz, Ar*H*NH), 7.05 – 7.25 (31H, m, Ar*H* & isophthalamide $H^5$), 6.38 (4H, d, $^3J$ = 9.0 Hz, hydroquinone Ar*H*), 6.11 (4H, d, $^3J$ = 9.0 Hz, hydroquinone Ar*H*), 4.44 (3H, s, $N^+CH_3$), 4.08 (4H, t, $^3J$ = 4.7 Hz, $CH_2$), 3.85 – 3.88 (12H, m, $CH_2$), 3.67 (4H, t, $^3J$ = 4.7 Hz, $CH_2$), 1.29 (36H, s, $^t$Bu). **$^{13}$C NMR** (75.5 MHz,

1:1 $CDCl_3/CD_3OD$) δ (ppm): 168.9, 159.5, 153.7, 152.5, 149.3, 147.7, 145.5, 144.4, 139.6, 135.5, 134.2, 133.5, 132.4, 132.1, 131.7, 131.4, 129.6, 128.1, 126.5, 125.0, 121.1, 115.3, 114.7, 71.6, 70.9, 67.9, 66.3, 64.6, 41.3, 34.9, 31.8, 30.3; **HRMS (ESI):** *m/z* calc. for $C_{104}H_{112}N_5O_{10}\cdot Cl$ $[M - Cl]^+$: 1591.8443; found: 1591.7578.

**Isophthalamide Rotaxane 4-oxygen polyether chain hexafluorophosphate salt (20·$PF_6$):**

Following the general procedure for anion exchange using rotaxane **20**·Cl (50 mg, 0.031 mmol) to give **20**·$PF_6$ as a yellow solid (53 mg, 100%).

**$^1$H NMR** (300 MHz, 1:1 $CDCl_3/CD_3OD$) δ (ppm): 9.91 (2H, s, axle N*H*), 9.27 (2H, s, pyridinium $H^2$ & $H^6$), 9.04 (1H, s, pyridinium $H^4$), 8.50 (1H, s, isophthalamide $H^2$), 8.10 (2H, br s, macrocycle N*H*), 7.94 (2H, dd, $^3J$ = 7.9 Hz, $^4J$ = 1.6 Hz, isophthalamide $H^4$ & $H^6$), 7.51 (4H, d, $^3J$ = 8.8 Hz, Ar*H*NH), 7.39 (1H, t, $^3J$ = 7.9 Hz, isophthalamide $H^5$), 7.26 – 7.06 (30H, m, Ar*H*), 6.43 (4H, d, $^3J$ = 9.1 Hz, hydroquinone Ar*H*), 6.22 (4H, d, $^3J$ = 9.1 Hz, hydroquninone Ar*H*), 4.51 (3H, s, $N^+CH_3$), 3.94 (4H, t, $^3J$ = 4.6 Hz, $CH_2$), 3.87 – 3.88 (12H, m, $CH_2$), 3.54 – 3.59 (4H, m, $CH_2$), 1.29 (36H, s, $^t$Bu); **$^{13}$C NMR** (75.5 MHz, 1:1 $CDCl_3/CD_3OD$) δ (ppm): 168.4, 159.2, 153.4, 152.2, 149.1, 147.5, 145.4, 144.1, 135.1, 134.1, 133.5, 132.3, 131.6, 131.2, 129.4, 127.9, 126.4, 125.3, 124.9, 121.5, 120.8, 115.2, 114.6, 71.3, 70.7, 67.7, 66.3, 64.4, 40.8, 34.8, 31.7; **$^{19}$F NMR** (282.4 MHz, 1:1 $CDCl_3/CD_3OD$) δ (ppm): −74.5 (d, $^1J$ = 710 Hz, $PF_6$); **$^{31}$P NMR** (121.6 MHz, 1:1 $CDCl_3/CD_3OD$) δ (ppm): −143.7 (sept, $^1J$ = 710 Hz, $PF_6$); **HRMS (ESI):** *m/z* calc. for $C_{104}H_{112}N_5O_{10}\cdot PF_6$ $[M - PF_6]^+$: 1591.8443; found: 1591.8391.

**Pyridine Rotaxane 4-oxygen polyether chain Chloride salt (21·Cl):**

Following the general procedure for rotaxane synthesis using bis-amine **17** (46 mg, 0.093 mmol), and 3,5-pyridine dicarbonyl dichloride (16 mg, 0.093 mmol). Preparative TLC (silica; 9:1 $CHCl_3$/MeOH) gave a yellow solid (55 mg, 36%).

**$^{1}$H NMR** (300 MHz, 1:1 $CDCl_3/CD_3OD$) δ (ppm): 9.58 (1H, s, pyridinium $H^4$), 9.51 (2H, s, pyridinium $H^2$ & $H^6$), 9.25 (1H, t, $^4J$ = 2.1 Hz, pyridine $H^4$), 9.09 (2H, d, $^4J$ = 2.1 Hz, pyridine $H^2$ & $H^6$), 7.68 (4H, d, $^3J$ = 8.8 Hz, NHAr*H*), 7.03 – 7.26 (30H, m, Ar*H*), 6.42 (4H, d, $^3J$ = 9.1 Hz, hydroquinone Ar*H*), 6.13 (4H, d, $^3J$ = 9.1 Hz, hydroquinone Ar*H*), 4.56 (3H, s, $N^+CH_3$), 4.06 (4H, t, $^3J$ = 4.6 Hz, C$H_2$), 3.90 – 3.86 (12H, m, C$H_2$), 3.66 (4H, t, $^3J$ = 4.6 Hz, C$H_2$), 1.29 (36H, s, $^t$Bu); **$^{13}$C NMR** (75.5 MHz, 1:1 $CDCl_3/CD_3OD$) δ (ppm): 166.5, 159.8, 153.7, 152.8, 152.6, 149.5, 147.8, 145.9, 144.5, 139.0, 135.5, 134.8, 133.6, 132.6, 131.8, 131.5, 129.4, 128.3, 126.7, 125.2, 121.6, 115.5, 114.8, 71.7, 71.0, 68.1, 66.4, 64.8, 41.6, 35.0, 31.9, 30.5; **HRMS (ESI):** *m/z* calc. for $C_{103}H_{111}N_6O_{10}\cdot Cl$ $[M - Cl]^+$: 1592.8395; found:1592.7850.

**Pyridine Rotaxane 4-oxygen polyether chain Hexafluorophosphate salt (21·$PF_6$):**

Following the general procedure for rotaxane anion exchange using rotaxane **21**·Cl (50 mg, 0.031 mmol) to give **21**·$PF_6$ as a yellow solid (53 mg, 100%).

**$^{1}$H NMR** (300 MHz, 1:1 $CDCl_3/CD_3OD$) δ (ppm): 9.36 (2H, s, pyridinium $H^2$ & $H^6$), 9.10 (2H, d, $^4J$ = 2.1 Hz, pyridine $H^2$ & $H^6$), 9.06 (1H, s, pyridinium $H^4$), 9.00 (1H, t, $^4J$ = 2.1 Hz, pyridine $H^4$), 7.55 (4H, d, $^3J$ = 8.8 Hz, HNAr*H*), 7.06 – 7.26 (30H, m, ArH), 6.43 (4H, d, $^3J$ = 9.1 Hz, hydroquinone Ar*H*), 6.22 (4H, d, $^3J$ = 9.1 Hz, hydroquinone Ar*H*), 4.58 (3H, s, $N^+CH_3$), 3.94 (4H, br s, C$H_2$), 3.87 – 3.89 (12H, m, C$H_2$), 3.55 (4H, br s, C$H_2$), 1.29 (36H, s, $^t$Bu); **$^{13}$C NMR** (75.5 MHz, 1:1 $CDCl_3/CD_3OD$) δ (ppm): 166.4, 159.5, 153.4, 152.4, 151.8, 149.4, 147.7, 147.4, 146.1, 144.3, 141.1, 135.2, 133.7, 132.6, 131.7, 131.4, 130.1, 128.2, 126.7, 125.1, 121.4, 115.6, 114.8, 71.4, 70.9, 68.0, 66.7, 64.7, 40.4, 35.0, 31.8; **$^{19}$F NMR** (282.4 MHz, 1:1 $CDCl_3/CD_3OD$) δ (ppm): −73.0 (d, $^1J$ = 712 Hz, P$F_6$); **$^{31}$P NMR** (121.6 MHz, 1:1 $CDCl_3/CD_3OD$) δ (ppm): −144.2 (sept, $^1J$ = 712 Hz, $PF_6$); **HRMS (ESI):** *m/z* calc. for $C_{103}H_{111}N_6O_{10}\cdot PF_6$ $[M - PF_6]^+$: 1592.8395; found: 1592.8319.

**Nitro Isophthalamide Rotaxane 4-oxygen polyether chain Chloride salt (22·Cl):**

Following the general procedure for rotaxane synthesis using bis-amine **17** (46 mg, 0.093 mmol), 5-nitroisophthaloyl dichloride (23 mg, 0.093 mmol). Preparative TLC (silica; 93:7 $CHCl_3$/MeOH) gave a yellow solid (64 mg, 41%).

**$^1$H NMR** (300 MHz, 1:1 $CDCl_3$/$CD_3OD$) δ (ppm): 9.62 (1H, s, pyridinium *H*$^4$), 9.52 (2H, s, pyridinium *H*$^2$ & *H*$^6$), 9.30 (1H, br t, $^4J$ = 1.4 Hz, isophthalamide *H*$^2$), 8.84 (2H, d, $^4J$ = 1.4 Hz, isophthalamide *H*$^4$ &*H*$^6$), 7.72 (4H, d, $^3J$ = 8.7 Hz, HNAr*H*), 6.99 – 7.25 (30H, m, Ar*H*), 6.42 (4H, d, $^3J$ = 9.1 Hz, hydroquinone Ar*H*), 6.13 (4H, d $^3J$ = 9.1 Hz, hydroquinone Ar*H*), 4.58 (3H, s, $N^+CH_3$), 4.10 (4H, t, $^3J$ = 4.4 Hz, C*H*$_2$), 3.89 – 3.84 (12H, m, C*H*$_2$), 3.69 (4H, t, $^3J$ = 4.4 Hz, C*H*$_2$) 1.30 (36H, s, $^t$Bu); **$^{13}$C NMR** (75.5 MHz, 1:1 $CDCl_3$/$CD_3OD$) δ (ppm): 165.7, 159.4, 153.6, 152.6, 149.3, 149.2, 147.5, 144.1, 135.8, 135.2, 133.4, 132.4, 131.6, 131.2, 128.0, 126.9, 126.5, 124.9, 121.2, 115.3, 114.6, 71.5, 70.9, 67.9, 66.1, 64.5, 41.8, 34.9, 31.8, 30.3; **HRMS (ESI):** *m/z* calc. for $C_{106}H_{114}N_7O_{12}$·Cl $[M - Cl]^+$: 1636.8394; found: 1636.7740.

**Nitro Isophthalamide Rotaxane 4-oxygen polyether chain Hexafluorophosphate salt (22·$PF_6$):**

Following the general procedure for rotaxane anion exchange using rotaxane **22**·Cl (50 mg, 0.030 mmol) to give **22**·$PF_6$ as a yellow solid (53 mg, 100%).

**$^1$H NMR** (300 MHz, 1:1 $CDCl_3$/$CD_3OD$) δ (ppm): 9.41 (2H, s, pyridinium *H*$^2$ & *H*$^6$), 9.15 (1H, s, pyridinium *H*$^4$), 9.06 (1H, s, isophthalamide *H*$^2$), 8.84 (2H, s, isophthalamide *H*$^4$ & *H*$^6$), 7.57 (4H, d, $^3J$ = 8.8 Hz, HNAr*H*), 7.03 – 7.25 (30H, m, Ar*H*), 6.43 (4H, d, $^3J$ = 8.4 Hz, hydroquinone Ar*H*), 3.58 – 3.97 (4H, d, $^3J$ = 8.4 Hz, hydroquinone Ar*H*), 4.59 (3H, s, $N^+CH_3$), 3.97 (4H, br s, C*H*$_2$), 3.87 – 3.89 (12H, m, C*H*$_2$), 3.58 (4H, br s, C*H*$_2$), 1.30 (36H, s, $^t$Bu); **$^{13}$C NMR** (125.5 MHz, 1:1 $CDCl_3$/$CD_3OD$) δ (ppm): 165.5, 159.2, 153.5, 152.4, 149.1, 147.4, 145.4, 144.0, 135.7, 135.1, 133.3, 132.2, 131.5, 131.1, 129.0, 127.9, 126.8, 126.3,

124.8, 121.0, 115.2, 114.4, 71.4, 70.7, 69.7, 66.0, 64.3, 53.5, 41.7, 34.7, 31.7; **$^{19}$F NMR** (282.4 MHz, 1:1 $CDCl_3/CD_3OD$) δ (ppm): −73.0 (d, $^1J$ = 712 Hz, P$F_6$); **$^{31}$P NMR** (121.6 MHz, 1:1 $CDCl_3/CD_3OD$) δ (ppm): −144.0 (sept, $^1J$ = 712 Hz, $P$$F_6$); **HRMS (ESI):** *m/z* calc. for $C_{106}H_{114}N_7O_{12}\cdot PF_6$ $[M - PF_6]^+$: 1636.8394; found: 1636.8242.

**Sulfonamide Rotaxane Chloride salt (23·**Cl**):**

Following the general procedure for rotaxane synthesis using bis-amine **17** (46 mg, 0.093 mmol), and 1,3-benzenedisulfonyl chloride (27 mg, 0.093 mmol). Preparative TLC (silica; 93:7 $CHCl_3$/MeOH) gave yellow solid (36 mg, 23%).

**$^1$H NMR** (300 MHz, 1:1 $CDCl_3/CD_3OD$) δ (ppm): 9.62 (2H, s, pyridine $H^2$ & $H^6$), 8.89 (1H, s, pyridine $H^4$), 8.55 (1H, s, sulfonamide $H^2$), 7.90 (2H, d, $^3J$ = 7.8 Hz, sulfonamide $H^4$ & $H^6$), 7.64, (4H, d, $^3J$ = 8.0 Hz, HNAr$H$), 7.12 – 7.29 (31H, m, Ar$H$ & sulfonamide $H^5$), 6.41 (4H, d, $^3J$ = 8.4 Hz, hydroquinone Ar$H$), 6.20 (4H, d, $^3J$ = 8.4 Hz, hydroquinone Ar$H$), 4.57 (3H, s, $N^+CH_3$), 3.87 (4H, br s, $CH_2$), 3.76 – 3.82 (12H, m, $CH_2$), 3.09 (4H, t, $^3J$ = 4.7 Hz, $CH_2$), 1.30 (36H, s, $^t$Bu); **$^{13}$C NMR** (75.5 MHz, 1:1 $CDCl_3/CD_3OD$) δ (ppm): 159.4, 153.2, 152.4, 149.4, 147.7, 145.5, 144.4, 142.8, 135.4, 133.3, 132.5, 131.7, 131.4, 131.0, 128.1, 126.5, 126.2, 125.0, 120.6, 116.1, 114.9, 71.4, 70.8, 67.9, 67.5, 64.6, 42.9, 34.9, 31.8, 30.3; **HRMS (ESI):** *m/z* calc. for $C_{102}H_{112}N_5O_{12}S_2\cdot Cl$ $[M - Cl]^+$: 1663.7782; found: 1663.7636.

**Sulfonamide Rotaxane Hexafluorophosphate salt (23·**$PF_6$**):**

Following the general procedure for rotaxane anion exchange using rotaxane **23**·Cl (30 mg, 0.018 mmol) to give **23**·$PF_6$ as a yellow solid (32 mg, 100%).

**$^1$H NMR** (300 MHz, 1:1 $CDCl_3/CD_3OD$) δ (ppm): 9.29 (2H, s, pyridine $H^2$ & $H^6$), 8.66 (1H, s, pyridine $H^4$), 8.49 (1H, br t, $^4J$ = 1.7 Hz, sulfonamide $H^2$), 8.01 (2H, dd, $^3J$ = 8.0 Hz, $^4J$ = 1.7 Hz, sulfonamide $H^4$ & $H^6$), 7.58 (4H, d, $^4J$ = 8.9 Hz, HNAr$H$), 7.12 – 7.29 (31H, m, Ar$H$ and sulfonamide $H^5$), 6.46 (4H, d, $^3J$ = 9.2 Hz, hydroquinone Ar$H$), 6.22 (4H, d, $^3J$ = 9.2 Hz, hydroquinone Ar$H$), 4.53 (3H, s, $N^+CH_3$), 3.88 – 3.97 (16H, m, $CH_2$), 3.16 (4H, t, $^3J$ = 5.3 Hz,

C$H_2$), 1.29 (36H, s, $^t$Bu); **$^{13}$C NMR** (75.5 MHz, 1:1 $CDCl_3$/$CD_3OD$) δ (ppm): 159.3, 153.2, 152.4, 149.4, 147.7, 145.8, 144.6, 143.0, 135.2, 133.8, 132.7, 131.8, 131.4, 131.1, 128.1, 126.6, 125.6, 125.1, 120.6, 116.2, 114.8, 71.2, 70.9, 67.7, 67.6, 64.6, 42.9, 34.9, 31.8, 30.3, 23.3; **$^{19}$F NMR** (282.4 MHz, 1:1 $CDCl_3$/$CD_3OD$) δ (ppm): −72.7 (d, $^1J$ = 712 Hz, P$F_6$); **$^{31}$P NMR** (121.6 MHz, 1:1 $CDCl_3$/$CD_3OD$) δ (ppm): −144.2 (sept, $^1J$ = 712 Hz, $P$F$_6$); **HRMS (ESI):** *m/z* calc. for $C_{102}H_{112}N_5O_{12}S_2 \cdot PF_6$ $[M - PF_6]^+$: 1663.7782; found: 1663.7624.

**2-(5-hydroxynaphthalen-1-yloxy)acetonitrile (24):**

NaOH (3.36 g, 84 mmol) and naphthalene-1,5-diol (6.73 g, 42 mmol) were dissolved in a degassed 1:1 dioxane/water mixture (100 mL) and stirred under $N_{2(g)}$. A solution of bromoacetonitrile (2.93 mL, 42 mmol) in dioxane (10 mL) was added to the above mixture. The reaction mixture was stirred for 1 h, and then acidified with 10% $HCl_{(aq)}$ and extracted with $CH_2Cl_2$ (3 × 100 mL). The solution was dried over anhydrous $MgSO_4$ and the solvent removed *in vacuo.* The resulting black oil was purified using column chromatography (silica; 98:2 $CH_2Cl_2$/MeOH) giving the product as a white solid (4.10 g, 49%).

**$^1$H NMR** (300 MHz, $CD_3OD$) δ (ppm): 7.92 (1H, d, $^3J$ = 8.5 Hz, Ar$H$), 7.79 (1H, d, $^3J$ = 8.5 Hz, Ar$H$), 7.44 (1H, t, $^3J$ = 8.1 Hz, Ar$H$), 7.37 (1H, d, $^3J$ = 8.1 Hz, Ar$H$), 6.97 (1H, d, $^3J$ = 7.7 Hz, Ar$H$), 6.90 (1H, d, $^3J$ = 7.7 Hz, Ar$H$), 4.98 (2H, s, C$H_2$CN); **$^{13}$C NMR** (300 MHz, $CD_3OD$) δ (ppm): 154.9, 154.0, 128.4, 127.9, 127.6, 125.4, 118.2, 117.4, 113.8, 110.4, 107.6, 55.0; **HRMS (Probe FI)** *m/z* calc. for $C_{12}H_9NO_2$ $[M]^{\cdot+}$: 199.0633; found: 199.0629.

**Napthoquinone bis-nitrile (25):**

Compound **24** (1.00 g, 5.0 mmol), bis-tosylate **2** (1.26 g, 2.5 mmol) and $K_2CO_3$ (0.83 g, 6.0 mmol) were added to dry MeCN (50 mL) and the mixture heated at reflux under $N_{2(g)}$ for 24 h. The mixture was cooled to RT, filtered and the solvent removed *in vacuo*. The resulting residue was redissolved in $CHCl_3$ (50 mL), filtered and the solvent removed *in*

*vacuo*. The resulting dark brown oil was purified by column chromatography (silica; 7:3 $CH_2Cl_2$/ EtOAc) to give a pale yellow oily solid (1.13 g, 81%).

**$^1$H NMR** (300MHz, $CDCl_3$) δ (ppm): 8.00 (2H, d, $^3J$ = 8.5 Hz, Ar*H*), 7.76 (2H, d, $^3J$ = 8.5 Hz, Ar*H*), 7.65 (4H, m, Ar*H*), 6.95 (2H, d, $^3J$ = 7.5 Hz, Ar*H*), 6.85 (2H, d, $^3J$ = 7.5 Hz, Ar*H*), 4.93 (4H, s, C*H*$_2$CN), 4.27 (4H, t, $^3J$ = 4.6 Hz, C*H*$_2$), 3.98 (4H, m, C*H*$_2$), 3.79 (4H, m, C*H*$_2$), 3.75 (4H, m, C*H*$_2$); **$^{13}$C NMR** (300MHz, $CDCl_3$) δ (ppm): 154.4, 152.1, 126.9, 126.3, 126.0, 124.5, 117.1, 115.1, 113.8, 106.4, 106.0, 71.0, 70.8, 69.7, 67.9, 53.8; **HRMS (ESI):** *m/z* calc. for $C_{32}H_{36}N_3O_7$ $[M + Na]^+$: 579.2102; found 579.2097.

**Napthoquinone bis-amine (26**·2HCl**):**

Bis-nitrile **25** (0.80 g, 1.43 mmol) was dissolved in dry THF (50 mL) and added dropwise to a solution of 1M $BH_3$·THF (7.5 mL) at 70 ºC. The solution was heated at reflux under $N_{2(g)}$ for 4 h, then cooled to RT and MeOH added until bubbling ceased. Gaseous HCl was bubbled through the solution for 30 min, and the resultant solid collected by vacuum filtration, washed with cold MeOH (3 × 30 mL) and dried *in vacuo* to give an off-white solid (0.74 g, 80%).

**$^1$H NMR** (300MHz, $d_6$-DMSO) δ: 8.22 (6H, br s, N*H*$_3$Cl), 8.00 (2H, d, $^3J$ = 8.5 Hz, Ar*H*), 7.77 (2H, d, $^3J$ = 8.5 Hz, Ar*H*), 7.36 – 7.41 (4H, m, Ar*H*), 6.99 (4H, d, $^3J$ = 7.3 Hz, Ar*H*), 4.30 – 4.33 (4H, m, C*H*$_2$), 4.22 – 4.25 (4H, m, C*H*$_2$), 3.86 – 3.89 (4H, m, C*H*$_2$), 3.65 – 3.68 (4H, m, C*H*$_2$), 3.58 – 3.61 (4H, m, C*H*$_2$); **$^{13}$C NMR** (300 MHz, $d_6$-DMSO) δ (ppm): 153.7, 153.4, 125.9, 125.6, 125.3, 125.3, 114.7, 114.3, 106.0, 105.8, 70.1, 69.9, 69.0, 67.7, 64.6. N.B. it was not possible to obtain MS data since the compound decomposes under the conditions required. Several techniques were attempted.

**Napthoquinone rotaxane chloride salt** (**27**·Cl):

Axle **13**·Cl (50 mg, 0.046 mmol), bis-amine **26**·2HCl (30 mg, 0.046 mmol) and $Et_3N$ (1 mL were dissolved in dry $CH_2Cl_2$ (20 mL) and stirred vigorously under $N_{2(g)}$ for 30 min. A solution of isophthaloyl dichloride (9.5 mg, 0.047 mmol) in dry $CH_2Cl_2$ (5 mL) was added

and the reaction stirred under $N_{2(g)}$ for 1 h before washing with 10% $HCl_{(aq)}$ (2 × 25 mL) and $H_2O$ (2 × 25 mL). The organic layer was dried over anhydrous $MgSO_4$, the solvent removed *in vacuo*, and the resulting crude yellow solid purified by preparative TLC (silica; 93:7 $CHCl_3$/MeOH) to give a yellow solid (46 mg, 56%).

**$^1$H NMR** (300MHz, $CDCl_3$) δ: 9.90 (2H, s, axle N*H*), 9.72 (1H, s, pyridinium $H^4$), 9.21 (1H, s, isophthalamide $H^2$), 9.08 (2H, br s, macrocycle N*H*), 8.16 (2H, s, pyridinium $H^2$ & $H^6$), 7.96 (2H, d, $^3J$ = 7.6 Hz, isophthalamide $H^4$ & $H^6$), 7.74 (4H, d, $^3J$ = 8.2 Hz, Ar*H*NH), 7.61 (2H, d, $^3J$ = 8.0 Hz, napthoquinone $H^8$), 7.05 – 7.30 (33H, m, isophthalamide $H^5$, napthoquinone $H^4$ & stopper Ar*H*), 6.88 (2H, t, $^3J$ = 8.0 Hz, napthoquinone $H^7$), 6.77 (2H, t, $^3J$ = 8.0 Hz, naphthoquinone $H^3$), 6.38 (2H, d $^3J$ = 8.0 Hz, napthoquinone $H^2$), 6.27 (2H, d $^3J$ = 8.0 Hz, napthoquinone $H^6$), 4.54 (3H, s, $N^+CH_3$), 4.01 – 4.05 (8H, m, C$H_2$), 4.77 – 3.85 (16H, m, C$H_2$), 1.32 (36H, s, $^t$Bu); **$^{13}$C NMR** (75.5MHz, $CDCl_3$) δ (ppm): 167.9, 157.6 154.9, 153.3, 145.9, 147.6, 144.5, 144.1, 135.6, 133.9, 132.1, 131.6, 131.1, 129.0, 127.8, 126.6, 126.2, 125.1, 124.7, 120.3, 116.1, 112.6, 109.0, 106.0, 105.7, 71.6, 71.4, 70.6, 68.4, 66.8, 64.3, 41.3, 36.6, 34.8, 31.8; **HRMS (ESI):** *m/z* calc. for $C_{114}H_{120}N_5O_{11}{\cdot}Cl$ $[M - Cl]^+$: 1735.9023; found: 1735.8798.

**Dicationic rotaxane Hexafluorophosphate salt (28·$(PF_6)_2$):**

Rotaxane **18**·$PF_6$ (50 mg, 0.030 mmol) was dissolved in MeI (5mL), and the solution was heated at reflux under $N_{2(g)}$ for 16 h. The solvent was removed *in vacuo* and the yellow residue redissolved in $CHCl_3$ then washed with 0.1 M $NH_4PF_{6(aq)}$ solution (10 × 10 mL) and $H_2O$ (2 × 10 mL). The organic layer was dried over anhydrous $MgSO_4$ and the solvent removed *in vacuo* to give a yellow solid (51 mg, 95%).

**$^1$H NMR** (500 MHz, 1:1 $CDCl_3$/$CD_3OD$) δ (ppm): 9.42 (1H, s, axle pyridinium $H^4$), 9.39 (2H, s, axle pyridinium $H^2$ & $H^4$), 9.19 (1H, s, macrocycle pyridinium $H^4$), 8.68 (4H, d, $^3J$ = 8.8 Hz, NHAr*H*), 7.11 – 7.32 (34H, m, stopper Ar*H*), 6.65 (4H, d, $^3J$ = 8.8 Hz

hydroquinone Ar*H*), 6.33 (4H, d, $^{3}J$ = 8.8 Hz hydroquinone Ar*H*), 4.48 (3H, s, axle $N^{+}CH_3$), 4.04 (4H, t, $^{3}J$ = 4.9 Hz, $CH_2$), 3.93 (3H, s, macrocycle $N^{+}CH_3$), 3.76 (4H, t, $^{3}J$ = 4.5 Hz, $CH_2$), 3.71 – 3.74 (8H, m, $CH_2$), 3.67 – 3.68 (4H, m, $CH_2$), 1.28 (36H, s, $^{t}$Bu); **$^{13}$C NMR** (75.5 MHz, $CDCl_3$) δ (ppm): 160.6, 158.5, 153.0, 151.8, 148.5, 147.0, 145.3, 144.2, 143.6, 135.4, 134.6, 133.8, 131.7, 131.1, 130.7, 127.3, 125.8, 124.2, 120.0, 115.4, 114.6, 70.6, 69.8, 67.5, 66.5, 63.8, 54.8, 49.7, 49.5, 40.3, 34.3 31.4; **$^{19}$F NMR** (282.4 MHz, $CDCl_3$) δ (ppm): −70.9 (d, $^{1}J$ = 710 Hz, $PF_6$); **$^{31}$P NMR** (121.6 MHz, $CDCl_3$) δ (ppm): −144.1 (sept, $^{1}J$ = 710 Hz, $PF_6$); **HRMS (ESI):** *m/z* calc. for $C_{106}H_{117}N_6O_{11}\cdot(PF_6)_2$ $[M - PF_6 - H]^{+}$: 1650.8814; found: 1650.9064.

**Pyridinium 5-oxygen polyether macrocycle iodide salt (29·I)**

Macrocycle **8** (100 mg, 0.168 mmol) was dissolved in MeI (4 ml) and heated at reflux under $N_{2(g)}$ for 16 h. The solution was cooled to RT, and the solvent removed *in vacuo* to yield the product as a bright yellow solid (124 mg, 100%).

**$^{1}$H NMR** (300MHz, $CD_3CN$) δ (ppm): 9.18 (3H, s, pyridinium $H^2$, $H^4$ & $H^6$), 8.24 (2H, br s, N*H*), 6.86 (4H, d, $^{2}J$ = 9.4 Hz hydroquinone Ar*H*), 6.80 (4H, d, $^{2}J$ = 9.4 Hz hydroquinone Ar*H*), 4.40 (3H, s, $N^{+}CH_3$), 4.12 (4H, t, $^{3}J$ = 4.6Hz, $CH_2$), 3.97 – 4.00 (4H, m, $CH_2$), 3.80 (4H, q, $^{3}J$ = 5.6 Hz, $CH_2$), 3.71 – 3.74 (4H, m, $CH_2$), 3.56 – 3.61 (8H, m, $CH_2$); **MS (ESI):** calc. for $C_{32}H_{40}N_3O_9\cdot I$ $[M - I]^{+}$: 610.3; found: 610.3.[2]

**Pyridinium 5-oxygen polyether macrocycle tetrafluoroborate salt (29·$BF_4$):**

Macrocycle **8** (100 mg, 0.168 mmol) was dissolved in dry $CH_2Cl_2$ (40 mL), $Me_3OBF_4$ (99 mg, 0.672 mmol) added and the mixture stirred under $N_{2(g)}$ for 24 h. The solution was poured onto ice water (50 mL) and extracted with $CH_2Cl_2$ (2 × 20 mL). The organic layer was dried over anhydrous $MgSO_4$ and the solvent removed *in vacuo*. The resulting residue was dissolved in MeCN (50 mL), filtered, and the filtrate concentrated *in vacuo* to give a yellow solid (53 mg, 45%).

**$^1$H NMR** (300MHz, $CD_3CN$) δ (ppm): 9.16 (2H, d, $^4J$ = 1.2 Hz, pyridinium $H^2$ & $H^6$), 8.98 (1H, s, pyridinium $H^4$), 7.72 (2H, br s, N*H*), 9.80 – 9.88 (8H, m, hydroquinone Ar*H*), 4.40 (3H, s, $N^+CH_3$), 4.12 (4H, t, $^3J$ = 5.0 Hz, $CH_2$), 3.98 – 4.02 (4H, m, $CH_2$), 3.72 – 3.82 (8H, m, $CH_2$), 3.56 – 3.62 (8H, m, $CH_2$); **HRMS (ESI):** calc. for $C_{32}H_{40}N_3O_9 \cdot BF_4$ $[M - BF_4]^+$: 610.2759; found: 610.2759.

**Pyridine 4-oxygen polyether macrocycle (30):**

3,5-Pyridine dicarbonyl dichloride (233 mg, 1.14 mmol) was dissolved in dry $CH_2Cl_2$ (10 mL) and added dropwise to a solution of bis-amine **17** (0.479 g, 1.14 mol), **6**·Cl (0.438 g, 1.14 mmol) and $Et_3N$ (0.5 mL) in dry $CH_2Cl_2$ (40 ml). The reaction mixture was stirred under $N_{2(g)}$ for 1 h and then cooled to RT. The solution was washed with 10% $HCl_{(aq)}$ (2 × 100 mL) and water (2 × 100 mL), and the organic layer dried over anhydrous $MgSO_4$, then the solvent was removed *in vacuo*. The resulting yellow solid was purified using column chromatography (silica; 95:5 $CH_2Cl_2$/MeOH) to give a white solid (0.292 g, 46%).

**$^1$H NMR** (300 MHz, $CDCl_3$) δ (ppm): 9.21 (2H, s, pyridinium $H^2$ & $H^6$), 8.19 (1H, s, pyridinium $H^4$), 6.77 (8H, s, hydroquinone Ar*H*), 6.69 – 6.74 (2H, m, N*H*), 4.11 (4H, t, $^3J$ = 5.0 Hz, $CH_2$), 4.05 (4H, t, $^3J$ = 5.0 Hz, $CH_2$), 3.82 – 3.90 (8H, m, $CH_2$), 3.72 (4H, s, $CH_2$); **$^{13}$C NMR** (75.5 MHz, $CDCl_3$): 165.0, 151.7, 136.4, 131.5, 129.2, 121.3, 115.8, 115.2, 70.9, 69.7, 68.2, 67.0, 39.7; **HRMS (ESI)**: *m/z* calc for $C_{29}H_{33}N_3O_8$ $[M + H]^+$: 552.2340; found: 552.2342.

**Pyridinium 4-oxygen polyether macrocycle iodide salt (31·I):**

Macrocycle **30** (50 mg, 0.09 mmol) and MeI (2 mL) were heated at reflux under $N_{2(g)}$ for 16 h. The reaction mixture was cooled to RT and the MeI removed *in vacuo* to yield a pale yellow solid (61 mg, 97%).

**$^1$H NMR** (300 MHz, $CDCl_3$) δ (ppm): 9.45 (1H, s, pyridinium $H^4$), 9.01 (2H, s, pyridinium $H^2$ & $H^6$), 8.96 (2H, t, $^3J$ = 5.3 Hz, N*H*), 6.76, (4H, d, $^3J$ = 8.8 Hz, hydroquinone Ar*H*), 6.60,

(4H, d, $^3J$ = 8.8 Hz, hydroquinone Ar*H*), 4.15 – 4.18 (8H, m, C*H*$_2$), 3.95 – 4.00 (4H, m, C*H*$_2$), 3.81 – 3.85 (8H, m, C*H*$_2$), 3.71 (3H, s, $N^+CH_3$); **$^{13}$C NMR** (75.5 MHz, $CDCl_3$) δ (ppm): 161.4, 152.4, 152.1, 147.3, 140.3, 134.0, 115.8, 114.7, 70.7, 69.9, 67.6, 65.9, 48.5, 40.1; **HRMS (ESI)**: *m/z* calc. for $C_{30}H_{36}N_3O_8$·I $[M - I]^+$: 556.2497; found: 566.2487.

**Isophthalamide Catenane 5-oxygen polyether chain Chloride salt** (**32**·Cl)**:**

Macrocycle **31**·I (75 mg, 0.108 mmol), and bis-amine **4** (50 mg, 0.108 mmol) were dissolved in dry $CH_2Cl_2$ (20 mL) and the solution stirred under $N_2$ for 5 min. Triethylamine (38 μL, 0.27 mmol) was added, followed immediately by isophthaloyl dichloride (22 mg, 0.108 mmol) in dry $CH_2Cl_2$ (2 mL) and the resulting solution stirred under $N_{2(g)}$ for 1 h at RT. The solution was washed with 10% $HCl_{(aq)}$ (2 × 20 mL) and $H_2O$ (2 × 20 mL), and the organic phase dried over anhydrous $MgSO_4$ then the solvent removed *in vacuo*. The crude yellow solid was purified by preparative TLC (9:1 $CH_2Cl_2$/MeOH & 9:1 EtOAc/MeOH) to give a pale yellow solid (45 mg, 35%).

**$^1$H NMR** (300 MHz, 1:1 $CDCl_3$/$CD_3OD$) δ (ppm): 9.14 (1H, s, pyridinium *H*$^4$), 8.77 (2H, s, pyridinium *H*$^2$ & *H*$^6$), 8.74 (1H, s, isophthalamide *H*$^5$), 8.51 (2H, t, $^3J$ = 5.3 Hz, pyridinium N*H*), 8.44 (2H, t, $^3J$ = 4.4 Hz, isophthalamide N*H*), 8.11 (2H, d, $^3J$ = 7.9 Hz, isophthalamide *H*$^4$ & *H*$^6$), 7.62 (1H, t, $^3J$ = 7.9 Hz, isophthalamide *H*$^2$), 6.72 (4H, d, $^3J$ = 9.4 Hz, pyridinium macrocycle hydroquinone Ar*H*), 6.67 (4H, $^3J$ = 9.4 Hz, pyridinium macrocycle hydroquinone Ar*H*), 6.39 (4H, d, $^3J$ = 9.1 Hz, isophthalamide macrocycle hydroquinone Ar*H*), 6.21 (4H, d, $^3J$ = 9.1 Hz, isophthalamide macrocycle hydroquinone Ar*H*), 4.25 (3H, s, $N^+CH_3$), 4.01 – 4.05 (8H, m, C*H*$_2$), 3.80 – 3.83 (8H, m, C*H*$_2$), 3.58 – 3.75 (28H, m, C*H*$_2$); **$^{13}$C NMR** (75.5 MHz, 1:1 $CDCl_3$/$CD_3OD$) δ (ppm): 168.4, 161.5, 153.9, 153.6, 153.4, 152.6, 146.2, 139.3, 134.5, 133.9, 132.1, 129.9, 125.7, 116.4, 115.6, 115.5, 115.3, 71.3, 71.2, 71.1, 70.6, 70.3, 68.6, 68.5, 66.8, 66.5, 50.1, 41.1, 40.9; **HRMS (ESI)**: *m/z* calc. for $C_{62}H_{74}N_5O_{17}$·Cl $[M - Cl]^+$: 1160.5074, found 1160.5225.

**Isophthalamide Catenane 5-oxygen polyether chain Hexafluorophosphate salt (32·$PF_6$):**

Catenane **32**·Cl (45 mg, 0.0376 mmol) was dissolved in $CHCl_3$ (20 ml) and washed with 0.1 M $NH_4PF_{6(aq)}$ (8 × 20 mL), and $H_2O$ (2 × 20 mL). The organic layer was dried over anhydrous $MgSO_4$, and the solvent removed *in vacuo* to give a yellow solid (47 mg, 95%).

**$^1$H NMR** (300 MHz, 1:1 $CDCl_3$/$CD_3OD$) δ (ppm): 9.00 (1H, s, pyridinium *H*$^4$), 8.54 (2H, s, pyridinium *H*$^2$ & *H*$^6$), 8.31 (2H, t, $^3J$ = 5.0 Hz, pyridinium N*H*), 8.29 (1H, s, isophthalamide *H*$^5$), 8.03 (2H, dd, $^3J$ = 7.8 Hz, $^4J$ = 1.7 Hz, isophthalamide *H*$^4$ & *H*$^6$), 7.94 (2H, t, $^3J$ = 5.5 Hz, isophthalamide N*H*), 7.62 (1H, t, $^3J$ = 7.8 Hz, isophthalamide *H*$^2$), 6.71 (4H, d, $^3J$ = 9.5 Hz, pyridinium macrocycle hydroquinone Ar*H*), 6.66 (4H, $^3J$ = 9.5 Hz, pyridinium macrocycle hydroquinone Ar*H*), 6.47 (4H, d, $^3J$ = 9.1 Hz, isophthalamide macrocycle hydroquinone Ar*H*), 6.29 (4H, d, $^3J$ = 9.1 Hz, isophthalamide macrocycle hydroquinone Ar*H*), 3.98 – 4.04 (11H, m , C*H*$_2$ & $N^+CH_3$), 3.87 (4H, t, $^3J$ = 4.7 Hz, C*H*$_2$), 3.73 – 3.81 (8H, m, C*H*$_2$), 3.64 – 3.67 (12H, m, C*H*$_2$), 3.56 – 3.60 (8H, m, C*H*$_2$), 3.48 – 3.49 (4H, m, C*H*$_2$); **$^{13}$C NMR** (75.5 MHz, 1:1 $CDCl_3$/$CD_3OD$) δ (ppm): 168.5, 161.8, 161.7, 153.7, 153.6, 153.2, 152.6, 146.1, 141.7, 134.9, 134.2, 131.6, 129.8, 125.6, 116.1, 115.8, 115.5, 115.3, 78.5, 71.2, 71.0, 70.5, 70.3, 68.5, 68.2, 67.1, 66.6, 41.2, 40.4; **$^{19}$F NMR** (282.4 MHz, 1:1 $CDCl_3$/$CD_3OD$) δ (ppm): −72.7 (d, $^1J$ = 710 Hz, P*F*$_6$); **$^{31}$P NMR** (121.6 MHz, 1:1 $CDCl_3$/$CD_3OD$) δ (ppm): -140.1 (sept, $^1J$ = 710 Hz, *P*$F_6$); **HRMS (ESI):** *m/z* calc. for $C_{62}H_{74}N_5O_{17}$·$PF_6$ $[M - PF_6]^+$: calc. 1160.5074, found 1160.5225.

**Isophthalamide Catenane 4-oxygen polyether chain Chloride salt (33·Cl):**

Macrocycle **31**·I (63 mg, 0.09 mmol), and bis-amine **17** (43 mg, 0.09 mmol) were dissolved in dry $CH_2Cl_2$ (20 mL) and the solution stirred under $N_{2(g)}$ for 5 min. Triethylamine (32 μL, 0.225 mmol) was added, followed immediately by isophthaloyl dichloride (18 mg, 0.09 mmol) in dry $CH_2Cl_2$ (2 mL) and the resulting solution stirred under $N_{2(g)}$ for 1 h at RT. The solution was washed with 10% $HCl_{(aq)}$ (2 × 20 mL) and $H_2O$ (2 × 20 mL), and the organic

phase dried over anhydrous $MgSO_4$ and the solvent removed *in vacuo*. The crude yellow solid was purified by preparative TLC (93:7 $CHCl_3$/MeOH & 8:2 EtOAc/MeOH) to give a pale yellow solid (28.3 mg, 29%).

**$^1$H NMR** (300 MHz, $CDCl_3$) δ (ppm): 9.55 (1H, s, pyridinium $H^4$), 9.23 (2H, s, pyridinium $H^2$ & $H^6$), 9.15 (1H, s, isophthalamide $H^2$), 8.61 (2H, s, isophthalamide N*H*), 8.50 (2H, s, pyridinium N*H*), 8.27 (2H, d, $^3J$ = 7.7 Hz, isophthalamide $H^4$ & $H^6$), 7.61 (1H, t, $^3J$ = 7.7 Hz, isophthalamide $H^5$), 6.75 (8H, q, $^3J$ = 9.3 Hz, pyridinium macrocycle hydroquinone Ar*H*), 6.24 (4H, d, $^3J$ = 8.8 Hz, isophthalamide macrocycle hydroquinone Ar*H*), 5.98 (4H, d, $^3J$ = 8.8 Hz, isophthalamide macrocycle hydroquinone Ar*H*), 4.56 (3H, s, $N^+CH_3$), 3.47 – 4.11 (40H, m, $CH_2$); **$^{13}$C NMR** (75.5 MHz, 1:1 $CDCl_3$/$CD_3OD$) δ (ppm): 168.3, 161.5, 153.4, 152.1, 147.0, 138.9, 134.4, 133.2, 132.0, 129.4, 125.9, 116.3, 115.5, 115.0, 114.3, 78.4, 71.4, 71.1, 70.7, 70.3, 68.5, 67.6, 66.7, 66.0, 41.1, 40.9, 40.7; **HRMS (ESI)**: *m/z* calc. for $C_{60}H_{70}N_5O_{16}Cl$ $[M - Cl]^+$ 1116.4812 found 1116.4756.

**Isophthalamide Catenane 4-oxygen polyether chain Hexafluorophosphate salt (33·$PF_6$):**

Catenane **33**·Cl (39 mg, 0.03 mmol) was dissolved in $CHCl_3$ (20 mL) and washed with 0.1M $NH_4PF_{6(aq)}$ (8 × 20 mL), and $H_2O$ (2 × 20 mL). The organic layer was dried over anhydrous $MgSO_4$, and the solvent removed *in vacuo* to give a yellow solid (42 mg, 100%). **$^1$H NMR** (300 MHz, $CDCl_3$) δ (ppm): 8.88 (2H, s, pyridinium $H^2$ & $H^6$), 8.73 (1H, s, pyridinium $H^4$), 8.36 (1H, s, isophthalamide $H^2$), 7.98 (2H, dd, $^3J$ = 7.8 Hz, $^4J$ = 1.6 Hz, isophthalamide $H^4$ & $H^6$), 7.61 (1H, t, $^3J$ = 7.8 Hz, isophthalamide $H^5$), 6.61 – 6.68 (8H, m, pyridinium macrocycle hydroquinone Ar*H*), 6.25 (4H, d, $^3J$ = 9.1 Hz, isophthalamide macrocycle hydroquinone Ar*H*), 6.14 (4H, d, $^3J$ = 9.1 Hz, isophthalamide macrocycle hydroquinone Ar*H*), 4.36 (3H, s, $N^+CH_3$), 3.93 – 4.00, (8H, m, $CH_2$), 3.82 (4H, s, $CH_2$), 3.68 – 3.76 (20H, m, $CH_2$), 3.65 (4H, s, $CH_2$), 3.52 (4H, br s, $CH_2$); **$^{13}$C NMR** (75.5 MHz, 1:1 $CDCl_3$/$CD_3OD$) δ (ppm): 168.4, 161.5, 153.6, 153.2, 153.1, 151.9, 146.6, 140.2, 134.7,

133.5, 131.4, 129.7, 126.3, 115.9, 115.5, 115.1, 114.4, 78.3, 71.3, 71.2, 70.6, 70.4, 68.4, 67.6, 66.5, 66.4, 40.9, 40.2; **$^{19}$F NMR** (282.4 MHz, 1:1 $CDCl_3/CD_3OD$) δ (ppm): −72.7 (d, $^1J$ = 710 Hz, P$F_6$); **$^{31}$P NMR** (121.6 MHz, 1:1 $CDCl_3/CD_3OD$) δ (ppm): −140.1 (sept, $^1J$ = 710 Hz, *P*$F_6$); **HRMS (ESI):** *m/z* calc. for $C_{60}H_{70}N_5O_{16}{\cdot}PF_6$ $[M - PF_6]^+$: 1116.4812; found: 1116.4815.

## 5.2.2 Experimental Details for Chapter 3

**Bipyridine Macrocycle (34)[5]:**

2,2'-bipyridine-4,4'-dicarboxylic acid (44 mg, 0.180 mmol) was suspended in $SOCl_2$ (10 mL), pyridine (cat.) was added, and the mixture heated at reflux for 16 h, by which time the solution had become homogeneous. The $SOCl_2$ was removed by distillation, and the residue redissolved in dry $CH_2Cl_2$ (5 mL) and added dropwise to a solution of bis-amine **17** (75 mg, 0.178 mmol), template **6**·Cl (69 mg, 0.180 mmol) and $Et_3N$ (63 µL, 0.452 mmol) in dry $CH_2Cl_2$ (20 mL). The reaction was stirred for 1 h under $N_{2(g)}$, washed with 10% $HCl_{(aq)}$ (2 × 50 mL), and $H_2O$ (2 × 50 mL), dried over anhydrous $MgSO_4$ and solvent removed *in vacuo*. The resulting crude material was purified by column chromatography (silica; 9:1 $CH_2Cl_2$/MeOH) to give a white solid (40 mg, 36 %).

**$^1$H NMR** (300 MHz, $CDCl_3$) δ (ppm): 8.83 (2H, d, $^3J$ = 5.0 Hz, bipy $H^6$), 8.47 (2H, s, bipy $H^3$), 7.73 (2H, dd, $^3J$ = 5.0 Hz, $^4J$ = 1.8 Hz, bipy $H^5$), 6.78 (10H, s, hydroquinone Ar*H* & N*H*), 4.14 (4H, t, $^3J$ = 4.4 Hz, C$H_2$), 4.02 (4H, t, $^3J$ = 4.4 Hz, C$H_2$), 3.89 (4H, q, $^3J$ = 4.4 Hz, C$H_2$), 3.78 (4H, t, $^3J$ = 4.4 Hz, C$H_2$), 3.67 (4H, s, C$H_2$); **$^{13}$C NMR** (125 MHz, $CDCl_3$) δ (ppm): 165.6, 156.6, 153.6, 153.2, 150.6, 142.9, 122.2, 118.4, 116.0, 115.8, 71.0, 69.9, 68.4, 67.4, 40.3; **HRMS (ESI):** *m/z* calc. for $C_{34}H_{36}N_4O_6$ $[M + Na]^+$: 651.2425; found: 651.2423.

**Rhenium Macrocycle (35):**

Macrocycle **34** (46 mg, 0.073 mmol) and $Re(CO)_5Cl$ (27 mg, 0.075 mmol) were dissolved in THF (10 mL) and heated at reflux under $N_2$ for 16 h. The mixture was filtered to give the product as an orange solid (64 mg, 95%).

**$^1$H NMR** (300 MHz, $d_6$-DMSO) δ (ppm): 9.44 (2H, t, $^3J$ = 5.2 Hz, N*H*), 9.18 (2H, d, $^3J$ = 5.8 Hz, bipy $H^6$), 9.09 (2H, s, bipy $H^3$), 8.07 (2H, dd, $^3J$ = 5.8 Hz, $^4J$ = 1.8 Hz, bipy $H^5$), 6.83 – 6.93 (8H, m, hydroquinone Ar*H*), 4.13 (4H, t, $^3J$ = 5.3 Hz, C$H_2$), 3.98 – 4.00 (4H, m, C$H_2$), 3.68 – 3.75 (8H, m, C$H_2$), 3.59 (4H, s, C$H_2$); **$^{13}$C NMR** (125 MHz, $d_6$-DMSO) δ (ppm): 197.5, 189.5, 163.5, 155.6, 153.8, 152.8, 152.3, 144.4, 125.8, 122.1, 115.5, 115.4, 70.0, 68.9, 67.7, 66.3; **HRMS (ESI)** calculated for $C_{37}H_{36}N_4O_{11}Re$ $[M + Na]^+$: 957.1512; found: 957.1514.

**Ruthenium Macrocycle (36·$(PF_6)_2$):**

Macrocycle **34** (30 mg, 0.048 mmol) and $Ru(bipy)_2Cl_2$ (23 mg, 0.048 mmol) were suspended in 9:1 EtOH/$H_2O$ (10 mL) and heated at reflux under $N_{2(g)}$ for 16 h. The red solution was cooled to RT and the solvent removed *in vacuo*. The resulting solid was redissolved in $H_2O$ (20 ml) and $NH_4PF_6$ added until precipitation ceased. The precipitate was collected by vacuum filtration and dried under vacuum for 2 h, giving a red solid (50 mg, 78%).

**$^1$H NMR** (300 MHz, $d_6$-acetone) δ (ppm): 9.20 (2H, s, macrocycle bipy $H^3$), 8.83 (4H, d, $^3J$ = 8.2 Hz, bipy $H^3$), 8.59 (2H, br s , N*H*), 8.19 – 8.27 (6H, m, macrocycle bipy $H^4$ & bipy $H^4$), 8.04 – 8.10 (4H, m, bipy $H^6$), 7.93 (2H, dd, $^3J$ = 5.8 Hz, $^4J$ = 1.8 Hz, macrocycle bipy $H^5$), 7.52 – 7.62 (4H, m, bipy $H^5$), 6.87 (8H, s, hydroquinone ArH), 4.13 (4H, t, $^3J$ = 5.3 Hz, C$H_2$), 4.04 – 4.07 (4H, m, C$H_2$), 3.79 – 3.81 (8H, m, C$H_2$), 3.67 (4H, s, C$H_2$); **$^{13}$C NMR** (125 MHz, $d_6$-acetone) δ (ppm): 164.5, 158.9, 158.2, 154.7, 154.0, 153.8, 153.2, 152.9, 143.8, 139.6, 129.2, 126.7, 125.7, 123.1, 116.8, 116.6, 71.8, 70.6, 69.4, 67.6, 40.9; **$^{19}$F NMR** (300 MHz, $d_6$-acetone) δ (ppm): −72.7 (d, $^1J$ = 710 Hz, P$F_6$); **$^{31}$P NMR** (300 MHz, $d_6$-acetone) δ (ppm):

−140.1 (sept, $^{1}J$ = 710 Hz, $PF_6$); **HRMS (ESI):** calc. for $C_{54}H_{52}N_8O_{11}Ru\cdot(PF_6)_2$ $[M - PF_6]^+$: 1187.2603; found: 1187.2431.

**Bipyridine Rotaxane (37·Cl):**

Following the general procedure for rotaxane formation using 2,2'-bipyridine-4,4'-dicarboxylic acid (24 mg, 0.097 mmol), bis-amine **17** (41 mg, 0.097 mmol), axle **13**·Cl (100 mg, 0.097 mmol), and $Et_3N$ (34 µL, 0.24 mmol). The resulting residue was redissolved in MeCN (50 mL), filtered and the solvent removed *in vacuo*. It was not possible to isolate the rotaxane from its component macrocycle using column chromatography (silica; 9:1 $CH_2Cl_2$/MeOH).

**Rhenium Rotaxane (38·$PF_6$):**

Following the procedure for bipyridine rotaxane (**37**·Cl) synthesis; the resulting residue and $Re(CO)_5Cl$ (9 mg, 0.025 mmol) were dissolved in THF (5 mL) and heated at reflux under $N_{2(g)}$ for 16 h. The solution was cooled to RT and the solvent removed *in vacuo*. The resulting residue was purified by preparative TLC (silica; 95:5 $CH_2Cl_2$/MeOH) then redissolved in $CHCl_3$ (10 mL) and washed with 0.1 M $NH_4PF_{6(aq)}$ (10 × 10 mL) and $H_2O$ (2 × 10 mL). The organic phase was dried over anhydrous $MgSO_4$ and the solvent removed *in vacuo* to give a bright orange solid (26 mg, 13%).

**$^{1}$H NMR** (300 MHz, $CDCl_3$) δ (ppm): 10.02 (2H, s, axle N*H*), 9.77 (1H, br s, pyridinium $H^2$), 9.27 – 9.29 (4H, m, pyridinium $H^4$ & $H^6$ & bipy $H^3$), 9.19 (2H, d, $^{3}J$ = 5.9 Hz, bipy $H^6$), 8.64 (2H, br s, macrocycle N*H*), 8.11 (2H, dd, $^{3}J$ = 5.9 Hz, $^{4}J$ = 1.8 Hz, bipy $H^5$), 7.72 (4H, d, $^{3}J$ = 6.7 Hz, Ar*H*NH), 7.11 – 7.37 (15H, m, stopper Ar*H*), 6.58 (4H, d, $^{3}J$ = 8.8 Hz, hydroquinone Ar*H*), 6.40 (4H, d, $^{3}J$ = 8.8 Hz, hydroquinone Ar*H*), 4.71 (3H, s, $N^+CH_3$), 4.07 (4H, t, $^{3}J$ = 5.3 Hz, C$H_2$), 4.00 – 4.01 (4H, m, C$H_2$), 3.91 (8H, s, C$H_2$), 3.66 (4H, br s, C$H_2$), 1.31 (36H, s, $^{t}$Bu); **$^{13}$C NMR** (125 MHz, $d_6$-acetone) δ (ppm): 198.5, 190.6, 164.7, 159.8, 157.5, 155.1, 153.8, 153.7, 149.8, 148.4, 145.7, 145.2, 145.1, 136.7, 135.1, 132.8, 132.7,

132.2, 131.9, 128.9, 127.3, 126.9, 125.8, 123.5, 121.4, 121.3, 117.2, 115.9, 71.9, 71.3, 68.9, 68.0, 65.2, 55.9, 40.8, 35.3, 32.1; **$^{19}$F NMR** (282.4 MHz, $d_6$-acetone ) δ (ppm): −72.4 (d, $^1J$ = 710 Hz, P$F_6$); **$^{31}$P NMR** (121.6 MHz, $d_6$-acetone) δ (ppm): −144.4 (sept, $^1J$ = 710 Hz, $P$F$_6$); **MS (ESI):** *m/z* calc. for $C_{111}H_{114}N_7O_{13}ReCl{\cdot}Cl$ $[M - Cl]^+$: 1975.77; found: 1975.79.

**Ruthenium Rotaxane (39·(PF$_6$)$_2$)**

Following the procedure for bipyridine rotaxane (**37**·Cl) synthesis; the resulting residue and Ru(bipy)$_2$Cl$_2$ (35 mg, 0.067 mmol) were suspended in 9:1 EtOH/$H_2O$ (10 mL) and heated at reflux under $N_{2(g)}$ for 16 h. The solution was cooled to RT and the solvent removed *in vacuo*. The resulting residue was purified by column chromatography (silica; 28:2:1 MeCN/$H_2O$/sat. $KNO_{3(aq)}$), the MeCN removed *in vacuo*, the resulting residue dissolved in $CHCl_3$ (25 mL) and $H_2O$ (25 mL) and $NH_4PF_6$ (10 mg, 0.061 mmol) added. The biphasic mixture was stirred for 30 min, the organic layer washed with $H_2O$ (2 × 30 mL), dried over anhydrous $MgSO_4$, and the solvent removed *in vacuo* to give a red solid (24 mg, 10%).

**$^1$H NMR** (300MHz, $d_6$-acetone) δ (ppm): 9.97 (2H, s, axle N*H*), 9.61 (1H, s, pyridinium $H^4$), 9.32 (2H, s, macrocycle bipy $H^3$), 9.24 (2H, s, pyridinium $H^2$ & $H^6$), 8.83 (4H, t, $^3J$ = 8.8 Hz, bipy $H^3$), 8.33 (2H, br s, macrocycle N*H*), 8.24 (4H, d, $^3J$ = 6.4 Hz, bipy Ar*H*), 8.12 (2H, t, $^3J$ = 7.7 Hz, bipy Ar*H*), 8.03 (2H, d, $^3J$ = 6.4 Hz, bipy Ar*H*), 7.98 (2H, d, $^3J$ = 5.3 Hz, bipy Ar*H*), 7.89 (2H, d $^3J$ = 5.3 Hz, bipy Ar*H*), 7.67 (4H, d, $^3J$ = 7.6 Hz, Ar*H*NH), 7.60 (2H, t, $^3J$ = 6.6 Hz, bipy Ar*H*), 7.12 – 7.35 (30H, m, stopper Ar*H*), 6.61 (4H, d, $^3J$ = 8.8 Hz, hydroquinone Ar*H*), 6.42 (4H, d, $^3J$ = 8.8 Hz, hydroquinone Ar*H*), 4.64 (3H, s, $N^+CH_3$), 3.98 – 4.02 (8H, m, C$H_2$), 3.93 (8H, s, C$H_2$), 3.63 (4H, br s, C$H_2$), 1.30 (36H, s, $^t$Bu); **$^{13}$C NMR** (125 MHz, $d_6$-acetone) δ (ppm): 164.4, 159.7, 158.6, 157.9, 157.9, 153.4, 153.3, 153.2, 152.6, 149.5, 147.9, 145.3, 144.7, 147.5, 143.4, 139.4, 139.3, 136.3, 134.9, 132.3, 131.7, 131.5, 129.0, 128.9, 128.5, 126.9, 126.5, 125.5, 125.4, 123.3, 121.1, 116.6, 115.5, 71.5, 70.9, 68.4, 67.5, 64.7, 55.5, 40.3, 35.0, 31.7; **$^{19}$F NMR** (300 MHz, $d_6$-acetone) δ (ppm): −72.2 (d, $^1J$ = 709 Hz, P$F_6$);

**$^{31}$P NMR** (300 MHz, $d_6$-acetone) δ (ppm): −140.1 (sept, $^1J$ = 709 Hz, $PF_6$); **MS (MALDI-TOF):** *m/z* calc. for $C_{128}H_{130}N_{11}O_{10}Ru{\cdot}(PF_6)_3$ $[M - PF_6]^+$: 2373.8; found: 2374.4.

**5-nitro-1,10-phenanthroline (40)[9]:**

1,10-Phenanthroline (1.0 g, 5.04 mmol) was dissolved in fuming $H_2SO_4$ (20 mL), conc. $HNO_3$ (10 mL) was added with care and the solution was heated at 120 °C for 1 h. The mixture was poured onto crushed ice (20 g) and once the ice had melted was treated with 30% $NaOH_{(aq)}$ until pH = 7. Sufficient conc. $HNO_3$ was added to allow for a weakly acidic solution and the resulting precipitate was filtered under reduced pressure and washed with cold $H_2O$ (2 × 100 mL). The solid was dried under vacuum and purified by column chromatography (silica; acetone, dry load) to yield an off-white solid (0.647 g, 57%).

**$^1$H NMR** (300 MHz, $CD_3OD$) δ (ppm): 9.28 (1H, dd, $^3J$ = 4.7 Hz, $^4J$ = 1.5 Hz, phen $H^4$), 9.24 (1H, dd, $^3J$ = 4.7 Hz, $^4J$ = 1.5 Hz, phen $H^2$), 9.03 (1H, dd, $^3J$ = 8.5 Hz, $^4J$ = 1.5 Hz, phen $H^9$), 8.90 (1H, s, phen $H^6$), 8.71 (1H, dd, $^3J$ = 4.7 Hz, $^4J$ = 1.5 Hz, phen $H^2$), 7.92 – 7.97 (2H, m, phen $H^3$ & $H^8$); **MS (ESI):** *m/z* calc. for $C_{12}H_7N_3O_2$ $[M + Na]^+$: 248.04; found: 248.05

**5-amino-1,10-phenanthroline (41)[10]:**

Hydrazine monohydrate (2.2 mL, 42.6 mmol) was added to a suspension of compound **40** (0.55 g, 2.44 mmol) and Pd/C (0.055 g, 10% by weight) in degassed EtOH (50 mL) and stirred at RT under $N_2$ for 1 h. The reaction was then heated at reflux for 24 h, cooled to RT and filtered to remove the catalyst. The solvent was removed *in vacuo* and the solid washed with $Et_2O$ (2 × 50 mL) to remove any remaining hydrazine then dried under vacuum. The resulting dark yellow solid was dissolved in $CHCl_3$ (100 mL), filtered, and the solvent removed *in vacuo* to give a bright yellow solid (0.40 g, 84%).

**$^1$H NMR** (200 MHz, $d_6$-DMSO) δ (ppm): 9.05 (1H, dd, $^3J$ = 4.4 Hz, $^4J$ = 1.7 Hz, phen $H^9$), 8.65 – 8.70 (2H, m, phen $H^2$ & $H^7$), 8.04 (1H, dd, $^3J$ = 8.2 Hz, $^4J$ = 1.7 Hz, phen $H^4$), 7.73 (1H, dd, $^3J_1$ = $^3J_2$ = 4.3 Hz, phen $H^8$), 7.50 (1H, dd, $^3J_1$ = $^3J_2$ = 4.3 Hz, phen $H^3$), 6.86 (1H, s,

phen $H^6$), 6.15 (2H, br s, N$H_2$). **MS (ESI):** *m/z* calc. for $C_{12}H_9N_3$ $[M + H]^+$: 196.09; found: 196.08.[10]

**Ruthenium Stopper 42**·$(PF_6)_2$:

Compound **41** (0.300 g, 1.54 mmol) and $Ru(bipy)_2Cl_2$ (0.745 g, 1.54 mmol) were suspended in 9:1 EtOH/$H_2O$ and heated at reflux under $N_{2(g)}$ for 16 h during which a colour change from dark purple to red was observed. The solution was cooled to RT, and the solvent removed *in vacuo*. The resulting red residue was dissolved in $H_2O$ (100 mL) and $NH_4PF_6$ added until no further precipitation was observed. The precipitate was collected by vacuum filtration and dried under vacuum giving a red solid (1.38 g, 100%).

**$^1$H NMR** (300 MHz, $d_6$-acetone) δ (ppm): 8.95 (1H, dd, $^3J$ = 8.5 Hz $^4J$ = 1.2 Hz, bipy Ar*H*), 8.80 – 8.86 (4H, m, bipy Ar*H*), 8.40 (1H, dd, $^3J$ = 5.3 Hz, $^4J$ = 1.2Hz, bipy ArH), 8.35 (1H, dd, $^3J$ = 8.2 Hz, $^4J$ = 1.2Hz, bipy ArH), 8.12 – 8.28 (5H, m, Ar*H*), 7.96 (1H, dd, $^3J$ = 5.3 Hz, $^4J$ = 1.2Hz, bipy ArH),7.85 – 7.93 (3H, m, ArH), 7.40 – 7.46 (2H, m, ArH), 7.30 (1H, s, phen H$^6$), 6.45 (2H, br s, N$H_2$); **$^{13}$C NMR** (300 MHz, $d_6$-acetone) δ (ppm): 158.1, 158.0, 157.9, 157.8, 152.9, 152.6, 152.6 (*sic*), 152.5, 152.4, 149.0, 147.9, 145.6, 142.4, 138.6, 138.5, 134.4, 133.7, 132.3, 128.5, 128.4, 128.4, 128.3, 126.7, 125.7, 125.0, 124.9, 124.9, 124.9, 124.6; **$^{19}$F NMR** (282.4 MHz, $d_6$-acetone) δ (ppm): −72.5 (d, $^1J$ = 700 Hz, P$F_6$); **$^{31}$P NMR** (121.6 MHz, $d_6$-acetone) δ (ppm): −144.2 (sept, $^1J$ = 700 Hz, $P$F$_6$); **HRMS (ESI):** *m/z* calc. for $C_{32}H_{25}N_7Ru$·$(PF_6)_2$ $[M - 2PF_6]^{2+}$ 304.5606, found 304.5598.

**Ruthenium Nicotinamide Stopper 43**·$(PF_6)_2$:

Nicotinic acid (0.274 g, 2.23 mmol) was suspended in dry $CH_2Cl_2$ (10 mL), $SOCl_2$ (1.05 mL, 14.4 mmol) and cat. DMF added and the reaction heated at reflux for 1.5 h under $N_{2(g)}$. The solution was cooled to RT, cooled to −32 °C for 2 h, the white crystals isolated by filtration, and washed with $CHCl_3$ (2 × 20 mL). This white solid was added to a solution of ruthenium stopper **42**·$(PF_6)_2$ (0.200 g, 0.223 mmol), $Et_3N$ (0.350 mL, 2.50 mmol) and cat. DMAP in dry

MeCN (8 mL) and the mixture subjected to microwave irradiation at 150 °C for 2 h. The solvent was removed *in vacuo* and the resulting residue purified by column chromatography (silica; 14:2:1 MeCN/$H_2O$/sat. $KNO_{3(aq)}$). The MeCN was removed *in vacuo* before adding $H_2O$ (30 mL) and $NH_4PF_6$ (0.218 g, 1.33 mmol), giving an orange precipitate which was filtered and re-dissolved in acetone (30 mL). The acetone was removed *in vacuo* to give the product as a red solid (0.206 g, 92%).

**$^1$H NMR** (300 MHz, $d_6$-acetone) δ (ppm): 10.51 (1H, br s, N*H*), 9.32 (1H, br s, pyridine $H^2$), 9.06 (1H, dd, $^3J$ = 8.8 Hz, $^4J$ = 1.2 Hz, pyridine $H^4$), 8.91 – 8.78 (6H, m, Ar*H*), 8.72 (1H, s, phen $H^6$), 8.54 – 8.46 (2H, m, Ar*H*), 8.40 (1H, dd, $^3J$ = 5.3 Hz, $^4J$ = 1.2 Hz, Ar*H*), 8.31– 8.10 (6H, m, Ar*H*), 7.98 – 7.88 (4H, m, Ar*H*), 7.68 – 7.58 (3H, m, Ar*H*), 7.46 – 7.37 (2H, m, Ar*H*); **$^{19}$F NMR** (282.4 MHz, $d_6$-acetone) δ (ppm): −72.6 (d, $^1J$ = 700 Hz, P$F_6$); **$^{31}$P NMR** (121.6 MHz, $d_6$-acetone) δ (ppm): −144.3 (sept, $^1J$ = 700 Hz, $PF_6$); **$^{13}$C NMR** (75.5 MHz, $d_6$-acetone) δ (ppm): 166.5, 158.4, 158.1, 153.8, 153.6, 153.0, 152.9, 150.0, 148.9, 148.7, 146.9, 139.0, 138.9, 137.5, 136.6, 135.2, 134.4, 131.6, 130.9, 128.8, 128.7, 128.3, 127.5, 126.8, 125.4, 125.3, 124.6, 122.9; **HRMS (ESI):** *m/z* calc. for $C_{38}H_{28}N_8ORu\cdot(PF_6)_2$ [M − $PF_6$]$^+$: 859.1076; found: 859.1072.

**Ruthenium Pyridinium Nicotinamide Thread 44**·$(PF_6)_3$:

Ruthenium nicotinamide stopper **43**·$(PF_6)_2$ (100 mg, 0.0996 mmol) and bromohexane (43 μL, 0.306 mmol) were dissolved in dry MeCN (4 mL) and the reaction was subjected to microwave irradiation at 175 °C for 1 h. The solvent was removed *in vacuo* and the resulting residue was purified by column chromatography (silica; 14:2:1 MeCN/$H_2O$/sat. $KNO_{3(aq)}$). The MeCN was removed *in vacuo*, the residue redissolved in $H_2O$ (10 mL) and $NH_4PF_6$ added until no further precipitate was observed. The precipitate was filtered and dried under vacuum for 3 h, giving a red solid (65.6 mg, 53%).

**$^{1}$H NMR** (300 MHz, $d_6$-acetone) δ (ppm): 10.79 (1H, br s, N*H*), 9.83 (1H, s, pyridinium $H^2$), 9.47 – 9.34 (2H, m, pyridinium $H^4$ & $H^5$), 9.04 – 8.99 (1H, m, pyridinium $H^6$), 8.90 – 8.80 (5H, m, Ar*H*), 8.71 (1H, s, phen $H^6$), 8.60 – 8.48 (3H, m, Ar*H*), 8.44 (1H, dd, $^3J$ = 5.3 Hz, $^4J$ = 1.1 Hz, Ar*H*), 8.32 – 8.23 (3H, m, Ar*H*), 8.22 – 8.12 (3H, m, Ar*H*), 7.97 – 7.88 (3H, m, Ar*H*), 7.68 – 7.61 (2H, m, Ar*H*), 7.44 – 7.37 (2H, m, Ar*H*), 4.99 (2H, t, $^3J$ = 7.8 Hz, $N^+CH_2$), 2.30 – 2.18 (2H, m, $N^+CH_2CH_2$), 1.57 – 1.27 (6H, m, $CH_2$), 0.88 (3H, t, $^3J$ = 7.1 Hz, $CH_3$); **$^{19}$F NMR** (282.4 MHz, $d_6$-acetone) δ (ppm): −72.5 (d, $^1J$ = 700 Hz, $PF_6$); **$^{31}$P NMR** (121.6 MHz, $d_6$-acetone) δ (ppm): −138.5 (sept, $^1J$ = 700 Hz, $PF_6$); **$^{13}$C NMR** (75.5 MHz, $d_6$-acetone) δ (ppm): 162.9, 158.4, 158.1, 154.4, 154.0, 153.4, 153.0, 149.0, 147.9, 147.2, 146.0, 145.4, 144.8, 139.1, 138.9, 137.7, 135.8, 134.2, 134.1, 131.4, 129.5, 128.8, 128.6, 127.6, 126.9, 125.4, 125.3, 123.6, 63.5, 32.1, 31.9, 26.5, 23.1, 14.2; **HRMS (ESI):** *m/z* calc. for $C_{44}H_{41}N_8ORu\cdot(PF_6)_3$ $[M - 2PF_6]^{2+}$: 943.2017 found 943.1994

**Dimethyl pyridine-3,5-dicarboxylate (45):**

3,5-Pyridine dicarboxylic acid (2.5 g, 15.0 mmol) and conc. $H_2SO_4$ (8.5 mL) were dissolved in MeOH (9 mL) and subjected to microwave irradiation at 120 °C for 20 min. The solution was cooled to RT, slowly poured onto ice (50 g) and $NH_4OH_{(aq)}$ was added until the solution was strongly alkaline. The solution was extracted with $Et_2O$ (3 × 50 mL) and the combined organic layers dried over anhydrous $MgSO_4$. The solvent was removed *in vacuo* to give a white solid (2.58 g, 88%).

**$^{1}$H NMR** (200 MHz, $CDCl_3$) δ (ppm): 9.38 (2H, d, $^4J$ = 2.0 Hz, pyridine $H^2$ & $H^6$), 8.89 (1H, t, $^4J$ = 2.0 Hz, pyridine $H^4$), 4.00 (6H, s, $CH_3$); **MS (ESI):** *m/z* calc. for $C_9H_9NO_4$: 196.06; found: 196.07 $[M + H]^+$.[11]

**5-(methoxycarbonyl)nicotinic acid (46)[12]:**

Compound **45** (1.24 g, 6.35 mmol) was dissolved in 0.1 M KOH solution in MeOH (104 mL) and stirred for 16 h before the solvent was removed *in vacuo*. The resulting residue was

dissolved in $H_2O$ (50 mL) and extracted with $Et_2O$ (3 × 50 mL) to remove the bis-ester starting material. The aqueous layer was adjusted to pH = 7 using 10% citric $acid_{(aq)}$, and the precipitate collected by vacuum filtration, then dried under vacuum to give a white solid (1.19 g, 69%).

**$^1$H NMR** (200 MHz, $d_6$-DMSO) δ (ppm): 9.24 – 9.26 (2H, m, pyridine $H^2$ & $H^6$), 8.63 (1H, t, $^4J$ = 2.0 Hz, pyridine $H^4$), 3.91 (3H, s, $CH_3$); **MS (ESI):** *m/z* calc. for $C_8H_7NO_4$ $[M - H]^-$: 180.03; found 180.04.[12]

**Methyl 5-(hexylcarbamoyl)nicotinate (47):**

Compound **46** (852 mg, 4.70 mmol), EDCI (992 mg, 5.17 mmol) and DMAP (cat.) were dissolved in $CH_2Cl_2$ (150 mL) and stirred for 1 h at 0 °C. Hexylamine (0.69 mL, 5.19 mmol) and $Et_3N$ (0.80 mL, 5.71 mmol) were added at 0 °C and the reaction was stirred for 4 days at RT under $N_{2(g)}$. It was then washed with 10% citric $acid_{(aq)}$ (2 x 100 mL), 10% $KOH_{(aq)}$ (2 x 100 mL) and $H_2O$ (100 mL), and dried over anhydrous $MgSO_4$. The solvent was removed *in vacuo* and the resulting residue purified by column chromatography (silica; 95:5 $CH_2Cl_2$/MeOH) to give a white solid (517 mg, 42%).

**$^1$H NMR** (300 MHz, $CDCl_3$) δ (ppm): 9.32 (1H, d, $^4J$ = 2.1 Hz, pyridine $H^6$), 9.18 (1H, d, $^4J$ = 2.3 Hz, pyridine $H^2$), 8.64 – 8.62 (1H, m, pyridine $H^4$), 6.28 (1H, br s, N*H*), 3.99 (3H, s, $CH_3$), 3.54 – 3.46 (2H, m, NHC$H_2$), 1.70 – 1.59 (2H, m, $NHCH_2CH_2$), 1.44 – 1.29 (6H, m, $CH_2$), 0.90 (3H, t, $^3J$ = 7.0 Hz, $CH_3$); **$^{13}$C NMR** (75.5 MHz, $CDCl_3$) δ (ppm): 165.0, 164.6, 152.7, 151.9, 135.5, 130.2, 125.7, 52.6, 40.3, 31.4, 29.4, 26.6, 22.5, 13.9; **HRMS (ESI):** *m/z* calc. for $C_{14}H_{20}N_2O_3$ $[M + Na]^+$: 287.1366; found: 287.1370.

**5-(hexylcarbamoyl)nicotinic acid (48):**

Compound **47** (200 mg, 0.757 mmol) was dissolved in 1:1 THF/$H_2O$ (40 mL), 2 M $KOH_{(aq)}$ (0.45 mL) was added and the reaction stirred for 16 h at RT under $N_{2(g)}$ The solution was washed with $Et_2O$ (3 × 50 mL) and 10% citric $acid_{(aq)}$ added to the aqueous layer until pH = 7.

The resulting precipitate was collected by vacuum filtration and dried under vacuum, giving a white solid (81.9 mg, 43%).

**$^{1}$H NMR** (300 MHz, $d_6$-DMSO) δ (ppm): 9.20 – 9.14 (2H, m, pyridine $H^2$ & $H^6$), 8.84 (1H, t, $^{3}J$ = 5.5 Hz, N*H*), 8.67 – 8.65 (1H, m, pyridine $H^4$), 3.31 – 3.21 (2H, m, NHC$H_2$), 1.59 – 1.46 (2H, m, NHCH$_2$C$H_2$), 1.36 – 1.22 (6H, m, C$H_2$), 0.86 (3H, t, $^{3}J$ = 6.7 Hz, C$H_3$); **$^{13}$C NMR** (75.5 MHz, $d_6$-DMSO) δ (ppm): 165.9, 163.7, 152.1, 152.0, 135.5, 129.9, 126.3, 39.4, 31.0, 28.9, 26.2, 22.1, 14.0; **HRMS (ESI):** *m/z* calc. for $C_{13}H_{18}N_2O_3$ $[M - H]^+$: 249.1245; found: 249.1240.

**Ruthenium pyridine thread (49·$(PF_6)_2$):**

Compound **48** (50.0 mg, 0.200 mmol) was added to an excess of $SOCl_2$ (5 mL) and the reaction was heated at reflux for 16 h under $N_{2(g)}$. Excess $SOCl_2$ was removed *via* distillation and the resulting residue was redissolved in dry MeCN (4 mL). Ruthenium stopper **42**·$(PF_6)_2$ (85 mg, 0.0946 mmol), $Et_3N$ (40 μL, 0.285 mmol) and DMAP (cat.) were added and the reaction subjected to microwave irradiation at 150 °C for 1 h. The solvent was removed *in vacuo* and the resulting residue purified by column chromatography (silica; 14:2:1 MeCN/$H_2O$/sat. $KNO_{3(aq)}$). The MeCN was removed *in vacuo*, $H_2O$ (20 mL), $CH_2Cl_2$ (50 mL) and $NH_4PF_6$ (46 mg, 0.30 mmol) added, and the biphasic mixture stirred for 10 min at RT. The organic phase was separated, washed with $H_2O$ (2 × 50 mL), dried over anhydrous $MgSO_4$, and the solvent was removed *in vacuo* to give the product as a red solid (90.0 mg, 84%).

**$^{1}$H NMR** (300 MHz, $d_6$-acetone) δ (ppm): 10.64 (1H, br s, phen N*H*), 9.37 (1H, d, $^{3}J$ = 2.1 Hz, pyridine $H^2$), 9.26 (1H, d, $^{3}J$ = 2.1 Hz, pyridine $H^6$), 9.11 – 9.07 (1H, m, pyridine $H^4$), 8.91 – 8.78 (6H, m, Ar*H* & N*H*CH$_2$), 8.72 (1H, s, phen $H^6$), 8.49 (1H, dd, $^{3}J$ = 5.3 Hz, $^{4}J$ = 1.2 Hz, Ar*H*), 8.41 (1H, dd, $^{3}J$ = 5.3 Hz, $^{4}J$ = 1.2 Hz, Ar*H*), 8.30 – 8.13 (8H, m, Ar*H*), 7.97 – 7.88 (3H, m, Ar*H*), 7.68 – 7.60 (2H, m, Ar*H*), 7.45 – 7.38 (2H, m, Ar*H*), 3.49 – 3.41

(2H, m, NHC$H_2$), 1.69 – 1.59 (2H, m, NHCH$_2$C$H_2$), 1.46 – 1.28 (6H, m, C$H_2$), 0.88 (3H, t, $^3J$ = 6.8 Hz, C$H_3$); **$^{19}$F NMR** (282.4 MHz, $d_6$-acetone) δ (ppm): −72.5 (d, $^1J$ = 700 Hz, P$F_6$); **$^{31}$P NMR** (121.6 MHz, $d_6$-acetone) δ (ppm): −144.3 (sept, $^1J$ = 700 Hz, $P$F$_6$); **$^{13}$C NMR** (125.5 MHz, $d_6$-acetone) δ (ppm): 166.1, 165.1, 158.5, 158.5(*sic*), 158.3, 158.2, 153.9, 153.1, 153.0, 152.1, 152.0, 149.0, 147.0, 139.1, 139.0, 137.6, 135.3, 135.2, 134.5, 131.7, 131.4, 130.5, 128.8, 128.7, 127.6, 126.8, 125.4, 125.3, 123.1, 40.7, 32.4, 30.7, 27.5, 23.3, 14.4; **HRMS (ESI):** *m/z* calc. for $C_{45}H_{41}N_9O_2Ru\cdot(PF_6)_2$ $[M - 2PF_6]^{2+}$: 420.6214; found: 420.6213.

**Ruthenium pyridinium thread (50·(PF$_6$)$_3$):**

Ruthenium pyridine thread **49**·(PF$_6$)$_2$ (31 mg, 0.0277 mmol) was dissolved in MeI (3 mL) and the reaction was heated at reflux for 64 h under $N_{2(g)}$. The solvent was removed *in vacuo* and the resulting residue redissolved in $H_2O$ (20 mL). $NH_4PF_{6(aq)}$ (15 mg, 0.0920 mmol) was added and the resulting precipitate was filtered and dried under vacuum to give the product as red solid (31 mg, 88%).

**$^1$H NMR** (300 MHz, $d_6$-acetone) δ (ppm): 10.78 (1H, br s, phen N$H$), 9.82 (1H, s, pyridinium $H^2$), 9.69 (1H, s, pyridinium $H^6$), 9.60 (1H, s, pyridinium $H^4$), 9.02 (1H, dd, $^3J$ = 8.7 Hz, $^4J$ = 1.1 Hz, Ar$H$), 8.90 – 8.79 (5H, m, Ar$H$), 8.72 (1H, s, phen $H^6$), 8.50 (1H, dd, $^3J$ = 5.3 Hz, $^4J$ = 1.1 Hz, Ar$H$), 8.46 – 8.42 (1H, m, Ar$H$), 8.37 (1H, br s, N$H$CH$_2$), 8.31 – 8.12 (6H, m, Ar$H$), 7.97 – 7.89 (4H, m, Ar$H$), 7.67 – 7.60 (2H, m, Ar$H$), 7.44 – 7.37 (2H, m, Ar$H$), 4.80 (3H, s, N$^+$C$H_3$), 3.53 – 3.45 (2H, m, NHC$H_2$), 1.69 – 1.60 (2H, m, NHCH$_2$C$H_2$), 1.40 – 1.27 (6H, m, C$H_2$), 0.88 (3H, t, $^3J$ = 7.1 Hz, C$H_3$); **$^{19}$F NMR** (283 MHz, $d_6$-acetone) δ (ppm): −74.4 (d, $^1J$ = 700 Hz, P$F_6$); **$^{31}$P NMR** (122 MHz, $d_6$-acetone) δ (ppm): −138.5 (sept, $^1J$ = 700 Hz, $P$F$_6$); **$^{13}$C NMR** (125.5 MHz, $d_6$-acetone) δ (ppm): 162.5, 161.5, 158.5, 158.3, 158.2, 154.1, 153.5, 153.1, 153.1(*sic*), 149.1, 148.5, 147.4, 142.9, 139.1, 139.0, 137.8, 135.7, 135.2, 134.2, 134.1, 131.5, 128.8, 128.7, 128.5, 127.7, 127.0, 125.4, 125.4(*sic*), 124.0, 50.1,

41.2, 32.3, 30.7, 27.4, 23.4, 14.4; **HRMS (ESI):** *m/z* calc. for $C_{46}H_{44}N_9O_2Ru\cdot(PF_6)_3$ $[M - PF_6]^+$: 1146.1952; found: 1146.1957.

**Ruthenium (II) bis-bipyridyl phenanthroline (51·($PF_6$)$_2$)[8]:**

1,10-Phenanthroline (20 mg, 0.011 mmol) and $Ru(bipy)_2Cl_2$ (55 mg, 0.011 mmol) were suspended in 9:1 EtOH/$H_2O$ (10 mL) and heated at reflux under $N_{2(g)}$ for 16 h. The solution was cooled to RT, the solvent removed *in vacuo* and the resulting residue purified by column chromatography (silica; 14:2:1 MeCN/$H_2O$/sat. $KNO_{3(aq)}$). The MeCN was removed *in vacuo*, $H_2O$ (20 mL) added followed by the addition of $NH_4PF_6$ until precipitation ceased. The precipitate was collected by vacuum filtration and dried under vacuum to give a red solid (38 mg, 37%).

**$^1$H NMR** (300 MHz, $d_6$-acetone) δ (ppm): 8.80 – 8.87 (6H, m, ArH), 8.45 (2H, dd, $^3J$ = 5.3 Hz, $^4J$ = 1.2 Hz, Ar*H*), 8.41 (2H, s, phen $H^4$ & $H^5$), 8.26 (2H, td, $^3J$ = 7.6 Hz, $^4J$ = 1.2 Hz, Ar*H*), 8.11 – 8.19 (4H, m, Ar*H*), 7.88 – 7.96 (4H, m, Ar*H*), 7.61 – 7.66 (2H, m, Ar*H*), 7.36 – 7.41 (2H, m, Ar*H*); **$^{19}$F NMR** (282.4 MHz, $d_6$-acetone) δ (ppm): −72.4 (d, $^1J$ = 700 Hz, P$F_6$); **$^{31}$P NMR** (121.6 MHz, $d_6$-acetone) δ (ppm): −144.3 (sept, $^1J$ = 700 Hz, $PF_6$).[8]

**Ferrocene bis-ester** (**52**)**:**

Ferrocene (2.00 g, 10.8 mmol) was dissolved in conc. $H_2SO_4$ (30 mL) and stirred for 3 h at RT. Meanwhile, dimethyl 5-aminoisophthalate (0.740 g, 3.54 mmol) was suspended in conc. HCl (10 mL) and $H_2O$ (10 mL), and $NaNO_2$ (1.00 g, 14.5 mmol) in $H_2O$ (20 mL) was added dropwise at 0 °C, and the solution stirred at 0 °C for 1 h. The ferrocenium solution was poured onto ice $H_2O$ (120 mL) and warmed to RT before adding Cu powder (1.00 g, 15.7 mmol). This was poured into the diazonium ion solution and stirred at 0 °C for 30 min and then at RT for 48 h (beware generation of $N_{2(g)}$). Ascorbic acid (6.00 g, 34.1 mmol) and $CH_2Cl_2$ (200 mL) were added before the mixture was filtered through celite® and washed with $CH_2Cl_2$ (2 × 50 mL). The aqueous layer was extracted with $CH_2Cl_2$ (2 × 200 mL) before

combining the organic phases and drying them over anhydrous $MgSO_4$. The solvent was removed *in vacuo* and the resulting residue purified by column chromatography (silica; $CH_2Cl_2$) to give the product as an orange solid (0.261 g, 19%).

**$^1$H NMR** (300 MHz, $CDCl_3$) δ (ppm): 8.48 (1H, s, isophthalamide $H^4$), 8.27 (2H, s, isophthalamide $H^2$ & $H^6$), 4.82 (2H, br s, Fc Cp$H^2$), 4.45 (2H, br s, Fc Cp$H^3$), 4.10 (5H, s, Fc Cp′*H*), 3.98 (6H, s, C$H_3$); **$^{13}$C NMR** (75.5 MHz, $CDCl_3$) δ (ppm): 166.4, 141.0, 130.8, 130.7, 127.8, 82.9, 69.9, 69.8, 66.8, 52.4; **HRMS (ESI):** *m/z* calc. for $C_{20}H_{18}FeO_4$ $[M + Na]^+$: 401.0447; found: 401.0446.

**Ferrocene bis-carboxylic acid (53):**

Ferrocene bis-ester **52** (241 mg, 0.637 mmol) was suspended in EtOH (25 mL) and KOH (179 mg, 3.19 mmol) in $H_2O$ (2.5 mL) was added. The reaction was heated at reflux for 16 h, cooled to RT and the solvent reduced by ½ *in vacuo*. Water (25 mL) was added, followed by sufficient 10% citric $acid_{(aq)}$ for pH = 5 to be achieved. The resulting precipitate was collected *via* filtration, washed with $H_2O$ (2 × 50 mL) and dried under vacuum to give the product as an orange solid (185 mg, 83%).

**$^1$H NMR** (300 MHz, $d_6$-DMSO) δ (ppm): 8.30 (1H, t, $^4J$ = 1.6 Hz, isophthalamide $H^5$), 8.18 (2H, d, $^4J$ = 1.6 Hz, isophthalamide $H^2$ & $H^6$), 4.85 (2H, t, $^3J$ = 2.1 Hz, Fc Cp$H^2$), 4.40 (2H, t, $^3J$ = 2.1 Hz, Fc Cp$H^3$), 4.03 (5H, s, Fc Cp′*H*); **$^{13}$C NMR** (75.5 MHz, $d_6$-DMSO) δ (ppm): 167.6, 139.6, 133.6, 129.4, 127.7, 83.5, 69.5, 69.5, 66.5; **HRMS (ESI):** *m/z* calc. for $C_{18}H_{14}FeO_4$ $[M - H]^-$: 349.0169; found 349.0167.[13]

***tert*-Butyl isophthalamide 5-oxygen polyether macrocycle (54)[5]:**

5-*tert*-Butylisophthalic acid (0.250 g, 1.12 mmol) was added to $SOCl_2$ (15 mL) and the reaction was heated at reflux under $N_{2(g)}$ for 16 h. The excess $SOCl_2$ was removed *via* distillation, and the resulting residue redissolved in dry $CH_2Cl_2$ (20 mL). Meanwhile bis-amine **4** (0.522 g, 1.12 mmol) and template **6**·Cl (0.432 g, 1.13 mmol) were dissolved in

dry $CH_2Cl_2$ (40 mL) and stirred for 10 min at RT. Triethylamine (0.390 mL, 2.78 mmol) was then added followed by immediate dropwise addition of the acid chloride solution. The reaction was stirred for 1 h at RT and washed with 10% $HCl_{(aq)}$ (50 mL) and $H_2O$ (2 x 50 mL). The organic phase was dried over anhydrous $MgSO_4$ and the solvent removed *in vacuo*. The resulting residue was purified by column chromatography (silica; 97:3 $CHCl_3$/MeOH), giving the product as a white solid (0.310g, 43%).

**$^1$H NMR** (200 MHz, $CDCl_3$) δ (ppm): 8.09 (2H, d, $^3J$ = 1.3 Hz, isophthalamide $H^4$ & $H^6$), 7.74 (1H, t, $^3J$ = 1.3 Hz, isophthalamide $H^2$), 6.84 – 6.68 (10H, m, hydroquinone Ar*H* & N*H*), 4.14 – 4.00 (8H, m, C$H_2$), 3.92 – 3.82 (8H, m, C$H_2$), 3.75 – 3.67 (8H, m, C$H_2$), 1.37 (9H, s, $^t$Bu); **MS (ESI):** *m/z* calc. for $C_{36}H_{46}N_2O_9$ $[M + Na]^+$: 673.31; found: 673.32.[14]

**Ferrocene isophthalamide 5-oxygen polyether macrocycle (55)[5]:**

Ferrocene bis-carboxylic acid **53** (77 mg, 0.286 mmol) was suspended in dry $CH_2Cl_2$ (10 mL) at 0 °C, oxalyl chloride (0.242 mL, 2.86 mmol) and DMF (cat.) added and the mixture stirred at RT for 16 h under $N_{2(g)}$ before removing the solvent *in vacuo*. The resulting residue was redissolved in dry $CH_2Cl_2$ (5 mL) and added dropwisely to a solution of bis-amine **4** (133 mg, 0.286 mmol), template **6.**Cl (110 mg, 0.286 mmol) and $Et_3N$ (0.100 ml, 0.714 mmol) in dry $CH_2Cl_2$ (30 mL). The solution was stirred at RT for 1 h under $N_{2(g)}$ before washing with 10% citric $acid_{(aq)}$ (2 × 20 mL) and $H_2O$ (20 mL). The organic phase was dried over anhydrous $MgSO_4$ and the solvent removed *in vacuo*. The resulting residue was purified by column chromatography (silica; 98:2 $CH_2Cl_2$/MeOH) to give the product as an orange solid (101 mg, 45%).

**$^1$H NMR** (200 MHz, 1:1 $CDCl_3$/$CD_3CN$) δ (ppm): 8.01 (2H, br s, isophthalamide $H^4$ & $H^6$), 7.79 (1H, br s, isophthalamide $H^2$), 7.23 (2H, t, $^3J$ = 4.9 Hz, N*H*), 6.84 – 6.73 (8H, m, hydroquinone Ar*H*), 4.89 (2H, br s, Fc Cp$H^1$), 4.48 (2H, br s, Fc Cp$H^2$), 4.16 – 4.05 (9H, m, Fc Cp′*H* & C$H_2$), 4.01 – 3.95 (4H, m, C$H_2$), 3.81 – 3.73 (8H, m, C$H_2$), 3.66 – 3.58 (8H, m,

C*H*$_2$); **$^{13}$C NMR** (125.5 MHz, 1:1 $CDCl_3$/$CD_3CN$) δ (ppm): 167.2, 153.7, 153.5, 141.5, 135.3, 128.4, 122.3, 116.1, 115.9, 78.6, 71.1, 70.6, 70.5, 70.1, 68.6, 67.6, 67.5, 40.2, 31.0; **HRMS (ESI):** *m/z* calc. for $C_{42}H_{46}FeN_2O_9$ $[M + Na]^+$: 801.2446; found: 801.2437.

**Phenol Stopper (56)[15]:**

Compound **10** (4.00 g, 10.7 mmol) was dissolved in phenol (15.5 g, 165 mmol), 36% $HCl_{(aq)}$ (0.5 mL) added and the reaction heated for 24 h at 110 °C. Water (50 mL) was then added and the aqueous layer extracted with toluene (3 x 100 mL). The toluene phase was washed with $NaOH_{(aq)}$ (3 x 200 mL) and $H_2O$ (3 x 200 mL), dried over anhydrous $Na_2SO_4$ and the solvent removed *in vacuo*. The resulting residue was purified *via* recrystallisation from 1:1 toluene/hexane, giving the product as an off-white solid (4.01 g, 83%).

**$^1$H NMR** (300 MHz, $CDCl_3$) δ (ppm): 7.26 – 7.15 (9H, m, Ar*H*), 7.13 – 7.03 (6H, m, Ar*H*), 6.72 (2H, d, $^3J$ = 8.9 Hz, Ar*H*), 4.63 (1H, s, O*H*), 1.31 (18H, s, $^t$Bu); **MS (ESI):** *m/z* calc. for $C_{33}H_{36}O$ $[M + Na]^+$: 471.27; found 471.28.[15]

**Bromo-stopper (57)[16]:**

Compound **56** (2.00 g, 4.46 mmol) and 1,3-dibromopropane (1.36 mL, 13.4 mmol) were dissolved in dry MeCN (100 mL), $K_2CO_3$ (1.85 g, 13.4 mmol) added and the reaction heated at reflux under $N_{2(g)}$ for 16 h. The solution was cooled to RT, filtered and the solid washed with $CH_2Cl_2$ (2 × 50 mL). The solvent was removed from the filtrate *in vacuo* and the resulting residue redissolved in $CH_2Cl_2$ (100 mL), washed with $H_2O$ (3 × 50 mL) and dried over anhydrous $MgSO_4$. The solvent was removed *in vacuo* and the resulting residue purified by column chromatography (silica; 2:1 petroleum ether/$CH_2Cl_2$), giving the product as a white solid (1.63 g, 64%).

**$^1$H NMR** (300 MHz, $CDCl_3$) δ (ppm): 7.26 – 7.17 (9H, m, Ar*H*), 7.13 – 7.07 (6H, m, Ar*H*), 6.81 – 6.75 (2H, m, Ar*H*OC$H_2$), 4.09 (2H, t, $^3J$ = 5.7 Hz, OC*H*$_2$), 3.61 (2H, t, $^3J$ = 6.5 Hz, BrC*H*$_2$), 2.36 – 2.27 (2H, m, BrCH$_2$C*H*$_2$), 1.31 (18H, s, $^t$Bu).

**Ruthenium pyridinium nicotinamide axle (58·$(PF_6)_3$):**

Compound **43**·$(PF_6)_2$ (150 mg, 0.149 mmol) and compound **57** (320 mg, 0.914 mmol) were dissolved in dry MeCN (10 mL) and the reaction was subjected to microwave irradiation at 175 °C for 4 h. The solvent was removed *in vacuo* and the resulting residue purified by column chromatography (silica; 14:2:1 MeCN/$H_2O$/sat. $KNO_{3(aq)}$). The MeCN was removed *in vacuo*, $H_2O$ (20 mL), $CH_2Cl_2$ (50 mL) and $NH_4PF_6$ (73 mg, 0.447 mmol) were added, and the resulting biphasic mixture was stirred for 10 min at RT. The organic phase was separated, washed with $H_2O$ (2 × 50 mL), dried over anhydrous $MgSO_4$ and the solvent removed *in vacuo* to give a red solid (144 mg, 58%).

**$^1$H NMR** (300 MHz, $d_6$-acetone) δ (ppm): 10.85 (1H, s, N*H*), 9.93 (1H, s, pyridinium $H^2$), 9.49 (1H, d, $^3J$ = 6.3 Hz, pyridinium $H^4$), 9.42 – 9.37 (1H, m, pyridinium $H^5$), 9.00 (1H, d, $^3J$ = 8.3 Hz, pyridinium $H^6$), 8.89 – 8.73 (6H, m, Ar*H*), 8.71 (1H, s, phen $H^6$), 8.54 – 8.41 (4H, m, Ar*H*), 8.30 – 8.23 (2H, m, Ar*H*), 8.19 – 8.12 (4H, m, Ar*H*), 7.95 – 7.83 (4H, m, Ar*H*), 7.67 – 7.61 (2H, m, Ar*H*), 7.42 – 7.06 (19H, m, Ar*H*), 6.78 – 6.74 (2H, m, Ar*H*), 5.24 (2H, t, $^3J$ = 7.0 Hz, $N^+CH_2$), 4.27 (2H, t, $^3J$ = 5.6 Hz, $OCH_2$), 2.80 – 2.69 (2H, m, $OCH_2CH_2$), 1.26 (18H, s, $^t$Bu); **$^{13}$C NMR** (126 MHz, $d_6$-acetone) δ (ppm): 162.8, 158.5, 158.2, 158.2(*sic*), 157.2, 154.0, 153.5, 153.1, 153.0, 152.9, 149.4, 149.0, 148.5, 148.3, 147.3, 146.5, 145.6, 145.1, 140.7, 139.1, 139.0, 137.8, 135.7, 134.1, 132.9, 131.7, 131.4, 129.5, 128.8, 128.7, 128.5, 128.4, 127.7, 127.0, 126.7, 125.4, 125.4(*sic*), 125.2, 123.7, 114.1, 65.8, 64.4, 61.7, 34.9, 31.7, 31.4; **$^{19}$F NMR** (282.4 MHz, $d_6$-acetone) δ (ppm): −72.5 (d, $^1J$ = 700 Hz, P$F_6$); **$^{31}$P NMR** (121.6 MHz, $d_6$-acetone) δ (ppm): −144.3 (sept, $^1J$ = 700 Hz, $PF_6$).

Axle **58**·$(PF_6)_3$ was observed (by TLC and $^1$H NMR) to decompose when left for relatively short periods in solution, and thus no $^{13}$C NMR or HRMS data could be obtained.

**Stoppered pyridine ester (59):**

Compound **46** (0.2 g, 1.11 mmol) was suspended in dry $CH_2Cl_2$ (30 mL), oxalyl chloride (0.19 mL, 2.22 mmol) and DMF (cat.) were added, and the mixture stirred under $N_{2(g)}$ for 1 h until homogenous. The solvent was removed *in vacuo*, the residue dissolved in dry $CH_2Cl_2$ (20 mL) and added dropwise to a solution of stopper **11** (0.52 g, 1.16 mmol), $Et_3N$ (0.28 mL, 2.0 mmol) and DMAP (cat.) in dry $CH_2Cl_2$ (30 mL). The resulting solution was stirred for 1 h, washed with 10% $HCl_{(aq)}$ (2 × 50 mL) and $H_2O$ (2 × 50 mL), dried over anhydrous $MgSO_4$ and the solvent removed *in vacuo*. The resulting brown oil was purified by column chromatography (silica; 95:5 $CH_2Cl_2$/MeOH) to yield an oily cream-coloured solid (0.60 g, 89%).

**$^1$H NMR** (300 MHz, $CDCl_3$) δ (ppm): 9.34 – 9.62 (2H, m, pyridine $H^2$ & $H^6$), 8.78 (1H, t, $^4J$ = 2.1 Hz, pyridine $H^4$), 8.05 (1H, br s, ArN*H*), 7.55 (2H, d, $^3J$ = 8.9 Hz, Ar*H*NH), 7.11 – 7.28 (17H, m, Ar*H*), 4.02 (3H, s, C$H_3$), 1.31 (18H, s, $^t$Bu); **$^{13}$C NMR** (300 MHz, $CDCl_3$) δ: 164.9, 162.8, 152.9, 151.9, 148.5, 146.9, 144.3, 143.5, 135.9, 134.9, 131.9, 131.1, 130.6, 127.3, 125.8, 124.3, 119.3, 63.8, 34.3, 33.3; **HRMS (ESI):** *m/z* calc. for $C_{41}H_{42}N_2O_3$ $[M + Na]^+$: 633.3088; found 633.3091.

**Stoppered pyridine carboxylic acid (60):**

Compound **59** (1.81 g, 2.96 mmol) was dissolved in 1:1 THF/$H_2O$ (50 mL), KOH (0.196 g, 3.5 mmol) was added, and the solution stirred for 16 h. 10% citric $acid_{(aq)}$ was added until the solution was pH = 7, and the aqueous mixture extracted with $CH_2Cl_2$ (3 x 50 mL). The combined organic layers were dried over anhydrous $MgSO_4$, and the solvent removed *in vacuo*. The resulting sticky brown solid was recrystallized from $CHCl_3$ to give an off-white solid (1.77 g, 100%).

**$^1$H NMR** (300 MHz, $d_6$-DMSO) δ (ppm): 11.70 (1H, s, COO*H*), 10.63 (1H, s, ArN*H*), 9.27 (1H, d, $^4J$ = 2.0 Hz, pyridine $H^2$), 9.21 (1H, d, $^4J$ = 2 Hz, pyridine $H^6$), 8.74 (1H, t, $^4J$ = 2 Hz,

pyridine $H^4$), 7.68 (2H, d, $^3J$ = 8.8 Hz, Ar*H*NH), 7.10 – 7.34 (17H, m, Ar*H*), 1.26 (18H, s, $^t$Bu); **$^{13}$C NMR** (300 MHz, $d_6$-DMSO) δ: 165.8, 163.1, 152.3, 147.9, 146.9, 143.6, 142.5, 136.4, 136.0, 130.7, 130.4, 130.1, 127.7, 126.4, 125.8, 124.5, 119.6, 34.9, 31.1; **HRMS (ESI):** *m/z* calc. for $C_{40}H_{40}N_2O_3$ $[M - H]^-$: 596.2966; found 595.2980.

**Ruthenium pyridine axle (61·$(PF_6)_2$):**

Acid **60** (316 mg, 0.529 mmol) was added to an excess of $SOCl_2$ (10 mL) and the reaction heated at reflux for 16 h under $N_{2(g)}$. Excess $SOCl_2$ was removed *via* distillation to give the corresponding acid chloride which was redissolved in dry MeCN (12 mL). To this, amine **42**·$(PF_6)_2$ (226 mg, 0.252 mmol), $Et_3N$ (0.105 mL, 0.751 mmol) and DMAP(cat.) were added and the reaction subjected to microwave irradiation at 150 °C for 2 h. The solvent was removed *in vacuo* and the resulting residue purified by column chromatography (silica; 14:2:1 MeCN/$H_2O$/sat. $KNO_{3(aq)}$ & 28:2:1 MeCN/$H_2O$/sat. $KNO_{3(aq)}$). The MeCN was removed *in vacuo* before adding $H_2O$ (20 mL), $CH_2Cl_2$ (30 mL) and $NH_4PF_6$ (123 mg, 0.756 mmol). The resulting biphasic mixture was stirred for 10 min at RT before the organic phase was separated, washed with $H_2O$ (2 × 50 mL) and dried over anhydrous $MgSO_4$. The solvent was removed *in vacuo* to give a red solid (149 mg, 40%).

**$^1$H NMR** (300 MHz, $d_6$-acetone) δ (ppm): 10.65 (1H, s, phen N*H*), 10.03 (1H, s, stopper N*H*), 9.39 (1H-, br s, pyridine $H^2$), 9.28 (1H, br s, pyridine $H^6$), 9.11 – 9.06 (1H, m, Ar*H*), 9.08 – 8.99 (1H, m, pyridine $H^4$), 8.89 – 8.73 (5H, m, Ar*H*), 8.70 (1H, s, phen $H^6$), 8.46 – 8.43 (1H, m, Ar*H*), 8.40 (1H, dd, $^3J$ = 5.3 Hz, $^4J$ = 1.2 Hz, Ar*H*), 8.29 – 8.22 (2H, m, Ar*H*), 8.21 – 8.12 (4H, m, Ar*H*), 7.97 – 7.81 (4H, m, Ar*H*), 7.79 – 7.74 (2H, m, Ar*H*), 7.67 – 7.61 (2H, m, Ar*H*), 7.45 – 7.15 (17H, m, stopper Ar*H*), 1.30 (18H, s, $^t$Bu); **$^{13}$C NMR** (126 MHz, $d_6$-acetone) δ (ppm): 165.9, 164.1, 158.4, 153.8, 153.0, 152.3, 149.8, 149.4, 149.0, 148.2, 147.2, 144.2, 139.1, 138.9, 137.6, 135.9, 135.6, 135.0, 134.3, 133.4, 132.2, 132.1, 131.8, 131.6, 131.5, 131.4, 131.3, 131.2, 128.8, 128.7, 128.6, 128.4, 127.5, 127.1, 127.0, 126.8, 125.6, 125.4,

125.3, 122.9, 120.2, 64.7, 34.9, 31.7; **$^{19}$F NMR** (283 MHz, $d_6$-acetone) δ (ppm): −72.4 (d, $^1J$ = 700 Hz, P$F_6$); **$^{31}$P NMR** (122 MHz, $d_6$-acetone, $P$F$_6$) δ (ppm): −144.3 (sept, $^1J$ = 700 Hz); **HRMS (ESI):** *m/z* calc. for $C_{72}H_{63}N_9O_2Ru\cdot(PF_6)_2$ $[M - PF_6]^+$: 1332.3804; found 1332.3834.

**Ruthenium pyridinium axle (62·$(PF_6)_3$):**

Compound **61**·$(PF_6)_2$ (61 mg, 0.0413 mmol) was dissolved in an excess of MeI (3 mL) and the reaction heated at reflux for 48 h under $N_{2(g)}$. The solvent was removed *in vacuo* and the resulting residue purified by column chromatography (silica; 28:2:1 MeCN/$H_2O$/sat. $KNO_{3(aq)}$) before removing the MeCN *in vacuo*. $H_2O$ (30 mL), $CH_2Cl_2$ (30 mL) and $NH_4PF_6$ (20.2 mg, 0.124 mmol) were added and the resulting biphasic mixture was stirred for 10 min at RT. The organic phase was separated, washed with $H_2O$ (2 × 30 mL) and dried over anhydrous $MgSO_4$ before the solvent was removed *in vacuo*. The resulting residue was redissolved in acetone (10 mL) and filtered. The solvent was removed from the filtrate *in vacuo* to give a red solid (47 mg, 70%).

**$^1$H NMR** (300 MHz, $d_6$-acetone) δ (ppm): 10.95 (1H, s, phen N*H*), 10.32 (1H, s, stopper N*H*), 9.86 (1H, s, pyridinium $H^2$), 9.83 – 9.79 (2H, m, pyridinium $H^4$ & $H^6$), 9.07 (1H, dd, $^3J$ = 8.8 Hz, $^4J$ = 1.1 Hz, Ar*H*), 8.89 – 8.79 (5H, m, Ar*H*), 8.73 (1H, s, phen $H^6$), 8.49 (1H, dd, $^3J$ = 5.3 Hz, $^4J$ = 1.1 Hz, Ar*H*), 8.43 (1H, dd, $^3J$ = 5.2 Hz, $^4J$ = 1.1 Hz, Ar*H*), 8.30 – 8.23 (2H, m, Ar*H*), 8.20 – 8.12 (4H, m, Ar*H*), 7.96 – 7.88 (4H, m, Ar*H*), 7.78 – 7.73 (2H, m, Ar*H*), 7.67 – 7.61 (2H, m, Ar*H*), 7.43 – 7.14 (17H, m, stopper Ar*H*), 4.84 (3H, s, $N^+CH_3$), 1.30 (18H, s, $^t$Bu); **$^{13}$C NMR** (75.5 MHz, $d_6$-acetone) δ (ppm): 162.4, 162.3, 161.0, 160.2, 158.3, 158.1, 158.0, 153.9, 153.2, 152.9, 149.7, 149.4, 149.0, 148.0, 147.3, 147.1, 147.0, 144.9, 144.8, 144.1, 139.0, 138.9, 137.6, 136.7, 135.8, 135.3, 132.2, 131.6, 131.5, 131.4, 131.3, 128.7, 128.6, 128.5, 128.4, 127.5, 126.8, 125.6, 125.3, 125.2, 120.3, 64.7, 34.9, 34.8, 31.6; **$^{19}$F NMR** (283 MHz, $d_6$-acetone) δ (ppm): −72.4 (d, $^1J$ = 700 Hz, P$F_6$); **$^{31}$P NMR** (122 MHz, $d_6$-

acetone) δ (ppm): −144.4 (sept, $^1J$ = 700 Hz, $P$$F_6$); **HRMS (ESI):** *m/z* calc. for $C_{73}H_{66}N_9O_2Ru\cdot(PF_6)_3$ $[M - 2PF_6 - H]^+$: 1346.3961; found 1346.3943.

**Isopthalamide rotaxane (63·$(PF_6)_3$):**

Bis-amine **4** (12 mg, 0.026 mmol) and axle **62·**$(PF_6)_3$ (43 mg, 0.026 mmol) were dissolved in dry $CH_2Cl_2$ (7 mL) and stirred at RT for 30 min. Triethylamine (9 μL, 0.0650 mmol) was added, immediately followed by the addition of isophthaloyl dichloride (5 mg, 0.026 mmol) in dry $CH_2Cl_2$ (2 mL). The mixture was stirred at RT for 1 h under $N_{2(g)}$, the solvent removed *in vacuo* and the resulting residue purified by column chromatography (silica; 28:2:1 MeCN/$H_2O$/sat. $KNO_{3(aq)}$). However it was not possible to separate the rotaxane from its component axle **62·**$(PF_6)_3$.

**Pyridine rotaxane (64·$(PF_6)_3$):**

Bis-amine **4** (12 mg, 0.026 mmol) and axle **62·**$(PF_6)_3$ (43 mg, 0.026 mmol) were dissolved in dry $CH_2Cl_2$ (7 mL) and stirred at RT for 30 min. Triethylamine (9 μL, 0.0650 mmol) was added, immediately followed by the addition of 3,5-pyridine dicarbonyl dichloride (5 mg, 0.026 mmol) in dry $CH_2Cl_2$ (2 mL). The mixture was stirred at RT for 1 h under $N_{2(g)}$. The solvent was removed *in vacuo* and the resulting residue purified by column chromatography (silica; 14:2 MeCN/$H_2O$ & 28:2:1 MeCN/$H_2O$/sat. $KNO_{3(aq)}$). The MeCN was removed *in vacuo*, $H_2O$ (20 mL), $CH_2Cl_2$ (20 mL) and $NH_4PF_6$ (13 mg, 0.078 mmol) added and the resulting biphasic mixture stirred for 10 min at RT. The organic phase was separated, washed with $H_2O$ (2 × 20 mL) and dried over anhydrous $MgSO_4$. The solvent was removed *in vacuo* to give a red solid (13 mg, 22%).

**$^1$H NMR** (500 MHz, $d_6$-acetone) δ (ppm): 11.07 (1H, s, phen N*H*), 10.28 (1H, s, axle ArHN*H*)), 10.06 (1H, s, axle pyridinium $H^4$), 9.48 (2H, br s, pyridinium $H^{2,6}$), 9.14 – 9.10 (2H, m, Ar*H*), 8.89 – 8.84 (4H, m, Ar*H*), 8.75 (1H, s, phen $H^6$), 8.67 – 8.63 (2H, m, Ar*H*), 8.44 – 8.41 (2H, m, Ar*H*), 8.32 – 8.21 (5H, m, Ar*H*), 8.16 – 8.09 (4H, m, Ar*H*), 7.94 – 7.88

(3H, m, Ar*H*), 7.80 (1H, br d, Ar*H*), 7.68 – 7.62 (3H, m, Ar*H*), 7.57 – 7.53 (1H, m, Ar*H*), 7.41 – 7.20 (17H, m, stopper Ar*H*), 6.68 – 6.63 (4H, m, hydroquinone Ar*H*), 6.42 – 6.37 (4H, m, hydroquinone Ar*H*), 4.94 (3H, m, $N^+CH_3$), 4.32 – 4.25 (2H, m, $CH_2$), 4.05 – 3.98 (2H, m, $CH_2$), 3.89 – 3.74 (16H, m, $CH_2$), 3.68 – 3.60 (2H, m, $CH_2$), 3.42 – 3.34 (2H, m, $CH_2$), 1.30 (18H, s, $^t$Bu); **$^{19}$F NMR** (282.4 MHz, $d_6$-acetone ) δ (ppm): −72.4 (d, $^1J$ = 700 Hz, $PF_6$); **$^{31}$P NMR** (121.6 MHz, $d_6$-acetone) δ (ppm): −144.3 (sept, $^1J$ = 700 Hz, $PF_6$); **HRMS (ESI):** *m/z* calc. for $C_{104}H_{103}N_{12}O_{11}Ru\cdot(PF_6)_3$ $[M - 2PF_6 - H]^+$: 1941.6500; found: 1941.6499.

### 5.2.3 Experimental Details for Chapter 4

**Tetraethylene glycol mono tosylate (65):**

A solution of NaOH (0.81 g, 20.3 mmol) in $H_2O$ (4.5 mL) was added to a mixture of THF (4.5 mL) and tetraethylene glycol (26.4 mL, 152 mmol), and the resulting mixture cooled to 0 ºC. A solution of TsCl (2.49 g, 13.1 mmol) in THF (15 mL) was added dropwise to the above mixture over 1 h and stirred at 0 ºC for 2 h before being poured onto ice water (75 mL). The organic layer was separated, and the aqueous phase washed with $CH_2Cl_2$ (3 × 30 mL). The combined organic layers were washed with $H_2O$ (3 × 30 mL), dried over anhydrous $MgSO_4$ and the solvent removed *in vacuo* giving a colourless oil (3.41 g, 75 %).

**$^1$H NMR** (300 MHz, $CDCl_3$) δ: 7.81 (2H, d, $^3J$ = 8.1 Hz, Ar*H*), 7.35 (2H, d, $^3J$ = 8.1 Hz, Ar*H*), 4.17 (4H, t, $^3J$ = 4.7 Hz, $CH_2$), 3.57 – 3.73 (12H, m, $CH_2$), 2.45 (3H, s, $CH_3$).[17]

**Tetraethylene glycol mono phthalimide (66)[17]:**

Potassium phthalimide (6.61 g, 36 mmol) was suspended in a solution of compound **65** (8.29 g, 24 mmol) in DMF (50 mL) and the mixture heated at 110 ºC under $N_{2(g)}$ for 18 h. The reaction was cooled to RT and the solvent removed *in vacuo*. The resulting residue was redissolved in EtOAc (30 mL), filtered and purified by column chromatography (silica; EtOAc → 95:5 EtOAc/MeOH) to give an oily white solid (5.65 g, 73 %).

**$^1$H NMR** (300 MHz, $CDCl_3$) δ: 7.78 – 7.82 (2H, m, Ar*H*), 7.65 – 7.70 (2H, m, Ar*H*), 3.85 (2H, t, $^3J$ = 5.3 Hz, C$H_2$), 3.69 (2H, t $^3J$ = 5.3 Hz, C$H_2$), 3.49 – 3.63 (12H, m, C$H_2$).[17]

**Tetraethyelene glycol phthalimide-tosylate (67)[17]:**

Compound **66** (5.65 g, 17.5 mmol), TsCl (3.32 g, 17.5 mmol), $Et_3N$ (3.5 mL, 25 mmol) and DMAP (cat.) were dissolved in $CH_2Cl_2$ (150 mL) and stirred for 16 h under $N_{2(g)}$. Water (20 mL) was added before the solution was adjusted to pH = 7 with 10% citric $acid_{(aq)}$. The organic layer was washed with $H_2O$ (2 × 150 mL) and sat. $NaCl_{(aq)}$ (150 mL), dried over anhydrous $MgSO_4$ and the solvent removed *in vacuo*. The resulting residue was washed with $Et_2O$ (2 × 50 mL) to give the product as a white oily solid (4.50 g, 54 %).

**$^1$H NMR** (300 MHz, $CDCl_3$) δ (ppm): 7.83 – 7.86 (2H, m, phthalimide Ar*H*), 7.80 (2H, d, $^3J$ = 8.8 Hz, tosyl Ar*H*), 7.71 – 7.74 (2H, m, phthalimide Ar*H*), 7.34 (2H, d, $^3J$ = 8.8 Hz, tosyl Ar*H*), 4.15 (2H, t, $^3J$ = 4.7 Hz, C$H_2$), 3.90 (2H, t, $^3J$ = 5.8 Hz, C$H_2$), 3.73 (2H, t, $^3J$ = 5.8 Hz, C$H_2$), 3.56 – 3.67 (6H, m, C$H_2$), 3.52 (4H, s, C$H_2$), 2.45 (3H, s, C$H_3$).[17]

**Tetraethyelene glycol phthalimide-azide (68)[18]:**

Compound **67** (1.00 g, 2.09 mmol), and $NaN_3$ (0.204 g, 3.14 mmol) were dissolved in dry degassed DMF (50 mL) and the solution heated at 85 °C under $N_{2(g)}$ for 16 h. The reaction was cooled to RT, added to $H_2O$ (50 mL) and extracted with $CH_2Cl_2$ (3 × 50 mL) to give an oily white solid (0.70 g, 96 %).

**$^1$H NMR** (300 MHz, $CDCl_3$) δ: 7.82 – 7.85 (2H, m, Ar*H*), 7.70 – 7.73 (2H, m, Ar*H*), 3.90 (2H, t, $^3J$ = 5.9 Hz, C$H_2$), 3.73 (2H, t, $^3J$ = 5.8 Hz, C$H_2$), 3.36 (2H, t, $^3J$ = 5.3 Hz, C$H_2$), 3.59 – 3.65 (10H, m, C$H_2$), 3.36 (2H, t, $^3J$ = 5.3 Hz, C$H_2$).[18]

**Tetraethyelene glycol amine-azide (69)[18]:**

Compound **68** (720 mg, 2.07 mmol) was suspended in EtOH (50 mL), hydrazine monohydrate (1.00 mL) was added and the suspension was heated at reflux under $N_{2(g)}$ overnight. The solution was cooled to RT, poured onto $H_2O$ (100 mL) and extracted with

$CH_2Cl_2$ (4 × 50 mL). The combined organic phases were dried over anhydrous $MgSO_4$ and the solvent removed *in vacuo* to give a colourless oil (460 mg, 100%).

**$^1$H NMR** (300 MHz, $CDCl_3$) δ: 3.62 – 3.70 (10H, m, C$H_2$), 3.52 (2H, t, $^3J$ = 5.3 Hz, C$H_2$), 3.40 (2H, t, $^3J$ = 4.8 Hz, C$H_2$), 2.87 (2H, t, $^3J$ = 4.8 Hz, C$H_2$).[18]

**Pyridine axle precursor (70):**

Acid **60** (250 mg, 0.419 mmol), EDCI (87 mg, 0.454 mmol) and DMAP (cat.) were suspended in $CH_2Cl_2$ (30 mL) and stirred under $N_{2(g)}$ until all solid had dissolved. A solution of compound **69** (100 mg, 0.454 mmol) and $Et_3N$ (0.10 mL, 0.713 mmol) in $CH_2Cl_2$ (20 mL) was added and the resulting solution stirred under $N_{2(g)}$ for 4 days. The solution was washed with 10% $HCl_{(aq)}$ (50 ml), 10% $NaOH_{(aq)}$ (50 mL) and $H_2O$ (2 × 50 mL), dried over $MgSO_4$, and the solvent removed *in vacuo*. Column chromatography (silica; 95:5 $CH_2Cl_2$/MeOH) gave the product as an orange oil (101 mg, 30%).

**$^1$H NMR** (300 MHz, $CDCl_3$) δ (ppm): 9.25 (1H, d, $^4J$ = 1.8 Hz, pyridine $H^2$), 9.18 (1H, d, $^4J$ = 1.8 Hz, pyridine $H^6$), 8.61 (1H, t, $^4J$ = 1.8 Hz, pyridine $H^4$), 8.42 (1H, s, ArHN*H*), 7.57 (2H, d, $^3J$ = 8.7 Hz, Ar*H*NH), 7.35 (1H, br s, N*H*$CH_2$), 7.11 – 7.24 (15H, m, stopper Ar*H*), 3.60 – 3.69 (12H, m, C$H_2$), 3.54 (4H, t, $^3J$ = 5.3 Hz, C$H_2$), 3.28 (4H, t, $^3J$ = 4.7 Hz, C$H_2$), 1.31 (18H, s, stopper $^t$Bu); **$^{13}$C NMR** (75.5 MHz, $CDCl_3$) δ (ppm): 165.0, 163.4, 148.4, 147.0, 143.8, 143.5, 135.5, 131.7, 131.0, 130.6, 127.3, 125.7, 124.2, 119.2, 70.6, 70.5, 70.4, 69.8, 69.4, 63.7, 50.5, 40.1, 34.2, 31.3; **HRMS (ESI):** calculated for $C_{48}H_{56}N_6O_5$ $[M + Na]^+$: 819.4204; found: 819.4209.

**Pyridinium axle precursor (71·Cl):**

Compound **70** (107 mg, 0.134 mmol) was dissolved in MeI (5 mL) and heated at reflux under $N_{2(g)}$ for 16 h. The solution was cooled to RT and the solvent was removed *in vacuo*. The yellow residue was redissolved in $CHCl_3$ (25 mL), washed with 1 M $NH_4Cl_{(aq)}$ (8 × 20 mL)

and $H_2O$ (2 × 20 mL), dried over anhydrous $MgSO_4$ and the solvent removed *in vacuo* to give a yellow oily solid (94 mg, 83%).

**$^1$H NMR** (300 MHz, $CDCl_3$) δ (ppm): 11.18 (1H, s, ArHN*H*), 10.47 (1H, t, pyridine *H*$^4$), 9.53 (1H, s, pyridine *H*$^2$), 9.44 (1H, t, $^3J$ = 4.7 Hz, N*H*$CH_2$), 9.04 (1H, s, pyridine *H*$^6$), 7.85 (2H, d, $^3J$ = 8.8 Hz, Ar*H*NH), 7.15 – 7.26 ( 15H, m, stopper Ar*H*), 4.29 (3H, s, $N^+CH_3$), 3.76 (2H, t, $^3J$ = 5.9 Hz, C$H_2$), 3.70 (4H, s, C$H_2$), 3.58 – 3.65 (8H, m, C$H_2$), 3.32 (2H, t, $^3J$ = 5.2 Hz, C$H_2$), 1.31 (18H, s, $^t$Bu); **$^{13}$C NMR** (75.5 MHz, $CDCl_3$) δ (ppm): 160.6, 158.4, 148.4, 147.2, 147.1, 146.5, 144.6, 143.7, 141.4, 135.2, 134.1, 133.9, 131.5, 131.0, 130.5, 127.4, 125.7, 124.3, 119.6, 77.2, 70.5, 70.4, 70.2, 69.7, 63.8, 50.6, 49.0, 40.4, 34.3, 31.3; **HRMS (ESI)** calculated for $C_{49}H_{59}N_6O_5 \cdot Cl$ $[M - Cl]^+$: 811.4541; found: 811.4545.

**Alkyne Stopper (72)[19]:**

Stopper **56** (2.0 g, 4.34 mmol) was dissolved in DMF (100 mL), followed by the addition of propargyl bromide solution (80% in toluene) and $K_2CO_3$. The mixture was heated at 80 °C under $N_2$ for 18 h, cooled to RT and the solvent removed in vacuo. Water (30 mL) was added and the solution extracted with EtOAc (3 x 30 mL), before the combined organic phase was removed *in vacuo*. The resulting brown residue was purified by silica plug ($CH_2Cl_2$) to yield a white solid (1.81 g, 86%).

**$^1$H NMR** (300 MHz, $CDCl_3$) δ (ppm): 7.12 – 7.30 (15H, m, stopper ArH), 6.89 (2H, d, $^3J$ = 8.8 Hz, Ar*H*$OCH_2$), 4.70 (2H, d, $^4J$ = 2.3 Hz, C$H_2$), 2.55 (1H, t, $^4J$ = 2.3 Hz, CC*H*), 1.35 (18H, s, $^t$Bu); **$^{13}$C NMR** (75.5 MHz, $CDCl_3$): 155.5, 148.4, 147.3, 143.8, 140.3, 132.2, 131.1, 130.7, 127.2, 125.7, 124.1, 113.4, 78.7, 75.4, 63.5, 55.7, 34.3, 31.4; **HRMS (ESI)** calc. for $C_{36}H_{38}O$ $[M + Na]^+$: 509.2815; found: 509.2821.[1]

**Rotaxane (73·$PF_6$):**

Axle precursor **71·**Cl (50 mg, 59 μmol), macrocycle **30**·I (41 mg, 59 μmol) and stopper **72** (29 mg, 59 μmol) were dissolved in degassed $CH_2Cl_2$ (15 mL), DIPEA (15 μL, 86 μmol),

$Cu(MeCN)_4PF_6$ (4 mg, 11 μmol) and TBTA (6 mg, 11 μmol) were added and the solution stirred under $N_{2(g)}$ for 16 h. The solution was washed with 10% $HCl_{(aq)}$ (2 × 20 mL) and $H_2O$ (2 × 20 mL), dried over anhydrous $MgSO_4$ and the solvent removed *in vacuo*. The crude material was purified by prep TLC (7:2:1 $CH_2Cl_2$/acetone/MeOH) to obtain a yellow solid which was then redissolved in $CHCl_3$ (10 mL) and washed with $NH_4PF_{6(aq)}$ (10 x 10 mL) and $H_2O$ (2 × 10 mL). The organic phase was dried over anhydrous $MgSO_4$ and the solvent removed *in vacuo* to give a yellow solid (51 mg, 40%).

**$^1$H NMR** (300 MHz, $d_6$-acetone) δ (ppm): 9.64 (1H, br s, axle ArHN*H*), 9.60 (3H, s, axle pyridinium $H^6$ & macrocycle pyridinium $H^2$ & $H^6$), 9.51 (1H, s, axle pyridinium $H^2$), 9.27 (1H, s, axle pyridinium $H^4$), 8.71 (1H, br s, macrocycle pyridinium $H^4$), 8.56 (2H, br s, macrocycle N*H*), 8.30 (1H, t, $^3J$ = 4.7 Hz, axle $CH_2NH$), 8.14 (1H, s, triazole C*H*), 7.74 (2H, d, $^3J$ = 8.8 Hz, Ar*H*NH), 7.10 – 7.39 (30H, m, stopper Ar*H*), 6.94 (2H, d, $^3J$ = 8.8 Hz, axle Ar*H*$OCH_2$), 6.50 (4H, d, $^3J$ = 8.8 Hz, hydroquinone Ar*H*), 6.31 (4H, d, $^3J$ = 8.8 Hz, hydroquinone Ar*H*), 5.63 (2H, s, axle ArHO$CH_2$), 4.76 (3H, s, macrocycle $N^+CH_3$), 4.67 (3H, s, axle $N^+CH_3$), 4.64 (2H, t, $^3J$ = 5.3 Hz, axle $CH_2$N), 4.00 – 4.12 (4H, m, $CH_2$), 3.84 – 3.98 (12H, m, $CH_2$), 3.77 – 3.82 (4H, m, $CH_2$), 3.62 – 3.65 (4H, m, $CH_2$), 3.56 – 3.59 (6H, m, $CH_2$), 3.45 (4H, br s, $CH_2$), 1.33 (18H, s, $^t$Bu), 1.30 (18H, s, $^t$Bu); **$^{13}$C NMR** (125 MHz, $d_6$-acetone) δ (ppm): 162.5, 161.6, 159.6, 157.6, 153.6, 152.7, 149.7, 149.5, 148.5, 148.5(*sic*), 148.2, 145.5, 144.9, 144.4, 140.7, 136.5, 135.2, 133.8, 133.1, 132.6, 131.3, 131.6, 129.9, 128.7, 128.5, 127.1, 126.9, 125.7, 125.5, 125.3, 121.3, 115.7, 115.1, 114.5, 71.6, 71.3, 71.3(*sic*), 71.2, 71.2(*sic*), 71.1, 68.2, 66.8, 65.0, 64.5, 62.5, 50.1, 49.7, 41.4, 41.1, 35.1, 35.1(*sic*), 31.9; **$^{19}$F NMR** (282.4 MHz, $d_6$-acetone ) δ (ppm): −72.3 (d, $^1J$ = 709 Hz, P$F_6$); **$^{31}$P NMR** (121.6 MHz, $d_6$-acetone) δ (ppm): −144.3 (sept, $^1J$ = 709 Hz, $PF_6$); **HRMS (ESI):** *m/z* calc. for $C_{115}H_{133}N_9O_{14}\cdot(PF_6)_2$ $[M - PF_6]^+$: 2009.9641; found: 2009.9694.

**4,4'-bis(azidomethyl)biphenyl (74):**

4,4′-*bis*(Chloromethane)-1,1′-biphenyl (2.5 g, 9.95 mmol) and $NaN_3$ (1.49 g, 24.9 mmol) was dissolved in DMSO (150 mL) and stirred for 16 h. The solution was poured onto $H_2O$ (300 mL) and the resulting precipitate collected by vacuum filtration. The precipitate was dried under vacuum for 4 h to give a white solid (2.48 g, 94 %).

**$^1$H NMR** (300 MHz, $CDCl_3$) δ: 7.63 (4H, d, $^3J$ = 8.5 Hz, Ar*H*), 7.41 (4H, d, $^3J$ = 8.5 Hz, Ar*H*), 4.41 (4H, s, C$H_2$).[20]

**(4'-(azidomethyl)biphenyl-4-yl)methanamine (75)[21]:**

Bis-azide **74** (300 mg, 1.14 mmol) was dissolved in 1:1 $Et_2O$/EtOAc (10 mL), 5% $HCl_{(aq)}$ (20 mL) was added and the biphasic mixture cooled to 0 ºC. A solution of $Ph_3P$ (295 mg, 1.13 mmol) in 1:1 $Et_2O$/EtOAc (10 mL) was added dropwise over 30 min, and the solution stirred for 18 h at RT. The precipitate was collected by vacuum filtration and washed with 1:1 $Et_2O$/EtOAc (2 × 50 mL). The resulting solid was suspended in $CH_2Cl_2$, 10% $NaOH_{(aq)}$ added and the biphasic mixture stirred for 30 min until all solid had dissolved. The organic layer was separated, washed with $H_2O$ (2 × 50 mL), dried over $MgSO_4$, and the solvent removed *in vacuo* to give a white waxy solid (100 mg, 37%).

**$^1$H NMR** (300 MHz, $CD_3OD$) δ: 7.59 – 7.66 (4H, m, Ar*H*), 7.42 (4H, d, $^3J$ = 8.2 Hz, Ar*H*), 4.40 (2H, s, C$H_2N_3$), 3.83 (2H, s, C$H_2NH_2$); **$^{13}$C NMR** (75.5 MHz, $CD_3OD$) δ: 142.6, 141.9, 140.3, 135.9, 129.8, 128.9, 128.1, 128.0, 55.1, 46.2; **HRMS (Probe FI)** calculated for $C_{14}H_{14}N_4$ $[M]^{\cdot+}$: 238.1218; found 238.1212.

**Pyridine axle precursor (76):**

Acid **60** (192 mg, 1.06 mmol) was suspended in dry $CH_2Cl_2$ (20 mL), then oxalyl chloride (0.190 mL, 2.12 mmol) and DMF (cat.) were added. The mixture was stirred for 1 h until all solid had dissolved. The solvent was removed *in vacuo*, then redissolved in dry $CH_2Cl_2$ (15 mL) and added dropwise to a solution of compound **75** (253 mg, 1.06 mmol) and $Et_3N$

(0.42 mL, 3 mmol) in $CH_2Cl_2$ (20 mL). The resulting solution was stirred for 1 h, washed with 10 % $HCl_{(aq)}$ (2 x 50 mL) and $H_2O$ (2 x 50 mL), dried over anhydrous $MgSO_4$, and the solvent removed *in vacuo*. The resulting brown oil was purified by column chromatography (silica; 95:5 $CH_2Cl_2$/MeOH) giving an oily orange solid (306 mg, 72 %).

**$^1$H NMR** (300MHz, $CDCl_3$) δ (ppm): 9.06 (2H, dd, $^3J$ = 8.2 Hz, $^4J$ = 2.1 Hz, pyridine $H^2$ & $H^6$), 8.90 (1H, s, ArHN*H*), 8.90 (1H, t, $^4J$ = 2.1 Hz, pyridine $H^4$), 7.48 – 7.54 (6H, m, stopper Ar*H*NH & 4 × biphenyl Ar*H*), 7.09 – 7.36 (20H, m, $CH_2$N*H*, 4 × biphenyl Ar*H* & stopper Ar*H*), 4.60 (2H, d, $^3J$ = 5.3 Hz, C$H_2$NH), 4.36 (2H, s, C$H_2N_3$), 1.30 (18H, s, $^t$Bu); **$^{13}$C NMR** (75.5 MHz, $CDCl_3$) δ (ppm): 165.1, 163.5, 150.8, 150.3, 148.5, 146.9, 144.1, 143.5, 140.3, 139.8, 136.6, 135.3, 134.5, 134.1, 131.8, 131.0, 130.6, 129.6, 128.6, 128.1, 127.3, 125.8, 124.2, 119.4, 63.7, 54.4, 43.8, 34.2, 31.3; **HRMS (ESI):** *m/z* calc. for $C_{54}H_{52}N_6O_2$ $[M + Na]^+$: 839.4044; found 839.4038.

**Pyridinium axle precursor (77·Cl):**

Compound **76** (100 mg, 0.12 mmol) was dissolved in MeI (5 mL), heated at reflux under $N_{2(g)}$ for 16 h, cooled to RT, and the solvent removed *in vacuo*. The residue was dissolved in $CHCl_3$ (30 mL), washed with 1 M $NH_4Cl_{(aq)}$ solution (5 × 50 mL) and $H_2O$ (2 × 50 mL), dried over anhydrous $MgSO_4$, and the solvent removed *in vacuo* to give a yellow oily solid (99 mg, 93%).

**$^1$H NMR** (300 MHz, $CDCl_3$) δ: 10.67 (1H, s, ArHN*H*), 10.32 (1H, s, pyridinium $H^6$), 9.94 (1H, t, $^3J$ = 5.9 Hz, $CH_2$N*H*), 9.26 (1H, s, pyridinium $H^2$), 8.47 (1H, s, pyridinium $H^4$), 7.66 (2H, d, $^3J$ = 8.9 Hz, Ar*H*NH), 7.54 (2H, d, $^3J$ = 8.2 Hz, biphenyl Ar*H*), 7.44 – 7.49 (4H, m, biphenyl Ar*H*), 7.34 (2H, d, $^3J$ = 8.2 Hz, biphenyl Ar*H*), 7.14 – 7.31 (15H, m, stopper Ar*H*), 4.58 (2H, d, $^3J$ = 5.9 Hz, C$H_2$NH), 4.33 (2H, s, C$H_2N_3$), 3.83 (3H, s, $N^+CH_3$), 1.29 (18H, s, $^t$Bu); **$^{13}$C NMR** (125 MHz, $CDCl_3$) δ (ppm): 160.4, 158.2, 148.7, 147.4, 147.3, 146.3, 145.1, 144.0, 141.6, 140.7, 139.6, 137.3, 135.4, 134.7, 134.7(*sic*), 134.3, 133.9, 131.7, 131.1, 130.7,

129.2, 128.9, 127.8, 127.3, 126.0, 119.5, 64.1, 54.6, 49.0, 44.0, 34.5; **HRMS (ESI)** *m/z* calc.for $C_{55}H_{55}N_6O_2$ $[M - Cl]^+$: 831.4381; found: 831.4366.

**Rotaxane (78·$(PF_6)_2$):**

Axle precursor **77**·Cl (65 mg, 78 μmol), macrocycle **30**·I (54 mg, 78 μmol) and stopper **72** (38 mg, 78 μmol) were dissolved in degassed $CH_2Cl_2$ (20 mL) and stirred for 15 min. DIPEA (20 μL, 115 μmol), $Cu(MeCN)_4PF_6$ (6 mg, 16 μmol) and TBTA (8 mg, 15 μmol) were added and the solution stirred under $N_{2(g)}$ for 16 h. The solution was washed with 10% $HCl_{(aq)}$ (2 × 20 mL) and $H_2O$ (2 × 20 mL), dried over anhydrous $MgSO_4$, and the solvent removed *in vacuo*. The crude material was purified by column chromatography (silica; 28:2:1 MeCN/$H_2O$/sat. $KNO_{3(aq)}$) and preparative TLC (silica; 9:1 $CH_2Cl_2$/MeOH) to obtain a yellow solid which was then redissolved in $CHCl_3$ (10 mL) and washed with $NH_4PF_{6(aq)}$ (10 × 10 mL) and $H_2O$ (2 × 10 mL). The organic phase was dried over anhydrous $MgSO_4$ and the solvent removed *in vacuo* to give a yellow solid (70 mg, 41%).

**$^1$H NMR** (500 MHz, $d_6$-acetone) δ (ppm): 9.61 (2H, s, axle pyridinium $H^2$ & $H^6$), 9.56 (1H, br s, axle ArHN*H*), 9.46 (1H, s, axle pyridinium $H^4$), 9.34 (2H, s, macrocycle pyridinium $H^2$ & $H^6$), 8.79 (2H, br s, macrocycle N*H*), 8.49 (1H, s, macrocycle pyridinium $H^4$), 8.15 (1H, s, triazole C*H*), 7.74 (1H, s, axle $CH_2NH$), 7.68 (4H, d, $^3J$ = 8.2 Hz, biphenyl Ar*H*), 7.63 (2H, d, $^3J$ = 8.2 Hz, Ar*H*NH), 7.49 (4H, d, $^3J$ = 8.2 Hz, biphenyl Ar*H*), 7.02 – 7.38 (30H, m, stopper Ar*H*), 6.93 (2H, d, $^3J$ = 9.4 Hz, Ar*H*$OCH_2$), 6.49 (4H, d, $^3J$ = 8.8 Hz, hydroquinone Ar*H*), 6.29 (4H, d, $^3J$ = 8.8 Hz, hydroquinone Ar*H*), 5.71 (2H, s, ArHOC$H_2$), 5.15 (2H, s, axle C$H_2$N), 4.70 (3H, s, macrocycle $N^+CH_3$), 4.34 (5H, br s, axle $N^+CH_3$ & C$H_2$NH), 3.73 – 4.02 (20H, m, macrocycle C$H_2$), 1.32 (18H, s, $^t$Bu), 1.29 (18H, s, $^t$Bu); **$^{13}$C NMR** (125 MHz, $CD_3CN$) δ (ppm): 161.9, 161.3, 159.5, 157.3, 153.4, 152.6, 149.9, 149.6, 148.6, 148.3, 147.8, 146.7, 145.9, 145.4, 145.1, 141.1, 140.9, 140.3, 138.2, 136.3, 135.9, 134.9, 133.4, 132.8, 132.4, 131.6, 131.3, 129.8, 128.8, 128.6, 128.4, 128.1, 127.1, 126.9, 125.8, 125.5, 121.6,

115.7, 115.0, 114.7, 71.4, 70.9, 68.2, 66.8, 64.5, 64.5(*sic*), 62.4, 54.2, 50.0, 49.7, 35.1, 35.0, 31.6; **$^{19}$F NMR** (282.4 MHz, $d_6$-acetone ) δ (ppm): −72.4 (d, $^1J$ = 702 Hz, P$F_6$); **$^{31}$P NMR** (121.6 MHz, $d_6$-acetone) δ (ppm): −144.3 (sept, $^1J$ = 702 Hz, $P$F$_6$); **HRMS (ESI):** *m/z* calc. for $C_{121}H_{129}N_9O_{11}\cdot(PF_6)_2$ $[M - 2PF_6 - H]^+$: 1883.9760; found: 1883.4697.

**Pyridine *N*-oxide thread (79):**

A solution of *m*CPBA (184 mg, 1.07 mmol) in dry $CH_2Cl_2$ (10 mL) was added to a solution of pyridine thread **5** (100 mg, 0.30 mmol) in dry $CH_2Cl_2$ (30 mL) at 0 °C. The solution was stirred under $N_{2(g)}$ at RT for 16 h, then washed with sat. $NaHCO_{3(aq)}$ (50 mL) and the aqueous layer extracted with $CH_2Cl_2$ (3 × 50 mL). The combined organic phase was dried over anhydrous $MgSO_4$, and the solvent removed *in vacuo*. The resulting residue was purified by column chromatography (silica; EtOAc → 95:5 EtOAc/MeOH) to give a white solid (50 mg, 48%).

**$^1$H NMR** (300 MHz, $CDCl_3$) δ (ppm): 8.89 (2H, s, pyridine $H^2$ & $H^6$), 8.24 (1H, s, pyridine $H^4$), 7.72 (2H, t, $^3J$ = 5.6 Hz, N$H$), 3.41 – 3.48 (4H, m, NHC$H_2$), 1.59 – 1.69 (4H, m, NHCH$_2$C$H_2$), 1.26 – 1.43 (8H, m, C$H_2$), 0.87 – 0.92 (6H, t, $^3J$ = 7.0 Hz, C$H_3$); **$^{13}$C NMR** (75.5 MHz, $CDCl_3$) δ (ppm): 162.2, 140.1, 134.1, 124.6, 40.7, 31.5, 29.3, 26.7, 22.6, 14.0; **HRMS (ESI):** *m/z* calc. for $C_{19}H_{31}N_3O_3$ $[M + Na]^+$: 372.2258; found: 372.2263.

**Pyridine *N*-oxide axle precursor (80):**

METHOD 1: A solution of *m*CPBA (92 mg, 0.531 mmol) in dry $CH_2Cl_2$ (10 mL) was added to a solution of compound **76** (122 mg, 0.149 mmol) in dry $CH_2Cl_2$ (30 mL) at 0 °C. The solution was stirred under $N_{2(g)}$ at RT for 16 h, then washed with sat. $NaHCO_{3(aq)}$ (50 mL). The combined organic phase was dried over anhydrous $MgSO_4$ and the solvent removed *in vacuo*. The resulting residue was purified by column chromatography (silica; 95:5 $CH_2Cl_2$/MeOH) to give a white solid (20 mg, 16%).

METHOD 2: Compound **76** (0.198 g, 0.24 mmol) and $NaHCO_3$ (1.03 g, 7.26 mmol) were dissolved in 1:1 2-butanone/$H_2O$ (50 mL) and a saturated solution of Oxone® (0.446 g, 0.726 mmol) in $H_2O$ (3 mL) was added dropwise. The solution was stirred vigorously for 2 h before addition of NaCl (1.70 g, 29.0 mmol) and extraction with $CHCl_3$ (3 × 50 mL). The organic layer was dried over anhydrous $MgSO_4$ and the solvent removed *in vacuo* to give a white solid (0.196 g, 97%).

**$^1$H NMR** (300MHz, $CDCl_3$) δ (ppm): 9.71 (1H, s, ArHN*H*), 8.88 (1H, s, pyridine $H^6$), 8.84 (1H, s, pyridine $H^2$), 8.38 (2H, br s, $CH_2NH$ & pyridine $H^4$), 7.63 (2H, d, $^3J$ = 8.8 Hz, Ar*H*NH), 7.55 (2H, d, $^3J$ = 8.2 Hz, biphenyl Ar*H*), 7.49 (2H, d, $^3J$ = 8.2 Hz, biphenyl Ar*H*), 7.15 – 7.35 (19H, m, stopper Ar*H*), 4.53 (2H, d, $^3J$ = 4.7 Hz, C$H_2$NH), 4.35 (2H, s, C$H_2N_3$), 1.36 (18H, s, $^t$Bu) **$^{13}$C NMR** (75.5 MHz, $CDCl_3$) δ (ppm): 162.0, 160.4, 148.5, 146.9, 144.5, 143.5, 140.2, 139.8, 136.3, 135.0, 134.5, 133.6, 131.8, 131.0, 130.6, 128.6, 128.3, 127.4, 127.3, 127.2, 125.8, 124.3, 119.5, 63.8, 54.4, 44.0, 34.3, 31.3; **HRMS (ESI):** *m/z* calc. for $C_{54}H_{52}N_6O_3$ $[M+Na]^+$: 855.3993; found: 855.3994.

***tert*-Butyl *N*-oxide rotaxane (81):**

Compound **80** (119 mg, 143 μmol), macrocycle **54** (23.2 mg, 36 μmol) and stopper **72** (17.5 mg, 36 μmol) were dissolved in degassed $CH_2Cl_2$ (10 mL) and stirred for 15 min. DIPEA (7 μL, 41 μmol), $Cu(MeCN)_4PF_6$ (3 mg, 8 μmol) and TBTA (4 mg, 7.5 μmol) were added and the solution stirred under $N_{2(g)}$ for 16 h. The solvent was removed *in vacuo* and the crude material purified by preparative TLC (silica; 1:1 MeCN/$CH_2Cl_2$) to obtain a white solid that was shown by $^1$H NMR spectroscopy to be contaminated by the component macrocycle. It was not possible to further purify this rotaxane, and therefore characterisation by $^{13}$C NMR is absent.

**$^1$H NMR** (300MHz, $CDCl_3$) δ (ppm): 8.76 (1H, s, isophthalamide $H^2$), 8.51 (1H, s, pyridine $H^6$), 8.48 (1H, s, pyridine $H^2$), 8.44 (1H, s, axle ArHN*H*), 8.34 (2H, t, $^3J$ = 3.5 Hz, macrocycle

N*H*), 8.27 (2H, d, $^4J$ = 1.2 Hz, isophthalamide $H^4$ & $H^6$), 7.94 (1H, t, $^3J$ = 5.3 Hz, axle $CH_2NH$), 7.57 – 7.68 (10H, m, 1 × pyridine $H^4$, 1 × triazole C*H*, 2 × axle Ar*H*NH & 6 × biphenyl Ar*H*), 7.37 (2H, d, $^3J$ = 8.2 Hz, biphenyl Ar*H*), 7.06 – 7.30 (30H, m, stopper Ar*H*), 6.84 (2H, d, $^3J$ = 8.8 Hz, axle Ar*H*$OCH_2$), 6.22 – 6.30 (8H, m, hydroquinone ArH), 5.58 (2H, s, axle $OCH_2$), 5.17 (2H, s, $CH_2N$), 4.71 (2H, d, $^3J$ = 5.3 Hz, axle $CH_2NH$), 3.78 – 3.93 (10H, m, macrocycle $CH_2$), 3.52 – 3.61 (10H, m, macrocycle $CH_2$), 3.38 (4H, br s, macrocycle $CH_2$), 1.32 (18H, s, $^t$Bu), 1.30 (18H, s, $^t$Bu); **HRMS (ESI):** *m/z* calc. for $C_{126}H_{136}N_8O_{13}$ $[M + Na]^+$: 1993.0152; found: 1993.0174.

**Pyridine *N*-oxide rotaxane (82):**

Compound **80** (178 mg, 214 μmol), macrocycle **8** (42 mg, 71 μmol) and stopper **72** (35 mg, 71 μmol) were dissolved in degassed $CH_2Cl_2$ (10 mL) and stirred for 15 min. DIPEA (14 μL, 82 μmol) and $Cu(MeCN)_4PF_6$ (5 mg, 13 μmol) were added and the solution stirred under $N_2$ for 16 h. The solvent was removed *in vacuo* and the crude material purified by column chromatography (silica; EtOAc) and preparative TLC (silica; 95:5 EtOAc/MeOH & 9:1 $CH_2Cl_2$/MeOH) to obtain a white solid (20 mg, 15%).

**$^1$H NMR** (300MHz, $CDCl_3$) δ (ppm): 9.39 (2H, d, $^4J$ = 2.2 Hz, macrocycle pyridine $H^2$ & $H^6$), 8.98 (1H, t, $^4J$ = 2.2 Hz, macrocycle pyridine $H^4$), 8.79 (1H, s, axle ArHN*H*), 8.52 (1H, s, axle pyridine $H^6$), 8.49 (1H, s, axle pyridine $H^2$), 8.32 (2H, t, $^3J$ = 4.3 Hz, macrocycle N*H*), 7.94 (1H, t, $^3J$ = 5.7 Hz, axle $CH_2NH$), 7.58 – 7.68 (10H, m, 1 × axle pyridine $H^4$, 1 × triazole C*H*, 2 × axle Ar*H*NH & 6 × biphenyl Ar*H*), 7.37 (2H, d, $^3J$ = 8.2 Hz, biphenyl Ar*H*), 7.07 – 7.30 (30H, m, stopper Ar*H*), 6.84 (2H, d, $^3J$ = 9.1 Hz, axle Ar*H*$OCH_2$), 6.23 – 6.29 (8H, m, hydroquinone Ar*H*), 5.58 (2H, s, axle $OCH_2$), 5.17 (2H, s, $CH_2N$), 4.71 (2H, d, $^3J$ = 5.7 Hz, axle $CH_2NH$), 3.91 (4H, t, $^3J$ = 4.7 Hz, macrocycle $CH_2$), 3.81 (4H, q, $^3J$ = 4.5 Hz, macrocycle $CH_2$), 3.55 – 3.61 (8H, m, macrocycle $CH_2$), 3.47 – 3.50 (4H, m, macrocycle $CH_2$), 3.35 – 3.42 (4H, m, macrocycle $CH_2$), 1.32 (18H, s, $^t$Bu), 1.30 (18H, s, $^t$Bu); **$^{13}$C NMR**

(125.5 MHz, $CDCl_3$) δ (ppm): 165.9, 160.8, 159.0, 156.1, 152.8, 152.6, 152.3, 148.7, 148.4, 147.3, 147.0, 144.8, 144.3, 143.8, 143.6, 140.9, 140.1, 140.0, 139.7, 137.6, 135.0, 133.9, 132.8, 132.3, 132.2, 132.1, 131.8, 131.1, 131.1(*sic*), 130.6, 129.2, 128.7, 128.4, 127.4, 127.4(*sic*), 127.2, 125.9, 125.7, 124.3, 124.1, 122.6, 120.5, 119.7, 114.9, 114.0, 113.2, 70.4, 70.0, 69.7, 66.8, 66.6, 63.8, 63.4, 62.0, 53.8, 43.6, 40.6, 34.3, 34.3(*sic*), 31.4, 31.3; **HRMS (ESI):** *m/z* calc. for $C_{119}H_{123}N_9O_{12}$ $[M + Na]^+$: 1937.9478; found: 1937.9468.

**Calixdiquinone *N*-oxide rotaxane (84):**

General procedure: Compound **80** (24 mg, 28.5 μmol), calixdiquinone macrocycle **83** (30 mg, 28.5 μmol) and stopper **72** (14 mg, 28.5 μmol) were dissolved in degassed $CH_2Cl_2$ (20 mL), (a solution of $M(ClO_4)_x$ (28.5 μmol) in) MeCN (0.25 mL) was added and the solution stirred for 15 min. DIPEA (5 μL, 29.3 μmol) and $Cu(MeCN)_4PF_6$ (2 mg, 5.4 μmol) were added and the solution stirred under $N_2$ for 16 h. The solvent was removed *in vacuo* and the crude material purified by preparative TLC (silica; 1:1 acetone/hexane & MeCN → 93:7 MeCN/MeOH) to obtain a yellow solid.

Without cation: Neat MeCN added i.e. no $M(ClO_4)_x$, giving a yield of 10% (7 mg).

With Barium: M = Ba, x = 2, giving a yield of 28% (18 mg). N.B. $Ba(ClO_4)_2$ mostly suspended throughout reaction

With Sodium: M = Na, x = 1, giving a yield of 50% (34 mg).

**$^1$H NMR** (300MHz, $CDCl_3$) δ (ppm): 9.12 (1H, s, axle ArHN*H*), 8.68 (2H, s, pyridine $H^6$ & isophthalamide $H^2$), 8.54 (1H, s, pyridine $H^2$), 8.52 (1H, t, $^3J$ = 5.6 Hz, axle $CH_2NH$), 8.39 (2H, br s, macrocycle N*H*), 8.23 (2H, dd, $^3J$ = 7.9 Hz, $^4J$ = 1.9 Hz, isophthalamide $H^4$ & $H^6$), 8.03 (1H, s, pyridine $H^4$), 7.92 (2H, d, $^3J$ = 8.8 Hz, Ar*H*NH), 7.64 (1H, s, triazole, C*H*), 7.59 (2H, d, $^3J$ = 7.5 Hz, biphenyl Ar*H*), 7.50 (2H, d, $^3J$ = 8.2 Hz, biphenyl Ar*H*), 7.37 – 7.41 (4H, m, biphenyl Ar*H*), 7.06 – 7.29 (31H, m, isophthalamide $H^5$ & stopper Ar*H*), 6.85 (2H, d, $^3J$ = 8.8 Hz, Ar*H*$OCH_2$), 6.55 – 6.56 (4H, m, calix Ar*H*), 6.50 (4H, d, $^3J$ = 9.1 Hz,

hydroquinone Ar*H*), 6.32 – 6.37 (8H, m, calix & hydroquinone Ar*H*), 5.60 (2H, s, axle OC$H_2$), 5.17 (2H, s, C$H_2$N), 4.59 (2H, d, $^3J$ = 5.6 Hz, axle C$H_2$NH), 4.29 (2H, d, $^2J$ = 12.9 Hz, calix C$H_2$), 4.21 (2H, t, $^3J$ = 8.7 Hz, macrcocycle C$H_2$), 4.09 (2H, d, $^2J$ = 12.9 Hz, calix C$H_2$) 3.96 – 3.99 (2H, m, macrocycle C$H_2$), 3.89 – 3.94 (6H, m, macrocycle C$H_2$), 3.82 – 3.85 (2H, m, macrocycle C$H_2$), 3.71 – 3.77 (4H, m, macrocycle C$H_2$), 2.92 (2H, $^2J$ = 12.9 Hz, calix C$H_2$), 2.73 (2H, $^2J$ = 12.9 Hz, calix C$H_2$), 1.32 (18H, s, axle $^t$Bu), 1.29 (18H, s, axle $^t$Bu), 0.95 (18H, s, calix $^t$Bu); **$^{13}$C NMR** (125 MHz, $CDCl_3$) δ (ppm): 187.9, 187.5, 185.0, 184.9, 167.9, 167.8, 161.6, 159.4, 156.4, 153.3, 152.8, 152.0, 149.0, 148.7, 148.2, 148.0, 147.5, 147.3, 147.0, 145.0, 144.4, 144.1, 143.5, 141.3, 140.9, 140.3, 140.2, 139.7, 137.9, 136.2, 134.1, 134.0, 132.5, 132.2, 132.1, 131.8, 131.4, 131.2, 130.9, 130.8, 129.5, 129.4, 129.2, 129.0, 128.0, 127.7, 127.7(*sic*), 127.5, 127.0, 126.3, 125.9, 125.4, 125.3, 124.9, 124.7, 124.5, 124.4, 122.9, 118.7, 115.4, 114.2, 113.5, 74.4, 67.7, 67.0, 64.0, 63.7, 62.3, 54.2, 53.7, 43.4, 41.0, 34.6, 34.5, 34.2, 31.6, 31.6(*sic*), 31.4; **HRMS (ESI):** *m/z* calc. for $C_{154}H_{154}N_8O_{16}$ $[M + Na]^+$: 2395.1414; found 2395.1450.

## 5.3 References


1. A. V. Leontiev, C. A. Jemmett and P. D. Beer, *Chem. Eur. J.*, 2011, **17**, 816-825.
2. K.-Y. Ng, V. Felix, S. M. Santos, N. H. Rees and P. D. Beer, *Chem. Commun.*, 2008, 1281-1283.
3. K. M. Bonger, R. van den Berg, L. H. Heitman, A. P. Izjerman, J. Oosterom, K. M. Timmers, H. S. Overkleeft and G. A. van der Marel, *Biorg. Med. Chem.*, 2007, **15**, 4841-4856.
4. J. A. Wisner, P. D. Beer and M. G. B. Drew, *Angew. Chem., Int. Ed.*, 2001, **40**, 3606-3609.
5. L. M. Hancock and P. D. Beer, *Chem. Eur. J.*, 2009, **15**, 42-44.
6. H. W. Gibson, S.-H. Lee, P. T. Engen, P. Lecavalier, J. Sze, Y. X. Shen and M. Bheda, *J. Org. Chem*, 1993, **58**, 3748-3756.
7. J. A. Wisner, P. D. Beer, M. G. B. Drew and M. R. Sambrook, *J. Am. Chem. Soc.*, 2002, **124**, 12469-12476.
8. W. Huang and T. Ogawa, *Polyhedron*, 2006, **25**, 1379-1385.
9. G. F. Smith and F. W. Cagle, *J. Org. Chem.*, 1947, **12**, 781-784.
10. K. Binnemans, P. Lenaerts, K. Driesen and C. Gorller-Walrand, *J. Mater. Chem.*, 2004, **14**, 191-195.
11. J. P. Collman, R. A. Decreau and S. Costanzo, *Org. Lett.*, 2004, **6**, 1033-1036.

12. K. M. Broadus and S. R. Kass, *J. Am. Chem. Soc.*, 2000, **122**, 9014-9018.
13. X. Li, W. Liu, H. Y. Zhang and B. L. Wu, *J. Organomet. Chem.*, 2008, **693**, 3295-3302.
14. M. R. Sambrook, P. D. Beer, J. A. Wisner, R. L. Paul, A. R. Cowley, F. Szemes and M. G. B. Drew, *J. Am. Chem. Soc.*, 2005, **127**, 2292-2302.
15. H. W. Gibson, S.-H. Lee, P. T. Engen, P. Lecavalier, J. Sze, Y. X. Shen and M. Bheda, *J. Org. Chem.*, 1993, **58**, 3748-3756.
16. Y. Zheng. H; Zhou. W; Lv. J; Yin. X; Li. Y; Liu. H; Li, *Chem. Eur. J.*, 2009, **15**, 13253-13262.
17. M. D. Lankshear, I. Dudley, K.-M. Chan, S. M. Santos, V. Felix and P. D. Beer, *Chem. Eur. J.*, 2008, **14**, 2248-2263.
18. M. Gonçalves, K. Estieu-Gionnet, T. Berthelot, G. Laïn, M. Bayle, X. Canron, N. Betz, A. Bikfalvi and G. Déléris, *Pharm. Res.*, 2005, **22**, 1411-1421.
19. V. Aucagne, K. D. Hänni, D. A. Leigh, P. J. Lusby and D. B. Walker, *J. Am. Chem. Soc.*, 2006, **128**, 2186-2187.
20. J. R. Thomas, X. Liu and P. J. Hergenrother, *J. Am. Chem. Soc.*, 2005, **127**, 12434-12435.
21. D. E. Phipps and P. D. Beer, *Tetrahedron Lett.*, 2009, **50**, 3454-3457.

# Appendices

## A.1 Titration Protocols

### A.1.1 $^1$H NMR Titrations

Proton NMR titration experiments were performed on a Varian Unity Plus 500 spectrometer. Typically, a solution of guest was added to a solution of the host at 293 K and the chemical shift(s) of particular host proton(s) was monitored for seventeen titration points (for 0, 0.2, 0.4, 0.6, 0.8, 1.0, 1.2, 1.4, 1.6, 1.8, 2.0, 2.5, 3.0, 4.0, 5.0, 7.0 and 10.0 equivalents of added guest). The resulting data were analysed using the winEQNMR2[1] computer programme in experiments where association of guest and host was fast on the NMR timescale.

A summary of the concentration of host and guest species, along with the solvent used for every $^1$H NMR titration described in this thesis is given in Table 1. The volumes of guest solution added were 10 × 2 μL, 2 × 5 μL, 2 × 10 μL, 1 × 20 μL, and 1 × 30 μL.

| HOST (concentration) | GUEST (concentration) | Solvent |
|---|---|---|
| Macrocycle **9** ($3.08 \times 10^{-3}$ M) | Thread **6**·Cl (0.154 M) | $CD_2Cl_2$ |
| Rotaxanes **14**·$PF_6$, **18**·$PF_6$, **19**·$PF_6$, **20**·$PF_6$, **21**·$PF_6$, **22**·$PF_6$, | TBA Cl, $H_2PO_4$, OAc | 45:45:10 $CDCl_3/CD_3OD/D_2O$ |
| Rotaxane **28**·$(PF_6)_2$ | TBA Cl | |
| Rotaxane **28**·$(PF_6)_2$ | TBA Cl, $H_2PO_4$, OAc | 65:35 $d_6$-acetone/$D_2O$ |
| Rotaxane **23**·$PF_6$ | TBA Cl | 1:1 $CDCl_3/CD_3OD$ |
| Catenanes **32**·$PF_6$, **33**·$PF_6$ | TBA Cl, $H_2PO_4$, OAc | |
| Thread **44**·$(PF_6)_3$, **50**·$(PF_6)_3$ ($1.91 \times 10^{-3}$ M) | TBA Cl, Br, $H_2PO_4$, OAc (0.094 M) | 9:1 $d_6$-acetone/$D_2O$ |
| Rotaxanes **38**·$PF_6$ | TBA Cl, $H_2PO_4$, OAc | 9:1 $d_6$-acetone/$D_2O$ |
| **39**·$PF_6$ | TBA Cl, $H_2PO_4$ | 7:3 $d_6$-acetone/$D_2O$ |
| Macrocycle **54** + 1 eq. TBACl | **44**·$(PF_6)_3$, **50**·$(PF_6)_3$ | $d_6$-acetone |
| Macrocycle **54** ($1.43 \times 10^{-3}$ M) | Thread **79**, **79** + 1 eq. TBACl (0.0715 M) | $CDCl_3$ |

***Table A1.*** *Host and guest concentrations, and solvent of NMR titrations.*

The values of the observed chemical shift and the guest concentration were entered into winEQNMR2 for every titration point, and estimates for the binding constant, limiting chemical shifts and binding stoichiometry made. The parameters were refined using non-linear least squares analysis to obtain the best fit between observed and calculated chemical shifts; the program plots the observed shift versus the guest concentration, revealing the accuracy of the experimental data and the suitability of the model used. The input parameters were varied until the best-fit values of the stability constants, together with their errors, converged.

### A.1.2 Luminescence titrations

Luminescence titration experiments were performed on a Perkin Elmer LS-55 spectrophotometer at 293 K. Equivalents of guest was added to a host solution (2.5 mL), with spectra being recorded after each addition of guest and thorough mixing.

Luminescence anion titrations used TBA salts as the guest species, and receptors **38**·$PF_6$, **39**·$(PF_6)_3$, **44**·$(PF_6)_2$, **50**·$(PF_6)_3$, and **51**·$(PF_6)_3$ as the host species. Equivalents of the 0.025 mol $dm^{-3}$ guest solution were added to a 1 x $10^{-4}$ mol $dm^{-3}$ host solution.

The luminescence pseudorotaxane study between macrocycle **55** and thread **44**·$(PF_6)_3$ involved the addition of equivalents of a 1.25 x $10^{-3}$ mol $dm^{-3}$ **44**·$(PF_6)_3$ solution to a 1 x $10^{-4}$ mol $dm^{-3}$ 1:1 **55**/TBACl host solution.

The titration data obtained was analysed using the SPECFIT computer programme to determine association constants. The parameters were refined using a global least squares fitting by the Levenberg-Marquardt method until the values for the stability constants converged.

### A.1.3 UV-vis Titrations

UV-visible experiments were performed on a T60U (PG Instruments Ltd) spectrophotometer at 293 K. The sample volume was 2.5 mL. Equivalents of a 2.5 x $10^{-3}$ mol $dm^{-3}$ TBA salt solution were added to 1 x $10^{-5}$ mol $dm^{-3}$ host solution and the sample was thoroughly mixed before each measurement was made.

## A.2 $^{1}$H NMR Job Plot Analysis

The titration data obtained could be used to determine the stoichiometry of the host-guest complex via Job Plot analysis,[2] which relies on the plotting of the mole fraction of a given component of the assembling system versus the difference in external observable from either that of the final or initial state of the system, as a function of mole fraction.

The mole fraction of host ($\chi_H$) was calculated for each data point by dividing the number of moles of the host present (constant) by the total number of moles present in the system. The difference in chemical shift of a given proton, $\Delta\delta$, was calculated for each point by the subtraction ($\delta[\chi_H=1] - \delta[\chi_H=n]$). The Job Plot was then produced by plotting the product of $\Delta\delta$ and $\chi_H$ against $\chi_H$.

## A.3 Crystal Structure Data

### A.3.1 Rotaxane 14·Cl

Crystals were grown by Dr. Nathan Kilah *via* gaseous diffusion of diisopropyl ether into dichloromethane solution of **14**·Cl, and solved by Dr. Christopher J. Serpell. Data were collected on the I19 beamline of the Diamond Light Source, Harwell, UK under an open flow of $N_2$ gas at 150 K.[3] Data were processed with the Crystal Clear Software package,[4] the structure solved with SIR92,[5] and refined on *F* with CRYSTALS.[6] All non-hydrogen atoms

were modelled with anisotropic displacement parameters, while hydrogen atoms were added geometrically and constrained in further refinement using a riding model. Vibrational, displacement and geometric restraints were applied where appropriate to ensure a physically reasonable model. A void of significant size containing highly disordered solvent was identified and modeled with SQUEEZE in PLATON (1483 $Å^3$ containing 325), approximating three diisopropyl ether molecules (348 electrons).[7]

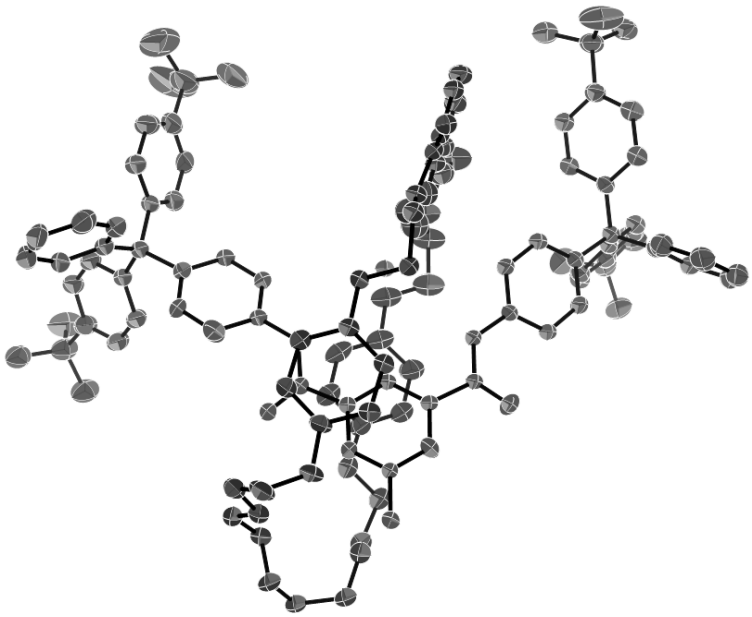


***Figure A1.*** *X-ray crystal structure of* ***14***·*Cl. Ellipsoids shown at 50% probability. Hydrogen atoms omitted for clarity.*

| Chemical formula | $C_{74}H_{78}N_3O_2 \cdot C_{32}H_{38}N_2O_9 \cdot Cl$ |
|---|---|
| Formula Mass | 1671.49 |
| Crystal system | Triclinic |
| *a*/Å | 12.186(7) |
| *b*/Å | 19.717(12) |
| *c*/Å | 25.205(15) |
| *α*/° | 105.937(9) |
| *β*/° | 93.453(3) |
| *γ*/° | 95.645(15) |
| Unit cell volume/Å$^3$ | 5771(6) |
| Temperature/K | 150 |
| Space group | $P\bar{1}$ |
| No. of formula units per unit cell, *Z* | 2 |
| No. of reflections measured | 75634 |
| No. of independent reflections | 35958 |
| $R_{int}$ | 0.052 |
| Final $R_1$ values ($I > 2\sigma(I)$) | 0.0800 |
| Final $wR(F^2)$ values ($I > 2\sigma(I)$) | 0.0906 |
| Final $R_1$ values (all data) | 0.1140 |
| Final $wR(F^2)$ values (all data) | 0.0767 |

### A.3.2 Rotaxane 22·Cl

Crystals were grown by Dr. Nathan Kilah *via* gaseous diffusion of diisopropyl ether into benzene solution of **22**·Cl, and solved by Dr. Nathan Kilah. Data were collected on the I19 beamline of the Diamond Light Source, Didcot, UK under an open flow of $N_2$ gas at 150 K.[3] Data were processed with the Crystal Clear Software package,[4] the structure solved with SIR92,[5] and refined on $F^2$ with CRYSTALS.[6] All non-hydrogen atoms were modelled with anisotropic displacement parameters, while hydrogen atoms were added geometrically and constrained in further refinement using a riding model. A MOGUL geometry check was also performed to identify unusual bond lengths and angles difficult to locate in large structures. Vibrational, displacement and geometric restraints were applied where appropriate to ensure a physically reasonable model. Two voids of significant size containing highly disordered solvent were identified and modelled with SQUEEZE in PLATON (220 and 1019 Å$^3$ containing 47 and 226 electrons respectively).[7]

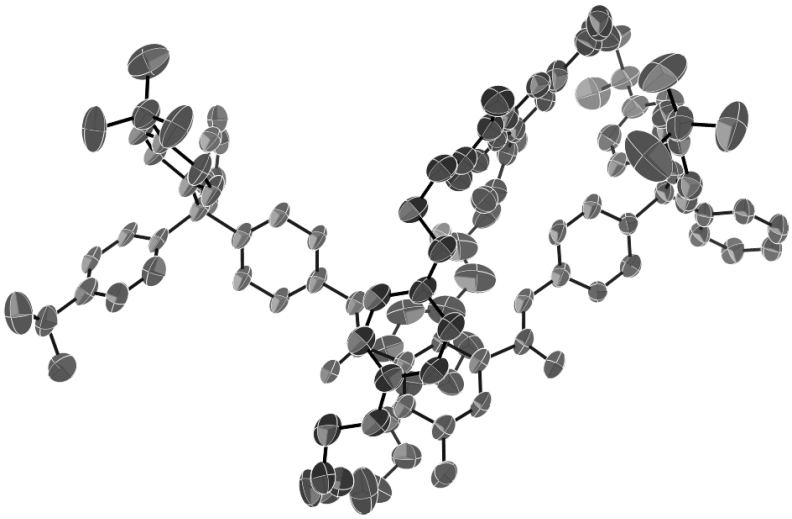


***Figure A2.*** *X-ray crystal structure of* ***22***·*Cl. Ellipsoids shown at 50% probability. Hydrogen atoms omitted for clarity.*

| Chemical formula | $C_{74}H_{78}N_3O_2{\cdot}Cl{\cdot}C_{30}H_{33}N_3O_{10}$ |
|---|---|
| Formula Mass | 1672.51 |
| Crystal system | Triclinic |
| *a*/Å | 11.591(8) |
| *b*/Å | 20.464(16) |
| *c*/Å | 23.83(2) |
| *α*/° | 88.49(3) |
| *β*/° | 77.61(2) |
| *γ*/° | 78.88(3) |
| Unit cell volume/Å$^3$ | 5416(7) |
| Temperature/K | 150 |
| Space group | $P\bar{1}$ |
| No. of formula units per unit cell, *Z* | 2 |
| No. of reflections measured | 37072 |
| No. of independent reflections | 15178 |
| $R_{int}$ | 0.181 |
| Final $R_1$ values ($I > 2\sigma(I)$) | 0.1371 |
| Final $wR(F^2)$ values ($I > 2\sigma(I)$) | 0.2533 |
| Final $R_1$ values (all data) | 0.1995 |
| Final $wR(F^2)$ values (all data) | 0.3387 |

## A.3.3 Catenane 32·Cl

Crystals were grown by slow evaporation of a $CHCl_3$/acetone solution of the **32**·Cl, and solved by Dr. Nathan Kilah. Data were collected using graphite monochromated Mo Kα radiation (λ = 0.71073 Å) on a Nonius KappaCCD diffractometer. The diffractometer was

equipped with a Cryostream $N_2$ open-flow cooling device,[3] and the data were collected at 150(2) K. Series of ω-scans were performed to a maximum resolution of 0.77 Å. Cell parameters and intensity data (including inter-frame scaling) were processed using the DENZO-SMN package.[8] The structures were solved with SUPERFLIP,[9] and refined on $F^2$ in CRYSTALS.[6] Molecular graphics were produced with CrystalMaker.

A portion of the five-oxygen macrocycle was disordered and was modelled over two sites with refined occupancy of 0.680(2) and 0.320(2). The cocrystallised chloroform was found to be related to the major component of the macrocycle disorder, and the occupancy of the chloroform and the disordered macrocycle were modelled together. Additional areas of electron density were observed near the chloroform, but no attempts gave a stable refinement even with considerable geometric and vibrational restraints. The residual electron density was therefore not modelled, and results in a level "C" alert in CheckCIF. Non-hydrogen atoms were refined with anisotropic displacement parameters.

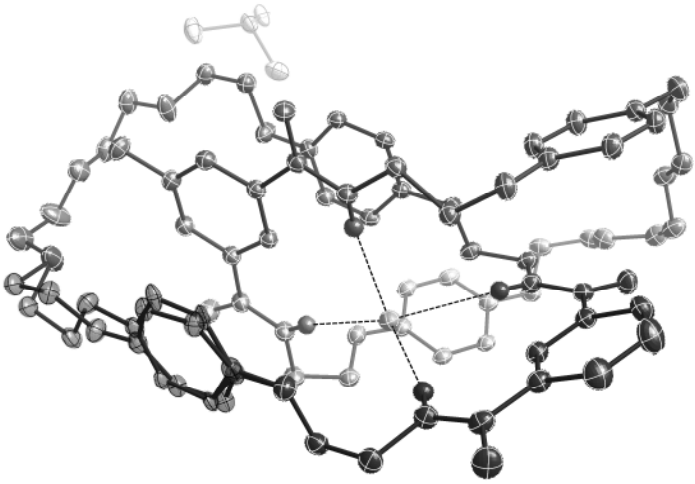


***Figure A3.*** *X-ray crystal structure of* ***32***·*Cl. Ellipsoids shown at 50% probability. Hydrogen atoms omitted for clarity.*

| Chemical formula | $C_{62.68}H_{74.68}N_5O_{17}\cdot Cl_{3.04}$ |
|---|---|
| Formula Mass | 1277.94 |
| Crystal system | Triclinic |
| *a*/Å | 11.8388(1) |
| *b*/Å | 17.4493(1) |
| *c*/Å | 17.8692(2) |
| *α*/° | 114.1468(4) |
| *β*/° | 97.4460(4) |
| *γ*/° | 102.6071(4) |
| Unit cell volume/Å$^3$ | 3186.35(5) |
| Temperature/K | 150 |
| Space group | $P\bar{1}$ |
| No. of formula units per unit cell, *Z* | 2 |
| No. of reflections measured | 26903 |
| No. of independent reflections | 14487 |
| $R_{int}$ | 0.025 |
| Final $R_1$ values ($I > 2\sigma(I)$) | 0.0512 |
| Final $wR(F^2)$ values ($I > 2\sigma(I)$) | 0.1217 |
| Final $R_1$ values (all data) | 0.0645 |
| Final $wR(F^2)$ values (all data) | 0.1342 |

### A.3.4 Catenane 33·$PF_6$

Crystals were grown by slow evaporation of a $CHCl_3$/MeOH solution of the **33**·$PF_6$, and solved by Dr. Christopher Serpell. Data were collected using graphite monochromated Mo Kα radiation (λ = 0.71073 Å) on a Nonius KappaCCD diffractometer. The diffractometer was equipped with a Cryostream $N_2$ open-flow cooling device,[3] and the data were collected at 150(2) K. Series of ω-scans were performed to a maximum resolution of 0.77 Å. Cell parameters and intensity data (including inter-frame scaling) were processed using the DENZO-SMN package.[8] The structures were solved with SUPERFLIP,[9] and refined on $F^2$ in CRYSTALS.[6] Molecular graphics were produced with CrystalMaker.

A water molecule was located in addition to the catenane. All hydrogens could be observed in the difference map, and after assigning geometric positions, they were refined against the data using restraints. The resulting positions were in keeping with hydrogen bonding requirements. Non-hydrogen atoms were refined with anisotropic displacement parameters.

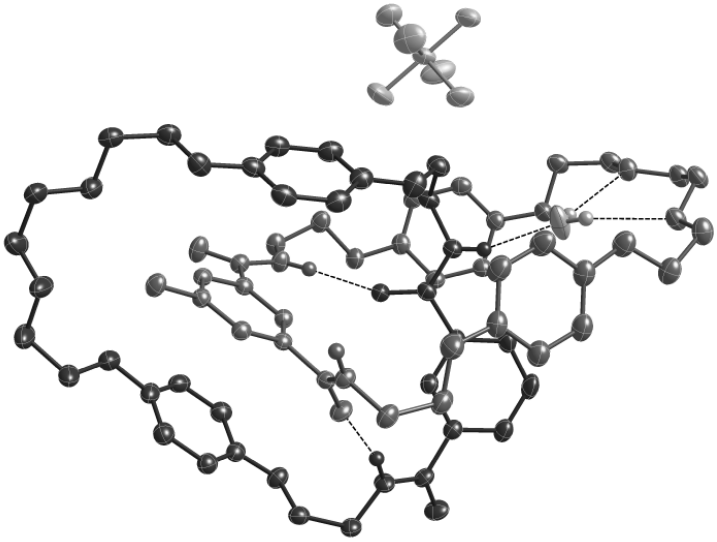


***Figure A4.*** *X-ray crystal structure of* ***33***$\cdot PF_6$*. Ellipsoids shown at 50% probability. Hydrogen atoms omitted for clarity.*

| Chemical formula | $C_{30}H_{36}N_3O_8 \cdot C_{30}H_{34}N_2O_8 \cdot F_6P \cdot H_2O$ |
|---|---|
| Formula Mass | 1280.22 |
| Crystal system | Triclinic |
| *a*/Å | 9.74820(10) |
| *b*/Å | 14.2731(2) |
| *c*/Å | 23.7801(3) |
| *α*/° | 74.5452(5) |
| *β*/° | 78.3493(5) |
| *γ*/° | 85.1917(5) |
| Unit cell volume/Å$^3$ | 3121.77(7) |
| Temperature/K | 150 |
| Space group | $P\bar{1}$ |
| No. of formula units per unit cell, *Z* | 2 |
| No. of reflections measured | 52283 |
| No. of independent reflections | 14264 |
| $R_{int}$ | 0.030 |
| Final $R_1$ values ($I > 2\sigma(I)$) | 0.0501 |
| Final $wR(F^2)$ values ($I > 2\sigma(I)$) | 0.1095 |
| Final $R_1$ values (all data) | 0.0785 |
| Final $wR(F^2)$ values (all data) | 0.1321 |

## A.3.5 Ruthenium Macrocycle 36·$(PF_6)_2$

Crystals were grown by slow evaporation of an acetone solution of **36·$(PF_6)_2$**, giving large red blocks and partially solved by Dr. Nathan Kilah. Unfortunately the data collected proved

unsuitable for a full solution to be obtained, and a great deal of disorder remains in the structure.

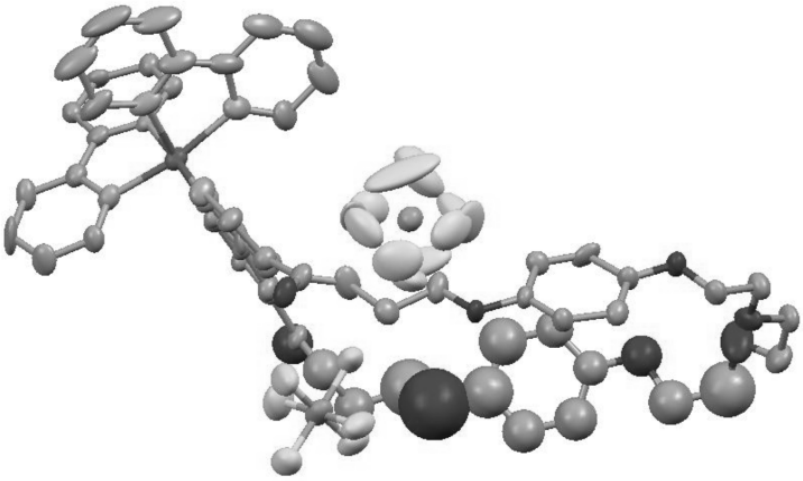


***Figure A5.*** *X-ray crystal structure of* ***36***$\cdot(PF_6)_2$*. Ellipsoids shown at 50% probability.*

## A.3.6 Ruthenium Nicotinamide Stopper 43·$(PF_6)(NO_3)$

Crystals were grown by slow evaporation of an acetone solution of **43·$(NO_3)(PF_6)$**, giving large red blocks, and solved by Dr. Christopher Serpell. Single crystal X-ray diffraction data were collected using graphite monochromated Mo Kα radiation (λ = 0.71073 Å) on a Nonius KappaCCD diffractometer. The diffractometer was equipped with a Cryostream $N_2$ open-flow cooling device,[3] and the data was collected at 150(2) K. Series of ω-scans were performed in such a way as to cover a sphere of data to a maximum resolution of 0.77 Å. Cell parameters and intensity data (including inter-frame scaling) were processed using the DENZO-SMN package.[10] The structure was solved by direct methods using the SIR92 software[5] and refined using full-matrix least-squares on $F^2$ within the CRYSTALS suite.[6] Although the majority of the structure was easily discerned, the acetone molecule O(64)-C(67) was difficult to resolve fully. It has been modelled as partially occupied, and required rigid-body refinement, as well as similarity restraints with respect to the other acetone molecule. All non-hydrogen atoms were refined with anisotropic displacement parameters.

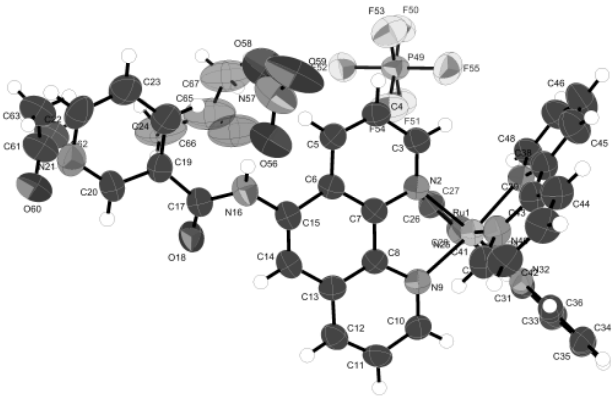


***Figure A6.*** *X-ray crystal structure of* ***43***$\cdot(NO_3)(PF_6)$*. Ellipsoids shown at 50% probability.*

| Chemical formula | $C_{38}H_{28}N_8ORu\cdot_{1.71}(C_3H_6O)\cdot F_6P\cdot NO_3$ |
|---|---|
| Formula Mass | 1019.82 |
| Crystal system | Monoclinic |
| *a*/Å | 11.8938(3) |
| *b*/Å | 13.4654(4) |
| *c*/Å | 26.7215(8) |
| *α*/° | 90 |
| *β*/° | 89.9032(12) |
| *γ*/° | 90 |
| Unit cell volume/Å$^3$ | 4279.6(2) |
| Temperature/K | 150 |
| Space group | *P*121/*c*1 |
| No. of formula units per unit cell, *Z* | 4 |
| No. of reflections measured | 49135 |
| No. of independent reflections | 9720 |
| $R_{int}$ | 0.033 |
| Final $R_1$ values ($I > 2\sigma(I)$) | 0.0653 |
| Final $wR(F^2)$ values ($I > 2\sigma(I)$) | 0.1409 |
| Final $R_1$ values (all data) | 0.0907 |
| Final $wR(F^2)$ values (all data) | 0.1636 |

## A.4 MD simulations: Experimental Details

Molecular dynamics simulations were carried out by Prof. Vitor Félix, Dr. Sergio Santos and Dr. Sílvia Carvalho at the University of Aveiro.

All MD simulations were carried out with the Amber 10 suite of programs.[11] The parameters for rotaxanes were taken from the General Amber Force Field (GAFF).[12] In our preliminary simulations it was observed that the default GAFF torsion parameters tend to lead to the

bending of the N-methyl group of the pyridinium axle from the ring plane. In order to correct this behavior, the default potential energy barrier ($V_n$), 0.3 kcal $mol^{-1}$, used to describe the X-ca-na-X torsion angles (where *ca* and *na* correspond to the pyridinium ring carbon and nitrogen atom, respectively, and × means any other atom) was increased to 1.5 $kcalmol^{-1}$ as found in AMBER parm99 force field for protonated histidine.[13] Partial atomic charges for the individual components of the rotaxanes (macrocycles and pyridinium axle) were fitted, according to the RESP methodology, on the electrostatic potential calculated at the HF/6-31G* level of theory with Gaussian03, using 10 concentric layer of points and a density of 10 points per layer.[14]

The methanol and chloroform solvent molecules were described using a full atom model with atomic charges and force field parameters taken from the literature.[15, 16] The TIP3P model was used for the water.[17] The chloride anion with charge of –1 was described with van der Waals parameters taken from the literature.[18] For the $OAc^-$ and $H_2PO_4^-$ polyatomic anions the atomic point charges were obtained from the literature[19, 20] and default GAFF atom types and parameters were used, except for the inorganic anion, in which the hydrogens were assigned with non-default GAFF atom type *hx*. This modification prevents the clash of the hydrogens in $H_2PO_4^-$ due to the absence of van der Waals parameters in the default atom type *ho*.

Low energy co-conformations were generated for rotaxane associations **14**·Cl, **14**·OAc, **14**·$H_2PO_4$, **20**·Cl and **11**·Cl, using gas phase simulations through quenched MD approach as follows. The individual interlocked rotaxane systems were submitted to a 2.5 ns molecular dynamics run at 2000 K with a 1 fs time-step. The use of this high temperature enables the system to cover all the conformational space since the energetic barriers are easily surmounted. 50000 structures were saved and subsequently minimized by molecular mechanics, through 1000 steps of the steepest descent method, followed by the conjugate

gradient method until a convergence criterion of 0.0001 kcal $mol^{-1}$ was achieved. The minimized structures were then sorted by molecular mechanics energy. For all anion interlocked rotaxanes, the lowest energy structure with *syn-syn*[21] co-conformation was selected and used in the solution MD simulations since that this conformation is the appropriated one to enable the chloride binding, as revealed by X-ray structure determinations of **14**·Cl and **22**·Cl.

The gas phase *syn-syn* conformations were solvated with a previously equilibrated cubic box of $CHCl_3/CH_3OH/H_2O$ (45/45/10). Subsequently, each solvated system was equilibrated under periodic boundary conditions as follows. The equilibration process started with the minimization of the solvent molecules by molecular mechanics keeping the solute fixed with a positional restrain of 500 kcal $mol^{-1}$ $Å^{-2}$. Then, the restraint was removed and the entire system was allowed to relax. The system was then heated up to 300 K over 100 ps in a NVT ensemble with a weak positional restraint (10 $mol^{-1}$ $Å^{-2}$) on the solute. The positional restraint was then removed and the system was allowed to equilibrate in a NPT ensemble at 300 K for 1 ns. At this stage, the box sizes of the solvated rotaxane systems were in the range of 46.2 to 53.8 Å. Finally, NPT data collection runs (300 K, 1 atm) were performed over 10 ns and snapshots were saved to a trajectory every 0.2 ps. Bond lengths involving all bonds to hydrogen atoms were constrained with the SHAKE algorithm.[22] The Particle Mesh Ewald method[23] was used to treat the long-range electrostatic interactions and the non-bonded van der Waals interactions were truncated with a 12 Å cut-off. The collected data were analyzed with the PTRAJ module implemented in the Amber package. The molecular modeling graphics were drawn with PyMOL.[24]

## A.5 References

1. M. J. Hynes, *J. Chem. Soc., Dalton Trans.*, 1993, 311-312.
2. M. T. Blanda, J. H. Horner and M. J. Newcomb, *J. Org. Chem.*, 1989, **54**, 4626-4636.

3. J. Cosier and A. M. Glazer, *J. Appl. Crystallogr.*, 1986, **19**, 105-107.
4. *CrystalClear: An Integrated Program for the Collection and Processing of Area Detector Data,*, Rigaku Corporation, 1997-2002.
5. A. Altomare, G. Cascarano, C. Giacovazzo, A. Guagliardi, M. C. Burla, G. Polidori and M. Camalli, *J. Appl. Crystallogr.*, 1994, **27**, 435.
6. P. W. Betteridge, J. R. Carruthers, R. I. Cooper, K. Prout and D. J. Watkin, *J. Appl. Crystallogr.*, 2003, **36**, 1487.
7. A. L. Spek, *J. Appl. Crystallogr.*, 2003, **36**, 7-13.
8. Z. Otwinoski and W. Minor, in *Macromolecular Crystallography, Pt A*, 1997, pp. 307-326.
9. L. Palatinus and G. J. Chapius, *Appl. Cryst.*, 1997, **40**, 786-790.
10. Z. Otwinowski and W. Minor, in *Macromolecular Crystallography, Pt A*, 1997, pp. 307-326.
11. D. A. Case, *AMBER 10*, University of California, San Francisco, 2008.
12. J. Wang, R. M. Wolf, J. W. Caldwell, P. A. Kollman and D. A. Case, *J. Comput. Chem.*, 2004, **25**, 1157-1174.
13. T. E. Cheatham III, P. Cieplak and P. A. Kollman, *J. Biomol. Struct. Dyn.*, 1999, **16**, 845-862.
14. M. J. Frisch, *Gaussian 03, Revision C.02*, Gaussian, Inc., Wallingford CT, 2004.
15. J. W. Caldwell and P. A. Kollman, *J. Phys. Chem.*, 1995, **99**, 6208-6219.
16. W. L. Jorgensen, J. M. Briggs and M. L. Contreras, *J. Phys. Chem.*, 1990, **94**, 1683-1686.
17. W. L. Jorgensen, J. Chandrasekhar, J. D. Madura, R. W. Impey and M. L. Klein, *J. Chem. Phys.*, 1983, **79**, 926-935.
18. I. S. Joung and T. E. Cheatham III, *J. Phys. Chem. B*, 2008, **112**, 9020-9041.
19. E. C. Meng, P. Cieplak, J. W. Caldwell and P. A. Kollman, *J. Am. Chem. Soc.*, 1994, **116**, 12061-12062.
20. J. R. Blas, M. Márquez, J. L. Sessler, F. J. Luque and M. Orozco, *J. Am. Chem. Soc.*, 2002, **124**, 12796-12805.
21. *The syn-syn co-conformation refers to the amide conformation in the macrocycle and pyridinium axle components of the rotaxane.*
22. J.-P. Ryckaert, G. Ciccotti and H. J. C. Berendsen, *J. Comput. Phys.*, 1977, **23**, 327-341.
23. U. Essmann, L. Perera, M. L. Berkowitz, T. Darden, H. Lee and L. G. Perdensen, *J. Chem. Phys.*, 1995, **103**, 8577-8593.
24. W. L. DeLano, *The PyMOL Molecular Graphics System 2002 on World Wide Web* http://www.pymol.org